ISSN 2071-4726
2071-0305

Инженерно-строительный журнал

НАУЧНОЕ ИЗДАНИЕ

№5(81) 2018

**Федеральное государственное автономное образовательное учреждение высшего образования
Санкт-Петербургский политехнический университет Петра Великого**

ПОЛИТЕХ
Санкт-Петербургский политехнический университет Петра Великого

**Инженерно-строительный институт
Центр дополнительных профессиональных программ**

***195251, г. Санкт-Петербург, Политехническая ул., 29,
тел/факс: 552-94-60, www.stroikursi.spbstu.ru,
stroikursi@mail.ru***

**Приглашает специалистов организаций, вступающих в СРО,
на курсы повышения квалификации (72 часа)**

Код	Наименование программы	Виды работ*
Курсы по строительству		
БС-01-04	«Безопасность и качество выполнения общестроительных работ»	**п.1,2, 3, 5, 6, 7, 9, 10, 11, 12, 13, 14**
БС-01	«Безопасность и качество выполнения геодезических, подготовительных и земляных работ, устройства оснований и фундаментов»	**1,2,3,5**
БС-02	«Безопасность и качество возведения бетонных и железобетонных конструкций»	**6,7**
БС-03	«Безопасность и качество возведения металлических, каменных и деревянных конструкций»	**9,10,11**
БС-04	«Безопасность и качество выполнения фасадных работ, устройства кровель, защиты строительных конструкций, трубопроводов и оборудования»	**12,13,14**
БС-05	«Безопасность и качество устройства инженерных сетей и систем»	**15,16,17,18,19**
БС-06	«Безопасность и качество устройства электрических сетей и линий связи»	**20,21**
БС-08	«Безопасность и качество выполнения монтажных и пусконаладочных работ»	**23,24**
БС-12	«Безопасность и качество устройства мостов, эстакад и путепроводов»	**29**
БС-13	«Безопасность и качество выполнения гидротехнических, водолазных работ»	**30**
БС-14	«Безопасность и качество устройства промышленных печей и дымовых труб»	**31**
БС-15	«Осуществление строительного контроля»	**32**
БС-16	«Организация строительства, реконструкции и капитального ремонта. Выполнение функций технического заказчика и генерального подрядчика»	**33**
Курсы по проектированию		
БП-01	«Разработка схемы планировочной организации земельного участка, архитектурных решений, мероприятий по обеспечению доступа маломобильных групп населения»	**1,2,11**
БП-02	«Разработка конструктивных и объемно-планировочных решений зданий и сооружений»	**3**
БП-03	«Проектирование внутренних сетей инженерно-технического обеспечения»	**4**
БП-04	«Проектирование наружных сетей инженерно-технического обеспечения»	**5**
БП-05	«Разработка технологических решений при проектировании зданий и сооружений»	**6**
БП-06	«Разработка специальных разделов проектной документации»	**7**
БП-07	«Разработка проектов организации строительства»	**8**
БП-08	«Проектные решения по охране окружающей среды»	**9**
БП-09	«Проектные решения по обеспечению пожарной безопасности»	**10**
БП-10	«Обследование строительных конструкций и грунтов основания зданий и сооружений»	**12**
БП-11	«Организация проектных работ. Выполнение функций генерального проектировщика»	**13**
Э-01	«Проведение энергетических обследований с целью повышения энергетической эффективности и энергосбережения»	
Курсы по инженерным изысканиям		
И-01	«Инженерно-геодезические изыскания в строительстве»	**1**
И-02	«Инженерно-геологические изыскания в строительстве»	**2,5**
И-03	«Инженерно-гидрометеорологические изыскания в строительстве»	**3**
И-04	«Инженерно-экологические изыскания в строительстве»	**4**
И-05	«Организация работ по инженерным изысканиям»	**7**

***(согласно приказам Минрегионразвития РФ N 624 от 30 декабря 2009 г.)**

По окончании курса слушателю выдается удостоверение о краткосрочном повышении квалификации установленного образца (72 ак. часа)

Для регистрации на курс необходимо выслать заявку на участие, и копию диплома об образовании по телефону/факсу: 8(812) 552-94-60, 535-79-92, , e-mail: stroikursi@mail.ru.

Инженерно-строительный журнал
НАУЧНОЕ ИЗДАНИЕ

ISSN 2071-4726, 2071-0305

Свидетельство о государственной регистрации: ПИ №ФС77-38070, выдано Роскомнадзором

Специализированный научный журнал. Выходит с 09.2008.

Включен в Перечень ведущих периодических изданий ВАК РФ

Периодичность: 8 раз в год

Учредитель и издатель:

Санкт-Петербургский политехнический университет Петра Великого

Адрес редакции:

195251, СПб, ул. Политехническая, д. 29, Гидрокорпус-2, ауд. 245

Дата выхода: 19.10.2018

Содержание

Контакты:
E-mail: mce@spbstu.ru
Web: http://www.engstroy.spbstu.ru

Magazine of Civil Engineering
SCHOLAR JOURNAL

ISSN 2071-4726, 2071-0305
Peer-reviewed scientific journal
Start date: 2008/09
8 issues per year

Publisher:
Peter the Great St. Petersburg Polytechnic University

Indexing:
Scopus, Russian Science Citation Index (WoS), Compendex, DOAJ, EBSCO, Google Academia, Index Copernicus, ProQuest, Ulrich's Serials Analysis System

Corresponding address:
245 Hydro Building, 29 Polytechnicheskaya st., Saint-Petersburg, 195251, Russia

Date of issue: 19.10.2018

Contents

E-mail: mce@spbstu.ru
Web: http://www.engstroy.spbstu.ru/eng/index.html

doi: 10.18720/MCE.81.1

Heating and charring of timber constructions with thin-layer fire protection

Прогрев и обугливание деревянных конструкций с тонкослойной огнезащитой

E.Yu. Polishchuk*,
A.B. Sivenkov,
S.K. Kenzhehan,
Fire Academy of Emercom of Russia, Moscow, Russia

Канд. техн. наук, докторант
Е.Ю. Полищук*,
д-р техн. наук, ученый секретарь
А.Б. Сивенков,
адъюнкт С.К. Кенжехан,
Академия ГПС МЧС России, г. Москва, Россия

Key words: timber construction; fire protection; charring; wood; fire resistance; prediction method

Ключевые слова: огнестойкость; пожарная опасность; деревянные конструкции; огнезащита; прогнозирование; обугливание; древесина

Abstract. The results of fire tests of constructions (beams) with fire retardant film coating in one-side fire effect under standard temperature fire regime are shown in this article. Intensity dynamics of samples heating and their charring process in thickness and along the perimeter were chosen as the key indicators. It is shown that the use of thin-layer non-swelling fire retardant coatings does not influence the intensity dynamics, in case of high-temperature exposure generates from the side of the bottom edge, however, but is able to localize the burning action effectively, thereby producing a positive impact on the level of fire hazard and fire resistance of building constructions. The directions of possible development of methodological approach to the calculation and analytical assessment of fire retardant indicators and classes of fire hazard of timber constructions with non-construction fire protection have been determined.

Аннотация. Приведены результаты огневых испытаний конструкций (балок) с огнезащитными пленочными покрытиями при одностороннем огневом воздействии в условиях стандартного температурного режима пожара. В качестве ключевых показателей были выбраны интенсивность динамики прогрева образцов и процесса их обугливания по толщине и по периметру образца. Показано, что применение тонкослойных не вспучивающихся огнезащитных покрытий не оказывает влияния на динамику прогрева, в случае действия источника высокотемпературного воздействия со стороны нижней грани, однако способно эффективно ограничивать распространение горения, оказывая общее положительное влияния на уровень пожарной опасности и огнестойкости строительных конструкций. Определены направления возможного развития методических подходов к расчетно-аналитической оценке показателей огнестойкости и классов пожарной опасности деревянных конструкций с неконструктивной огнезащитой.

1. Introduction

For many years buildings and constructions fire protection problem with the use of timber constructions attracts attention of researchers from different countries [1–8]. Through these research papers, quite abundant knowledge about patterns of wood burning process, the influence of various individual chemical substances and their mixtures on the processes of thermal decomposition of timber-based material, interrelations of charring parameters with constructions fire retardant indicators and also, methods and types of fire protection have been formed [9].

However, researches, as a rule, are limited to the study of timber constructions properties on its base under high temperature effect with the use of relatively small samples (hinges, beams and construction elements) [10, 11], including in the presence of fire retardant materials [12]. For all of those purposes the complex of physicochemical methods of investigation such as thermal analysis and various calorimetric methods are as actively used as laboratory methods of assessment of fire and technical materials characteristics (combustibility, flammability, flame spread, smoke-forming ability and toxicity of combustion products) [13–17].

Полищук Е.Ю., Сивенков А.Б., Кенжехан С.К. Прогрев и обугливание деревянных конструкций с тонкослойной огнезащитой // Инженерно-строительный журнал. 2018. № 5(81). С. 3–14.

In majority cases these methods allow to assess the capacity of relatively thin (10–15 mm, rarely – to 70 mm) wooden samples with fire protection to resist the effect of ignition sources of different power. However, the characteristics obtained as a result cannot usually be scaled for the purposes of predicting the behaviour of timber constructions of different sections, areas, humidity and ages under standard or real fire regimes.

Certainly, it is possible to attract large scale fire tests for these purposes. In different countries methodological approaches to the assessment of fire hazard and fire resistance of building constructions are similar [18–23], and, as a rule, such researches involve the need to prepare full-scale constructions [24–26] and test results of not more than 2 or 3 identical constructions, what makes it difficult to perform statistical analysis and to assess the reliability or the relevance of the experimental data obtained. In particular, in recent years, during a series of experiments, the authors have shown the capacity of fire retardant impregnating compositions including surface coating to increase the class of timber constructions fire hazard and fire resistance [27–29]. There are some works devoted to the study of fire hazard and fire retardant of timber constructions processed by intumescent [30, 31] and thick coating [32, 33], as well as with construction fire protection [34, 35]. However, the presented results need to be further approved, and their interpreting remain challenges of methodological and technical nature, in particular, an assessment of such an important indicator of timber construction as the charring dynamics is often carried out with the basis on indirect criteria, such as the heating dynamics in the places where thermocouples are situated [29, 34], since it is not possible to examine constructions after completion of the test.

In the light of wooden house buildings development and the need to provide objects with fire safety using wood as the main construction material [36, 37] the development of methodological approaches to the integrated assessment of indicators that characterized fire resistance of timber constructions and necessary for mathematical modelling of constructions behavior under standard and real thermal fire regimes gain special pertinence and significance.

The development of capabilities of systems and means of mathematical modelling and computer-aided design of multi – layered systems through various options of possible impacts that call for a need of improving constructions and their fragments test methods are relevant to the current circumstances. The review of approaches to the evaluated estimate of rationed indicators taking into account the development of numerical modelling methods should be provided [25].

Under the current principals [38–41] to the evaluated estimate of timber constructions fire resistance, it is assumed that the construction is subject to three- or four-side fire effect (Figure 1), and the effect of fire protection is determined by the ability to provide heat insulation of the protected surface [38, 42]. The impact of non-constructive fire protection is not actually taken into consideration, it is assumed that losing the thermal insulating capacity by the facing leads to “the instant complete charring” of the construction, after which the charring rate of all the sides becomes higher or equal to the standard rate (0.65 mm for wood of coniferous trees, in case of one-side heating) [38], regardless of the presence of surface or deep flameproofing that seems to be not in conformity with their effective role [28, 29].

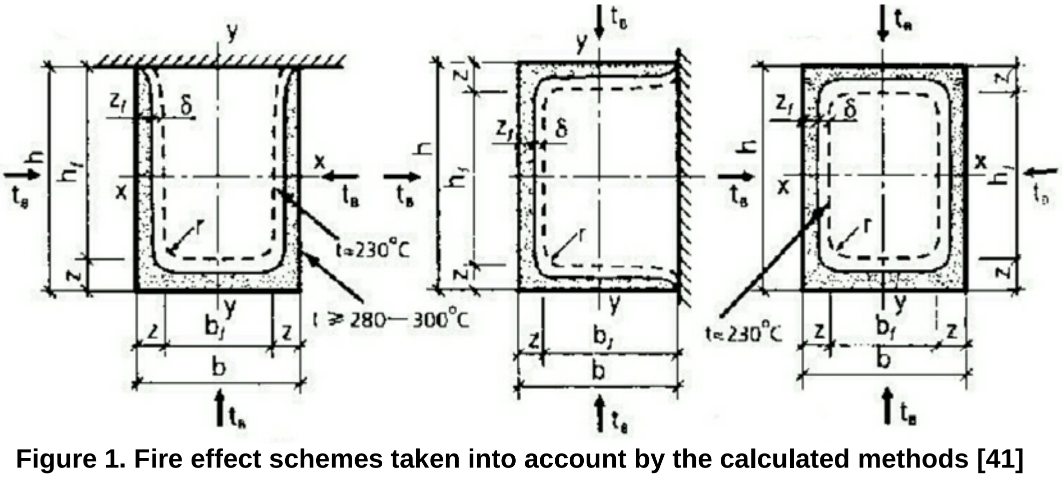

Figure 1. Fire effect schemes taken into account by the calculated methods [41]

The aim of the work is the formation of the methodological approaches to the evaluated estimate of the influence of flameproofing on the indexes of the fire hazard and fire resistance of timber constructions.

Allowances and simplifications made in the calculated methods are related in many ways to the imperfection of the methods of fire resistance experimental evaluation. As a result, the possibility to apply methods of calculated prediction of non-standard constructions used in the modern timber construction is strictly limited. In fact, it is possible to say that, under the following frameworks, convenient correcting factors are selected for each technical solution, according to the test results.

In the current work the following tasks of influence of flameproofing with the use of thin film coating on the indexes are being solved:

- Dynamics of timber constructions heating under one-sided fire effect of the standard fire temperature control;
- Flame spread on the surface outside the zone of fire effect;
- Charring rate of timber constructions under one-sided fire effect.

These parameters are defined for both unprocessed constructions and fire-proofing constructions with the use of thin-coat roll film coating (thickness 1.5 mm).

To explore the behaviour of timber constructions with non-thermal-insulting fire protection under one-sided fire effect, to develop methodological approaches to the assessment of fire protection efficiency in relation to the constructions and the predictive assessment of fire hazard and fire resistance of constructions with non-construction and thin-layer fire protection new film fire retardant coatings on the base of commercially produced film-forming oligomer systems laid on glass-cloth reinforcing framework have been chosen [43, 44]. The mechanism of fire-protection action of the applied coatings is determined by forming a filter barrier, which prevents the mass transfer between the flammable substrate and the environment, on the surface of the protected material.

This coating, combined with vinyl and acetate glue system, provides I – II groups of fire protection effectiveness with from 5.5 up to 13 % mass loss, in accordance with adopted in Russia methods of effectiveness assessment of wood fire retardant materials according to the national standard of the Russian State Standard GOST R 53292-2009 [45], provides the transfer of wood and materials based on it into a group of inflame-resistant materials (the critical surface density of heat flux is more than 20 kW/m^2) which have moderate smoke-forming ability and do not spread flame on the surface.

2. Methods

To study features of influence of fire retardant means and materials on the fire hazard and timber constructions fire resistance indicators the approach that includes quantitative assessment of the tested beams heating dynamic and the levels of their thermal damage on the indicator of perimeter change of the cross sections are being offered. For this purpose the installation for thermophysical studies and tests of small fragments of flat constructions and individual components of their joining transition and fixing was used in the work [46].

The experiment was carried out in parallel for two samples of pine wood beams with a specific gravity of 455 kg/m^3 and equilibrium humidity of 12% with the actual sizes 135x135x600 mm without fire protection (sample # 0) and with fire retardant film coating (sample # 1).

The scheme of samples layout is shown in the Figure 2, to prevent (decrease) the mutual influence. The area between the samples was filled with two gypsum sheets with a thickness of 10 mm each, mechanically attached to the tested samples. Foam concrete blocks were used as non-combustible fill.

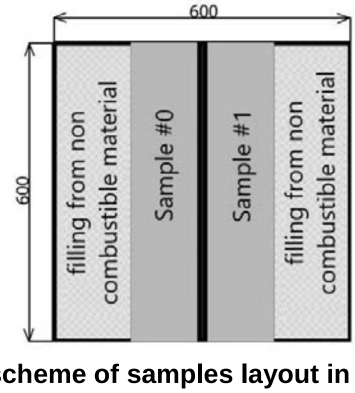

Figure 2. The scheme of samples layout in the test furnace

Each sample had thermoelectric converters (TS) at a depth of from 10 to 50 mm from the exposed surface in accordance with the scheme shown in the Figure 3.

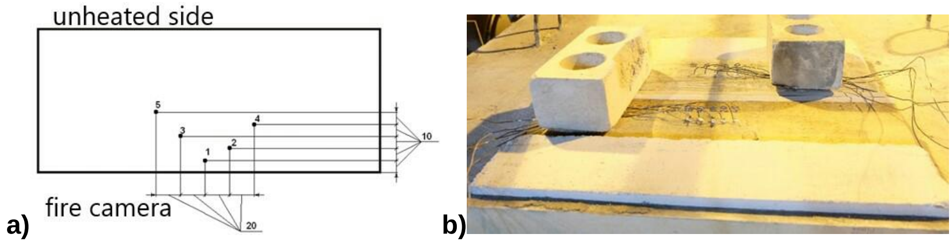

Figure 3. The scheme of technical support (TS) installation in wood beams: a) in cut; b) top view at the place of installation

Tests, lasting 60 minutes were conducted in the conditions of the standard temperature regime in accordance with the requirements of ISO 834. Fire-resistance tests — Elements of building construction — Part 1: General requirements. The fixing of heating dynamics was conducted during the experiment. After fire exposure, the samples were subjected to forced suppression, the samples and char layers state was recorded and the charring depth was evaluated as well.

3. Results and Discussion

The comparative analysis of the heating dynamics of the tested samples (Figures 4-5) shows that fire retardant coating does not actually affect the heating dynamics of the samples in the temperature range of the decomposition of wood (150–200 °C [32]). In the specified temperature range, the growth rate of the temperatures is apparently determined by the features of the wood specific samples.

These results show that there is higher heating dynamics for the sample with fire retardant coating in the surface layer (Figure 4a). This phenomenon involves most likely the use as a reinforcing base of incombustible heat-retardant glass cloth and can be attributed to the difficulty of heat and mass transfer between the sample surface and the environment in the direction of decreasing the dissipation of heat, i.e. in fact, its accumulation takes place in the volume between the fire retardant coating and wood surface that is able to influence on the overall level of fire hazard of such a construction reducing its contribution to the formation of dangerous fire factors.

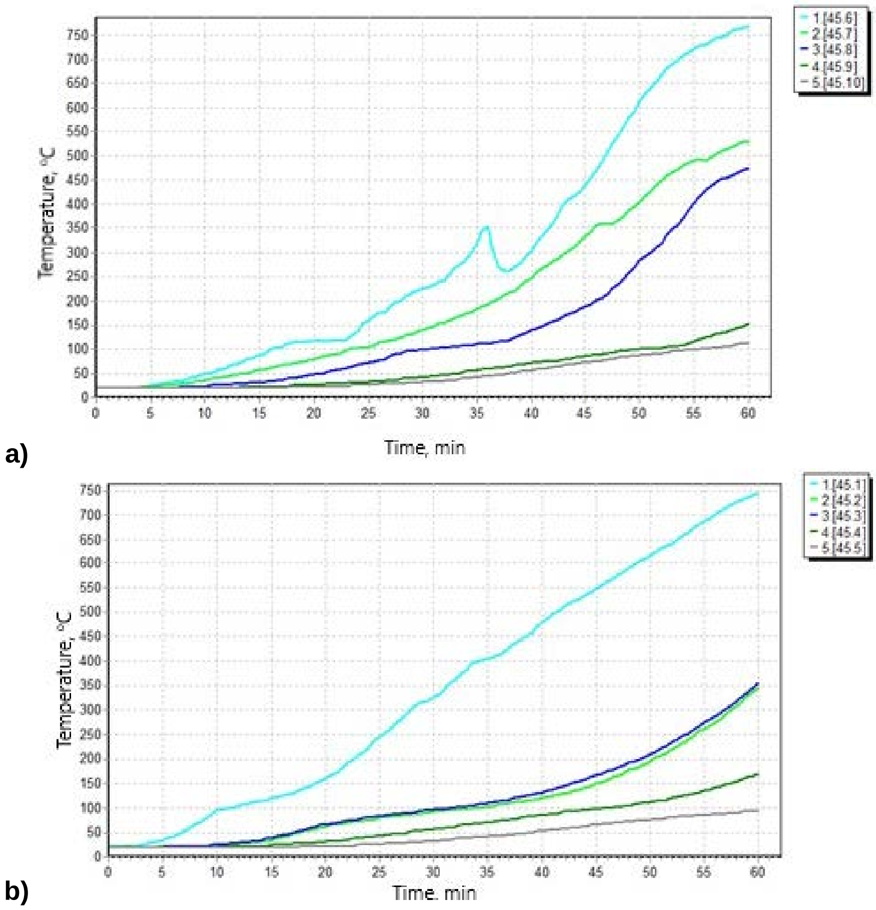

Figure 4. The dynamics of beam heating without fire protection (a) and with fire retardant film coating (b): 1, 2, 3, 4, 5 –numbers of thermocouple in accordance with the Figure 2

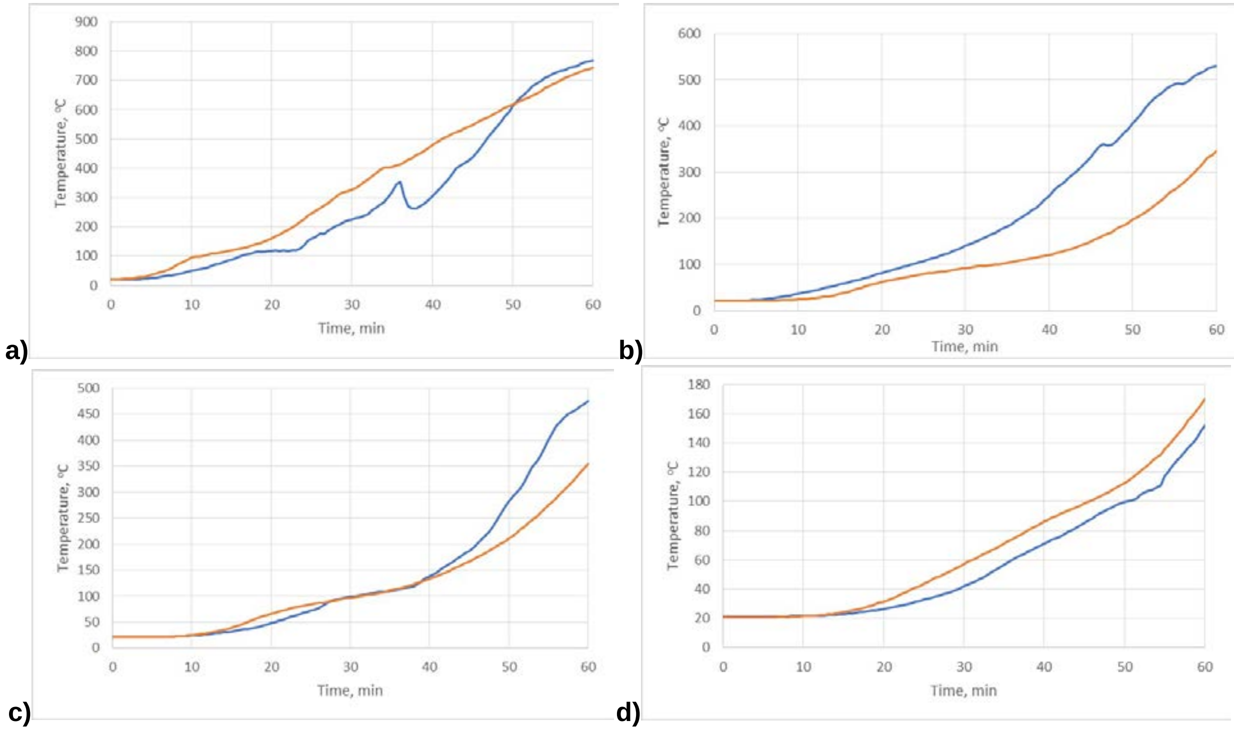

Figure 5. The dynamics of wooden beam heating at a depth of (a) 10, (b) 20, (c) 30, (d) 40 and (e) 50 mm from the exposed surface: 0 - without fire protection; 1 - with fire retardant film coating

In this case, the estimated average speeds of charring for unprotected wooden beams are in the range of 0.27 mm/min at the surface (TS No. 1) to 0.61 mm/min at a depth of 30 mm from the exposed surface (TS No. 3). For the sample with fire retardant coating the corresponding values are from 0.38 to 0.54 mm/min. Thus, according to the objective observations with one-sided fire exposure from the side of the bottom edge of the charring speed for both samples was in the same range.

Both tested samples had the same dynamics of achieving temperature of 100 °C in the sample volume (Figure 6), and thus [39, 40] the zone, overheated more than this temperature, is necessary to exclude from the fire retardant calculation.

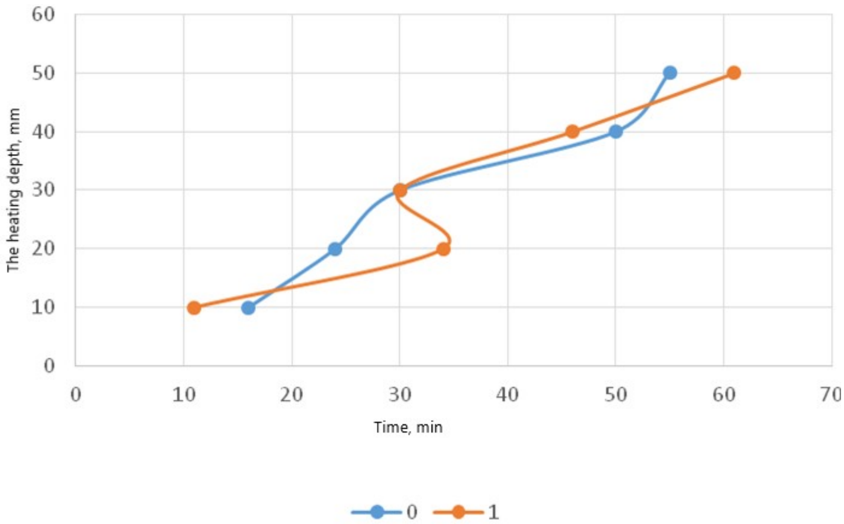

Figure 6. The dynamics of wooden beam heating with one-sided fire exposure: 0 – sample without fire protection; 1 – sample with film fire retardant coating

Minor differences in the heating dynamics, represented in the Figure 6, are most likely determined by the characteristics of timber constructions, the presence of cracks and defects (the type of wood). The combination of obtained data allows identifying the linear dependence of the heating depth from the time of fire exposure (Figure 7).

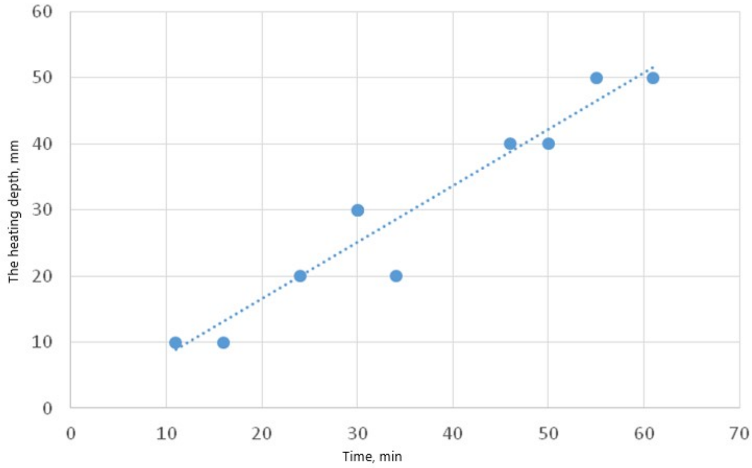

Figure 7. The dependence of the depth of wooden beam heating up to 100 °C from time of fire exposure from the side of the bottom face

Taking into account the obtained data, the intensity of the construction heating and charring process can be represented in the form of the equation 1 with the value of reliability of approximation 0.9235:

$$h = 0.8551 * t - 0.5261 - Z \tag{1}$$

where *h* is the depth of heating to 100 °C; *t* – time of fire exposure (standard temperature fire regime) on the bottom edge of a wooden beam, min.; *Z* is the depth of charring, determined as the product of the regulatory rate of charring [38, 41] at the time of fire exposure.

In accordance with the mathematical relation, looking at "normative" values of charring rate (0.65 mm/min) [33], at the time of fire exposure of the charring depth is 39 mm and overheated layer thickness is more than 11 mm. At the present time accepting under calculations the thickness of overheated layer is 7 mm [40, 41] that corresponds to 20–25 minutes of fire exposure.

Thus, according to the analysis of the data of objective control of dynamics of wooden beam heating with fire protection and fire resistance, the conclusion about absence of positive influence of the tested fire retardant coating on the level of fire hazard and fire resistance of timber constructions can be made. The similar conclusions can be made according to the results of the charring current depth changes from the side of exposed surface where the charring speed status for both samples were also close to 0.63 and 0.5–0.83 mm/min for both the untreated and fire retardant samples.

At the same time, the obtained data analysis allows identifying the range features in the behavior of investigated timber samples that need to be considered under fire hazard assessment and fire resistance of timber constructions with fire protection, and namely:

– before the violation of the integrity of film fire retardant coating there was no the features of flaming combustion above the sample surface (Figure 8b);

a)  b) 

Figure 8. The samples surface condition with fire protection (from the bottom) and without fire protection (at the top) through: a) 20 minutes after fire exposure start-up; b) 50 minutes after fire exposure start-up

– in 40 minutes after fire exposure start-up there was both side and frontal surfaces fire outlet without fire protection (Figure 9), and for the sample with the fire retardant coating there was burning outlet only from the side of one of the frontal surfaces that had not undergone the flameproofing.

Figure 9. Fire outlet outside the fire camera in 40 – 45 minutes after fire exposure star-up

As a result of experiment the damage area for fire retardant coating sample did not exceed 40 % (Figure 10b), while the sample without fire protection had two totally charred frontal and side edges (Figure 10a) and the total area of damages exceeded 60 %.

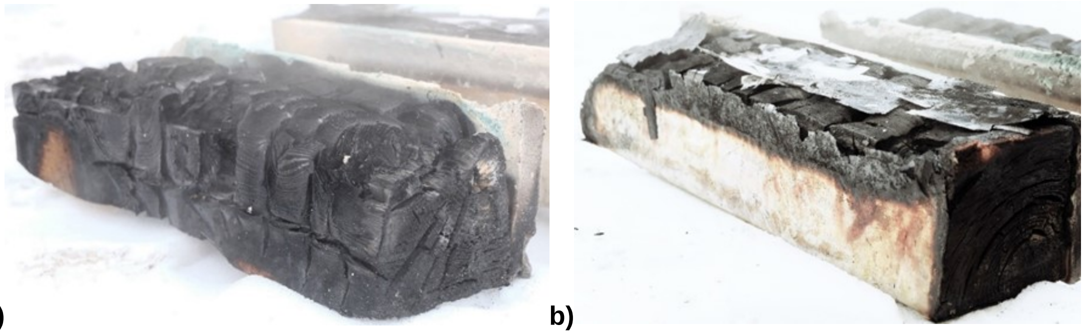

a) b)

Figure 10. Samples appearance after testing: a) without fire protection; b) with film fire retardant coating

The rate of the sample charring without fire protection in the central part of one of the side edges has been reached 0.5 - 0.6 mm/min (Figure 11) while the sample of fire retardant coating of the side edge have remained intact.

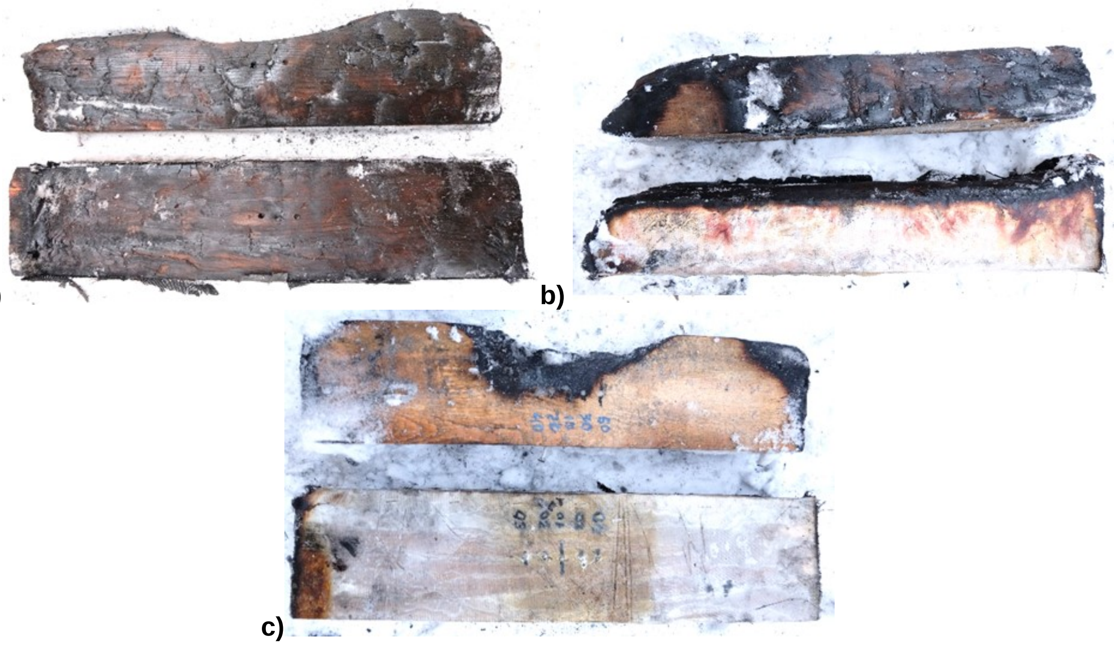

a) b) c)

Figure 11. Appearance of the samples without fire protection (at the top) and with film fire retardant coating (at the bottom) after char seams removal: a) view from the side of exposed surface; b) view from the side of the top (unheated) surface (Figure 2)

The analysis of obtained data allows making the conclusions that the modern approach to the definition of the charring average speed indicator (mm/min) does not fully characterize the behavior of timber constructions in the terms of fire exposure (fire) and does not take into consideration the material features to propagate burning on the surface and support the burning without external heat flux. In majority cases the researchers consider that only exposed surface is charred [24, 25, 39, 40].

The impact of fire retardant materials on the construction behavior in the conditions of fire is able to be considered by the authors according to the size changes of the working sample cross section within the rate of the area reducing or perimeter cross section. Thus, before and after experiment the control of the perimeter length of the working cross section samples has shown that for the sample without fire protection the maximum perimeter reducing in the central part has been reached 160 mm, from 540 up to 380 mm. The rate of loss of the cross section was 2.7 mm/min that corresponds to two-side heating (perimeter calculated changes under one-side heating 1.3 mm/min) under standard charring rate is 0.65 mm/min. The maximum cross section reducing for the sample with fire protection was 80 mm, and the perimeter decreasing rate was 1.3 mm/min.

Making the analysis regarding the linear parameters of the process of thermal damage of timber constructions elements demonstrates uneven loss of the value of cross section sample, and also the impact of features of applying fire retardant materials technology for timber constructions, for instance, film fire retardant coating. The more objective assessment of fire retardant materials effectiveness for the constructions can be considered in assessing both samples heating dynamics and thermal burnout (charring) of their surface layer.

The main disadvantage of the perimeter length changes rate of the perimeter cross section is the difficulty of its standardization in the relation of the constructions with different rates of width and height. The possible solution to the problem can be the introduction of universal indicator that allows more accurately estimate the residual load capacity of timber construction in the process of fire impact (fire). Such an indicator can be "sector rate", characterizing the changes of timber constructions cross-section area. To this end, the cross-section was divided into 8 sectors (Figure 12), each monitoring the residual cross – sectional area with features of the temperature effect focus on the construction sample.

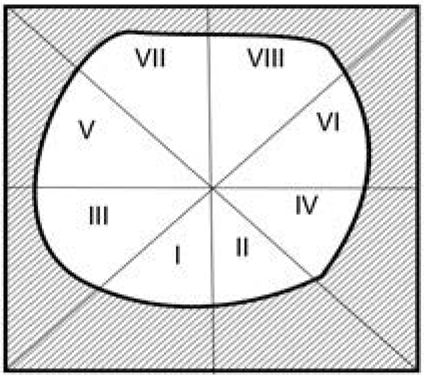

Figure 12. The example of dividing element cross-section of timber constructions on the sector

Methodological assessment of fire resistance of timber constructions may involve the solution of two main tasks:

- determining directly the square of residual (non – charred) cross-section, but not the thickness of the charring surface [40];
- assessment of strength characteristics of the residual cross - section with the temperature gradient. It is assumed that the individual indicators of the calculated retardants have to be applied for each temperature zone [47].

Thus, the changes rate of its area with the use of the finite elements method can be determined for each sector. It will allow with the use of hardware and software solve the task of identifying the residual value of the construction cross-section and its load capacity in the terms of fire depending on the direction and intensity of fire exposure, presence, type and method of fire protection. In future, this field requires very careful methodological work based on the opportunity of computer software use [48–50], focused on prediction of classification indicators of fire hazard and fire resistance of timber constructions.

4. Conclusions

The undertaken study and the obtained results lead to the following conclusions:

1. Under one-sided fire effect of the standard temperature fire regime on the side of the lower edge difference in heating dynamic of samples without fire protection and with thin - layer fire- protection do not have significant differences;
2. The presence of surface non-thermal-insulting flameproofing allows reducing the area of thermal damages by localizing them in the zone of external fire effect;
3. Flameproofing with the use of thin-layer non-thermal-insulting fire retardant materials and coatings does not significantly influence the index of average linear charring rate of timber constructions which is ranged from 0.5 to 1.25 mm/min for samples with or without flameproofing;
4. The use of thin-layer fire retardant coatings and materials allows slowing down the rate of the area reducing of the cross section of timber construction by limiting the flame spread outside the zone of fire effect. The use of thin-layer fire retardant coating for fire protection allowed reducing the rate from 2.7 mm/min for the sample without fire protection to 1.3 mm/min for the one with fire retardant film coating.

References

1. Terzal, E., Kartal, S.N., White, R.H., Shinoda, K., Imamura, Y. Fire performance and decay resistance of solid wood and plywood treated with quanternary ammonia compounds and common fire retardants. Eur. J. Wood Prod. 2011. Vol. 69. Pp. 41–51.
2. Ozdemir, F., Tutus, A. Effects of fire retardants on the combustion behavior of high-density fiberboard. Bio Ressources. 2013. Vol. 8(2). Pp. 1665–1674.
3. Wang, Q., Li, J., Winandy, J.E. Chemical mechanism of fire retardantce of boric acid on wood. Wood Sci Technol. 2004. Vol. 38. Pp. 375–389
4. Boruszewski, P. Characteristics of selected fireproof properties of particleboard made from particles impregnated with salt agent. Annals of Warsaw university of Life Science – SGGW Forestry and Wood technology. 2011. No. 73. Pp. 142–146.
5. Harada, T., Kamikawa, D., Miyatake, A., Momohara, I., Miybayashi, M., Imamura, Y. Fire resistance of structural glued laminated timber treated with wood preservatives. Mokuzai Gakkaishi. 2015. Vol. 61. No. 2. Pp. 82–87. (jap, Resume, Fig., Table: Eng.)
6. Saknite, T., Serdjuks, D., Goremikins, V., Pakrastins, L., Vatin, N.I. Fire design of arch-type timber roof. Magazine of Civil Engineering. 2016. No. 4(64). Pp. 26–39.
7. Vilguts, O.A., Serdjuks, D., Pakrastins, L. Design Methods of Elements from Cross- Laminated Timber Subjected to Flexure. Saint-Petersburg: Proceedings of the "International Scientific Conference - Urban Civil Engineering and Municipal Facilities". Procedia Engineering. 2015. Vol. 117. Pp. 10–19.
8. Chernenko, V.A. Technology of wood impregnation by polymeric compositions. Construction of Unique Buildings and Structures. 2017. No. 7(58). Pp. 32–52. doi: 10.18720/CUBS.58.3
9. Lowden, L.A., Hull, T.R. Flammability behaviour of wood and a review of the methods for its reduction. Fire Science Reviews. 2013. 2:4. DOI 10.1186/2193-0414-2-4
10. Vermasi, I., DiDomizio, M.J., Richter, F., Weckman, E.J. Pyrolysis and spontaneous ignition of wood under transient irradiation: Experiment and a-priori predictions. Fire safety journal. 2017. Vol. 91. Pp. 218–225.
11. Yang, Z., Yi, A., Liu, J., Zhao, X. Study of fire hazard of flooring materials on data of cone calorimetr. Procedia Engineering. 2016. Vol. 135. Pp. 584–587.
12. Garay, R., Henriquez, M. Fire performance of boards and pine radiata wood with and without flame retardant paint. Ciencia y technologia. 2010. Vol. 12(1). Pp. 11–24.
13. Ukaszek, A., Polka, M., Konecki, M. Analysis of the visibility range in smoke generated in the course of the

Литература

1. Terzal E., Kartal S.N., White R.H., Shinoda K., Imamura Y. Fire performance and decay resistance of solid wood and plywood treated with quanternary ammonia compounds and common fire retardants // Eur. J. Wood Prod. 2011. Vol. 69. Pp. 41–51.
2. Ozdemir F., Tutus A. Effects of fire retardants on the combustion behavior of high-density fiberboard // Bio Ressources. 2013. Vol. 8(2). Pp. 1665–1674.
3. Wang Q., Li J., Winandy J.E. Chemical mechanism of fire retardantce of boric acid on wood // Wood Sci Technol. 2004. Vol. 38. Pp. 375–389.
4. Boruszewski P. Characteristics of selected fireproof properties of particleboard made from particles impregnated with salt agent // Annals of Warsaw university of Life Science – SGGW Forestry and Wood technology. 2011. № 73. Pp.142–146.
5. Harada T., Kamikawa D., Miyatake A., Momohara I., Miybayashi M., Imamura Y. Fire resistance of structural glued laminated timber treated with wood preservatives // Mokuzai Gakkaishi. 2015. Vol. 61. № 2. Pp. 82–87. (jap, Resume, Fig., Table: Eng.)
6. Сакните Т., Сердюк Д.О., Горемыкин В.В., Пакрастиньш Л., Ватин Н.И. Проектирование огнестойких арочных деревянных покрытий // Инженерно-строительный журнал. 2016. № 4(64). С. 26–39. DOI: 10.5862/MCE.64.3
7. Vilguts O.A., Serdjuks D., Pakrastins L. Design Methods of Elements from Cross- Laminated Timber Subjected to Flexure // Saint-Petersburg: Proceedings of the "International Scientific Conference - Urban Civil Engineering and Municipal Facilities". Procedia Engineering. 2015. Vol. 117. Pp. 10–19.
8. Черненко В.А. Технологии пропитки древесины полимерными композициями // Строительство уникальных зданий и сооружений. 2017. № 7(58). С. 32–52. DOI: 10.18720/CUBS.58.3
9. Lowden L.A., Hull T.R. Flammability behaviour of wood and a review of the methods for its reduction // Fire Science Reviews. 2013. 2:4. DOI 10.1186/2193-0414-2-4
10. Vermasi I., DiDomizio M.J., Richter F., Weckman E.J. Pyrolysis and spontaneous ignition of wood under transient irradiation: Experiment and a-priori predictions // Fire safety journal. 2017. Vol. 91. Pp. 218–225.
11. Yang Z., Yi A., Liu J., Zhao X. Study of fire hazard of flooring materials on data of cone calorimetr // Procedia Engineering. 2016. Vol 135. Pp. 584–587.
12. Garay R., Henriquez M. Fire performance of boards and pine radiata wood with and without flame retardant paint // Ciencia y technologia. 2010. Vol. 12(1). Pp. 11–24.

combustion of oak wood protected by selected fire retardants. Annals of Warsaw University of Life Sciences – SGGW Forestry and Wood Technology 2011. No. 75. Pp. 59–63.
14. Vasiljevich, J., Jerman, I., Jaksa, G., Alongi, J., Malucelli, G., Zorko, M., Tomshich, B., Simonchic, B. Functionalization of cellulose fibres with DOPO-polysilsesquioxane flame retardant nanocoating. Cellulose. 2015. Vol. 22. Pp. 1893–1910. DOI 10.1007/s10570-015-0599-x
15. Kim, J., Lee, J.-H., Kim, S. Estimating the fire behavior of wood flooring using a cone calorimeter. J Therm Anal Calorim. 2012. Vol. 110. Pp. 677–683. DOI 10.1007/s10973-011-1902-1
16. Merk, V., Chanana, M., Keplinger, T., Gaand, S., Burgert, I. Hybrid wood materials with improved fire retardance by bio-inspired mineralisation on the nano- and submicron level. Green Chem. 2015. Vol. 17. Pp. 1423–1428. DOI: 10.1039/c4gc01862a
17. Merryweather, G., Spearpoint, M.J. Flame spread measurements on wood products using the ASTM E 1321 LIFT apparatus and a reduced scale adaptation of the cone calorimeter. Fire and materials. 2010. Vol. 34. Pp. 109–136. DOI: 10.1002/fam.1001
18. Gravit, M.V. Garmonizatsiya rossiyskikh i yevropeyskikh normativnykh dokumentov, reglamentiruyushchikh metody ispytaniy na ognestoykost stroitelnykh konstruktsiy s ispolzovaniyem sredstv ognezashchity [Harmonization of Russian and European regulatory documents establishing the methods of fire tests of building structures with the use of fire protection]. Fire and Explosion Safety. 2014. Vol. 23. No. 5. Pp.38–46. (rus)
19. Gravit, M.V., Nedryshkin, O.V., Vaytitskiy, A.A., Shpakova, A.M., Nigmatullina, D.G. Fire technical characteristics of building materials in the European and Russian regulatory documents. Problems of harmonization of research methods and classification. Fire and Explosion Safety. 2016. Vol. 25. No. 10. Pp. 16–29. DOI: 10.18322/PVB.2016.25.10.16-29. (rus)
20. International standart of Commonwealth of Independent States GOST 30247.0 Konstruktsii stroitelnyye. Metody ispytaniy na ognestoykost. Obshchiye trebovaniya [Elements of building constructions. Fire-resistance test methods. General requirements]. (rus)
21. International standart of Commonwealth of Independent States GOST 30247.1 Konstruktsii stroitelnyye. Metody ispytaniy na ognestoykost. Nesushchiye i ograzhdayushchiye konstruktsii [Elements of building constructions. Fire-resistance test methods. Loadbearing and separating constructions]. (rus)
22. ENV 13381-7:2002 Test methods for determining the contribution to the fire resistance of structural members - Part 7: Applied protection to timber members
23. BS EN 1365-2-2000: Fire resistance tests for loadbearing elements - Part 2 Floors and roofs
24. O'Neill, J.W., Abu, A.K., Carradine, D.M., Moss, P.J., Buchanan, A.H. Modelling the fire performance of structural timber floors. 7th International conference on structures in fire. Zurich, Switzerland, June 6-8, 2012. [Online] URL: https://ir.canterbury.ac.nz/handle/10092/7354 (date of reference: 20.01.2018)
25. Menis, A. Fire resistance of laminated veneer lumber (LVL) and Cross-laminated timber (XLAM) elements. SSD, ICAR 09, Technica delle Construzioni, 2012. 248 p.
26. Suzuki, J., Mizukami, T., Naruse, T., Araki, Y. Fire resistance of timber panel structures under standard fire exposure. Fire Technology. 2016. No. 52. Pp. 1015–1034.
27. Nigmatullina, D.M., Polishchuk, E.Yu., Sivenkov, A.B., Stenina, E.I., Balakin, V.M. Pozharnaya opasnost derevyannykh konstruktsiy s glubokoy propitkoy ognebiozashchitnymi sostavami [The fire hazard of

13. Ukaszek A., Polka M., Konecki M. Analysis of the visibility range in smoke generated in the course of the combustion of oak wood protected by selected fire retardants // Annals of Warsaw University of Life Sciences – SGGW Forestry and Wood Technology. 2011. № 75. Pp. 59–63.
14. Vasiljevich J., Jerman I., Jaksa G., Alongi J., Malucelli G., Zorko M., Tomshich B., Simonchic B. Functionalization of cellulose fibres with DOPO-polysilsesquioxane flame retardant nanocoating // Cellulose. 2015. Vol. 22. Pp. 1893–1910. DOI 10.1007/s10570-015-0599-x
15. Kim J., Lee J.-H., Kim S. Estimating the fire behavior of wood flooring using a cone calorimeter // J Therm Anal Calorim. 2012. Vol. 110. Pp. 677–683. DOI 10.1007/s10973-011-1902-1
16. Merk V., Chanana M., Keplinger T.,Gaand S., Burgert I. Hybrid wood materials with improved fire retardance by bio-inspired mineralisation on the nano- and submicron level // Green Chem. 2015. Vol. 17. Pp. 1423–1428. DOI: 10.1039/c4gc01862a
17. Merryweather G., Spearpoint M.J. Flame spread measurements on wood products using the ASTM E 1321 LIFT apparatus and a reduced scale adaptation of the cone calorimeter // Fire and materials. 2010. Vol. 34. Pp. 109–136. DOI: 10.1002/fam.1001
18. Гравит М.В. Гармонизация российских и европейских нормативных документов, регламентирующих методы испытаний на огнестойкость строительных конструкций с использованием средств огнезащиты // Пожаровзрывобезопасность. 2014. Т. 23. № 5. С. 38–46.
19. Gravit M.V., Nedryshkin O.V., Vaytitskiy A.A., Shpakova A.M., Nigmatullina D.G. Fire technical characteristics of building materials in the European and Russian regulatory documents. Problems of harmonization of research methods and classification // Fire and Explosion Safety. 2016. Vol. 25. № 10. Pp. 16–29. DOI: 10.18322/PVB.2016.25.10.16-29.
20. ГОСТ 30247.0 Конструкции строительные. Методы испытаний на огнестойкость. Общие требования.
21. ГОСТ 30247.1 Конструкции строительные. Методы испытаний на огнестойкость. Несущие и ограждающие конструкции
22. ENV 13381-7:2002 Test methods for determining the contribution to the fire resistance of structural members - Part 7: Applied protection to timber members
23. BS EN 1365-2-2000: Fire resistance tests for loadbearing elements - Part 2 Floors and roofs
24. O'Neill J.W., Abu A.K., Carradine D.M., Moss P.J., Buchanan A.H. Modelling the fire performance of structural timber floors // 7th International conference on structures in fire. Zurich, Switzerland, 2012. [Электронный ресурс] URL: https://ir.canterbury.ac.nz/handle/10092/7354 (дата обращения: 20.01.2018)
25. Menis A. Fire resistance of laminated veneer lumber (LVL) and Cross-laminated timber (XLAM) elements // SSD, ICAR 09, Technica delle Construzioni. 2012. P. 248.
26. Suzuki J., Mizukami T., Naruse T., Araki Y. Fire resistance of timber panel structures under standard fire exposure // Fire Technology. 2016. № 52. Pp. 1015–1034.
27. Нигматуллина Д.М., Полищук Е.Ю., Сивенков А.Б., Стенина Е.И., Балакин В.М. Пожарная опасность деревянных конструкций с глубокой пропиткой огнебиозащитными составами // Электронный журнал: Технологии техносферной безопасности. 2017. № 3(73). [Электронный ресурс]. Сист.требования: AdobeAcrobatReader. URL: http://agps-2006.narod.ru/ttb/2017-3/30-03-17.ttb.pdf (дата обращения: 13.01.2018).
28. Арцыбашева О.В., Анохин Е.А., Полищук Е.Ю., Сивенков А.Б. Повышение огнестойкости деревянных конструкций путем применения огнебиозащитных пропиточных составов // Полимерные материалы

wooden structures with deep fire and bio protective impregnation compositions]. Internet journal: Tekhnology tekhnosfernoy bezopasnost. Vol. 73. No. 3. [Online] URL: http://agps-2006.narod.ru/ttb/2017-3/30-03-17.ttb.pdf (date of reference: 13.01.2018). (rus)

28. Artsybasheva, O.V., Anokhin, E.A., Polishchuk, E.Yu., Sivenkov, A.B. Povysheniye ognestoykosti derevyannykh konstruktsiy putem primeneniya ognebiozashchitnykh propitochnykh sostavov [Increase of fire resistance of timber constraction with fire retardant processing]. Polimernyye materialy ponizhennoy goryuchesti: materialy VIII mezhdunarodnoy konferentsii pamyati akademika Zhubanova B.A. Alma-Ata: KTI KChS MVD RK, 2017. Pp. 153–155. (rus)
29. Anokhin, E.A. Povysheniye klassa pozharnoy opasnosti derevyannykh konstruktsiy dlitelnogo sroka ekspluatatsii [Increasing of fire safety of aged timber construction]: Dissertation of candidate of technical science. Moscow, 2017. 236 p. (rus)
30. Garashchenko, N.A. Issledovaniya effektivnosti ognezashchity derevokleyenykh konstruktsiy [Investigation of effectivness of fire protection of timber construction]: Dissertation of candidate of technical science. Moscow, 2007. 157 p. (rus)
31. Gravit, M., Gumenyuk, V., Sychov, M., Nedryshkin, O. Estimation of the pores dimensions of intumescent coatings for increase the fire resistance of building structures // Procedia Engineering. 2015. Vol. 117. Pp. 119–125.
32. Aseyeva, R.M., Serkov, B.B., Sivenkov A.B. Goreniye drevesiny i yeye pozharoopasnyye svoystva [Wood burning and they fire properties]. Moscow. Akademy of State fire service of EMERCOM of Russia, 2010. 262 p. (rus)
33. Korolchenko, A.Ya. i dr. Raschety tolshchin ognezashchity, obespechivayushchiye trebuyemyye pokazateli pozharnoy opasnosti derevokleyenykh konstruktsiy [Calculations of fire protection thickness, providing the required indicators of fire danger of wood-glued structures]. Fire and Explosion Safety. 2005. Vol. 17. No. 3. Pp. 49–56. (rus)
34. White, R.H. Fire resistance of wood members with directly applied protection. Proceedings of the fire and materials. Conference. 26-28 January 2009. Pp. 13–19.
35. Kruglov, E.Yu. et al. Ognestoykost ograzhdayushchikh legkikh derevyannykh karkasnykh konstruktsiy s teploizolyatsiyey iz penokompozita Penocom [The fire resistance of cladding light wood frame structures with insulation from penaconite Penocom]. Pozhary i chrezvychaynyye situatsii: predotvrashcheniye, likvidatsiya. 2015. No. 3. Pp. 63–70. (rus)
36. Gorvett, Z. “Plyscrapers”: The rise of the wooden skyscraper. BBC future. October 31, 2017. [Online]. URL: http://www.bbc.com/future/story/20171026-the-rise-of-skyscrapers-made-of-wood (date of reference: 27.03.2018).
37. Marsh, J. Spreading like wildfire: why wooden skyscrapers are springing up across the world. CNN style. 2016. [Online] URL: http://edition.cnn.com/2016/04/26/design/wooden-skyscrapers-timber-trend-catching-fire/ (date of reference: 27.03.2018).
38. EN 1995-1-2:2004 Eurocode 5: Design of timber structures — Part 1-2: General. Structural fire design
39. Cachim, P.B., Franssen, J.-M. Assessment of Eurocode 5 charring rate calculation methods. Fire Technology. 2010. No. 46. Pp. 169–181.
40. Frangy, A. Eurocodes: Background & Applications structural fire design. Chapter 6: Fire resistance assessment of timber structures. JRC science and policy reports, European Union. 2014. Pp. 215–238.

пониженной горючести: материалы VIII международной конференции памяти академика Жубанова Б.А. Алма-Ата: КТИ КЧС МВД РК, 2017. С. 153–155.

29. Анохин Е.А. Повышение класса пожарной опасности деревянных конструкций длительного срока эксплуатации: дис. … канд. техн. наук: 05.26.03 // Анохин Евгений Анатольевич. М.: 2017. 236 с.
30. Гаращенко Н.А. Исследования эффективности огнезащиты деревоклееных конструкций: дис. … канд. техн. наук: 05.26.03 // Гаращенко Никита Анатольевич. М.: 2007. 157 с.
31. Gravit, M., Gumenyuk, V., Sychov, M., Nedryshkin, O. Estimation of the pores dimensions of intumescent coatings for increase the fire resistance of building structures // Procedia Engineering. 2015. Vol. 117. Pp. 119–125.
32. Асеева Р.М., Серков Б.Б., Сивенков А.Б. Горение древесины и ее пожароопасные свойства. Монография. М.: Академия ГПС МЧС России, 2010. 262 с.
33. Корольченко А.Я. и др. Расчеты толщин огнезащиты, обеспечивающие требуемые показатели пожарной опасности деревоклееных конструкций // Пожаровзрывобезопасность. 2015. Т. 17. № 3. С. 49–56.
34. White R.H. Fire resistance of wood members with directly applied protection // Proceedings of the fire and materials. Conference. 26-28 January 2009. Pp. 13–19.
35. Круглов Е.Ю. и др. Огнестойкость ограждающих легких деревянных каркасных конструкций с теплоизоляцией из пенокомпозита Penocom // Пожары и чрезвычайные ситуации: предотвращение, ликвидация. 2015. № 3. С. 63–70.
36. Gorvett Z. “Plyscrapers”: The rise of the wooden skyscraper // BBC future. October 31, 2017. [Электронный ресурс]. URL: http://www.bbc.com/future/story/20171026-the-rise-of-skyscrapers-made-of-wood (Дата обращения: 27.03.2018).
37. Marsh J. Spreading like wildfire: why wooden skyscrapers are springing up across the world // CNN style. August 9, 2016. [Электронный ресурс]. URL: http://edition.cnn.com/2016/04/26/design/wooden-skyscrapers-timber-trend-catching-fire/ (Дата обращения 27.03.2018).
38. EN 1995-1-2:2004 Eurocode 5: Design of timber structures — Part 1-2: General. Structural fire design.
39. Cachim P.B., Franssen J.-M. Assessment of Eurocode 5 charring rate calculation methods // Fire Technology. 2010. Vol. 46. Pp. 169–181.
40. Frangy A. Eurocodes: Background & Applications structural fire design. Chapter 6: Fire resistance assessment of timber structures // JRC science and policy reports. European Union, 2014. Pp. 215–238.
41. СП 64.13330.2017. Деревянные конструкции. Актуализированная редакция СНиП II-25-80.
42. Мосалков И.Л., Плюснина Г.Ф., Фролов А.Ю. Огнестойкость строительных конструкций. М.: ЗАО «Спецтехника», 2001. 496 с.
43. Полищук Е.Ю., Асеева Р.М., Анохин Е.А., Серков Б.Б., Сивенков А.Б., Сахаров П.А. Перспективы применения древесных композиционных материалов в строительстве // Полимерные материалы пониженной горючести. Материалы VIII международной конференции. Алматы: Казахский Национальный университет им. аль-Фараби, 2017. С. 168–170.
44. Полищук Е.Ю., Сивенков А.Б. Новые технические решения при обеспечении пожарной безопасности и огнестойкости конструкций из древесины и материалов

41. Russian building codes SP 64.13330.2017. Derevyannyye konstruktsii. Aktualizirovannaya redaktsiya SNiP II-25-80 [Timber construction. Actual redaction of SNiP II-25-80] (rus)
42. Mosalkov, I.L., Plyusnina, G.F., Frolov, A.Yu. Ognestoykost stroitelnykh konstruktsiy [Fire resistance of building concstruction]. Moscow, ZAO «Spetstekhnika», 2001. 496 p. (rus)
43. Polishchuk, E.Yu., Aseyeva, R.M., Anokhin, E.A., Serkov, B.B., Sivenkov, A.B., Sakharov, P.A. Perspektivy primeneniya drevesnykh kompozitsionnykh materialov v stroitelstve [Perspectives of wooden composition in building]. Polimernyye materialy ponizhennoy goryuchesti. Materialy VIII mezhdunarodnoy konferentsii. Almaty: Kazakhskiy Natsionalnyy universitet im. al-Farabi, 2017. Pp. 168–170. (rus)
44. Polishchuk, E.Yu., Sivenkov, A.B. Novyye tekhnicheskiye resheniya pri obespechenii pozharnoy bezopasnosti i ognestoykosti konstruktsiy iz drevesiny i materialov na yeye osnove [New technical solution for timber construction fire resistance and wooden materials fire safety providing]. Materialy XXIX Mezhdunarodnoy nauchno-prakticheskoy konferentsii, posvyashchennoy 80-letiyu FGBU VNIIPO MChS Rossii. 2017. Pp. 60–62. (rus)
45. National Russian Standart GOST R 53292-2009 Ognezashchitnyye sostavy i veshchestva dlya drevesiny i materialov na yeye osnove. Obshchiye trebovaniya. Metody ispytaniy. [Fire retardant compositions and substances for wood. General requirements. Test methods]. (rus)
46. Sobur, S.V. Ognezashchita materialov i konstruktsiy. Spravochnik [Fire protection of materials and construction. Handbook]. Moscow: Pozhkniga, 2003. 256 p. (rus)
47. Kharitonov, V.S. Nesushchaya sposobnost izgibayemykh kleyenykh derevyannykh konstruktsiy massivnogo secheniya pri teplovom vozdeystvii [Bearing capacity of bent laminated wood structures of solid cross section under thermal influence]. Abstract of dissertation of candidate of technical science. Moscow, 1992. 24 p. (rus)
48. Kovredov, A.V., Kudryavtsev, K.S., Nechaev, A.V. Work of wood on crumpling in a programmatic complex APM. Construction of Unique Buildings and Structures. 2017. 52(1). Pp. 7–16. (rus)
49. Rasha, I.K., Pertseva, O.N., Lazareva, A.Yu., Martynov, G.V. Computational modelling of random distribution of stresses for wooden structures. Magazine of Civil Engineering. 2017. 69(1). Pp. 23–33. doi: 10.18720/MCE.69.2
50. Lazarevska, M., Cvetkovska, M., Knezevic, M., Trombeva Gavriloska, A., Milanovic, M., Murgul, V., Vatin, N. Neural network prognostic model for predicting the fire resistance of eccentrically loaded RC columns. Applied Mechanics and Materials. 2014. Vol. 627. Pp. 276–282. DOI: 10.4028/www.scientific.net/AMM.627.276

на ее основе // Материалы XXIX Международной научно-практической конференции, посвященной 80-летию ФГБУ ВНИИПО МЧС России, 2017. С. 60–62.
45. ГОСТ Р 53292-2009 Огнезащитные составы и вещества для древесины и материалов на ее основе. Общие требования. Методы испытаний.
46. Собурь С.В. Огнезащита материалов и конструкций. Справочник. М.: Пожкнига, 2003. 256 с.
47. Харитонов В.С. Несущая способность изгибаемых клееных деревянных конструкций массивного сечения при тепловом воздействии: автореферат дис. ... кандидата технических наук : 05.26.01 // Харитонов Виктор Сергеевич. М: 1992. 24 с.
48. Ковредов А.В., Кудрявцев К.С., Нечаев А.В. Работа древесины на смятие в программном комплексе АРМ // Строительство уникальных зданий и сооружений. 2017. № 1(52). С. 7–16. doi 10.18720/CUBS.52.1
49. Раша И.К., Перцева О.Н., Лазарева А.Ю., Мартынов Г.В. Численное моделирование случайного распределения напряжений для деревянных конструкций // Инженерно-строительный журнал. 2017. № 1(69). С. 23–33. doi: 10.18720/MCE.69.2
50. Lazarevska M., Cvetkovska M., Knezevic M., Trombeva Gavriloska A., Milanovic M., Murgul V., Vatin N. Neural network prognostic model for predicting the fire resistance of eccentrically loaded RC columns // Applied Mechanics and Materials. 2014. Vol. 627. Pp. 276–282. DOI: 10.4028/www.scientific.net/AMM.627.276

Evgeniy Polishchuk,*
+7(967)638-53-21; epyur@ya.ru

Andrey Sivenkov,
+7(916)174-52-44; sivenkov01@mail.ru

Samat Kenzhehan,
+7(777)846-62-62; kenzhehan85@mail.ru

Евгений Юрьевич Полищук,*
+7(967)638-53-21; эл. почта: epyur@ya.ru

Андрей Борисович Сивенков,
+7(916)174-52-44;
эл. почта: sivenkov01@mail.ru

Самат Кенжеханулы Кенжехан,
+7(777)846-62-62;
эл. почта: kenzhehan85@mail.ru

Polishchuk, E.Yu., Sivenkov, A.B., Kenzhehan, S.K. Heating and charring of timber constructions with thin-layer fire protection. *Magazine of Civil Engineering*. 2018. 81(5). Pp. 3–14. doi: 10.18720/MCE.81.1.

doi: 10.18720/MCE.81.2

Site-selection on the basis of territorial analysis methods

Выбор участка строительства на основе методов территориального анализа

N.S. Bolshakov*,
V.L. Badenko,
Peter the Great St. Petersburg Polytechnic University, St. Petersburg, Russia
A. Celani,
Politecnico di Milano, Milano, Italia

Студент Н.С. Большаков*,
д-р техн. наук, профессор В.Л. Баденко,
Санкт-Петербургский политехнический университет Петра Великого, г. Санкт-Петербург, Россия
PhD, научный сотрудник А. Челани,
Политекнико ди Милано, Милан, Италия

Key words: site-selection; territorial analysis; urban planning; regional economics; decision-making; location quotient; rental house

Ключевые слова: выбор участка строительства; территориальный анализ; градостроительство; региональная экономика; принятие решений; коэффициент локации; аренда

Abstract. The object of research is the site-selection process for the rental housing construction. This form of real estate is becoming more widespread in the west, while in Russia it's development is currently on initial stage. The article proposes the site-selection solution on the basis of existing methods of territorial analysis, calculation of employment shares, location quotients, Hirschmann-Herfindahl index and Kano model application, as well as application examples of the obtained databases in the conditions of a narrowly formulated problem. The research results are the mechanisms for solving three types of problems depending on the nature of the initial data according to correspondence between the properties of the object under construction and the urban territories.

Аннотация. Объектом исследования является процесс выбора участка капительного строительства жилого здания с целью последующей сдачи в аренду. Данная форма недвижимости получает все более широкое распространение на западе, в то время, как в России только зарождается. В статье предлагается решение задачи размещения существующими методами территориального анализа, применением расчетов долей трудоустройства, коэффициентов локации, индекса Хиршманна-Херфиндаля и модели Кано, а также иллюстрируются примеры применения полученных баз данных в условиях узко сформулированной задачи. Результатом исследования являются механизмы решения трех типов задач в зависимости от природы исходных данных на основе исследования соответствия свойств строящегося объекта и территорий города.

1. *Introduction*

Site selection is the initial stage of any construction process. It indicates the tools of placing new objects, both for business and for government. Site selection involves measuring the needs of a new project. Rationally chosen area maximizes the profitability and efficiency of facility. It can be analyzed from several points of view, one of them is the economic analysis of regions and areas which potentially can be chosen as a site.

Each region differs from others in size, location, morphology, diversity of population and donations of factors. Due to these characteristics and some exogenous factors, the regions have become specialized in their sectors over time. Indicators such as employment share [1, 2], location quotients [3–6] and the Hirschman-Herfindahl index [7, 8] are useful tools for analyzing the level of specialization and diversification in the region in order to understand how this affects economic indicators and how it behaves with respect to the reference area. This article is aimed to apply these methods during site selection process. The scale of large Russian city Saint-Petersburg with its 111 local regions (municipal sectors) is analyzed in some parts of the article as an example.

In this particular investigation the following calculations are considered as a part of decision-making process [9]. Results of calculations are used as coefficients describing economical rationality of choosing a site for construction. Still these methods and all the formed databases may be applied in other cases. In

Большаков Н.С., Баденко В.Л., Челани А. Выбор участка строительства на основе методов территориального анализа // Инженерно-строительный журнал. 2018. № 5(81). С. 15–24.

our work particularly we focused on choosing a site for specific object – middle-class rental house. This type of business becomes more and more popular in European countries and United States of America [10, 11] and represented in Saint Petersburg only by one house. Population of large agglomerations such as Saint Petersburg become more convenient with sharing apartments. Renting real estate in a lot of cases becomes more profitable and thus popular than buying it for the citizens [12]. That is why we find actual our attempts to apply existing methods of territorial analysis to site-selection of this modern type of real estate. In addition to this we find it necessary to have an instrument which values the site without expert review, only on the basis of statistical data (in this article all the initial data is taken from Rosstat which is main statistical database in the country [13]). At the same time suggested methodology can be applied for large variety of cases by identifying sectors related to specific features of investigated object. From this perspective we consider the sites or generally the whole urban territory which consists of different sites the object of this research.

In this research we were interested in economic parameters of the sites. In particular we tried to evaluate numerical values for these economic parameters and different municipal authorities using methods of territorial analysis. One of the research tasks is to describe the process of creating databases of these parameters.

All the parameters mentioned above calculated for each municipal authority and investigated sector combined all together create databases of investigated city. To sum up these parameters are:

1. $Sh_{i,j}^{K}$ – shares;
2. $LQ_{i,j}^{K}$ – location quotients;
3. G_{i}^{K} – growth;
4. HHI_{i} - Hirschmann-Herfindahl Index.

The scale of territorial analysis provides an ability to apply such methods for other large urban territories with population over one million citizens and area more than one thousand square kilometers. Our investigation is based on comparison between the properties of municipal authorities (which consist of sites) and objects that are expected to be placed in urban area. In this case we can formulate 3 types of tasks:

- Municipal authority – object (which considers municipal authority as an input factor and provides suiting objects as an output on the basis of municipal authority parameters);
- Object + municipal authority (which compares parameters of the given municipal authority and object as an input factor and provides conclusion about their compatibility);
- Object – municipal authority (which considers object as an input factor and provides suiting municipal authorities on the basis of object properties).

While the 4 object parameters mentioned above are represented by numerical values the suitability of the sites (or a number of sites united in municipal authority) for a certain type of construction is a logical parameter of the object. We aim to identify the relation between suitability of the site and numerical parameters of the site in 3 different cases descried above.

Some examples of approaches in case of site selection are already described in investigations of one of the authors, Vladimir Badenko, Nikolay Arefiev [14–16] and W. Nann [17]. The significance of economical aspect and financial risks in real estate projects is also highlighted in the investigations of our colleagues [18]. Still such modern type of construction as rental houses are not mentioned in the previous works. Valuable contribution in the tasks of site-selection is also made by Jacek Malczewski [19–21] whose experience is also taken into account in this work. Some solution on the intersections of decision-making and site-selection cases may be found in his articles. As we focused on the real estate analysis our investigation is also based on some researches of this market provided by our colleagues [22–26]. The concept of site selection as a part of rational development process also relates to value-oriented management of investment and housing projects investigated by our colleagues [27].

As a result we find it necessary to identify the weaknesses of research in order to formulate and understand further researches that are necessary in this area. All the results concerning Saint Petersburg territories are represented in this article only as an example in order to explain the application of obtained databases in real case.

2. Methods

Analytical method of this research deals with interpretation and analysis of data related to municipal authorities of the city in order to evaluate economic parameters for the sites and to make conclusion of the site suitability during site selection process.

The source of data that can be used in developing this methodology varies due to the territory. In Europe the data is well-organized and available in Eurostat for all the regions while the Russian analogue is Rosstat. It is based on the employment statistics in territories. The following data is available for all the Russian cites and can be applied for each region. For example in the boundaries of Saint Petersburg there are 111 city municipal authorities: 81 municipal districts (some of them have names, some are called by numbers), 9 cities (Zelenogorsk, Kolpino, Krasnoe Selo, Kronstadt, Lomonosov, Pavlovsk, Peterhof, Pushkin, Sestroretsk) and 21 settlements. Databases both in Europe and in Russia are normally classified also according to the industries. In case of Russian statistics databases divide employment in following Industries:

- Industry A: Agriculture, hunting and forestry;
- Industry B: Fisheries, fish farming;
- Industry C: Mining;
- Industry D: Manufacturing Processes;
- Industry E: Production and distribution of electricity, gas and water;
- Industry F: Construction;
- Industry G: Wholesale and retail trade; repair of motor vehicles, motorcycles, household goods and personal items;
- Industry H: Hotels and restaurants;
- Industry I: Transport and Communications;
- Industry J: Financial activities;
- Industry K: Real estate transactions, leasing and provision of services;
- Industry L: Public administration and military security; social insurance;
- Industry M: Education;
- Industry N: Healthcare and the provision of social services;
- Industry O: Provision of other communal, social and personal services.

In order to clarify the application model in our investigation we focused on two main industries connected with rental house type of construction: K (real estate transactions, leasing and provision of services) and H (hotels and restaurants). The last only partly gave us representation of renting activities in the sector because we were interested only in hotel business employment, not restaurant. It also proves that Russian statistics databases do not provide actual information for such type of business activities yet. More detailed and focused data could have given more exact results and conclusions about municipal employment statistics.

On the basis of employment data we have an ability to calculate a number of parameters for investigated municipal authorities. If $E_{i,j}^{K}$ is employment in industry *K*, municipal authority *i*, year *j* then appropriate share is equal

$$Sh_{i,j}^{K} = \left(\frac{E_{i,j}^{K}}{E_{i,j}^{T}}\right) \tag{1}$$

where *T* stands for Total sum of the industries.

The created database of shares for each year, municipal authority and industry allowes us to calculate location quotients which represent a measure of relative specialization by comparing the degree of municipal authority specialization taking Saint Petersburg as reference:

$$LQ_{i,j}^{K} = \left(\frac{Sh_{i,j}^{K}}{Sh_{S,j}^{K}}\right) \tag{2}$$

where S stands for reference municipal authority (Saint Petersburg) representing data for the whole employment statistics of the city.

In order to investigate growth for the past six years an useful tool is Shift and Share Analysis. Growth G_i^K for each industry and municipal authority can be calculated as follows:

$$G_i^K = \left(\frac{E_{i,2016}^K}{E_{i,2011}^K}\right) - 1 \quad (3)$$

In addition in order to make some conclusions about specialization intensity for different part of the city we have calculated The Hirschmann-Herfindahl Index. We used the freshest data available, so this index represents situation in 2016 year:

$$HHI_i = \sum_K (Sh_{i,2016}^K)^2 \quad (4)$$

Analysis of created databases and comparison of the calculated parameters for different municipal authorities give the researcher an opportunity to evaluate economical suitability of each site during site selection process. As a result it is possible to formulate recommendations for selection of the most rational site for rental house or any other specific type of construction with its specific properties.

Another possible method that can respond to the need of a decision needs process must be retrieved from different disciplinary fields, fields that already responded with proper methodologies to the need of understanding: “what user want”. Kano model is part of a general strategy for assessing quality in manufacturing environment, starting from the assumption that is possible to provide a precise definition of what the potential customer wants. Application of this model is a current plan for the future research in this field.

3. Results and Discussion

All the collected data and all the calculations can be formed in a database. For each numerical parameter mentioned in the previous chapter we have a table in three dimensions: location (111 municipal authorities in case of Saint Petersburg in total), time (we collected as much data available as possible for the last six years) and industry (the full list is mentioned in the introduction). All the examples mentioned below are just pieces of information that was valuable for us in context of site-selection task for rental home.

The example of shares analysis is represented on the Figure 1. In order to form this graph we cut the comparison between Saint Petersburg and only one of the 111 municipal authorities mentioned in the database. This data can be found in the Table 1.

Table 1. Employment shares in MO “Akademicheskoye” and Saint Petersburg

Industry		Saint Petersburg	MO “Akademicheskoye”
Agriculture	A	0.002747948	-
Fisheries, fish farming	B	0.000209577	-
Mining	C	0.000980395	-
Manufacturing Processes	D	0.153864461	0.061920173
Energy	E	0.025424909	-
Construction	F	0.041754879	-
Wholesale and retail trade	G	0.106701781	0.010248112
Hotels and restaurants	H	0.019455867	0.008144552
Transport and Communications	I	0.107680045	-
Financial activities	J	0.035154973	-
Real estate	K	0.146704026	0.147572816
Public administration	L	0.061593668	0.014131607
Education	M	0.141012052	0.466450917
Healthcare	N	0.113000463	0.216990291
Other	O	0.043714958	0.074541532

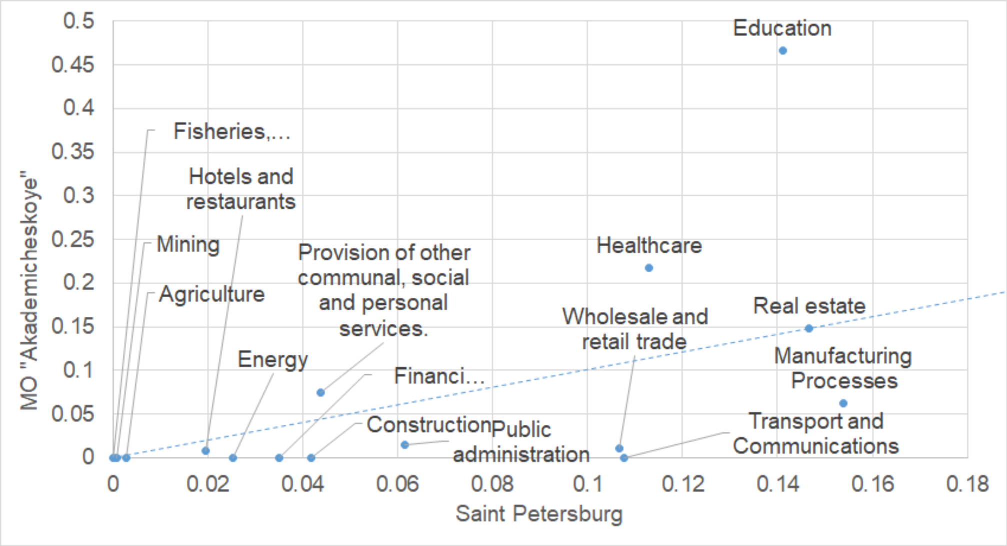

Figure 1. Shares of MO "Akademicheskoe"

This example represents a decision for the first type of tasks mentioned in the introduction (Municipal authority – object). All the industries that are situated above the bisecting line represent higher employment share than the reference area (Saint Petersburg). Assuming that we are interested particularly in municipal authority "Akademicheskoye" we can make conclusion about the industry that dominates and suppose that this region is more predisposed for such types of business activities as education and healthcare. It leads to the consequence that this municipal authority suits more for selection of the sites for types of construction connected with education or healthcare. Still one of the industries we are interested in (real estate) lies on the bisecting line thus representing normal employment for Saint Petersburg). Hotels and restaurants is slightly lower than the bisecting line. This information gives us a signal, that Akademicheskoye is not the most favorable municipal area for rental house construction. At the same time we can make conclusions that selection of sites for types of construction related to Manufacturing processes, wholesale and retail trade or public administration may be not rational due to the shares statistics of this part of the city. This leads us to conclusions about logical parameter of investigated object which is suitability of the site for specific type of construction.

The fact that some of the industries perform zero shares may be explained by lack of data about employment in these industries in Russian statistics databases.

The location quotients of the industry that we were interested in during our investigation is represented below on the Figure 2.

This graph represents a decision for the third task that is mentioned in the introduction. On the basis of Saint Petersburg example we were given real estate industry and hotels and restaurants industry as input factors. The numbers from 1 to 111 represent 111 municipal authorities in the same order that is provided by Rosstat. The graph mentioned above provides an ability to make conclusions about municipal authorities that are favorable for such type of construction. By analyzing such numerical object parameter as location quotient for two investigated industries and determining municipal authorities on their intersection we could postpone which of them suit for selection of the site for rental home type of construction linking numerical parameters of the site to its logical parameter which is suitability for specific type of construction.

Some of the municipal authorities have not provided information about 2016 year yet. That is why we can find some points on the horizontal axis in this example.

Shift-share analysis is represented on the following Figure 3. In order to form this graph we cut the comparison between Saint Petersburg and only of the 111 municipal authorities mentioned in the database. This data is presented in the Table 2.

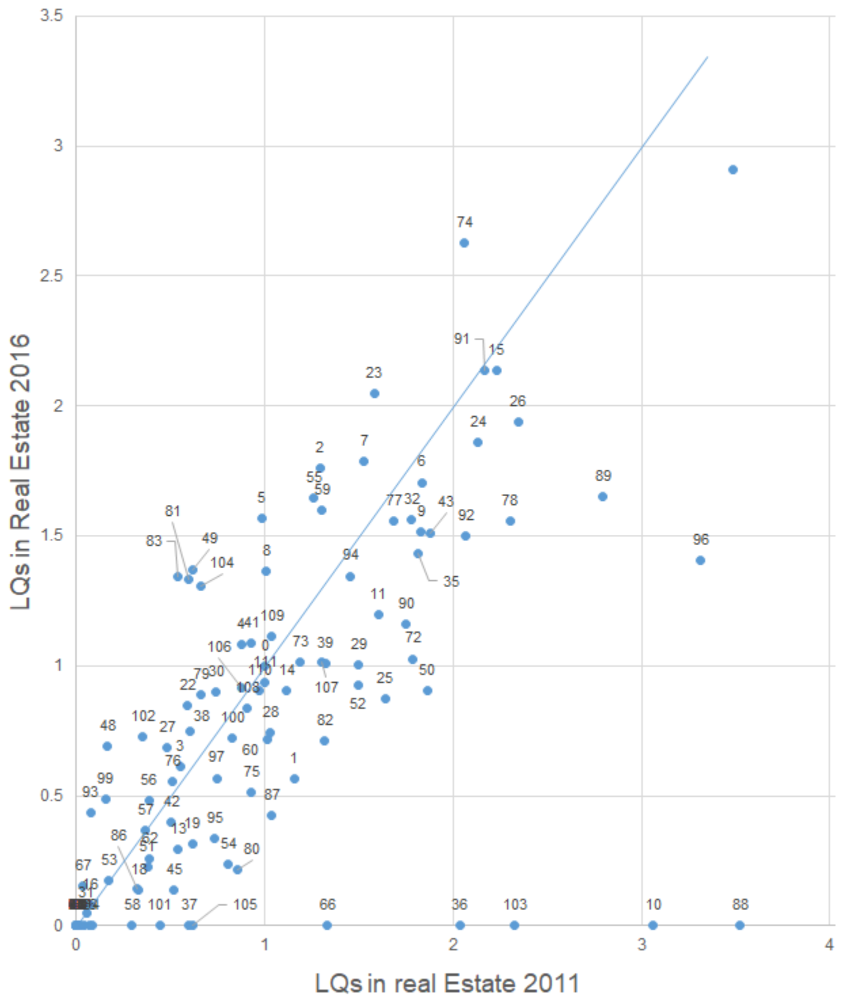

Figure 2. LQ development in real estate 2011-2016

Table 2. Change in employment shares in MO “Akademicheskoye” and Saint Petersburg

Industry		Saint Petersburg	MO "Akademicheskoye"
Agriculture	A	-0.281708449	-1
Fisheries, fish farming	B	0.378504673	-
Mining	C	2.942857143	-
Manufacturing Processes	D	-0.001935493	0.654178674
Energy	E	-0.099333082	-
Construction	F	-0.02891415	-1
Wholesale and retail trade	G	0.124342169	-0.086538462
Hotels and restaurants	H	0.174659003	0.424528302
Transport and Communications	I	0.00785967	-
Financial activities	J	0.023094258	-
Real estate	K	0.102444597	-0.151890887
Public administration	L	-0.080731182	-0.15483871
Education	M	-0.035599932	0.317088029
Healthcare	N	0.038325456	0.058962885
Other	O	0.026850678	1.592870544

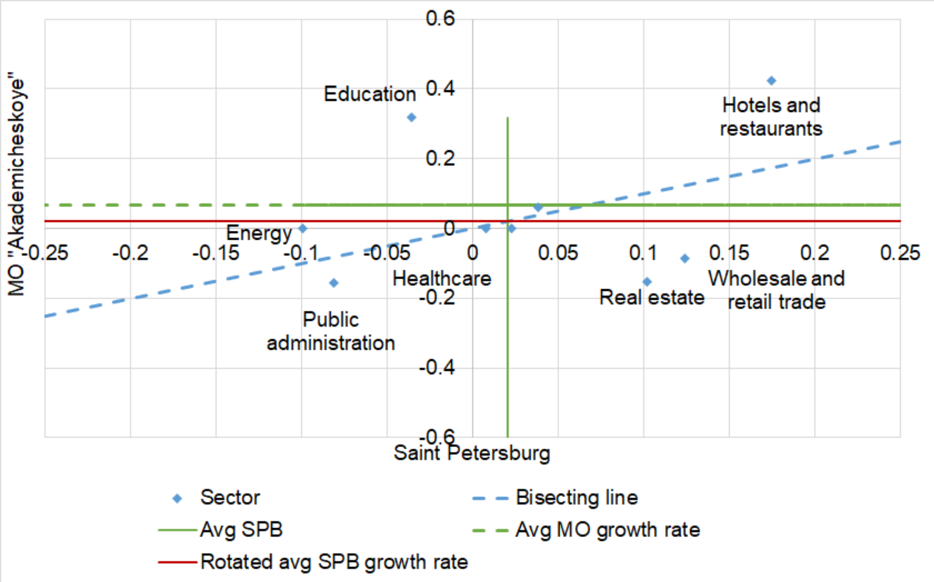

Figure 3. Shift-share analysis for MO "Akademicheskoe"

For all the determined municipal authorities and the industries we are interested it became possible to solve the second type of the tasks mentioned in the introduction. By considering them both as an input factor and using Shift-Share Analysis Chart as an instrument we can analyze the growth rate for the last 5 years comparing to the whole territory of Saint Petersburg which was chosen as a reference area. As we can see the hotels and restaurants industry performs growth rate higher than Saint Petersburg average and higher than this industry on the whole territory of the city.

Hirschmann-Herfindahl Index analysis is represented on the Figure 4.

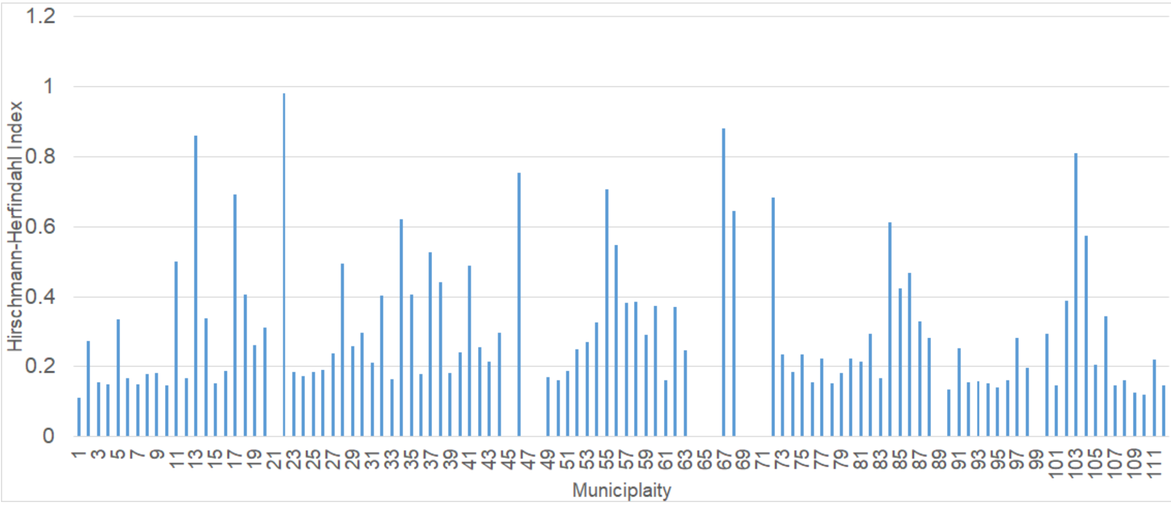

Figure 4. Hirschmann-Herfindahl Index for Saint Petersburg municipal authorities

The created databases also provide possibility to analyze intensity of municipal authorities specialization by the Hirschmann-Herfindahl Index which is another numerical parameter of investigated object. The closer it is to 1, the higher specialization of the regions in partcular industries. For example if we consider municipal authority "Akademicheskoye" we will find out that its Hirschmann-Herfindahl Index is approximately 0.3 which is a bit above average. We can explain it by the fact that this area is more specialized in education industry.

The application of the method presented in this paper, combined with the Quality Function Deployment techniques can cover almost all the complexity of the topic and completing the pattern of decision support tools for the Engineer and the project leader. The definition of the needs of the potential user is the natural complement of the research, driven to understand the potential offer in an area to rate the success of an operation in an ex-ante approach.

4. Conclusions

1. The created databases of such numerical parameters of the urban sites as shares, location quotients and employment provide an ability link economical characteristics of the sites with their suitability. In our particular research we determined some areas of the city which may be selected as the site for such type of modern construction as rental houses by linking them to suitability of the site which is a logical parameter of investigated object. The technique proposed in the article is applicable for any large urban area in Russia as the Rosstat data is available. Following points refer to Saint Petersburg application in order to clarify kind of conclusions that might be identified.

2. Considering municipal authority as an input factor it is possible to provide the most suitable objects as an output on the basis of municipal authority numerical parameters. In this case it is necessary to analyze the most suitable sectors for fixed location according to database. In the introduction this task was mentioned as “municipal authority – object”. The higher share in relation to reference area is represented by the municipal authority – the higher suitability of this municipal authority for relative type of construction. Visually suitability refers to the sectors which lie above the bisecting line in the shares graph.

3. Comparing parameters of the given municipal authority and construction object type as an input factors in shift-share analysis becomes possible by analyzing economic parameters of given municipal authority and sector in the related database. As a consequence it is possible to make conclusions about site suitability of the object related to particular sector in particular urban area. In the introduction this task was mentioned as “object + municipal authority”.

4. An ability to choose the most suiting areas among 111 municipal authorities is provided as we were given two industries as an input factor by analyzing increase of location quotient for the last 5 years choosing the sites where this parameter is the highest. Than we analyzed selected areas more precisely in the context of particular industries with the help of shift-share analysis. All the calculated coefficients may be used as indicators in the general task of site-selection which describe economical rationality of decision-making and thus site suitability. As a result we could make conclusions that such municipal authorities of Saint Petersburg as “Adimiralteyskiy”, MO 7, “Smolninskoye” perform good parameters on the intersection of real estate and hotel industries thus suiting more for rental home types of construction. This is a clear example of the third task mentioned in the introduction which is the main (object – municipal authority, which considers object as an input factor and provides suiting municipal authorities on the basis of object properties).

5. One of the weaknesses that we faced during our investigation was imperfection of databases. Some information was unavailable or not updated. The results of researches also strongly depend on the reliability of data used. The lack of content in Rosstat databases only proves the actuality of regional analysis of economical activities in Saint Petersburg. Scientific society doesn’t even have an access to initial statistics about employment, labor and some other statistical data which can be used for site-selection investigations while identifying economic parameters of urban sites and municipal authorities in general.

6. In further research it will be assessed the side of the supply/demand equilibrium, understanding with qualitative-quantitative way the potential demand for the built object and the area, this typology of tools helps the researcher to overcome the market failures, or lowering the market risk of built objects, It can be studied in parallel with similar researches the possibility to adapt Kano model to the study case, providing to Engineers and Project leaders technical information for a project able to understand the market needs as well, giving completeness to the overall design.

References

1. Khusaini, M. A shift-share analysis on regional competitiveness – a case of Banyuwangi District, East Java, Indonesia Procedia – Social and Behavioral Sciences. 2015. Vol. 211. Pp. 738–744.
2. Goschin, Z. Regional growth in Romania after its accession to EU: A shift-share analysis approach. Procedia Economics and Finance. 2014. Vol. 15. Pp. 169–175.
3. Billings, S.B., Johnson, E.B. The location quotient as an estimator of industrial concentration. Regional Science and Urban Economics. 2012. Vol. 42. Pp. 642–647.
4. Morrissey, K. Producing regional production multipliers for Irish marine sector policy: A location quotient approach. Ocean & Coastal Management. 2014. Vol. 91. Pp. 58–64.

Литература

1. Khusaini M. A shift-share analysis on regional competitiveness – a case of Banyuwangi District, East Java, Indonesia // Procedia – Social and Behavioral Sciences. 2015. Vol. 211. Pp. 738–744.
2. Goschin Z. Regional growth in Romania after its accession to EU: A shift-share analysis approach // Procedia Economics and Finance. 2014. Vol. 15. Pp. 169–175.
3. Billings S.B., Johnson E.B. The location quotient as an estimator of industrial concentration // Regional Science and Urban Economics. 2012. Vol. 42. Pp. 642–647.
4. Morrissey K. Producing regional production multipliers for Irish marine sector policy: A location quotient approach // Ocean & Coastal Management. 2014. Vol. 91. Pp. 58–64.
5. Berawi M.A., Zagloel T.Y., Miraj P., Mulyanto H. Producing alternative concept for the trans-sumatera toll road project

5. Berawi, M.A., Zagloel, T.Y., Miraj, P., Mulyanto, H. Producing alternative concept for the trans-sumatera toll road project development using location quotient method. Procedia Engineering. 2017. Vol. 171. Pp. 265–273.
6. Trappey, A., Trappey, C.V., Liu, P., Hsiao, C.-T., Ou, J., Chen, K. Location quotient EIO-LCA method for carbon emission analysis. Concurrent Engineering Approaches for Sustainable Product Development in a Multi-Disciplinary Environment. Springer London. 2013. Pp. 367–377.
7. Sun, H., Shao, R. Herfindahl index applied to Fourier analysis. Digital Signal Processing. 2009. Vol. 19. Pp. 726–730.
8. Yiğit, I., Tür, S. Relationship between diversification strategy applications and organizational performance according to Herfindahl Index criteria. Procedia – Social and Behavioral Sciences. 2012. Vol. 58. Pp. 118–127.
9. Bolshakov, N.S., Badenko, V.L. Site selection problem solution using multicriteria analysis and GIS. Topical areas of fundamental and applied research XI: Proceedings of the Conference. North Charleston, SC, USA: CreateSpace. 2017. Pp. 14–21.
10. Gilbert, A. Rental housing: The international experience. Habitat International. 2016. Vol. 54. Pp. 173–181.
11. Femi, A.B., Khan, T.H., Ahmad, A., Udin, A. Impact of Tertiary Institutions on house rental value in developing city. Procedia – Social and Behavioral Sciences. 2015. Vol. 172. Pp. 323–330.
12. The New York Times. Sharing an apartment with strangers. [Online]. URL: https://www.nytimes.com/2017/05/05/realestate/rent-long-island-city-room-share.html (date of reference: 05.05.2017).
13. Federalnaya sluzhba gosudarstvennoy statistiki [Federal State Statistics Service] [Online]. System requirements: Microsoft Excel. URL: http://www.gks.ru/ (date of reference: 20.08.2017).
14. Arefiev, N., Terleev, V., Badenko, V. GIS-based fuzzy method for urban planning. Procedia Engineering. 2015. Vol. 117. Pp. 39–44.
15. Arefiev, N., Garmanov, V., Bogdanov, V., Ryabov, Y., Terleev, V., Badenko, V. A market approach to the evaluation of the ecological-economic damage to the urban lands. Procedia Engineering. 2015. Vol. 117. Pp. 26–31.
16. Fedorov, M., Badenko, V., Maslikov, V., Chusov, A. Site selection for flood detention basis with minimum environmental impact. Procedia Engineering. 2016. Vol. 165. Pp. 1629–1636.
17. Nann, W. Review of T. Glatte's book "International Production Site Selection". Construction of Unique Buildings and Structures. 2014. 24(9). Pp. 7–10.
18. Zolotova, J.S., Tereshchenko, A.G., Kimetova, N.R. Financial risk insurance while participating in shared investment construction of other real estate. Construction of Unique Buildings and Structures. 2014. 25(10). Pp. 123–133. (rus)
19. Malczewski, J. GIS-based multicriteria decision analysis: a survey of the literature. International Journal of Geographical Information Science. 2006. Vol. 20. Pp. 703–726.
20. Malczewski, J. Liu, X. Local ordered weighted averaging in GIS-based multicriteria analysis. Annals of GIS. 2014. Vol. 20. Pp. 117–129.
21. Jelokhani-Niaraki, M., Malczewski, J. Decision complexity and consensus in Web-based spatial decision making: A case study of site selection problem using GIS and multicriteria analysis. Cities. 2015. Vol. 45. Pp. 60–70.
22. Vatin, N.I., Gamayunova, O.S., Nemova, D.V. Analysis of the real estate market of St. Petersburg. Applied

development using location quotient method // Procedia Engineering. 2017. Vol. 171. Pp. 265–273.
6. Trappey A., Trappey C.V., Liu P., Hsiao C.-T., Ou J., Chen K. Location quotient EIO-LCA method for carbon emission analysis // Concurrent Engineering Approaches for Sustainable Product Development in a Multi-Disciplinary Environment. Springer London. 2013. Pp. 367–377.
7. Sun H., Shao R. Herfindahl index applied to Fourier analysis // Digital Signal Processing. 2009. Vol. 19. Pp. 726–730.
8. Yiğit I., Tür S. Relationship between diversification strategy applications and organizational performance according to Herfindahl Index criteria // Procedia - Social and Behavioral Sciences. 2012. Vol. 58. Pp.118–127.
9. Bolshakov N.S., Badenko V.L. Site selection problem solution using multicriteria analysis and GIS // Topical areas of fundamental and applied research XI Proceedings of the Conference. North Charleston, SC, USA: CreateSpace. 2017. Pp. 14–21.
10. Gilbert A. Rental housing: The international experience // Habitat International. 2016. Vol. 54. Pp. 173–181.
11. Femi A.B., Khan T.H., Ahmad A., Udin A. Impact of Tertiary Institutions on house rental value in developing city // Procedia – Social and Behavioral Sciences. 2015. Vol. 172. Pp. 323–330.
12. The New York Times. Sharing an apartment with strangers. [Электронный ресурс]. URL: https://www.nytimes.com/2017/05/05/realestate/rent-long-island-city-room-share.html (дата обращения: 05.05.2017)
13. Федеральная служба государственной статистики [Электронный ресурс]. Систем. требования: Microsoft Excel. URL: http://www.gks.ru/ (дата обращения: 20.08.2017)
14. Arefiev N., Terleev V., Badenko V. GIS-based fuzzy method for urban planning // Procedia Engineering. 2015. Vol. 117. Pp. 39–44.
15. Arefiev N., Garmanov V., Bogdanov V., Ryabov Y., Terleev V., Badenko V. A market approach to the evaluation of the ecological-economic damage to the urban lands // Procedia Engineering. 2015. Vol. 117. Pp. 26–31.
16. Fedorov M., Badenko V., Maslikov V., Chusov A. Site selection for flood detention basis with minimum environmental impact // Procedia Engineering. 2016. Vol. 165. Pp. 1629–1636.
17. Нанн В. Обзор книги Т.Глатта "Выбор площадки строительства для объекта производственного назначения с учетом анализа международного строительного рынка" // Строительство уникальных зданий и сооружений. 2014. № 9(24). С. 7–10.
18. Золотова Ю.С., Терещенко А.Г., Киметова Н.Р. Страхование финансового риска при участии в долевом строительстве объектов недвижимости // Строительство уникальных зданий и сооружений. 2014. № 10(25). С. 123–133.
19. Malczewski J. GIS-based multicriteria decision analysis: a survey of the literature // International Journal of Geographical Information Science. 2006. Vol. 20. Pp. 703–726.
20. Malczewski J. Liu X. Local ordered weighted averaging in GIS-based multicriteria analysis // Annals of GIS. 2014. Vol. 20. Pp. 117–129.
21. Jelokhani-Niaraki M., Malczewski J. Decision complexity and consensus in Web-based spatial decision making: A case study of site selection problem using GIS and multicriteria analysis // Cities. 2015. Vol. 45. Pp. 60–70.
22. Vatin N.I., Gamayunova O.S., Nemova D.V. Analysis of the real estate market of St. Petersburg // Applied Mechanics and Materials. 2014. Vol. 638–640. Pp. 2460–2464.

Mechanics and Materials. 2014. Vol. 638–640. Pp. 2460–2464.

23. Brzezicka, J., Wisniewski, R. Translocality on the real estate market. Land use policy. 2016. Vol. 55. Pp. 166–181.
24. Vatin, N.I., Gamayunova, O.S. Real estate abroad: how to make the right choice. Applied Mechanics and Materials. 2014. Vol. 670–671. Pp. 1612–1615.
25. Popovic S.G., Vukanic S., Komatina D.F., Alihodzic-Jasarevic E., Vatin N. Models of landscape shaping in exploited quarries of urban area. Procedia Engineering. 2015. Vol. 117(1). Pp. 614–620.
26. Urbanavičienė, V., Kaklauskas, A., Zavadskas, E.K., Šliogerienė, J., Naimaviciene, J., Vatin, N.I. Facilitating the housing bargaining with the help of the bargaining decision support system. International Journal of Strategic Property Management. 2014. Vol. 18(3). Pp. 213–224.
27. Azarova, I. The main aspects of the value-oriented management of investment and construction housing projects. Magazine of Civil Engineering. 2015. 59(7). Pp. 18–29.

23. Brzezicka J., Wisniewski R. Translocality on the real estate market // Land use policy. 2016. Vol. 55. Pp. 166–181.
24. Vatin N.I., Gamayunova O.S. Real estate abroad: how to make the right choice // Applied Mechanics and Materials. 2014. Vol. 670–671. Pp. 1612–1615.
25. Popovic S.G., Vukanic S., Komatina D.F., Alihodzic-Jasarevic E., Vatin N. Models of landscape shaping in exploited quarries of urban area // Procedia Engineering. 2015. Vol. 117(1). Pp. 614–620.
26. Urbanavičienė V., Kaklauskas A., Zavadskas E.K., Šliogerienė J., Naimaviciene J., Vatin, N.I. Facilitating the housing bargaining with the help of the bargaining decision support system // International Journal of Strategic Property Management. 2014. Vol. 18(3). Pp. 213–224.
27. Азарова И.Б. Основные аспекты ценностно-ориентированного управления инвестиционно-строительными жилищными проектами // Инженерно-строительный журнал. 2015. № 7(59). С. 18–29.

Nikolai Bolshakov,*
+7(921)357-70-91;
nikolaybolshakov7@gmail.com

Vladimir Badenko,
+7(921)309-41-00; vbadenko@gmail.com

Alberto Celani,
+7(999)711-82-87; alberto.celani@polimi.it

Николай Сергеевич Большаков,*
+7(921)357-70-91;
эл. почта: nikolaybolshakov7@gmail.com

Владимир Львович Баденко,
+7(921)309-41-00;
эл. почта: vbadenko@gmail.com

Альберто Челани,
+7(999)711-82-87;
эл. почта: alberto.celani@polimi.it

doi: 10.18720/MCE.81.3

Reliability assessment of the construction schedule by the critical chain method

Модель надежности календарного графика строительства

M.V. Petrochenko*,
V.Z. Velichkin,
Peter the Great St. Petersburg Polytechnic University, St. Petersburg, Russia
Y.N. Kazakov,
St. Petersburg State University of Architecture and Civil Engineering, St. Petersburg, Russia
Y.B. Zavodnova,
Peter the Great St. Petersburg Polytechnic University, St. Petersburg, Russia

Канд. техн. наук, доцент
М.В. Петроченко*,
д-р техн. наук, профессор В.З. Величкин,
Санкт-Петербургский политехнический университет Петра Великого, г. Санкт-Петербург, Россия
д-р техн. наук, профессор Ю.Н. Казаков,
Санкт-Петербургский государственный архитектурно-строительный университет, г. Санкт-Петербург, Россия
ассистент Е.Б. Заводнова,
Санкт-Петербургский политехнический университет Петра Великого, г. Санкт-Петербург, Россия

Key words: project management; schedule control; baseline term; critical path; Goldratt's method; project buffer; construction project; critical chain; theory of constraints; construction management

Ключевые слова: управление проектами; контроль расписания; базовый план; критический путь; метод Голдрата; буфер проекта; строительный проект; критическая цепь; теория ограничений; управление строительством

Abstract. Implementation of the construction projects is associated with significant current material, technical and financial costs. They increase significantly in case of the breaking deadlines the large stages of projects and putting buildings into operation. The main aim of the current research is development the new approach for reliability model of the construction schedule for increasing reliability of the calendar planning regarding the meeting the construction projects on time. The following task were solved: the model of technical, labor and time reserves was developed; the algorithm of effective operational management system for the entire construction production process was offered. The probability of task completion was assessed by the E.M. Goldratt method, the probability function, based on the beta distribution was used. Initiating a shorter work execution period as a more stringent control action leads to an increase in the reliability of the construction program in the established settlement (contract) time from 50% probability to the normative 90% probability. Probabilistic approach allows to assess the achieved effect of applying the methodology of EM. Goldratt for the streamlined construction and to take a measured deadline for the execution of tasks in the development of the construction project.

Аннотация. Условия реализации строительных программ определяют текущие материальные, технические и финансовые издержки, которые существенно возрастают при несвоевременной сдаче крупных этапов работ и при нарушении сроков ввода завершенных строительством объектов в эксплуатацию. Целью исследования является разработка нового подхода к оценке модели надежности календарного плана строительства для повышения вероятности своевременного выполнения проекта. Для оценки надежности выполнения работ, организованных по методу Э.М. Голдратта, была использована функция вероятности на основе бета-распределения. инициирование уменьшенного срока выполнения работ и более жесткое управляющие воздействия приводят к повышению надежности выполнения строительной программы в установленные расчетные (контрактные) сроки с 50 % вероятности до нормативной 90 % вероятности. Разработанный подход позволяет оценить достигаемый эффект при применении методологии Э.М. Голдратта для поточной организации строительства и принять взвешенные сроки выполнения работ при разработке строительной программы.

Петроченко М.В., Величкин В.З., Казаков Ю.Н., Заводнова Е.Б. Модель надежности календарного графика строительства // Инженерно-строительный журнал. 2018. № 5(81). С. 25–31.

1. Introduction

Implementation of the construction projects is associated with significant current material, technical and financial costs. They increase significantly in case of the breaking deadlines the large stages of projects and putting buildings into operation. All current construction costs determined by designers and estimated in documentation are compensated by the investor while making the advance and final payments for the completed construction projects. Late commissioning the buildings into operation, an intensive work at the final stages of the projects lead to the additional costs over the estimated one in the calculation. Exceeded expenses are refunded by the internal resources of the contractor construction organizations. Penalties, fines and forfeits for the untimely completion the project stages become the additional expenses of the construction companies. For this reason, project managers devote the considerable attention to the investigation of methods and approaches for meeting the deadline of construction projects on time [1–4].

The theory of constraints (TOC) and the method of critical chains were formulated and proved by E.M. Goldratt [5–8]. They belong to the category of methods aimed at the formation the logical management procedures to achieve the quality and timeliness performing the various programs [9–12]. TOC and the method of critical chains are designed to take into account possible constraints and disruptions that may arise during the plan implementation, as well as to identify the restraining process for project development [13–16].

At the same time, realization all stages and tasks can be calculated without any delays in conditions of the intensive fulfillment the processes. Taking into account the accompanying factors, the deadlines for the performance of tasks become significantly shortened and their critical chain is determined. For this reason, the measures are provided: the expansion of bottlenecks and the temporary time reserves buffer is formed only before the end of the program at the end of the critical chain [17–20]. Lack of accounting the possible difficulties and delays in determination the individual tasks duration with intensive implementation lead to performing them in a tight schedule. If failures and delays occur, they are compensated by the final program buffer in the form of the provided amount of time and resource reserves [21].

Described organizational approach for the implementation stages and tasks according to the technological program (project) significantly increases the volume of organizational and managerial activities. Therefore, a preliminary effectiveness assessment of this system implementation are required. One of the approaches for assessing the critical chain method can be the usage the probability indicator of the implementation the reduced deadlines for accepted programs and reliability indicator of the project completion at the target deadline.

The main aim of the current research is development the new approach for reliability model of the construction schedule for increasing reliability of the calendar planning regarding the meeting the construction projects on time. The following task were solved:

– construction schedule reliability was assessed by the critical chain method.

2. Methods

To assess the probability of task completion by the E.M. Goldratt method, the probability function, based on the beta distribution was used. Application of critical chain approach of E.M. Goldratt proves its effectiveness not in all calculation cases [22, 23]. The indicators of increasing the of program reliability implementation in fixed dates were obtained experimentally and have positive values. But they were obtained for a small number of tests and have a wide space of data at small values. For a wide application of the critical chain method, it is necessary to obtain a sufficiently convincing apparatus for the effectiveness evaluating of its use. In this connection, it is proposed to apply a stochastic-mathematical model for the reliability assessing of the construction plan (schedule) execution, developed and calculated on the base of critical chains method by E.M. Goldratt.

Initiation of tight deadlines for performing the stages and tasks corresponds to certain functions of the management system and can be considered as a direction for improvement the reliability of meeting the deadlines. In this case, the final temporary buffer plays a secondary supporting role and contributes to the reliability of the project. It is possible to estimate the risk reduction of untimely project completion (construction plan) on the basis the beta distribution function of the probability construction and installation tasks within the established timeframes [24, 25]. This function was widely used in the construction when the methods of network planning and management were frequently used.

The methodology for assessing the construction program reliability in accordance with the approved calendar plan, formed by the critical chain method, can be based on the beta distribution function of the frequency distribution function of a random variable [26]. In general, the probability of executing a work plan can be calculated using the PERT methodology, with the appointment the optimistic and pessimistic estimates terms of tasks performance. In the critical chain method under consideration, the control effect on the work program should be taken into account in order to evaluate the results. It is expedient to use the beta-distribution function taking into account the influence of control solutions. The function has the following form:

$$\varphi(x) = \frac{(\xi+1)(\xi+2)(\xi+3)}{2(b-a)^{\xi+3}}(x-a)^{\xi}(b-x)^{2} \quad (1)$$

where $\varphi(x)$ – density frequency function of a random variable;

x – value of the random variable deadline milestone;

a – minimum possible deadline of the milestone;

b – maximum possible end date of the milestone;

ξ – function parameter that takes into account the system performance effectiveness.

It is possible to determine the mathematical expectation for the beta distribution function of the random variable that takes into account the impact of the control system:

$$T_{me} = \frac{b\xi + b + 3a}{\xi + 4} \quad (2)$$

Dispersion of the deadline for the construction program implementation for this function is calculated by the formula:

$$\sigma^2 = \frac{3(\xi+1)(b-a)^2}{(\xi+4)^2(\xi+5)} \quad (3)$$

Parameter of the considered function ξ counts the different operating level of the control system. When $\xi = 1$ a standard form of the beta distribution function is formed, which arises in the normal operation the control system in terms of the frequency and force impact. The decrease in the value of this parameter characterizes the influence strengthening the management system. It contributes to a more complete, timely and early completion the all planned tasks. The value $\xi = 0$ characterizes the state of the most active management. In this case it is impossible the further reducing the failures risks and increase the reliability the timely tasks while forecasting by means of management activities without additional labor and technical resources. In this case, a well-organized technological process is considered without failures, delays and failures.

Increasing the value parameter ξ to 2 or more indicates a decrease in the level of control and its effectiveness. The parameter ξ value is established on the basis of its correlation with the process monitoring level and the frequency of the influence the control decisions. If the making decisions are made less than one per five days, it is advisable to take this parameter at least 1.5.

When the value of the parameter ξ is decreasing, the area under the curve of the beta distribution function moved towards an optimistic evaluating « a » and accordingly decreases the expectation value (2). In case $\xi=0$,

$$T_{me} = (b + 3a)/4 \quad (4)$$

The tight terms of tasks performance which are less then established by the standards indicate a high management level and, in accordance with the function (1), the value of the parameter ξ should be taken less than 1 (for example 0; 0.3; 0.5; 0.7). According to the E.M. Goldratt recommendations, the duration of operations is assumed to be 50% shorter than the normative value, and therefore the value of the control parameter can be chosen close to the zero. Reduction of technically based standards used in the plans for construction processes in the general case is possible by approximately 30%. Possible failures and delays can extend task completion time to 50 %.

Reduction of the value the mathematical expectation in comparison with the initial value, determined on the basis of the current standards, forms an additional time reserve (buffer). The created time reserve (buffer) contributes to the plan fulfillment within the approved timeframe and increase of its reliability level.

Consequently, the critical chain method promotes to reduce risks and timely completion of the project in two ways. In the first case, reliability is enhanced by creating the ideal conditions for the construction process and encouraging workers to perform work in a shorter time. In the second case, the reliability increase is provided by the terminal reserve (buffer) at the final stage of project execution.

3. Results and Discussion

Application method for the probability-mathematical model

A set of tasks execution was considered to illustrate the performance ability of this mathematical model.

Determine the project duration by calculating of each separate construction process according to technical standards. Join the processes in a complex and get a plan with a deadline of 160 days.

Assuming that an optimistic project duration is $a=(1-0.3)\cdot 160=112$ days and a pessimistic assessment of the plan fulfillment is $b=(1+0.5)\cdot 160=240$ days.

Assign for executors the term of the plan fulfillment 120 days (25 % reduction in terms). At the same time, the contract has a deadline set by technical standards – 160 days. During this period, the contractor is legally responsible. Considering the contraction of the construction plan for the executors, a pessimistic estimate of the completion time of tasks will be $b=1.25\cdot 160=200$ days. (25 % overall reduction in terms).

Determine the reliability (probability) of the plan in contractual period of 160 days with the regular approach and the critical chain method.

The probability of completion the set of tasks for given optimistic and pessimistic estimates for any period can be calculated by the expression:

$$\rho(T)=0.5\alpha^{\xi+1}[\alpha^2(\xi+1)(\xi+2)-2\alpha(\xi+1)(\xi+3)+(\xi+2)(\xi+3)], \qquad (5)$$

where $\rho(T)$ – the probability of execution the tasks in the period T;

$$\alpha=\frac{T-a}{b-a}$$

ξ – a parameter of control system.

- Define the efficiency in the form of the construction plan reliability for the regular standard conditions of work organization for contractual conditions. Accept $\xi=1$.

$$\alpha=\frac{160-112}{240-112}=0.375$$

$$P(160)=0.14(0.14\cdot 3-0.375\cdot 8+6)=0.48$$

- The effectiveness of the plan under standard conditions using the critical chain method for contractual terms will be:

Petrochenko, M.V., Velichkin, V.Z., Kazakov, Y.N., Zavodnova, Y.B. Reliability assessment of the construction schedule by the critical chain method. *Magazine of Civil Engineering*. 2018. 81(5). Pp. 25–31. doi: 10.18720/MCE.81.3.

$$\alpha = \frac{160-112}{200-112} = 0.545$$

$$P(160) = 0.297(0.297\cdot 3 - 0.545\cdot 8 + 6) = 0.752$$

Determine the effectiveness (reliability) of implementation the deadline for performers is 120 days by the critical path method:

$$\alpha = \frac{120-112}{200-112} = 0.091$$

$$P(120) = 0.0083(0.0083\cdot 3 - 0.091\cdot 8 + 6) = 0.25$$

Define the effectiveness (reliability) of the plan implementation taking into account the using the critical chain method. Calculating of the duration should be made on the basis of labor input standards for 120 days under ideal conditions of work organization and fixed deadlines. Accept $\xi = 0$.

1. $$P(120) = 0.091(0.0083 - 0.091\cdot 3 + 3) = 0.25$$

Consequently, by setting the shorter terms of tasks execution and forming a temporary buffer, it is possible to get a significant increase in reliability of completion all tasks in the directive dates. It is shown at the graph in Figure 1.

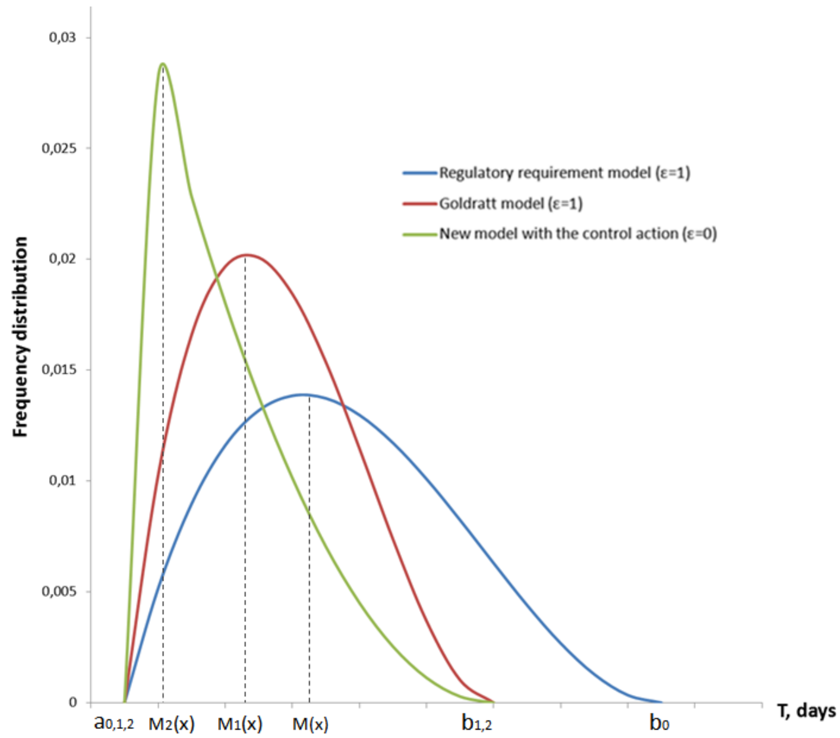

Figure 1. Comparison of normal distribution curves for the mathematical models of the project execution

Existing research examples of the application the critical chain method indicate an increase in reliability by 15–20 %, but the reference frame is not indicated [6, 9, 10]. The conducted studies show the possibility for increasing reliability by 40-45% in comparison with the regulatory base.

4. Conclusions

1. The considered example of the application of the mathematical model shows that initiating a shorter work execution period as a more stringent control action leads to an increase in the reliability of the construction program in the established settlement (contract) time from 50 % probability to the normative 90 % probability.

2. Described probabilistic approach allows to assess the achieved effect of applying the methodology of E.M. Goldratt for the streamlined construction and to take a measured deadline for the execution of tasks in the development of the construction project.

References

1. Kalugin, Yu.B. Reasons of delays in construction projects. Magazine of Civil Engineering. 2017. 74(6). Pp. 61–69.
2. Yaghootkar, K., Gil, N. The effects of schedule – driven project management in multi – project environment. Int Journal of Project Management. 2012. No. 30. Pp. 127–140.
3. Bolotin, S., Birjukov, A. Time Management in Drafting Probability Schedules for Construction Work. World Applied Sciences Journal. 2013. No. 13. Pp. 1–4.
4. Czarnigowska, A., Sobotka, A. Time-cost relationship for predicting construction duration. Archives of Civil and Mechanical Engineering. 2013. No. 13(4). Pp. 518–526.
5. Goldratt, E.M. Łańcuch krytyczny. Projekty na czas [Critical Chain]. Warszawa, 2009. 220 p.
6. Goldratt, E. M. Critical Chain. USA, 1997. 160 p.
7. Kalko, D.V. Teoriya ogranicheniy Goldratta kak instrument poiska i upravleniya rezervami proizvodstva [The theory of Goldratt's limitations as a tool for the search and management of production reserves]. Logisticheskiye sistemy v globalnoy ekonomike. 2017. No. 7. Pp. 170–173.
8. Ponsteen, A., Kusters, R.J. Classification of Human and Automated Resource Allocation Approaches in Multi-Project Management. Proceedia – Social and Behavioral Sciences. 2015. No. 194. Pp. 165–173.
9. Araszkiewicz, K. Application of Critical Chain Management in Construction Projects Schedules in a Multi-Project Environment: A Case Study. Procedia Engineering. 2017. No. 182, Pp. 33–41.
10. Roghanian, E., Alipour, M., Rezaei, M. An improved fuzzy critical chain approach in order to face uncertainty in project scheduling. International Journal of Construction Management. 2018. Vol. 18(1). Pp. 1–13.
11. Bevilacqua, M., Ciarapica, F.E., Mazzuto, G., Paciarotti, C. Robust multi-criteria project scheduling in plant engineering and construction. Handbook on Project Management and Scheduling. 2015. No. 2(1). Pp. 1291–1305.
12. Ghazvini, M.S., Ghezavati, V., Raissi, S., Makui, A. An integrated efficiency-risk approach in sustainable project control. Sustainability (Switzerland). 2017. No. 9(9). Pp. 1–20.
13. Wei, C.-S., Wei, C.-C., Wei, S.-T. The design of an activity buffer that minimises project delay. International Journal of Industrial and Systems Engineering. 2016. Vol. 24(4). Pp. 510–528.
14. Ghaffari, M., Emsley, M.W. Current status and future potential of the research on Critical Chain Project Management Surveys in Operations. Research and Management Science. 2015. Vol. 20(2). Pp. 43–54.
15. Połoński, M., Pruszyński, K. Impact of baseline terms on the course of critical paths and time buffers in the modified goldratt's method. Archives of Civil Engineering. 2013. Vol. 59(3). Pp. 313–320.
16. Bie, L., Cui, N., Zhang, X. Buffer sizing approach with dependence assumption between activities in critical chain scheduling. International Journal of Production Research. 2012. Vol. 50(24). Pp. 7343–7356.
17. Guerrero, M.A., Carbonell, M.A., Carbonell, M.M. Applying EVM and Es metrics to analyze and forecast schedule performance in the spanish context of the building sector. Construction and Building Research. 2014. No. 1. Pp. 49–56.

Литература

1. Калугин Ю.Б. Причины отставаний строительных проектов // Инженерно-строительный журнал. 2017. № 6(74). С. 61–69.
2. Yaghootkar K., Gil N. The effects of schedule – driven project management in multi – project environment // Int Journal of Project Management. 2012. № 30. Pp. 127–140.
3. Bolotin S., Birjukov A. Time Management in Drafting Probability Schedules for Construction Work // World Applied Sciences Journal. 2013. № 13. Pp. 1–4.
4. Czarnigowska A., Sobotka A. Time-cost relationship for predicting construction duration // Archives of Civil and Mechanical Engineering. 2013. № 13(4). Pp. 518–526.
5. Goldratt E.M. Łańcuch krytyczny. Projekty na czas [Critical Chain]. Warszawa, 2009. 220 p.
6. Goldratt E. M. Critical Chain. USA, 1997. 160 p.
7. Калько Д.В. Теория ограничений Голдратта как инструмент поиска и управления резервами производства // Логистические системы в глобальной экономике. 2017. № 7. С. 170–173.
8. Ponsteen A., Kusters R.J. Classification of Human and Automated Resource Allocation Approaches in Multi-Project Management // Proceedia – Social and Behavioral Sciences. 2015. № 194. Pp. 165–173.
9. Araszkiewicz K. Application of Critical Chain Management in Construction Projects Schedules in a Multi-Project Environment: A Case Study // Procedia Engineering. 2017. № 182. Pp. 33–41.
10. Roghanian E., Alipour M., Rezaei, M. An improved fuzzy critical chain approach in order to face uncertainty in project scheduling // International Journal of Construction Management. 2018. Vol. 18(1). Pp. 1–13.
11. Bevilacqua M., Ciarapica F.E., Mazzuto G., Paciarotti C. Robust multi-criteria project scheduling in plant engineering and construction // Handbook on Project Management and Scheduling. 2015. Vol. 2(1). Pp. 1291–1305.
12. Ghazvini M.S., Ghezavati V., Raissi S., Makui A. An integrated efficiency-risk approach in sustainable project control // Sustainability (Switzerland). 2017. Vol. 9(9). Pp. 1–20.
13. Wei C.-S., Wei C.-C., Wei S.-T. The design of an activity buffer that minimises project delay // International Journal of Industrial and Systems Engineering. 2016. Vol. 24(4). Pp. 510–528.
14. Ghaffari M., Emsley M.W. Current status and future potential of the research on Critical Chain Project Management Surveys in Operations // Research and Management Science. 2015. Vol. 20(2). Pp. 43–54.
15. Połoński M., Pruszyński K. Impact of baseline terms on the course of critical paths and time buffers in the modified goldratt's method // Archives of Civil Engineering. 2013. Vol 59(3). Pp. 313–320.
16. Bie L., Cui N., Zhang X. Buffer sizing approach with dependence assumption between activities in critical chain scheduling // International Journal of Production Research. 2012. Vol. 50(24). Pp. 7343–7356.
17. Guerrero M.A., Carbonell M.A., Carbonell M.M. Applying EVM and Es metrics to analyze and forecast schedule performance in the spanish context of the building sector // Construction and Building Research. 2014. № 1. Pp. 49–56.

Petrochenko, M.V., Velichkin, V.Z., Kazakov, Y.N., Zavodnova, Y.B. Reliability assessment of the construction schedule by the critical chain method. *Magazine of Civil Engineering*. 2018. 81(5). Pp. 25–31. doi: 10.18720/MCE.81.3.

18. Bruni, M.E., Beraldi, P., Guerriero, F., Guerriero, F. A scheduling methodology for dealing with uncertainty in construction projects. Engineering Computations (Swansea, Wales). 2011. Vol. 28(8). Pp. 1064–1078.
19. Liu, H.-B. Schedule risk management method of construction project based on critical chain. International Conference on Electric Technology and Civil Engineering, ICETCE 2011 – Proceedings. 2011. Pp. 2561–2563.
20. De Marco, A., Briccarello, D., Rafele, C. Cost and schedule monitoring of industrial building projects: Case study. Journal of Construction Engineering and Management. 2009. Vol. 135(9). Pp. 853–862.
21. Luiz, J.V.R., De Souza, F.B., Luiz, O.R. PMBOK® and critical chain practices: Antagonisms and opportunities for complementation. Gestao e Producao. 2017. Vol. 24(3). Pp. 464–476.
22. Kahmann, A., Kloeckner, A.P. Theory of restrictions and project management - critical chain: A systematic review of the literature. Espacios. 2014. Vol. 35(13). Pp. 1–20.
23. Duan, Q., Liao, T.W. Improved ant colony optimization algorithms for determining project critical paths. Automation in Construction. 2010. Vol. 19(6). Pp. 676–693.
24. Połoński, M., Pruszyński, K. The time buffers location and critical chain concepts in civil engineering network schedule. Part I. Theoretical background. Przegląd Budowlany. 2008. No. 2. Pp. 5–49.
25. Martens, A., Vanhoucke, M. A buffer control method for top-down project control. European Journal of Operational Research. 2017. Vol. 262(1). Pp. 274–286.
26. Ma, G., Wang, A., Li, N., Gu, L., Ai, Q. Improved Critical Chain Project Management Framework for Scheduling Construction Projects. Journal of Construction Engineering and Management. 2014. Vol. 140(12). Pp. 31–58.

18. Bruni M.E., Beraldi P., Guerriero F., Guerriero F. A scheduling methodology for dealing with uncertainty in construction projects // Engineering Computations (Swansea, Wales). 2011. Vol. 28(8). Pp. 1064–1078.
19. Liu H.-B. Schedule risk management method of construction project based on critical chain // International Conference on Electric Technology and Civil Engineering, ICETCE 2011 – Proceedings. 2011. Pp. 2561–2563.
20. De Marco A., Briccarello D., Rafele, C. Cost and schedule monitoring of industrial building projects: Case study // Journal of Construction Engineering and Management. 2009. Vol. 135(9). Pp. 853–862.
21. Luiz J.V.R., De Souza F.B., Luiz O.R. PMBOK® and critical chain practices: Antagonisms and opportunities for complementation // Gestao e Producao. 2017. Vol. 24(3). Pp. 464–476.
22. Kahmann A., Kloeckner A.P. Theory of restrictions and project management - critical chain: A systematic review of the literature // Espacios. 2014. Vol. 35(13). Pp.1–20.
23. Duan Q., Liao T.W. Improved ant colony optimization algorithms for determining project critical paths // Automation in Construction. 2010. Vol. 19(6). Pp. 676–693.
24. Połoński M., Pruszyński K. The time buffers location and critical chain concepts in civil engineering network schedule. Part I. Theoretical background // Przegląd Budowlany. 2008. № 2. Pp. 5–49.
25. Martens A., Vanhoucke M. A buffer control method for top-down project control // European Journal of Operational Research. 2017. Vol. 262(1). Pp. 274–286.
26. Ma G., Wang A., Li N., Gu L., Ai Q. Improved Critical Chain Project Management Framework for Scheduling Construction Projects // Journal of Construction Engineering and Management. 2014. Vol. 140(12). Pp. 31–58.

Marina Petrochenko,*
+7(812)552-94-60; mpetroch@mail.ru

Viktor Velichkin,
+7(921)654-54-68; V.Velichkin2011@yandex.ru

Yuryi Kazakov,
+7(981)757-57-77; kazakov@spbgasu.ru

Yevgeniya Zavodnova,
+7(965)761-58-24; yavtushenko_89@mail.ru

Марина Вячеславовна Петроченко,*
+7(812)552-94-60; эл. почта: mpetroch@mail.ru

Виктор Захарович Величкин,
+7(921)654-54-68;
эл. почта: V.Velichkin2011@yandex.ru

Юрий Николаевич Казаков,
+7(981)757-57-77;
эл. почта: kazakov@spbgasu.ru

Евгения Борисовна Заводнова,
+7(965)761-58-24;
эл. почта: yavtushenko_89@mail.ru

doi: 10.18720/MCE.81.4

Evolutionary optimization of prestressed steel frames

Эволюционная оптимизация предварительно напряженных стальных рам

A.V. Alekseytsev*,
National Research Moscow State Civil Engineering University, Moscow, Russia
S.A. Akhremenko,
Bryansk State University of Engineering and Technology, Bryansk. Russia

Канд. техн. наук, доцент
А.В. Алексейцев*,
Национальный исследовательский Московский государственный строительный университет, г. Москва, Россия
канд. техн. наук, профессор
С.А. Ахременко,
Брянский государственный инженерно-технологический университет, г. Брянск, Россия

Key words: prestressed frames; evolutionary optimization; a mixed account of constraints; weakly interacting populations; adaptive genetic operators

Ключевые слова: преднапряженные рамы; эволюционная оптимизация; комбинированный учет ограничений; слабовзаимодействующие популяции; адаптивные генетические операторы

Abstract. A method for the optimal synthesis of prestressed steel frame structures is developed. The search for a solution is being carried out by applying discrete sets of variable parameters, including cross-sections of structural rods and cross-sections of prestressing tie-rods. It is possible to vary the location of the prestressing system. To optimize the cost of the objects under consideration, an improved meth-od of evolutionary simulation has been used, including a combined scheme for constraints set and an unusual scheme for the formation of populations. Strength and stiffness considerations for a number of objects within a population are not strict, and for variants with breached constraints, a penalty function has been applied. In forming the current population used to modify the individuals, multipoint genetic operators, random generation, and a strategy of elitism have been applied. To vary the location of the prestressing system and take into account the multivariance of loads, parallel evolving populations have been introduced, between which a limited exchange of individuals is allowed. Examples of optimization of prestressed frames with girders and trusses were considered.

Аннотация. Разрабатывается методика оптимального синтеза преднапряженных стальных рамных конструкций. Поиск решения осуществляется на дискретных множествах варьируемых параметров, включающих сечения стержней конструкции и сечения преднапрягающих затяжек. Предусматривается возможность варьирования расположения системы преднапряжения. Для оптимизации стоимости рассматриваемых объектов используется усовершенствованная схема эволюционного моделирования, включающая комбинированную схему учета ограничений и неординарную схему формирования популяций. Учет ограничений по прочности и жесткости для ряда объектов в популяции не является строгим, при этом для вариантов, имеющих нарушение ограничений, используется штрафная функция. При формировании текущей популяции для модификации объектов используются многоточечные генетические операторы, случайная генерация и стратегия элитизма. Для варьирования расположения системы преднапряжения и учета многовариантности нагружений вводятся параллельно эволюционирующие популяции, между которыми допускается ограниченный обмен особями. Рассмотрены примеры оптимизации преднапряженных рам с балочным и ферменным ригелями.

1. Introduction

Reduction of materials used in steel structures is one of the topical problems arising during building and structure design. At present, algorithms of evolutionary simulation established on the basic principles of the evolution of species in an animated nature can be successfully used to optimize designs, by applying discrete sets of variants of structures and design parameters (dimensions, cross-sections sizes of rod, coordinates of nodal joints, grades of steels, etc.). Studies have proven that this approach to optimization for this class of problems is quite effective.

Reduced costs of frame structures can be attained via prestressing. The issue of optimization of prestressed rod, plate, and shell objects is crucial and has been a focus of close attention for many researchers. Numerous papers have been devoted to the optimization of prestressed reinforced concrete slabs [1–4], beams [5–10], trusses [11, 12], bridge structures [13–15], tensegrity systems [16], cable-stayed domes [17], membrane [18] structures and poles with prestressed anchor stays [19]. It is describes the two-stage general approach to optimization of reinforced concrete structures [20], where, at the first stage, linear programming is applied to select the prestressing force, and at the second stage - the specific dimensions of an element.

This method of cable-stayed trusses optimization based on evolutionary simulation has been developed [21] with variables divided into three groups: prestressing force, sizes of cross-sections, and location of structural elements. In [11], steel trusses were optimized according to a two-stage scheme, where, at the first stage, cross-sections of elements were selected, and, at the second stage, prestress was calculated via linear programming.

A number of important research areas are related to prestressed structure optimization issues. Primarily, assessment of the prestressed systems technical condition, which can be performed, for example, by an oscillatory method [22], as well as through experimental studies. For example, in [23], an experimental analysis of the behavior of steel trusses was made by taking into account different ways of linking ropes and prestressed elements. For such trusses with tubular cross-sections of elements, the effect of prestressing compressed and tensioned rods made of various steel grades was studied [24]. The stability of prestressed steel columns was investigated [25, 26].

This paper suggests a method for optimizing prestressed frame structures based on a multi-threaded iterative procedure. At the same time, based on the use of parallel populations, the issue of finding the minimum cost of construction is being solved. The distinctive feature of the suggested approach is that single computational process is applied to vary the standard sizes of the bar cross-section, location, and dimensions of the prestressing system, as well as the values of prestressing forces.

2. Methods

2.1. Formulation of the optimization problem

We consider the steel frame structure, which includes the prestressing system in the form of stops, tie-ropes, and elements fixing the tie-rope position. The design model is discretized according to the scheme of the finite element method, with rigid consoles (inserts) used to attach ropes to rods. System prestressing is taken into account by introducing multidirectional paired forces, the points of application of which coincide with the stops location, and the lines of such forces action coincide with the rope longitudinal axis. Technological characteristics, which depend on the conditions of initial loading and step-by-step prestressing, have not been taken into account. Frame bars are described by means of multilayer bar finite elements, in which each layer can be subject to tension-compression strains [27]. In general, Bernoulli's hypothesis of flat sections is used for the layer assembly. We set the following tasks.

Personal objective **(I)**: cost C of the prestressed structure, for which the value of prestress force and location of the prestressing system does not change, is minimized.

$$C(\{X\}, P) \to \min, \ \{X\} = \{X_1, ..., X_n\}, \tag{1}$$

where $\{X\}$ – set of variable sizes of cross-section profiles in rods represented by integral geometric characteristics, n – the number of variable parameters; P – constant parameters of the prestressing system.

Alekseytsev, A.V., Akhremenko, S.A. Evolutionary optimization of prestressed steel frames. *Magazine of Civil Engineering*. 2018. 81(5). Pp. 32–42. doi: 10.18720/MCE.81.4.

Variable

$$X_i = \{A_i; x_{i1}, y_{i1}, ..., x_{ik}, y_{ik}\},\ i = 1..n, \tag{2}$$

where A_i – bar cross-section i, $x_{i1}, y_{i1}, ..., x_{ik}, y_{ik}$ – coordinates of points in bar cross-section i, k – number of cross-section points in which stresses are calculated.

Personal objective **(II)**: Search for optional design with minimum cost.Taking into account the change in the prestressing system location. The prestress force remains constant.

$$\begin{gathered} C(\{X\}, P, \{Y\}) \to \min, \\ \{Y\} = \{Y_1, ..., Y_R\}, \\ \{Y_i\} = \{B_i(x_{bi}, y_{bi}),\ E_i(x_{ei}, y_{ei})\}, i = 1..R, \end{gathered} \tag{3}$$

where $\{Y\}$ – set of the prestressing system locations, R – the number of such variant in the structure, B_i, E_i – points of prestressing forces application.

The considered private objectives allow us to formulate the ***general objective*** **(III):** minimization of the frame construction cost C by taking into account the variable level of prestress and variations in the prestressing system location. The species target function is minimized

$$\begin{gathered} C(\{X\}, P, \{Y\}, \{N\}) \to \min, \\ \{N\} = \{N_1, ..., N_D\}, i = 1..D, \end{gathered} \tag{4}$$

where $\{N\}$ – set of values of prestressing forces, D – number of prestress levels of the structure which, in a particular case, may coincide with the number of tie-rope standard dimensions used.

For all the tasks set, constraints on the strength, stability, and stiffness of the frame structure should be taken into account, in accordance with current design standards. It is required from the prestressing system not to exceed the value of the tensile strength of the rope above the permissible design value. Conditions of the symmetry, unification, and design features of the object should also be taken into account.

2.2. Solving algorithm

The optimization algorithm is based on a modification of the combined evolution strategy detailed in [28]. We perform a number of steps.

1. *Formation of the structure finite element model*. In this case, for private objective achieving (I), this model shall be constructed traditionally. Stiffness of the prestressing ropes is set to be constant. Necessary design values (topology, material characteristics, loads, kinematic constraints, etc.) need to be entered.

In solving the objective tasks (II), a R of variants of finite element models with its own location of the prestressing system shall be formed. In this case, all variants are considered in a single multi-threaded iterative scheme and are united by a common system of constraints. For each R variant of the prestressing system location, an evolving population, for which a limited exchange of individuals from other populations is allowed, should be organized in the genetic algorithm in parallel.

For general formulation of the task, the process of the computational model formation is similar to the one described in the objective (II), but, in this event, in calculations, for each reinforcement system location variant, D different loads formed by prestressing forces shall be taken into consideration. Each value of the force can be associated with a certain rope cross-section. In this event, stiffness of the rope also changes, depending on the current value of the force.

At this stage, information on the operational loads applied to the structure, the sets of values of variable parameters that can be chosen, and other data necessary for the implementation of optimization and evaluation procedures for the object stress-strain state shall also be entered.

2. *Random generation of the initial pool of prestressed system variants*. Values required for problem solving in various constructive solutions of the object have been obtained from the corresponding sets of variable parameters. In this event, the possibility of grouping the elements by taking into account the symmetry of the system, constructive, and technological requirements shall be made use of. As a result, for each of the tasks posed, the first generation of individuals (set of the object variants) further considered in the genetic iterative procedure can be represented as (5):

$$G_1^{(I)} = \begin{array}{c|ccc} F_1: & X_{1\tilde{i}}, & \ldots, & X_{n\tilde{i}} \\ \hline \ldots & \ldots, & \ldots, & \ldots \\ \hline F_{ng}: & X_{1\tilde{i}}, & \ldots, & X_{n\tilde{i}} \end{array}; \quad G_1^{(II)} = \begin{array}{c|cccc} F_1: & X_{1\tilde{i}}, & \ldots, & X_{n-1\tilde{i}}, & Y_{n\tilde{j}} \\ \hline \ldots & \ldots, & \ldots, & \ldots, & \ldots \\ \hline F_{ng}: & X_{1\tilde{i}}, & \ldots, & X_{n-1\tilde{i}}, & Y_{n\tilde{j}} \end{array};$$

$$G_1^{(III)} = \begin{array}{c|ccccc} F_1: & X_{1\tilde{i}}, & \ldots, & X_{n-2\tilde{i}}, & Y_{n-1\tilde{j}}, & N_{n\tilde{k}} \\ \hline \ldots & \ldots, & \ldots, & \ldots, & \ldots, & \ldots, \\ \hline F_{ng}: & X_{1\tilde{i}}, & \ldots, & X_{n-2\tilde{i}}, & Y_{n-1\tilde{j}}, & N_{n\tilde{k}} \end{array}, \qquad (5)$$

where $G_1^{(I)}, G_2^{(II)}, G_1^{(III)}$ – initial populations for the formulation of tasks I, II, III, respectively;

$\tilde{i}$, $\tilde{j}$, $\tilde{k}$ – whole numbers randomly selected at intervals $[1..np_i], [1..R], [1..D]$, np_i – number of values permitted for selected variable parameter i. Number ng of the project variants is presumed to be equal to 20 for the first and subsequent generations.

3. *Calculation of the stress-strain state and the fitness of the objective function for each structure variant*. The decision shall be made on a system of linear algebraic equations for the discretized object finite-element method to determine displacements, and then, forces and stresses in structural elements. If the object meets the set constraints, calculations of its cost *C* shall be made. Based on the value *C,* a decision shall be made as to the acceptance of the structure variant for further stages of the genetic iterative procedure. The cost shall include conditional cost values of materials and construction.

4. *Creating the Elite Objects Database (EOB).* EOB shall include structure variants with the best *C* value. Initially, objects from the initial pool generated at stage 2 shall be placed there, provided that all constraints have been met. This stage shall be implemented if the EOB has not been created, otherwise the next stage is to be started.

5. *EOB correction*. For any object to be entered into the database the following requirements shall be met:

– the cost of the object-applicant intended for inclusion in the database should be less than the maximum cost of the objects already existing in the EOB;
– The object-applicant should not be a copy of any object from the EOB.

6. *Formation of the current pool (generation) of individuals (structure variants)*. New variants of the object are obtained through the implementation of genetic operators on the objects with the best cost values randomly selected from the EOB. Selection shall be made via the roulette wheel method, depending on the *C* value. The mechanism for the structure variant change is demonstrated by example of 20 objectives making up the pool in Table 1.

7. Check of compliance with the calculation termination criterion. If the contents of the EOB for 200-300 iterations does not change, then the solution obtained after checking passive constraints and verification calculations, taking into account physical, geometric, and constructive nonlinearities, for example by [29], can be deemed final. Otherwise, stages 3, 5-7 shall be repeated.

Table 1 Principle of population formation

Individuals number	Name and description of the operator
1	Single-point mutation
2	Ditto
3	- // -
4	Two-point mutation
5	Ditto
6	- // -
7	Regulated *n*-point mutation [30]
8	Ditto
9	- // -
10	Single point crossover
11	Ditto
12	Two-point crossover
13	Ditto
14	Regulated *n*-point crossover and inversion [31]
15	Ditto
16	Single-point inversion
17	Multipoint inversion
18	Random generation of the object. Values of variable parameters are randomly selected from a discrete set of corresponding acceptable values.
19	Ditto
20	- // -

3. Results and Discussion

3.1. Example 1. Optimal design of the steel frame with the search for the prestressing tie-rod position (personal objective (I))

The object in question is shown in Figure 1,a. It is assumed that the frame has become unfastened through the loss of stability from the plane by longitudinal girders and capping beams. The rods with the cross-section area shown in Figure 1,b are made of Fe 430 steel. Mechanical characteristics: modulus of elasticity $E_a = 2.06 \cdot 10^5$ MPa, yield strength $\sigma_y = 255$ MPa. In calculating structure variants during the course of the optimization process, stresses were limited by the value $\sigma = 235$ MPa. Restrictions on displacements were imposed: $\delta_x \leq 0.012$ m, $\delta_y \leq 0.072$ m. The tie-rod 3 is made of a spiral rope (Figure 1,c) of grade SS45 as per EN12385-10, with a modulus of elasticity $E_r = 1.7 \cdot 10^5$ MPa. The prestressing force was assumed to be 1000 kN, making up 84 % of the design load. The structure model was discretized into finite elements measuring 1 m.

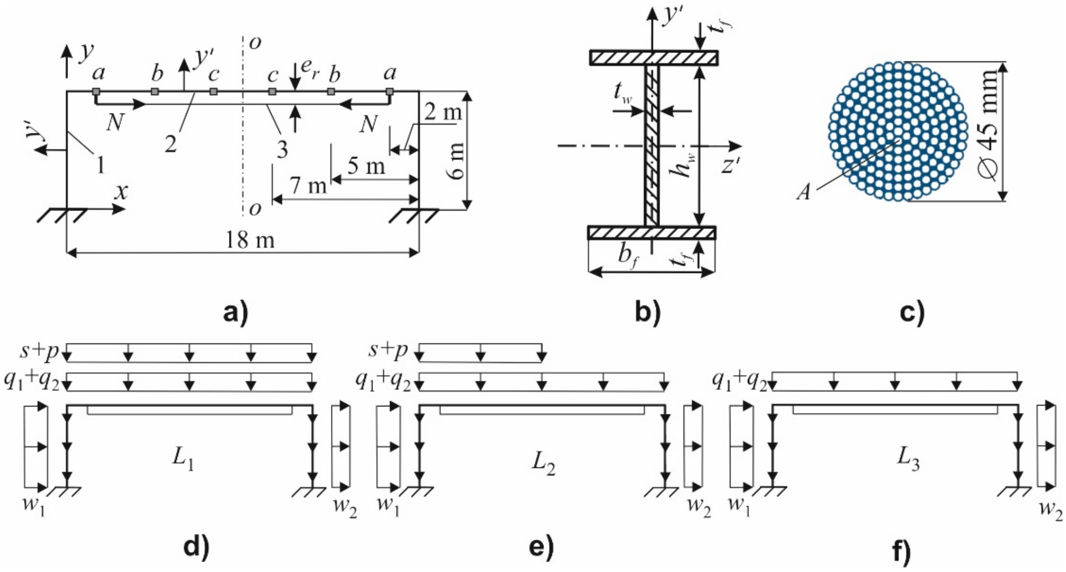

Figure 1. Geometric model of the object and considered load combinations

The frame was designed for the following loads: structure weight q_1, wind loads $w_1 = 1.1\,\mathrm{kN/m}$ $w_2 = 0.83\,\mathrm{kN/m}$, decking weight $q_2 = 12\,\mathrm{kN/m}$, snow load $s = 10.8\,\mathrm{kN/m}$, and payload $p = 7.2\,\mathrm{kN/m}$ acting on the entire span of the frame, snow $\bar{s}$ and payload $\bar{p}$ acting on half the span of the frame and having the same intensity as loads s and p (Figure 1,d-f).

The following loading combinations (6) were considered:

$$L_1 = q_1 + q_2 + p + 0{,}9(s + w_1 + w_2)\,;\; L_2 = q_1 + q_2 + \bar{s} + 0{,}9(\bar{p} + w_1 + w_2)\,;$$
$$L_3 = q_1 + q_2 + 0{,}9(w_1 + w_2)\,. \tag{6}$$

Sizes of profiles in the rod cross-sections and location of the prestressing tie-rods 3 were varied. Grade profiles were as per ASTM A6. The tie-rod can be located in positions a-a, b-b or c-c (Figure 1, a). Four groups of structural elements were introduced: columns 1 and three equal parts of beam 2. For each group of elements, cross-sections were varied independently. A discrete set of parameters acceptable for selection during the course of the optimization process is presented in Table 2.

Table 2. Variable cross-sections of rods

N	Designation	Cross-sections in Fig. 1,b, 10^{-2} m			
W1	W 8x8x31	18.1	0.72	20.3	1.1
W2	W10x10x49	22.46	0.86	25.4	1.42
W3	W12x12x65	27.72	0.99	30.5	1.54
W4	W14x10x68	32.04	1.05	25.5	1.83
W5	W16x10.25x77	38.14	1.16	26.1	1.93
W6	W18x11x86	42.78	1.22	28.2	1.96
W7	W21x8.25x93	50.18	1.47	21.4	2.36
W8	W24x9x94	57.26	1.31	23	2.22
W9	W27x10x102	64.58	1.31	25.4	2.11
W10	W30x10.5x108	71.94	1.38	26.6	1.93
W11	W33x11.5x118	79.74	1.4	29.2	1.88
W12	W36x12x135	86.28	1.52	30.4	2.01

Alekseytsev, A.V., Akhremenko, S.A. Evolutionary optimization of prestressed steel frames. *Magazine of Civil Engineering*. 2018. 81(5). Pp. 32–42. doi: 10.18720/MCE.81.4.

In varying sizes of profiles, the eccentricity of tie-rod e_r relative to the longitudinal axis of the frame girder was defined as $e_{ri} = h_{wi} / 2 + t_{fi}$, $i = [1;12]$. Vertical frame rods with length e_{ri} connecting tie-rod 3 to beam 2, by their integral characteristics were considered to be close to absolutely rigid bodies. To assess prestress efficiency, optimal synthesis of the frame without prestressing was performed, with the results shown in Figure 2,a. Optimal solutions for the frame with prestressing are shown in Figure 2,b-d.

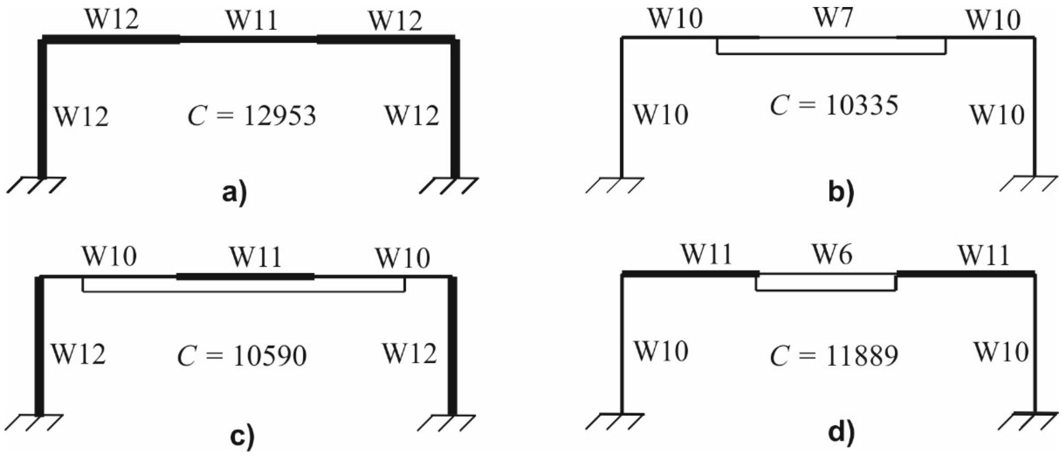

Figure 2. Solution results: W6-W12 – cross-section numbers from Table 2

The optimization process required the performance of no more than 100 iterations of the evolutionary algorithm, and 2000 variants of the frame were calculated. For the considered conditions for the solution, the location of b-b tie-rod 3 was the most expedient (Figure 1,a). Figure 2 illustrates that prestressing makes it possible to reduce the conventional cost of the considered frame structure by more than 20 %.

3.2. Example 2. Search for the optimal frame solution by taking into account variations in tie-rod stiffness and tension force (personal objective (II))

The frame of example 1 is considered. The tie-rod is fixed to the structure in the b-b position, and its position does not change. Materials, loads, kinematic constraints, and the variable parameters of rods remain the same as in Example 1. In addition, the values of tie-rod section 3 and corresponding tension forces are independently varied. Permissible values for the tie-rods variable parameters are given in Table 3.

Some typical results of optimal frame design are shown in Fig. 3. Analysis of the results obtained indicate that the most efficient level of the prestressing value is *N* = 1400 kN. The optimization process required execution of no more than 120 iterations of the evolutionary algorithm, which allowed calculating 2400 variants of the frame.

Table 3. Design characteristics of spiral ropes

Discrete sets of variable parameters of spiral SS ropes: diameter – *D*, 10^{-3} m; axial stiffness – *EA*, MN; design load – *P*, kN; prestressing force – *N*, kN									
D	25	30	35	40	45	50	55	60	65
EA	66	95	124	160	204	242	295	350	413
P	370	524	719	931	1190	1460	1770	2100	2470
N	300	500	700	900	1100	1400	1700	2000	2400

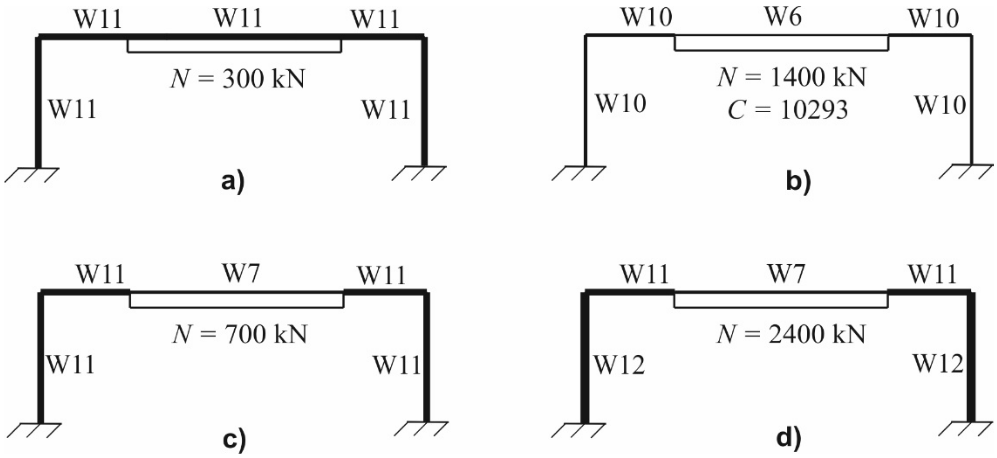

Figure 3. Results of the problem solution: W6-W12 – cross-section numbers from Table 2

3.3. Example 3. Optimization of the constructive solution for a single-story building frame by varying the location of the tie-rod and the level of its prestress (personal objective (III)).

To prevent the loss of stability from plane, the frame is fastened by spacers along the upper and lower belts of the roof truss and capping beams along the column length. Action of two combinations of loads L_1 and L_2, and g of the frame weight, decking structure, and snow load S. The frame rods are made of A529 steel, Grade 55, yield strength $\sigma_y = 380\ \mathrm{MPa}$. In calculating the structure variants, stresses were limited by $\sigma = 360\ \mathrm{MPa}$. Dimensions of the profiles shown in Table 2 were varied for the columns and the top chord of truss, rectangular pipe profiles as per ASTM A500 were used for the remaining elements of the truss, dimensions which are given in Table 4.

Table 4. Discrete set of rods cross-sections

N	Designation	Cross-sectional dimensions in Fig. 4,b, 10^{-2} m		
		d_1	d_2	$t_1 = t_2$
T1	4x3	6.7056	9.2456	0.457
T2	5x3	6.7056	11.7856	0.457
T3	6x4	9.2456	14.3256	0.457
T4	7x5	11.1099	16.18996	0.795
T5	8x6	14.3256	19.4056	0.457
T6	10x6	14.3256	24.4856	0.457
T7	10x8	18.4150	23.4950	0.953
T8	12x8	19.0500	29.2100	0.635
T9	14x10	23.4950	33.6550	0.953
T10	16x12	28.5750	38.7350	0.953

Tie-rods were allowed to be made of grades SS 30, SS 40, SS 50 with the initial prestress forces equal to 500, 900, and 1400 kN, respectively. The tie-rod could be located in one of three possible positions (1, 2, 3) shown in Figure 4, a by the dashed line. Considering the object symmetry, the following group of variable parameters was used: group provided g_1 - g_8 – (Figure 4,a), within the limits of which the rod cross-section is assumed to be the same. Here, group g_1 – columns, g_2 contains all elements of the top chord of truss, g_3 - g_6 – are elements of the bottom chord, g_7 – all pillars, g_8 – all of the web members. A total of 10 parameters were varied independently. The optimization process was completed in no more than 200 iterations of genetic algorithm. The best solution found is shown in Figure 4,c.

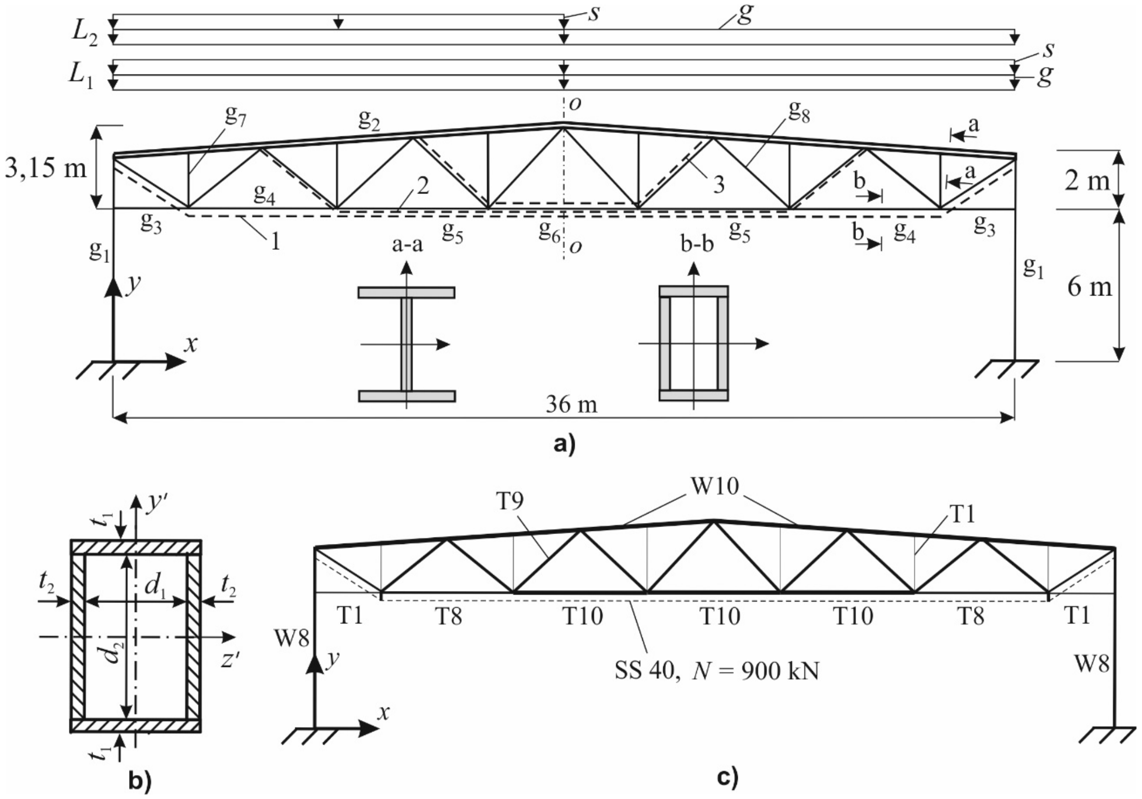

Figure 4. Input data and results of optimization of the frame with a roof truss: W8, W10 – section numbers from table. 2; T1 – T10 – section numbers from table 4.

3.4. Discussion

Problems of prestressed structures optimization were effectively solved based on various modifications of genetic algorithms, as those presented in [21, 22]. The step-by-step decision-making process was applied. The presented algorithm contains the unified iteration scheme for all design stages, to make possible obtaining the solution of very complex problems with a large number of variable parameters. Comparison of solutions obtained through the use of our proposed computational scheme with the results obtained by other authors [4], where is concluded that the amounts of the material and the cost of a steel plane truss can be reduced up to 19.9 %, guarantees very good results regarding objective function and convergence values. At the same time, one of the factors improving repeatability is the introduction of the penalty function described in [10].

4. Conclusions

1. The novel search method for a rational construction solution for steel frames with prestressed structural elements was developed on the basis of evolutionary simulation. The optimization algorithm enables consideration of different loading variants, independent variation of configurations and parameters of the projected structures and the prestressing system in one iterative process.

2. The effect of cost reduction compared with the same structure designed without prestress, considering the requirements of design standards, exceeded 18–20 %.

3. Considered examples demonstrated that theproposed algorithm used for specific structures allows determining the rational prestressing force value and the prestressing system location. This algorithm is recommended for use in computer-aided design engineering of buildings and structures made of steel frames.

5. Acknowledgement

The authors express their cordial gratitude to the Honorable worker of science and engineering of the Russian Federation, Distinguished scholar of Bryansk Oblast, head of the scientific school “Increase of reliability, design safety, vibration protection and service life of building systems and engineering products”, head of the mechanics department of Bryansk State Engineering and Technology University, professor, doctor of engineering Serpik Igor Naftolevich for the benevolent attitude and assistance in scientific research. Work was performed under the grant program of the Russian Fundamental Research Fund as project 16-38-00041.

References

1. El Semelawy, M., Nassef, A.O., El Damatty, A.A. Design of prestressed concrete flat slab using modern heuristic optimization techniques. Expert Systems with Applications. 2012. No. 39. Pp. 5758–5766.
2. Ivashenko, I.A. Optimization of the Prestress Value in Binding of Rein-forced Concrete Structures. Procedia Engineering. 2016. No. 150. Pp. 1771–1775.
3. Talaei, A.S., Nasrollahi, A., Ghayekhloo, M. An automated approach for optimal design of prestressed concrete slabs using PSOHS. KSCE Journal of Civil Engineering. 2017. No. 21(3). Pp. 782–791.
4. Kaveh, A., Talaei, A.S., Nasrollahi, A. Application of Probabilistic Particle Swarm in Optimal Design of Large-Span Prestressed Concrete Slabs. Iranian Journal of Science and Technology-Transactions of Civil Engineering. 2016. No. 40(1). Pp. 33–40.
5. Eurviriyanukul, S., Askes, H. Tendon layout optimization through configurational forces equilibration in plane stress analysis of prestressed concrete structures. Computers & Structures. 2011. No. 89. Pp. 1673–1680.
6. Barakat, S., Bani-Hani, K., Taha, M.Q. Multi-objective reliability-based optimization of prestressed concrete beams. Structural Safety. 2004. No. 26. Pp. 311–342.
7. Steensels, R., Vandewalle, L., Vandoren, B., Degée, H. A two-stage modelling approach for the analysis of the stress distribution in anchorage zones of pre-tensioned, concrete elements. Engineering Structures. 2017. No. 15. Pp. 384–397.
8. Khaleel, M.A., Itani, R.Y. Optimization of partially prestressed concrete girders under multiple strength and serviceability criteria. Computers & Structures. 1993. No. 49. Pp. 427–438.
9. Turkeli, E., Ozturk, H.T. Optimum design of partially prestressed concrete beams using Genetic Algorithms. Structural Engineering and Mechanics. 2017. No. 64(5). Pp. 274–291.
10. Schnellenbach-Held, M., Steiner, D. Self-Tuning Closed-Loop Fuzzy Logic Control Algorithm for Adaptive Prestressed Structures. Structural Engineering International. 2014. No. 24(2). Pp. 163–172.
11. Levy, R., Hanaor, A. Optimal design of prestressed trusses. Computers & Structures. 1992. No. 43. Pp. 741–744.
12. Aydin, Z., Cakir, E. Cost minimization of prestressed steel trusses considering shape and size variables. Steel and Composite Structures. 2015. No. 19(1). Pp. 43–58.
13. Martí, J.V., Gonzalez-Vidosa, F., Yepes, V., Alcalá, J. Design of prestressed concrete precast road bridges with hybrid simulated annealing. Engineering Structures. No. 2013. Pp. 342-352.
14. Rana, S., Islam, N., Ahsan, R., Ghani, S.N. Application of evolutionary operation to the minimum cost design of continuous prestressed concrete bridge structure. Engineering Structures. 2013. No. 46. Pp. 38–48.
15. Eom, G.-H., Kim, S.J., Lee, T.-H. Design Optimization and Structural Performance Evaluation of Plate Girder Bridge Constructed Using a Turn-Over Process. Materials. 2017. No. 10(3). art. No. 283.
16. Zhang, P., Feng, J. Initial prestress design and optimization of tensegrity systems based on symmetry and stiffness. International Journal of Solids and Structures. 2017. No. 106. Pp. 68–90.
17. Quagliaroli, M., Malerba, P.G., Albertin, A., Pollini, N. The role of prestress and its optimization in cable domes design. Computers & Structures. 2015. No. 161. Pp. 17–30.
18. Dutta, S., Ghosh, S., Inamdar, M.M. Reliability-Based Design Optimization of Frame-Supported Tensile Membrane Structures. ASCE-ASME Journal of Risk and

Литература

1. El Semelawy M., Nassef A.O., El Damatty A.A. Design of prestressed concrete flat slab using modern heuristic optimization techniques // Expert Systems with Applications. 2012. № 39. Pp. 5758–5766.
2. Ivashenko I.A. Optimization of the Prestress Value in Binding of Rein-forced Concrete Structures // Procedia Engineering. 2016. № 150. Pp. 1771–1775.
3. Talaei A.S., Nasrollahi A., Ghayekhloo M. An automated approach for optimal design of prestressed concrete slabs using PSOHS // KSCE Journal of Civil Engineering. 2017. № 21(3). Pp. 782–791.
4. Kaveh A., Talaei A.S., Nasrollahi A. Application of Probabilistic Particle Swarm in Optimal Design of Large-Span Prestressed Concrete Slabs // Iranian Journal of Science and Technology-Transactions of Civil Engineering. 2016. № 40(1). Pp. 33–40.
5. Eurviriyanukul S., Askes H. Tendon layout optimization through configurational forces equilibration in plane stress analysis of prestressed concrete structures // Computers & Structures. 2011. № 89. Pp. 1673–1680.
6. Barakat S., Bani-Hani K., Taha M.Q. Multi-objective reliability-based optimization of prestressed concrete beams // Structural Safety. 2004. № 26. Pp. 311–342.
7. Steensels R., Vandewalle L., Vandoren B., Degée H. A two-stage modelling approach for the analysis of the stress distribution in anchorage zones of pre-tensioned, concrete elements // Engineering Structures. 2017. № 15. Pp. 384–397.
8. Khaleel M.A., Itani R.Y. Optimization of partially prestressed concrete girders under multiple strength and serviceability criteria // Computers & Structures. 1993. № 49. Pp. 427–438.
9. Turkeli E., Ozturk H.T. Optimum design of partially prestressed concrete beams using Genetic Algorithms // Structural Engineering and Mechanics. 2017. № 64(5). Pp. 274–291.
10. Schnellenbach-Held M., Steiner D. Self-Tuning Closed-Loop Fuzzy Logic Control Algorithm for Adaptive Prestressed Structures // Structural Engineering International. 2014. № 24(2). Pp. 163–172.
11. Levy R., Hanaor A. Optimal design of prestressed trusses // Computers & Structures. 1992. № 43. Pp. 741–744.
12. Aydin Z., Cakir E. Cost minimization of prestressed steel trusses considering shape and size variables // Steel and Composite Structures. 2015. № 19(1). Pp. 43–58.
13. Martí J.V., Gonzalez-Vidosa F., Yepes V., Alcalá J. Design of prestressed concrete precast road bridges with hybrid simulated annealing // Engineering Structures. № 2013. Pp. 342–352.
14. Rana S., Islam N., Ahsan R., Ghani S. N. Application of evolutionary operation to the minimum cost design of continuous prestressed concrete bridge structure // Engineering Structures. 2013. № 46. Pp. 38–48.
15. Eom G.-H., Kim S.J., Lee, T.-H. Design Optimization and Structural Performance Evaluation of Plate Girder Bridge Constructed Using a Turn-Over Process // Materials. 2017. № 10(3). art. No. 283.
16. Zhang P., Feng J. Initial prestress design and optimization of tensegrity systems based on symmetry and stiffness // International Journal of Solids and Structures. 2017. № 106. Pp. 68–90.
17. Quagliaroli M., Malerba P.G., Albertin A., Pollini N. The role of prestress and its optimization in cable domes design // Computers & Structures. 2015. № 161. Pp. 17–30.
18. Dutta S., Ghosh S., Inamdar M.M. Reliability-Based Design Optimization of Frame-Supported Tensile Membrane Structures // ASCE-ASME Journal of Risk and Uncertainty

Uncertainty in Engineering Systems Part a-Civil Engineering. 2017. No. 3(2). art. No. G4016001.
19. Guo, J., Jiang, J. An algorithm for calculating the feasi-ble pre-stress of cable-struts structure. Engineering Structures. 2016. No. 118. Pp. 228–239.
20. Kirsch, U. Two-level optimization of prestressed structures. Engineering Structures. 1997. No. 19. Pp. 309–317.
21. Ailin, Z., Haijun, Y., Guojun, Z., Chuancheng, Z. The shape optimization design of prestressed cable-truss structure based on evolutionary method of nodes. Fourth International Conference on Advances in Steel Structures. 2005. No. II. Pp. 1335–1340.
22. Ruocci, G., Cumunel, G., Le, T., Argoul, P., Point, N., Dieng, L. Damage assessment of prestressed structures: A SVD-based approach to deal with time-varying loading. Mechanical Systems and Signal Processing. 2014. No. 47. Pp. 50–65.
23. Alekseytsev, A.V., Kurchenko, N.S. Deformations of steel roof trusses under shock emergency action. Magazine of Civil Engineering. 2017. No. 5(73). Pp. 3–13. doi: 10.5862/MCE.73.1.
24. Wang, J., Afshan, S., Gardner, L. Axial behaviour of prestressed high strength steel tubular members. Journal of Constructional Steel Research. 2017. No. 133. Pp. 547–563.
25. Li, P., Wadee, M.A., Yu, J., Christie, N.G., Wu, M. Stability of prestressed stayed steel columns with a three branch crossarm system. Journal of Constructional Steel Research. 2016. No. 122. Pp. 274–291.
26. Yu, J., Wadee, M.A. Optimal prestressing of triple-bay prestressed stayed columns. Structures. 2017. No. 12. Pp. 132–144.
27. Serpik, I.N., Kurchenko, N.S. Nakhozhdeniye predelnykh nagruzok dlya sistem tonkostennykh sterzhney otkrytogo profilya [Search of ultimate loads for systems of thin-walled rods of an open profile]. Vestnik Bryanskogo gosudarstvennogo tekhnicheskogo universiteta. 2013. No. 1(37). Pp. 41–48. (rus)
28. Serpik, I.N., Alekseytsev, A.V., Balabin, P.Yu., Kurchenko, N.S. Flat rod systems: optimization with overall stability control. Magazine of Civil Engineering. 2017. No. 8. Pp. 181–192. doi: 10.18720/MCE.76.16.
29. Serpik, I.N., Kurchenko, N.S., Alekseytsev, A.V., Lagutina, A.A. Analiz v geometricheski, fizicheski i konstruktivno nelineynoy postanovke dinamicheskogo povedeniya ploskikh ram pri zaproyektnykh vozdeystviyakh [The analysis in geometrically, physically and structurally non-linear statement of dynamic behavior of flat frames at emergency actions]. Promyshlennoye i grazhdanskoye stroitelstvo. 2012. No. 10. Pp. 49–51. (rus)
30. Serpik, I.N., Alekseytsev, A.V. Optimization of flat steel frame and foundation posts system]. Magazine of Civil Engineering. 2016. No. 1. Pp. 14–24. doi: 10.5862/MCE.61.2
31. Alekseytsev, A.V, Serpik, I.N. Optimizatsiya ploskikh ferm na osnove geneticheskogo poiska i iterativnoy protsedury triangulyatsii [Optimization of plane trusses on the basis of genetic search and the iterative procedure of a triangulation]. Stroitelstvo i rekonstruktsiya. 2011. No. 2. Pp. 3–8. (rus)

in Engineering Systems Part a-Civil Engineering. 2017. № 3(2). art. No.G4016001.
19. Guo J., Jiang J. An algorithm for calculating the feasible pre-stress of cable-struts structure // Engineering Structures. 2016. № 118. Pp. 228–239.
20. Kirsch U. Two-level optimization of prestressed structures // Engineering Structures. 1997. № 19. Pp. 309–317.
21. Ailin Z., Haijun Y., Guojun Z., Chuancheng Z. The shape optimization design of prestressed cable-truss structure based on evolutionary method of nodes // Fourth International Conference on Advances in Steel Structures. 2005. № II. Pp. 1335–1340.
22. Ruocci G., Cumunel G., Le T., Argoul P., Point N., Dieng L. Damage assessment of prestressed structures: A SVD-based approach to deal with time-varying loading // Mechanical Systems and Signal Processing. 2014. № 47. Pp. 50–65.
23. Алексейцев А.В., Курченко Н.С. Деформации стальных стропильных ферм при ударных аварийных воздействиях // Инженерно-строительный журнал. 2017. № 5(73). С. 3–13. doi: 10.5862/MCE.73.1.
24. Wang J., Afshan S., Gardner L. Axial behaviour of prestressed high strength steel tubular members // Journal of Constructional Steel Research. 2017. № 133. Pp. 547–563.
25. Li P., Wadee M.A., Yu J., Christie N.G., Wu M. Stability of prestressed stayed steel columns with a three branch crossarm system // Journal of Constructional Steel Research. 2016. № 122. Pp. 274–291.
26. Yu J., Wadee M.A. Optimal prestressing of triple-bay prestressed stayed columns // Structures. 2017. № 12. Pp. 132–144.
27. Серпик И.Н., Курченко Н.С. Нахождение предельных нагрузок для систем тонкостенных стержней открытого профиля // Вестник Брянского государственного технического университета. 2013. № 1(37). С. 41–48.
28. Серпик И.Н., Алексейцев А.В., Балабин П.Ю., Курченко Н.С. Плоские стержневые системы: оптимизация с контролем общей устойчивости // Инженерно-строительный журнал. 2017. № 8(76). С. 181–192. doi: 10.18720/MCE.76.16.
29. Серпик И.Н., Курченко Н.С., Алексейцев А.В., Лагутина А.А. Анализ в геометрически, физически и конструктивно нелинейной постановке динамического поведения плоских рам при запроектных воздействиях // Промышленное и гражданское строительство. 2012. № 10. С. 49–51.
30. Серпик И.Н., Алексейцев А.В. Оптимизация системы стальной плоской рамы и столбчатых фундаментов // Инженерно-строительный журнал. 2016. № 1(61). С. 14–24
31. Алексейцев А.В, Серпик И.Н. Оптимизация плоских ферм на основе генетического поиска и итеративной процедуры триангуляции // Строительство и реконструкция. 2011. № 2. С. 3–8.

Anatoly Alekseytsev,
+7(960)564-33-58; aalexw@mail.ru

Sergey Akhremenko,
+7(960)564-33-58; aalexw@mail.ru

Анатолий Викторович Алексейцев,*
+7(960)564-33-58; эл. почта: aalexw@mail.ru

Сергей Аврамович Ахременко,
+7(960)564-33-58; эл. почта: aalexw@mail.ru

Алексейцев А.В., Ахременко С.А. Эволюционная оптимизация предварительно напряженных стальных рам // Инженерно-строительный журнал. 2018. № 5(81). С. 32–42.

doi: 10.18720/MCE.81.5

Productivity of microalgae as biofuel for bioadaptive systems of facades

Продуктивность микроводорослей, как биотоплива для биоадаптивных систем фасадов

E.S. Zalata*,
Y.Y. Shavrov,
K.I. Strelets,
Peter the Great St. Petersburg Polytechnic University, St. Petersburg, Russia
M.S. Emelyanova,
St. Petersburg State University, St. Petersburg, Russia

Студент Е.С. Залата*,
студент Ю.Ю. Шавров,
канд. техн. наук, заместитель директора по дополнительному профессиональному образованию К.И. Стрелец,
Санкт-Петербургский политехнический университет Петра Великого, г. Санкт-Петербург, Россия
ведущий специалист М.С. Емельянова,
Санкт-Петербургский государственный университет, г. Санкт-Петербург, Россия

Key words: energy efficient façade; microalgae; biofuel; biogas

Ключевые слова: энергоэффективный фасад; микроводоросли; биотопливо; биогаз

Abstract. Microalgae are one of the promising fuel sources and many specialists associate it with the future of alternative energy. A promising area of application of photobiological devices is their conjugation with the architectural covers of a building and formation of bio-adaptive facades. The determining criteria for the organization of the microalgae biomass production process in the facade structure is solar radiation, ratio of light and dark growth phase and ambient temperature. The goal of this work is to study the productivity of microalgae Chlorella of CALU 157 strain at low temperatures and low illumination, as well as to calculate the amount of biofuel that can be produced under such climatic conditions. In the first stage of the experiment the algae cultivation was studied at different illumination values – 3500 lx, 1750 lx and 930 lx. In the second stage of the experiment cultivation of algae at different temperatures was studied: +2 °C, +10 °C, +19 °C and +25 °C. Total number of cells in the suspension was determined using the method of direct cell counting in Goryaev chamber. As a result of the experiment microalgae productivity data were obtained at different illumination and temperature. It was found that at a temperature of 2 °C and 10 °C, an almost stable state of algae was observed, the concentration increased very slowly, however the culture did not die. Also the calculation of the amount of energy and biogas, which can be obtained from the biomass of microalgae under the growing conditions of 3500 lx and 23 °C was also made.

Аннотация. Микроводоросли являются одним из перспективных топливных источников. Одним из направлений применения фотобиологических устройств на основе микроводорослей является сопряжение их с архитектурными оболочками здания и образование биоадаптивных фасадов. Определяющими критериями для организации процесса производства биомассы микроводорослей в фасадной конструкции является солнечная радиация, соотношение световой и темновой фазы роста, температура окружающей среды. Целью данной работы является изучение продуктивности микроводорослей Chlorella vulgaris Beijer., штамм CALU-157 при различных температурах и различном количестве освещения, а также расчет количества биотоплива, которое можно получить при таких условиях. Первый этап эксперимента заключался в расчете концентрации и продуктивности микроводорослей при освещенности 3500 Лк, 1750 Лк и 930 Лк. Второй этап эксперимента заключался в расчете концентрации и продуктивности микроводорослей при температурах +2 °C, +10 °C, +19 °C и +25 °C. Общее количество клеток в суспензии определялось с помощью метода прямого подсчета клеток в камере Горяева. В результате эксперимента получены данные продуктивности микроводорослей при различной освещенности и различной температуре. Было выявлено, что при температуре 2 °C и 10 °C состояние водорослей было стабильным, концентрация увеличивалась очень медленно, однако гибели культуры не произошло. Также сделан расчет количества энергии и биогаза, которое можно получить из биомассы микроводорослей при условиях выращивания 3500 Лк и 23 °C.

Залата Е.С., Шавров Ю.Ю., Стрелец К.И., Емельянова М.С. Продуктивность микроводорослей, как биотоплива для биоадаптивных систем фасадов // Инженерно-строительный журнал. 2018. № 5(81). С. 43–51.

1. Introduction

In many countries the cost of heat network and boiler plants operation is increasing every year. The known problems of operation of centralized heat supply urgently require accelerated introduction of non-traditional methods of energy supply. The use of biofuel in recent decades has attracted increasing interest. At present, attention is drawn to the use of third-generation biofuel obtained on the basis of microalgae [1–5].

Microalgae are one of the promising fuel sources and many specialists associate it with the future of alternative energy [6]. They are tiny, mostly unicellular organisms about 5 micrometers in size. Like other plants, microalgae use sunlight as a source of energy to create biomass. This process is called photosynthesis which in nature occurs identically in all plants. However, microalgae are much more efficient in converting light energy into biomass than multicellular plants, since the microalgae are unicellular, and each individual cell performs photosynthesis. Microalgae can divide up to once a day doubling their biomass which is an energy carrier. 1 gram of dry biomass contains about 21 kJ of energy [7]. In the work [8] it is justified that microalgae will become the main raw renewable source of technical lipids for biofuel production.

A promising area of application of photobiological devices is their conjugation with the architectural covers of a building and formation of bio-adaptive facades [9, 10–12]. Creating such building structures allows to reduce power consumption and to provide comfortable conditions in the premises. This direction is completely new in the world of architecture and has not yet become widespread [13, 14]. The use of such structures can significantly improve biosphere compatibility of modern megalopolises. However, many external factors affect their efficiency such as: level of solar radiation, temperature, amount of available nitrogen and phosphorus compounds and availability of carbon dioxide sources [15-18]. Therefore, one of the main criteria for the high efficiency of the photobioreactor is the choice of a suitable area.

The determining criteria for the organization of the microalgae biomass production process in the facade structure is solar radiation equal to 4.0 kWh/m^2/day or approximately 14 MJ/m^2, ratio of light and dark growth phase is not less than 6:18, ambient temperature is not lower than 12 °C [13]. Analysis of the cartographic material at the research initial stage showed that there are many places in Europe with suitable climate conditions however in the coldest days of the year it can be necessary to use additional heating. [13, 19] The climatic conditions can be found in such places as Nice, Marsel (France), Malta and Cyprus islands, San Remo, Sicily (Italy), Sochi (Russia) and others.

Further research was conducted using the example of climatic conditions of the city of Sochi which is located in Russia. The average annual solar radiation in Sochi is 4.0 kWh/m^2/day. The maximum amount of solar radiation is in July and is 7.24 kWh/m^2/day, the minimum amount is in December – 1.29 kWh/m^2/day. The average annual temperature is 15 °C. The average temperature in the hottest month (August) is 24.9 °C, in the coldest month – 6.95 °C [20]. Thus, this region fully meets the criteria for microalgae cultivation in summer but in winter additional heating may be necessary. To clarify this issue it is necessary to study the behavior of algae at low temperatures and low illumination. For this purpose, two stages of the experiment are planned:

1. Calculation of microalgae productivity with a small amount of illumination;
2. Calculation of microalgae productivity at low temperatures.

The experiment results will allow to determine under what climatic conditions the environment heating for microalgae is mandatory for the algae life.

In articles [21, 22] it is stated that the optimum temperature for chlorella is 33–36 °C. There are no data on the behavior of microalgae at low temperatures. Therefore, in this article, for the first stage of the experiment the following temperature values were chosen: +2 °C, +10 °C, +19 °C and +25 °C. In the article [21-23] it is stated that the optimal illumination for chlorella is 20-30 thousand lx. According to the data [24] the values of 20–30 lx are commensurable with a clear, sunny afternoon at noon in the middle latitudes. When cultivating microalgae in real weather conditions, the illumination will fluctuate from 0.2 lx at night to 30 lx in the daytime. There are no data on the behavior of microalgae with a small amount of illumination (0–5000 lx). Therefore, in this article, for the second stage of the experiment the following values of illumination were chosen: 3500 lx, 1750 lx and 930 lx.

Thus, the goal of this work is to study the productivity of microalgae at low temperatures and low illumination, as well as to calculate the amount of biofuel that can be produced under such climatic conditions. To achieve the goal, the following tasks are set and solved:

- calculation of concentration and productivity of microalgae at illumination of 3500 lx, 1750 lx and 930 lx;

- calculation of concentration and productivity of microalgae at temperatures of +2 °C, +10 °C, +19 °C and +25 °C;
- calculation of amount of energy that can be obtained under the above-described growing conditions, as well as calculation of amount of biogas that can be obtained under the same conditions.

2. Methods

Unicellular green alga Chlorella of CALU 157 strain was used as a test organism in the experiments. This alga was taken from the collection of algae of the Microbiology Laboratory of the Biological Institute of St. Petersburg University. It is not demanding to nutrient medium, carbon dioxide, mechanical stirring and has high productivity [25]. Sterility is not required for cultivation. During cultivation it observes the strain monoculture. In addition, it is widely spread in nature and well studied by scientists. [22, 26, 27].

Medium Tamiya was used as a nutrient medium which was singled out by many researchers as the most optimal for the growth of chlorella [28, 29]. The medium is characterized by the following composition of salts and microelements:

Table 1. Composition of nutrient medium Tamiya

No	Components	Per 1 liter of medium
1	K2HPO4	66.6 mg
2	MgSO4 × 7H2O	33.3 mg
3	KNO3	100 mg
4	Solution with microelements × 1000	1 ml

Table 2. Solution with microelements × 1000

No	Components	Per 1 liter of solution
1	NaBO3 × 4H2O	2.63 g
2	MnSO4 × 5H2O	1.81 mg
3	ZnSO4 × 7H2O	0.22 mg
4	(NH4)6Mo7O24 × 4H2O	1.0 ml
5	CuSO4 × 5H2O	0.079 g
6	Co(NO3)2 × 6H2O	0.02 g
7	CaCl2	1.2 g
8	FeSO4 × 7H2O	9.3 g
9	Na2EDTA × 2H2O (Trilon B)	10 g

The nutrient medium and salt solutions were prepared on distilled water and were not sterilized. To avoid precipitation the sample of each substance was first dissolved in a small amount of water, and then the solutions were poured together in the above sequence and the water was added to the desired volume.

To prepare 1 liter of medium, sample of K_2HPO_4 was dissolved in 800 ml of distilled water. Sample of $MgSO_4 \times 7H_2O$ was dissolved separately in 100 ml of water and poured into K_2HPO_4 solution while stirring. Sample of KNO_3 was added to the mixture. After the sample complete dissolution, 1 ml of microelement solution was added. After that the volume was brought to a liter with distilled water. Total number of cells in the suspension was determined using the method of direct cell counting in Goryaev chamber [30] for 10 days. For the biomass cultivation 250 ml conical flasks were used.

The first stage of the experiment was conducted in the educational and scientific center for the utilization of industrial and domestic waste in St.Petersburg Polytechnic University. The algae cultivation was studied at different illumination values – 3500 lx, 1750 lx and 930 lx. For this purpose, 30 W fluorescent lamp LBU 30 (U-shaped) was used. Temperature of all three samples was the same: 23 °C. Initial concentration in all three flasks was 2.125 million of cells/ml. Position of each flask with the suspension was determined with a luxmeter. The first flask was at a distance of 50 mm from the lamp, the illumination was 3500 lx. The second flask was at a distance of 170 mm, the illumination was 1750 lx. The third flask was at a distance of 245 mm, the illumination was 930 lx. All three flasks were illuminated for 12 hours per day.

The second stage of the experiment was conducted in the Microbiology Laboratory of the Biological Institute of St. Petersburg University. Cultivation of algae at different temperatures was studied: +2 °C, +10 °C, +19 °C and +25 °C. Chlorella suspension was placed in a thermostat, while the illumination for all samples was the same: 600 lx (Figure 1). Initial concentration of all samples was 130 thousand of cells/ml. The suspension was illuminated for 24 hours a day.

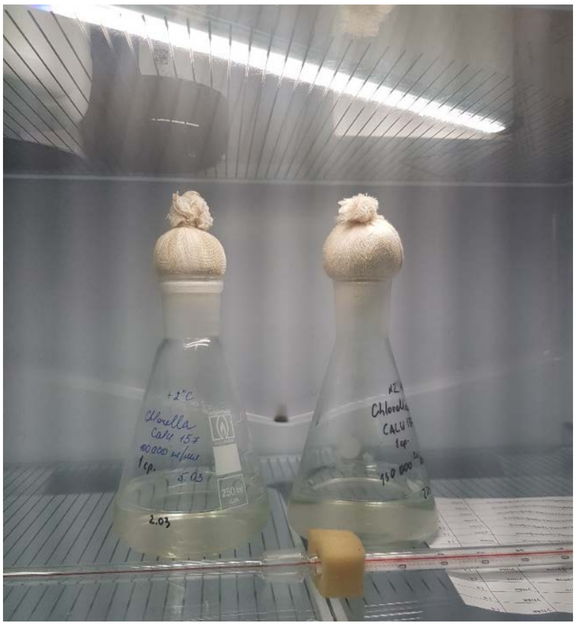

Figure 1. Cultivation of algae at the temperature +2 °C

3. Results and Discussion

The results of the first stage are given in Table 3 and Figure 2.

Table 3. Concentration of microalgae as a function of illumination, mln. of cells/ml

Illumination\t, days	1	2	3	4	5	6	7	8	9	10
3500 lx	2.125	2.76	3.56	4.61	5.12	5.41	6.3	7.02	6.75	6.61
1750 lx	2.125	2.48	3	3.55	3.78	4.02	4.7	5	4.9	5
930 lx	2.125	2.34	2.68	2.96	3.07	3.3	3.6	4.11	4.02	4

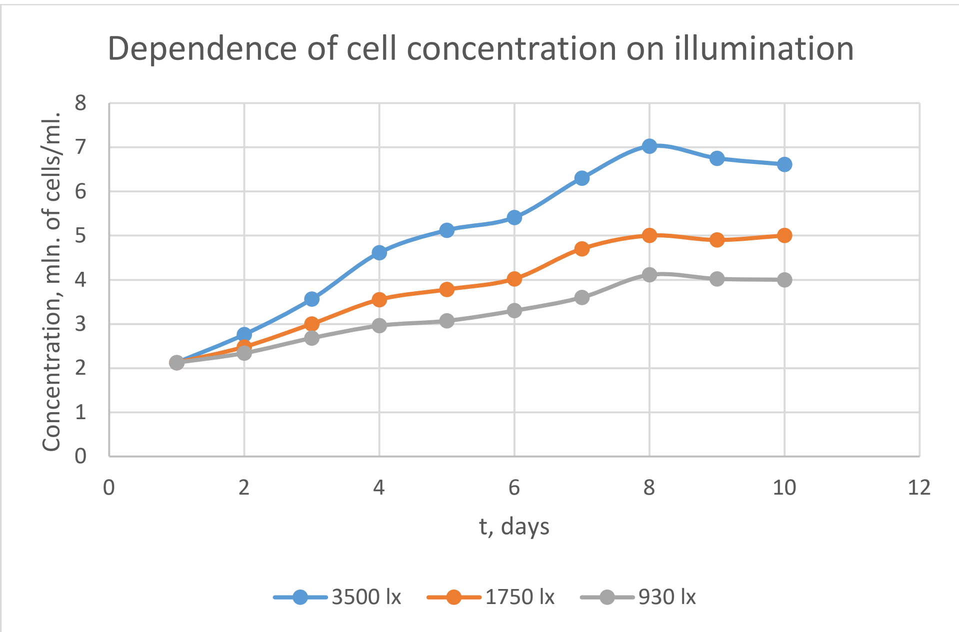

Figure 2. Dependence of cell concentration on illumination

Figure 2 shows that as the amount of illumination increases, the growth rate of microalgae increases, which coincides with the results of other investigators [22]. It can also be noted that the maximum concentration was observed on day 8, after which it began to decrease. This may be due to the onset of a stationary phase of growth. On day 8, the number of algae under illumination of 3500 lx was 7.02 million of cells/ml, with illumination of 1750 lx – 5 million of cells/ml, with illumination of 930 lx – 4.11 million of cells/ml.

In the article [16] it is said that the optimal illumination of chlorella lies within 20–25 klx, the threshold of light saturation is (25…90) $\cdot 10^3$ lx. Also, the authors note that chlorella can adapt to different light intensities, while the value of optimal illumination is closely related to the design of the photobioreactor. In the article [22] it is noted that the strain growth occurs more intensively with uniform illumination and a small thickness of the suspension. In our experiment illumination was carried out from one side of the flask, the diameter of the flask was 12 cm, i.e. the results can be improved by uniform illumination and by choosing a vessel with a smaller diameter. Another way to optimize the insolation can be to maintain intensive bubbling of the suspension so that all cells were in the area with a high level of illumination for sufficient time.

The microalgae biomass productivity was calculated based on the results of the first stage.

Productivity (P) is the amount of biomass formed by growing and multiplying microalgae cells per 1 day in 1 liter of cell suspension. [PRODUCTIVITY OF MICROALGAE CULTIVATION SYSTEM AT NATURAL LIGHTING]

$$\mathrm{P} = \frac{\mathrm{B_2} - \mathrm{B_1}}{\mathrm{t}},\ [\mathrm{P}] = [\text{million of cells}/(\mathrm{l} \cdot \text{day})],$$

where B_1 is the suspension density on the first day of measurement, million of cells/l; B_2 is the suspension density on the last day of measurement, million of cells/l; t is the duration of measurements, days.

Based on the results of the experiment, the average productivity of microalgae at an illumination of 3500 lx before the onset of the stationary phase (day 8) is:

$$\mathrm{P} = \frac{7.02 - 2.125}{7} \approx 0.7\ \text{million of cells}/(\mathrm{ml} \cdot \text{day}) = 700\ \text{million of cells}/(\mathrm{l} \cdot \text{day})$$

The average productivity of microalgae at an illumination of 1750 lx before the onset of the stationary phase is:

$$\mathrm{P} = \frac{5.0 - 2.125}{7} \approx 0.411\ \text{million of cells}/(\mathrm{ml} \cdot \text{day}) = 411\ \text{million of cells}/(\mathrm{l} \cdot \text{day})$$

The average productivity of microalgae at an illumination of 930 lx before the onset of the stationary phase is:

$$\mathrm{P} = \frac{4.11 - 2.125}{7} \approx 0.283\ \text{million of cells}/(\mathrm{ml} \cdot \text{day}) = 283\ \text{million of cells}/(\mathrm{l} \cdot \text{day})$$

The results of the second stage are given in Table 4 and Figure 3.

Table 4. Concentration of microalgae as a function of temperature, thous. of cells/ml

Temperature\t, days	1	2	3	4	5	6	7	8	9	10	11
2°C	130	300	360	460	210	420	500	450	510	540	500
10°C	130	320	430	520	370	550	600	620	700	750	800
19°C	130	500	700	880	870	1300	1700	2500	2900	3100	3470
25°C	130	560	800	940	1150	1480	2230	2850	3340	3670	4100

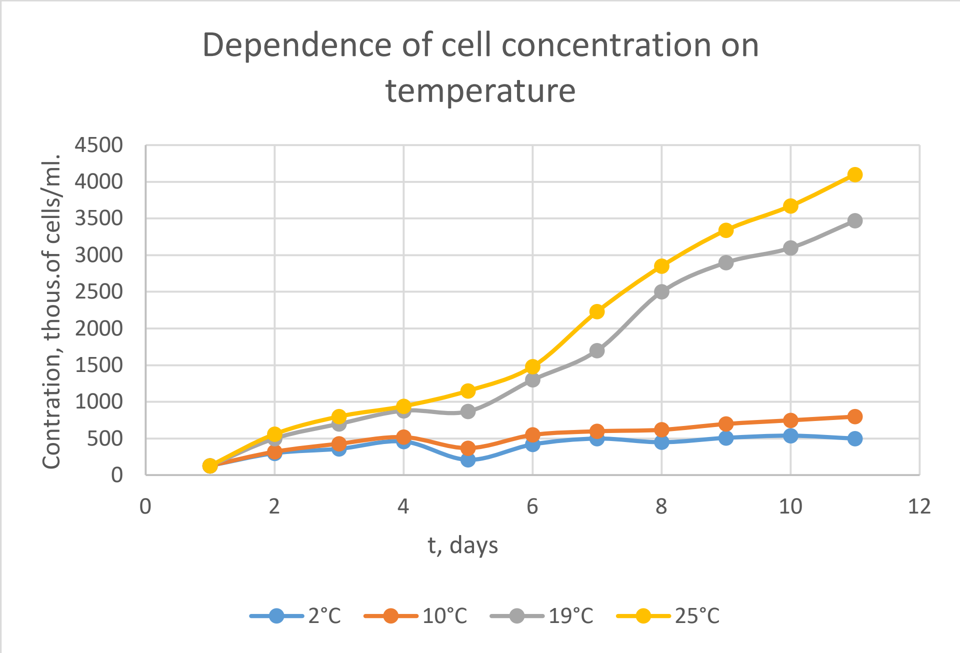

Figure 3. Dependence of cell concentration on temperature

Figure 3 shows that as the temperature increases, the growth rate of biomass increases, which coincides with the results of other investigators [21]. The maximum increase in biomass was at a temperature of 25 °C and amounted to 4.1 million of cells/ml. on day 11 of cultivation. At a temperature of 2 °C and 10 °C, an almost stable state of algae is observed, the concentration increases very slowly but the cells remain active, the culture does not die. In the article [27] it is stated that different species of microalgae grow in a wide range of temperatures, but as a rule, they are all sensitive to freezing, and therefore, the temperature shall not drop below 0 °C, at which the culture will die.

The microalgae biomass productivity was calculated based on the results of the second stage.

The average productivity of microalgae at a temperature of 25 °C is:

$$\mathrm{P} = \frac{4.1 - 0.13}{10} = 0.397 \text{ million of cells}/(\text{ml} \cdot \text{day}) \ = 397 \text{ million of cells}/(\text{l} \cdot \text{day})$$

The average productivity of microalgae at a temperature of 19°C is:

$$\mathrm{P} = \frac{3.47 - 0.13}{10} = 0.334 \text{ million of cells}/(\text{ml} \cdot \text{day}) \ = \ 334 \text{ million of cells}/(\text{l} \cdot \text{day})$$

The average productivity of microalgae at a temperature of 10 °C is:

$$\mathrm{P} = \frac{0.8 - 0.13}{10} = 0.067 \text{ million of cells}/(\text{ml} \cdot \text{day}) \ = \ 67 \text{ million of cells}/(\text{l} \cdot \text{day})$$

The average productivity of microalgae at a temperature of 10 °C is:

$$\mathrm{P} = \frac{0.5 - 0.13}{10} = 0.037 \text{ million of cells}/(\text{ml} \cdot \text{day}) \ = \ 37 \text{ million of cells}/(\text{l} \cdot \text{day})$$

After that the amount of biofuels that can be obtained from the microalgae biomass was calculated. To calculate the maximum amount of biofuel under the conditions tested in the experiment, we take the results of growth of microalgae from the first stage with an illumination of 3500 lx. As it was already calculated above, the productivity in this case was 700 million of cells/(l·day).

In the publication [27] it is said that 100 million of cells in a dry form weigh 1.3 gram, which allows these calculations:

$$\mathrm{P} = \frac{700}{100} \cdot 1.3 = 9.1 \text{ g of dry biomass}/(\text{l} \cdot \text{day})$$

Thus, 700 million of cells is 9.1 grams of dry biomass. The average caloric value of 1 gram of dry biomass of microalgae Chlorella, Spirulina, Synechococcus and Platymonas is 5 kcal (21 kJ) [7], then the amount of energy will be:

$$9.1 \cdot 21 = 191.1 \frac{\text{kJ}}{\text{l} \cdot \text{day}} = 191100 \frac{\text{kJ}}{\text{m}^3 \cdot \text{day}} = 53083 \frac{\text{kWh}}{\text{m}^3 \cdot \text{day}}$$

Taking into account all losses during processing of biomass into biogas, it can be assumed that 1 g of dry biomass corresponds to 0.68 liter of methane [31, 32]. Thus, the amount of biogas will be equal to:

$$9.1 \cdot 0.68 = 6.188 \frac{\text{l of methane}}{\text{l of medium} \cdot \text{day}}$$

4. Conclusions

1. As the illumination increases, the growth rate of microalgae increases. On day 8, the number of algae under illumination of 3500 lx was 7.02 million of cells/ml, with illumination of 1750 lx – 5 million of cells/ml, with illumination of 930 lx – 4.11 million of cells/ml. The productivity of microalgae at an illumination of 3500 lx is 700 million of cells/(l·day), at an illumination of 1750 lx is 411 million of cells/(l·day), at an illumination of 930 lx is 283 million of cells/(l·day).

2. As the temperature increases, the biomass increases. The maximum concentration of biomass was at a temperature of 25 °C and amounted to 4.1 million of cells/ml. on day 11 of cultivation. At a temperature of 2 °C and 10 °C, an almost stable state of algae is observed, the concentration increases very slowly, however the culture does not die. The productivity of microalgae at a temperature of 25 °C was 397 million of cells/(l·day), at a temperature of 19 °C – 334 million of cells/(l·day), at a temperature of 10 °C – 67 million of cells/(l·day), at a temperature of 2 °C – 37 million of cells/(l·day).

3. The amount of energy that can be obtained from the microalgae biomass under the growing conditions of 3500 lx and 23 °C is 53083 (kWh)/(m^3·day). The biogas amount that can be obtained from the same amount of biomass is 6.188 l of methane/(l of medium·day).

References

1. Lundquist, T.J., Woertz, I.C., Quinn, N.W.T., Benemann, J.R. A Realistic Technology and Engineering Assessment of Algae Biofuel. Energy Biosciences Institute University of California. 2010. Pp. 37–125.
2. Dvoretskiy, D.S., Dvoretskiy, S.I., Temnov, M.S., Peshkova, Ye.V., Akulinin, Ye.I. Tekhnologiya polucheniya lipidov iz mikrovodorosley [Technology of obtaining lipids from microalgae]. Tambov.: Izd-vo FGBOU VPO TGTU. 2015. 99 p. (rus)
3. Dvoretsky, D.S. Optimization of the Process of Cultivation of Microalgae Chlorella Vulgaris Biomass with High Lipid Content for Biofuel Production. Chemical Engineering Transactions. 2015. No. 43. Pp. 361–366.
4. Li, Y., Horsman, M., Lan, C.Q., Dubois-Calero, N. Biofuels from microalgae. Biotechnol Prog. 2008. No. 24. Pp. 815–820.
5. Temnov, M.S., Santalov, R.D., Androsova, A.A. Razrabotka tekhnologii kultivirovaniya biomassy mikrovodorosley chlorella vulgaris s povyshennym soderzhaniyem lipidov [Development of technology for cultivation of biomass of microalgae chlorella vulgaris with an increased lipid content]. Uspekhi v khimii i khimicheskoy tekhnologii. 2015. Vol. 29. No. 8. Pp. 116–117. (rus)
6. Kotelev, M.S., Novikov, A.A., Afonin, D.S., Vinokurov, V.A. Polucheniye vysokoenergonasyshchennoy biomassy mikrovodorosley Botryococcus braunii i Chlorella v fotobioreaktore [Production of high-energy-saturated biomass of microalgae Botryococcus braunii and Chlorella in a photobioreactor]. Khimiya i tekhnologiya topliv i masel. 2012. No. 1(569). (rus)
7. Zarei Darki, B., Korol, O.N., Gevorgiz, R.G. Proizvoditelnost sistemy kultivirovaniya mikrovodorosley pri yestestvennom osveshchenii [Productivity of the

Литература

1. Lundquist T.J., Woertz I.C., Quinn N.W.T., Benemann J.R. A Realistic Technology and Engineering Assessment of Algae Biofuel // Energy Biosciences Institute University of California. 2010. Pp. 37–125.
2. Дворецкий Д.С., Дворецкий С.И., Темнов М.С., Пешкова Е.В., Акулинин Е.И. Технология получения липидов из микроводорослей. Тамбов.: Изд-во ФГБОУ ВПО ТГТУ. 2015. 99 с.
3. Dvoretsky D.S. Optimization of the Process of Cultivation of Microalgae Chlorella Vulgaris Biomass with High Lipid Content for Biofuel Production // Chemical Engineering Transactions. 2015. № 43. Pp. 361–366.
4. Li Y., Horsman M., Lan C.Q., Dubois-Calero N. Biofuels from microalgae // Biotechnol Prog. 2008. № 24. Pp. 815–820.
5. Темнов М.С., Санталов Р.Д., Андросова А.А. Разработка технологии культивирования биомассы микроводорослей chlorella vulgaris с повышенным содержанием липидов // Успехи в химии и химической технологии. 2015. Т. 29. № 8. С. 116–117.
6. Котелев М.С., Новиков А.А., Афонин Д.С., Винокуров В.А. Получение высокоэнергонасыщенной биомассы микроводорослей Botryococcus braunii и Chlorella в фотобиореакторе // Химия и технология топлив и масел. 2012. № 1(569).
7. Зареи Дарки Б., Король О.Н., Геворгиз Р.Г. Производительность системы культивирования микроводорослей при естественном освещении // Biotechnologia Acta. 2014. № 3. С. 109–114.
8. Gouveia L. Microalgae as a Feedstock for Biofuels // Springer. 2011. Pp. 68–100.
9. Wilkie Ann C., Smith P.H., Bordeaux F.M. An economical bioreactor for evaluating biogas potential of particulate

microalgae cultivation system under natural light]. Biotechnologia Acta. 2014. No. 3. Pp. 109–114. (rus)

8. Gouveia, L. Microalgae as a Feedstock for Biofuels. Springer. 2011. Pp. 68–100.
9. Wilkie Ann, C., Smith, P.H., Bordeaux, F.M. An economical bioreactor for evaluating biogas potential of particulate biomass. Bioresourse Technology. 2004. No. 92. Pp. 103–109.
10. Petrichenko, M.R., Nemova, D.V., Kotov, E.V., Tarasova, D.S., Sergeev, V.V. Ventilated facade integrated with the HVAC system for cold climate. Magazine of Civil Engineering. 2018. No. 1. Pp. 47–58. doi: 10.18720/MCE.77.5.
11. Petrichenko, M.R., Kotov, E.V., Nemova, D.V., Tarasova, D.S., Sergeev, V.V. Numerical simulation of ventilated facades under extreme climate conditions. Magazine of Civil Engineering. 2018. No. 1. Pp. 130–140. doi: 10.18720/MCE.77.12.
12. Petritchenko, M.R., Subbotina, S.A., Khairutdinova, F.F., Reich, E.V., Nemova, D.V., Olshevskiy, V.Ya., Sergeev, V.V. Impact of rustication joints interval on air mode in the air gap of ventilated facades. Magazine of Civil Engineering. 2017. No. 5. Pp. 40–48. doi: 10.18720/MCE.73.4.
13. Zalata, Ye.S., Shavrov, Yu.Yu., Marichev, A.P., Maslikov, V.I., Strelets, K.I. Ispolzovaniye fotobiologicheskikh ustroystv v razlichnykh sistemakh zdaniy [The use of photobiological devices in various building systems]. Materialy V Mezhdunarodnoy nauchno-prakticheskoy konferentsii Komsomolsk-na-Amure. 2017. Pp. 468-474. (rus)
14. Janssen, M., Tramper, J., Mur, L.R., Wijffels, R.H. Enclosed outdoor photobioreactors: light regime, photosynthetic efficiency, scale-up, and future prospects. Biotechnol Bioeng. 2003. No. 81. Pp. 193–210.
15. Chernova, N.I., Kiseleva, S.V., Rafikova, Yu.Yu. Vliyaniye klimaticheskikh i infrastrukturnykh faktorov na resursnyy potentsial proizvodstva biotopliva iz mikrovodorosley [The influence of climatic and infrastructural factors on the resource potential of biofuel production from microalgae]. Kongress reencon – XXI «Vozobnovlyayemaya energetika XXI VEK». 2016. Pp. 45–49. (rus)
16. Dvoretskiy, D.S., Peshkova, Ye.V., Temnov, M.S. Eksperimentalnoye opredeleniye tekhnologicheskikh rezhimov rosta biomassy mikrovodorosli khlorella s povyshennym soderzhaniyem lipidov [Experimental determination of technological regimes of growth of biomass of microalgae chlorella with a high content of lipids]. Tekhnologii pishchevoy i pererabatyvayushchey promyshlennosti APK - produkty zdorovogo pitaniya. 2014. No. 2. Pp. 32–38. (rus)
17. Fedyukhin, A., Sultanguzin, I., Gyul'Maliev, A., Sergeev, V. Biomass pyrolysis and gasification comprehensive modeling for effective power generation at combined cycle power plant. Eurasian Chemico-Technological Journal. 2017. Vol. 19(3). Pp. 245–253.
18. Anikina, I.D., Sergeyev, V.V., Amosov, N.T., Luchko, M.G. Use of heat pumps in turbogenerator hydrogen cooling systems at thermal power plant. International Journal of Hydrogen Energy. 2017. Vol. 42(1). Pp. 636–642.
19. Andreyenko, T.I., Gabderakhmanova, T.S., Danilova, O.V. Atlas resursov vozobnovlyayemoy energii na territorii Rossii: nauch. Izdaniye [Atlas of renewable energy resources in Russia: scientific. Edition]. RKhTU im. D.I. Mendeleyeva. Moskva. 2015. P. 160. (rus)
20. SP 131.13330.2012 Stroitelnaya klimatologiya. Aktualizirovannaya redaktsiya SNiP 23-01-99* [SP 131.13330.2012 Construction climatology. Updated edition of SNiP 23-01-99 *]. (rus)
21. Nagornov, S.A., Meshcheryakova, Yu.V. Issledovaniye usloviy kultivirovaniya mikrovodorosli khlorella v trubchatom fotobioreaktore [Investigation of the

biomass // Bioresourse Technology. 2004. № 92. Pp. 103–109.

10. Петриченко М.Р., Немова Д.В., Котов Е.В., Тарасова Д.С., Сергеев В.В. Вентилируемые фасады, интегрированные с инженерными системами здания для холодного климата // Инженерно-строительный журнал. 2018. № 1(77). С. 47–58.
11. Петриченко М.Р., Котов Е.В., Немова Д.В., Тарасова Д.С., Сергеев В.В. Численное моделирование вентилируемых фасадов в экстремальных климатических условиях // Инженерно-строительный журнал. 2018. № 1(77). С. 130–140.
12. Петриченко М.Р., Субботина С.А., Хайрутдинова Ф.Ф., Рейх Е.В., Немова Д.В., Ольшевский В.Я., Сергеев В.В. Влияние рустов на воздушный режим в вентилируемом фасаде // Инженерно-строительный журнал. 2017. № 5(73). С. 40–48.
13. Залата Е.С., Шавров Ю.Ю., Маричев А.П., Масликов В.И., Стрелец К.И. Использование фотобиологических устройств в различных системах зданий // Материалы V Международной научно-практической конференции Комсомольск-на-Амуре. 29 – 30 ноября 2017 года. С. 468–474.
14. Janssen M., Tramper J., Mur L.R., Wijffels R.H. Enclosed outdoor photobioreactors: light regime, photosynthetic efficiency, scale-up, and future prospects // Biotechnol Bioeng. 2003. № 81. Pp. 193–210.
15. Чернова Н.И., Киселева С.В., Рафикова Ю.Ю. Влияние климатических и инфраструктурных факторов на ресурсный потенциал производства биотоплива из микроводорослей // Конгресс reencon–XXI «Возобновляемая энергетика XXI ВЕК». С. 45–49.
16. Дворецкий Д.С., Пешкова Е.В., Темнов М.С. Экспериментальное определение технологических режимов роста биомассы микроводоросли хлорелла с повышенным содержанием липидов // Технологии пищевой и перерабатывающей промышленности АПК - продукты здорового питания. 2014. № 2. С. 32–38.
17. Fedyukhin, A., Sultanguzin, I., Gyul'Maliev, A., Sergeev, V. Biomass pyrolysis and gasification comprehensive modeling for effective power generation at combined cycle power plant // Eurasian Chemico-Technological Journal. 2017. Vol. 19(3). Pp. 245–253.
18. Anikina, I.D., Sergeyev, V.V., Amosov, N.T., Luchko, M.G. Use of heat pumps in turbogenerator hydrogen cooling systems at thermal power plant // International Journal of Hydrogen Energy. 2017. Vol. 42(1). Pp. 636–642.
19. Андреенко Т.И., Габдерахманова Т.С., Данилова О.В. Атлас ресурсов возобновляемой энергии на территории России: науч. издание. РХТУ им. Д.И. Менделеева. Москва. 2015. 160 с.
20. СП 131.13330.2012 Строительная климатология. Актуализированная редакция СНиП 23-01-99*
21. Нагорнов С.А., Мещерякова Ю.В. Исследование условий культивирования микроводоросли хлорелла в трубчатом фотобиореакторе // Вестник ТГТУ. 2015. Т. 21. № 4. С. 653–659.
22. Мещерякова Ю.В., Нагорнов С.А. Культивирование микроводоросли хлорелла с целью получения биотоплива // Вопросы современной науки и практики. 2012. Специальный выпуск (43). С. 33–36.
23. Яковлев А.Н., Савинова Д.М., Кругликова Л.Л. Влияние фотометрических характеристик источника излучения на эффективность выращивания микроводоросли chlorella // Высокие технологии в современной науке и технике. 2014. С. 225–228.
24. Прохоров А.М. Люкс. М.: Советская энциклопедия.1990. Т. 2. С. 623.
25. Ауджанова В.К. Морфологические и систематические характеристики хлореллы. Ее производство и

conditions for the cultivation of chlorella microalgae in a tubular photobioreactor]. Vestnik TGTU. 2015. No. 4. Pp. 653–659. (rus)

22. Meshcheryakova, Yu.V., Nagornov, S.A. Kultivirovaniye mikrovodorosli khlorella s tselyu polucheniya biotopliva [Cultivation of chlorella microalgae to produce biofuels]. Voprosy sovremennoy nauki i praktiki. Spetsialnyy vypusk. 2012. No. 43. Pp. 33–36. (rus)
23. Yakovlev, A.N., Savinova, D.M., Kruglikova, L.L. Vliyaniye fotometricheskikh kharakteristik istochnika izlucheniya na effektivnost vyrashchivaniya mikrovodorosli chlorella [The effect of the photometric characteristics of the radiation source on the growth efficiency of chlorella]. Vysokiye tekhnologii v sovremennoy nauke i tekhnike. Tomsk.: Izd-vo Natsionalnyy issledovatelskiy Tomskiy politekhnicheskiy universitet. 2014. Pp. 225–228. (rus)
24. Prokhorov, A.M. Lyuks [Lux]. M.: Sovetskaya entsiklopediya.1990. P. 623. (rus)
25. Audzhanova, V.K. Morfologicheskiye i sistematicheskiye kharakteristiki khlorelly. Yee proizvodstvo i primeneniye [Morphological and systematic characteristics of chlorella. The production and use]. Nauchnyy vestnik. 2014. No. 1(1). Pp. 113 – 126. (rus)
26. Sorokina, K.N. Potentsial primeneniya mikrovodorosley v kachestve syrya dlya bioenergetiki [The potential of microalgae as a raw material for bioenergy]. Kataliz v promyshlennosti. 2012. No. 2. Pp. 63–72. (rus)
27. Bodnar, O.I., Burega, N.V., Palchyk, A.O., Viniarska, H.B., Grubinko, V.V. Optimization of Chlorella vulgaris Beij. Cultivation in a bioreactor of continuous action. Biotechnologia acta. 2016. No. 4. Pp. 42–49.
28. Tamiya, H. Mass culture of algae. Ann Rev Plant Physiol.1957. No. 8. Pp. 309–334.
29. Temnov, M.S. Razrabotka tekhnologii polucheniya biotopliva iz mikrovodorosli chlorella vulgaris [Development of technology for biofuel production from microalgae chlorella vulgaris]. Tezisy doklada na konferentsii. Tambovskiy gosudarstvennyy tekhnicheskiy universitet, Tambov. 2015. No. 8. Pp. 201–202. (rus)
30. Sirenko, L.A. Metody fiziologo-biologicheskogo issledovaniya vodorosley v gidrobiologicheskoy praktike [Methods of physiological and biological study of algae in hydrobiological practice]. Kiyev.: Nauk. Dumka.1975. 247 p. (rus)
31. Smart Material House BIQ. Published by: IBA Hamburg GmbH. July 2013.
32. Baltrėnas, P., Misevičius, A. Biogas production experimental research using algae. Journal of Environmental Health Science and Engineering. 2015. URL: https://doi.org/10.1186/s40201-015-0169-z

применение // Научный вестник. 2014. № 1(1). С. 113–126.

26. Сорокина К.Н. Потенциал применения микроводорослей в качестве сырья для биоэнергетики // Катализ в промышленности. 2012. № 2. С. 63–72.
27. Bodnar O.I., Burega N.V., Palchyk A.O., Viniarska H.B., Grubinko V.V. Optimization of Chlorella vulgaris Beij. Cultivation in a bioreactor of continuous action // Biotechnologia acta. 2016. Vol. 9. № 4. Pp. 42–49.
28. Tamiya H. Mass culture of algae // Ann Rev Plant Physiol. 1957. № 8. Pp. 309–334.
29. Темнов М.С. Разработка технологии получения биотоплива из микроводоросли chlorella vulgaris // Тезисы доклада на конференции. Тамбовский государственный технический университет, Тамбов. С. 201–202.
30. Сиренко Л.А. Методы физиолого-биологического исследования водорослей в гидробиологической практике. Киев.: Наук. Думка.1975. 247 с.
31. Smart Material House BIQ. Published by: IBA Hamburg GmbH. July 2013.
32. Baltrėnas P., Misevičius A. Biogas production experimental research using algae // Journal of Environmental Health Science and Engineering. 2015. URL: https://doi.org/10.1186/s40201-015-0169-z

Ekaterina Zalata,*
+7(921)407-81-84; ekaterinazalata@gmail.com

Yurii Shavrov,
+7(981)937-11-13; Sharohka@mail.ru

Kseniya Strelets,
+7(812)552-94-60; kstrelets@mail.ru

Maria Emelyanova,
+7(812)428-40-10; margar9@mail.ru

Екатерина Сергеевна Залата,*
+7(921)407-81-84;
эл. почта: ekaterinazalata@gmail.com

Юрий Юрьевич Шавров,
+7(981)937-11-13; эл. почта: Sharohka@mail.ru

Ксения Игоревна Стрелец,
+7(812)552-94-60; эл. почта: kstrelets@mail.ru

Мария Сергеевна Емельянова,
+7(812)428-40-10; эл. почта: margar9@mail.ru

Залата Е.С., Шавров Ю.Ю., Стрелец К.И., Емельянова М.С. Продуктивность микроводорослей, как биотоплива для биоадаптивных систем фасадов // Инженерно-строительный журнал. 2018. № 5(81). С. 43–51.

doi: 10.18720/MCE.81.6

Bearing capacity of pasted anchors in the masonry walls of natural limestone

Несущая способность вклеиваемых анкеров в кладке стен из природного известняка

V.N. Alekseenko*,
O.B. Zhilenko,
V.I. Vernadsky Crimean Federal University, Simferopol, Crimea, Russia
M. Al Ali,
Technical University in Košice, Košice, Slovak Republic

Канд. техн. наук, доцент В.Н. Алексеенко*,
канд. техн. наук, доцент О.Б. Жиленко,
Крымский федеральный университет им. В.И. Вернадского, Симферополь, Россия
канд. техн. наук, заведующий кафедры М. Ал Али,
Технический университет г. Кошице, г. Кошице, Словакия

Key words: natural limestone; pasted steel anchor; anchor mixture; physical experiment; calculation; Civil Engineering; Construction Industry; Buildings

Ключевые слова: природный известняк; клеевой стальной анкер; анкерный состав; физический эксперимент; расчет; гражданское строительство; строительная индустрия; здания

Abstract. The joint work of pasted steel anchors and wall masonry elements from natural limestone is discussed in the article. The aim of the scientific work is the development of a technique for calculating the load-bearing capacity of anchors in masonry walls from natural limestone and the development of nomograms for the rapid evaluation of the bearing capacity of anchors. The state of the problem of the work of pasted anchors in various materials was studied. It is established that the known methods for calculating the strength of pasted steel anchors do not take into account the joint work of the natural limestone and pasted steel anchor. Previous studies have focused on the study of anchor joints in concrete, and the work of the pasted joint in the masonry walls of natural limestone has not been investigated. In the present work, for the experimental study of the work of pasted steel anchors in the masonry of walls made of natural limestone, the following materials were accepted: natural limestone, periodic profile reinforcement and anchor mixture. General methods of experimental and theoretical research: analysis, synthesis, deduction, induction, analogy. To solve the set tasks, in the experimental part, the strength of the adhesive joint for pulling in stone elements after the strength of the anchor mixture was established, when fitting the fixture ø 12 mm A 500C into it. Experimental samples, tested to determine the strength of the adhesive joint, were destroyed by breaking the stone. This fact confirms the higher strength of the adhesive bond than the stone element. The results of the physical experiment performed by the authors for determining the parameters of the joint work of the pasted steel anchor and the stone elements from natural limestone are presented in article. It has been experimentally established that 0.4 mm is the criterion for the limiting displacement of anchors, in which splitting of stones from the effect of transverse tensile stresses caused by pulling out pasted steel anchors is not allowed. The estimated evaluation of the joint work of pasted steel anchors and wall masonry elements from natural limestone was proposed.

Аннотация. В статье рассматривается совместная работа стальных анкеров и элементов кладки стен из природного известняка. Целью научной работы является разработка методики расчета несущей способности анкеров в каменной кладке стен из природного известняка и разработка номограмм для оперативной оценки несущей способности анкеров. Изучено состояние вопроса о работе клеевых стальных анкеров в различных материалах. Установлено, что известные методики расчета прочности стальных анкеров не учитывают совместную работу природного камня известняка и стального анкера. Предыдущие исследования направлены на изучение анкерных соединений в бетоне, а работа клеевого соединения в каменной кладке стен из природного известняка не исследована. В настоящей работе, для экспериментального исследования работы клеевых стальных анкеров в каменной кладке стен из природного известняка, приняты следующие материалы: камень известняк, арматура периодического профиля и анкерная смесь. Общие методы экспериментальных и теоретических исследований: анализ, синтез, дедукция, индукция, аналогия. Для решения поставленных задач, в экспериментальной части исследованы прочность клеевого

Алексеенко В.Н., Жиленко О.Б., Ал Али М. Несущая способность вклеиваемых анкеров в кладке стен из природного известняка // Инженерно-строительный журнал. 2018. № 5(81). С. 52–63.

соединения на выдергивание в каменных элементах после набора прочности анкерного состава, при установке в него арматуры ø 12 мм А 500С. Опытные образцы, испытанные для определения прочности клеевого соединения разрушились путем раскола камня. Это обстоятельство подтверждает более высокую прочность клеевого соединения, чем каменного элемента. В статье представлены результаты физического эксперимента выполненного авторами для определения параметров совместной работы стального анкера и камней природного известняка. Опытным путем установлено, что 0,4 мм – это тот критерий предельного смещения анкеров, при котором не допускается раскол камней от воздействия поперечных напряжений растяжения, возникших при выдергивании стальных анкеров. Предложена расчетная оценка совместной работы стальных анкеров и элементов кладки стен из природного известняка.

1. Introduction

The object of research of scientific work is a technical solution for the reliable fastening of modern hinged facades to buildings with walls of natural limestone.

Research subject: glued joint of a steel anchor in a stone element of natural limestone.

In accordance with the Decree of the Government of the Russian Federation No. 1636 of December 27, 1997 [1] only such anchors are allowed to be used on responsible construction sites whose suitability for use in construction is confirmed by the relevant technical certificate of the Ministry of Construction of the Russian Federation. Anchors that do not have a technical certificate are not allowed for use in critical construction sites [2].

The work of steel anchors fixed in a concrete base, which perceive the tensile and shearing forces from static loads, including their joint action, has been fairly well studied [3–18]. Leading world manufacturers of anchor fasteners Hilti, Fisher, Spit, etc. [19–21], offer methods for calculating and predicting the long-term bearing capacity of anchors fixed in a concrete base. In the recommendations for the design and installation of anchor fastenings of hinged facade systems developed by V.N. Vorobyov [2], the versions of the fastenings of front systems are described quite fully, however, the types of anchorage considered do not contain information on the operation of the glued steel anchor in the walls of natural limestone. Tests of anchor bolts on modified acrylic adhesives in determining the strength of their laying in concrete for short-term, long-term and dynamic loads, conducted by G.A. Molodchenko, V.A. Sklyarov, L.N. Shutenko, M.S. Zolotov and others [22–29] have shown the possibility of using them for fixing building structures and equipment under the action of various combinations of loads on them. In this case, the application of the above-mentioned known techniques for calculating and constructing anchor fasteners on an adhesive basis in elements of masonry of walls made of natural limestone is incorrect. To ensure the reliability of anchorages, it is necessary to account for the joint work of the glue shell of the anchor and the base of natural stone material [30–35].

At present, a large number of works have been devoted to the investigation of the thermal protection properties of hinged ventilated facades [36–38], while the methods for determining the bearing capacity of fastenings of facade systems have not been studied enough and need improvement.

The relevance of the research is that at present there are no methods that take into account the conditions for the joint work of the glue shell of the anchor and the natural limestone stone.

The aim of the scientific work is the development of a technique for calculating the load-bearing capacity of anchors in masonry walls from natural limestone and the development of nomograms for the rapid evaluation of the bearing capacity of anchors.

Objectives:

1. To carry out an experimental study of the joint work of the glue joint of steel anchor and natural limestone stones.

2. Develop proposals for the calculation of steel anchors in the masonry walls of natural limestone.

2. Materials and Methods

The method of full-scale tests and rules for determining the capacity of anchors in relation to longitudinal axial pulling loads with reference to the actual building base are set out in SRT 44416204-010-2010 "Anchor fasteners. The method of determining the bearing capacity by the results of full-scale tests" [39].

The essence of this method is that the tests of the anchorage on the pulling force applied to the anchor along its axis determine the resistance to fastening of the load and the deformation corresponding to the limiting states characteristic for it, and then the load-bearing capacity of the anchors is calculated by processing the test results.

Installation of anchorages in hinged façade systems should be carried out on the basis of a project developed in accordance with the requirements of STO NOSTROY [40] and taking into account the recommendations of the anchor manufacturer. The anchor mark must be indicated in the design documentation [40].

Previous studies have been directed to the study of anchor joints in concrete, the work of the glue joint in the masonry walls of natural limestone was not considered. In the present work, for the experimental study of the joint work of glue steel anchors in the masonry of walls made of natural limestone, the following materials were accepted: a nomulite limestone stone, a periodic profile armature and an anchor mixture.

A natural physical experiment was carried out. The strength of the glued joint is determined when installing anchors in the base of natural limestone stones. General methods of experimental and theoretical research: analysis, synthesis, deduction, induction, analogy.

Based on the analysis and processing of the results obtained, the following strength characteristics are determined:

The physical and mechanical properties of the natural limestone stone used in the manufacture of prototypes are determined by testing a stone element 120x108 mm; h = 156 mm; the volume weight is 1750 kg/m^2. The test was carried out in accordance with Russian State Standard GOST 8.136-74 [41] on the hydraulic press P-125.

Based on the analysis and processing of the results obtained, the strength characteristics of the stone of natural limestone are determined (Table 1).

Table 1. Physical and mechanical properties of natural limestone stone.

Geometric characteristics: ***axbxh*, *m***	**Weight** ***m*, *kN***	**Volumetric weight:** $\rho, kg/m^3$	**Destructive load:** ***F*, *kN***	**Ultimate Compressive Strength:** σ_{cm}, MPa	**Stone mark**
1	2	3	4	5	6
0.12x0.10x0.15	0.035	1750	88.26	6.8	M 50

The physical and mechanical properties of the A 500C armature used in the manufacture of prototypes are determined by testing the rods with a length of 350 mm. The test was carried out in accordance with Russian State Standard GOST 1497-84 [42] on an explosive device MP-500.

Based on the analysis and processing of the results obtained, the following strength and deformation characteristics of the reinforcement are determined: the physical yield strength $\boldsymbol{\sigma_y}$, the time resistance $\boldsymbol{\sigma_u}$, the elastic modulus E_s, the limiting relative deformations ε_{ux} corresponding to class A 500C.

A mortar mixture for anchoring and fixing various building elements in the Ceresit CX 5 masonry has been applied.

According to the manufacturer's data, compressive strength is:

- after 6 hours more than 12.0 MPa;
- after 1 day more than 22.5 MPa;
- after 28 days more than 22.5 MPa.

Flexural strength is:

- after 6 hours more than 2.2 MPa;
- after 1 day more than 2.6 MPa;
- after 28 days more than 8.0 MPa.

Testing of the samples was carried out after the strength of the solution mixture was collected after 28 days.

To solve the set tasks, in the experimental part, glued joints of A-500C armature are investigated when pulled from a stone base. Destruction determined the bearing capacity and deformation of glue joints of steel anchors in stone elements from natural limestone. The depth of the anchoring of the reinforcing bar, to obtain objective results, was taken differently on the basis of technological considerations for attaching hinged ventilated facade systems to the walls of multi-storey buildings.

The scope of the experiment was planned, allowing to obtain the number of experimental data necessary for statistical analysis and processing of the results ensuring the solution of the problems posed in this study.

The test facility is a R-20 rupture machine, into which a prototype is installed in an inventory metal cage. MIG-1 clock indicators are used to measure the deformation of the anchor shear relative to the outer surface of the stone base perpendicular to it.

To assign the load during testing of the adhesive joint, a numerical model was constructed in the PC "LIRA" and the forces acting in the anchor rods during the fastening of hinged ventilated facades to the walls of multi-storey buildings of stones and blocks of saw limestone were determined.

The tests were carried out in accordance with the requirements of Russian State Standard GOST 1497-84 [42].

The load was applied in steps of 0.1 from the expected destructive value to track the dynamics of failure and deformation of the adhesive bond in the test sample.

In prototypes tested after 28 days, the growth of deformations also depended on the anchoring depth. The displacement of the anchor passed along the contact zone "rock stone – anchor".

3. Results and Discussion

The destruction of anchorages can be as follows [2]:

- failure to connect the anchor to the base (in cases where the size or the anchor mark does not correspond to the pulling load, with insufficient anchoring depth, if the anchor installation technology is violated);
- failure of the base material (with insufficient strength of the base material, non-observance of the minimum axial distances);
- cleavage of the base in angular zones (with insufficient edge distances, high proppant force, high shear load);
- destruction of the steel anchor (the rarest case of failure).

The maximum permissible deformations in the test specimen occurred at a load from 24.52 kN to 30.4 kN.

Experimental samples tested to determine the strength of the adhesive bond were destroyed by slipping the glue joint through the contact zone "glue shell – the surface of the stone" and was followed by a subsequent split of fragments of stones. This circumstance confirms the need to take into account the joint work of anchoring elements in the contact area of materials.

It is established that the exhaustion of the bearing capacity of the adhesive joint should be considered when the anchor is displaced relative to the surface of the stone reaching a value of 0.4 mm.

With further load application, the anchor was pulled out of the previously drilled hole instantly, and followed by a split stone (Figures 1, 2).

Figure 1. Type of prototype when the anchor displacement is relative to the upper surface of the stone 0.4 mm

Figure 2. When the anchor was displaced more than 0.4 mm, it was pulled out, followed by a subsequent split of the stones

Splitting of stones occurred at loads exceeding by 15–20 % the load of depletion of the bearing capacity of the adhesive joint (according to the limiting displacement of the anchor 0.4 mm).

Thus, under the action of tensile forces in an anchor glued to a stone wall masonry element from natural limestone, a "glue shell – stone surface" breakdown occurs on the contact.

To develop proposals for calculating the strength of steel anchors in the masonry walls of natural limestone, criteria for limiting the displacement of anchors (0.4 mm) should be adopted, in which the joint work of materials is not allowed.

In connection with the natural variability of the structure of natural limestone stones formed as a deposit product, it is expedient to operate with the factors of joint work of the anchoring elements, proceeding from the assumptions only of the elastic stage of work [3–18]. It should be emphasized that taking into account the inelastic work of the elements can lead to an unreasonable and very dangerous overestimation of the design strength characteristics of anchor joints in natural limestone.

Based on the results of the experiment, the ultimate bonding tension of the glue shell of the steel anchor with the surface of the stone hole of natural limestone is determined by the strength corresponding to the M50 grade.

$$\tau_{cl(0.95)} = \frac{P}{\pi \cdot d_h \cdot h_{ef}} \tag{1}$$

where: d_h – is diameter of the hole previously drilled in stone, mm;

h_{ef} – is depth of anchoring of the anchor (effective anchoring depth), mm;

P – is destructive load, kN.

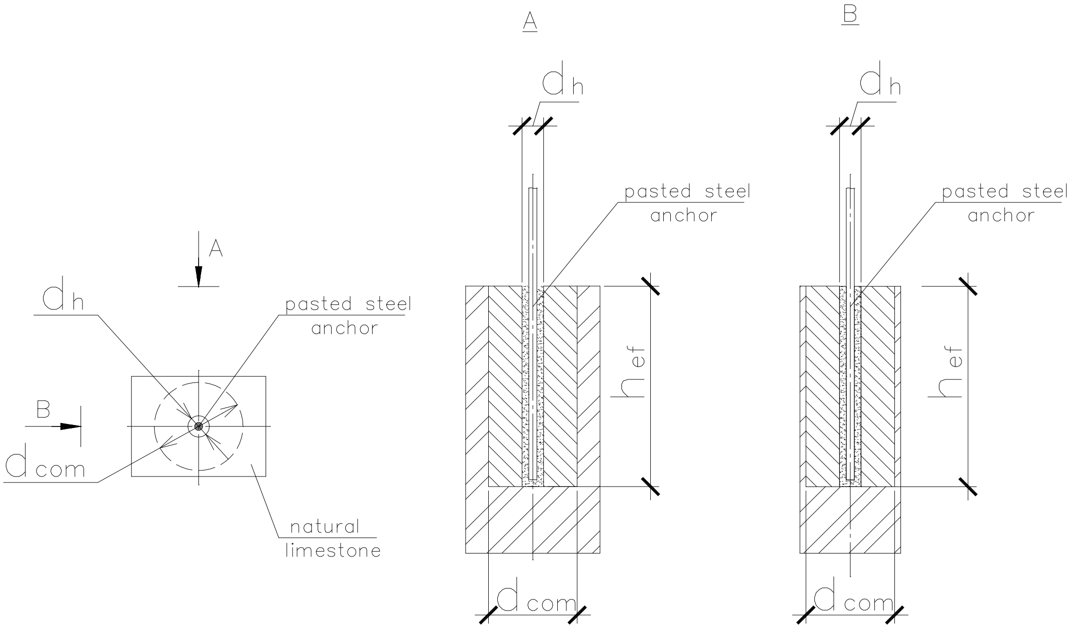

Figure 3. Scheme of a prototype of a natural limestone stone with an adhesive steel anchor

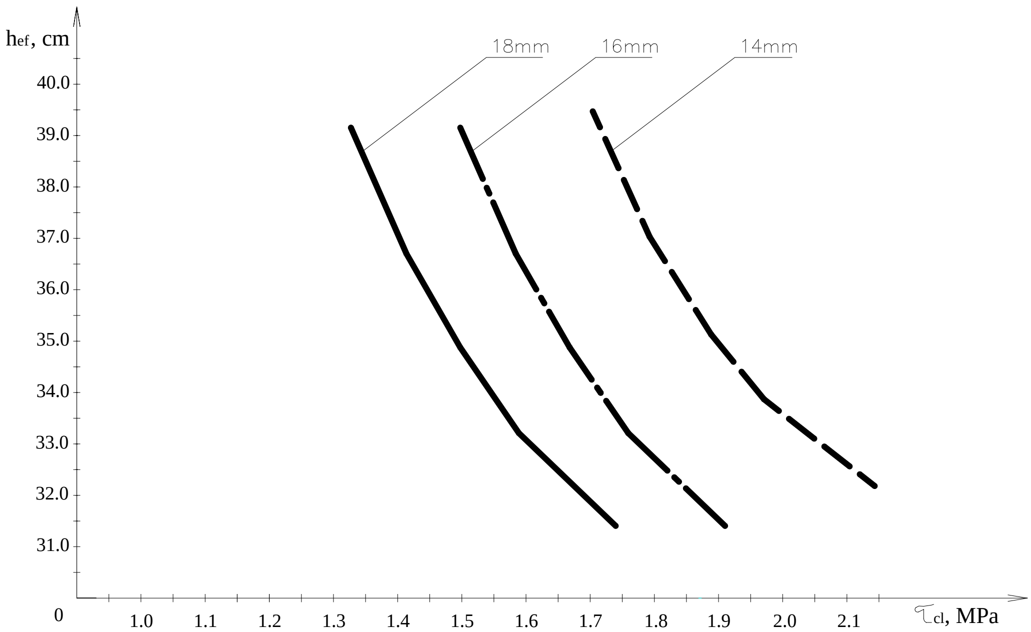

Figure 4. Experimental dependence of the ultimate bonding tension of the glue shell with the surface of the hole in the stone of natural limestone with the strength corresponding to the M50 grade

From the foregoing, when taking into account only the elastic stage of the work, it follows that calculation of the depth of anchoring of the anchor in the stones of saw limestone is determined by the formula:

$$h_{ef} = \frac{P}{\tau_{cl(0,95)} \cdot \pi \cdot d_h} \tag{2}$$

The area of the stone element, subject to compression from pulling the anchor, is determined by the diameter of the conventional stone shell, which is involved in the adhesive work of the anchor in joint work:

$$A_{com} = \frac{\pi}{4}(d_{com}^2 - d_h^2) \tag{3}$$

where d_{com} – is diameter of the conventional stone shell, involved in the glue shell of the anchor in the joint work.

Maximum allowable compression area for M50 stones is:

$$A_{ult.com.} = \frac{P}{M} \tag{4}$$

where P – is breaking load (tensile force in the anchor), kN;

M – is grade of stone, MPa.

$$\frac{\pi}{4}(d_{com}^2 - d_h^2) = \frac{P}{M} \tag{5}$$

From the equality 5, we determine the diameter of the conventional stone shell, which is involved in the adhesive work of the anchor in joint work:

$$d_{com} = \sqrt{0.025 \cdot P + d_h^2} \tag{6}$$

The minimum permissible distance between the holes or to the outer edge of the stone (Figure 5) is determined as follows:

$$B_{min} = d_{com} + 2d_h \tag{7}$$

The recommended distance between the holes or to the outer edge of the stone (Figure 5) is determined by the formula:

$$B_{opt} = 2(d_{com} + d_h) \tag{8}$$

The design load-bearing capacity of the anchor for pulling in the saw limestone of the M50 strength grade will be:

$$P_f=1.75*h_{ef}*\cdot \pi \cdot d_h \tag{9}$$

where 1.75 MPa – is a cautious value with a guaranteed probability of 0.95 of the maximum permissible adhesion stress of the anchor glue shell with the surface of the hole in the stone of the limestone of the numulite with strength corresponding to M50 [43].

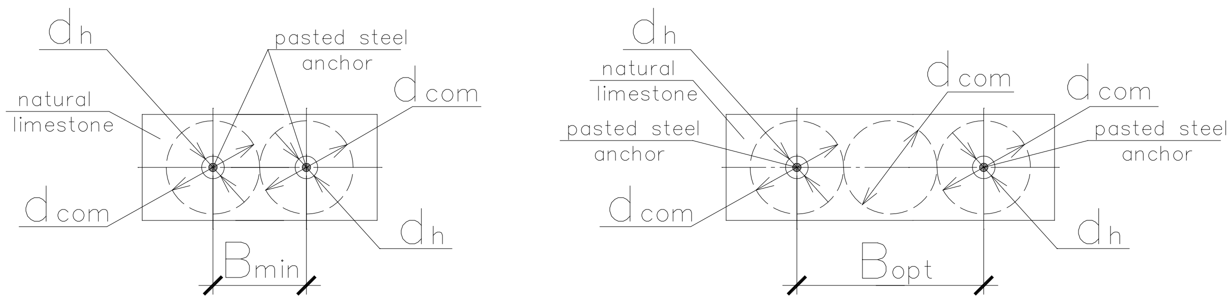

Figure 5. Calculation scheme

To quickly assess the bearing capacity of anchors of different diameters, it is convenient to use nomograms (Figure 6), developed by the authors on the basis of the conducted experiments and statistical processing of the results obtained.

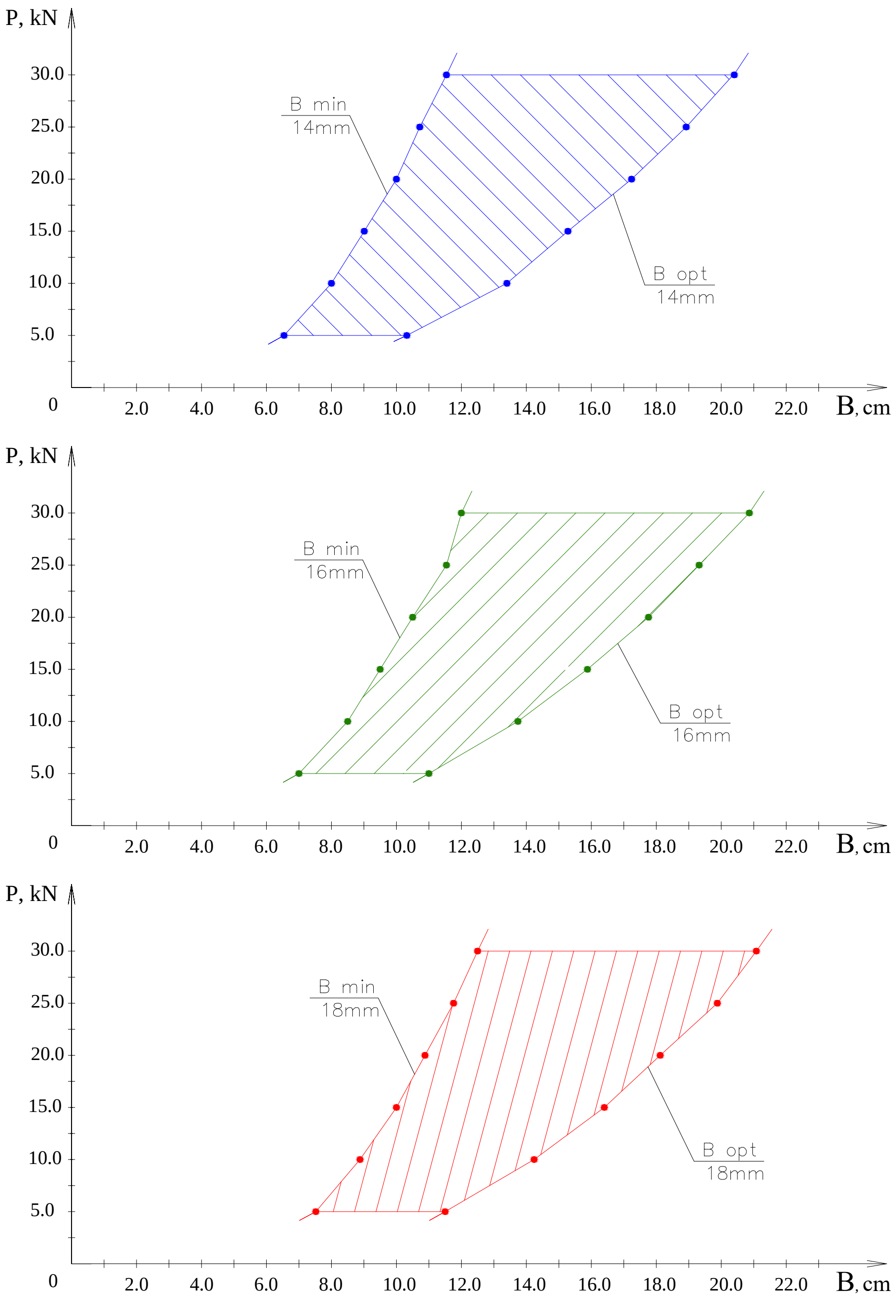

Figure 6. Recommended spacing between the holes (diameter 14 mm, 16 mm, 18 mm) or to the outer edge of the stone (for glue steel anchors) in natural limestone stone with strength corresponding to the M50 grade

4. Conclusions

1. An experimental study of the strength of glue joints of steel anchors and natural limestone stones was carried out. It has been experimentally established that 0.4 mm is the criterion for the limiting displacement of anchors, in which the joint work of the glue joint is preserved in the contact zone "glue shell – stone surface". The obtained research results are relevant for calculating and constructing anchor fastenings of hinged ventilated facades on the walls of buildings made of stones and blocks of saw limestone.

2. In connection with the natural variability of the structure of natural limestone stones formed as a deposit product, taking into account the inelastic work of the elements can lead to an unreasonable and very dangerous overestimation of the design strength characteristics of anchor joints in natural limestone.

3. Proposals for the calculation of steel anchors in masonry walls made of natural limestone have been developed.

4. When calculating and constructing anchors in natural stones of a different structure or age, it is necessary to perform control tests that specify the actual parameters of the joint operation of the elements in the contact zone "glue shell – stone surface".

References

1. Postanovleniye Pravitelstva RF № 1636 ot 27 dekabrya 1997 g. «O pravilakh podtverzhdeniya prigodnosti novykh materialov, izdeliy, konstruktsiy i tekhnologiy dlya primeneniya v stroitelstve» [Decree of the Government of the Russian Federation No. 1636 of December 27, 1997 "On the rules for confirming the suitability of new materials, products, structures and technologies for use in construction"]. (rus)
2. Vorobyov, V.N. Navesnyye fasadnyye sistemy. Rekomendatsii po proyektirovaniyu i montazhu ankernykh krepleniy [Suspended facade systems. Recommendations for the design and installation of anchorages]. LLC PortActivStroy. Vladivostok. 2017. 44 p. (rus)
3. STO 36554501-048-2016. Ankernyye krepleniya k betonu. Pravila proyektirovaniya [STO 36554501-048-2016. Anchoring fastenings to concrete. Design rules]. Moscow: OAO "HIC "Stroitelstvo". 2014. 37 p. (rus)
4. STO SRO-P 60542948 00036-2015. Proyektirovaniye ankerov, ustanavlivayemykh v zatverdevshiy beton zhelezobetonnykh konstruktsiy [STO SRO-P 60542948 00036-2015. Design of anchors installed in hardened concrete reinforced concrete structures]. Moscow: SRO NP «SOUZATOMPROEKT». 2015. 65 p. (rus)
5. MDS 31-4.2000. Posobiye po proyektirovaniyu ankernykh boltov dlya krepleniya stroitelnykh konstruktsiy i oborudovaniya (k SNiP 2.09.03-85) [MDS 31-4.2000. A manual on the design of anchor bolts for fixing building structures and equipment (к СНиП 2.09.03-85)]. Moscow: CNIIpromzdaniy. 2001. 105 p. (rus)
6. Shin, J., Kim, J., Chang, H.-J. Anchor plate effect on the breakout capacity in tension for thin-walled concrete panels. Engineering Structures. 2016. No. 106. Pp. 147–153.
7. Epackachi, S., Esmaili, O., Mirghaderi, S.R., Behbahani, A.A.T. Behavior of adhesive bonded anchors under tension and shear loads. Journal of Constructional Steel Research. 2015. No. 114. Pp. 269–280.
8. Ashoura, A.F., Alqedra, M.A. Concrete breakout strength of single anchors in tension using neural networks. Advances in Engineering Software. 2005. No. 36. Pp. 87–97.
9. Pitrakkos, T., Tizani, W. Experimental behaviour of a novel anchored blind-bolt in tension. Engineering Structures. 2013. No. 49. Pp. 905–919.
10. Tizani, W., Rahman, N.A., Pitrakkos, T. Fatigue life of an anchored blind-bolt loaded in tension. Journal of Constructional Steel Research. 2014. No. 93. Pp. 1–8.
11. González, F., Fernández, J., Agranati, G., Villanueva, P. Influence of construction conditions on strength of post installed bonded Anchors. Construction and Building Materials. 2018. No. 165. Pp. 272–283.
12. Upadhyaya, P., Kumar, S. Pull-out capacity of adhesive anchors: Ananalytical solution. International Journal of Adhesion & Adhesives. 2015. No. 60. Pp. 54–62.
13. Wang, D., Wu, D., Ouyang, C., He, S., Sun, X. Simulation analysis of large-diameter post-installed anchors in concrete. Construction and Building Materials. 2017. No. 143. Pp. 558–565.
14. Mohyeddin, A., Gad, E.F., Yangdon, K., Khandu, R., Lee, J. Tensile load capacity of screw anchors in early age concrete. Construction and Building Materials. 2016. No. 127. Pp. 702–711.
15. CINTEC Anchor In Action, September, 2000. [Electronic resource]. URL: http: //www, cintec. com

Литература

1. Постановление Правительства РФ № 1636 от 27 декабря 1997 г. «О правилах подтверждения пригодности новых материалов, изделий, конструкций и технологий для применения в строительстве».
2. Воробьев В.Н. Навесные фасадные системы. Рекомендации по проектированию и монтажу анкерных креплений. Владивосток: «ПортАктивСтрой». 2017. 44 с.
3. СТО 36554501-048-2016. Анкерные крепления к бетону. Правила проектирования. М: ОАО "НИЦ "Строительство". 2014. 37 с.
4. СТО СРО-П 60542948 00036-2015. Проектирование анкеров, устанавливаемых в затвердевший бетон железобетонных конструкций. М: СРО НП «СОЮЗАТОМПРОЕКТ». 2015. 65 с.
5. МДС 31-4.2000. Пособие по проектированию анкерных болтов для крепления строительных конструкций и оборудования (к СНиП 2.09.03-85). М: ЦНИИпромзданий. 2001. 105 с.
6. Shin J., Kim J., Chang H.-J. Anchor plate effect on the breakout capacity in tension for thin-walled concrete panels // Engineering Structures. 2016. Vol. 106. Pp. 147–153.
7. Epackachi S., Esmaili O., Mirghaderi S.R., Behbahani A. Asghar Taheri. Behavior of adhesive bonded anchors under tension and shear loads // Journal of Constructional Steel Research. 2015. Vol. 114. Pp. 269–280.
8. Ashoura A.F., Alqedra M.A. Concrete breakout strength of single anchors in tension using neural networks // Advances in Engineering Software. 2005. Vol. 36. Pp. 87–97.
9. Pitrakkos T., Tizani W. Experimental behaviour of a novel anchored blind-bolt in tension // Engineering Structures. 2013. Vol. 49. Pp. 905–919.
10. Tizani W., Rahman N.A., Pitrakkos T. Fatigue life of an anchored blind-bolt loaded in tension // Journal of Constructional Steel Research. 2014. Vol. 93. Pp. 1–8.
11. González F., Fernández J., Agranati G., Villanueva P. Influence of construction conditions on strength of post installed bonded Anchors // Construction and Building Materials. 2018. Vol. 165. Pp. 272–283.
12. Upadhyaya P., Kumar S. Pull-out capacity of adhesive anchors: Ananalytical solution // International Journal of Adhesion & Adhesives. 2015. Vol. 60. Pp. 54–62.
13. Wang D., Wu D., Ouyang C., He S., Sun X. Simulation analysis of large-diameter post-installed anchors in concrete // Construction and Building Materials. 2017. Vol. 143. Pp. 558–565.
14. Mohyeddin A., Gad E.F., Yangdon K., Khandu R., Lee J. Tensile load capacity of screw anchors in early age concrete // Construction and Building Materials. 2016. Vol. 127. Pp. 702–711.
15. CINTEC Anchor In Action, September, 2000. [Электронный ресурс]. URL: http://www.cintec.com.
16. Павлова М.О. Прочность и деформативность кладки стен из различных материалов в зоне заделки анкеров при действии на них продольных и поперечных сил. М.: ГУЛ ЦНИИСК им. В.А. Кучеренко, 2000.
17. Элигенхаузен Р., Малле Р. Крепления в бетонных конструкциях и в каменной кладке // Строительная инженерная практика. Берлин: изд. «Вильгельм Эрнст&Сын», 2000.

Алексеенко В.Н., Жиленко О.Б., Ал Али М. Несущая способность вклеиваемых анкеров в кладке стен из природного известняка // Инженерно-строительный журнал. 2018. № 5(81). С. 52–63.

16. Pavlova, M.O. Prochnost i deformativnost kladki sten iz razlichnykh materialov v zone zadelki ankerov pri deystvii na nikh prodolnykh i poperechnykh sil [Strength and deformation of the masonry of walls from various materials in the zone of anchoring of the anchors under the action of longitudinal and transverse forces on them]. Moscow: GUL TsNIISK V.A. Kucherenko. 2000. (rus)
17. Eligenhausen, R., Malle, R. Krepleniya v betonnykh konstruktsiyakh i v kamennoy kladke [Fixings in concrete structures and in masonry]. J. "Building engineering practice", ed. "Wilhelm Ernst & Son" Berlin. 2000.
18. Eligehausen, R., Hoehler, M., Testing of post-installed fastenings to concrete structures in seismic regions. Conference Proceedings of the fib Symposium on Concrete Structures in Seismic Regions. Athens, Greece. 2003.
19. Rukovodstvo po ankernomu krepezhu Hilti [Guide to anchor fasteners Hilti]. Principality of Liechtenstein: Corporation Hilti. FL-9494 Schaan. 2008. 419 p.
20. Tekhnicheskiy spravochnik Fisher dlya fasadov s vozdushnym zazorom [Technical Reference Fisher for facades with air gap]. Release. 2007. 78 p.
21. Tekhnicheskoye rukovodstvo po ankernoy tekhnike SPIT [Technical Guide to Anchor Technology SPIT]. Release. 2010. 33 p.
22. Molodchenko, G.A., Sklyarov, V.A. Kratkovremennaya prochnost ankernykh boltov na modifitsirovanykh akrilovykh kleyakh [Short-term strength of anchor bolts on modified acrylic adhesives]. Municipal economy of cities. Kiev: Equipment. 2000. No. 25. Pp. 109–111. (rus)
23. Molodchenko, G.A., Sklyarov, V.A. Dlitelnaya prochnost ankernykh boltov na modifitsirovannykh akrilovykh kleyakh [Long-term strength of anchor bolts on modified acrylic adhesives]. Resource-saving materials, constructions, buildings and structures. Rivne. 2000. No. 5. Pp. 75–81. (rus)
24. Molodchenko, G.A., Sklyarov, V.A. Vliyaniye glubiny zadelki na prochnost kleyevogo ankera [Effect of embedment depth on the strength of the adhesive anchor]. Modeling and optimization in materials science. Odessa. 2001. Pp. 90–91. (rus)
25. Molodchenko, G.A., Sklyarov, V.A. Raschetnyye kharakteristiki ankernykh boltov na akrilovykh kleyakh [Calculation characteristics of anchor bolts on acrylic adhesives]. Thesis. reports XXXI scientific and technical conference of teachers, post-graduate students and employees of the Kharkov State Academy of Municipal Economy. Part 1. Kharkiv: KGAGH. 2002. Pp. 11-13. (rus)
26. Sklyarov, V.A. Issledovaniye na vynoslivost ankernykh boltov [Study on the endurance of anchor bolts]. Thesis. reports XXX scientific and technical conference of teachers, post-graduate students and employees of the Kharkov State Academy of Municipal Economy. Part 2. Kharkiv: KGAGH. 2000. Pp. 57–58. (rus)
27. Shutenko, L.N., Zolotov, M.S., Sklyarov, V.A. Prochnost ankernykh boltov na akrilovykh kleyakh pri dinamicheskikh nagruzheniyakh [Strength of anchor bolts on acrylic adhesives under dynamic loading]. Resource-saving materials, constructions, buildings and structures. Rivne: NUVHtaP, 2005. No. 12. Pp. 346–354. (rus)
28. Shutenko, L.N., Zolotov, M.S., Sklyarov, V.A. Raschetnyye kharakteristiki ankernykh boltov na akrilovykh kleyakh [Calculation characteristics of anchor bolts on acrylic adhesives] Perfection of the quality of building materials and structures (models, compositions, properties, operational durability). Novosibirsk: NSAU. 2005. Pp. 39–42. (rus)
29. Eligenhausen, R., Okelo, R. Proyektirovaniye gruppovykh krepleniy dlya rezhimov razrusheniya v rezultate vydergivaniya ili protalkivaniya dlya otdelnykh ankerov iz gruppy [Design of group fastenings for failure modes as a result of pulling or pushing for individual anchors from the

18. Eligehausen R., Hoehler M. Testing of post-installed fastenings to concrete structures in seismic regions // Conference Proceedings of the fib Symposium on Concrete Structures in Seismic Regions. Athens, Greece, 2003.
19. Руководство по анкерному крепежу Hilti. Княжество Лихтенштейн: Корпорация Hilti. FL-9494 Schaan. 2008. 419 с.
20. Технический справочник Fisher для фасадов с воздушным зазором. Выпуск 2007. 78 с.
21. Техническое руководство по анкерной технике SPIT. Выпуск 2010. 33 с.
22. Молодченко Г.А., Скляров В.А. Кратковременная прочность анкерных болтов на модифицированых акриловых клеях // Коммунальное хозяйство городов. К.: Техніка. 2000. № 25. С. 109–111.
23. Молодченко Г.А., Скляров В.А. Длительная прочность анкерных болтов на модифицированных акриловых клеях // Ресурсозберігаючі матеріали, конструкції, будівлі та споруди. Рівне. 2000. № 5. С. 75–81.
24. Молодченко Г.А., Скляров В.А. Влияние глубины заделки на прочность клеевого анкера // Моделирование и оптимизация в материаловедении. Одесса. 2001. С. 90–91.
25. Молодченко Г.А., Скляров В.А. Расчетные характеристики анкерных болтов на акриловых клеях // Тез. докладов XXXI науч.-техн. конф. преподавателей, аспирантов и сотрудников Харьковской государственной академии городского хозяйства. Ч. 1. Харьков: ХГАГХ. 2002. С. 11–13.
26. Скляров В.А. Исследование на выносливость анкерных болтов // Тез. докладов XXX науч.-техн. конф. преподавателей, аспирантов и сотрудников Харьковской государственной академии городского хозяйства. Ч.2. Харьков. 2000. С. 57–58.
27. Шутенко Л.Н., Золотов М.С., Скляров В.А. Прочность анкерных болтов на акриловых клеях при динамических нагружениях // Ресурсоекономні матеріали, конструкції, будівлі та споруди. Рівне: НУВГтаП, 2005. № 12. С. 346–354.
28. Шутенко Л.Н., Золотов М.С., Скляров В.А. Расчетные характеристики анкерных болтов на акриловых клеях // Совершенствование качества строительных материалов и конструкций (модели, составы, свойства, эксплуатационная стойкость). Новосибирск: НГАУ. 2005. С. 39–42.
29. Элигенхаузен Р., Окело Р. Проектирование групповых креплений для режимов разрушения в результате выдергивания или проталкивания для отдельных анкеров из группы. Отчет № 18/1-96/20, Институт строительных материалов, Университет Штутгарта, 1996.
30. Guerreiro J., Gago A.S., Ferreira J., Proença J. An innovative anchoring system for old masonry buildings // Journal of Building Engineering. 2017. Vol. 13. Pp. 184–195.
31. Ceroni F., Cuzzilla R., Pecc M. Assessment of performance of steel and GFRP bars as injected anchors in masonry walls // Construction and Building Materials. 2016. Vol. 123. Vol. 78–98.
32. Contrafatto L., Cosenza R. Behaviour of post-installed adhesive anchors in natural stone // Construction and Building Materials. 2014. Vol. 68. Pp. 355–369.
33. Muñoz R., Lourenço P.B., Moreira S. Experimental results on mechanical behaviour of metal anchors in historic stone masonry // Construction and Building Materials. 2018. Vol. 163. Pp. 643–655.
34. Streeter K., Luscinski K. Mechanical Anchor Strength in Stone Masonry // STRUCTURE magazine. 2013. Pp. 14–16.

Alekseenko, V.N., Zhilenko, O.B., Al Ali, M. Bearing capacity of pasted anchors in the masonry walls of natural limestone. *Magazine of Civil Engineering*. 2018. 81(5). Pp. 52–63. doi: 10.18720/MCE.81.6.

group]. Report No. 18 / 1-96 / 20, Institute of Building Materials, University of Stuttgart. 1996.

30. Guerreiro, J., Gago, A.S., Ferreira, J., Proença, J. An innovative anchoring system for old masonry buildings. Journal of Building Engineering. 2017. No. 13. Pp. 184–195.
31. Ceroni, F., Cuzzilla, R., Pecc, M. Assessment of performance of steel and GFRP bars as injected anchors in masonry walls. Construction and Building Materials. 2016. No. 123. Pp. 78–98.
32. Contrafatto, L., Cosenza, R. Behaviour of post-installed adhesive anchors in natural stone. Construction and Building Materials. 2014. No. 68. Pp. 355–369.
33. Muñoz, R., Lourenço, P.B., Moreira, S. Experimental results on mechanical behaviour of metal anchors in historic stone masonry. Construction and Building Materials. 2018. No. 163. Pp. 643–655.
34. Streeter, K., Luscinski, K. Mechanical Anchor Strength in Stone Masonry. STRUCTURE magazine. 2013. Pp. 14–16.
35. Pisani M.A. Theoretical approach to the evaluation of the load-carrying capacity of the tie rod anchor system in a masonry wall. Engineering Structures. 2016. No. 124. Pp. 85–95.
36. Petrichenko, M.R., Nemova, D.V., Kotov, E.V., Tarasova, D.S., Sergeev, V.V. Ventilated facade integrated with the HVAC system for cold climate. Magazine of Civil Engineering. 2018. No. 1. Pp. 47–58. doi: 10.18720/MCE.77.5.
37. Petrichenko, M.R., Kotov, E.V., Nemova, D.V., Tarasova, D.S., Sergeev, V.V. Numerical simulation of ventilated facades under extreme climate conditions. Magazine of Civil Engineering. 2018. No. 1. Pp. 130–140. doi: 10.18720/MCE.77.12.
38. Petritchenko, M.R., Subbotina, S.A., Khairutdinova, F.F., Reich, E.V., Nemova, D.V., Olshevskiy, V.Ya., Sergeev, V.V. Impact of rustication joints interval on air mode in the air gap of ventilated facades. Magazine of Civil Engineering. 2017. No. 5. Pp. 40–48. doi: 10.18720/MCE.73.4.
39. STO FGU FTsS 44416204-10-2010 Krepleniya ankernyye. Metod opredeleniya nesushchey sposobnosti po rezultatam naturnykh ispytaniy [STO FGU FTSS 44416204-10-2010 Anchoring fastenings. The method of determining the load-bearing capacity by the results of full-scale tests].
40. STO NOSTROY 2.14.96-2013 «Navesnyye fasadnyye sistemy. Montazh ankernykh krepleniy» [STO NOSTROY 2.14.96-2013 "Suspended facade systems. Mounting of anchorages»].
41. GOST 8.136-74 Gosudarstvennaya sistema obespecheniya yedinstva izmereniy (GSI). Pressy gidravlicheskiye dlya ispytaniy stroitelnykh materialov. Metody i sredstva poverki (s Izmeneniyem N 1) [Russian State Standard GOST 8.136-74 State system for ensuring the uniformity of measurements. Hydraulic presses for testings building materials. Verification methods and means]. Moscow: Publishing house of standards. 2015. 75 p.
42. GOST 1497-84. (ISO 6892-84, ST SEV 471-88) Metally. Metody ispytaniy na rastyazheniye (s Izmeneniyami N 1, 2, 3) [Russian State Standard GOST 1497-84. (ISO 6892-84, ST SEV 471-88) Metals. Tensile test methods (with Changes N 1, 2, 3)]. Moscow.: Publishing house of standards. 1985. Pp. 3–37.
43. DBN V.1.1 - 1 – 94. Proyektirovaniye i stroitelstvo grazhdanskikh zdaniy iz blokov i kamney pilenykh izvestnyakov krymskikh mestorozhdeniy v seysmicheskikh rayonakh. [DBN V.1.1 - 1 – 94. Designing and building of civil buildings from blocks and stones of sawed limestones

35. Pisani M.A. Theoretical approach to the evaluation of the load-carrying capacity of the tie rod anchor system in a masonry wall // Engineering Structures. 2016. Vol. 124. Pp. 85–95.
36. Петриченко М.Р., Немова Д.В., Котов Е.В., Тарасова Д.С., Сергеев В.В. Вентилируемые фасады, интегрированные с инженерными системами здания для холодного климата // Инженерно-строительный журнал. 2018. № 1(77). С. 47–58. DOI: 10.18720/MCE.77.5.
37. Петриченко М.Р., Котов Е.В., Немова Д.В., Тарасова Д.С., Сергеев В.В. Численное моделирование вентилируемых фасадов в экстремальных климатических условиях // Инженерно-строительный журнал. 2018. № 1(77). С. 130–140.. DOI: 10.18720/MCE.77.12.
38. Петриченко М.Р., Субботина С.А., Хайрутдинова Ф.Ф., Рейх Е.В., Немова Д.В., Ольшевский В.Я., Сергеев В.В. Влияние рустов на воздушный режим в вентилируемом фасаде // Инженерно-строительный журнал. 2017. № 5(73). С. 40–48. DOI: 10.18720/MCE.73.4
39. СТО ФГУ ФЦС 44416204-10-2010 Крепления анкерные. Метод определения несущей способности по результатам натурных испытаний.
40. СТО НОСТРОЙ 2.14.96-2013 «Навесные фасадные системы. Монтаж анкерных креплений».
41. ГОСТ 8.136-74 Государственная система обеспечения единства измерений (ГСИ). Прессы гидравлические для испытаний строительных материалов. Методы и средства поверки (с Изменением N 1). М.: Издательство стандартов. 2015. 75 с.
42. ГОСТ 1497-84. (ИСО 6892-84, СТ СЭВ 471-88) Металлы. Методы испытаний на растяжение (с Изменениями N 1, 2, 3). М.: Издательство стандартов. 1985. С. 3–37.
43. ДБН В.1.1 - 1 – 94. Проектирование и строительство гражданских зданий из блоков и камней пиленых известняков крымских месторождений в сейсмических районах. К.: КиевЗНИИЭП. 43 с.
44. Сердюков В.М., Григоренко А.Г. Испытание сооружений. К.: Будівельник. 1976. 200 с.
45. Рекомендации по проектированию навесных фасадных систем с вентилируемым воздушным зазором для нового строительства и реконструкции зданий, Москомархитектура, Москва, 2002 г.
46. Фасадные теплоизоляционные системы с воздушным зазором. Рекомендации по составу и содержанию документов и материалов, представляемых для технической оценки пригодности продукции, ГОССТРОЙ России, Москва, 2004 г.
47. Опыт, проблемы и пути совершенствования применения навесных фасадных систем в московском строительстве, Городской координационной экспертно-научный центр «Энлаком», Москва, 2005 г.

of the Crimean deposits in seismic regions]. Кiev: KyivZNIIEP. 43 p.

44. Serdyukov, V.M., Grigorenko, A.G. Ispytaniye sooruzheniy [Testing of structures]. Кiev: Bydivelnik. 1976. 200 p.
45. Rekomendatsii po proyektirovaniyu navesnykh fasadnykh sistem s ventiliruyemym vozdushnym zazorom dlya novogo stroitelstva i rekonstruktsii zdaniy [Recommendations on the design of hinged facade systems with ventilated air gap for new construction and reconstruction of buildings]. Moscomarchitectura, Moscow, 2002.
46. Fasadnyye teploizolyatsionnyye sistemy s vozdushnym zazoroMoscow Rekomendatsii po sostavu i soderzhaniyu dokumentov i materialov, predstavlyayemykh dlya tekhnicheskoy otsenki prigodnosti produktsii [Facade thermal insulation systems with air gap. Recommendations on the composition and content of documents and materials submitted for technical evaluation of the suitability of products]. GOSSTROY of Russia, Moscow, 2004.
47. Opyt, problemy i puti sovershenstvovaniya primeneniya navesnykh fasadnykh sistem v moskovskom stroitelstve [Experience, problems and ways to improve the application of hinged facade systems in Moscow construction]. City Coordination Expert-Scientific Center "Enlakom", Moscow, 2005.

Vasiliy Alekseenko,*
+7(978)712-18-07; avn108@mail.ru

Oksana Zhilenko,
+7(978)706-89-77; o.b.zhilenko@mail.ru

Mohamad Al Ali,
+421905359228; mohamad.alali@tuke.sk

Василий Николаевич Алексеенко,*
+7(978)712-18-07; эл. почта: avn108@mail.ru

Оксана Борисовна Жиленко,
+7(978)706-89-77;
эл. почта: o.b.zhilenko@mail.ru

Мохамад Ал Али,
+421905359228;
эл. почта: mohamad.alali@tuke.sk

Alekseenko, V.N., Zhilenko, O.B., Al Ali, M. Bearing capacity of pasted anchors in the masonry walls of natural limestone. *Magazine of Civil Engineering*. 2018. 81(5). Pp. 52–63. doi: 10.18720/MCE.81.6.

doi: 10.18720/MCE.81.7

Method for calculating strongly damped systems with non-proportional damping

Метод расчета сильно демпфированных систем с непропорциональным демпфированием

O.P. Nesterova*,
A.M. Uzdin,
Petersburg State Transport University, St. Petersburg, Russia
M.Yu. Fedorova,
St.Petersburg State University of Film and Television, St. Petersburg, Russia

Аспирант О.П. Нестерова*,
д-р техн. наук, профессор А.М. Уздин,
Петербургский государственный университет путей сообщения Императора Александра I, Санкт-Петербург, Россия
канд. физ.-мат. наук, доцент М.Ю. Федорова,
Санкт-Петербургский государственный университет кино и телевидения, Санкт-Петербург, Россия

Key words: earthquake engineering; calculation; strongly damped system

Ключевые слова: землетрясение; расчет; сильно демпфированные системы

Abstract. The calculation of systems under seismic excitations is performed both dynamically by time integration and quasistatically under inertial seismic loads using linear response-spectra method (RSM). Dynamic timing calculation can be performed either using direct integration of the initial system of motion equations, or by using the spectral decomposition of motion equations by shape modes. RSM is completely based on spectral decomposition. However, the spectral decomposition was worked out only for systems with proportional damping, when the eigenvectors of the undamped and damped systems coincide. With regard to RSM, even for proportional damping, the existing Guide Lines do not allow to take into account the actual damping in the system. There are proposals for the explicit calculation of damping within the framework of the RSM for proportional damping in literature. Their results can be used both for constructing RSM and for integrating motion equations with arbitrary damping using the spectral decomposition of the motion equations. But so far the mentioned mathematical results have not been connected with calculating structures. The authors propose a variant of the RSM for calculating highly damped systems under earthquake impact. To this aim, complex eigenvectors and eigenvalues of the motion equation system were obtained, and this system was reduced to a tridiagonal form. As a result, the assumed equation system of the order equal to N was decomposed into N pairs of independent real equations. The base oscillation accelerogram and its derivative present the input in the right part of the motion equations. In this way two matrices of seismic forces are generally obtained. To sum up these forces, the shape mode correlation coefficients were analyzed. An example of mass damper calculation is given in the paper. For 4-6-story buildings constructed in ordinary conditions the proposed variant of the RSM leads to the same data that existing Guide Lines. But the proposed variant of RSM makes it possible to calculate systems with heterogeneous damping including seismic isolated systems, mass dampers and systems with soil-structure interaction which is impossible to do on the base of the existing Guide Lines.

Аннотация. Расчет систем на сейсмическую нагрузку выполняется динамически, путем интегрирования по времени, и квазистатически, по инерционным сейсмическим нагрузкам с использованием линейно-спектрального метода (ЛСМ). Динамический расчет может быть выполнен либо путем прямого интегрирования исходной системы уравнений движения, либо с использованием спектрального разложения уравнений движения по формам. ЛСМ полностью основан на спектральном разложении. Однако спектральное разложение было разработано только для систем с пропорциональным затуханием, когда собственные векторы незатухающих и затухающих систем совпадают. Что касается ЛСМ, даже для пропорционального демпфирования существующая методика в нормативной документации не позволяет учитывать фактическое демпфирование в системе. В литературе существуют предложения по явному учету затухания в рамках ЛСМ для пропорционального затухания. Данные результаты могут быть использованы в расчетах как по ЛСМ, так и путем интегрирования уравнений движения с произвольным затуханием с использованием спектрального разложения уравнений движения. Но до сих пор упомянутые математические результаты не были использованы при расчете конструкций зданий и сооружений. Авторы предлагают вариант ЛСМ для расчета сильно демпфированных систем при расчете на землетрясения. С этой целью были получены комплексные собственные векторы и собственные значения системы уравнений движения, и эта система была сведена к трехдиагональной форме. В результате принятая система уравнений порядка N была разложена на N пар независимых вещественных уравнений. Правая часть уравнения представляет собой ускорение основания и его производную. Таким образом, получается две матрицы сейсмических сил. Чтобы суммировать эти силы, были проанализированы коэффициенты корреляции форм. В статье приведен пример расчета здания с динамическим гасителем. Для 4-6-этажных зданий, построенных в обычных условиях, предлагаемый вариант ЛСМ приводит к тем же данным, что и нормативный вариант ЛСМ. Но предлагаемый вариант ЛСМ позволяет рассчитать системы с неоднородным затуханием, включая системы с сейсмоизоляцией, с динамическими гасителями и системы с учетом основания, что невозможно сделать на основе существующей нормативной документации.

1. Introduction

The object of the study is the method of calculating damping for analyzing seismic stability of strongly damped systems.

In the past 20 years, various kinds of dampers have been increasingly used to decrease dynamic loads on building structures in earthquake engineering in particular [1–7]. However, in the theory and practice of seismic load calculations, the problem of allowing for damping causes certain difficulties. At present, the basic method for evaluating the seismic stability of structures is the method of decomposition by vibration modes. In this case, in the process of calculating it is necessary to build a damping matrix, write down the system of seismic oscillation equations, expand the system according to vibration modes, estimate loads for each mode and sum up these loads taking into account the random nature of the impact. When calculating the structure by the linear spectral method (LSM), the response spectra are used to estimate the seismic loads, and in the case of dynamic calculation a package of accelerograms with further averaging of the result or some deliberately dangerous accelerogram [8, 9] is used. At present the construction of linear system damping matrix is not a difficult problem. This task is included in program complexes, for example, MicroFE [10], Midas [11], etc. Some aspects of this problem were considered by the authors in [1]. As a result, the system of seismic oscillation equations has the following form

$$M\ddot{q} + B_{eq}\dot{q} + Rq = -M\ddot{Y}_0, \tag{1}$$

where M is inertia matrix; B_{eq} is the matrix of equivalent viscous damping;

R is the stiffness matrix; q is the column of generalized displacements;

$\ddot{Y}_0$ is the column of kinematic inputs

To solve equation (1), the decomposition of motion by the oscillation modes of the undamped system is used in research on the subject [1, 11]. Such decomposition is admissible at damping of less than 15 % of the critical value, or in the case when the matrices $M^{-1}R$ and $M^{-1}B$ have the same eigenvector matrices [12]. Damping, which allows the decomposition of the motion equations by the oscillation modes of the undamped system, is called proportional.

Calculating structures with a non-proportional damping have caused certain difficulties so far. Meanwhile, this kind of calculations is necessary for seismic-protection systems, tuned mass dampers, structures consisting of different materials, soil-structure interaction analysis etc. Especially relevant are such calculations for selecting parameters of special seismic protection at the early stages of its designing, when no design accelerograms for the building site are available yet.

The aim of investigation is bringing out features of calculating systems with a non-proportional damping using the motion decomposition by oscillation modes. To do this, it is necessary to solve the following problems

1. Building the spectral distribution of strongly damped systems and developing the response spectra method (RSM) for their calculating.
2. Presenting some example of proposed method

Nesterova, O.P., Uzdin, A.M., Fedorova, M.Yu. Method for calculating strongly damped systems with non-proportional damping. Magazine of Civil Engineering. 2018. 81(5). Pp. 64–72. doi: 10.18720/MCE.81.7.

2. Methods

System (1) is reduced to a system of equations of the first order.

$$A \cdot \dot{\Theta} = Q\,, \tag{2}$$

where

$$A = \begin{Vmatrix} -M^{-1}B_{eq} & -M^{-1}R \\ E & 0 \end{Vmatrix}; \qquad \Theta = \begin{pmatrix} q \\ \dot{q} \end{pmatrix}; \quad Q = \begin{pmatrix} \ddot{Y}_0 \\ 0 \end{pmatrix}$$

System (2) is characterized by a set of complex eigenvalues presented in the following form

$$\Lambda = \left/ -\frac{\gamma_1 k_1}{2}, -\frac{\gamma_2 k_2}{2}, \dots -\frac{\gamma_n k_n}{2}, -\frac{\gamma_1 k_1}{2}, -\frac{\gamma_2 k_2}{2}, \dots -\frac{\gamma_n k_n}{2} \right/ + i \left/ \omega_1, \omega_2, \cdots \omega_n, -\omega_1, -\omega_2, \cdots - \omega_n \right/, \tag{3}$$

where n is the number of the system degree of freedom

$$\lambda_{i,i+1} = -\frac{\gamma_i k_i}{2} \pm i\omega_i\,, \ \omega_i = k_i \sqrt{1 - \frac{\gamma_i^2}{4}} \tag{4}$$

$\lambda, k, \omega, \gamma$ are an eigenvalue, eigenfrequency, the frequency of damped oscillations, and the modal inelastic resistance coefficient of the system respectively.

Peculiarities of constructing the damping matrix and determining the eigenvalues and vectors of the matrix A were considered in [12]

For strongly damped systems, appearance of real eigenvalues is possible. This aspect of the problem was considered in [13].

According to [14], there exists a real transformation of the variables of the equation system (2)

$$T = \begin{pmatrix} V_1 & W_1 & T_1 \\ V_2 & W_2 & T_2 \end{pmatrix}, \tag{5}$$

by replacing the original variables $\{q, \dot{q}\}$ with new ones $\{\Xi, \mathrm{H}, \mathrm{I}\}$

$$\begin{cases} \dot{q} = V_1\Xi + W_1\mathrm{H} + T_1\mathrm{I} \\ q = V_2\Xi + W_2\mathrm{H} + T_2\mathrm{I} \end{cases}, \tag{6}$$

and reducing the matrix A to a tridiagonal form.

In transformation (5), the matrices $\{V_1, V_2\}$ and $\{W_1, W_2\}$ are respectively real and imaginary parts of the eigenvector matrix of the matrix A.

In new variables, the system of equations (2) takes the form:

$$\begin{cases} \dot{\Xi} = -\dfrac{1}{2}\Gamma\Lambda\Xi + \Lambda_*\mathrm{H} - P_1\ddot{Y}_0 \\ \dot{\mathrm{H}} = -\Lambda_*\Xi - \dfrac{1}{2}\Gamma\Lambda\mathrm{H} - Q_1\ddot{Y}_0 \\ \dot{\mathrm{I}} = NI - U_1\ddot{Y}_0 \end{cases} \tag{7}$$

In the system of equations (7)

$\Gamma=\lceil\gamma_1,\ \gamma_2,\ \ldots\ \gamma_{nc}\rfloor$ is the diagonal matrix of inelastic resistance modal coefficients; $\Lambda=\lceil k_1,\ k_2,\ldots\ k_{nc}\rfloor$ is the diagonal matrix of natural frequencies of system oscillations; $\Lambda=\lceil k_1,\ k_2,\ldots\ k_{nc}\rfloor$ is the diagonal matrix of frequencies of the damped system; $N=\lceil \nu_1,\ \nu_2,\ldots\ \nu_{nr}\rfloor$ is the diagonal matrix of the real eigenvalues of the matrix A, where nc is the number of complex eigenvalues pairs, nr is the number of real eigenvalues ($2\cdot nc+nr=n$).

$P_{1,2}$, $Q_{1,2}$, $U_{1,2}$ are blocks of the matrix inverse to transformation matrix (5)

$$T^{-1}=\begin{bmatrix} P_1 & P_2 \\ Q_1 & Q_2 \\ U_1 & U_2 \end{bmatrix} \tag{8}$$

The decoupling of oscillation equations similar to (7) is known in the vibration theory [13, 15–17].

The last matrix equation of system (7) is a system of independent first-order equations of the form

$$\dot{\upsilon}_j-\nu_j\upsilon=-d_j^{(U)}\ddot{y}_0 \tag{9}$$

Here the variable υ_j is an element of the vector of variables I.

The kinematic input vector is written in the form $\ddot{Y}_0=V_p\ddot{y}_0$, where $\ddot{y}_0$ is the accelerogram of base oscillations, V_p is the vector of excitation projections on the directions of generalized coordinates; $d_j^{(U)}$ is an element of the vector U_1V_p.

The first two equations of system (7) are written down in pairs of independent second-order equations

$$\begin{aligned}\ddot{\xi}_j+\gamma_j k_j\dot{\xi}_j+k_j^2\xi_j&=-d_j^{(1)}\ddot{y}_0+d_j^{(2)}\dddot{y}_0\\ \ddot{\eta}_j+\gamma_j k_j\dot{\eta}_j+k_j^2\eta_j&=-d_j^{(3)}\ddot{y}_0+d_j^{(4)}\dddot{y}_0\end{aligned} \tag{10}$$

The coefficients $d_j^{(1)}$, $d_j^{(2)}$, $d_j^{(3)}$, $d_j^{(4)}$ are the elements of the vectors $(\Lambda*Q_1+0.5\Gamma\Lambda P_1)V_p$; P_1V_p; $(\Lambda*P_1+0{,}5\Gamma\Lambda Q_1)V_p$ и Q_1V_p respectively.

If damping in the system is proportional, i.e. condition (11) takes place,

$$B_{eq}=RX\Phi X^{-1}, \tag{11}$$

then the coefficients $d_j^{(2)}$, $d_j^{(3)}$, $d_j^{(4)}$ become 0.

In condition (1), Φ is an arbitrary real diagonal matrix.

For arbitrary damping, movement in the direction of i-th generalized coordinate is presented as the sum

$$y_i=\sum_j \chi_{ij}^{(1)}\xi_j^{(1)}+\chi_{ij}^{(2)}\xi_j^{(2)}+\chi_{ij}^{(3)}\eta_j^{(3)}+\chi_{ij}^{(4)}\eta_j^{(4)}+\sum_s \chi_{is}^{(5)}\upsilon_s \tag{12}$$

$\chi_{ij}^{(k)}$ are coefficients similar to the mode coefficient η_{ij} introduced in the applied earthquake engineering theory and used in the existing Guidelines [14], they are defined as follows: $\chi_{ij}^{(1)}=v_{ij}d_j^{(1)}$, $\chi_{ij}^{(2)}=v_{ij}d_j^{(2)}$, $\chi_{ij}^{(3)}=w_{ij}d_j^{(3)}$, $\chi_{ij}^{(4)}=w_{ij}d_j^{(4)}$, $\chi_{ij}^{(5)}=u_{ij}d_j^{(U)}$;

$\xi_j^{(1)}$ and $\eta_j^{(3)}$ are determined from the solution of the following equations:

$$\ddot{\xi}_j^{(1)} + \gamma_j k_j \dot{\xi}_j^{(1)} + k_j^2 \xi_j^{(1)} = \ddot{y}_0 \text{ and } \ddot{\eta}_j^{(3)} + \gamma_j k_j \dot{\eta}_j^{(3)} + k_j^2 \eta_j^{(3)} = \ddot{y}_0; \tag{13}$$

$\xi_j^{(2)}$ and $\eta_j^{(4)}$ are determined from the solution of the following equations:

$$\ddot{\xi}_j^{(1)} + \gamma_j k_j \dot{\xi}_j^{(1)} + k_j^2 \xi_j^{(1)} = \dddot{y}_0 \text{ and } \ddot{\eta}_j^{(3)} + \gamma_j k_j \dot{\eta}_j^{(3)} + k_j^2 \eta_j^{(3)} = \dddot{y}_0; \tag{14}$$

The function υ_j is obtained from the solution of equation (9).

We note that the appearance of the derivative of the load (the third derivative of the base displacements) in the right-hand side of presentation (10) was mentioned in paper on damping forced oscillations [1].

The obtained presentation of solution (11) makes it possible both numerical integration of the equations of motion with retention of the required number of vibration modes and the application of the response spectra method (RSM) with some refinement.

When the RSM is used, seismic forces in the absence of real eigenvalues should be summed up according to the formula

$$s_i = \left[\sum_{k=1}^{nf} \sum_{j=1}^{nf} \sum_{m=1}^{2} \sum_{n=1}^{2} s_{ij}^{(m)} s_{ik}^{(n)} \varepsilon_{jk}^{(m,n)} \right]^{1/2} \tag{15}$$

where ‘nf’ is the number of the considered oscillation modes;

m = 1, 2 is the index of the displacement component ξ or η;

N = 1, 2 the index of the component of the displacement caused by $\ddot{y}_0$ or $\dddot{y}_0$;

$\varepsilon_{jk}^{(m,n)}$ is the corresponding correlation coefficient.

If we take into account that the correlation coefficient of functions ξ_j or η_j is equal to 1, and the correlation coefficient between the function and its derivative is equal to 0, then expression (15) is simplified and with the account of damped modes of oscillations takes the form

$$s_i = \left[\sum_j \sum_k s_{ij} s_{ik} \varepsilon_{jk} + \sum_j \sum_k s'_{ij} s'_{ik} \varepsilon''_{jk} + \sum_{j_{j \neq k}} \sum_k s_{ij} s'_{ik} \varepsilon'_{jk} + \sum_s \sum_r s^*_{is} s^*_{ir} \varepsilon^*_{rs} + \right]^{1/2} \tag{16}$$

In formula (16), the first term is conventional seismic force, determined on the basis of equations (13) and having a standard form for a system with concentrated masses m_i: [2]

$$s_{ij} = A \cdot g \cdot m_i \cdot \beta(T_j) \cdot K_\psi(\gamma_j) \cdot \left(\chi_{ij}^{(1)} + \chi_{ij}^{(2)} \right) \tag{17}$$

The second term in formula (17) is completely analogous to the first, but is obtained on the basis of equations (14), in which the derivative of the input accelerogram is used as the input excitation. In this case, the seismic forces formula is the following

$$s'_{ij} = A \cdot g \cdot m_i \cdot \beta(T_j) \cdot K_\psi(\gamma_j) \cdot \frac{\left(\chi_{ij}^{(3)} + \chi_{ij}^{(4)} \right)}{k_j} \tag{18}$$

The third term appears due to a possible correlation between seismic forces S_{ij} and S'_{ij} for i≠j.

Finally, the fourth term is determined on the basis of equation (9). For seismic forces, it is also possible to obtain an analogue of the dynamic factor by presenting seismic load in the form

$$s_{ij}^{*} = A \cdot g \cdot m_i \cdot \beta\left(\nu_j\right) \cdot \chi_{ij}^{(5)} \tag{19}$$

If the modes are not correlated, then from (16) we obtain a formula similar to that used in the current Russian standards of earthquake-proof construction.

$$s_i = \left[\sum s_{ij}^2 + \sum s_{ij}'^2 + \sum\left(s_{ij}^*\right)^2\right]^{1/2} \tag{20}$$

An important problem of estimating seismic loads on a damped system is calculating correlation coefficients, which are determined by formulas

$$\varepsilon_{ij} = \int_0^\infty \frac{S(\omega)e^{i\omega t}d\omega}{Z_i Z_j};\quad \varepsilon_{ij}' = \int_0^\infty \frac{\omega S(\omega)e^{i\omega t}d\omega}{Z_i Z_j};\quad \varepsilon_{ij}'' = \int_0^\infty \frac{\omega^2 S(\omega)e^{i\omega t}d\omega}{Z_i Z_j}; \tag{21}$$

Here $S(\omega)$ is the input spectral density, $Z_j=(\omega^2-k_j^2)^2-\gamma_j^2\, k_j^2\, \omega^2$.

For $\varepsilon_{ij}*$ the correlation coefficient has the following form

$$\varepsilon_{ij}^{*} = \int_0^\infty \frac{S(\omega)e^{i\omega t}d\omega}{\left(\omega-\nu_i\right)\left(\omega-\nu_j\right)} \tag{22}$$

Many studies have been devoted to the problem of calculating integrals (21–22). Due to the fact that Zj functions have a pronounced peak at $\omega = kj$, the form of the function $S(\omega)$ does not play an important role. The results obtained by formulas of A.A. Petrov [18], A. Ter Kuryugian [19, 20] and other authors diverge by 3–7%. The authors of this paper prefer to use the formula of A.A. Petrov. The development of formulas of A. Petrov and A. Ter Kurrigyan is presented in [21].

3. Results and Discussion

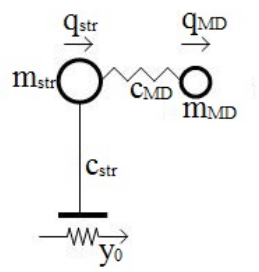

Figure 1. The design diagram for analyzing systems with the MD

The above proposed method allows one to consider linear systems with inhomogeneous and non-proportional damping. The most important area of application of the proposed technique is calculating the tuned mass damper (MD) and the soil- structure-interaction. For example, let us consider calculating the MD, shown in Figure 1. The MD is considered for tuning equal to 0.98 and the relative mass equal to 0.1 and damping equal to 5% of the critical value. The MD tuning $\kappa = \frac{k_{MD}}{k_{str}}$, where $k_{MD} = \sqrt{\frac{C_{MD}}{m_{MD}}}$, $k_{str} = \sqrt{\frac{C_{str}}{m_{str}}}$; the relative mass $\nu = \frac{m_{MD}}{m_{str}} = 0.1.$

In Figure 2 the graphs show the dependence of the MD efficiency (relative decrease of the shearing force on the structure base) on damping in the MD spring. The first graph (curve 1) shows the conventional solution with the motion decomposition by the oscillation modes of the undamped system obtained earlier

[22], the second graph (curve 2) shows the exact solution with harmonic excitation and the third graph (curve 3) - the proposed solution.

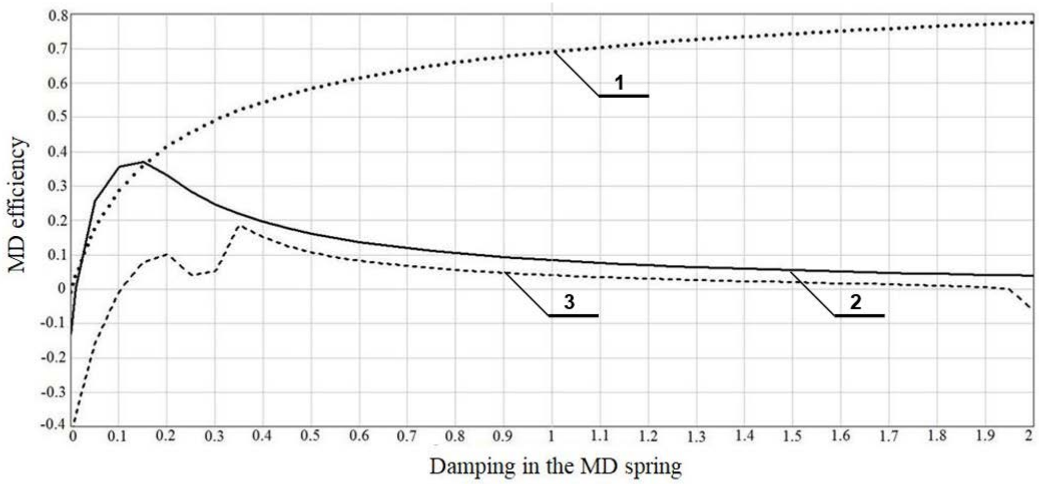

Fig.2. Dependence of the MD efficiency on damping in the MD spring;
Curve 1 – conventional solution with the motion decomposition by the oscillation modes of the undamped system;
Curve 2 – solution with harmonic excitation;
Curve 3 – the proposed solution

In the proposed solution, a normative spectral curve is used to set the input excitation. It can be seen from Figure 2 that the motion equation decomposition by to the oscillation modes of the undamped system is acceptable for solving the problem under consideration with damping of less than 0.2 of the critical value, but for greater damping such decomposition gives a qualitatively incorrect result that does not provide the safety margin. The exact solution with a harmonic excitation qualitatively coincides with the proposed one, and the existing difference between the solutions is due to the difference in the spectra of the given inputs.

4. Conclusions

1. The method for calculating strongly damped systems using their spectral distribution and estimating seismic loads on the basis of the RSM is proposed.

2. The proposed method of calculating systems with a non-proportional damping allows one to carry out linear calculations of a wide range of systems, including seismoprotection systems, the MD, structures h a soil massif, structures consisting of different materials, etc. The use of conventional methods for culating this sort of structures can result in significant errors, distorting calculation results by 2 or more times. The peculiarities of the proposed method are calculating complex eigenvalues and complex eigenvectors of the system under consideration, introducing an amendment to seismic forces for each oscillation mode and taking into account the mode correlation

3. Using this method, one can set the design input excitation by the normative response spectrum. This makes it possible to select the parameters of special seismic protection at the initial stages of designing, when no design accelerograms for the building site are available.

4. Proposed results are illustrated as applied to the calculating the tuned mass damper

5. Acknowledgements

The authors are grateful to S.R. Grebenshchikova for her help in preparing the English version of the paper.

The authors are grateful to the RFFI. The investigations were carried out with the support of the RFFI grant No. 16-58-53095 "Development of the theory of limiting states for ensuring seismic stability of railway bridges under construction and operation".

References

1. Uzdin, A.M., Fedorova, M.Y., Durseneva, N.V. Ocenka sei`smostoi`kosti spetcial`ny`kh dempfirovanny`kh sistem [Estimation of seismic stability of special damped systems]. VI Poliahovskie chteniia. Mezhdunarodnaia konferentciia po mehanike, posviashchennaia 95-letiiu so dnia rozhdeniia S.V. Vallandera. Izbranny`e trudy` [VI Polyahovskie readings. International Conference on mechanics, dedicated to the 95th anniversary of the birth of S. Wallander. Selected works]. St. Petersburg. 31.01.2012-03.02.2012. 2012. Pp. 52–53. (rus)
2. Uzdin, A.M., Elizarov, S.V., Belash, T.A., Sei`smostoi`kie konstruktcii transportny`kh zdanii` i sooruzhenii`. [Earthquake resistant design of transport buildings and structures]. FGOU «Uchebno-metodicheskii` centr po obrazovaniiu na zheleznodorozhnom transporte». 2012. 500 p. (rus)
3. Aiken, I.D., Kelly, J.M. Mahmoodi P. The application of viscoelastic dampers to seismically resistant structures. Proceedings of Fourth U.S. National conference on Earthquake Engineering. May 20-24. 1990. Palm Springs, California. Vol. 3. Pp. 459–468.
4. Christopoulos, C., Rotunno M., de Callafon R.A. Semi-active tuned mass damper for seismic protection of MDOF structures: Controlling the damping. 12th European Conference on Earthquake Engineering. Elsevier Science Ltd. Oxford. UK. 2002. No. 178.
5. Durseneva, N.V., Indeykin, A.V., Kuznetsova, I.O., Uzdin, A.M., Fedorova, M.Yu. Peculiarities of Calculating Bridges with Seismic Isolation Including Spherical Bearings and Hydraulic Dampers in Russia. Journal of Civil Engineering and Archtecture. 2015. Vol. 9. No. 4. Pp. 401–409.
6. Jerónimo, E., Guerreiro, L. Seismic displacement analysis of bridges with viscous dampers. Proc. of 12-th European Conference on Earthquake Engineering. Paper Reference 373.
7. Skinner, R.I., Kelly, J.M., Heine, A.Y. Hysteresis damper for earthquake resistant structures. Earthquake Eng. Struct. Dyn. No. 1974. Vol. 3.3. Pp. 287–296.
8. Uzdin, A.M. Zadanie sei`smicheskogo vozdei`stviia. Vzgliad inzhenera-stroitelia. [Earthquake input setting. The view of a civil engineer]. Sei`smostoi`koe stroitel`stvo. Bezopasnost` sooruzhenii`. 2005. No. 1. Pp. 27–31. (rus)
9. Dolgaya, A.A., Indeykin, A.V., Uzdin, A.M. Earthquake accelerations for construction calculating with different responsibility degrees. Structural Dynamics – EURODYN'96. 1996 Balkema, Rotterdam. ISBN 9054108134. Pp. 143–147.
10. Soldatov, A.Y., Lebedev, V.L., Semenov, V.A. Uchet dempfirovaniia pri raschetakh sooruzhenii` na kinematicheskie vozdei`stviia. [The account of damping in calculating the facilities for kinematic effects]. VII Savinovskie chteniia, Tezisy` docladov. PGUPS [VII Savinovsky reading. Abstracts. “PGUPS”]. 2014. Pp. 21–22. (rus)
11. MIDAS Civil 2018 http://manual.midasuser.com/EN_Common/Civil/865/index.htm
12. Nesterova, O.P., Nikonova, N.V., Fedorova, M.Yu., Uzdin, A.M., Vorobyova, K.V. Taking account of damping in estimating structure earthquake stability. Materials Physics and Mechanics. 2016. Vol. 26. Pp. 57–60.
13. Uzdin, A.M. Uchet dempfirovaniia kolebanii` v ramkakh linei`no-spektral`noi` teorii sei`smostoi`kosti [Damping accounting within the framework of the response spectra method]. Materialy` konferentcii` i soveshchanii` po gidrotekhnike. Metody` issledovanii` i raschetov sei`smostoi`kosti gidrotekhnicheskikh i e`nergeticheskikh sooruzhenii`. VNIIG im. B.E.Vedeneeva [Proceedings of conferences and meetings on hydraulic engineering. Methods of research and calculations of seismic resistance

Литература

1. Уздин А.М., Федорова М.Ю., Дурсенева Н.В. Оценка сейсмостойкости специальных демпфированных систем // VI Поляховские чтения. Международная конференция по механике, посвященная 95-летию со дня рождения С.В. Валландера. Избранные труды. СПб. 31.01.2012-03.02.2012. С. 52–53.
2. Уздин А.М., Елизаров С.В., Белаш Т.А. Сейсмостойкие конструкции транспортных зданий и сооружений. Учебное пособие. ФГОУ «Учебно-методический центр по образованию на железнодорожном транспорте». 2012. 500 с.
3. Aiken I.D., Kelly J.M., Mahmoodi P. The application of viscoelastic dampers to seismically resistant structures // Proceedings of Fourth U.S. National conference on Earthquake Engineering. May 20-24. 1990. Palm Springs, California. Vol.3. Pp. 459–468.
4. Christopoulos C., Rotunno M., de Callafon R.A. Semi-active tuned mass damper for seismic protection of MDOF structures: Controlling the damping // 12th European Conference on Earthquake Engineering. Elsevier Science Ltd. Oxford. UK. 2002. № 178.
5. Durseneva N.V., Indeykin A.V., Kuznetsova I.O., Uzdin A.M., Fedorova M.Yu. Peculiarities of Calculating Bridges with Seismic Isolation Including Spherical Bearings and Hydraulic Dampers in Russia // Journal of Civil Engineering and Archtecture. 2015. Vol. 9. № 4. Pp. 401–409.
6. Jerónimo E., Guerreiro L. Seismic displacement analysis of bridges with viscous dampers // Proc. of 12-th European Conference on Earthquake Engineering. Paper Reference 373.
7. Skinner R.I., Kelly J.M., Heine A.Y. Hysteresis damper for earthquake resistant structures // Earthquake Eng. Struct. Dyn. No. 1974. Vol. 3.3. Pp. 287–296.
8. Уздин А.М. Задание сейсмического воздействия. Взгляд инженера-строителя // Сейсмостойкое строительство. Безопасность сооружений. 2005. № 1. С. 27–31.
9. Dolgaya A.A., Indeykin A.V., Uzdin A.M. Earthquake accelerations for construction calculating with different responsibility degrees // Structural Dynamics – EURODYN'96. 1996 Balkema, Rotterdam. ISBN 9054108134 Pp. 143–147.
10. Солдатов А.Ю., Лебедев В.Л., Семенов В.А. Учет демпфирования при расчетах сооружений на кинематические воздействия // VII Савиновские чтения. Тезисы докладов. ПГУПС. 2014. С. 21–22.
11. MIDAS Civil 2018 [Электронный ресурс] http://manual.midasuser.com/EN_Common/Civil/865/index.htm
12. Nesterova O.P., Nikonova N.V., Fedorova M.Yu., Uzdin A.M., Vorobyova K.V. Taking account of damping in estimating structure earthquake stability // Materials Physics and Mechanics. 2016. Vol. 26. Pp. 57–60.
13. Уздин А.М. Учет демпфирования колебаний в рамках линейно-спектральной теории сейсмостойкости // Материалы конференций и совещаний по гидротехнике. Методы исследований и расчетов сейсмостойкости гидротехнических и энергетических сооружений. ВНИИГ им. Б.Е.Веденеева. 1982. С. 29–34.
14. СП 14.13330.2014 Строительство в сейсмических районах СНиП II-7-81* (актуализированного СНиП II-7-81* "Строительство в сейсмических районах" (СП 14.13330.2011))
15. Morzfeld M., Ma F. The decoupling of linear dynamical systems // III ECCOMAS Thematic Conference on Computational Methods in Structural Dynamics and Earthquake Engineering. 2011.

hydraulic and power structures. B.E.Vedeneev VNIIG]. 1982. Pp. 29–34. (rus)

14. SP 14.13330.2014 Stroitel`stvo v sei`smicheskikh rai`onakh. Aktualizirovannaia redaktciia SNiP II-7-81* [Guidelines “SP 14.13330.2014 Construction in seismic areas. The updated edition of Guidelines II-7-81*”]. (rus)
15. Morzfeld, M., Ma, F. The decoupling of linear dynamical systems. III ECCOMAS Thematic Conference on Computational Methods in Structural Dynamics and Earthquake Engineering. 2011.
16. Patil, M.J. Decoupled second-order equations and modal analysis of a general nonconservative system. AIAA Dynamics Specialists Conference. 2000.
17. Igusta, T., Kiureghian, A., Sackman, C.A. Modal decomposition method for stationary response of non-classically damped systems. Earthquake Engineering and Structural Dynamics. 1984. No. 12. Pp. 121–136.
18. Petrov, A.A., Bazilevsky, S.V. Vliianie vzaimnoi` korreliatcii mezhdu obobshchenny`mi koordinatami pri sluchai`ny`kh kolebaniiakh linei`ny`kh sistem. [Influence of cross correlation between generalized coordinates for random oscillations of linear systems]. Stroitel`naia mehanika i raschet sooruzhenii. 1979. No. 4. Pp. 52–56. (rus)
19. Kiureghian, A. Response spectrum method for random vibration analysis of MDF systems. Earthquake Engineering and Structural Dynamics. 1981. Vol. 9. No. 5. Pp. 419–435.
20. Kiureghian. A., Nakamuro, Y. CQC modal combination rule for high-frequency modes. Earthquake Engineering and Structural Dynamics. 1993. No. 22. Pp. 943–956.
21. Chen, H., Tan, P., Zhou, F. An improved response spectrum method for non-classically damped systems. Earthquake engineering. 2017. Vol. 15. No. 10. Pp. 4375–4397.
22. Uzdin, A.M., Sandovich, T.A., Al`-Naser-Mohomad Samikh Amin. Osnovy` teorii sei`smostoi`kosti i sei`smostoi`kogo stroitel`stva zdanii` i sooruzhenii`. [Fundamentals of the theory of seismic resistance and earthquake-proof construction of buildings and structures] S.Peterburg, Izd. VNIIG. [St. Petersburg, VNIIG]. 1993. 175 p. (rus)

16. Patil M.J. Decoupled second-order equations and modal analysis of a general nonconservative system // AIAA Dynamics Specialists Conference. 2000.
17. Igusta T., Kiureghian. A., Sackman C.A. Modal decomposition method for stationary response of non-classically damped systems // Earthquake Engineering and Structural Dynamics. 1984. № 12. Pp. 121–136.
18. Петров А.А., Базилевский С.В. Влияние взаимной корреляции между обобщенными координатами при случайных колебаниях линейных систем // Строительная механика и расчет сооружений. 1979. № 4. С. 52–56.
19. Kiureghian A. Response spectrum method for random vibration analysis of MDF systems // Earthquake Engineering and Structural Dynamics. 1981. Vol. 9. № 5. Pp. 419–435.
20. Kiureghian. A., Nakamuro Y. CQC modal combination rule for high-frequency modes // Earthquake Engineering and Structural Dynamics. 1993. № 22. Pp. 943–956.
21. Chen H., Tan P., Zhou F. An improved response spectrum method for non-classically damped systems // Earthquake engineering. 2017. Vol. 15. № 10. Pp. 4375–4397.
22. Уздин А.М., Сандович Т.А., Аль-Насер-Мохомад Самих Амин. Основы теории сейсмостойкости и сейсмостойкого строительства зданий и сооружений. С.Петербург: Изд. ВНИИГ, 1993. 175 с.

Olga Nesterova,*
+7(960)280-59-75; neona975@yandex.ru

Alexander Uzdin,
+7(812)310-70-14; uzdin@mail.ru

Maria Fedorova,
+7(812)428-69-44; mgfed@mail.ru

Ольга Павловна Нестерова,*
+7(960)280-59-75;
эл. почта: neona975@yandex.ru

Александр Моисеевич Уздин,
+7(812)310-70-14; эл. почта: uzdin@mail.ru

Мария Юрьевна Федорова,
+7(812)428-69-44; эл. почта: mgfed@mail.ru

doi: 10.18720/MCE.81.8

Survivability of structural systems of buildings with special effects

Живучесть конструктивных систем сооружений при особых воздействиях

V.I. Travush,
Russian Academy of Architecture and Building Sciences, Moscow, Russia
N.V. Fedorova*,
National Research Moscow State Civil Engineering University, Moscow, Russia

Д-р техн. наук, вице-президент РААСН В.И. Травуш,
Российская академия архитектуры и строительных наук, г.Москва, Россия
д-р техн. наук, профессор Н.В. Федорова,
Национальный исследовательский Московский государственный строительный университет, г. Москва, Россия

Key words: survivability of structures; survivability parameter; structural system; static and dynamic diagram; added dynamic loading

Ключевые слова: живучесть сооружений; параметр живучести; конструктивная система; статико-динамическая диаграмма; динамическое догружение

Abstract. The technique of calculation analysis of survivability of reinforced concrete statically indeterminate beams and rod structural systems of buildings and structures under emergency influences is given. The statement of the problem of the computational analysis of the survivability of such constructive systems and the algorithm for determining the survivability parameter under special influences in the form of a sudden shutdown of one of the constructions is expounded. The criteria of the bearing capacity for a particular limiting state for the considered constructive systems arising under such influences are proposed, the excess of which can cause a progressive destruction of the constructive system. An example of a computational analysis of the survivability of a statically indeterminate reinforced concrete continuous beam in comparison of the theoretical results obtained with the results of its experimental studies is considered. However, the problem can be used for determining the parameter of the survivability of buildings and structures for the examined impacts.

Аннотация. Приведена методика расчетного анализа живучести железобетонных статически неопределимых балочных и стержневых конструктивных систем зданий и сооружений при аварийных воздействиях. Изложена постановка задачи расчетного анализа живучести таких конструктивных систем и алгоритм определения параметра живучести при особых воздействиях в виде внезапного выключения одной из конструкций. Предложены критерии несущей способности при особом предельном состоянии для рассматриваемых конструктивных систем возникающие при таких воздействиях, превышение которых может вызвать прогрессирующее разрушение конструктивной системы. Рассмотрен пример расчетного анализа живучести статически неопределимой железобетонной неразрезной балки в сопоставлении полученных теоретических результатов с результатами ее экспериментальных исследований. Приведенные расчетные зависимости могут быть использованы для определения параметра живучести зданий и сооружений при рассматриваемых воздействиях.

1. Introduction

The existing methods for structural analysis of survivability [1–4] and progressive collapse [5–9] of reinforced concrete frames of buildings and structures do not take into consideration additional dynamic loading in structural elements in case of abrupt failure of one of the bearing elements or consider it nominally. The impact on this additional loading of the prestress in structural reinforced concrete elements and brittle fracture of the tensile zone of concrete at the moment of cracking is not assessed either. At the same time survivability experimental data analysis of such structures in accidental limit state [10–14] shows that the impact of these factors while assessing survivability of buildings and structures can be rather significant.

Травуш В.И., Федорова Н.В. Живучесть конструктивных систем сооружений при особых воздействиях // Инженерно-строительный журнал. 2018. № 5(81). С. 73–80.

Let us consider a method for survivability analysis for redundant reinforced concrete framed structures with normal and stressed reinforcement considering the mentioned above factors.

The analysis is aimed at the determination of the survivability parameter of structural systems, criteria of reinforced structural elements in such systems in accidental limit state and determination of an additional dynamic loading factor in bearing element sections due to abrupt failure of one of the structures.

Here, the term survivability of a constructive system (λ) will be defined as a factor equal to the load acting on the structure, with the value of which, in case of switching off one of the load-bearing elements in the structural system, structural changes (failures) leading to local or progressive destruction begin.

Accidental limit state is meant as a state occurring under accident impact beyond which a local or progressive collapse of the structure can take place [15, 16]. Survivability parameter enables quantitative assessment of a building structural system load level under which, in case of accident impact, structural changes can occur, and assessment of these changes regarding stability of geometrical shape.

For calculation analysis and determination of the survivability parameter of a reinforced concrete statically indeterminate constructive system, a calculation algorithm including the following steps is proposed.

For a given structural system a primary design diagram for a given design load specified according to the regulatory requirements is built (Figure 1,a, b).

2. Methods

On the basis of a mixed-mode method for redundant systems, a system of fundamental equations as proposed in [1,2] is formed. Load coefficients of equations are presented in the form of two summands:

$$\left.\begin{aligned}\vec{A}\mathrm{M}+\vec{B}Z+\overrightarrow{\Delta_p}+\lambda\overrightarrow{\delta_p}=0\\ \vec{C}\mathrm{M}+0+\overrightarrow{R_p}+\lambda\overrightarrow{r_p}=0\end{aligned}\right\}, \tag{1}$$

where $\vec{A}, \vec{B}, \overrightarrow{\Delta_p}, \vec{C}, \overrightarrow{R_p}$ are the matrices of coefficients of the unknowns of the mixed-mode method; $\overrightarrow{\delta_p}$ are the matrices of displacements in the direction of the removed elements from the external parametric loads P at $\lambda=1$: $\overrightarrow{r_p}$ are the matrices of the responses in the constraints of the main system from the external parametric load at $\lambda=1$ (Fig.1, b).

Considering fundamental equation features of the mixed-mode method C=-BT (where "T" means operation of transposition), the system (1) is written as follows

$$\begin{Vmatrix}A & B\\ -B^T & 0\end{Vmatrix}\cdot\begin{Vmatrix}\vec{M}\\ \vec{Z}\end{Vmatrix}+\begin{Vmatrix}\overrightarrow{\Delta_p}\\ \overrightarrow{R_p}\end{Vmatrix}+\lambda\begin{Vmatrix}\overrightarrow{\delta_p}\\ \overrightarrow{r_p}\end{Vmatrix}=0. \tag{2}$$

The equation system solution (2) is as follows:

$$\begin{Vmatrix}\vec{M}\\ \vec{Z}\end{Vmatrix}=\begin{Vmatrix}\overrightarrow{M_p}\\ \overrightarrow{Z_p}\end{Vmatrix}+\lambda\begin{Vmatrix}\overrightarrow{m_p}\\ \overrightarrow{r_p}\end{Vmatrix}, \tag{3}$$

where

$$\begin{Vmatrix}\overrightarrow{M_p}\\ \overrightarrow{Z_p}\end{Vmatrix}=-\begin{Vmatrix}A & B\\ -B^T & 0\end{Vmatrix}^{-1}\cdot\begin{Vmatrix}\overrightarrow{\Delta_p}\\ \overrightarrow{R_p}\end{Vmatrix}, \tag{4}$$

$$\begin{Vmatrix}\overrightarrow{m_p}\\ \overrightarrow{r_p}\end{Vmatrix}=-\begin{Vmatrix}A & B\\ -B^T & 0\end{Vmatrix}\cdot\begin{Vmatrix}\overrightarrow{\delta_p}\\ \overrightarrow{r_p}\end{Vmatrix}, \tag{5}$$

A combined stresses (forces, moments) diagram in a set *n*- times redundant structural system due to the design load and prestressing force is built (diagram M_n^c in Figure 1 c, d).

In the given structural system loaded with a design load, accident impact in the form of abrupt failure of one of vertical structural elements, for instance, support 2, is applied. The so called *secondary design diagram* with an excluded vertical element is built (Figure 1, e). Due to the instantaneous character of the accident impact, vertical reaction of support R_2 obtained on the basis of the design load is applied in the secondary design diagram with the opposite sign, supposing that on the first semi-oscillation of the beginning of beam vibrations after support removal this reaction and accordingly the moment from this reaction (Figure 1, f) reaches its maximum value. Calculation according to the secondary design diagram is made and new stresses diagrams of all loads and prestress are built (diagram $M^{d}_{n-1,\Sigma,}$ in Figure 1, g).

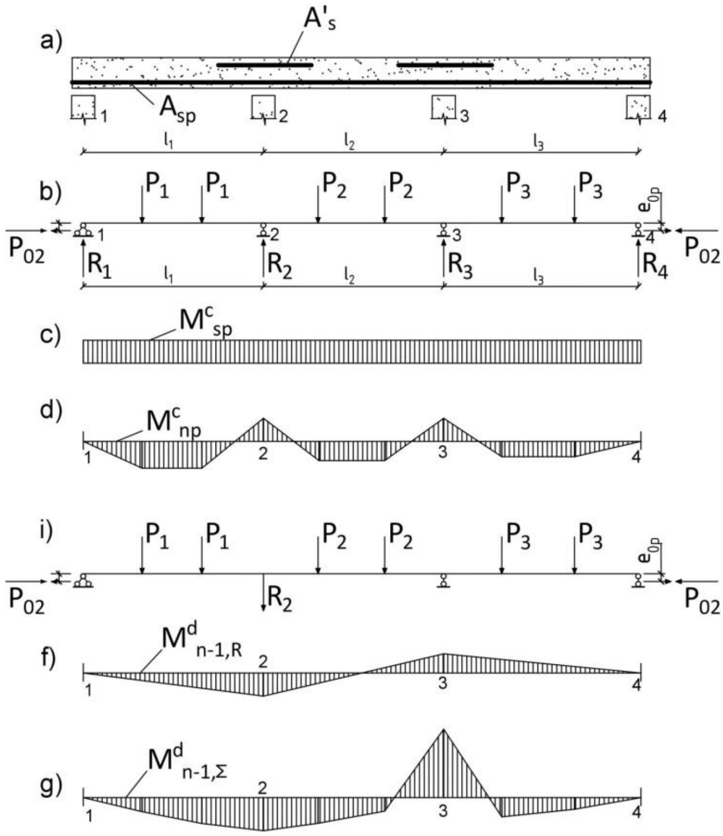

Figure 1. Continuous reinforced concrete beam survivability analysis: a, b – structural and design diagrams respectively; c, d – moment diagrams due to prestressing force and external loading in the primary design diagram; e, f, g – secondary design diagram and moment diagrams in the secondary design diagram

Failure of any section (tie) in a new structure will occur if deformation stress in this element reaches the limit value as per the criteria of accidental limit state (see below). Then, for all forces in failing elements the system of inequalities shall be satisfied:

$$|M_j| = |M_{jq} + \lambda m_{jp}| \le M_{j,u} \quad (j = 1,2, \ldots k) \tag{6}$$

where M_{ju} is the limit value of the force in the failing element taking into account the dynamic strength of the materials. M_{jq}, m_{jp} are the matrix elements of columns M_p and m_p. (In case of ductility of structural system elements, material strength increase under dynamic loads in the secondary design diagram is not taken into consideration).

In the left-hand side of inequality (6), value of the moments M_j is taken in absolute magnitude since the negative sign at M_j indicates that the direction of this force is opposite to accepted in the basic system of the mixed-mode method limit force value.

The minimum value of the survivability parameter $\lambda = \lambda_m$, when in the most loaded *j*- th element the limit value is reached and is found according to the formula

$$\lambda_{(m)} = \min\left(M_{j,u} \pm |M_{jq}|\right) / |m_{jp}| \,, \, (j = 1,2, \ldots k). \tag{7}$$

Sign "minus" in the numerator is applied if M_{jq} and m_{jp} signs are the same, and sign "plus" is applied if these signs are opposite.

When the survivability parameter changes in the most loaded *j*-th element $\lambda \in [0, \lambda_{(m)j}]$, initial structural system with all included ties works. If $\lambda > \lambda_{(m)j}$, the j-th tie fails and the degree of redundancy of the structure decreases by *1* which is equivalent to the exclusion of constraints (6) from the system of equations (1) and the *j*- th unknown. And the initial matrices shall be transformed as follows:

– in matrix *A* the *j*-th row and *j*-th column are excluded;

– in matrix *B* the *j*-th row is excluded;

– in matrix columns the values of load coefficients $\overrightarrow{\Delta_p}$ and $\overrightarrow{R_p}$ are specified according to the following equations:

$$\Delta_{jp}^{(1)} = \Delta_{iq} + \delta_{ip} \cdot \lambda_{(m)} + \delta'_{ij} \cdot (\pm M_{j,u}), \quad (8)$$

$$R_{jp}^{(1)} = R_{iq} + r_{ip} \cdot \lambda_{(m)} + r'_{ij} \cdot (\pm M_{j,u}), \quad (9)$$

where $\delta_{ip}, \delta'_{ij}, r'_{ij}$ and Δ_{iq}, R_{iq} are the factors at the unknowns (unit deflection and responses) and load coefficients (of displacement and response) of the mixed-mode method of redundant structures analysis. In expression (9) sign at $M_{j,u}$ is taken in line with the sign of $m_{j,p}$.

To find the next failing tie, matrices are changed in the described way and the calculation procedure repeats. After the second failing tie is found the system of equations is transformed taking as initial a system of equations obtained after transformation at the first step of the solution. And at the second and subsequent steps the increment of the survivability parameter $\Delta_{(m)}$ is obtained, i.e. the parameter at which the second and subsequent ties fail. These parameters values are calculated by formulae:

$$\begin{aligned} \lambda_m^{(2)} &= \lambda_m^{(1)} + \Delta\lambda_{(m)}^1, \\ \lambda_m^{(3)} &= \lambda_m^{(2)} + \Delta\lambda_{(m)}^2, \\ \lambda_m^{(k)} &= \lambda_m^{(k-1)} + \Delta\lambda_{(m)}^{k-1}. \end{aligned} \quad (10)$$

The sign of the solution completion, i.e. exhaustion of the system survivability is the formation of an unstable frame after subsequent tie failure. This sign at each step of the fracture $\Delta\lambda_m$ is found by means of calculation of the determinant of a matrix of coefficients at the unknowns. If the determinant equals to zero, then the structure has exhausted its vitality and turned into unstable system.

Calculating limit forces in the structure sections ($M_{j,u}$) the following constraints for dynamic stresses are taken as criteria of the accidental limit state of a reinforced concrete structure. Fist, constraints for dynamic stresses in the reinforcement (Figure 2, a):

$$\sigma_s^d < R_{s,ser}^d, \quad (11)$$

where σ_s^d are the dynamic loading stresses in the positive reinforcement of the considered design section calculated according to the secondary design diagram, considering additional dynamic loading [17, 18] at the moment of cracking; $R_{s,ser}^d$is the standard value of the reinforcement dynamic strength specified as per the recommendations [1]. Second, constraints for dynamic stresses in compressed concrete (Figure 2, b):

$$\sigma_b^d < R_{b,ser}^d, \quad (12)$$

where σ_b^d are the dynamic stresses in compressed concrete in the considered section, calculated as per the secondary design diagram taking into account additional dynamic loading of compressed concrete at the moment of cracking [18]; $R_{b,ser}^d$ is the standard value of the concrete dynamic strength specified according to the recommendations [1,2].

If both strength criteria for reinforcement (11) and concrete (12) for the most stressed sections of the span of a continuous beam are satisfied (Figure 2 a, b), a deformation criterion of accidental limit state is checked:

$$f \le \frac{1}{\rho} l, \quad (13)$$

where $f$and ρ are the deflection and the curvature in the beam span l respectively.

The value of ρ is found by formula

$$\rho = 80 - 2\frac{l}{h}, \quad (14)$$

but is not less than 30,

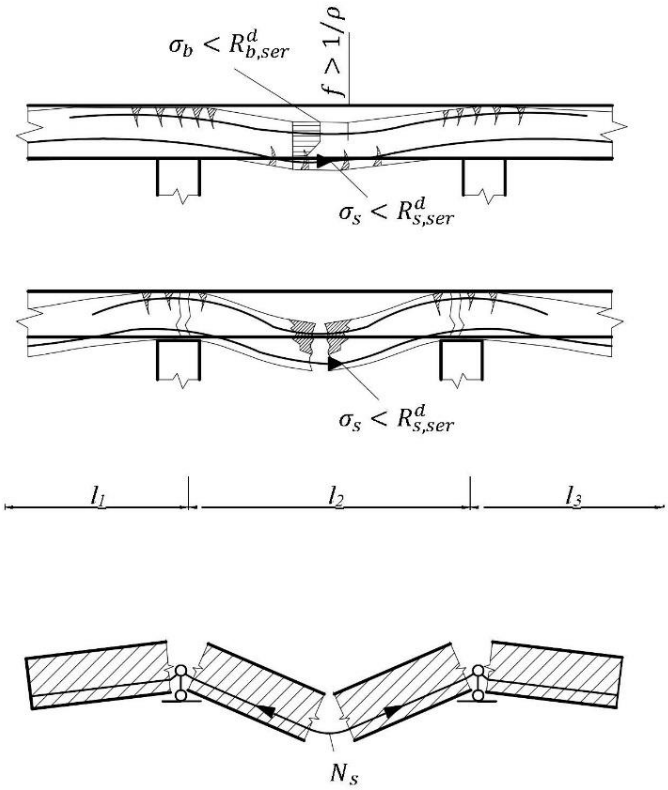

Figure 2. Defining criteria for beam system failure in accidental limit state: a – design diagram for "mild" section failure, b – for compressed concrete brittle fracture, c – for suspended system

where l, h are respectively the span and the depth of section of the structural element.

If compressed concrete fracture (criterion 12) occurs in more than three sections of the beam, then, if thrust bearing is structurally possible, a rigid structure turns into a suspended structure (Figure 2, c). Survivability of such a system for accidental limit state is checked as per condition:

$$N_s < A_s R^d_{s,ser}, \tag{15}$$

where N_s is the force in positive reinforcement of the span I of the continuous beam calculated as for a suspended cable for the design load applied to the continuous beam in the span considering additional dynamic loading in the considered design section. And sections of connection of rigid blocks (disks), the beam span is divided into in case of compressed concrete zone brittle fracture in the most stressed beam sections, are taken as the design ones (Figure 2, c). If condition (15) is not fulfilled, a local fracture of the considered span occurs (element) of the constructive system.

Calculation Example. Let us consider the survivability analysis of the reinforced continuous beam which test results are given in [11].

A three-span continuous beam consisted of three prefabricated unstressed reinforced elements of concrete B25, with section of 120x40 mm and length of 1200 mm. Prefabricated element reinforcement involves two-dimensional welded reinforcing mats with main reinforcement of 8 mm diameter, grade A400. Crosswise reinforcement of the prefabricated elements was of wire with diameter 1.5 mm and spacing 60 mm. Assembling of prefabricated elements into a continuous beam was performed as per the inserts, with butt joint grouting between the edges of the prefabricated elements using the same concrete as was used for prefabricated elements.

The structural system was loaded with two concentrated forces P_i (i =1, 2, 3) in each span according to diagram Figure 1b. As an impact beyond design basis a moment tie failure (section fracture) above the first intermediate support 2 was studied.

3. Results and Discussion

The result data of the calculation based on the described algorithm are presented in the diagram "moment- curvature" (Figure 3).

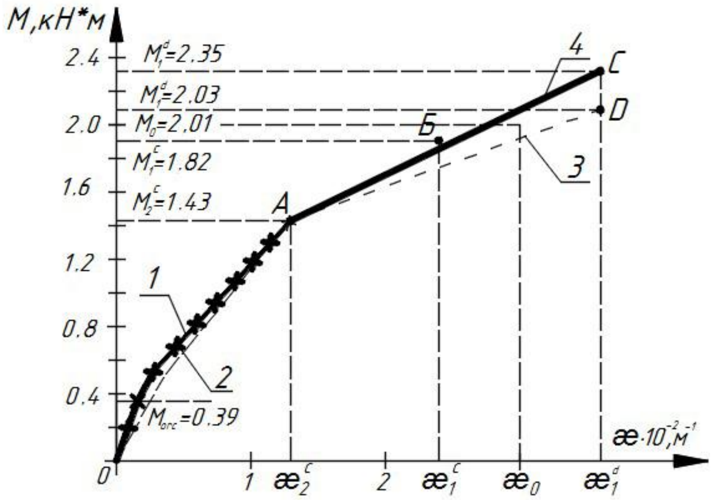

Figure 3. Moment-curvature diagram in the most stressed section of the first span of the beam

Here, curve 1 shows an experiment diagram in the most stressed span section of the first span of the continuous beam when it was loaded with the design load; curve 2 shows the design diagram for static loading of the beam with the set load P_i, up to the impact beyond design basis (point A), and before the bearing capacity exhaustion in the section subject to static deformation of the section after failure of the moment tie (section AB), 3 and 4 are the design and experiment diagrams of the dynamic deformation of the section of the first span after the impact beyond design basis and before the failure of this section due to the working reinforcement fracture (the criterion defined by the formula (11)). In the diagrams "moment-curvature", parameters $æ_2^c$,$æ_1^c$,$æ_1^d$,M_2^c, M_1^c, M_1^d are the curvatures and moments in the initial redundant to the second degree beam and those in the beam with a failed moment tie above the support 2 in static and dynamic states of the structure. Moment M_{crc} characterized the beginning of cracking in the continuous beam system, moment M_0 corresponded to the design value of the limit beam curvature.

It is pertinent to note that in well-known publications on the problem, determination of dive dynamics in the design of buildings is more often, or through the use of direct methods of structural dynamics, e.g. [19, 20], or the dynamics is taken into account in a simplified way – the introduction of dynamic factor [21, 22]. In the first case, for complex structural systems, the solution is relatively time consuming. In the second case, the result is relatively close. The proposed variant of the quasi-static method for determining the dive dynamics makes it relatively easy to accurately determine the parameter survivability of structures and load dynamics in its structural elements.

The obtained in [11] experiment pattern of the failure of the beam system (Figure 4) after the impact beyond design basis in the form of abrupt failure of the moment tie above the second support of the continuous beam were marked by the fracture of the working reinforcement in the first and third spans and above the second intermediate support, and completely complied with the design value of the survivability parameter and the criterion (11) for accidental limit state.

Figure 4. General view of the secondary structure failure

4. Conclusion

1. The proposed algorithm for survivability analysis of redundant beam structural systems under accident impact and the accidental limit state criteria for redundant systems make it possible to determine the minimum level of loading of a structural system (survivability parameter λ) at which in a structural system in case of a sudden removal of one of the load-bearing structural elements (a tie) structural changes – failures leading to structural local or progressive collapse begin.

2. Comparison of the calculation data and experimental data of static – dynamic loading of a continuous three-span reinforced concrete beam with a suddenly failed in it moment tie, showed the efficiency of the developed algorithm for quantitative assessment of the survivability parameter of a structural system and suitability of the accepted criteria for accidental limit state under accident impact.

References

1. Geniyev, G.A., Kolchunov, V.I., Klyueva, N.V., Nikulin, A.I., Pyatikrestovskiy, K.P. Prochnost i deformativnost zhelezobetonnykh konstruktsiy pri zaproyektnykh vozdeystviyakh [Strength and deformability of reinforced concrete structures under beyond design impacts]. Moscow: ASV, 2004. 216 p. (rus)
2. Kolchunov, V.I., Androsova, N.B., Klyueva, N.V., Bukhtiyarova, A.S. Zhivuchest zdaniy i sooruzheniy pri zaproyektnykh vozdeystviyakh [Effervescence of buildings and structures under beyond-design impacts]. Moscow: ASV, 2014. 208 p. (rus)
3. Travush, V.I., Fedorova, N.V Survivability parameter calculation for framed structural systems. Russian Journal of Building Construction and Architecture. 2017. No. 1(33). Pp. 6–14.
4. Perelmuter, A.V., Pichugin, S.F. Issues on estimation of building structure vulnerability. Magazine of Civil Engineering. 2014. No. 5(49). Pp. 5–14. (rus)
5. Rudenko, D.V., Rudenko, V.V. Zashchita karkasnykh zdaniy ot progressiruyushchego obrusheniya [Protection of frame buildings from progressive collapse]. Magazine of Civil Engineering. 2009. No. 3(5). Pp. 38–41. (rus)
6. Kodysh, E.N., Trekin, N.N., Chesnokov, D.A. Zashchita mnogoehtazhnyh zdanij ot progressiruyushchego obrusheniya [Protection of Multistory Buildings from Progressing Collapse]. Industrial and Civil Engineering. 2016. No. 6. Pp. 8–13. (rus)
7. Kokot, S., Anthoine, F., Negro, P., Solomos, G. Static and dynamic analysis of a reinforced concrete flat slab frame building for progressive collapse. Engineering Structures. 2012. Vol. 40. Pp. 205–217.
8. Liu, M. A new dynamic increase factor for nonlinear static alternate path analysis of building frames against progressive collapse. Engineering Structures. 2013. Vol. 48. Pp. 666–673.
9. Livingston, E., Sasani, M., Bazan, M., Sagiroglu, S. Progressive collapse resistance of RC beams. Engineering Structures. 2015. Vol. 95. Pp. 61–70.
10. Lew, H.S., Yihai, B., Fahim, S., Main, J., Pujol, S., Sozen, M.A. An experimental and computational study of reinforced concrete assemblies under a column removal scenario. Boulder: Natl. Inst. Stand. Technol. Tech. Note 1720, 2011. 104 p.
11. Geniyev, G.A., Klyueva, N.V. Eksperimentalno-teoreticheskiye issledovaniya nerazreznykh balok pri avariynom vyklyuchenii iz raboty otdelnykh elementov [Experimental and theoretical studies of continuous beams in case of emergency shutdown of individual elements of work]. News of higher educational institutions. Construction. 2000. No. 10. Pp. 25–27. (rus)
12. Forquin, P., Chen, W. An experimental investigation of the progressive collapse resistance of beam-column RC sub-assemblages. Construction and Building Materials. 2017. Vol. 152. Pp. 1068–1084.

Литература

1. Гениев Г.А., Колчунов В.И., Клюева Н.В., Никулин А.И., Пятикрестовский К.П. Прочность и деформативность железобетонных конструкций при запроектных воздействиях. М.: АСВ, 2004. 216 с.
2. Колчунов В.И., Андросова Н.Б., Клюева Н.В., Бухтиярова А.С. Живучесть зданий и сооружений при запроектных воздействиях. М.: АСВ, 2014.208 с.
3. Travush V.I., Fedorova N.V Survivability parameter calculation for framed structural systems // Russian Journal of Building Construction and Architecture. 2017. № 1(33). Pp. 6–14.
4. Перельмутер А.В., Пичугин С.Ф. Об оценке уязвимости строительных конструкций // Инженерно-строительный журнал. 2014. № 5(49). С. 5–14.
5. Руденко Д.В., Руденко В.В. Защита каркасных зданий от прогрессирующего обрушения // Инженерно-строительный журнал. 2009. № 3(5). С. 38–41.
6. Кодыш Э.Н., Трекин Н.Н., Чесноков Д.А. Защита многоэтажных зданий от прогрессирующего обрушения // Промышленное и гражданское строительство. 2016. № 6. С. 8–13.
7. Kokot S, Anthoine F., Negro P., Solomos G. Static and dynamic analysis of a reinforced concrete flat slab frame building for progressive collapse // Engineering Structures. 2012. Vol. 40. Pp. 205–217.
8. Liu M. A new dynamic increase factor for nonlinear static alternate path analysis of building frames against progressive collapse // Engineering Structures. 2013. Vol. 48. Pp. 666–673.
9. Livingston E., Sasani M., Bazan M., Sagiroglu S. Progressive collapse resistance of RC beams // Engineering Structures. 2015. Vol. 95. Pp. 61–70.
10. Lew H.S., Yihai B., Fahim S., Main J., Pujol S., Sozen M.A. An experimental and computational study of reinforced concrete assemblies under a column removal scenario. Boulder: Natl. Inst. Stand. Technol. Tech. Note 1720, 2011. 104 p.
11. Гениев Г.А., Клюева Н.В. Экспериментально-теоретические исследования неразрезных балок при аварийном выключении из работы отдельных элементов // Известия вузов. Строительство. 2000. № 10. С. 25–27.
12. Forquin P. Chen W. An experimental investigation of the progressive collapse resistance of beam-column RC sub-assemblages // Construction and Building Materials. 2017. Vol. 152. Pp. 1068–1084.
13. Fascetti A., Kunnath S.K., Nistico N. Robustness evaluation of RC frame buildings to progressive collapse // Engineering Structures. 2015. Vol. 86. Pp. 242–249.
14. Алексейцев А.В., Курченко Н.С. Деформации стальных стропильных ферм при ударных аварийных воздействиях // Инженерно-строительный журнал. 2017. № 5(73). С. 3–13.

Травуш В.И., Федорова Н.В. Живучесть конструктивных систем сооружений при особых воздействиях // Инженерно-строительный журнал. 2018. № 5(81). С. 73–80.

13. Fascetti, A., Kunnath, S.K., Nistico, N. Robustness evaluation of RC frame buildings to progressive collapse. Engineering Structures. 2015. Vol. 86. Pp. 242–249.
14. Alekseytsev, A.V., Kurchenko, N.S. Deformations of steel roof trusses under shock emergency action. Magazine of Civil Engineering. 2017. No. 5. Pp. 3–13. doi: 10.5862/MCE.73.1.
15. Svod Pravil 296.1325800.2017 Zdaniya i sooruzheniya. Osobyye vozdeystviya [Code of Regulations 296.1325800.2017 Buildings and structures. Special effects]. Minstroy Rossii. Moscow, 2017. 23 p. (rus)
16. Minimum Design Loads for Buildings and Other Structures, ASCE 7-10. ASCE/SEI. American Society of Civil Engineers. 2010. 658 p.
17. Kolhunov, V.I., Androsova, N.B. Calculation of additional dynamic stresses in rebars of flexural reinforced concrete structural elements caused by fragile failure of tensed concrete. Scientific Herald of the Voronezh State University of Architecture and Civil Engineering. Construction and Architecture. 2016. No. 4(32). Pp. 6–16. (rus)
18. Fedorova, N.V., Khalina, T.A. Issledovanie dinamicheskih dogruzhenij v zhelezobetonnyh konstruktivnyh sistemah pri vnezapnyh strukturnyh perestrojkah [Study of Dynamic Loadings in Reinforced Concrete Structural System at Sudden Structural Reorganizations]. Industrial and Civil Engineering. 2017. No. 5. Pp. 45–49. (rus)
19. Brunesi, E., Nascimbene, R., Parisi, F., Augenti, N. Progressive collapse fragility of reinforced concrete framed structuresthrough incremental dynamic analysis. Engineering Structures. 2015. Vol. 104. Pp. 65–79.
20. Masoero, E., Daro, P, Chiaia, B.M. Progressive collapse of 2D framed structures: An analytical model. Engineering Structures. 2013. Vol. 54. Pp. 94–102.
21. Dat, P.X., Hai, T.K., Jun, Y. A simplified approach to assess progressive collapse resistance of reinforced concrete framed structures. Engineering Structures. 2015. Vol. 101. Pp. 45–57.
22. Perelmuter, A.V., Kriksunov, E.Z., Mosina, N.V. Realizatsiya rascheta monolitnykh zhilykh zdaniy na progressiruyushcheye (lavinoobraznoye) obrusheniye v srede vychislitelnogo kompleksa "SCAD OFFICE" [Realization of the calculation of monolithic residential buildings for a progressive (avalanche) collapse in the environment of the computer complex "SCAD OFFICE]. Magazine of Civil Engineering. 2009. No. 2. Pp. 13–18. (rus)

15. СП 296.1325800.2017 Здания и сооружения. Особые воздействия. Минстрой России. М., 2017. 23 с.
16. Minimum Design Loads for Buildings and Other Structures, ASCE 7-10. ASCE/SEI. American Society of Civil Engineers. 2010. 658 p.
17. Kolhunov V.I., Androsova N.B. Calculation of additional dynamic stresses in rebars of flexural reinforced concrete structural elements caused by fragile failure of tensed concrete // Scientific Herald of the Voronezh State University of Architecture and Civil Engineering. Construction and Architecture. 2016. № 4(32). C. 6–16.
18. Федорова Н.В., Халина Т.А. Исследование динамических догружений в железобетонных конструктивных системах при внезапных структурных перестройках // Промышленное и гражданское строительство. 2017. № 5. С. 45–49.
19. Brunesi E., Nascimbene R., Parisi F., Augenti N. Progressive collapse fragility of reinforced concrete framed structuresthrough incremental dynamic analysis // Engineering Structures. 2015. Vol. 104. Pp. 65–79.
20. Masoero E., Daro P, Chiaia B.M. Progressive collapse of 2D framed structures: An analytical model // Engineering Structures. 2013. Vol. 54. Pp. 94–102.
21. Dat P.X., Hai T.K., Jun, Y. A simplified approach to assess progressive collapse resistance of reinforced concrete framed structures // Engineering Structures. 2015. Vol. 101. Pp. 45–57.
22. Перельмутер А.В., Криксунов Э.З., Мосина Н.В. Реализация расчета монолитных жилых зданий на прогрессирующее (лавинообразное) обрушение в среде вычислительного комплекса "SCAD OFFICE" // Инженерно-строительный журнал. 2009. № 2(4). С. 13–18.

Vladimir Travush,
+7(495)625-73-16; travush@raasn.ru

Nataliya Fedorova,
+7(960)697-12-30; fenavit@mail.ru

Владимир Ильич Травуш,
+7(495)625-73-16; эл. почта: travush@raasn.ru

Наталия Витальевна Федорова,
+7(960)697-12-30; эл. почта: fenavit@mail.ru

Travush, V.I., Fedorova, N.V. Survivability of structural systems of buildings with special effects. Magazine of Civil Engineering. 2018. 81(5). Pp. 73–80. doi: 10.18720/MCE.81.8.

doi: 10.18720/MCE.81.9

Aerodynamics of building structures for flue gas removal

Аэродинамика строительных сооружений для удаления дымовых газов

V.K. Akhmetov*,
National Research Moscow State Civil Engineering University, Moscow, Russia
V.Ya. Shkadov,
Lomonosov Moscow State University, Moscow, Russia
P.N. Konon,
Belarusian State University, Minsk, Belarus

Д-р техн. наук, профессор В.К. Ахметов*,
Национальный исследовательский Московский государственный строительный университет, Москва, Россия
д-р физ.-мат. наук, профессор В.Я. Шкадов,
Московский государственный университет им. М.В. Ломоносова, Москва, Россия
канд. физ.-мат. наук, доцент П.Н. Конон,
Белорусский государственный университет, Минск, Беларусь

Key words: high-rise buildings; power engineering; cooling tower; smokestack; gas dynamics; numerical method

Ключевые слова: высотные сооружения; энергетическое строительство; градирня; дымовая труба; газовая динамика; численный метод

Abstract. Natural fuel burning in modern heat power plants with flue gas formation is accompanied with harmful environmental impact and potential opportunity of acid fallout. This can lead to local or even global catastrophe under adverse circumstances. High-rise structures combining a smokestack and a cooling tower are used for ecological natural fuel burning. The most important problem of these structures design is to study gas-dynamic behavior of flue gas mixing with warm ambient air flow during its movement along exhaust duct. Mathematical model and efficient numerical technique for problem solution have been developed in this work. The flowfields and the temperature and concentration distributions are calculated for various inlet conditions. Swirl flow ratio influence on flow nature has been studied. Obtained solutions have been compared with available experimental data and numerical researches. Calculation results can be used in search of optimum building structures.

Аннотация. Сжигание природного топлива в современных тепловых электростанциях с образованием дымовых газов сопровождается вредным воздействием на окружающую среду и потенциальной возможностью выпадения кислотных дождей. При неблагоприятных обстоятельствах это может приводить к локальным или даже к глобальным катастрофам. Для экологически чистого процесса сжигания природного топлива применяются комбинированные высотные сооружения, объединяющие дымовую трубу и мокрую градирню. Важнейшей задачей проектирования таких устройств является изучение газодинамических характеристик процесса смешения дымовых газов с потоком окружающего теплого воздуха при движении по газоотводящему каналу. В данной работе разработана математическая модель и эффективный численный метод решения поставленной задачи. Рассчитаны поля течений, распределения температур и концентраций при различных условиях на входе в канал. Изучено влияние закрутки потока на характер течения. Представлено сравнение полученных решений с известными экспериментальными данными и численными исследованиями. Результаты расчетов могут быть использованы для поиска оптимальной конструкции возводимых сооружений.

1. Introduction

Investigations on combined high-rise structures development for ecological fuel burning have been carried out since the seventies. Such structures have the following principle of operation. At the base of the stack flue gas, from which the sulfur has been removed, is fed into a flow of air heated in a heat exchanger. As it moves through the stack, the gas mixes with the hot air and is carried into the atmosphere by the natural draft. This design has the following advantages. The energy consumption for re-heating of the smoke in this case is reduced. The pollutant concentrations and temperature of the gas at the stack outlet is significantly reduced, because the volume of heated air is much greater than the volume of flue gas (ratio 5:1 – 25:1). Combined high-rise structures provide better draft due to the mixing process in comparison with conventional smokestacks. Problems of external aerodynamics of high-rise buildings were investigated in [1–3].

One promising means of enhancing the efficiency of combined high-rise structures is to swirl the flue gas ahead of the stack inlet. Swirling flows are widely used in various technical applications and are observed in natural phenomena. They have been the object of a great deal of theoretical and experimental study. The most important properties of swirling flows are described in [4, 5]. Swirling flows in channels were investigated numerically in [6–8], in an unbounded medium in [9, 10] and experimentally in [11–13].

The problem of the interaction between two axisymmetric swirling flows is topical in the context of the problems of modeling flows in combustion chambers and gas turbines [14, 15] and in vortex chambers and gas curtains [16–18]. An important feature of these flows is the formation of axial recirculation zones when the initial swirl reaches a critical value. The shape and the character of these zones resemble those formed in swirling streams upon the breakdown of vortex flow [19, 20]. The results of experiments on the stability of swirling flows and the structure of the axial recirculation zone are presented in [21–24].

Thus, the object of research of this work is a combined high-rise structure. The subject of the study is a turbulent flow consisting of smoke and heated air. The task of the research is to study the effect of swirling flow on the mixing and heat transfer processes in a combined high-rise structures. The aim of the research is to ensure minimal environmental damage from burning natural fuels.

The purpose of this work is to develop mathematical model and study the gas-dynamic process of turbulent mixing of flue gas and hot air in the structure under consideration. The general formulation of the problem of the mixing of two nonisothermal turbulent flows is based on the complete Reynolds equations. This system closed by a turbulence model is fairly complicated and its solution is laborious. So we will use a simplified model is based on the parabolized Navier-Stokes equations. In this paper, an efficient numerical method for solution of the problem is presented.

2. Methods

We will consider the problem of mixing of hot gases in the axisymmetric pipe, whose lateral surface is specified in the cylindrical coordinate system r, φ, z by the equation $R(z)$. A swirled flow of flue gas is fed into the central part $(0 \le r \le R_1)$ of the inlet cross-section $(z = 0)$ of this pipe. An outer unswirled hot air flow is introduced into the peripheral part $(R_1 \le r \le R_0 = R(0))$. To investigate the gas dynamic processes of turbulent mixing of heated gases, we use the system of conservation equations for mixture mass, momentum, energy, and admixture mass in the form of boundary layer approximation

$$
\begin{gathered}
\frac{\partial(r\rho U)}{\partial z}+\frac{\partial(r\rho V)}{\partial r}=0,\\
\frac{\partial[(p+\rho U^2)r]}{\partial z}+\frac{\partial(\rho rUV)}{\partial r}=\frac{\partial}{\partial r}(r\tau)-\rho g r,\\
\frac{\partial(r\rho\, UH)}{\partial z}+\frac{\partial(r\rho\, VH)}{\partial r}=\frac{\partial(rq)}{\partial r}+\rho V W^2+\mu r\left(\frac{\partial W}{\partial r}-\frac{W}{r}\right)^2,\\
\frac{\partial(r\rho\, UH)}{\partial z}+\frac{\partial(r\rho\, VH)}{\partial r}=\frac{\partial(rq)}{\partial r},\\
\frac{\partial(r\rho\, UE)}{\partial z}+\frac{\partial(r\rho\, VE)}{\partial r}=\frac{\partial(\mu r\gamma_\alpha)}{\partial r},\\
\frac{\partial(r\rho\, UW)}{\partial z}+\frac{\partial(r\rho\, VW)}{\partial r}=\frac{\partial}{\partial r}\left(\mu r\frac{\partial W}{\partial r}\right)-\frac{\rho V W}{r}-\mu\frac{W}{r^2},\\
h=c_p T,\ H=h+\frac{U^2}{2}+gz,\ q=\frac{1}{\sigma}\mu\frac{\partial}{\partial r}(h+0.5\sigma U^2),\ \gamma_\alpha=\frac{1}{\sigma_\alpha}\frac{\partial E}{\partial r},\ \sigma=\frac{1}{\lambda}\mu c_p,\\
\tau=\mu\frac{\partial U}{\partial r}.
\end{gathered}
\tag{1}
$$

Here, the following notation is used: U, V and W are the axial, radial, and azimuthal velocity components, respectively, μ is the dynamic viscosity, g is the gravity acceleration, T is the temperature, c_p is the specific heat, h is the enthalpy, H is the total enthalpy, q is the heat flux, E_i is the admixture concentration, γ_i is the admixture mass flow-rate, σ and σ_α are Prandtl numbers, and τ is the friction force.

We will use Shkadov method of equal flow-rate surfaces [25]. In the cylindrical coordinate system r, φ, z we define smooth lines $r = \delta_n(z)$, $n = 0,1,2,\ldots,N$, each of which is a streamline and satisfies the equation

$$U\frac{\partial \delta_n}{\partial z} = V \text{ for } r = \delta_n(z). \tag{2}$$

The grid of lines $\delta_n(z)$ is constructed together with the solution. Obviously, $\delta_0 = 0$ is the symmetry axis and $\delta_N = R(z)$ is the pipe wall. The gas dynamic functions can be calculated on the intermediate lines

$$r = \delta_{n+1/2}(z) = 0.5(\delta_n + \delta_{n+1}),\ n = 0, 1, 2, \ldots, N-1.$$

Each equation from the system (1) can be written in the form

$$\frac{\partial(r\rho\, UA)}{\partial z} + \frac{\partial(r\rho\, VA)}{\partial r} = \frac{\partial Q}{\partial r} - \varepsilon_A\, \omega\, r, \tag{3}$$

$$A = \{1, U, H, E, W\},\quad Q = \{0, r\tau, rq, r\mu\gamma_\alpha, \mu r \partial W/\partial r\},$$

$$\varepsilon_A = 1,\ \omega = \frac{\partial p}{\partial z} + \rho g z, \text{ for } A = U,$$

$$\varepsilon_A = 1,\ \omega = -\frac{\rho V W^2}{r} - \mu\left(\frac{\partial W}{\partial r} - \frac{W^2}{r}\right), \text{ for } A = H,$$

$$\varepsilon_A = 1,\ \omega = \frac{\rho V W}{r} + \mu\frac{W}{r}, \text{ for } A = W,$$

$$\varepsilon_A = 0 \text{ for } A = 1, E.$$

Integrating equation (3) with respect to r from $r = \delta_n$ to $r = \delta_{n+1}$, taking into account equation (2) and the Leibniz rule

$$\frac{d}{d\lambda}\int_{U(\lambda)}^{V(\lambda)} f(x,\lambda)\, dx = \int_{U(\lambda)}^{V(\lambda)} \frac{\partial}{\partial\lambda}(f(x,\lambda))\, dx + f(V(\lambda),\lambda)\frac{dV}{d\lambda} - f(U(\lambda),\lambda)\frac{dU}{d\lambda},$$

we obtain

$$\frac{d}{dz}\int_{\delta_n}^{\delta_{n+1}}(r\rho UA)\, dr = -Q\Big|_{\delta_n}^{\delta_{n+1}} - \varepsilon_A\, \omega\frac{1}{2}(\delta_{n+1}^2 - \delta_n^2), \qquad \frac{d}{dz}\int_{\delta_n}^{\delta_{n+1}}(r\rho U)\, dr = 0. \tag{4}$$

Integrals are approximated by finite-difference expressions

$$\int_{\delta_n}^{\delta_{n+1}}(r\rho UA)\, dr = 0.5(\delta_{n+1}^2 - \delta_n^2)\,(\rho UA)_{n+1/2}.$$

Considering as unknown functions

$$f_{n+1/2}=0.5(\delta_{n+1}^2-\delta_n^2),\ n=0,1,2,\ldots,N-1,$$

we obtain expressions for $\delta_n(z)$

$$\delta_1^2=2f_{1/2},\quad \delta_2^2=2(f_{1/2}+f_{3/2}),\quad \ldots,\quad \delta_N^2=2\sum_{n=1}^{N}f_{n-1/2}.$$

Taking this into account we deduce from (4) the system of ordinary differential equations on each line $r=\delta_{n+1/2}(z)$

$$U\dot{U}=\frac{1}{\rho f}R_u-(1-\frac{1}{\gamma})\pi_T\frac{1}{\rho}\dot{p}-\pi_g,$$

$$U\dot{T}=\frac{1}{\rho f}R_T-(1-\frac{1}{\gamma})U\frac{1}{\rho}\dot{p}+\frac{1}{\rho}\frac{\pi_w^2}{\pi_T}G_T,$$

$$U\dot{E}=\frac{1}{\rho f}R_E, \tag{5}$$

$$U\dot{W}=\frac{1}{\rho f}R_w+\frac{1}{\rho}G_w,$$

$$\frac{\dot{f}}{f}=-\frac{\dot{p}}{p}+\frac{\dot{T}}{T}-\frac{\dot{U}}{U}.$$

Here a dot denotes differentiation with respect to z. The system of equations (5) is written in the dimensionless form. The quantities U, T, ρ, E, p and W are scaled by their maximum values U_1, T_1, ρ_1, E_1, p_1 and W_1 in the inner jet at the pipe inlet and f is scaled by R_0^2. The three dimensionless parameters in (5) $\pi_g=R_0 g/U_1^2$, $\pi_w=W_1/U_1$, $\pi_T=c_p T_1/U_1^2$ are the Froude number, the swirl parameter and the analog of the Mach number M.

For flows without swirl, equation for the pressure is written as

$$\frac{\dot{p}}{p}\left[-\frac{1}{2\gamma}R^2+\left(1-\frac{1}{\gamma}\right)\pi_T p\sum_{n=0}^{N-1}\frac{f_{n+1/2}}{\rho U^2}\right]=R\dot{R}-\sum_{n=0}^{N-1}\left(\pi_g\frac{f_{n+1/2}}{U^2}+\frac{R_T}{\rho UT}-\frac{R_u}{\rho U^2}\right). \tag{6}$$

For swirling flows, the pressure is determined by the equation

$$\frac{\partial p}{\partial r}=\frac{\gamma}{\gamma-1}\frac{\pi_w^2}{\pi_T}\rho\frac{W^2}{r}$$

which can, after integration, be written in the form:

$$p(z,r)=p^w(z,r)+p_0(z),\quad p^w(z,r)=\frac{\gamma}{\gamma-1}\frac{\pi_w^2}{\pi_T}\int_0^r\rho\frac{W^2}{r}dr.$$

In order to find $p(z,r)$, we calculate $p^w(z,r)$ from the mean value theorem and $\dot{p}^w(z,r)$ from the recurrence relations

$$\dot{p}_1^w=\alpha_{1/2}f_{1/2},\quad \dot{p}_{n+1}^w=\dot{p}_n^w+\alpha_{n+1/2}f_{n+1/2},\quad n=1,2,\ldots,N-1,$$

$$\dot{p}_{n+1/2}^w=0.5(\dot{p}_n^w+\dot{p}_{n+1}^w),\quad n=0,1,2,\ldots,N-1,$$

$$\alpha_{n+1/2} = \frac{\gamma}{\gamma-1}\frac{\pi_w^2}{\pi_T}\frac{\rho f}{r^2}\left(2W\dot{W} - W^2\frac{\dot{U}}{U}\right)\Bigg|_{\delta_{n+1/2}},$$

and determine $p_0(z)$ by integrating the equation

$$\dot{p}_0\sum_{n=0}^{N-1} g_{n+1/2} + \sum_{n=0}^{N-1}\dot{p}^w g_{n+1/2} = R\dot{R} - \sum_{n=0}^{N-1}\left(\pi_g\frac{f_{n+1/2}}{U^2} + \frac{R_T}{\rho UT} + \frac{f_{n+1/2}}{\rho UT}\pi_w^2\frac{G_T}{\pi_T} - \frac{R_u}{\rho U^2}\right), \quad (7)$$

$$g_{n+1/2} = -\frac{f_{n+1/2}}{\gamma(p^w + p_0)} + \left(1 - \frac{1}{\gamma}\right)\pi_T f_{n+1/2}\frac{1}{\rho U^2}.$$

Expression (7) is obtained by summing equations (5) for all grid points with the account of equality

$$\sum_{n=0}^{N-1} f_{n+1/2} = \frac{1}{2}R^2(z).$$

Density on each line is calculated by the formula

$$\rho(z,\delta_{n+1/2}) = \frac{p(z,\delta_{n+1/2})}{T(z,\delta_{n+1/2})}. \quad (8)$$

Equations (5)–(7) contain the dissipative terms

$$R_u = [r\mu\frac{\partial U}{\partial r}], \quad R_w = [r\mu\frac{\partial W}{\partial r}], \quad R_E = \frac{1}{\sigma_\alpha}[r\mu\frac{\partial E}{\partial r}],$$

$$R_T = \frac{1}{\sigma}[r\mu\frac{\partial T}{\partial r}] + \frac{1}{\pi_T}\left([r\mu U\frac{\partial U}{\partial r}] - U[r\mu\frac{\partial U}{\partial r}]\right), \quad (9)$$

$$G_T = \mu\left(\frac{\partial W}{\partial r} - \frac{W}{r}\right)^2 + \frac{\rho V W^2}{r}, \quad G_w = -\frac{\rho V W}{r} - \mu\frac{W}{r^2}.$$

where the quantity in brackets means $[Q] = Q_{n+1} - Q_n$.

The boundary conditions on the flow axis for the unknown quantities $A = \{U, T, E, W\}$ of system (5) follow from the symmetry conditions. In the wall region we assume that the boundary layer is thin and the uniform flow zone extends to the wall. Therefore, we have

$$\frac{\partial A}{\partial r} = 0 \text{ for } \delta = 0,\ \delta = R(z). \quad (10)$$

To determine the derivatives with respect to r in expressions (10), we use the following algorithm. We will assume that the unknown functions $A' = \partial A/\partial r$, where $A = \{U,\ W, T, E\}$, on the segments $\Delta_n = \delta_n - \delta_{n-1}$ have the form

$$A' = a_n + b_n\eta_n, \quad \eta_n = \frac{r - \delta_{n-1}}{\delta_n - \delta_{n-1}}, \quad r \in [\delta_{n-1}, \delta_n], \quad \eta_n \in [0, 1]. \quad (11)$$

Obviously, $a_n = A'_{n-1}$, $a_n + b_n = A'_n$, $b_n = A'_n - A'_{n-1}$. After integration, the expression (11) takes the form

$$A(\eta_n) = A_{n-1} + \Delta_n(a_n\eta_n + \frac{b_n\eta_n^2}{2}), \quad \eta_n \in [0, 1], \quad n = 1, 2, \ldots, N. \quad (12)$$

Substituting in (12) the values $\eta_n = 1$ and $\eta_n = 0.5$, we obtain

$$A_n = A_{n-1} + \frac{1}{2}\Delta_n(A'_{n-1} + A'_n), \quad n = 0, 1, 2, \ldots, N,$$

$$A_{n-1/2} = A_{n-1} + \frac{1}{8}\Delta_n(3A'_{n-1} + A'_n), \quad n = 1, 2, \ldots, N.$$

Excluding unknowns in integer nodes, we obtain a system of three-point equations with respect to unknowns A'_n:

$$\Delta_n A'_{n-1} + 3(\Delta_n + \Delta_{n+1})A'_n + \Delta_{n+1}A'_{n+1} = 8(A_{n+1/2} - A_{n-1/2}), \quad n = 1, 2, \ldots, N-1. \quad (13)$$

The values A'_0 и A'_N for the flow in a channel, in accordance with expression (10), are assumed to be zero. The system of equations (13) is effectively solved by the sweep method.

The system of equations (5)–(9) must be closed by specifying a turbulence model. We will use an algebraic model based on the Prandtl mixing length l_i which for swirling flows is linked with the turbulent viscosity ν_{ti} as follows:

$$l_i^2 = \nu_{ti}\left\{\left(\frac{\partial V_z}{\partial r}\right)^2 + \left[r\frac{\partial}{\partial r}\left(\frac{V_\varphi}{r}\right)\right]^2\right\}^{-1/2}, \quad (14)$$

where the subscript i has the values z for the axial and φ for the azimuthal direction. The dimensionless empirical constants were taken to be equal to $l_z / R_0 = 0.068$, $l_\varphi / R_0 = 0.034$. These values were obtained experimentally [16] for swirling flows of the gas-curtain type. Investigations presented in [16] showed that the numerical results based on these values of l_z and l_φ are in good agreement with the experimental data.

The system (5), (7) from $5N+1$ differential equations is solved numerically by the Runge-Kutta method. In most calculations we used $N = 50$.

3. Results and Discussion

This method of calculating for unswirled flows was tested using numerical solutions [26] obtained on the basis of the complete Navier-Stokes equations and the differential $k - \varepsilon$ turbulence model. The velocity distribution over the inlet cross-section $z = 0$ was specified as follows:

$$U = U_1 = 1, \quad 0 \le r \le r_1; \qquad U = U_2 = 0.1, \quad r_1 < r \le 1, \quad (15)$$

where $r_1 = 0.12$. The velocity profiles obtained from a numerical solution of problem (5), (7)–(10) with conditions (15) are presented in Figure 1,a. The velocity distributions are only slightly different from the results of [26].

For swirled flows, this method was tested using experimental data [27] on the mixing of two coaxial isothermal flows in the absence of admixtures. The flow in an annular channel $(0.5 \le r \le 1)$, which the inner flow entered pre-swirled and the outer flow unswirled, was considered. At $z = 0$, the velocity distribution was specified as follows:

$$U = 1.2,\ W = 1,\ 0.5 \le r \le 0.75; \quad U = 0.8568,\ W = 0,\ 0.75 \le r \le 1. \quad (16)$$

Here, U is divided by the mean-flow velocity and W by the maximum azimuthal velocity at the channel inlet. In this case, the inner to outer mass flow-rate ratio was equal to unity and the swirl parameter $\pi_w = 0.833$.

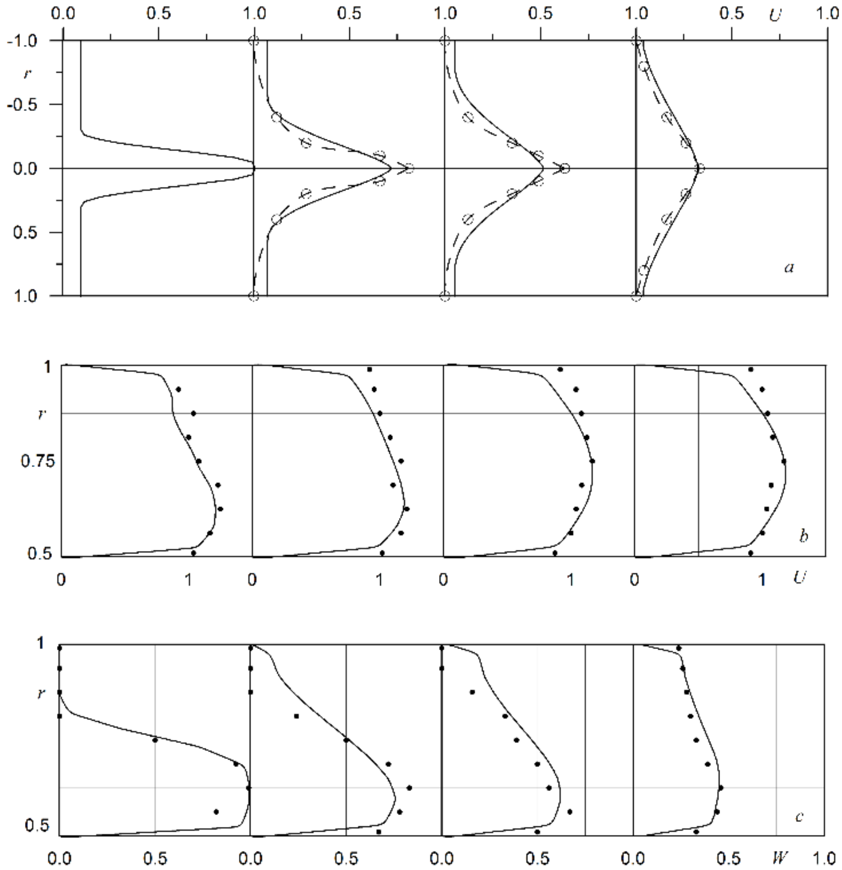

Figure 1. Comparison of the calculated profiles (solid lines) for unswirled flows with the data of [26] (dashed lines) for $z = 0.1,\ 2,\ 3,\ 4$ (a) and for swirled flows with experiments [27] for $z = 0.06,\ 1.56,\ 3.06,\ 4.56$ (b)

The profiles of the axial and azimuthal velocities found from the numerical solution of problem (5), (7)–(10) with conditions (16) are presented in Figure 1,b. The data of experiments [27] are indicated by the points. A comparison shows fairly good agreement between theory and experiment and confirms the possibility of using the mathematical model to describe the process of mixing of two turbulent flows in the presence of swirling.

The main part of the calculations was performed for the following distributions over the inlet cross-section $z = 0$:

$$\begin{aligned} &U(r) = U_1 = 1,\ W(r) = W_1(r),\ T(r) = T_1 = 1,\ E(r) = E_1 = 1,\ 0 \le r \le r_1, \\ &U(r) = U_2, \quad W(r) = W_2, \quad T(r) = T_2, \quad E(r) = E_2, \quad r_1 < r \le 1, \end{aligned} \tag{17}$$

where $r_1 = R_1 / R_0$. The solution domain was determined by the length $z_0 = 2.2 R_0$ and the lateral surface was either assumed to be cylindrical $R_0 = 1$ or specified by the equation $R(z) = 1 - 0.15 z$.

For high-rise structures of the kind described, typical values of the parameters are as follows: base diameter 90 m, height 100 m, flow-rate of the flue gases in the inner flow 300 m^3/s at a gas temperature of 120^{0}C, and air flow-rate in the outer flow 5000 m^3/s at a gas temperature of 70^{0}C. Therefore, in the calculations the values of the dimensionless quantities were taken to be equal to

$$U_2 = 0.05 - 0.4,\ T_2 = 0.5 - 0.9,\ E_2 = 0 - 1,$$

$$\sigma = 0.72,\ \pi_g = 6.45,\ \pi_T = 5754,\ \pi_w = 0 - 1.35.$$

In investigating the process of mixing of two hot gases, our attention was focused on the effect of the inner jet swirl on the flow parameters. In the axial velocity distribution (Figure 2) an important effect can be detected: swirling of the inner jet leads to a deceleration of the flow. When the swirl $\pi_w > 1.35$, we were unable to carry out further calculations on the basis of the parabolized equations, and the complete Navier-Stokes equations had to be used.

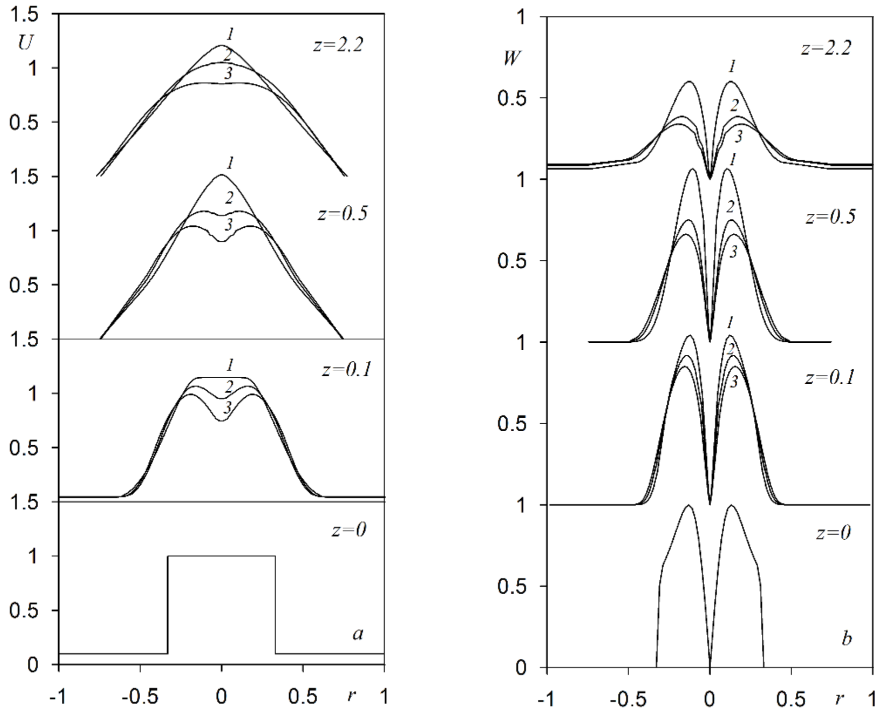

Figure 2. Axial and azimuthal velocities profiles for $\pi_w = 0,\ 1,\ 1.3$ (a), $\pi_w = 0.2,\ 1,\ 1.3$ (b) (curves 1-3) in sections z=const

Another effect discernible in the axial velocity distribution is that associated with jet acceleration under the action of a lift force (Figure 3,a). In the distribution of the azimuthal velocity the most important property is as follows. For a weak swirl $\pi_W = 0.2$, under the action of the lift force produced by the temperature difference the flow rotation velocity increases The effects of flow acceleration and increase in the rotation velocity on an initial segment of the channel are manifested even more clearly with increase in the inner gas jet to outer air flow temperature ratio T_1 / T_2 (Figure 3,b).

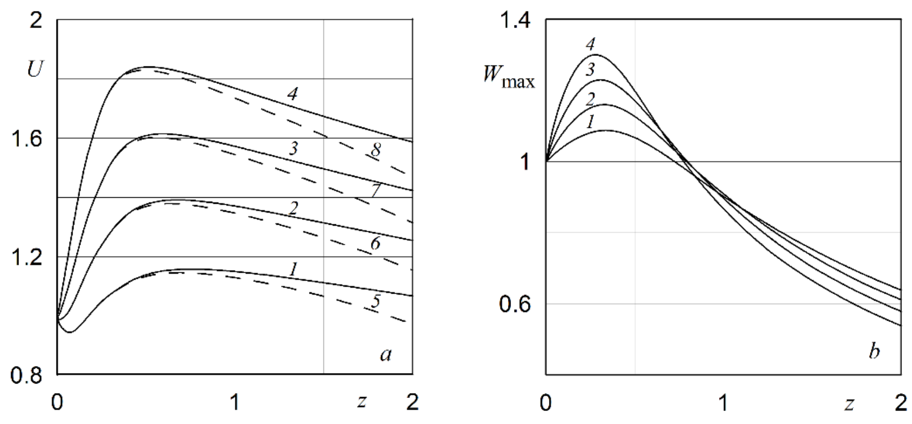

Figure 3. Distributions of the axial velocity over the axis $r = 0$ for $\pi_w = 1$ (a) and the maximum azimuthal velocity (b) for $\pi_w = 0.2,\ T_2 = 0.8,\ 0.7,\ 0.6,\ 0.5$ (curves1–4), $R(z) = 1 - 0.15z$ (curves 5–8)

A favorable effect can be detected in the variation of the admixture concentration along the flow axis, which is almost halved at the channel outlet as compared with its initial value. With increase in the swirl, due to efficient mixing of the flows, the admixture concentration falls closer to the inlet cross-section. At the stack mouth the concentration depends only slightly on the initial swirl of the inner jet. In all cases, the temperature decreases with increase in z (Figure 4).

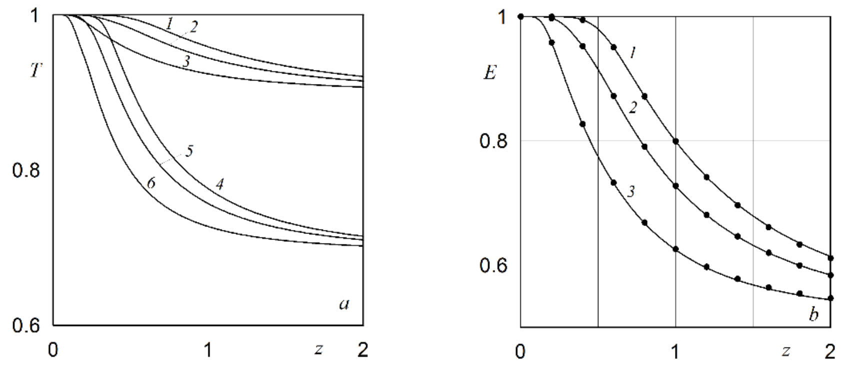

Figure 4. Distributions of the temperature (a) and the concentration (b) over the axis $r = 0$ $\pi_w = 0.2,\ 0.5,\ 1.3$, $T_2 = 0.8$ (curves1–3) and $T_2 = 0.5$ (curves1–4)

A graphic representation of the flow pattern inside the ventilation pipe can be seen in Figure 5. The streamlines converge fairly rapidly toward the center with increase in the distance z. This information can be used in profiling the stack walls in order to reduce the dimensions of the structure, cut costs, and make the structure more stable.

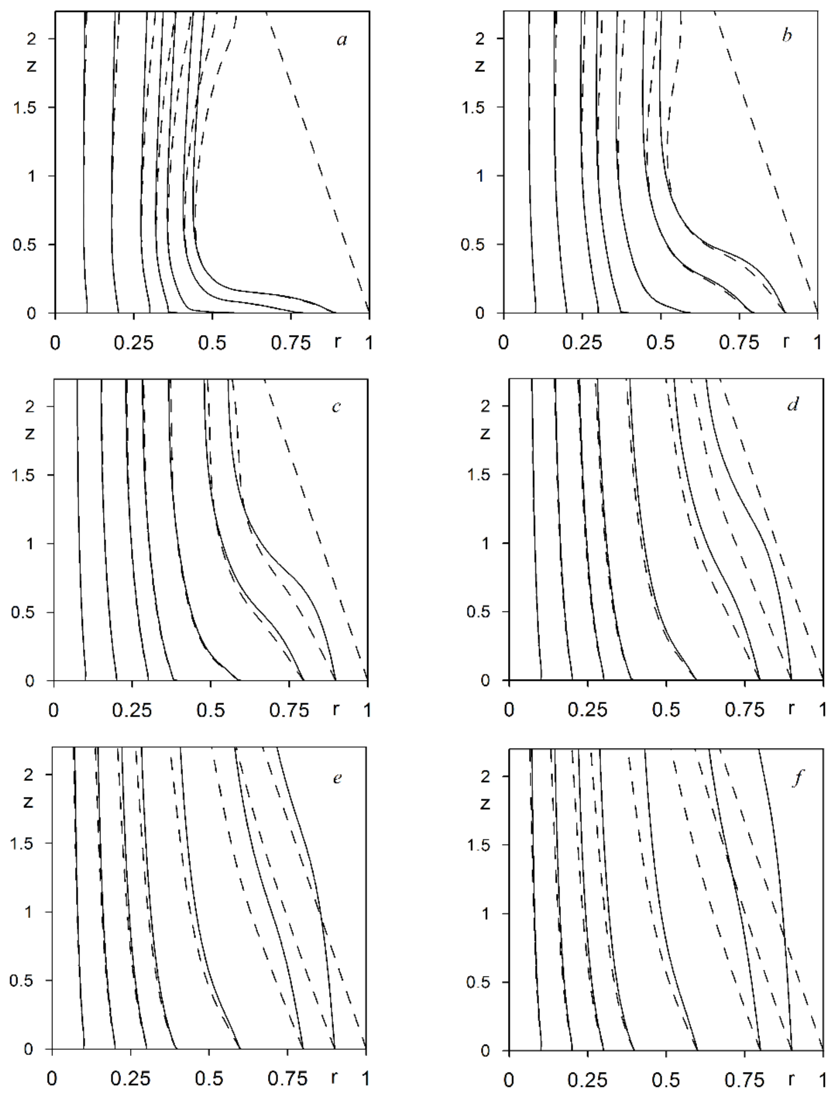

Figure 5. Streamlines for $\pi_w = 1$, $r_1 = 0.33$, $T_2 = 0.8$, $U_2 = 0.1,\ 0.2,\ 0.3,\ 0.4,\ 0.5,\ 0.6$ (a-e), $R(z) = 1$ – solid lines, $R(z) = 1 - 0.15z$ – dashed lines

Obtained critical swirl flow ratio $\pi_W = 1.35$ can be compared with calculation results based on complete Navier-Stokes equations system. Let us define two characteristic values: r_* – vortex core radius over the inlet cross-section $z = 0$ (distance from the axis, at which azimuthal velocity W has maximum value), and U_* – flow axial velocity at $r = r_*$, $z = 0$. Then we introduce dimensionless parameters that determine viscous swirling flow

$$\mathrm{Re} = \frac{U_* r_*}{\nu}, \qquad \mathrm{Ro} = \frac{U_*}{r_* \omega}. \tag{18}$$

where ω is flow angular velocity at $r \to 0$. Rossby number Ro is inversely proportional to swirl parameter. Critical Rossby number value dependence from Reynolds number, which results in axial recirculation zone formation in a flow, is represented in Figure 6. Solid line corresponds to swirling flow calculation results in cylindrical channel with impermeable walls, obtained on the basis of complete Navier-Stokes equations system solution [10]. Data of works [28], [29], recalculated by formula (18), are marked with circles and rhombs. Critical swirl ratio $\pi_W = 1.35$, obtained by means of parabolized Navier-Stokes equations (5), is represented in Figure 6 by dashed line and corresponds to $\mathrm{Ro} = 0.43$.

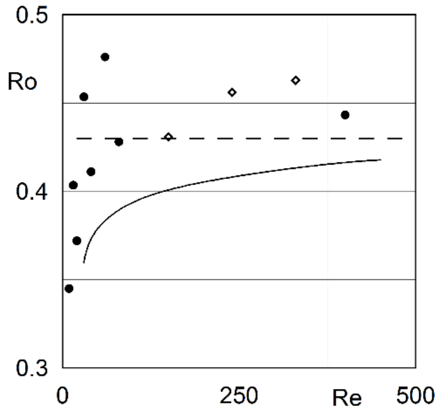

Figure 6. Critical values of Rossby numbers

4. Conclusions

1. Mathematical model is developed and boundary value problem is formulated for studying the process of turbulent mixing of flue gas and heated air in combined high-rise structure.

2. An efficient method of solving the parabolized Navier-Stokes equations, which reduces the initial system to ordinary differential equations written on the streamlines, is proposed.

3. Algorithm and computer calculation program have been developed. Verification of the program was carried out.

4. All fundamental flow characteristics have been calculated: velocity profiles, temperature distribution and harmful impurities concentration distribution for different flow cross-sections. The results of calculations showed the following important features of the flows. Initial inner swirl flow serves to mixing process intensification. Weak and moderate swirling of the inner flue gas, which causes additional rotation in flow, is of special interest for stack flue stream. Strong swirl results in abrupt flow deceleration and possible formation of an axial reverse-flow zone. This effect is undesirable.

5. The positive effect discernible in the axial velocity distribution is that associated with jet acceleration under the action of a lift force. The flow swirl promotes a more rapid temperature equalization over the channel length. In the cases considered, the admixture concentration at the channel outlet decreases by a factor of 2-4.

6. Streamline flow patterns have been obtained. These patterns can be used for smokestack wall profiling to shorten structure dimensions and reduce construction costs. The results of this work allow us to seek the optimal flow regimes in high-rise structures for ejecting pollutant-containing smokes and gases into the atmosphere with a view to minimizing environmental damage.

References

1. Isaev, S.A., Vatin, N.I., Baranov, P.A., Sudakov, A.G., Usachov, A.Ye., Yegorov, V.V. Razrabotka i verifikatsiya mnogoblochnykh vychislitelnykh tekhnologiy dlya resheniya nestatsionarnykh zadach stroitelnoy aerodinamiki vysotnykh zdaniy v ramkakh podkhoda URANS [Development and verification of multiblock computational technologies for solution of unsteady problems of high building aerodynamics in the framework of URANS approach]. Magazine of Civil Engineering. 2013. No. 1(36). Pp. 103–109.
2. Isaev, S.A., Vatin, N.I., Lebiga, V.A., Zinoviev, V.N., Chang, K.-C., Miau, J.-J. Zadachi i metody chislennogo i fizicheskogo issledovaniya aerodinamiki vysotnykh zdaniy v pribrezhnoy zone «more-susha» [Problems and methods of numerical and experimental investigation of high rise constructions' aerodynamics in the coastal region "sea-land"]. Magazine of Civil Engineering. 2013. No. 2(37). Pp. 54–61.
3. Mikhaylova, M.K., Dalinchuk, V.S., Bushmanova, A.V., Dobrogorskaya, L.V. Proyektirovaniye, stroitelstvo i ekspluatatsiya vysotnykh zdaniy s uchetom aerodinamicheskikh aspektov [Design, construction and operation of high-rise buildings, taking into account the aerodynamic aspects]. Construction of Unique Buildings and Structures. 2016. No. 10(49). Pp. 59–74. (rus)
4. Lucca-Negro, O., O'Doherty, T. Vortex breakdown: a review. Progress in Energy and Combustion Science. 2001. Vol. 27. Pp. 431–481.
5. Escudier, M.P. Vortex breakdown: observations and explanations. Progress in Aerospace Sciences. 1988. Vol. 25. No. 2. Pp. 189–229.
6. Wang, Y., Xingjian Wang, X., Yang, V. Evolution and transition mechanisms of internal swirling flows with tangential entry. Physics of Fluids. 2018. Vol. 30. 013601.
7. Ogus, G., Baelmans, M., Vanierschot, M. On the flow structures and hysteresis of laminar swirling jets. Physics of Fluids. 2016. Vol. 28. 123604.
8. Akhmetov, V.K., Medvedev, Yu.V., Shkadov, V.Ya. Effect of the inertia terms in sliding bearing calculation problems. Fluid Dynamics. 2014. Vol. 49. No. 3. Pp. 320–329.
9. Orlandi, P. Two-dimensional and three-dimensional direct numerical simulation of co-rotating vortices. Physics of Fluids. 2007. Vol. 19. 013101.
10. Akhmetov, V.K., Shkadov, V.Ya. Ustoychivost svobodnykh i ogranichennykh zakruchennykh techeniy s zonami retsirkulyatsii [Stability of free and bounded swirling flows with recirculation zones]. Inzhenernaya fizika. 2008. No. 6. Pp. 6–13. (rus)
11. Oberleithner, K., Paschereit, C., Seele, R., Wygnanski, T. Formation of turbulent vortex breakdown: intermittency, criticality, and global instability. AIAA Journal. 2012. Vol. 50. No. 7. Pp. 1437–1452.
12. Escudier, M.P., Nickson, A.K., Poole, R.J. Influence of outlet geometry on strongly swirling turbulent flow through a circular tube. Physics of Fluids. 2006. Vol. 18. 125103.
13. Mergheni, M.A., Riahi, Z., Sautet, J.C., Nasrallah, S.B. Swirl effects on dynamics characteristics of a coaxial jet. Thermal Science. 2017. Vol. 21. No. 6. Pp. 2543–2552.
14. Alekseyenko, S.V., Shtork, S.I., Yusupov, R.R. Izotermicheskoye modelirovaniye aerodinamicheskoy struktury zakruchennogo techeniya v dvukhstupenchatom gorelochnom ustroystve [Isothermal modeling of aerodynamic structure of the swirling flow in two-stage vortex burner device]. Izvestiya Tomskogo politekhnicheskogo universiteta. Inzhiniring georesursov. 2017. Vol. 328. No. 7. Pp. 6–18. (rus)
15. Mansouri, Z., Aouissi, M., Boushaki, T. A numerical study of swirl effects on the flow and flame dynamics in a lean

Литература

1. Исаев С.А., Ватин Н.И., Баранов П.А., Судаков А.Г., Усачов А.Е., Егоров В.В. Разработка и верификация многоблочных вычислительных технологий для решения нестационарных задач строительной аэродинамики высотных зданий в рамках подхода URANS // Инженерно-строительный журнал. 2013. № 1(36). С. 103–109.
2. Исаев С.А., Ватин Н.И., Лебига В.А., Зиновьев В.Н., Кэ-Чин Чан, Цзюн-Цзи Мяу. Задачи и методы численного и физического исследования аэродинамики высотных зданий в прибрежной зоне «море-суша» // Инженерно-строительный журнал. 2013. № 2(37). С. 54–61.
3. Михайлова М.К., Далинчук В.С., Бушманова А.В., Доброгорская Л.В. Проектирование, строительство и эксплуатация высотных зданий с учетом аэродинамических аспектов // Строительство уникальных зданий и сооружений. 2016. № 10(49). С. 59–74.
4. Lucca-Negro O., O'Doherty T. Vortex breakdown: a review // Progress in Energy and Combustion Science. 2001. Vol. 27. Pp. 431–481.
5. Escudier M.P. Vortex breakdown: observations and explanations // Progress in Aerospace Sciences. 1988. Vol. 25. № 2. Pp. 189–229.
6. Wang Y., Xingjian Wang X., Yang V. Evolution and transition mechanisms of internal swirling flows with tangential entry // Physics of Fluids. 2018. Vol. 30. 013601.
7. Ogus G., Baelmans M., Vanierschot M. On the flow structures and hysteresis of laminar swirling jets // Physics of Fluids. 2016. Vol. 28. 123604.
8. Ахметов В.К., Медведев Ю.В., Шкадов В.Я. Влияние инерционных членов в задачах расчета опор скольжения // Известия РАН. Механика жидкости и газа. 2014. № 3. С. 26–36.
9. Orlandi P. Two-dimensional and three-dimensional direct numerical simulation of co-rotating vortices // Physics of Fluids. 2007. Vol. 19. 013101.
10. Ахметов В.К., Шкадов В.Я. Устойчивость свободных и ограниченных закрученных течений с зонами рециркуляции // Инженерная физика. 2008. № 6. С. 6–13.
11. Oberleithner K., Paschereit C., Seele R., Wygnanski T. Formation of turbulent vortex breakdown: intermittency, criticality, and global instability // AIAA Journal. 2012. Vol. 50. № 7. Pp. 1437–1452.
12. Escudier M.P., Nickson A.K., Poole R.J. Influence of outlet geometry on strongly swirling turbulent flow through a circular tube // Physics of Fluids. 2006. Vol. 18. 125103.
13. Mergheni M.A., Riahi Z., Sautet J.C., Nasrallah S.B. Swirl effects on dynamics characteristics of a coaxial jet // Thermal Science. 2017. Vol. 21. № 6. Pp. 2543–2552.
14. Алексеенко С.В., Шторк С.И., Юсупов Р.Р. Изотермическое моделирование аэродинамической структуры закрученного течения в двухступенчатом горелочном устройстве // Известия Томского политехнического университета. Инжиниринг георесурсов. 2017. Т. 328. № 7. С. 6–18.
15. Mansouri Z., Aouissi M., Boushaki T. A numerical study of swirl effects on the flow and flame dynamics in a lean premixed combustor // International journal of heat and technology. 2016. Vol. 34. № 2. Pp. 227–235.
16. Кутателадзе С.С., Волчков Э.П., Терехов В.И. Аэродинамика и тепломассообмен в ограниченных вихревых потоках. Новосибирск: Институт теплофизики, 1987. 283 с.
17. Lu X., Wang S., Sung H.G., Hiseh S.Y., Yang V. Large-eddy simulation of turbulent swirling flow injected into

premixed combustor. International journal of heat and technology. 2016. Vol. 34. No. 2. Pp. 227–235.

16. Kutateladze, S.S., Volchkov, E.P., Terekhov, V.I. Aerodinamika i teplomassoobmen v ogranichennykh vikhrevykh potokakh [Aerodynamics and heat and mass exchange in bounded vortex flows]. Novosibirsk: Institut teplofiziki, 1987. 283 p. (rus)
17. Lu, X., Wang, S., Sung, H.G., Hiseh, S.Y., Yang, V. Large-eddy simulation of turbulent swirling flow injected into dump chamber. Journal of Fluid Mechanics. 2005. Vol. 527. Pp. 171–195.
18. Wang, P., Bai, X.S., Wessman, M., Klingmann, J. Large eddy simulation and experimental studies of a confined turbulent swirling flow. Physics of Fluids. 2004. Vol. 16. No. 9. Pp. 3306–3324.
19. Rukes, L., Sieber, M., Paschereit, C., Oberleithner, K. The impact of heating the breakdown bubble on the global mode of a swirling jet: experiments and linear stability analysis. Physics of Fluids. 2016. Vol. 28. 104102.
20. Gallaire, F., Ruith, M., Meiburg, E., Chomaz, J., Huerre, P. Spiral vortex breakdown as a global mode. Journal of Fluid Mechanics. 2006. Vol. 549. Pp. 71–80.
21. Blanco-Rodríguez, F.J., Rodríguez-García, J.O., Parras, L., del Pino, C. Optimal response of Batchelor vortex. Physics of Fluids. 2017. Vol. 29. 064108.
22. Yadav, N.K., Samanta, A. The stability of compressible swirling pipe flows with density stratification. Journal of Fluid Mechanics. 2017. Vol. 823. Pp. 689–715.
23. Delbende, I., Rossi, M. Nonlinear evolution of a swirling jet instability. Physics of Fluids. 2005. Vol. 17. 044103.
24. Akhmetov, V.K. Gidrodinamicheskaya ustoychivost kontrvikhrevykh techeniy [Hydrodynamic stability of counter vortex flows]. Gidrotekhnicheskoye stroitelstvo. 2018. No. 2. Pp. 13–18. (rus)
25. Shkadov, V.Ya. Nekotoryye metody i zadachi teorii gidrodinamicheskoy ustoychivosti [Some methods and problems of hydrodynamic stability theory]. Trudy instituta mekhaniki MGU. 1973. No. 25. 160 p. (rus)
26. Khodadadi, J.M., Vlachos, N.S. An experimental investigation of confined coaxial turbulent jets. AIAA. 1987. Paper No. 1380. 11 p.
27. Mattingly, J.D., Oates, G.C. An experimental investigation of the mixing of co-annular swirling flows. AIAA. 1985. Paper No. 186. 9 p.
28. Kopecky, R.M., Torrance, K.E. Initiation and structure of axisymmetric eddies in a rotating stream. Computers and Fluids. 1973. Vol. 1. No. 3. Pp. 289–300.
29. Uchida, S., Nakamura, Y., Suehiro, F. Numerical calculations of swirling flows for vortex breakdown. Transactions of the Japan Society for Aeronautical and Space Sciences. 1981. Vol. 24. No. 63. Pp. 17–25.

dump chamber // Journal of Fluid Mechanics. 2005. Vol. 527. Pp. 171–195.

18. Wang P., Bai X.S., Wessman M., Klingmann J. Large eddy simulation and experimental studies of a confined turbulent swirling flow // Physics of Fluids. 2004. Vol. 16. № 9. Pp. 3306–3324.
19. Rukes L., Sieber M., Paschereit C., Oberleithner K. The impact of heating the breakdown bubble on the global mode of a swirling jet: experiments and linear stability analysis // Physics of Fluids. 2016. Vol. 28. 104102.
20. Gallaire F., Ruith M., Meiburg E., Chomaz J., Huerre P. Spiral vortex breakdown as a global mode // Journal of Fluid Mechanics. 2006. Vol. 549. Pp. 71–80.
21. Blanco-Rodríguez F.J., Rodríguez-García J.O., Parras L., del Pino C. Optimal response of Batchelor vortex // Physics of Fluids. 2017. Vol. 29. 064108.
22. Yadav N.K., Samanta A. The stability of compressible swirling pipe flows with density stratification // Journal of Fluid Mechanics. 2017. Vol. 823. Pp. 689–715.
23. Delbende I., Rossi M. Nonlinear evolution of a swirling jet instability // Physics of Fluids. 2005. Vol. 17. 044103.
24. Ахметов В.К. Гидродинамическая устойчивость контрвихревых течений // Гидротехническое строительство. 2018. № 2. С. 13–18.
25. Шкадов В.Я. Некоторые методы и задачи теории гидродинамической устойчивости // Труды института механики МГУ. 1973. № 25. 160 с.
26. Khodadadi J.M., Vlachos N.S. An experimental investigation of confined coaxial turbulent jets // AIAA. 1987. Paper № 1380. 11 p.
27. Mattingly J.D., Oates G.C. An experimental investigation of the mixing of co-annular swirling flows // AIAA. 1985. Paper № 186. 9 p.
28. Kopecky R.M., Torrance K.E. Initiation and structure of axisymmetric eddies in a rotating stream // Computers and Fluids. 1973. Vol. 1. № 3. Pp. 289–300.
29. Uchida S., Nakamura Y., Suehiro F. Numerical calculations of swirling flows for vortex breakdown // Transactions of the Japan Society for Aeronautical and Space Sciences. 1981. Vol. 24. № 63. Pp. 17–25.

Vadim Akhmetov,*
+7(916)812-46-50; vadim.akhmetov@gmail.com

Viktor Shkadov,
+7(495)939-39-49; vshkadov@yandex.ru

Pavel Konon,
+375(29)505-09-03; kononp@tut.by

Вадим Каюмович Ахметов,*
+7(916)812-46-50;
эл. почта: vadim.akhmetov@gmail.com

Виктор Яковлевич Шкадов,
+7(495)939-39-49;
эл. почта: vshkadov@yandex.ru

Павел Николаевич Конон,
+375(29)505-09-03; эл. почта: kononp@tut.by

Akhmetov, V.K., Shkadov, V.Ya., Konon, P.N. Aerodynamics of building structures for flue gas removal. Magazine of Civil Engineering. 2018. 81(5). Pp. 81–92. doi: 10.18720/MCE.81.9.

doi: 10.18720/MCE.81.10

Composition and rheological characteristics of bitumen in short-term and long-term aging

Состав и реологические характеристики битума при кратковременном и длительном старений

B.B. Teltayev*,
Kazakhstan Highway Research Institute, Almaty, Republic of Kazakhstan
C.O. Rossi,
University of Calabria, Cozenza, Calabria, Italy
S.Zh. *Ashimova*
Kazakhstan Highway Research Institute, Almaty, Republic of Kazakhstan

Д-р техн. наук, президент Б.Б. Телтаев*,
Казахстанский дорожный научно-исследовательский институт, Алматы, Республика Казахстан
PhD, профессор Ч.О. Росси,
Университет Калабрии, г. Козенца, Калабрия, Италия
инженер С.Ж. Ашимова
Казахстанский дорожный научно-исследовательский институт, Алматы, Республика Казахстан

Key words: blown bitumen; short-term aging; long-term aging; dynamic shear rheometer; bending beam rheometer; complex shear modulus; phase angle; stiffness

Ключевые слова: окисленный битум; кратковременное старение; длительное старение; динамический сдвиговой реометр; реометр с изгибаемой балкой; комплексный сдвиговой модуль; фазовый угол; жесткость

Abstract. This paper investigates the impact of sequential short-term and long-term aging of blown bitumen of the grade BND 70/100 on its mechanical characteristics in the temperature interval from 76°C to -36 °C. Group chemical composition of the bitumen has been determined by the method of liquid adsorption chromatography by the chromatograph “Gradient M”. Short-term aging has been performed in the vertical rolling thin film oven (RTFOT) under the standard of AASHTO T 240-08, and the long-term aging - in the pressure aging vessel (PAV) under the standard of ASTM D 6521-08. Mechanical characteristics of the bitumen are complex shear modulus G^* and phase angle δ at the mean and high temperatures (from 4 °C to 76 °C) have been measured by dynamic shear rheometer (DSR) under the standard of AASHTO T 315-08. Bitumen stiffness S at low temperatures (from -24 °C to -36 °C) has been measured by bending beam rheometer (BBR) under the standard of AASHTO T 313-08. It has been determined that during short-term aging the content of oils in the bitumen has been decreased for 1.5 %, and the content of asphaltenes has been increased for 2 %. After the long-term aging, performed after the short-term aging, the content of oils in the bitumen has been decreased for 7 %, and the content of asphaltenes has been increased for 6.3 %. The content of resins in the bitumen remains practically constant at both types of aging. At the mean and high temperatures the short-term and long-term aging increase the complex shear modulus up to 2 and 7 200 times respectively and decrease the phase angle at average for 4-6° and 8-10° respectively. At low temperatures the short-term aging and long-term aging increase the bitumen stiffness in 1.5 and 2.5 times respectively.

Аннотация. В настоящей работе исследовано влияние последовательных кратковременного и длительного старений окисленного битума марки БНД 70/100 на его механические характеристики в температурном интервале от 76 °C до -36 °C. Групповой химический состав битума был определен методом жидкостно-адсорбционной хроматографии на хроматографе «Градиент М». Кратковременное старение было осуществлено в вертикальной тонкопленочной вращающейся печи (RTFOT) по стандарту AASHTO T 240-08, а длительное старение - в сосуде высокого давления и температуры (PAV) по стандарту ASTM D 6521-08. Механические характеристики битума – комплексный сдвиговой модуль G* и фазовый угол δ при средних и высоких температурах (от 4 °C до 76 °C) были измерены динамическим сдвиговым реометром (DSR) по стандарту AASHTO T 315-08. Жесткость битума S при низких температурах (от -24 °C до -36 °C) была измерена реометром с изгибаемой балкой (BBR) по стандарту AASHTO T 313-08. Установлено, что при кратковременном старении содержание масел в битуме уменьшается на 1,5 %, а содержание

Телтаев Б.Б., Росси Ч.О., Ашимова С.Ж. Состав и реологические характеристики битума при кратковременном и длительном старений // Инженерно-строительный журнал. 2018. № 5(81). С. 93–101.

асфальтенов увеличивается на 2 %. После длительного старения, осуществленного после кратковременного старения, содержание масел в битуме уменьшается на 7 %, а содержание асфальтенов увеличивается на 6,3 %. При обоих видах старения содержание смол в битуме остается практически постоянным. При средних и высоких температурах кратковременное и длительное старения повышают комплексный сдвиговой модуль до 2 и 7 200 раз соответственно и уменьшают фазовый угол в среднем на 4-6° и 8-10° соответственно. При низких температурах кратковременное и длительное старения повышают жесткость битума в 1,5 и 2,5 раза соответственно.

1. Introduction

It is well-known that bitumens in the conditions of their storage, preparation of an asphalt concrete mix, its transportation, laying, and compaction and during operation of an asphalt concrete pavement are subject to aging [1–3]. Due to aging bitumens usually become more viscous and more brittle at low temperatures. Therefore, the quantitative evaluation of the impact of bitumen aging on their properties is important for road engineering.

At present many countries of the world use widely three methods of artificial aging for bitumens. The first two of them [4] imitate the aging of a bitumen during preparation of an asphalt concrete mix, its transportation, laying, compaction, and the third method models the aging of a bitumen during operation of an asphalt concrete pavement. The latter two methods have been developed quite recently and included into the known American technical system Superpave [5].

The review of the published works [6–13] has shown that at present the intensive investigation is performed for the impact of bitumen aging on the properties of the bitumens themselves [8–10] and asphalt concretes with their use [11–15]. Meanwhile, practically always bitumen aging has been performed under the methods, included into Superpave. Practically all investigations are experimental ones and the impact of short-term and long-term aging has been evaluated in them on the rheological properties [5, 8–12], structural changes [9], standard characteristics [11, 12] of bitumens and asphalt concretes [9–13].

This paper investigates and gives the quantitative evaluation of the impact of short-term and long-term aging of the blown bitumen of grade BND 70/100 on its group chemical composition and mechanical (rheological) characteristics within the temperature interval from 76 °C to -36 °C by dynamic shear rheomoter (DSR) and bending beam rheometer (BBR).

2. Materials and Methods

2.1. Bitumen

Bitumen of grade BND 70/100 has been selected for experimental research of its rheological characteristics at various temperatures in three conditions: non-aged, after short-term aging (RTFOT) and after long-term aging (RTFOT+PAV). Bitumen has been produced at Pavlodar petrochemical plant from crude oil of Western Siberia (Russia) by method of direct oxidation. Its characteristics satisfy the requirements of the standard of Kazakhstan ST RK 1373-2013 [16]. Grade of bitumen under Superpave: PG 64-40 [5]. The main standard characteristics of the bitumen in the initial condition are shown in the Table 1.

Table 1. Main standard characteristics of bitumen in initial condition

Indicator	Measurement unit	Requirements of ST RK 1373-2013	Values
Penetration depth of the needle, 25°C, l00 g, 5s	0.1 mm	70–100	75
Penetration Index	-	-1.0...+1.0	-0.87
Ductility at the temperature of:			
25°C		≥75	118
0°C		≥3.8	5.2
Softening point	°C	≥ 45	47.5
Fraas brittle point	°C	≤ -20	-28.5
Dynamic viscosity at 60°C	Pa·s	≥145	229
Kinematic viscosity at 135 °C	mm^2/s	≥250	428

2.2. Short-term aging

Short-term aging of the bitumen in the vertical rolling thin film oven have been performed under the standard of AASHTO T 240-08, which models the bitumen aging during preparing of an asphalt concrete mix, its transportation, laying and compaction. The samples of the bitumen were in the oven at the temperature of 150 °C for 75 minutes.

2.3. Long-term aging

Long-term aging of the bitumen in the special pressure aging vessel has been performed under the standard of ASTM D 6521-08, which models the bitumen aging during operation of the asphalt concrete pavement. The samples of the bitumen, after the short-term aging, were in the vessel under the pressure of 2070 kPa and at the temperature of 100 °C for 20 hours.

2.4. Dynamic shear rheometer

The mechanical characteristics of the bitumen at the mean and high temperatures (from +4 °C to +76 °C) have been measured by dynamic shear rheometer (Figure 1) under the standard of AASHTO T 315-08. The samples of the bitumen in the shape of round plate with diameter of 25 mm and thickness of 1 mm have been tested under the impact of sinusoidal varied strain, which has the amplitude of 12 % and frequency of 10 rad/s. Before testing the samples have been kept at the specified temperature not less than for 10 minutes. Shear deformation γ, shear stress τ and the phase angle δ have been measured as the test results.

The value of the complex shear modulus G* of the bitumen has been calculated under the formula [17–19]:

$$G^* = \frac{\tau_{\max} - \tau_{\min}}{\gamma_{\max} - \gamma_{\min}}, \tag{1}$$

where $\tau_{\max} - \tau_{\min}$ are maximum and minimum shear stresses respectively;

$\gamma_{\max} - \gamma_{\min}$ are maximum and minimum shear strains respectively.

The shear stresses τ_{max}, τ_{min} and shear strains γ_{max}, γ_{min} occur on the same plane, and their differences in the values are caused by sinusoidal load.

Figure 1. Dynamic shear rheometer (DSR)

2.5. Bending beam rheometer

The mechanical characteristics of the bitumen at low temperatures (-24, -30 and -36°C) have been measured by bending beam rheometer (Figure 2) under the standard of AASHTO T 313-08. The samples of the bitumen for tests had the shape of a beam with dimensions of 6.25x12.5x125 mm. Before testing the samples have been kept at the tested temperature for 60 minutes. In the beginning of the test the load, equal to 980 mN, has been applied automatically for 1 second and it has been kept as the constant one for the following 240 seconds. The maximum deflection of the middle of the beam has been measured automatically.

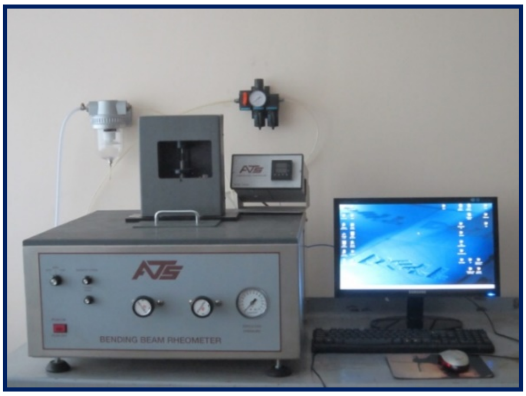

Figure 2. Bending beam rheometer (BBR)

Maximum stress on the bottom surface of the bituminous beam in its middle has been calculated under the formula:

$$\sigma = \frac{3 \cdot P \cdot \ell}{2 \cdot b \cdot h^2} \tag{2}$$

where P is a load, mN;

h, b, ℓ are height, width and length of the beam respectively, mm.

Maximum strain of the bottom surface of the bituminous beam in its middle at the time moment *t* has been calculated under the formula:

$$\varepsilon(t) = \frac{6 \cdot h}{\ell^2} f(t) \tag{3}$$

where $f(t)$ is the maximum deflection of the middle of the bituminous beam, mm.

The stiffness of the bituminous beam at the time moment *t* has been calculated under the formula

$$S(t) = \frac{P \cdot \ell^3}{4 \cdot b \cdot h^3 \cdot f(t)}. \tag{4}$$

2.6. Group chemical composition of bitumen

Group chemical composition of the bitumen has been determined by liquid adsorption chromatography method on the chromatograph “Gradient M” (Figure 3), manufactured by the Institute of petrochemical processing of the Republic of Bashkortostan (Russia). Chromatograph consists of two parts: analytical and detecting. The analytical part is the glass capillary column with the length of 300±5 mm and diameter of 1.2–1.4 mm, filled with the modified silica gel. Separating of the sample into maltenes (oils and resins) and asphaltenes with the use of complicated mixes of the solvents taken in different proportions (isooctane, dichloroethane, diisomayl ether, ethyl acetat, ethyl hydroxide and chlorbenzene). Detection for the groups of chemical compounds has been performed according to their heat conductivity at the temperature of 680 °C.

Figure 3. Liquid adsorption chromatograph

3. Results and Discussion

3.1. Group chemical composition of bitumen

Group chemical compositions of the investigated bitumen in three conditions has been shown in the Figure 4, where the impact of aging on the chemical composition is clearly seen: one can consider that the content of resins is practically constant at double aging (short-term and long-term); short-term and long-term aging decrease the content of oils for 1.5 % and 5.5 % respectively and increase the content of asphaltenes for 2.0 % and 4.3 % respectively. In general, the sequential double aging decreased the content of oils for 7.0 %, and the content of asphaltenes has been increased for 6.3 %.

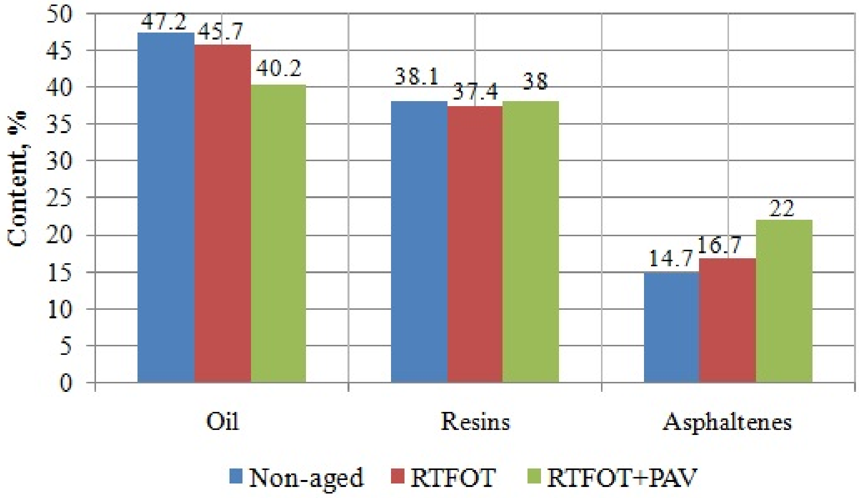

Figure 4. Group chemical composition of bitumen

3.2. Mechanical characteristics

3.2.1. At the mean and high temperatures

The graphs for dependence of the complex shear modulus G* and phase angle *δ* of the bitumen in three conditions on the temperature have been represented in Figures 5 and 6. It is seen that the aging changes the mechanical characteristics of the bitumen. Thus, after the short-term aging G* has been increased at the temperatures of 4 °C and 76 °C in 1.3 and 2.1 times respectively. And the impact of long-term aging on G* was great: the increase of G* was 5 300 and 7 200 times at the temperatures of 40 °C and 76 °C respectively.

In semi-logarithmic coordinates the temperature dependences of G* of the bitumen in the initial condition and after the short-term aging are nearly the straight lines. These straight lines are nearly parallel, i.e. the thermal sensitivity of the bitumen G* is practically similar in the specified conditions. Dependence of G* on the temperature after the long-term aging is of some other nature: within the range of temperatures from 26 °C to 76 °C it is a straight line, but with the less thermal sensibility; from 4 °C to 13 °C it is also described by the equation of straight line, but with considerably less thermal sensitivity; and temperature range from 13 °C to 26 °C is a transition one, within which the non-linear decrease of thermal sensitivity of the bitumen G* occurs.

Thus, the short-term aging of the bitumen, during which the content of oils has been decreased for 1.5 %, and the content of asphaltenes has been increased for 2 %, determined the increase of shear modulus G* at the mean and high temperatures in 1.3 and 2.1 times; long-term aging, resulting in the oil content decrease for 7 %, and the asphaltenes content increase for 6.3 %, has lead to the increase of G* at high temperatures up to 7 200 times.

The graphs in Figure 6 show clearly the impact of temperature and aging on phase angle *δ*. The phase angle is an important mechanical characteristic of the viscoelastic materials [20–22]. It shows the ratio of the elastic and non-elastic deformations. Its value varies from 0° to 90°. For the pure elastic material it is equal to 0° and for pure plastic material it is equal to 90°.

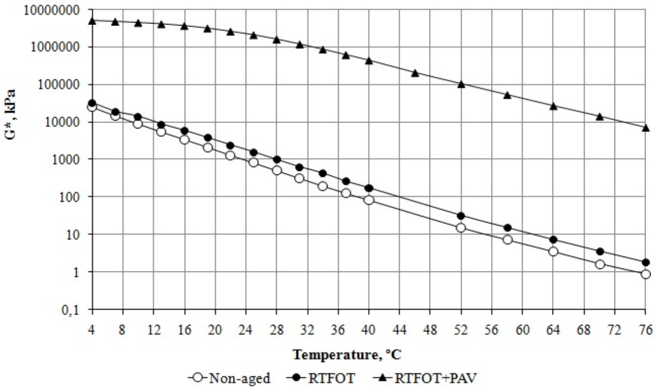

Figure 5. Dependence of complex shear modulus of bitumen on temperature

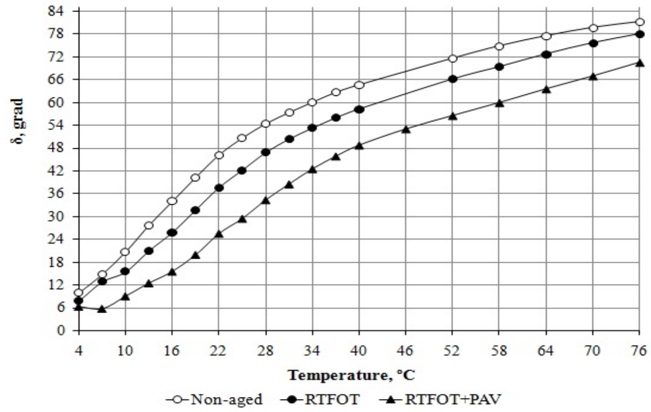

Figure 6. Dependence of phase angle of bitumen on temperature

It can be said that the short-term and long-term aging in the whole considered interval of temperatures (from 4 °C to 76 °C) decrease the phase angle of the bitumen at average for 4-6° and 8-10° respectively.

As could be expected, δ increases with the temperature increase. Temperature dependence of δ can be considered as bilinear one. There is a transition section in each condition of the bitumen (non-aged, RTFOT, RTFOT+PAV) between the first (at mean temperatures) and the second (at high temperatures) linear sections. The first linear section is characterized by higher indicator of thermal sensitivity of δ, and the second one has some lower thermal sensitivity. Smooth non-linear decrease for the indicator of thermal sensitivity of the phase angle occurs within the transition section. As it is seen from the Table 2, with the increase of aging level of the bitumen the position and characteristic (mean) temperature of the transition section on the temperature dependence of the phase angle shifts towards higher temperatures, and the width of the section has been decreased.

Table 2. Characteristics of transition section in temperature dependence of phase angle of bitumen

Condition of bitumen	Characteristics of transition section			
	initial temperature, °C	final temperature, °C	width of section, °C	conventional temperature of transition, °C
Non-aged	24	52	28	30
RTFOT	28	50	22	35
RTFOT+PAV	36	40	4	38

The works [9, 11–14] according to the results of experimental investigations determine that at high temperatures the short-term, as well as the long-term aging, increase complex shear modulus G* and decrease phase angle δ of the bitumens. But the authors do not mention numerical value for variation of G* and δ of the bitumens, provided by the impact of aging. It is obvious that it is connected with the fact that the issue of impact of aging on mechanical and other properties of bitumens is on the stage of studying and accumulating of experimental data, and researchers refrain themselves from general conclusions.

3.2.2. At low temperatures

The graphs for the stiffness of the bitumen at various low temperatures and conditions according to the aging are represented in Figures 7–9, where it can be clearly seen that the short-term and long-term aging impact essentially on deformability of the bitumen at low temperatures. At all low temperatures and conditions the bitumen stiffness decreases essentially under the exponential law within the time interval from 8 s to 240 s. At small load durations (8 s) the short-term aging increases the bitumen stiffness at the temperatures of -24 °C, -30 °C and -36 °C in 2.2; 1.3 and 1.5 times respectively, and the long-term aging in 2.8; 2.5 and 2.3 times respectively. Averaging the data, mentioned above, one can adopt that at average the short-term and long-term aging at small load durations increase the bitumen stiffness in 1.7 and 2.5 times respectively.

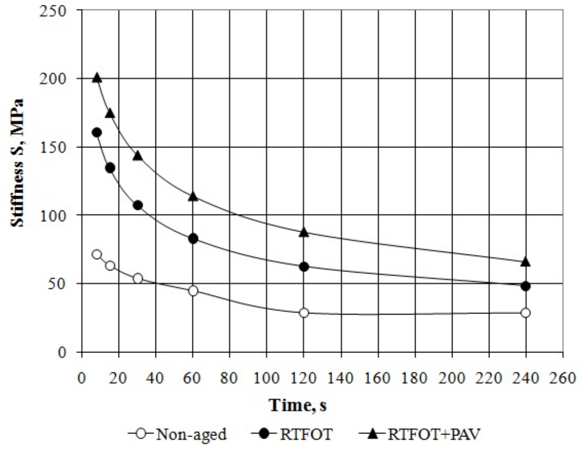

Figure 7. Time dependence of bitumen stiffness at the temperature of – 24 °C

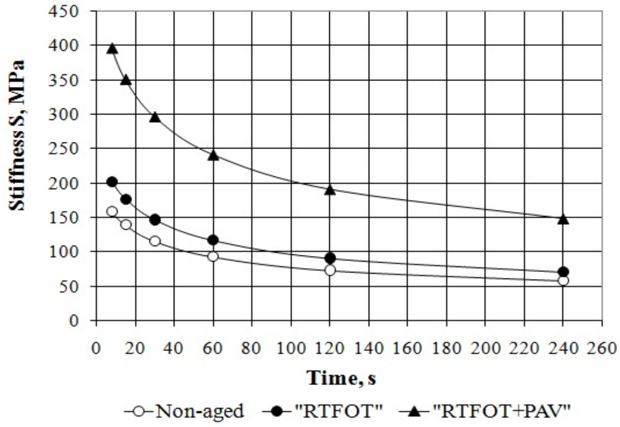

Figure 8. Time dependence of bitumen stiffness at the temperature of – 30 °C

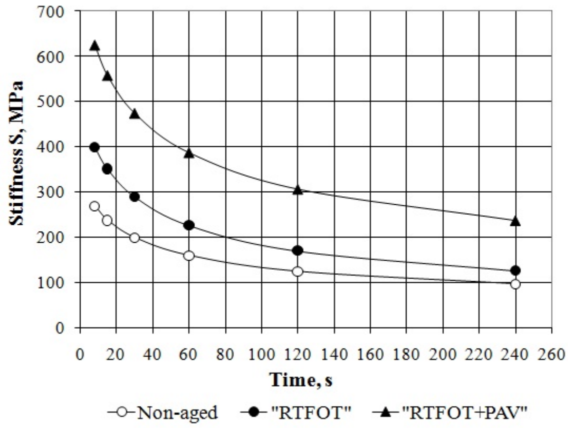

Figure 9. Time dependence of bitumen stiffness at the temperature of - 36°C

As it is known, one of the modern methodological systems in the world, aimed at more differentiated recording of the climatic conditions when defining the operational grade for the road bitumens, is Superpave [2]. The stiffness has been adopted at load duration of 60 seconds in Superpave as one of the bitumen indicators, characterizing its stability at low temperatures. For the tested bitumen the values of specific stiffness (at 60 s) at various low temperatures and aging conditions have been shown in Figure 10. The Figure shows clearly the cooperative effect of short-term and long-term aging and low temperature on specific stiffness of the bitumen: the specific stiffness has been increased with the aging level increase. For example, at the temperatures of -24 °C, -30 °C and -36 °C the short-term aging increases the specific stiffness of the bitumen in 1.8; 1.3 and 1.4 times respectively, and the long-term aging - in 2.5; 2.6 and 2.4 times respectively. At average the short-term aging and long-term aging increase the specific stiffness of the bitumen in 1.5 and 2.5 times respectively.

The literature review has shown that the investigations of the impact of aging on mechanical and other properties of bitumens at low temperatures are strictly limited. Only the work [10] investigates the impact of short-term and long-term aging on stiffness of bitumen PMB 45/80-65, modified by liquid surface substance on the basis of amines within the temperature range from -10 °C to -28 °C. It has been determined that the long-term aging does not almost impact on bitumen stiffness, and the short-term aging increases it slightly: critical temperature, at which the bitumen stiffness is equal to 300 MPa, is increased only for 2.5 °C.

Our work investigates pure (unmodified) bitumen. It is obvious, that modification reduces the process of aging for bitumens, which can be a subject for future investigations.

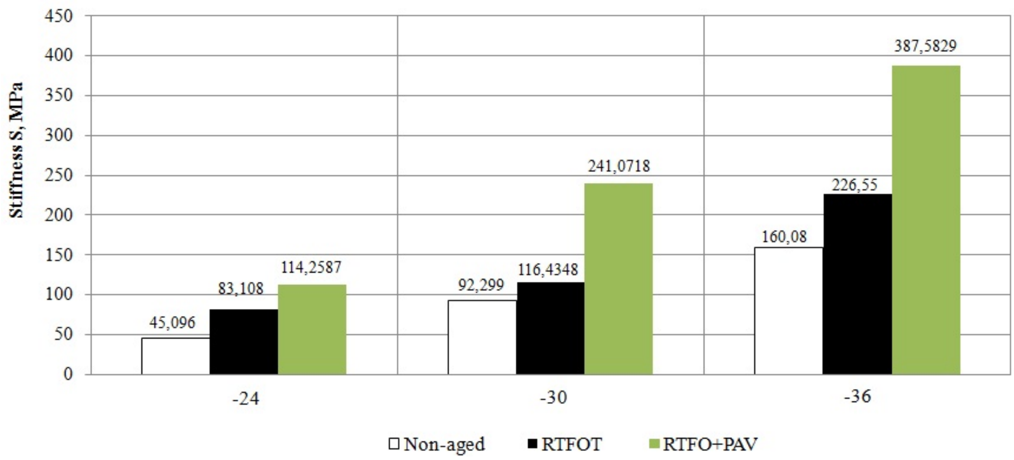

Figure 10. Bitumen stiffness at various low temperatures and aging conditions

4. Conclusion

1. At short-term aging of blown bitumen of grade BND 70/100 the content of oils in it has been decreased for 1.5 %, and the content of asphaltenes has been increased for 2 %. The long-term aging of the bitumen, performed after its short-term aging, compared with its initial condition, decreases the content of oils for 7 %, and the content of asphaltenes increases for 6.3 %. After two types of aging the content of resins in the bitumen remains practically constant.
2. The short-term aging determined the complex shear modulus G* increase at the mean and high temperatures (from 4 °C to 76 °C) in 1.3 and 2.1 times respectively, and the long-term aging increased G* at high temperatures in 7 200 times.
3. The short-term and long-term aging decrease the phase angle *δ* of the bitumen at the mean and high temperatures at average for 4-6° and 8-10° respectively.
4. The short-term and long-term aging increase the bitumen stiffness S at low temperatures (from -24 °C to -36 °C) in 1.5 and 2.5 times respectively.

References

1. Yoder, E.J., Witczak, M.W. 1975. Principles of pavement design. John Wiley & Sons, Inc. New Jersey. 736 p.
2. Papagiannakis, A.T., Masad, E.A. Pavement design and materials. John Wiley & Sons, Inc.: New Jersey, NJ, USA, 2008.
3. MS-4. The asphalt handbook. 7th ed.; Asphalt Institute: Lexington, MA, USA, 2008.
4. ST RK 1552-2006. Bitumy i bitumnyye vyazhushchiye. Metody opredeleniya izmeneniya massy posle progreva. Tekhnicheskiye usloviya. [Bitumens and bituminous binders. Methods of definition for weight variation after heating. Technical specifications]: Astana. 2006. Astana, 2006. (rus)
5. Superpave series No. 1. Performance graded asphalt binder specification and testing. Asphalt Institute, Lexington. 2003.
6. Radovskiy, B., Teltayev, B. Visco-elastic properties of asphalt based on penetration and softening point. Springer International Publishing AG, 2018. 115 p.
7. Teltayev, B., Radovskiy, B. Predicting thermal cracking of asphalt pavements from bitumen and mix properties. Road Materials and Pavement Design. 2017. Pp. 1–16.
8. Falchetto, A.C., Alisov, A., Goeke, M., Wistuba, M.P. Identification of structural changes in bitumen due to aging

Литература

1. Yoder E.J., Witczak M.W. 1975. Principles of pavement design. John Wiley & Sons, Inc. New Jersey. 736 p.
2. Papagiannakis A.T., Masad E.A. Pavement design and materials; John Wiley & Sons, Inc.: New Jersey, NJ, USA, 2008.
3. MS-4. The asphalt handbook. 7th ed.; Asphalt Institute: Lexington, MA, USA, 2008.
4. СТ РК 1552-2006. Битумы и битумные вяжущие. Методы определения изменения массы после прогрева. Технические условия. Астана, 2006.
5. Superpave series No. 1. Performance graded asphalt binder specification and testing. Asphalt Institute, Lexington, 2003.
6. Radovskiy B., Teltayev B. Visco-elastic properties of asphalt based on penetration and softening point. Springer International Publishing AG, 2018. 115 p.
7. Teltayev B., Radovskiy B. Predicting thermal cracking of asphalt pavements from bitumen and mix properties. // Road Materials and Pavement Design. 2017. Pp. 1–16.
8. Falchetto A.C., Alisov A., Goeke M., Wistuba M.P. Identification of structural changes in bitumen due to aging and fatigue // Proceedings of the 6th Euroasphalt and Eurobitumen Congress. Prague, Czech Republic, 2016.

Teltayev, B.B., Rossi, C.O., Ashimova, S. Composition and rheological characteristics of bitumen in short-term and long-term aging. Magazine of Civil Engineering. 2018. 81(5). Pp. 93–101. doi: 10.18720/MCE.81.10.

and fatigue. Proceedings of the 6th Euroasphalt and Eurobitumen Congress. Prague, Czech Republic. 2016.
9. Hofko, B., Falchetto, A.C., Grenfell, J., Huber, L., Lu, X., Porot, L., Poulikakos, L.D. Effect of short-term aging temperature on bitumen properties. Road Materials and Pavement Design. 2017. No. 18. Pp. 108–117.
10. Iwanski, M., Choiewinska, M., Mazurek, G. Impact of the aging on viscoelastic properties of bitumen with the liquid active agent on operating temperature. IOP Conference series: Materials science and engineering. 2017. Vol. 245. Pp. 1–8.
11. Molenaar, A.A.A., Hagos, E.T., van de Ven, M.F.C. Effect of aging on the mechanical characteristics of bituminous in PAC. Journal of Materials in Civil Engineering. 2017. No. 8. Pp. 779–887.
12. Ramadan, K.Z., Abo-Qudais, S.A. Effect of Superpave short-term aging on binder and asphalt mixture rheology. Periodica Polytechnica Transportation Engineering. 2017. No. 45(4). Pp. 196–205.
13. Pasandin, A.R., Perez, I., Oliveira, J.R.M., Silva, H.M.R.D., Pereira, P.A.A. Influence of aging on the properties of bitumen from asphalt mixture with recycled concrete aggregates. Journal of Cleaner Production. 2017. Pp. 165–173.
14. Saoula, S., Saoudani, K., Haddadi, S., Munoz, M.E., Santamaria, A. Analysis of the rheological behavior of aging bitumen and predicting the risk of permanent deformation of asphalt. Materials Sciences and Applications. 2013. No. 4. Pp. 312–318.
15. Sarsam, S.I., Adbulmajeed, S.M. Influence of aging time on asphalt pavement performance. Journal of Engineering. 2014. No. 12. Pp. 1–12.
16. ST RK 1373-2013. Bitumy i bitumnyye vyazhushchiye. Bitumy neftyanyye dorozhnyye vyazkiye. Tekhnicheskiye usloviya.[Bitumens and bituminous binders. Oil road viscous bitumens. Technical specifications]: Astana. 2013. Astana, 2013. (rus)
17. Cristensen, R.M. Theory of viscoelasticity: An introduction. New York, Academic Press. 1971.
18. Tschoegl, N.W. The phenomenological theory of linear viscoelastic behavior. An Introduction. Berlin, Springer. 1989.
19. Ferry, J.D. Viscoelastic properties of polymers. New York, Willey & Sons, Inc. 1980.
20. King, G.N., Radovskiy, B.S. Properties of polymer bituminous binders and their test methods developed in the USA. Materials and Structures. 2004. Pp. 16–27.
21. Radovskiy, B.S. Modern condition of development for Superpave method of designing of asphalt concrete mixes. Road Machinery. 2008. Pp. 12–22.
22. Van der Poel C. A general system describing the visco-elastic properties of bitumens and its relation to routine test data. Applied Chemistry. London. 1954. Vol. 4. Pp. 221–236.

Bagdat Teltayev,*
+7(701)760-67-01; bagdatbt@yahoo.com

Cesare Rossi,
+39(327)833-28-61; cesare.oliviero@unical.it

Saltanat Ashimova
+7(778)955-75-55; salta_32@mail.ru

9. Hofko B., Falchetto A.C., Grenfell J., Huber L., Lu X., Porot L., Poulikakos L.D. Effect of short-term aging temperature on bitumen properties // Road Materials and Pavement Design. 2017. No. 18. Pp. 108–117.
10. Iwanski M., Choiewinska M., Mazurek G. Impact of the aging on viscoelastic properties of bitumen with the liquid active agent on operating temperature // IOP Conference series: Materials science and engineering. 2017. Vol. 245. Pp. 1–8.
11. Molenaar A.A.A., Hagos E.T., van de Ven M.F.C. Effect of aging on the mechanical characteristics of bituminous in PAC // Journal of Materials in Civil Engineering. 2017. No. 8. Pp. 779–887.
12. Ramadan K.Z., Abo-Qudais S.A. Effect of Superpave short-term aging on binder and asphalt mixture rheology // Periodica Polytechnica Transportation Engineering. 2017. No. 45(4). Pp. 196–205.
13. Pasandin A.R., Perez I., Oliveira J.R.M., Silva H.M.R.D., Pereira P.A.A. Influence of aging on the properties of bitumen from asphalt mixture with recycled concrete aggregates // Journal of Cleaner Production. 2017. Pp. 165–173.
14. Saoula S., Saoudani K., Haddadi S., Munoz M.E., Santamaria A. Analysis of the rheological behavior of aging bitumen and predicting the risk of permanent deformation of asphalt // Materials Sciences and Applications. 2013. No. 4. Pp. 312–318.
15. Sarsam S.I., Adbulmajeed S.M. Influence of aging time on asphalt pavement performance // Journal of Engineering, 2014. No. 12. Pp. 1–12.
16. СТ РК 1373-2013. Битумы и битумные вяжущие. Битумы нефтяные дорожные вязкие. Технические условия. Астана, 2013.
17. Cristensen R.M. Theory of viscoelasticity: An introduction. New York, Academic Press, 1971.
18. Tschoegl N.W. The phenomenological theory of linear viscoelastic behavior. An Introduction. Berlin, Springer, 1989.
19. Ferry J.D. Viscoelastic properties of polymers. New York, Willey & Sons, Inc., 1980.
20. King G.N., Radovskiy B.S. Properties of polymer bituminous binders and their test methods developed in the USA // Materials and structures. 2004. Pp. 16–27.
21. Radovskiy B.S. Modern condition of development for Superpave method of designing of asphalt concrete mixes. Road machinery. 2008. Pp. 12–22.
22. Van der Poel C. A general system describing the visco-elastic properties of bitumens and its relation to routine test data // Applied Chemistry. London. 1954. Vol. 4. Pp. 221–236.

Багдат Бурханбайулы Телтаев,*
+7(701)760-67-01;
эл. почта: bagdatbt@yahoo.com

Чезаре Оливиеро Росси,
+39(327)833-28-61;
эл. почта: cesare.oliviero@unical.it

Салтанат Жандарбековна Ашимова
+7(778)955-75-55; эл. почта: salta_32@mail.ru

Телтаев Б.Б., Росси Ч.О., Ашимова С.Ж. Состав и реологические характеристики битума при кратковременном и длительном старений // Инженерно-строительный журнал. 2018. № 5(81). С. 93–101.

doi: 10.18720/MCE.81.11

Energy intensity of parts made from polyurethane elastomers

Энергоемкость деталей из полиуретановых эластомеров

V.G. Artiukh,
E.A. Galikhanova*,
Peter the Great St. Petersburg Polytechnic University, St. Petersburg, Russia
V.M. Mazur,
LLC 'Saint-Petersburg Electrotechnical Company', Saint-Petersburg, Pushkin, Russia
S.B. Kargin,
Pryazovskyi State Technical University, Mariupol, Ukraina

Д-р техн. наук, профессор В.Г. Артюх,
студент Э.А. Галиханова*,
Санкт-Петербургский политехнический университет Петра Великого, г. Санкт-Петербург, Россия
главный специалист технического управления В.О. Мазур,
ООО «Научно-производственное объединение «Санкт-Петербургская Электротехническая Компания», г. Санкт-Петербург, г. Пушкин, Россия,
канд. техн. наук, доцент С.Б. Каргин,
Приазовский государственный технический университет, г. Мариуполь, Украина

Key words: energy consumption; polyurethane; elastomer; shock absorber; elastic element

Ключевые слова: поглощение энергии; полиуретан; эластомер; амортизатор; упругий элемент

Abstract. Laboratory testing with determination of strength and energy characteristics of materials for elastic elements of shock absorbers helped to establish that polyurethane elastomers, having the highest values of specific energy consumption and a wide range of alternating dissipation and rigidity characteristics were the best materials. It will allow to create a series of efficient shock absorbers for different elements and units of building constructions. As the result of the analysis performed of different types of steel springs a coefficient of spring's quality in volume was obtained, as well as coefficient of spring's quality in weight, coefficients of shape for cylindrical, crew-type and plate springs. These coefficients can help to arrive at the conclusion, regarding the appropriateness of this spring for a particular elements and units of building constructions.

Аннотация. Лабораторные испытания с определением прочностных и энергетических характеристик материалов для упругих элементов амортизаторов позволили установить, что лучшими материалами являются полиуретановые эластомеры, обладающие наибольшими значениями удельной энергоемкости и широким диапазоном изменения диссипативных и жесткостных характеристик. Это позволит создать ряд эффективных амортизаторов для различных элементов и узлов строительных конструкций. В результате проведенного анализа различных типов стальных пружин получены коэффициент качества пружины по объему, коэффициент качества пружины по весу, коэффициенты формы для цилиндрических винтовых и тарельчатых пружин. На основании этих коэффициентов можно сделать заключение о пригодности данной пружины для конкретных элементов и узлов строительных конструкций.

1. Introduction

The use of polymeric materials, including polyurethane elastomers, is continuously increasing in different fields of science such as engineering, transport and construction. It could be explained by the unique qualities of elastomers in terms of their strength, elasticity, energy intensity and other mechanical characteristics. The most upcoming elastomers are injection molded structural polyurethanes, the use of which in construction is expanding very fast.

The energy intensity of elements and units of building structures is the most important characteristic that affects the ability to protect elements from dynamic effects, for example, seismic. The overwhelming majority of such elements have insufficient energy intensity and excessive rigidity.

In metallurgical machinery high levels of parasitic (not technological) loads are often observed. Good example of such drives are drives of continuous wide strip mill (WSM) 1700, where dynamic loads during strip bite by work rolls are in 3...4 times exceed technological loads at steady rolling. One of the most effective solutions to reduce dynamic loads is significant increase of energy intensity of main drive lines; the most real way of energy intensity increase is installation of energy-intensive (active) parts [1] in drive.

Maximum possible energy intensity, with loads not exceeding standards, able to significantly increase the energy intensity of the entire drive, characterizes this kind of detail.

General issues of machines loading and arising overloads are considered in [1–6]. Elastomer-metallic dampers and their elastic elements began to be scrutinized long time ago, and these researches are ongoing so far [7, 8]. The selection of polymeric (elastomeric) materials for elastic elements of active devices, study their mechanical characteristics are shown in articles [9–12]. Different types of protective devices for metallurgical machines described in [13, 14]. Mechanical and temperature properties of polyurethane elastomers are described in articles [15–21].

It is possible to achieve the maximum energy intensity of detail (assembly, unit) modernizing it in three ways:

1. Selection of detail material with the highest specific energy intensity;
2. Ensuring uniform distribution of stresses in detail;
3. Provision of sufficient size (volume, mass) of this detail.

Below these options of energy intensity increase are considered and the greatest interest is active parts that can affect values of parasitic loads.

2. Methods

Modern machinery is based on numerous classes of materials having different (often substantially different) mechanical characteristics. These are steel, non-ferrous metals and their alloys, plastics, ceramics, elastomers and so on. These materials vary in strength by tenfold and in rigidity by hundreds or thousands times. Common for all construction materials is a lack of information about their energy intensity in any literature. It shows that question of energy intensity of shock absorbers not found not only the proper solution, but also the relevant description. It needs to start this task with selection of material.

Let us consider any simple detail (beam), where there is a simple stress state (such as uniaxial stretching or compression). Specific (per volume unit) energy intensity can be represented as

$$u_v = \frac{U}{V} = \frac{\sigma^* \cdot \varepsilon^*}{2}, \quad (1)$$

where U is energy intensity of detail;

V is volume of detail;

σ^* is stress limit value;

ε^* is deformation limit value.

Keeping in mind that

$$\sigma^* = E \cdot \varepsilon^* \text{ and } \varepsilon^* = \frac{\sigma^*}{E}, \quad (2)$$

Finally

$$u_v = \alpha \frac{\left(\sigma^*\right)^2}{E}, \quad (3)$$

where α is a numeric factor depending on kind of stress condition (quality factor of stress condition). For uniaxial stretching and compression α = 0.5 (i.e., for such loading which provides uniform stress distribution throughout the volume of the elastic element [2]).

Stress limit value can be chosen depending on purpose of calculated detail. For fragile metal materials it is value close to strength limit σ_B, for ductile metal materials it is yield strength σ_t, for high-strength metal materials it is conditional yield strength $\sigma_{0.2}$. Comparative analysis of different materials on energy intensity can be performed by formula (3) with the same coefficient α, for example, taking α = 0.5. Thus we compare samples of various materials but in the same tense condition.

In the vast majority of real structures of shock absorbers as materials which accumulate energy special spring steel grades are used. These are (according to their description in CIS countries) carbon constructional steel grades 65G, 70G, siliceous alloy spring steel grades 60C2, 70C2, 60C2HFA and other. Listed steel grades are characterized by high strength limit values (after thermal treatment) σ_B = 1100...1900 MPa and conditional yield strength $\sigma_{0.2}$ = 700...1500 MPa. For widely spread spring steel grades having $\sigma_{0.2} \approx$ 1200MPa, we get taking into account $\sigma^* = \sigma_{0.2}$

$$u_v = 0.5\frac{1200^2}{2 \cdot 10^5} = 3.6\frac{MJ}{m^3} = 3.6MPa. \tag{4}$$

For decades, steel was practically the only material for springs and other energy-intensive items. Comparing energy intensity of different steel grades actually we consider only their strength because modulus of elasticity of different steel grades are insensitive structural characteristics, i.e. practically permanent. For all low-alloyed steel grades normal modulus of elasticity value may be taken as $E = 2.0 \cdot 10^5$ MPa. Therefore, the improvement of springs and other energy-intensive steel elements went in a way only to increase their strength. This process led to undoubted success. Best spring steels are superior to ordinary low-carbon steels (which are the most widely spread) on strength by 4...5 times and on energy intensity by 20 times, that is a major achievement of specialists working with metal.

However, this way of specific energy intensity improve is not the only one. Apart from steel and considering broader class of materials it needs to take into stiffness of material into account (in addition to strength) stated by normal elasticity module. It is better to search materials with high strength and low stiffness. Such materials can be found among polymers and elastomers in particular that relate to low-modulus materials. Energy-intensive materials can be found in groups of polyamides, lavsanov, ultra-high-molecular polyethylene as well as urethane rubbers-polyurethanes.

It should be noted that specific energy intensity is absent in the list of mechanical characteristics of these materials. So it can be concluded that the listed materials (unlike steels) on “energy intensity” parameter were not selected and not improved. In this regard, low-modulus materials have great chances for meaningful improvements [10]. As an example, we consider such material as molding structural polyurethane CKU-PFL-100 (description in CIS countries) which has normal compressive modulus E_c = 60 MPa. This material is quite widely spread and produced by domestic industry in CIS countries. There are foreign analogues of this material (for example, adiprene L 167).

For polyurethane elastic elements working on compression (with single loading that is typical for buffer devices), it is allowable to consider elastic deformation equal to 20...35 % [11]. Allowable deformation with one-time loading can be found in experiments on samples (e.g., cylindrical samples under their compression). Measuring dimensions of sample before and after loading it is possible to find deformation when after its removal initial sample size fully recovers. For low-hardness polyurethane elastomers (E_c = 10…30 MPa) this value is ε^* = 0.35, for medium-hardness polyurethane elastomers (E_c = 35…60 MPa) ε^* = 0.30 and so on. Let us take the maximum allowable stress σ^* = 0.3E, then specific energy intensity:

$$u_v = \frac{(0.30E_c)^2}{2E} = \frac{0.09E_c}{2} = 2.7MPa; \tag{5}$$

It is clear from shown figures that energy intensity of given polyurethane corresponds to energy intensity of special spring steel grades. It is about specific energy intensity per unit volume. Meanwhile, there are objects in machinery engineering practice (mainly vehicles), for which a very important parameter is their own weight. In this case, to characterize suitability of material it is better to use specific energy intensity per unit weight

$$u_p = \frac{u_v}{\gamma_м} = \alpha\frac{\left(\sigma^*\right)^2}{E \cdot \gamma_м}, \tag{6}$$

where γ_m is specific weight of elastic element material, MN/m^3.

For material considered above:

- steel, $\gamma_s = 78 \cdot 10^{-3}$ MN/m^3;
- polyurethane, $\gamma_p = 11 \cdot 10^{-3}$ MN/m^3.

Respectively, values of specific energy intensity are:

- for spring steel (σ^*= 1200 MPa; E = 2·10⁵ MPa); $u_p = \dfrac{3.6}{78\cdot 10^{-3}} = 46m$;
- polyurethane CKU-PFL -100 (σ^*= 0.35E; E = 60 MPa), $u_p = \dfrac{2.7}{11\cdot 10^{-3}} = 245m$.

3. Results and Discussion

Figures convincingly show that according to u_p elastomers have a clear advantage over special spring steel grades [11]. There are values of energy intensity of some common plastics below in Table 1. From Table 1 it is clear that all these materials have high energy intensity, therefore, can be effectively used in machines with significant levels of parasitic loads.

Table 1. Energy intensity of elastic elements materials

Elastic element material (description as per CIS countries)	Normal elastic modulus (E), MPa	Maximum (limit) deformation ε^*, %	Limit stress σ^*, MPa	Specific weight of material γ_M, kN/m³	Specific intensity of material under compression	
					per unit volume u_v, MPa	per unit weight, u_p, m
Spring steel 65G	$2\cdot 10^5$	0.45	900	78	2.03	26.0
Spring steel 60C2	$2\cdot 10^5$	0.60	1200	78	3.60	46.2
Spring steel 60C2HFA	$2\cdot 10^5$	0.80	1600	78	6.40	82.0
Rubber B-14	14	35	4.90	13	0.855	66.0
Polyurethane CKU-7L	20	35	7.0	11	1.21	110
Adiprene L 100	30	32	9.60	11	1.53	126.0
Polyurethane CKU-PFL-100	60	30	18.0	11	2.70	245
Polyethylene CBMPE	300	10	30.0	9.5	1.50	158

Note. The best options are highlighted.

From Table 1 it is clear that the highest energy intensity (color highlighted) per unit of weight have low-modulus materials: molded structural polyurethanes and polyethylene CBMPE. The most strength spring steel is slightly better compared to rubber B-14 in terms of specific energy intensity. At the same time, high-strength spring steel grades still are not better compared to elastomers in terms of energy intensity per unit volume. Question about choosing particular material for engineered shock absorber will be resolved below, where in addition to specific energy intensity of material other significant factors would be considered [14].

Energy intensity is maximum energy of elastic deformation accumulated by detail with this form of loading. The same item can show varying energy intensities in different loading variants depending on load stress state arising in this detail. Specific energy intensity of different materials on the example of uniaxial stress state with a uniform distribution of stresses was considered above.

For arbitrary stress state specific (per unit volume) energy intensity is

$$u_v = \frac{1}{2}\left(\sigma_1\varepsilon_1 + \sigma_2\varepsilon_2 + \sigma_3\varepsilon_3\right), \tag{7}$$

where σ_1, σ_2, σ_3 are principal stresses;

ε_1, ε_2, ε_3 are principal deformations.

When use the generalized Hooke's law and exclude from formula (7) deformations:

$$u_V = \frac{1}{2E}\left[\sigma_1^2 + \sigma_2^2 + \sigma_3^2 - 2\mu\left(\sigma_1 \cdot \sigma_2 + \sigma_1 \cdot \sigma_3 + \sigma_2 \cdot \sigma_3\right)\right]. \qquad (8)$$

From formula (8) it is possible to get special cases for simple stress states: stretch-compression, torsion, bending and other.

Total energy intensity of detail can be found by summing formula (8) throughout volume of the detail. To do this it needs to know all stress states of the detail of analytical expressions for the main stresses depending on detail coordinates of points:

$$U = \int_V u_V \cdot dV\,; \qquad (9)$$

$$\left.\begin{aligned} \sigma_1 &= f_1(x, y, z) \\ \sigma_2 &= f_2(x, y, z) \\ \sigma_3 &= f_3(x, y, z) \end{aligned}\right\}. \qquad (10)$$

Difficulties in practical application of formula (9) is that for the majority of details (except those that operate at very simple stress conditions) it is difficult to get functions (10) with sufficient accuracy and in a form convenient for integration.

Quite simply result can be achieved when it comes to uniaxial tensile-compression, when it comes to torsion and bend it is more complicated. For such energy-intensive items as disk springs calculation of energy intensity is strongly difficult, for objects of type similar to slotted springs it becomes virtually impossible (if not take numerical methods into consideration that can be used for making special cases).

At the same time, energy intensity of any details or units can be found experimentally or approximately by values of limit loads and deformations. If working characteristic of researched detail (in coordinates “force P and draught λ”) is available and it is for all λ and ensure the absence of residual deformations then target energy intensity represents area of working characteristic limited by values $0 \le \lambda \le \lambda^*$, where λ^* is maximum draught, causing arise of plastic deformation in detail.

$$U = \int_0^{\lambda^*} P(\lambda) \cdot d\lambda\,, \qquad (11)$$

where $P(\lambda)$ is a variable force value.

In most cases, expression $P(\lambda)$ is easier than expression (10) and integral (11) is easier to calculate; function $P(\lambda)$ may be approximate.

Finally, energy intensity of detail can be found on the basis of internal loading factors and elastic movements. For linearly deformable systems (consisting of rods) energy intensity of detail can be found by formula

$$U = P^* \cdot \frac{\lambda^*}{2}\,, \qquad (12)$$

Where P^* is force appropriating loading when $\sigma_{max} = \sigma^*$;

λ^* is limit value of generalized displacement in direction of force P^*.

So, for elastic element constituting the beam on two supports and under loading by force in the middle by equation (11) it is

$$U = \frac{\left(P^*\right)^2 \cdot l^3}{96 E I_x}. \qquad (13)$$

It would be interesting to compare energy intensity of the same detail under different loading. Let the detail has simple form that is a cylinder with diameter d and length l, and $l >> d$, so our detail is beam which can be calculated by methods of strength of materials.

This beam can be stretched, compressed, bent in different ways (such as doubly or cantilever beam) and tighten. It is possible to produce cylindrical coil spring from long beam, and so on. The energy intensity of these beams can be represented as

$$U = \alpha \cdot \frac{\left(\sigma^*\right)^2}{E} \cdot V. \tag{14}$$

More value of α, bigger energy intensity of the beam, more it is suitable for manufacture of shock absorber. Let us start with tension-compression (meaning a case of compression, when there is no loss of stability)

$$U = \frac{1}{2} P^* \cdot \Delta l^* = \frac{1}{2} P^* \cdot \frac{P^* \cdot l}{EF}, \tag{15}$$

where Δl^* is maximum allowable deformation at which there is no permanent deformation.

Here $P^* = \sigma^* \cdot F$. Accordingly,

$$U = \frac{1}{2} \sigma^* \cdot F \cdot \frac{\sigma^* \cdot F \cdot l}{EF} = \frac{1}{2} \cdot \frac{\left(\sigma^*\right)^2}{E} \cdot V. \tag{16}$$

Thus, in this case $\alpha = 0.5$, which was already mentioned above. Note that stresses in the above example are considered uniformly distributed throughout the volume of the cylinder.

Further, bending of the beam (as beam on two pivot supports) by concentrated force P applied to the middle is considered. In this case

$$U = \frac{1}{2} P \cdot f = \frac{1}{2} P^* \cdot \frac{P^* \cdot l^3}{48 E I_x}, \tag{17}$$

where f is deflection of the beam.

Here P^* has to be found considering conditions of strength at bending.

$$\sigma^* = \frac{P^* \cdot l}{4 W_x}, \tag{18}$$

where W_x is axial section modulus of the beam. At the same time

$$P^* = 4 W_x \cdot \frac{\sigma^*}{l}.$$

Substituting it into formula (18)

$$U = \frac{1}{2} \cdot 4 W_x \cdot \frac{\sigma^*}{l} \cdot 4 W_x \cdot \frac{\sigma^*}{l} \cdot \frac{l^3}{48 E I_x} = \frac{1}{6} \cdot \frac{\left(\sigma^*\right)^2}{E} \cdot \frac{W_x^2 \cdot l}{I_x}. \tag{19}$$

Factor $\frac{W_x^2 \cdot l}{I_x}$ has dimension m³, it is proportional to volume. In other words, volume of the detail can be isolated from expression (19). Thus, for the cylinder

$$W_x = \frac{\pi d^3}{32};\ I_x = \frac{\pi d^4}{64}. \tag{20}$$

Then $\frac{W_x^2 \cdot l}{I_x} = \frac{\pi d^3 \cdot \pi d^3 \cdot 64}{32 \cdot 32 \cdot \pi d^4} \cdot l = \frac{\pi d^2 \cdot l}{4 \cdot 4} = \frac{1}{4} V$. Formula (19) begins to be in a form

$$U = \frac{1}{24} \cdot \frac{\left(\sigma^*\right)^2}{E} \cdot V. \tag{21}$$

From formulas (16) and (21) it is seen that energy intensity of the same detail (the cylinder) decreased by 12 times at the transition from stretching to bending. If consider this detail as a shaft its energy intensity is equal to

$$U = \frac{1}{2} M^* \cdot \varphi^*, \quad (22)$$

where M^* is torque corresponding to maximum stress $\tau_{max} = \tau^*$. This value is related to the equivalent stress σ^* that is a strength criteria (e.g., energy)

$$\sigma^* = \sqrt{3} \cdot \tau^*, \quad (23)$$

φ^* − the angle of shaft twist which corresponds to torque M*. This angle can be found by the formula

$$\varphi^* = \frac{M^* \cdot l}{GI_p}, \quad (24)$$

where G is shear modulus of the shaft material

$$G = \frac{E}{2(1+\mu)}, \quad (25)$$

where μ is Poisson coefficient of the material;

I_p is polar moment of inertia of the shaft cross-section.

$$I_p = \frac{\pi d^4}{32}. \quad (26)$$

Considering (25) and (26) it comes from (24

$$U = \frac{1}{2} M^* \cdot \frac{M^* \cdot l}{GI_p}. \quad (27)$$

Here

$$M^* = \tau^* \cdot W_p. \quad (28)$$

W_p is polar section modulus

$$W_p = \frac{\pi d^3}{16}. \quad (29)$$

Putting (28) and (29) into (27) it comes to

$$U = \frac{1}{2} \tau^* \cdot W_p \cdot \frac{\tau^* \cdot W_p \cdot l}{GI_p}. \quad (30)$$

If put in expression (30) values τ^* and G, taken from (23) and (25) it comes to

$$U = \frac{1}{2} \cdot \frac{\sigma^*}{\sqrt{3}} \cdot \frac{\pi d^3}{16} \cdot \frac{\sigma^* \cdot \pi d^3 \cdot l \cdot 32 \cdot 2(1+\mu)}{\sqrt{3} \cdot 16 \cdot \pi d^4 \cdot E} = 0.208 \frac{\left(\sigma^*\right)^2}{E} \cdot V. \quad (31)$$

This result is 2.4 times less than in case of tension or compression; but it is significantly higher than for case of bending. However, it should be noted that considered cross section (circle) is advantageous (optimal) in case of torsion and disadvantageous in case of bending.

If cross-section of square is taken, then as per formula (16) for case of uniaxial stretching or compression it comes to obtaining of α = 0.5 (as well as for other forms of cross-sections). For case of bending from formula (29) it comes to

$$U = \frac{1}{6} \cdot \frac{\left(\sigma^*\right)^2}{E} \cdot \frac{\left(b^3\right)^2 \cdot l \cdot 12}{6^2 \cdot b^4} = \frac{1}{18} \cdot \frac{\left(\sigma^*\right)^2}{E}. \quad (32)$$

Here, quality factor of the stress state $\alpha = \frac{1}{18}$ compared with $\alpha = \frac{1}{24}$ of the circle. For case of torsion of shaft with square cross-section let us take formula (30) wherein W_p should be replaced by W_k and I_p should be replaced by I_K respectively, wherein:

$$W_{\kappa} = 0.208 \cdot a^3;$$
$$I_{\kappa} = 0.141 \cdot a^4.$$

Then

$$U = \frac{1}{2} \cdot \frac{\sigma^*}{\sqrt{3}} \cdot 0.208 \cdot a^3 \frac{\sigma^* \cdot 0.208 a^3 \cdot l \cdot 2(1+0,25)}{\sqrt{3} \cdot E \cdot 0.141 \cdot a^4} = 0.128 \frac{\left(\sigma^*\right)^2}{E} \cdot V, \quad (33)$$

that is the quality of the stress state which became almost 2 times less than one of a round shaft.

These values are listed in Table 2; wherein in all cases, quality factors of elastic elements are calculated. This refers not only to the quality of the stress state but also to a real opportunity to implement this stress state for particular material and particular design. Thus, for steel springs it is practically impossible to implement loading case by tensile or compressive force. Such devices would have extremely large (unacceptable for real conditions) stiffness. Practically all steel springs (cylindrical coil, disk, slotted, torsions) work in torsion or bending. Exception is ring springs working in tension and compression which, however, have significant irremovable drawbacks. These exceptions will be discussed below.

Table 2. The specific energy intensity of the elastic elements

Material of the elastic element (description as per CIS countries)	Shape and form of deformation	Coefficient of quality of the stress state α	Specific energy c intensity per unit of volume u_v, MPa	Quality coefficient of the elastic element β	Overall energy intensity u_r, MPa
Steel 65G	Twisting (torsion)	0.208	0.844	0.208	0.844
	Cylindrical coil spring	0.208	0.844	0.085	0.343
	Bending of rectangular beam	0.055	0.223	0.055	0.223
Steel 60C2	Twisting (torsion)	0.208	1.50	0.208	1.50
	Cylindrical coil spring	0.208	1.50	0.085	0.620
	Bending of rectangular beam	0.055	0.396	0.055	0.396
Steel 60C2HFA	Twisting (torsion)	0.208	2.66	0.208	2.66
	Cylindrical coil spring	0.208	2.66	0.085	1.10
	Bending of rectangular beam	0.055	0.704	0.055	0.704
Rubber B-14	Compression	0.500	0.855	0.500	0.855
Polyurethane CKU-7L	Compression	0.500	1.21	0.500	1.21
Adiprene L-100	Compression	0.500	1.53	0.500	1.53
Polyurethane CKU-PFL-100	Compression	0.500	2.70	0.500	2.70
Polyethylene CBMPE	Compression	0.500	1.50	0.500	1.50

Note. The most perspective options of elastic elements are highlighted.

Table 2 shows values of specific energy intensity related to the elastic element. For case of bending bar with rectangular cross section is taken (which gives the same results as the square bar), and in case of torsion round is optimum.

This takes into account the quality factor of the stress state, weight and dimensions of the elastic element. The latter is especially important when one element is replaced by another and available slots for their installation are preserved. In this case, it may be found so-called overall specific energy intensity

$$u_0 = \alpha \cdot \frac{\left(\sigma^*\right)^2}{E} \cdot \frac{V}{V_0}, \tag{34}$$

where V_o is overall volume of elastic element.

Relation between $\frac{V_0}{V}$ can be called a coefficient of form of elastic element, for example, of spring. Spring shape can be considered optimal if this coefficient equals one.

Further, in Table 2 quality coefficient of elastic element is shown

$$\beta = \alpha \frac{V}{V_0}, \tag{35}$$

which takes into account nature of the stress state and shape of the elastic element (spring). For cylindrical coil spring actual volume is equal to

$$V = \frac{\pi d^2}{4} \cdot \pi D \cdot n, \tag{36}$$

where D is diameter of the cylindrical coil spring;

d is diameter of the rod (bar);

n is number of coils.

Overall volume of the spring is

$$V_0 = \frac{\pi \left(D + d\right)^2}{4} \left(n \cdot d + \lambda^*\right), \tag{37}$$

where λ^* is maximum spring draught corresponding to maximum stress τ^*.

Then shape factor of the spring is

$$k_{sh} = \frac{V_0}{V} = \frac{\left(D + d\right)^2 \cdot \left(n \cdot d + \lambda\right)}{\pi \cdot D \cdot n \cdot d^2}. \tag{38}$$

According to the formula (38) value of k_{sh} can be calculated for any given spring. For example, there is a spring with the parameters: D = 128 mm; d = 32 mm; n = 6; λ^* = 40 mm. For this spring

$$k_{sh} = \frac{(128 + 32)^2 \cdot (6 \cdot 32 + 40)}{3.14 \cdot 128 \cdot 6 \cdot 32^2} = 2.4. \tag{39}$$

In general, for all springs of the same type it is

$$2.0 \le k_{sh} \le 6.0 \tag{40}$$

The highest values of k_{sh} correspond to low stiffness springs, lower levels correspond to high stiffness springs. As a rule, high stiffness springs are used for metallurgical equipment; in this case it can be limited by

$$2.0 \le k_{sh} \le 3.0 \tag{41}$$

Formula (38) can be simplified if value $nd+\lambda^*$ (which represents height of spring in free state) is shown in form

$$nd + \lambda^* = nd \cdot \xi, \tag{42}$$

where $\xi = \dfrac{H}{n \cdot d}$ is relative height of spring depending on its stiffness.

$$1.1 \le \xi \le 1.5 \tag{43}$$

Then formula (38) has form

$$k_{sh} = \frac{\left(D^2 + d^2\right)\xi}{\pi \cdot D \cdot d} \tag{44}$$

Analysis of results presented in Table 2 allows to finally evaluate material in terms of its effectiveness to produce shock absorbers. Table 2 shows that efficiency of polymer materials in particular of class of polyurethane elastomers significantly increases when quality of stress state and dimensions of elastic elements are taken into account. This advantage is certain. Even the best spring steel grades (obtained as a result of numerous researches and action focused on obtaining the highest energy intensity) yield to polyurethane elastomers for which corresponding selection has not being conducted and characteristics as energy intensity is not available in standard set of their mechanical characteristics. It is understood that upon receipt of relevant order technologists and polyurethane developers for new elastomers can significantly improve parameter such as energy intensity. Nowadays, it is believed that elastomers of polyurethane type have a great future in terms of amortization of metallurgical equipment [3, 5, 6].

Practice of last two decades of development and implementation of shock absorbers done from molded structural polyurethanes fully confirms this. Designed and manufactured in Peter the Great St. Petersburg Polytechnic University compression shock absorbers for frames of housings rollers and rollers supports of roller tables have been introduced in almost all roughing mills in Ukraine and similar technical solutions will be implemented soon for roughing mills in Russia. These dampers have elastic elements made of polyurethane type CKU-PFL, adiprene, vibrathane and others with normal compressive elastic modulus E_c = 5...500 MPa. This rigidity of the material makes it possible to use elastic element in a form of a monoblock (thick-walled cylinder) and allows it for axial compression.

All similar elastic elements have been installed to replace existing steel disk springs or cylindrical coil springs in existing slots. Thus, overall dimensions of new shock absorbers do not exceed the old ones that greatly simplifies the process of replacing. At the same time, due to significantly higher energy intensity (refer to Table 2) dampers with elastic elements made of polyurethanes provide better protection from dynamic loads and increased resource of elastic elements.

In a future, process of replacing metal springs by polyurethane elastic elements will continue to expand. However, steel springs fully will not be pushed out. This is because of many reasons. All these features refer to mechanical characteristics of elastomers from which it should be noted that use of elastomers is limited by many factors such as heat and cold resistance, internal friction, rheological effects and so on.

Therefore, steel springs for a number of objects remain. To the point, there is another issue that is the choice of optimal design of steel springs. Wherein spring material is excluded from consideration. It is necessary to analyze quality of stress state, filling out of overall dimensions and some of the technological and operational characteristics.

From Table 3 it is clear that elastic element in a form of torsion in terms of its parameters is better than cylindrical coil springs. At the same time, torsion bars are rarely used because of inconvenient form that is long round shaft which is not always possible to successfully fit into the size of protected unit. To the point, the element has greater rigidity. If twisted into a spiral these elements become with acceptable size and stiffness, but lost in optimum use of the overall volume.

Table 3. Features steel springs

Spring type	Strain type	Stress state quality coefficient α	Shape factor k_{sh}	Quality coefficient of the elastic element β
Torsion (Elastic shaft)	Torsion	0.208	1.0	0.208
Cylindrical coil	Torsion	0.208	2.0…3.0	0.083
Disk	Plane stress	0.055	1.5…1.7	0.0345
Ring	Tension and compression	0.5	4.0…6.0	0.109
Multi-sheet	Bend	0.083	1.8…2.0	0.054

Steel springs also need to be analyzed in terms of their effectiveness when working in shock absorbers. First of all, it is necessary to answer the question why on practice with a large number of constructions of steel springs in metallurgical machines are used 1...2 types of springs. Mainly these are various sizes cylindrical coil springs, sometimes these are disk springs. At the same time, torsions, slotted and ring springs are used very rarely and multi-sheet springs are used almost exclusively on some vehicles.

Table 3 shows basic characteristics of the most popular springs. Wherein it takes into account quality factor of stress state and form factors. Obtained results of the analysis are:

1. Quality factor of the elastic element (spring) by volume

$$\beta = \frac{\alpha}{k_{sh}}. \tag{45}$$

2. Quality ratio by weight of the elastic element

$$\beta_m = \frac{\alpha}{k_{sh} \cdot \gamma_m}. \tag{46}$$

On the basis of these coefficients suitability of spring for a specific machine or unit can be concluded. Coefficients of various forms of springs are calculated:

- for cylindrical coil springs (with high stiffness) in the formula (39);
- for disc springs it follows.

Actual volume of spring

$$V = \frac{\pi}{4}\left(D^2 - d^2\right)\delta_S, \tag{47}$$

where D and d are outer and inner diameters of the spring;

δ_S is thickness of spring sheet.

Overall volume of the spring (the volume of cylinder into which it fits)

$$V_0 = \frac{\pi}{4} D^2 \left(\delta_S + \lambda^*\right), \tag{48}$$

where λ^* is maximum spring draught corresponding to maximum stress σ^*. Value of λ^* for disc springs can be taken as draught *S* defined in accordance with Russian State Standard GOST (standard in CIS countries).

Then a shape factor

$$k_{sh} = \frac{D^2\left(\delta_S + \lambda^*\right)}{\left(D^2 - d^2\right)\delta_S}. \tag{49}$$

For increased rigidity of springs (which are mainly used in metallurgy) it is $1.5 \le k_{sh} \le 1.8$. Formula (49) can be simplified when put relative draught for spring

$$\eta = \frac{\delta_S + \lambda^*}{\delta_S}. \tag{50}$$

Quantity for hard springs ranges

$$1.4 \le \eta \le 1.6. \tag{51}$$

Then (49) takes the form

$$k_{sh} = \frac{D^2}{\left(D^2 - d^2\right)}\eta. \tag{52}$$

For slotted spring with dimensions:

D and d are outer and inner diameters;

$\delta = \dfrac{D-d}{2}$ – is thickness of the pipe; H is height of the spring;

ς is relative density of slots

$$\varsigma = \frac{F_h}{F_s}, \tag{53}$$

where F_h is area of holes in pipe wall; F_s is area of side of the pipe.

Usually,

$$0.1 \le \varsigma \le 0.3. \tag{54}$$

In this notation

$$V = \pi(D-d)\cdot\delta\cdot H(1-\varsigma), \tag{55}$$

and the overall volume

$$V_0 = \pi\frac{D^2}{4}\cdot H. \tag{56}$$

Thus the shape factor

$$k_{sh} = \frac{D^2}{4\left(D-d\right)\cdot\delta\cdot\left(1-\varsigma\right)}. \tag{57}$$

For actual size of slotted springs it is.

$$3.0 \le k_{sh} \le 6.0 \tag{58}$$

For a preliminary assessment it can be $k_{sh} \approx 5.0$.

4. Conclusions

1. Laboratory tests for determination of strength and power characteristics of materials for elastic elements of shock absorbers revealed that the best materials are polyurethane elastomers having the largest values of specific energy intensity and wide range of dissipative and stiffness characteristics. It makes possible to create a wide number of effective shock absorbers for different machines.
2. As a result of the analysis of various types of steel springs quality coefficient by volume of spring, coefficient of spring quality by weight, form coefficient for cylindrical coil springs and disk springs are obtained. On the basis of these coefficients conclusions about suitability of certain spring for specific machine or elements and units of building structures.

5. Acknowledgments

The reported study was funded by RFBR according to the research project No. 16-08-00845a "Verification and development of models of inelastic deformation at the passive loading". The authors declare that there is no conflict of interest regarding the publication of this paper.

References

1. Mazur, V., Artyukh, V., Artyukh, G., Takadzhi, M. Current Views on the Detailed Design of Heavily Loaded Components for Rolling Mills. Engineering Designer. 2012. Vol. 37. No.1. Pp. 26–29.
2. Gharaibeh, N.S., Matarneh, M.I, Artyukh, V.G. Loading Decrease in Metallurgical Machines. Research Journal of Applied Sciences, Engineering and Technology. 2014. No. 8(12). Pp.1461–1464.
3. Artiukh, V., Mazur, V., Prakash, R. Increasing Hot Rolling Mass of Steel Sheet Products, Solid State Phenomena. 2016. Vol. 871. Pp. 3–8.

Литература

1. Mazur V., Artyukh V., Artyukh G., Takadzhi M. Current Views on the Detailed Design of Heavily Loaded Components for Rolling Mills // Engineering Designer. 2012. Vol. 37. № 1. Pp. 26–29.
2. Gharaibeh N.S., Matarneh M.I, Artyukh V.G. Loading Decrease in Metallurgical Machines // Research Journal of Applied Sciences, Engineering and Technology. 2014. № 8(12). Pp.1461–1464.
3. Artiukh V., Mazur V., Prakash R. Increasing Hot Rolling Mass of Steel Sheet Products // Solid State Phenomena. 2016. Vol. 871. Pp. 3–8.

Artiukh, V.G., Galikhanova, E.A., Mazur, V.M., Kargin, S.B. Energy intensity of parts made from polyurethane elastomers. Magazine of Civil Engineering. 2018. 81(5). Pp. 102–115. doi: 10.18720/MCE.81.11.

4. Sorochan, E., Artiukh, V., Melnikov, B., Raimberdiyev, T. Mathematical Model of Plates and Strips Rolling for Calculation of Energy Power Parameters and Dynamic Loads. MATEC Web of Conferences. 2016. Vol. 73. 04009.
5. Artiukh, V., Mazur, V., Pokrovskaya, E. Influence of Strip Bite Time in Work Rolls Gap on Dynamic Loads in Strip Rolling Stands. MATEC Web of Conferences. 2016. Vol. 86. 01030.
6. Artiukh, V., Mazur, V., Matarneh, M.I. Horizontal Force During Rolling as Indicator of Rolling Technology and Technical Conditions of Main Rolling Equipment. Procedia Engineering. 2016. No. 165. Pp. 1722–1730.
7. Gharaibeh, N.S., Matarneh, M.I, Artyukh, V.G. Effectiveness of Flexible Pin Type Couplings. International Journal of Engineering Science and Innovative Technology (IJESIT). 2015. Vol. 4. Pp. 1–7.
8. Belkin, A.E., Dashtiev, I.Z., Semenov, V.K. Matematicheskaia model' viazkouprugogo povedeniia poliuretana pri szhatii s umerenno vysokimi skorostiami deformirovaniia [Mathematical Model of Viscoelastic Behavior of Polyurethane under Compression with Moderately High Strain Rates]. Vestnik MGTU im. N.E.Baumana. Ser. Mashinostroenie [Herald of the Bauman Moscow State Technical University. Mechanical Engineering]. 2014. No. 6. Pp. 44–58. (rus)
9. Bergstrom, J., Boyce, M.C. Mechanical behavior of particle filled elastomers. Rubber Chem. Tech. 1999. Pp. 633–656.
10. Artiukh, V.G., Karlushin, S.Yu., Sorochan, E.N. Peculiarities of Mechanical Characteristics of Contemporary Polyurethane Elastomers. Procedia Engineering. 2015. No. 117. Pp. 938–944.
11. Al-Quran, F.M.F., Matarneh, M.E., Artukh, V.G. Choice of Elastomeric Material for Buffer Devices of Metallurgical Equipment. Research Journal of Applied Sciences, Engineering and Technology. 2012. No. 4(11). Pp. 1585–1589.
12. Maniak, I., Melnikov, B., Semenov, A., Saikin, S. Experimental Investigation and Finite Element Simulation of Fracture Process of Polymer Composite Material with Short Carbon Fibers. Applied Mechanics and Materials. 2015. Vol. 725–726. Pp. 943–948.
13. Belkin, A.E., Narskaya, N.L. Raschet elastomernogo tsilindricheskogo amortizatora s uchetom vyazkih svoistv materiala [Analysis of an Elastomer Cylindrical Shock-Absorber with Regard to Viscous Properties of the Material]. Universities News: Engineering. 2015. No. 8(665). Pp. 12–18. (rus)
14. Pestryakov, I.I., Gumerova, E.I., Kupchin, A.N. Assessment of efficiency of the vibration damping material «Teroson WT 129». Construction of Unique Buildings and Structures. 2016. No. 5(44). Pp. 46–57.
15. Govorčin Bajsić, E., Rek, V., Agić, A. Thermal Degradation of Polyurethane Elastomers: Determination of Kinetic Parameters. Journal of Elastomers and Plastics. 2003. Vol. 35. Pp. 311–323.
16. Agić, A., Govorčin Bajsić, E., Rek, V. Kinetic Parameters Estimation for Thermal Degradation of Polyurethane Elastomers. Journal of Elastomers and Plastics. 2006. Vol. 38. Pp. 105–118.
17. Zhang, H., Chen, Y., Zhang, Y., Sun, X., Ye, H. Synthesis and Characterization of Polyurethane Elastomers. Journal of Elastomers and Plastics. 2008. Vol. 40. Pp. 161–177.
18. Datta, J. Synthesis and Investigation of Glycolysates and Obtained Polyurethane Elastomers. Journal of Elastomers and Plastics. 2010. Vol. 42. Pp. 117–127.
19. Bergstrom, J.S., Boyce, M.C. Large strain time-dependent behavior of filled elastomers. Mech. Mater. 2000. Vol. 32. Pp. 627–644.
20. Petrovic, Z., Ferguson, J. Polyurethane Elastomers. Prog. Polym. Sci. 1991. Vol. 16. Pp. 695–836.

4. Sorochan E., Artiukh V., Melnikov B., Raimberdiyev T. Mathematical Model of Plates and Strips Rolling for Calculation of Energy Power Parameters and Dynamic Loads // MATEC Web of Conferences. 2016. Vol. 73. 04009.
5. Artiukh V., Mazur V., Pokrovskaya E. Influence of Strip Bite Time in Work Rolls Gap on Dynamic Loads in Strip Rolling Stands // MATEC Web of Conferences. 2016. Vol. 86. 01030.
6. Artiukh V., Mazur V., Matarneh M.I. Horizontal Force During Rolling as Indicator of Rolling Technology and Technical Conditions of Main Rolling Equipment // Procedia Engineering. 2016. № 165. Pp. 1722–1730.
7. Gharaibeh N.S., Matarneh M. I, Artyukh V.G. Effectiveness of Flexible Pin Type Couplings // International Journal of Engineering Science and Innovative Technology (IJESIT). 2015. Vol. 4. Pp. 1–7.
8. Белкин А.Е., Даштиев И.З., Семенов В.К. Математическая модель вязкоупругого поведения полиуретана при сжатии с умеренно высокими скоростями деформирования // Вестник МГТУ им. Н.Э. Баумана. Серия «Машиностроение». 2014. № 6. С. 44–58.
9. Bergstrom J., Boyce M.C. Mechanical behavior of particle filled elastomers // Rubber Chem. Tech. 1999. Pp. 633–656.
10. Artiukh V.G., Karlushin S.Yu., Sorochan E.N. Peculiarities of Mechanical Characteristics of Contemporary Polyurethane Elastomers // Procedia Engineering. 2015. № 117. Pp. 938–944.
11. Al-Quran F.M.F., Matarneh M.E., Artukh V.G. Choice of Elastomeric Material for Buffer Devices of Metallurgical Equipment // Research Journal of Applied Sciences, Engineering and Technology. 2012. № 4(11). Pp. 1585–1589.
12. Maniak I., Melnikov B., Semenov A., Saikin S. Experimental Investigation and Finite Element Simulation of Fracture Process of Polymer Composite Material with Short Carbon Fibers // Applied Mechanics and Materials. 2015. Vol. 725–726. Pp. 943–948.
13. Белкин А.Е., Нарская Н.Л. Расчет эластомерного цилиндрического амортизатора с учетом вязких свойств материала // Известия высших учебных заведений. Машиностроение. 2015. № 8(665). С.12–18.
14. Пестряков И.И., Гумерова Э.И., Купчин А.Н. Оценка эффективности вибродемпфирующего материала «Teroson WT 129» // Строительство уникальных зданий и сооружений. 2016. № 5(44). С. 46–57.
15. Govorčin Bajsić E., Rek V., Agić A. Thermal Degradation of Polyurethane Elastomers: Determination of Kinetic Parameters // Journal of Elastomers and Plastics. 2003. № 35. Pp. 311–323.
16. Agić A., Govorčin Bajsić E., Rek V. Kinetic Parameters Estimation for Thermal Degradation of Polyurethane Elastomers // Journal of Elastomers and Plastics. 2006. Vol. 38. Pp. 105–118.
17. Zhang H., Chen Y., Zhang Y., Sun X., Ye H. Synthesis and Characterization of Polyurethane Elastomers // Journal of Elastomers and Plastics. 2008. Vol. 40. Pp. 161–177.
18. Datta J. Synthesis and Investigation of Glycolysates and Obtained Polyurethane Elastomers // Journal of Elastomers and Plastics. 2010. Vol. 42. Pp. 117–127.
19. Bergstrom J.S., Boyce M.C. Large strain time-dependent behavior of filled elastomers // Mech. Mater. 2000. Vol. 32. Pp. 627–644.
20. Petrovic Z., Ferguson J. Polyurethane Elastomers // Prog. Polym. Sci. 1991. Vol. 16. Pp. 695–836.
21. Govorcin Bajsic E., Rek V., Sendijarevic A., Sendijarevic V., Frisch K.C. DSC Study of Morphological Changes in

21. Govorcin Bajsic, E., Rek, V., Sendijarevic, A., Sendijarevic, V., Frisch, K.C. DSC Study of Morphological Changes in Segmented Polyurethane Elastomers. Journal of Elastomers and Plastics. 2000. No. 32. Pp. 162–182.
22. Kukhar, V., Artiukh, V., Butyrin, A., Prysiazhnyi, A. Stress-Strain State and Plasticity Reserve Depletion on the Lateral Surface of Workpiece at Various Contact Conditions During Upsetting. In: Murgul V., Popovic Z. (eds) International Scientific Conference Energy Management of Municipal Transportation Facilities and Transport EMMFT 2017. EMMFT 2017. Advances in Intelligent Systems and Computing. 2018. Vol. 692. Pp. 201–211. doi: https://doi.org/10.1007/978-3-319-70987-1_22
23. Balalayeva, E., Artiukh, V., Kukhar, V., Tuzenko, O., Glazko, V., Prysiazhnyi, A., Kankhva, V. Researching of the Stress-Strain State of the Open-Type Press Frame Using of Elastic Compensator of Errors of “Press-Die” System. In: Murgul V., Popovic Z. (eds) International Scientific Conference Energy Management of Municipal Transportation Facilities and Transport EMMFT 2017. EMMFT 2017. Advances in Intelligent Systems and Computing. Vol. 692. Pp. 212–219. doi: https://doi.org/10.1007/978-3-319-70987-1_24
24. Yakovlev, S.N., Mazurin, V.L. Vibroisolating properties of polyurethane elastomeric materials, used in construction. Magazine of Civil Engineering. 2017. No. 6. Pp. 53–60. doi: 10.18720/MCE.74.5
25. Artiukh, V., Nikitchenko, A., Ignatovich, I., Prykina, L. The prospects of creation of the draft gear with the polyurethane resin elastic element for the rolling stock. IOP Conf. Series: Earth and Environmental Science 90. 2017. 012191. doi: 10.1088/1755-1315/90/1/012191

Segmented Polyurethane Elastomers // Journal of Elastomers and Plastics. 2000. № 32. Pp. 162–182.
22. Kukhar V., Artiukh V., Butyrin A., Prysiazhnyi A. Stress-Strain State and Plasticity Reserve Depletion on the Lateral Surface of Workpiece at Various Contact Conditions During Upsetting. In: Murgul V., Popovic Z. // International Scientific Conference Energy Management of Municipal Transportation Facilities and Transport EMMFT 2017. EMMFT 2017. Advances in Intelligent Systems and Computing. 2018. Vol. 692. Pp. 201–211. doi: https://doi.org/10.1007/978-3-319-70987-1_22
23. Balalayeva E., Artiukh V., Kukhar V., Tuzenko O., Glazko V., Prysiazhnyi A., Kankhva V. Researching of the Stress-Strain State of the Open-Type Press Frame Using of Elastic Compensator of Errors of “Press-Die” System. In: Murgul V., Popovic Z. // International Scientific Conference Energy Management of Municipal Transportation Facilities and Transport EMMFT 2017. EMMFT 2017. Advances in Intelligent Systems and Computing. Vol. 692. Pp. 212–219. doi: https://doi.org/10.1007/978-3-319-70987-1_24
24. Яковлев С.Н., Мазурин В.Л. Виброизолирующие свойства полиуретановых эластомеров, применяемых в строительстве // Инженерно-строительный журнал. 2017. № 6(74). С. 53–60. doi: 10.18720/MCE.74.5
25. Artiukh V., Nikitchenko A., Ignatovich I., Prykina L. The prospects of creation of the draft gear with the polyurethane resin elastic element for the rolling stock // IOP Conf. Series: Earth and Environmental Science 90. 2017. 012191. doi: 10.1088/1755-1315/90/1/012191

Viktor Artiukh,
+7(931)579-70-53; artiukh@mail.ru

Elina Galikhanova,*
+7(905)004-41-99; elinlvs.g@gmail.com

Vladlen Mazur,
+7(921)369-17-60; mazur@spbec.com

Sergey Kargin,
+38(098)480-51-15; vbudar1973@gmail.com

Виктор Геннадиевич Артюх,
+7(931)579-70-53; эл. почта: artiukh@mail.ru

Элина Азатовна Галиханова,*
+7(905)004-41-99;
эл. почта: elinlvs.g@gmail.com

Владлен Олегович Мазур,
+7(921)369-17-60;
эл. почта: mazur@spbec.com

Сергей Борисович Каргин,
+38(098)480-51-15;
эл. почта: vbudar1973@gmail.com

doi: 10.18720/MCE.81.12

Protection of construction materials based on acrylates from biodeterioration

Защита строительных материалов на основе акрилатов от биоповреждений

N.A. Anikina*,
V.F. Smirnov,
O.N. Smirnova,
E.A. Zaharova,
Lobachevsky State University of Nizhny Novgorod, Nizhny Novgorod, Russia

Канд. биол. наук, научный сотрудник Н.А. Аникина*,
д-р биол. наук, заведующий отделом В.Ф. Смирнов,
канд. биол. наук, старший научный сотрудник О.Н. Смирнова,
научный сотрудник Е.А. Захарова,
Нижегородский государственный университет им Н.И. Лобачевского, г. Нижний Новгород, Россия

Key words: construction materials based on acrylates; funginertness; microfungi; enzyme activity; biodeterioration of buildings and construction; fungicidal additives; protection from biodeterioration

Ключевые слова: строительные материалы на основе акрилатов; грибостойкость; микроскопические грибы; активность ферментов; биоповреждение зданий и сооружений; фунгицидные присадки; защита от биодеградации

Abstract. The article is dedicated to the funginertness of different construction materials based on acrylates: emulsions Lakroten E-21, Lakroten E-31, Latacryl ZM-1, and Latacryl AF, as well as metacrylate, metacrylate copolymer with metacrylic acid, and n-chlorophenylmetacrylate acrylic glasses. All studied materials, except the Latacryl ZM-1 and copolymer acrylic glasses, demonstrated susceptibility to biodeterioration by microfungi. Multi-compound acrylic compositions appeared to exhibit the emergence, i.e. their funginertness cannot be predicted based on stability of their individual components. Fungal exo-oxidoreductases (catalase, peroxidase) were defined to contribute into the biodegradation processes in construction materials based on acrylates by micromycetes. The biocides Nuosept 78 and Rosima 243 demonstrated the ability to suppress exo-catalase and exo-peroxidase activity (exo-catalase and exo-peroxidase participate in the biodeterioration of the studied materials) in the fungus Aspergillus terreus; thus, they can be recommended for use as means of bioprotection. The non-fungi-resistant acrylic materials were protected from biodeterioration in a targeted and scientifically-grounded way by the introduction of the abovementioned biocidal additives into their compositions. The bioprotection is based on biochemical aspects of biodestructive microfungal activity.

Аннотация. Исследована грибостойкость ряда рецептур строительных материалов на основе акрилатов: эмульсий Лакротэн Э-21, Лакротэн Э-31, Латакрил ЗМ-1, Латакрил АФ и органических стекол на основе метилметакрилата и сополимеров метилметакрилата с метакриловой кислотой и n-хлорфенилметакрилатом. Показано, что все исследованы материалы, за исключением акриловой эмульсии Латакрил ЗМ-1 и сополимерных органических стекол, способны подвергаться биодеструкции микроскопическими грибами. Выявлено, что многокомпонентные акриловые композиции обладают свойством эмерджентности, и их грибостойкость не может быть спрогнозирована, исходя из устойчивости отдельных компонентов рецептур. Установлено участие грибных экзооксидоредуктаз (каталазы, пероксидазы) в процессах биодеградации микромицетами строительных композиций на основе акрилатов. Показано, что биоциды Nuosept 78 и Rosima 243 способны подавлять у гриба Aspergillus terreus активность экзокаталазы и экзопероксидазы, участвующих в деструкционном процессе изучаемых материалов, и, следовательно, могут быть рекомендованы в качестве средств защиты от биоповреждений. Осуществлена научно обоснованная и целенаправленная защита негрибостойких материалов на основе акрилатов от биоповреждений путем введения вышеуказанных биоцидных добавок в состав композиций, основанная на учете биохимических аспектов жизнедеятельности микроскопических грибов-биодеструкторов.

Аникина Н.А., Смирнов В.Ф., Смирнова О.Н., Захарова Е.А. Защита строительных материалов на основе акрилатов от биоповреждений // Инженерно-строительный журнал. 2018. № 5(81). С. 116–124.

1. Introduction

Construction materials based on acrylates (acrylicglasses, paints and lacquers) with increased thermostability, high water and atmospheric resistance are broadly used in various industrial fields and in construction [1–5]. Particularly, acrylic glasses are used as various elements of interior of buildings and structures, advertising materials, illuminating devices, vehicle glazing, instrumentation; acrylic emulsions are used for concrete water-proofing, drenching of porous structural materials, as the basis for paints and lacquers for interior and exterior works, for preparation of water putties, glues, fillers [6–8].

In the course of transportation, storage and use these materials are exposed to the destructive effects of microorganisms, which use them as a nutrient source [9–13]. Microfungi are the most active destructors of different synthetic materials, as they have powerful and labil enzyme systems (oxidoreductases, liases, hydrolases, etc.) enabling to metabolise different polymers, including acrylic-based polymers [14–18]. Biodeterioration of materials is accompanied by change of their decorative, physical and chemical properties, including cracking and layering of coatings, cavitation, foreign odour, deliquation, settling, jellification, viscosity loss, and colour change, which negatively affects appearance and functioning of building constructions [19–22].

Currently, there are no biological resistance (fungal resistance) polymeric acrylate-base compositions [23]. The assortment of acrylic materials is being constantly updated. The new formulations will have different resistance to activity of microorganisms, in particular, microfungi, depending on their chemical composition [24, 25]. The non-fungi-resistant compositions need to be protected from biodeterioration caused by microfungi. There are various methods of material/product bioprotection (mechanical, physical, chemical), with the chemical methods being the most wide-spread. The chemical method features an introduction of special biocidal additives into the material/product composition [26, 27]. Unfortunately, now such additives are selected by trial-and-error method, based only on the information about their fungicidal properties. However, task-orientated and systematic additives selection based on studying the mechanisms of the suppression of the activity of fungal aggressive metabolites, in particular, enzymes taking part in construction materials biodeterioration is required.

In this respect, the purpose of this study is to evaluate funginertness of different construction materials based on acrylates and to develop a targeted and systematic approach to protection of non-fungi-resistant materials from biodeterioration based on biochemical aspects of microorganisms' activity. For this purpose the following objectives have been set:

- Evaluation of the degree of degradation of constructional materials based on acrylates by microscopic fungi
- Revealing the effect of components of acrylic compositions on the degree of their funginertness
- Identification of the most active mycodestructor of the research materials
- Protection of the test materials from microbiological deterioration based on used fungicides ability to suppress the activity of aggressive metabolites taking part in the biodeterioration of construction materials based on acrylates.

2. Methods

The following construction materials based on acrylates were used as the subject of this study: acrylic glasses based on metacrylate copolymer, metacrylicacid, and n-chlorophenylmetacrylate; acrylic emulsions used as film-forming basis for paints for interior and exterior works: Lakroten E-21 (butylacrylate-styrene-acrylicacid copolymer), Lakroten E-31 (butylacrylate-methylmetacrylate-metacrylicacid copolymer), Latacryl ZM-1 (butylacrylate-metacrylicacid-methylmetacrylate copolymer), and Latacryl AF (butylacrylate-methylmetacrylate-styrene-metacrylicacid copolymer).

The preparations Nuosept 78 and Rosima 243 were used as biocides. The active substances of the preparations Nuosept 78 and Rosima 243 are triazine and thyasolinone, respectively.

Funginertness of lacquers and paints, their components, and acrylic glasses was defined using the method described in the literature [28, 29]. This method allows estimating the natural resistance of the materials to microfungal activity, i.e. the possibility to use them by micromycetes as a nutrient source. The biodeterioration level of the polymer materials was studied both in respect to separate microfungal species, and to the mixed culture (mixture of fungi). Samples purified from external contaminations were infected with an aqueous suspension of fungal spores and allowed to stay for 28 days under conditions optimum for their growth. Tests of paints and their components were performed with the use of the following kinds of fungi: Aspergillus terreus, A. niger, A. ustus, Alternaria alternata, Fusarium moniliforme, Penicillium ochrochloron, P. chrysogenum, P. funiculosum, P. martensii, P. brevicompactum, Trichoderma viride, Gliocladium virens; acrylic glasses: Aspergillus niger, A. oryzae, A. terreus, Chaetomium globosum, Penicillium funiculosum, P. chrysogenum, P.cyclopium, Trichoderma viride, Paecilomyces variotii. These species of fungi are active biodegradants of different construction materials, including based on acrylates [30]. Given fungi are mandatory testing cultures, which are used in national and international standard test methods for the degree of polymers and paint-and-lacquer materials biodeterioration. Fungal resistance was estimated from the intensity of fungal development (0-6 points). A material was considered to be fungi-resistant, if it acquired 0–2 points.

Exo-enzyme activity was studied by cultivation of the fungus Aspergillus terreus, one of the most aggressive biodestructor of acrylate-based materials, on carbon-depleted liquid Czapek-Dox medium with the following composition (g/L): $NaNO_3$– 2.0, KH_2PO_4– 0.7, K_2HPO_4– 0.3, KCl – 0.5, $MgSO_4 {*} 7H_2O$ – 0.5, $FeSO_4 {*} 7H_2O$ – 0.01, sucrose – 1.5. The modified Czapek-Dox medium which additionally contained the acrylic emulsion Lakroten E-21 as a nutrient source was used in some experiments. The biocidal preparations were introduced to the media on the fourth day of the fungus cultivation.

The enzymatic activity was defined by spectrophotometric method (UV-mini 1240, Shimadzy, Australia): catalase activity – by consumption of H_2O_2 (λ=240 nm) [31], peroxidase activity – by oxidation of n–phenylenediamine (λ=535 nm) in presence of H_2O_2 [32]. The enzymatic activity was expressed in conventional units (c.u.). Change of optical density of the reaction mixture taken per 1 mg of protein in 1 minute was considered to be an activity unit for each of the abovementioned enzymes. The protein content in my celium and culture fluid were defined by Lowry – Folin method [33].

The statistical processing of results and the reliability assessment of differences in mean values were carried out according to the criteria of a student's test for the probability level of no less than 95% with the use of Microsoft Excel 2007 and Statistica 10.0 software.

3. Results and Discussion

The information on evaluation of funginertness of acrylic polymers (both to mixture of different cultures and to individual cultures) is represented in Table 1.

The obtained results demonstrated, that in the case influence of a mixture of fungal cultures, Latacryl ZM-1 revealed fungi-resistant characteristics; other tested acrylates did not demonstrate funginertness to micromycetic activity and can be consumed by them as a nutrient source. Comparison of destructive abilities of fungus strains posed an interesting task. In this regard, we evaluated funginertness of compositions to activity of various fungus cultures. The tested materials demonstrated different levels of resistance to particular fungus species. The fungi Aspergillus terreus, Fusarium moniliforme, Penicillium funiculosum appeared to be the most active biodegradants of acrylic emulsions.

Table 1. Evaluation of growth of individual fungus species and their mixture on the tested materials

	Growth level, points			
Material / Fungus species	Lakroten E-21	Lakroten E-31	Latacryl AF	Latacryl ZM-1
Mixture of fungus cultures	3	3	3	2
Aspergillus terreus	3	3	3	3
A. niger	2	2	2	2
A. ustus	1	2	2	2
Alternaria alternate	1	2	3	3
Fusarium moniliforme	2	3	2	3
Penicillium ochrochloron	1	1	2	2
P. chrysogenum	2	1	3	2
P. funiculosum	3	3	3	3
P. martensii	2	2	3	2
P. brevicompactum	2	2	2	3
Trichoderma viride	1	1	2	2
Gliocladium virens	1	1	2	2

The funginertness of acrylic glasses of various acrylate-based compositions was studied in the same way (Table 2).

Table 2. Evaluation of growth of individual fungus species and their mixture on the acrylic glasses

	Growth level, points		
Material / Fungus species	Polymethylmetacrylate	Polymethylmetacrylate – metacrylic acid – n-chlorophenyl-metacrylate copolymer	Polymethylmetacrylate – metacrylic acid copolymer
Mixture of fungus culture	4	2	2
Chaetomium globosum	2	3	4
Penicillium funiculosum	2	3	4
Aspergillus terreus	4	3	3
P. chrysogenum	3	3	4
P. cyclopium	3	3	4
Trichoderma viride	2	3	3
A. oryzae	4	3	3
A. niger	1	1	1
Paecilomyces variotii	4	4	3

Among acrylic glasses, copolymer formulations of acrylic compositions appeared to be resistant to activity of mixture of fungus cultures. Tests for individual fungus species proved that all studied compositions of acrylic glasses appeared to be non-fungi-resistant, i.e. they are susceptible to biodeterioration by microfungi (except the variants with Aspergillus niger). The most intensive growth on these materials was expressed by the fungi Paecilomyces variotii, P. chrysogenum.

Notably, the biodeterioration process is more intensive for acrylic glasses in comparison with emulsions, as in this case the observed growth of fungi on the materials was evaluated as 4 points (the fungus growth covers less than 25% of the surface and can be observed with the naked eye). Various levels of biodeterioration of polymer acrylate materials, in our opinion, may be caused either by difference in their compositions, or by physiological and biochemical characteristics of the biodestroying fungi.

We tested individual components of acrylic emulsions for funginertness (Table 3).

Table 3. Funginertness of components of acrylic emulsions

Components of acrylic emulsions	Growth level, points	Evaluation of funginertness
Methylmetacrylate	3	Non-fungi-resistant
Ethylacrylate	0	Fungi-resistant
Methacrylic acid	0	Fungi-resistant
Butylacrylate	0	Fungi-resistant
Butylmetacrylate	0	Fungi-resistant
Styrene	3	Non-fungi-resistant
Vinylidene dichloride – vinyl chloride copolymer latex (VDVC-65 latex)	1	Fungi-resistant
Emulsifier S-10	5	Non-fungi-resistant
Neonol (emulsifier)	0	Fungi-resistant
Sulphonol (emulsifier)	4	Non-fungi-resistant

The experiment results represented in Table 3 demonstrated that ethylacrylate, butylmetacrylate, VDVC-65 latex, neonol, metacrylic acid, and butylacrylate have fungi-resistance characteristics. Meanwhile, such compounds as methylmetacrylate, emulsifier S-10, styrene, and sulphonol appeared to be non-fungi-resistant (the observed fungus growth was evaluated as 5 and 4 points, respectively).

According to the data presented in literature, biodeterioration of polymers is mainly an enzymatic process [8, 19]. Many acrylate-based materials are suspected to micromycetic destruction by activity of exo-oxidoreductases (catalase and peroxidase). In this regard, on the next stage of the study peroxidase and catalase activity of A. terreus, one of the most active biodestructors of the tested materials, was analysed during the cultivation in the medium with acrylate (Figure 1).

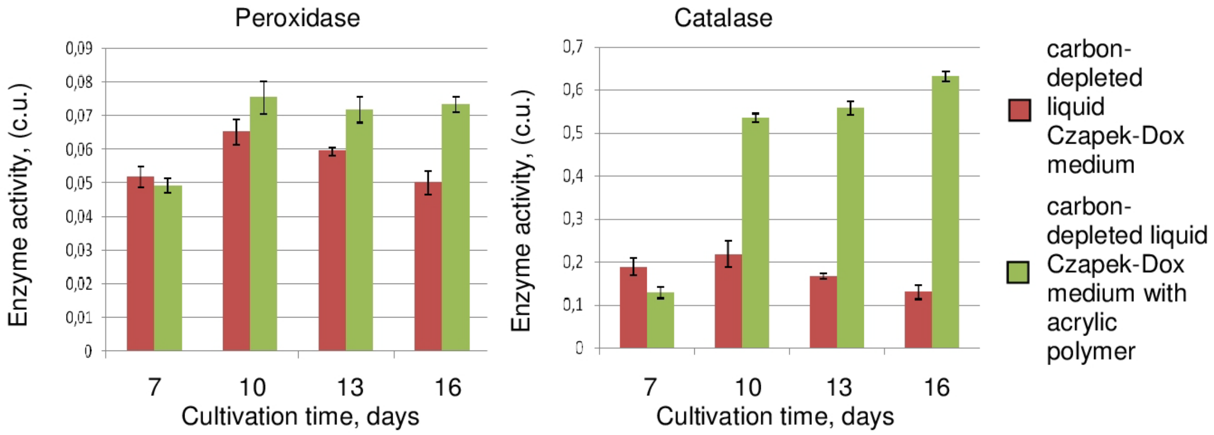

Figure 1. Peroxidase and catalase activity of A. terreus in the course of cultivation on media with different composition

We discovered peroxidase and catalase activity in A. terreus, where the latter exceeded the peroxidase activity significantly. It was demonstrated, that adding acrylic materials to the nutrient medium causes the increase in exo-catalase and exo-peroxidase activity compared with the control experiment, which shows the possibility of participation of these exo-oxidoreductases in the deterioration of the examined acrylic polymer.

On the next stage of this study, the influence of Nuosept 78 and Rosima 243, biocides widely used presently for bioprotection of various construction and industrial materials from mycodestructors, on exo-catalase and exo-peroxidase activity of A. terreus was defined on carbon-depleted liquid Czapek-Dox medium enriched with an acrylic polymer (Figure 2).

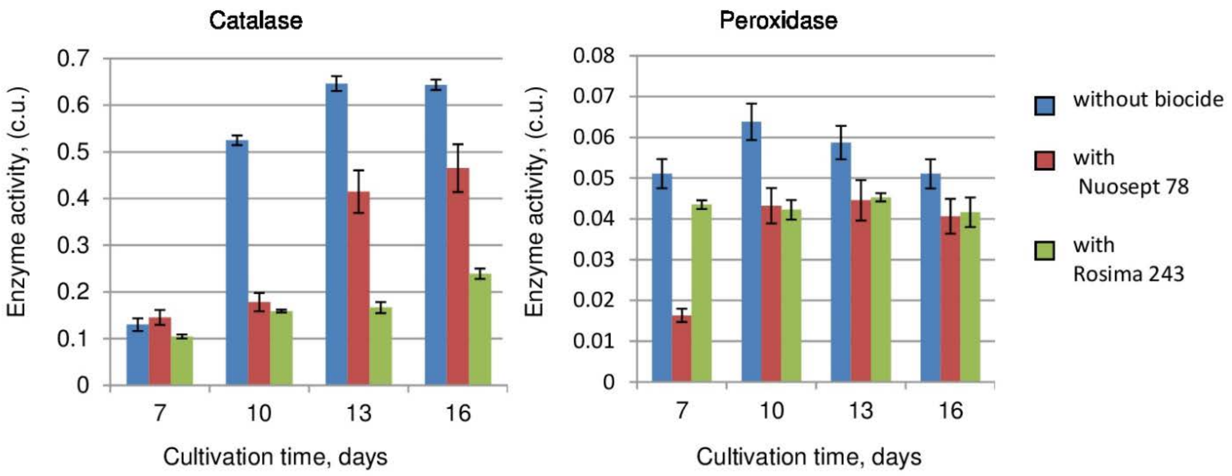

Figure 2. Catalase activity during cultivation of A. terreus on carbon-depleted liquid medium with added acrylic polymer

The experiment results showed that adding biocides to the acrylate-rich cultivation medium causes inhibition of catalase and peroxidase activity. The maximum inhibiting effect of the Rosima 243 in respect of catalase and peroxidase developed on the 13-th – 16-th day of cultivation, and of the Nuosept 78 – on the 7-th – 10-th day of exposure.

Due to the fact that the examined compounds inhibited the activity of fungal exo-oxidoreductases involved into the deterioration of acrylic polymer compositions, it was interesting to assess the possibility to use Rosima 243 and Nuosept 78 as the biodeterioration protective means for non-fungi-resistant acrylic polymer compositions. These biocides were added to the acrylic compositions. The effective biocide concentrations providing resistance of the examined materials to fungal activity were selected by experiment. The results of these experiments are given in Table 4.

Table 4. Funginertness of acrylic polymer compositions with added biocidal additives

	Growth level, points	
Biocide / Material	Rosima 243 (0.5 % w/w)	Nuosept 78 (0.5 % w/w)
Lakroten E-21	0	0
Lakroten E-31	0	1
Latacryl AF	1	1
Latacryl ZM-1	1	0
Polymethylmethacrylate	2	2
Polymethylmethacrylate copolymer - metacrylic acid - n-chlorophenylmethacrylate	2	2
Polymethylmethacrylate copolymer - metacrylicacid	2	2

The results given in the table showed that adding Nuosept 78 and Rosima 243 biocides to the non-fungi-resistant polymer compositions (in the concentration not more than 0.5 % w/w) gave them resistance to microfungal activity. The achieved results justify to the full extent our approach to targeted and systematic protection of specific materials (in this case acrylic polymers) and building construction s on their basis from microbiological deterioration based on used protection means (fungicides) ability to suppress the activity of aggressive metabolites (exoenzymes) taking part in the biodeterioration of construction materials based on acrylates.

Currently, a number of various methods based on microbiological, physical, and chemical principles is used for biodeterioration evaluation for industrial and construction materials [34]. The funginertness evaluation method used by us is based on the visual evaluation of fungal growth on the materials. Although the long time required for this method (28–30 days) is its drawback, its advantage is evident, i.e. only this method allows concluding quite reliably on the possibility to use the material by fungi as a nutrient source. This principle is broadly used both in original and in conventional studies of fungal resistance [35–37].

The question of the possibility to predict funginertness of the whole formulation, if funginertness of separate components is known, needs to be answered. The obtained data show that it is not possible. All tested formulations of acrylic emulsions contain both fungi-resistant and non-fungi-resistant components. However, the fungus growth levels are different on these materials. Consequently, the biodegradation level of the final formulation may depend on the quantitative ratio of initial ingredients, i.e. in this case the phenomenon of emergence was observed. The same situation was observed by us before, when we studied funginertness of acrylic emulsions of the trademarks Acremos and MBM [38]. In case if a non-fungi-resistant polymeric composition needs to acquire fungi-resistant properties, an additive with fungicidal effect should be introduced into this composition.

As mentioned before, now construction and industrial materials are protected not by scientifically-grounded means, but bytrial-and-error method, i.e. a fungicidal additive is selected from the existing list of technical biocides used as the means of protection from biodeterioration. In this case not always an effective biocide can be selected immediately; this process can be time-sapping. Besides, this method is not ecologically safe, as the biocidal effect of the selected protective mean may have the “total” effect and induce extinction of fungi, which are not engaged into the biodestruction process. In our opinion, the physiological and biochemical approach based on the study of mechanisms of biocidal inhibiting effects on fungal metabolites (exoenzymes), involved in biodegradation of materials, provides the optimal and targeted protection from biodeterioration. Nowadays biochemical approach is present in studying the process of construction materials biodeterioration in particular Serova T.A. et al. propose a wood deterioration diagnostic technique based on the determination of its lignin and cellulose content [39].

Our approach was tested by us for protection of acrylates from biodeterioration, as an example. As noted above, the fungi Aspergillus terreus are the most aggressive among the destructors of the studied materials. These micromycetes are known to be good producers of such extracellular enzymes as catalase and peroxidase [29]. These enzymes are able to participate in biodestruction of such materials as acrylates, polystyrenes, epoxide resins [30, 11].The biocides Nuosept 78 and Rosima 243 are broadly used for protection of these materials. The investigation on the dependence of their high bioprotective effect and their ability to inhibit such enzymes as catalase and peroxidase was a matter of a particular interest.

Actually, the results of our experiments confirmed this assumption; and it allowed using the abovementioned biocides as the effective protective means for acrylates against fungal biodeterioration. The physiological and biochemical approach can be successfully extrapolated for the targeted protection of other construction materials, used in construction of various buildings and structures, to enhance its efficiency and reduce the biocidal additives' selection period.

4. Conclusions

In the work, it was revealed that the most of the studied compositions of acrylic emulsions and acrylic glasses widely used in construction industry for creation of various buildings and structures can be subjected to fungal biodeterioration i.e. be used as a nutrient source. Acrylic emulsion Latacryl 3M-1 and copolymer glasses (copolymer polymethylmethacrylate-methacrylic acid- n-chlorophenyl methacrylate and polymethyl methacrylate copolymer – methacrylic acid) have exhibited funginertness. The scientifically based and task-orientated protection of acrylic materials against biodeterioration by adding biocidal additives into the mixture was achieved with respect to physiology-biochemical aspects (the activity of exo-oxidoreductases participating in the biodeterioration) of fungi-decomposers. In the connection with these facts, Nuosept 78 and Roisma 243 were recommended for the protection of non-funginert acrylates against biodeteriorations. Given biocides are able to suppress oxidoreductase activity. This approach will allow considerably optimize and specify the search of biocidal agents for the protection of materials against fungal biodegradation. With the use of the new approach based on the consideration of a biocides ability to inhibit fungal aggressive metabolites in particular exoenzymes that are capable of participating in construction materials biodeterioration, effective biodeterioration protective means (Nuosept 78 and Roisma 243) were selected. The incorporation of given biocides into acrylate compositions provided their persistence to fungal biodeterioration.

References

1. Yeskov, A.A., Lebedeva, T.A., Belova, M.V. Lakokrasochnyye materialy s ponizhennym soderzhaniyem letuchikh veshchestv (obzor) [Paint-and-lacquer materials with lowered content of volatile organic compounds (review)]. Trudy VIAM. 2015. No. 6. St. 08. (rus)
2. Seo, J.Y., Han, M. Multi-functional hybrid coatings containing silica nanoparticles and anticorrosive acrylate monomer for scratch and corrosion resistance. Nanotechnology. 2011. No. 22. Pp. 1–9.
3. Shcherbakova, M.S., Shutilin, Yu.F., Moiseyev, V.V. Vliyaniye sostava lakokrasochnogo materiala na svoystva pokrytiy [Influence of the composition of paint on the properties of coatings]. Vestnik VGUIT. 2013. No. 1(55). Pp. 137–139. (rus)
4. Abrosimova, L.F., Shakirova, O.G. Antikorrozionnyy lakokrasochnyy material na osnove akrilovykh sopolimerov [Anticorrosive paint based on acrylic copolymers]. Yevraziyskiy soyuz uchenykh. 2016. No. 1-2(22). Pp. 21–23. (rus)
5. Shirakawa, M.A., Loh, K., John, V.M., Silva, M.E.S., Gaylarde, C.C. Biodeterioration of painted mortar surfaces in tropical urban and coastal situations: Comparison of four paint formulations. International Biodeterioration and Biodegradation. 2011. Vol. 65(5). Pp. 669–674.
6. Sentyurin, Ye.G., Mekalina, I.V., Ayzatulina, M.K., Bogatov, V.A. Akrilatnyye vysokoteplostoykiye organicheskiye stekla. Opyt primeneniya. Perspektivy [Acrylate high-temperature resistant organic glass. Experience of application. Prospects]. Izvestiya vysshikh uchebnykh zavedeniy. Seriya "Khimiya i khimicheskaya tekhnologiya". 2015. No. 58(8). Pp. 22–24. (rus)
7. Petrov, A.A., Klimova, S.F., Mekalina, I.V., Sentyurin, Ye.G., Bogatov, V.A. Novyye akrilatnyye organicheskiye stekla chastichno sshitoy struktury [New acrylate organic glass partially cross-linked structure]. Uspekhi v khimii i khimicheskoy tekhnologii. 2012. No. 4(133). Pp. 70–72. (rus)
8. Sharma, M., Sharma, P., Sharma, A., Chandra, S. Microbial Degradation Of Plastic - A Brief Review. CIBTech Journal of Microbiology. 2015. Vol. 4(1). Pp. 85–89.

Литература

1. Еськов А.А., Лебедева Т.А., Белова М.В. Лакокрасочные материалы с пониженным содержанием летучих веществ (обзор) // Труды ВИАМ. 2015. № 6. Ст. 08.
2. Seo J.Y., Han M. Multi-functional hybrid coatings containing silica nanoparticles and anticorrosive acrylate monomer for scratch and corrosion resistance // Nanotechnology. 2011. № 22. Pp. 1–9.
3. Щербакова М.С., Шутилин Ю.Ф., Моисеев В.В. Влияние состава лакокрасочного материала на свойства покрытий // Вестник ВГУИТ. 2013. № 1(55). С. 137–139.
4. Абросимова Л.Ф., Шакирова О.Г. Антикоррозионный лакокрасочный материал на основе акриловых сополимеров // Евразийский союз ученых. 2016. № 1–2(22). С. 21–23.
5. Shirakawa M.A., Loh K., John V.M., Silva M.E.S., Gaylarde C.C. Biodeterioration of painted mortar surfaces in tropical urban and coastal situations: Comparison of four paint formulations // International Biodeterioration and Biodegradation. 2011. Vol. 65(5). Pp. 669–674.
6. Сентюрин Е.Г., Мекалина И.В., Айзатулина М.К., Богатов В.А. Акрилатные высокотеплостойкие органические стекла. Опыт применения. Перспективы // Известия высших учебных заведений. Серия "Химия и химическая технология". 2015. № 58(8). С. 22–24.
7. Петров А.А., Климова С.Ф., Мекалина И.В., Сентюрин Е.Г., Богатов В.А. Новые акрилатные органические стекла частично сшитой структуры // Успехи в химии и химической технологии. 2012. № 4(133). С. 70–72.
8. Sharma M., Sharma P., Sharma A., Chandra S. Microbial Degradation Of Plastic - A Brief Review // CIBTech Journal of Microbiology. 2015. Vol. 4(1). Pp. 85–89.
9. Elumalai P., Elumalai E., David E. Fungi associated with deteriorations of painted wall surfaces: isolation and identification // European Journal of Academic Essays. 2014. Vol. 1(3). Pp. 48–50.
10. Gautam R. A review of biodegradation of synthetic plastic and foams // Applied Biochemistry and Biotechnology. 2007. Vol. 141(1). Pp. 85–108.

9. Elumalai, P., Elumalai, E., David, E. Fungi associated with deteriorations of painted wall surfaces: isolation and identification. European Journal of Academic Essays. 2014. Vol. 1(3). Pp. 48-50.
10. Gautam, R. A review of biodegradation of synthetic plastic and foams. Applied Biochemistry and Biotechnology. 2007. Vol. 141(1). Pp. 85–108.
11. Shah, A.A. Biological degradation of plastics: A comprehensive review. Biotechnology Advances. 2008. Vol. 26. Pp. 246–265.
12. Grassi, N., Skott, Dzh. Destruktsiya i stabilizatsiya polimerov [Destruction and stabilization of polymers]. Moskva: Mir, 1988. 446 p. (rus)
13. English, S.E., Fjelde, S., Greenhalgh, M., McCabe, R.W., McKenna, T., Morton, L.H.G., Schmidt, B., Sherrington, I. Laboratory and field studies on thin paint films. International Biodeterioration and Biodegradation. 2003. Vol. 52(40). Pp. 247–253.
14. Okunye, O.L., Morakinyo, K.O., Ayedun, J.S. Isolation and Characterization of Fungi Associated with in Can Degradation of Paint. Journal of Environment and Earth Science. 2013. Vol. 3(12). Pp. 142–145.
15. Sabadakha, Ye.N., Prokopchuk, N.R., Goncharova, I.A. Vliyaniye metabolitov gribov na fiziko-mekhanicheskiye svoystva lakokrasochnykh pokrytiy [Influence of metabolites of fungi on the physico-mechanical properties of paint and varnish coatings]. Trudy BGTU. Seriya 4: Khimiya i tekhnologiya organicheskikh veshchestv. 2010. No. 4. Pp. 306–309. (rus)
16. Shimao, M. Biodegradation of plastics. Current Opinion in Biotechnology. 2001. Vol. 12(3). Pp. 242–247.
17. Pathak, V.M., Navneet. Review on the current status of polymer degradation: a microbial approach. Bioresources and Bioprocessing. 2017. No. 4(15). Pp. 1–31.
18. Gu, J.D. Microbiological deterioration and degradation of synthetic polymeric materials: recent research advances. International Biodeterioration and Biodegradation. 2003. Vol. 52(2). Pp. 69–91.
19. Ravikumar, H.R., Shwetha, S.R., Karigar, C.S. Biodegradation of paints: a current status. Indian Journal of Science and Technology. 2012. Vol. 5(1). Pp. 1977–1987.
20. Ishfaq, S., Ali, N., Tauseef, I., Khattak, M.N.K., Shinwari, Z.K., Ali, M.I. Analysis of paint degradation by fungal and bacterial species. Pakistan Journal of Botany. 2015. Vol. 47(2). Pp. 753–760.
21. Obidi, O.F., Aboaba, O.O., Makanjuola, M.S., Nwachukwu, S.C.U. Microbial evaluation and deterioration of paints and paint-products. Journal of Environmental Biology. 2009. Vol. 30(5). Pp. 835–840.
22. Mai, C., Schormann, W., Majcherczyk, A., Hüttermann, A. Degradation of acrylic copolymers by white-rot fungi. Applied Microbiology and Biotechnology. 2004. No. 65(4). Pp. 479–487.
23. Kurowski, G., Vogt, O., Ogonowski, J. Paint-degrading microorganisms. Technical Transactions. 2017. Vol. 12. Pp. 81–92.
24. Kutz, M. Handbook Of Environmental Degradation Of Materials. USA: William Andrew Publishing, 2012. 936 p.
25. Shumaila, I., Naeem, A., Isfahan, T., Muhammad, N.K.K., Zabta, K.S., Muhammad, I.A. Analysis of paint degradation by fungal and bacterial species. Pakistan Journal of Botany. 2015. No. 47(2). Pp. 753–760.
26. Edge, M., Allen, N.S., Turner, D., Robinson, J., Seal, K. The enhanced performance of biocidal additives in paints and coatings. Progress in Organic Coatings. 2001. No. 43. Pp. 10–17.
27. Cappitelli, F., Sorlini, C. Microorganisms Attack Synthetic Polymers in Items Representing Our Cultural Heritage. Applied and Environmental Microbiology. 2008. Vol. 74(3). Pp. 564–569.

11. Shah A.A. Biological degradation of plastics: A comprehensive review // Biotechnology Advances. 2008. Vol. 26. Pp. 246–265.
12. Грасси Н., Скотт Дж. Деструкция и стабилизация полимеров. Москва: Мир, 1988. 446 с.
13. English S.E., Fjelde S., Greenhalgh M., McCabe R.W., McKenna T., Morton L.H.G., Schmidt B., Sherrington I. Laboratory and field studies on thin paint films // International Biodeterioration and Biodegradation. 2003. Vol. 52(40). Pp. 247–253.
14. Okunye O.L., Morakinyo K.O., Ayedun J.S. Isolation and Characterization of Fungi Associated with in Can Degradation of Paint // Journal of Environment and Earth Science. 2013. Vol. 3(12). Pp. 142–145.
15. Сабадаха Е.Н., Прокопчук Н.Р., Гончарова И.А. Влияние метаболитов грибов на физико-механические свойства лакокрасочных покрытий // Труды БГТУ. Серия 4: Химия и технология органических веществ. 2010. № 4. С. 306–309.
16. Shimao M. Biodegradation of plastics // Current Opinion in Biotechnology. 2001. Vol. 12(3). Pp. 242–247.
17. Pathak V.M., Navneet. Review on the current status of polymer degradation: a microbial approach // Bioresources and Bioprocessing. 2017. № 4(15). Pp. 1–31.
18. Gu J.D. Microbiological deterioration and degradation of synthetic polymeric materials: recent research advances // International Biodeterioration and Biodegradation. 2003. Vol. 52(2). Pp. 69–91.
19. Ravikumar H.R., Shwetha S.R., Karigar C.S. Biodegradation of paints: a current status // Indian Journal of Science and Technology. 2012. Vol. 5(1). Pp. 1977–1987.
20. Ishfaq S., Ali N., Tauseef I., Khattak M.N.K., Shinwari Z.K., Ali M.I. Analysis of paint degradation by fungal and bacterial species // Pakistan Journal of Botany. 2015. Vol. 47(2). Pp. 753–760.
21. Obidi O.F., Aboaba O.O., Makanjuola M.S., Nwachukwu S.C.U. Microbial evaluation and deterioration of paints and paint-products // Journal of Environmental Biology. 2009. Vol. 30(5). Pp. 835–840.
22. Mai C., Schormann W., Majcherczyk A., Hüttermann A. Degradation of acrylic copolymers by white-rot fungi // Applied Microbiology and Biotechnology. 2004. № 65(4). Pp. 479–487.
23. Kurowski G., Vogt O., Ogonowski J. Paint-degrading microorganisms // Technical Transactions. 2017. Vol. 12. Pp. 81–92.
24. Kutz M. Handbook Of Environmental Degradation Of Materials. USA:William Andrew Publishing, 2012. 936 p.
25. Shumaila I., Naeem A., Isfahan T., Muhammad N.K.K., Zabta K.S., Muhammad I.A. Analysis of paint degradation by fungal and bacterial species // Pakistan Journal of Botany. 2015. Vol. 47(2). Pp. 753–760.
26. Edge M., Allen N.S., Turner D., Robinson J., Seal K. The enhanced performance of biocidal additives in paints and coatings // Progress in Organic Coatings. 2001. № 43. Pp. 10–17.
27. Cappitelli F., Sorlini C. Microorganisms Attack Synthetic Polymers in Items Representing Our Cultural Heritage // Applied and Environmental Microbiology. 2008. Vol. 74(3). Pp. 564–569.
28. Mochalova A.E., Kruglova E.N., Yunin P.A., Apryatina K.V., Smirnova O.N., Smirnova L.A. Graft and block copolymers of chitosan with vinyl monomers: Synthesis, structure, and properties // Polymer Science Series B. 2015. Vol. 57(2). Pp 93–105.
29. Smirnov V.F., Smirnova L.A., Mochalova A.E., Kryazhev D.V., Tsverova N.E., Zotov K.A. Destrction of compositions based on chitosan copolymers with vinyl monomers by micromycetes // Biotekhnologiya. 2011. № 4. Pp. 47–56.

28. Mochalova, A.E., Kruglova, E.N., Yunin, P.A., Apryatina, K.V., Smirnova, O.N., Smirnova, L.A. Graft and block copolymers of chitosan with vinyl monomers: Synthesis, structure, and properties. Polymer Science Series B. 2015. Vol. 57(2). Pp. 93–105.
29. Smirnov, V.F., Smirnova, L.A., Mochalova, A.E., Kryazhev, D.V., Tsverova, N.E., Zotov, K.A. Destrction of compositions based on chitosan copolymers with vinyl monomers by micromycetes. Biotekhnologiya. 2011. No. 4. Pp. 47–56.
30. Chiellini, E., Meisel, I. Resent advances in biodegradable polymers and plastics. Wiley, Somerset New Jersey U.S.A.: John and Sons, 2003. 446 p.
31. Li, Y., Shellhorn, H.E. Rapid kinetic microassay for catalase activity. Journal of Biomolecular Techniqes. 2007. Vol. 18. Pp. 185–187.
32. Nagaraja, P., Shivakumar, A., Kumar, S.A. Development and evaluation of kinetie spectrophotometric assays for horseradish peroxidase by catalytic coupling of paraphenylendiamine and mequinol. Analytical Scienses. 2009. Vol. 25. Pp. 1243–1248.
33. Doson, R., Elliot, D., Elliot, U., Dzhons, K. Spravochnik biokhimika [Biochemistry handbook]. Moskva: Mir, 1991. 544 p. (rus)
34. Ermolovich, O.A., Makarevich, A.V., Goncharova, E.P., Vlasova, G.M. Methods for Analyzing of Biodegrability of Polymeric Materials. Biotechnology in Russia. 2005. No. 4. Pp. 62–72.
35. ASTM G 21 Standard Practice for Determining Resistance of Synthetic Polymeric Materials to Fungi. American Society for Testing and Materials. 2002. 6 p.
36. ASTM D5590-00 Standard Test Method for Determining the Resistance of Paint films and Related Coatings to Fungal Defacement by Accelerated Four-Week Agar Plate Assay. 2010. 4 p.
37. ISO 846 Plastics — Evaluation of the action of microorganisms. 1997. 27 p.
38. Smirnov, V.F., Berezhnaya, Ye.V., Semin, I.V., Frantsuz, Z.S., Tsendrovskiy, D.V. Gribostoykiye akrilovyye emulsii dlya vodno-dispersionnykh materialov razlichnogo naznacheniya [Fungi-resistant acrylic emulsions for water-dispersive materials for various purposes]. Lakokrasochnyye materialy i ikh primeneniye. 1993. No. 6. Pp. 15–16. (rus)
39. Serova, T.A., Titova, J.A., Shenin, J.D. Chemical method of assessing the degree of biodegradation of wooden structural elements. Magazine of Civil Engineering. 2014. No. 3(47). Pp. 77–89.

30. Chiellini E., Meisel I. Resent advances in biodegradable polymers and plastics. Wiley, Somerset New Jersey U.S.A.: John and Sons, 2003. 446 p.
31. Li Y., Shellhorn H.E. Rapid kinetic microassay for catalase activity // Journal of Biomolecular Techniqes. 2007. Vol. 18. Pp. 185–187.
32. Nagaraja P., Shivakumar A., Kumar S.A. Development and evaluation of kinetie spectrophotometric assays for horseradish peroxidase by catalytic coupling of paraphenylendiamine and mequinol // Analytical Scienses. 2009. Vol. 25. Pp. 1243–1248.
33. Досон Р., Эллиот Д., Эллиот У., Джонс К. Справочник биохимика. Москва: Мир, 1991. 544 с.
34. Ermolovich O.A., Makarevich A.V., Goncharova E.P., Vlasova G.M. Methods for Analyzing of Biodegrability of Polymeric Materials // Biotechnology in Russia. 2005. № 4. Pp. 62–72.
35. ASTM G 21 Standard Practice for Determining Resistance of Synthetic Polymeric Materials to Fungi. American Society for Testing and Materials. 2002. 6 p.
36. ASTM D5590-00 Standard Test Method for Determining the Resistance of Paint films and Related Coatings to Fungal Defacement by Accelerated Four-Week Agar Plate Assay. 2010. 4 p.
37. ISO 846 Plastics — Evaluation of the action of microorganisms. 1997. 27 p.
38. Смирнов В.Ф., Бережная Е.В., Семин И.В., Француз З.С., Цендровский Д.В. Грибостойкие акриловые эмульсии для водно-дисперсионных материалов различного назначения // Лакокрасочные материалы и их применение. 1993. № 6. С. 15–16.
39. Серова Т.А., Титова Ю.А., Шенин Ю.Д. Химический метод оценки степени биодеградации древесины конструктивных элементов // Инженерно-строительный журнал. 2014. №3(47). С. 77–89.

Nadezhda Anikina,
+7(904)045-06-08; undinaf@gmail.com

Vasiliy Smirnov,
+7(951)917-10-15; biodeg@mail.ru

Olga Smirnova,
+7(905)668-71-31; protectfun@mail.ru

Elena Zaharova,
+7(960)184-05-46;
zaharova_elena_aleksandrovna@mail.ru

Надежда Андреевна Аникина,
+7(904)045-06-08;
эл. почта: undinaf@gmail.com

Василий Филиппович Смирнов,
+7(951)917-10-15; эл. почта: biodeg@mail.ru

Ольга Николаевна Смирнова,
+7(905)668-71-31;
эл. почта: protectfun@mail.ru

Елена Александровна Захарова,
+7(960)184-05-46; эл. почта:
zaharova_elena_aleksandrovna@mail.ru

Аникина Н.А., Смирнов В.Ф., Смирнова О.Н., Захарова Е.А. Защита строительных материалов на основе акрилатов от биоповреждений // Инженерно-строительный журнал. 2018. № 5(81). С. 116–124.

doi: 10.18720/MCE.81.13

Structurization processes of cement composites modified with electrolytic additives

Процессы структурообразования цементных композитов, модифицированных добавками электролитов

T.S. Shepelenko*,
N.P. Gorlenko,
O.A. Zubkova,
Tomsk State University of Architecture and Building, Tomsk, Russia

Канд. хим. наук, доцент Т.С. Шепеленко*,
д-р техн. наук, профессор Н.П. Горленко,
канд. техн. наук, доцент О.А. Зубкова,
Томский государственный архитектурно-строительный университет, Томск, Россия

Key words: cement; electrolytic solutions; aluminium and ferric chloride solutions; additives; strength

Ключевые слова: цемент; растворы электролитов; хлориды алюминия и железа; добавки; прочность

Abstract. There has been research on the impact of $AlCl_3$ and $FeCl_3$ solutions on kinetics of cement hardening. The research was carried out in two comparative versions, one of which had the saline solutions introduced into cement as gauge liquid (“water–1% electrolytic solution”), the other had them as additives, synthesized in suspensions “cement – (water–1% electrolytic solution)”. It has been stated that the use of $AlCl_3$ and $FeCl_3$ solutions as gauge liquids leads to reduction of compression resistance values of modified cement rocks. The value of 28-day hardness, compared to plain cement, is reduced by 18 % in case of cement gauging with $AlCl_3$ solution, and by 27% in case of binder gauging with $FeCl_3$ solution. On the contrary, the composites, produced by means of introducing the additives, synthesized within suspensions, into cement paste, have shown a significant boost in 28-day hardness compared to plain sample – by 30 and 23 % accordingly. The analysis of the result studies of the additives by means of XPA and IR-spectral analysis has shown that within the structurization of additives the interrelated changes take place, due to the rapid decrease of portlandite amount and carbonization. The authors suppose the acceleration of setting and the higher strength of cement composite with the introduced additive, synthesized by means of cement exposure to 1 % $AlCl_3$ solution, to take place due to synergic influence of a number of factors: intensive growth of ettringite crystal seeds and badly crystallized phases of hydrated calcium silicates of tobermorite-like structure; reduction of $Ca(OH)_2$ in the hard phase of a cement rock; and carbonization effect, which includes the formation of crystal phase for $Ca_8Al_{12}Fe_2C_{12}(CO_3)\cdot(OH)_2\cdot 22H_2O$. The improvement of density properties of a cement composite after introducing the additive, synthesized by means of cement exposure to 1 % $FeCl_3$ solution, is probably facilitated by gauging of $Ca(OH)_2$, or may be explained by “working” $CaCO_3$ and ettringite microcrystals, catalyzing the intergrowth of composite skeletal frame, or by “working” gelatinous hydrated calcium ferrites and silicates, characterized by a high surface area, which facilitate and boost interphase contacts, increasing the density of cement systems.

Аннотация. Изучено влияние добавок электролитов – хлоридов трехвалентных железа и алюминия на кинетику твердения цемента. Исследование проведено в двух сравнительных вариантах, в одном из которых растворы солей вводились в цемент в качестве жидкостей затворения («вода – 1%-й раствор электролита»), в другом – в качестве добавок, синтезированных в составе суспензий «цемент – вода – 1%-й раствор электролита». Установлено, что использование растворов $AlCl_3$ и $FeCl_3$ в качестве жидкости затворения приводит к уменьшению значений прочности при сжатии модифицированных цементных камней во всем интервале твердения. Величина 28-ми суточной прочности по сравнению с бездобавочным цементным камнем снижается на 18% в случае затворения цемента раствором хлорида алюминия и на 27% – в случае затворения вяжущего раствором хлорида железа. Композиты, полученные введением в цементное тесто добавок, синтезированных в составе суспензий, напротив, показали значительный прирост 28-ми суточной прочности относительно бездобавочного образца – на 30 и 23%, соответственно. Анализ результатов изучения добавок методами РФА и ИК-спектроскопии показал, что в структурообразовании добавок имеют место взаимозависимые изменения, связанные с резким уменьшением количества портландита и карбонизацией. Авторы предположили, что ускорение

Шепеленко Т.С., Горленко Н.П., Зубкова О.А. Процессы структурообразования цементных композитов, модифицированных добавками электролитов // Инженерно-строительный журнал. 2018. № 5(81). С. 125–134.

схватывания и увеличение прочности цементного композита при введении добавки, синтезированной экспозицией цемента в 1%-м растворе $AlCl_3$, реализуется благодаря синергетическому влиянию нескольких факторов: интенсивному росту зародышей кристаллов эттрингита – главного армирующего компонента цементной системы и слабо закристаллизованных фаз гидросиликатов кальция тоберморитоподобной структуры, уменьшению количества $Ca(OH)_2$ в твердой фазе цементного камня и эффекту карбонизации, включая образование кристаллической фазы $Ca_8Al_{12}Fe_2O_{12}(CO_3)\cdot(OH)_2\cdot22H_2O$. Улучшение прочностных характеристик цементного композита при введении добавки, синтезированной экспозицией цемента в 1%-м растворе $FeCl_3$, вероятно происходит благодаря связыванию $Ca(OH)_2$, а также может быть объяснено «работой» микрокристаллов эттрингита и $CaCO_3$, катализирующих прорастание скелетного каркаса композита, а также с «работой» гелеобразных гидроферритов и гидросиликатов кальция, обладающих высокой удельной поверхностью, которые облегчают и улучшают межфазовые контакты, увеличивая плотность цементных систем.

1. *Introduction*

The construction of high-quality and most advanced concretes is one of the main tasks of construction materials engineering. Contemporary construction science employs a wide range of methods [1–12], allowing the targeted exposure of a cement rock (CR) structure, which in a number of ways determines operational parameters of cement concrete and products thereof. The easiest and most efficient means of regulating the gauging properties is the application of additives. Nowadays additives of various purposes are as essential components of a concrete mix, as gauge liquids, aggregate and water. Therefore the approach, devoted to engineering of new, competitive local concrete additives, increasing the strength, corrosive resistance, and providing the durance of concrete, requires special attention.

The analysis of science and research literature has shown, that the concrete technology has a lasting importance of additives, boosting the setting and hardening of concrete – chlorides, carbonates, sulfates, nitrates, silicates, phosphates, and other electrolytic and non-electrolytic solutions and their various combinations. The most common and effective of this far from complete list of chemical additives are still the muriates and their compounds: ultimate advantages of chloride modifiers are their high solubility, reliable performance, availability and low cost.

Experimental research has stated the results of such additives applications to increase at the increase of saline cationic charge: polyvalent cations are by far more effective than the low-valent ones [13–16]. There has also been stated, that the salts of three-valence metals combine the properties of hardening boosters and concrete imporosity boosters (colmatants). The disadvantage of chloride additives is the so-called chloride aggression to the steel fittings. The analytical research of scientific results, presented by foreign and Russian scientists from 1973 to 2004 [17] shows, that the critical concentration of chlorides in concrete is the range of 0.15 % to 3 %, depending on the operational conditions of engineering constructions. According to the standard, effective on the Russian territory (Construction Rules SP 28.13330.2012), as well as the European standard BS EN 206, the maximum allowed amount of chlorides, calculated as ions of Cl^-, should not exceed 1 % of cement mass in plain concrete, 0.4 % in concrete with prestressed reinforcement, 0.1 % with nonprestressed reinforcement. The corrosion risks may be eliminated by means of simultaneous application of inhibitory agents – nitrates and nitrites of calcium, borates, chromates, katapine [13, 14]. Without any risk chlorides may be applied in aerated concrete technology (cellular and pumice concrete), in construction of concrete slabs, paving elements, construction of outdoor amenities.

The conventional way of applying setting and hardening boosters is their immersion into the gauging liquid. The research [18] has described a scientific approach, according to which the increase of cement rock strength is obtained by means of introducing the additives, synthesized in “cement–water–sugar” suspensions.

The goal of the present study is to examine the influence water solutions of ferric and aluminium chlorides have on structurization processes and compression strength of cement rocks with the application of the given scientific approach. The synthesis of additives has been carried out in “cement-electrolytic solution” suspension. As for the electrolytes, 1 % solutions of $AlCl_3$ and $FeCl_3$ have been used. The additives were introduced into “water-cement” system at the stage of cement paste batching. To support the proposed means of introducing the electrolytic solutions into cement systems (CS) scientifically, 1 % solutions of aluminium and ferric chlorides were also used as gauging liquids.

2. Methods

In the functioning of a gauge liquid portland cement CEM II / A-Sh 32.5H produced by Topkinsk plant has been used, in correspondence with the Russian State Standard GOST 31108-2003.

Plain Cement Rocks (PCR) and Modified Cement Rocks (MCR): $MFeCl_3$, $MAlCl_3$, MFe and MAl have been produced as cubes with the side of 2 cm in regular hardening conditions. The ratio of liquid and solid phases (L/S) was 0.34.

Table 1. Properties of additives and MCR

No.	Additive composition	Saline solution pH	Additive code	Means of cement modification	CR code
1	1% $FeCl_3$ solution	2.5	$FeCl_3$	Cement + (1% $FeCl_3$ solution, as a gauge liquid)	$MFeCl_3$
2	cement + (1% $FeCl_3$ solution)		CFe	(Cement – H_2O) + 5% (mass) CFe additive	MFe
3	1% $AlCl_3$ solution	3.8	$AlCl_3$	Cement + (1% $AlCl_3$ solution, as a gauge liquid)	$MAlCl_3$
4	cement + 1% $AlCl_3$ solution		CAl	(Cement – H_2O) + 5% (mass) CAl additive	MAl
5	cement + H_2O (check)	–	CV	–	–

MCR production was different by the way of electrolytic introduction into the “cement-water” system. For instance, the rocks $MFeCl_3$ and $MAlCl_3$ were produced by means of gauging the plain cement with 1% solutions of $FeCl_3$ and $AlCl_3$, accordingly; for MFe and MAl rocks it was the introduction of CFe and CAl additives accordingly into the “water-cement” system; the additives were introduced at the stage of cement paste batching, in amounts of 5% of dry cement mass.

CFe additive was synthesized through the belowmentioned method.

The samples of basic gauge liquid were exposed to 1% ferric chloride with the ratio L/S = 1:5 for 24 hours, having thoroughly mixed the suspension;

After the exposure time was out, the solid part of suspension was separated from the liquid part by means of filtering. To abort the hydration processes the solid residue was processed with acetone and dried in a dessicator over $CaCl_2$ until reaching a fixed mass;

The additive, prepared in such a manner, was ground in a porcelain mortar until reduced to the size of 008 sieve according to State Standard GOST 6613.

CAl was synthesized by means of exposure of plain cement to 1 % aluminium chloride, and then according to steps 1–4.

Ferric and aluminium chlorides were used as hexaqua hydrates $FeCl_3 \cdot 6H_2O$ (GOST 4147-74) and $AlCl_3 \cdot 6H_2O$ (GOST 3759-75). While these salts are hydroscopic, before the production of 1% solutions hydrates were brought to fixed mass in a dessicator at the constant temperature (110±5)° C (GOST 5382-91).

Test sample CV was synthesized by means of exposing the plain cement to distilled water under the conditions, completely identical to the abovementioned method of additives preparation.

Table 1 presents the means of additives synthesizing and the ways of cement modification with the additives. Table 2 shows the compression strength values (R, MPa) and density changes in MCR (reduction or increase, ΔR, %) compared to PCR. Compression strength values of CR aged 1-3-7-28 days were determined based on 6 parallel measurements at every checkpoint. Arithmetical average of strength was calculated from three closest values, providing the margin of error under 4.8 %.

Physical and chemical analysis of CFe and CAl additives was carried out in comparison to test sample CV.

Figure 1 and Table 2 present the data on additives and test sample CV examination, obtained by means od IR-spectral analysis. Figure 2 and Table 4 show the results of x-ray phase analysis. IR spectral analysis of the additives were carried out by means of Fourier spectrometer “*Varian Excalibur HE* 3600” at the frequency range 400–4000 cm^{-1}; for XPA it was X-ray diffraction meter Shimadzu XRD-700 with a copper anode in range of 5–90 deg.

Table 2. Compression strength R, (MPa) and density increase (reduction) values ΔR (%) of MCR compared to PCR

No.	**CR**	**Period of hardening, days**							
		1		3		7		28	
		R	Δ*R*, %	*R*	Δ*R*, %	*R*	Δ*R*, %	*R*	Δ*R*, %
1	PCR	4.1	–	31.2	–	37.3	–	43.2	–
2	$MFeCl_3$	2.7	–33	24.2	–22	24.4	–34	31.4	–27
3	MFe	5.0	+25	40.3	+29	43.4	+16	53.4	+23
4	$MAlCl_3$	3.4	–16	35.0	+13	34.4	–7	35.3	–18
5	MAl	5.1	+25	41.2	+32	44.3	+19	56.4	+30

3. Results and Discussion

Results presented in table 2 prove that the application of 1 % ferric and aluminium chloride solutions as gauge liquids provide the reduction of compression strength of cement rocks $MAlCl_3$ and $MFeCl_3$ at the whole period of hardening. In addition to that the value of 28-day strength compared to PCR is reduced by 18 % for the $MAlCl_3$ rock, produced by means of adding aluminium chloride into cement, and by 27 % for $MFeCl_3$ rock, produced by mixing the gauge liquid with ferric chloride. MAl and MFe rocks, produced by introducing into “cement-water” system the additives, synthesized in suspensions “cement – 1 % saline solution ($AlCl_3$ or $FeCl_3$)”, on the contrary, have shown a significant increase in strength compared to PCR – by 30 % and 23 % accordingly.

The process of three-valence metal saline solutions interacting with cement is rather complex and has a number of common things and differences, depending on the character of saline cation. Thus, due to the heavy charge and a small diameter (for Al^{3+} – 0.057 nm, for Fe^{3+} – 0.067 nm), cations of these metals in water solutions are highly hydrated. In acidic conditions aquatic complexes of ferric and aluminium ions are coordinated to six ligands – water molecules. Through the example of Al^{+3} cation it reads as following:

$$Al^{3+} + 6H_2O \rightarrow [Al(H_2O)_6]^{3+}{}_{\text{(wat.)}},\ \Delta H_{\text{hydro.}} = –4640 \text{ kJ/mole [19]}$$

Aquatic complex of aluminium hexahydrate easily enters hydrolysis reaction, which undergoes with co-production of various products in acidic and alkaline conditions, provided by amphoteric character of aluminium. If, for the sake of simplification, water molecules included into complex salts, produced during the hydrolysis, are left out, and hydronium ion H_3O^+ is supplemented with hydrogen ion H^+ among the reaction products, that will be read as follows:

$$Al^{3+} + H_2O \leftrightarrow AlOH^{2+} + H^+;$$

$$AlOH^{2+} + H_2O \leftrightarrow Al(OH)_2^+ + H^+;$$

$$Al(OH)_2^+ + H_2O \leftrightarrow Al(OH)_3\downarrow + H^+.$$

The ratio of hydrolysis products depends on pH value. Aquatic complex $[Al(H_2O)_6]^{3+}$ is stable at pH ranging from 0 to 4, then its amount in hydrolysis products is reducing, and at pH = 6 aluminium hexahydrate is not registered; $AlOH^{2+}$ appears at pH = 3, its value peaks at pH = 5, and at pH = 6.5 divalent cation disappears; $Al(OH)_2^+$ is produced at pH = 4, its maximum amount is registered at pH = 6, while at pH= 7.5 it is already nonexistent; $Al(OH)_3$ appears at pH = 4.5, peaks at pH = 7.5, reaching pH = 11 aluminium hydroxide is not registered [20].

Contacting cement, hydrolysis of aluminium chloride is boosted, while pore liquid ions $OH^–$ gauge nascent ions H^+ (or, more precisely, hydronium ions H_3O^+), emitting water (neutralization reaction). Simultaneous ion-exchange reaction of $AlCl_3$ with $Ca(OH)_2$ is also possible:

$$2\ AlCl_3 + 3Ca(OH)_2 \rightarrow 3CaCl_2 + 2Al(OH)_3\downarrow.$$

While alkaline properties of liquid phase of cement are quickly restored to regular values (pH ≈ 12 [13, 15, 16]), residual alminium hydroxide, produced by means of hydrolysis and ion-exchange reactions, transforms into soluble aluminate-ion $[Al(OH)_4]^–$:

$$Al(OH)_3 + H_2O \leftrightarrow [Al(OH)_4]^- + H^+.$$

According to [19, 20] $Al(OH)_3$ starts the transformation into $[Al(OH)_4]^-$ at pH = 7.5 already, while the maximum amounts of aluminate-ion are registered having reached pH = 11 and higher.

Ferric hexahydrate $[Fe(H_2O)_6]^{3+}$ is also susceptible to hydrolysis and may partake in the neutralization reaction while contacting cement. The authors [21] remark the difficulties in studying hydrolysis products of $FeCl_3$, different from $AlCl_3$, due to the rapid speed of hydrolysis reactions and $Fe(OH)_3$ setting. Theoretically it is also possible to have an ion-exchange reaction between calcium hydroxide and ferric chloride solution ($2FeCl_3 + 3Ca(OH)_2 = 2Fe(OH)_3\downarrow + 3CaCl_2$). However, low solubility product of ferric hydroxide ($SP_{Fe(OH)_3} = 3.8 \cdot 10^{-38}$) facilitates its settling since the first contact of saline solution with the gauge liquid, before the reactions in question. It has been stated in [22] that $Fe(OH)_3$ from 1 % $FeCl_3$ solution settles at pH ≈ 2.5 already, its maximum amount is registered at pH = 4–5 (according to data of [23] – within the range of pH = 4.5–5.5). With the increase of pH in $FeCl_3$ solutions the existence of a polycation has been proved, with the compound $[Fe_{24}O_{12}(OH)_{32}]^{+16}$, which environment is similar to the structure of crystalline ferric oxyhydroxide β-FeOOH [21].

Having recovered the regular pH values of cement porous liquid, Al^{+3} and Fe^{+3} cations, bearing amphoteric properties, are included into the corresponding oxygen-containing anions. Moreover, while aluminium cation at pH = 11 completely enters a soluble aluminate, ferric cation transforms into calcium hydroferrite (CHF) of low solubility [13]:

$$3Ca^{+2} + 2Fe^{+3} + 12OH^- \rightarrow 3CaO \cdot Fe_2O_3 \cdot 6H_2O \downarrow.$$

Settling CHF has a gelatinous structure and may clog CR pores.

The differences in additives structurization are reflected in the results, obtained by means of IR spectral analysis and XPA. Thus, IR-spectre of CAl additive is different from test sample CV spectre by the significant increase of absorption in every area, characteristic for cement systems (Figure 1).

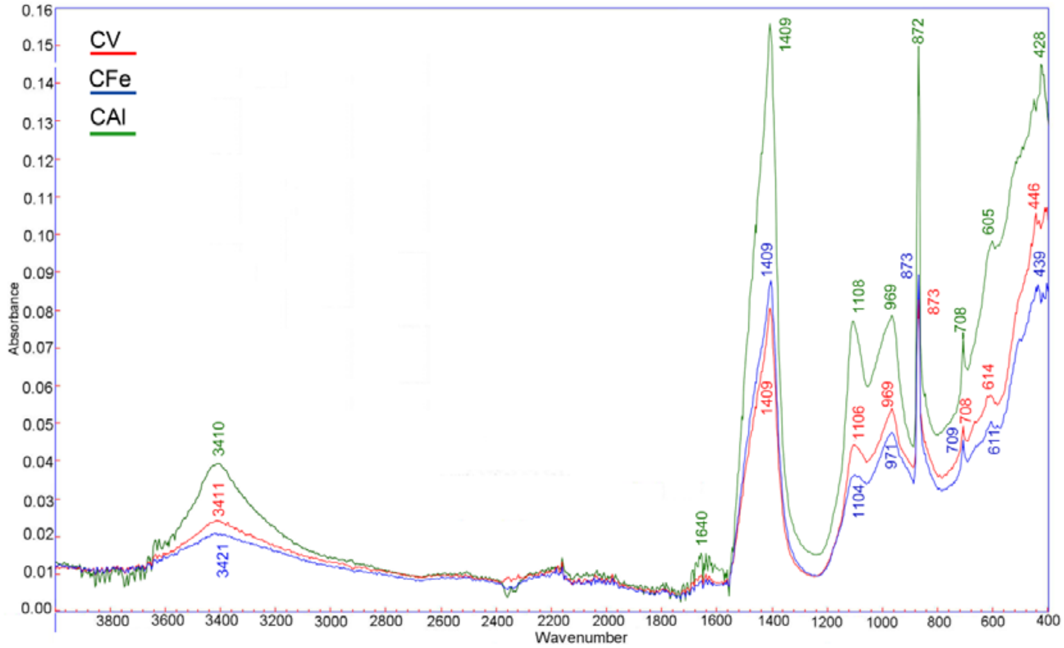

Figure 1. IR-spectres of CAl and CFe additives and test sample CV

Increase of peak height with the maximum of 3410 cm^{-1} indicates a more intensive formation of hydrated calcium sulfoaluminates (HCSA), hydrated calcium sulfates (HCS) and other hydrated phases, which have crystallization water in their molecules, appearing at the reaction of gauge liquid with aluminium chloride solution. Ettringite is also registered in the existence of adsorption bands in spectral areas of 1000–1100 cm^{-1} and 400–600 cm^{-1} [24, 25]. Spectral lines intensity in all the abovementioned intervals compared to the test sample CV is significantly increased (table 3). According to X-ray microanalisys high fuzziness of absorption profile 400-600 cm^{-1} proves the irregular structure of octahedral Al–O_6 groups [25], determined by the high amount of aluminium ions in ettringite crystals. The differences, found in oscillation spectre, are corresponding to the XPA data (Figure 2, table 4) – the height of HCSA reflexes in CAl additive compared to CV is raised by 40–54 % (the measurements were carried out on 2θ with reflection angles: 9.016^0, 15.530^0, 19.988 and 22.962^0).

There has also been registered the increase in analytical signal, responsible for the formation of low-crystallized phases of HCS of tobermorite-like structure (969 cm^{-1}). In IR records of CAl this signal is increased by 51 % compared to CV. It is difficult to determine HCS by means of XPA, while the reflections of these phases are overriden by the reflexes of other plain and hydrated crystalline phases of the gauge liquid.

Table 3. IR-analysis results for MAl and MFe additives, and test sample CV

Adsorption band, cm^{-1}	**Assignment**	**$I_{additives}$ / I_{CV}·100%**	
		MAl	MFe
3640	Stretching vibrations $(OH)^-$	present	abcent
3410	Stretching and deformational vibrations of H_2O in crystallohydrates	+60	Under CV level
1650	Characteristic adsorption region of H_2O	+50	CV level
1409	$CaCO_3$	+90	+9
872	Symmetrical stretching vibrations $(CO_3)^{2-}$	+83	+10
1108	Coupled vibrations S–O of $(SO_4)^{2-}$ compounded in ettringite and stretching vibrations of $(AlO_4)^-$	+77	Under CV level
969	Asymmetric vibrations of bridge bonds of Si–O–Si and symmetric and asymmetric vibrations of end bonds of Si–O	+51	
614	(600–700 cm^{-1}) – deformational vibrations of $(AlO_4)^-$	+69	
605		+45	
428		+34	

Figure 1 and the data of Table 3 show that cement exposure in $AlCl_3$ solution (CAl additive) facilitates the rapid boost in gauge structure carbonization: the intensity of absorption bands of 1409 and 872 cm^{-1} compared to test sample CV, produced by cement exposure to distilled water, is increased by 90 % and 83 % correspondingly. X-ray evidence also registers the increase of reflection height, corresponding to $CaCO_3$ (Figure 2).

It is known, that out of cement hydrated phases the most susceptible to carbonization is $Ca(OH)_2$. Thermodynamic calculations [26] have shown the reaction between $Ca(OH)_2$ and CO_2 with its transformation into $CaCO_3$ to have the most negative value of Gibbs thermodynamic potential. The presented data may be quite a reasonable proof to explain the significant reduction in intensity of portlandite reflections: from 35 to 100 % (17.978^0, 34.061^0, 50.976^0) in CAl X-ray evidence compared to CV (Table 4). A typical feature of the additive is the existence of one more crystalline phase, containing carbonate ions: $Ca_8Al_{12}Fe_2O_{12}(CO_3)·(OH)_2·22H_2O$, registered in low-angle region (Figure 2).

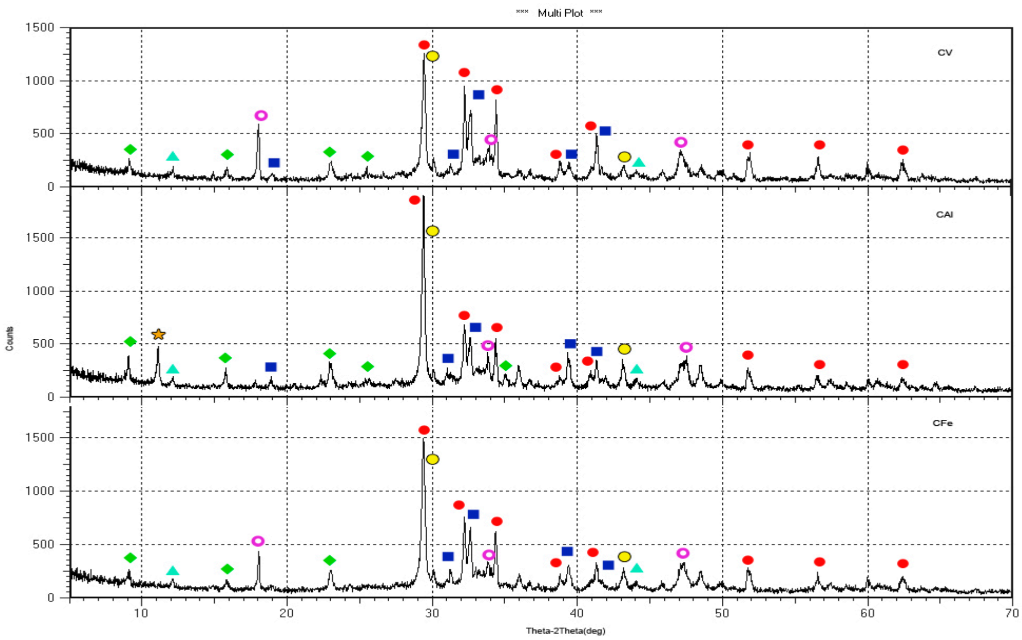

Phases: ● – Ca_3SiO_5; ■ – Ca_2SiO_4; ▲ – Ca_2FeAlO_5; ○ – $Ca(OH)_2$; ○ – $CaCO_3$;
◆ – $CaCO_3 \cdot Ca_6Al_2(SO_4)_3(OH)_{12} \cdot 26H_2O$; ☆– $Ca_8Al_{12}Fe_2O_{12}(CO_3) \cdot (OH)_2 \cdot 22H_2O$.

Figures 2. XPA graphs of CAl and CFe additives and test sample CV

The analysis of the obtained data allows to come to the conclusion, that the reaction of the gauge liquid with 1 % $AlCl_3$ solution is followed with the activation of hydration processes, increase in amounts of ettringite microcrystals and tobermorite-like compounds, as well as the gauging of portlandite and structure carbonization. Introduction of CAl additive, enriched with ettringite microcrystals, carbonized phases and HCS, into cement paste launches the mechanism of early structurization of cement composite MAl and significantly (by 30 %) increases the strength of the hardening system.

As can be seen from Figure 1, oscillatory spectre of CFe additive, synthesized by means of cement exposure to 1 % ferric chloride solution, contrary to the changes, found out in the spectre of CAl additive, is characterized by the reduction of the lines intensity compared to the test sample CV at the whole range of wavenumbers, except for the ones responsible for the existence of carbonade-containing phases in gauge structure. The height of adsorption bands 1409 and 872 cm^{-1} compared to CV, produced by means of cement exposure to distilled water, is increased by 9 and 10 % accordingly. X-ray evidence also shows some increase in the intensity of reflections, corresponding to $CaCO_3$ (Figure 2). The intensity of ettringite reflections as a part of CFe stays at the level of the test sample, portlandite reflections intensity is reduced from 23 % to 100 % (Table 4).

Therefore, the common detail in structurization of the additives, produced by modifying the gauge liquid with aluminium and ferric solutions, is the presence of interdependent changes, caused by rapid reduction of portlandite amounts and carbonization.

According to [27] the half of the solid phase of hydrated newgrowths of a cement gauge liquid is presented by secondary calcium hydroxide, forming dense layered packs or hexagonal, well-formed crystals, filling the porous area of a cement rock. There has been research presented in [25], showing that more than a half of 28-day rock cleavage surface is occupied with $Ca(OH)_2$ crystals, while the crush cut goes through the cleavage plains of these crystals, as through the weakest areas of the solid "cement-water" system. Large crystalline blocks increase the deficiency, reduce the deformability and accumulate structural stress, reducing the uniformity, strength and corrosion resistance of a CR [25, 27, 28].

The inclusion of carbonate-containing phases in cement composite structurization, those being formed first of all and mostly due to the gauging of porous liquid calcium hydroxide by carbonate dioxide, is on the other hand, considered a beneficiary process, facilitating the reduction of shrinking deformations, and crack resistance of CR and concrete, and the significant improvement of carbonate and sulfate corrosion operational resistance [10, 25, 30]. The authors [31], considering the benefits of carbonization, have proposed to apply industrial CO_2 as a facilitating additive foe concrete. Operational testing of the approach has shown the introduction of carbon dioxide into the concrete paste (slag portlandcement has been used as a gauge) to provide the increase in compression strength up to 14 % at the day age and up to 26 % at the period of 28 days. Based on the results of isometric calorimetric test and microstrucrural analysis the authors have stated that nanosized carbonization products activate the hydration and provide the development of stronger concrete microstructure.

Table 4. The intensity of $Ca(OH)_2$ and ettringite reflexes as additive parts compared to the test sample CV according to XPA data

No.	The intensity of additives crystalline phases reflexes compared to the test sample, $I_{additives} / I_{CV} \cdot 100$ %			
	Phase	2θ,⁰	MAl	MFe
1	Ettringite	9.016	+54	CV level
		15.530	+50	
		19.988	+50	
		22.962	+40	
2	Portlandite	17.978	–50	–25
		34.061	–35	–23
		47.045	CV level	CV level
		50.976	–100	–100

In the application of ferric chloride solution for CFe additive synthesis the authors relied on the well-known thesis [13], that the ferric salts not just facilitate the pore clogging and improve CR structure, but also increase the deformability and long-time performance of construction composites. And despite the fact that oscillatory spectre shows slower hydration processes in the "cement – $FeCl_3$ solution" system, and XPA results of the additive present no phases, different from the one, forming in the "cement-water" system (test sample CV), the introduction of CFe into cement paste provides not only faster settling, but also a significant (23 %) increase in cement composite MFe strength compared to PCR. That may on the one hand stem from the "performance" of ettringite and $CaCO_3$ microcrystals, like with CAl instance catalyzing the growth of composite skeletal structure, and, on the other hand, with the "performance" of such gelatinous phases as HCS and dicalcium phosphate, characterized with a high specific surface, facilitating and improving interphase contacts, increasing the density of CR.

4. Conclusions

The research undertaken and the interpretation of the results, provided in the given paper, allow the following conclusions:

1. The application of 1 % ferric and aluminium chloride solutions as gauge liquids leads to the reduction of compression strength of $MAlCl_3$ and $MFeCl_3$ cement rocks. At the 28-day age the value of strength reduction compared to PCR was 18 % and 27 % accordingly.

2. Faster settling and increase in strength of MAl cement composite by 30 % at the introduction of CAl additive, synthesized by means of cement exposure to 1 % $AlCl_3$ solution, is provided by means of synergic influence of a number of factors: intensive growth of ettringite crystal seeds – the main reinforcing component of a cement system and tobermorite-like phases of HCS, the reduction of $Ca(OH)_2$ amounts in the solid phase of a cement rock, and carbonization effect. A certain impact on the structurization is facilitated by a discovered as a part of an additive the crystalline phase of $Ca_8Al_{12}Fe_2O_{12}(CO_3)\cdot(OH)_2\cdot 22H_2O$, formed during alumoferrite hydration.

3. Faster settling and strengthening of MFe cement composite by 23 % at the introduction of CFe additive, synthesized by means of cement exposure to 1 % of $FeCl_3$ solution, is probably facilitated by the gauging of calcium hydroxide, or may as well be explained by the "performance" of ettringite and $CaCO_3$ microcrystals, like in CAl instance catalyzing the growth of composite skeletal structure, and by the "performance" of such gelatinous phases like dicalcium hydrophosphates and HCS, characterized with a high specific surface, facilitating and improving interphase contacts, increasing the density of CR.

The engineered additives intensify structurization and solidify the structure of cement composites, from the early hardening periods, and may be recommended to improve the operational properties of cement systems.

References

1. Sobolev, K., Shah, S.P. Nanotechnology of concrete: recent developments and future perspectives. American Concrete Institute: SP-254. 2008. 160 p.
2. Li, Z., Wang, H., He, S., et. al. Investigations on the preparation and mechanical properties of the nano-alumina reinforced cement composite. Mater. Lett. 2006. Vol. 60(3). Pp. 356–359.
3. Kuo, W.-Y., Huang, J.-S., Lin, C.-H. Effects of organo-modified montmorillonite on strengths and permeability of cement. Cem. Concr. Res. 2006. Vol. 36(5). Pp. 886–95.
4. Shishkin, A., Shishkina, A., Vatin, N. Low-shrinkage alcohol cement concrete (2014). Applied Mechanics and Materials. No. 633-634, Pp. 917–921.
5. Tarig, A., Yanful, E.K. A review of binders used in cemented paste tailings for underground and surface disposal practices. J. of Environmental Management. 2013. Vol. 131. No. 12. Pp. 138–149.
6. Suzdaltsev, O.V. Dolgovechnyye arkhitekturno-dekorativnyye poroshkovo-aktivirovannyye betony s ispolzovaniyem otkhodov kamnedrobleniya gornykh porod porod [Long-term performance fair-faced powder-activated concretes with the application of crusher rock run]. Ph.D. Thesis in Engineering Science. Penza, 2015. 237 p. (rus)
7. Larsen, L.O., Naruts, V.V. Self-compacting concrete with limestone powder for transport infrastructure. Magazine of Civil Engineering. 2016. No. 8. Pp. 76–85. doi: 10.5862/MCE.68.8
8. Degirmenci, N., Yilmaz, A. Use of diatomite as partial replacement for Portland cement in cement mortars. Construction and Building Materials. 2009. No. 23. Pp. 284–288.
9. Ibe, Ye.Ye. Gidrotekhnicheskiy beton na kompozitsionnom portlandtsemente s mineralnymi dobavkami, soderzhashchimi vysokoglinozemistyye shlaki [Hydrotechnical concrete on composite portlandcement with mineral additives, containing high-alumina slags]. Ph.D. thesis in Engineering Science. Barnaul, 2016. 152 p. (rus)
10. Shepelenko, T.S., Zubkova, O.A., Subbotina, N.V. et al. Kompozitsionnyye tsementy, soderzhashchiye sakharozu [Composite cements, containing sucrose]. Vestnik TGASU. 2017. No. 5. Pp. 151–158. (rus)
11. Ponomarev, A., Knezević, M., Vatin, N., et. al. Nanosize scale additives mix influence on the properties of the high performance concretes. Journal of Applied Engineering Science. 2014. No. 12(3). Pp. 227–231.
12. Justs, J., Bajare, D., Korjakins, A., et. al. Microstructural investigations of UHPC obtained by pressure application within the first 24 hours of hardening. Construction Science. 2013. No. 8. Pp. 50–57.
13. Ratinov, V.B., Rozenberg, T.I. Dobavki v beton [Concrete additives]. Moskva: Stroyizdat, 1989. 188 p .(rus)
14. Ruzhinskiy, S., Portik, A., Savinykh, A. Vse o penobetone [Complete guide on aerated concrete]. Sankt-Peterburg: OOO «Stroy-beton», 2006. 630 p. (rus)
15. Berdov, G.I., Ilina, L.V. Vzaimodeystviye alyuminatnykh klinkernykh mineralov s vodnymi rastvorami elektrolitov [Reaction of aluminate clinker minerals with aqueous electrolyte solutions]. Izvestiya vuzov. Stroitelstvo. 2012. No. 9. Pp. 13–19. (rus)
16. Berdov, G.I., Ilina, L.V., Rakov, M.A. Povysheniye prochnosti tsementnykh materialov putem vvedeniya dobavok elektrolitov [Increasing cement material strength by means of introducing electrolytic additives]. StroyPROFI. 2014. No. 12. Pp. 1–10. (rus)
17. Leonovich, S.N., Prasol, A.V. Zhelezobeton v usloviyakh khloridnoy korrozii: deformirovaniye i razrusheniye [Reinforced concrete under chloride corrosion:

Литература

1. Sobolev K., Shah S.P. Nanotechnology of concrete: recent developments and future perspectives // American Concrete Institute: SP-254. 2008. 160 p.
2. Li Z., Wang H., He S., et. al. Investigations on the preparation and mechanical properties of the nano-alumina reinforced cement composite // Mater. Lett. 2006. Vol. 60(3). Pp. 356–359.
3. Kuo W.-Y., Huang J.-S., Lin C.-H. Effects of organo-modified montmorillonite on strengths and permeability of cement // Cem. Concr. Res. 2006. Vol. 36(5). Pp. 886–95.
4. Shishkin A., Shishkina A., Vatin N. Low-shrinkage alcohol cement concrete (2014) // Applied Mechanics and Materials. № 633-634, Pp. 917–921.
5. Tarig A., Yanful E.K. A review of binders used in cemented paste tailings for underground and surface disposal practices // J. of Environmental Management. 2013. Vol. 131. № 12. Pp. 138–149.
6. Суздальцев О.В. Долговечные архитектурно-декоративные порошково-активированные бетоны с использованием отходов камнедробления горных пород: дисс …. на соиск. учен. степ. к.т.н.: Спец. 05. 23.05. Пенза, 2015. 237.с.
7. Ларсен О.А., Наруть В.В. Самоуплотняющийся бетон с карбонатным наполнителем для объектов транспортной инфраструктуры // Инженерно-строительный журнал. 2016. № 8(68). С. 76–85
8. Degirmenci N., Yilmaz A. Use of diatomite as partial replacement for Portland cement in cement mortars // Construction and Building Materials. 2009. № 23. Pp. 284–288.
9. Ибе Е.Е. Гидротехнический бетон на композиционном портландцементе с минеральными добавками, содержащими высокоглиноземистые шлаки: дисс. … на соиск. учен. степ. к. т. н.: Спец. 05.23.05. Барнаул, 2016. 152 с.
10. Шепеленко Т.С., Зубкова О.А., Субботина Н.В. и др. Композиционные цементы, содержащие сахарозу // Вестник ТГАСУ. 2017. № 5. С. 151–158.
11. Ponomarev A., Knezević M., Vatin N., et. al. Nanosize scale additives mix influence on the properties of the high performance concretes // Journal of Applied Engineering Science. 2014. № 12(3). Pp. 227–231.
12. Justs J., Bajare D., Korjakins A., et. al. Microstructural investigations of UHPC obtained by pressure application within the first 24 hours of hardening // Construction Science. 2013. № 8. Pp. 50–57.
13. Ратинов В.Б., Розенберг Т.И. Добавки в бетон. М.: Стройиздат, 1989. 188 с.
14. Ружинский С., Портик А., Савиных А. Все о пенобетоне. Санкт-Петербург: ООО «Строй-бетон», 2006. 630 с.
15. Бердов Г.И., Ильина Л.В. Взаимодействие алюминатных клинкерных минералов с водными растворами электролитов // Известия вузов. Строительство. 2012. № 9. С. 13–19.
16. Бердов Г.И., Ильина Л.В., Раков М.А. Повышение прочности цементных материалов путем введения добавок электролитов // СтройПРОФИ. 2014. № 12. С. 1–10.
17. Леонович С.Н., Прасол А.В. Железобетон в условиях хлоридной коррозии: деформирование и разрушение // Строительные материалы. 2013. № 5. С. 94–95.
18. Шепеленко Т.С., Саркисов Ю.С., Горленко Н. П., Цветков Н.А., Зубкова О.А. Процессы структурообразования цементных композиций, модифицированных добавками сахарозы // Инженерно-строительный журнал. 2016. № 6(66). С. 3–11.

deformation and destruction]. Stroitelnyye materialy. 2013. No. 5. Pp. 94–95. (rus)

18. Shepelenko, T.S., Sarkisov, U.S., Gorlenko, N.P., et. al. Structure-forming processes of cement composites, modified by sucrose additions. Magazine of Civil Engineering. 2016. No. 6. Pp. 3–11.
19. Sokolova, T.A., Tolpeshta, I.I., Trofimov, S.Ya. Pochvennaya kislotnost. Kislotno-osnovnaya bufernost pochv. Soyedineniya alyuminiya v tverdoy faze pochvy i v pochvennom rastvorerastvore [Soil acidity. Acid-base buffer characteristics of soils. Aluminium compounds in soil solid phase and solutions]. Tula: Grifi K, 2012. 124 p. (rus)
20. Mikhaylov, V.I. Polucheniye i fiziko-khimicheskiye svoystva materialov na osnove nanodispersnykh oksidov alyuminiya i zheleza (III) [Production and physical and chemical properties of materials based on nanodispersed aluminium and ferric (III) oxides]. Ph.D. thesis in Engineering Science. Syktyvkar, 2016, 129 p. (rus)
21. Zhy, M., Frandsen, A.F., Wallace, A.F., et all. Precipitation Pathways for Ferrihydrite Formation in Acidic Solutions. Geochimica et Cosmochimica Acta. 2016. Vol. 172. Pp. 244–264.
22. Starov, V.M. Nanoscience: Colloidal and Interfaciel Aspects. London, New York: CRC Press Taylor @Francis Group. 2010. 1187 p.
23. Svatovskaya, L.B., Solovyev, V.Ya., Stepanova, I.V., et al. Vysokoprochnyy beton [High-strengh concrete]. Patent Russia No. 2323910, 2008. (rus)
24. Taylor, H.F.W. Cement Chemistry. London: Academic Press, 1964. 560 p.
25. Samchenko, S.V. Formirovaniye i genezis struktury tsementnogo kamnya: monografiya. M.: MGSU, Ay Pi Er Media, EBS ASV, 2016. 248 p. (rus)
26. Babushkin, V.I., Matveyev, G.M., Mchedlov-Petrosyan, O.P. Termodinamika silikatov [Silicate thermodynamics]. Moskva: Stroyizdat, 1986. 351 p. (rus)
27. Trofimov, B.Ya., Mushtakov, M.I. Korroziya betona: monografiya [Concrete corrosion: monograph]. Chelyabinsk: Izd-vo YuUrGU, 2008. 310 p.
28. Shpynova, L.G., Chikh, V.I., Sanitskiy, M.A., et al. Fiziko-khimicheskiye osnovy formirovaniya struktury tsementnogo kamnya [Physical and chemical foundations of cement rock structurization]. Lvov: Vishcha shkola, 1981. 160 p. (rus)
29. Pashchenko, A.A. Teoriya tsementa [Cement theory]. Kiyev: Budivelnik, 1991. 196 p. (rus)
30. Malova, Ye.Yu. Kompozitsionnyye portlandtsementy s karbonatsoderzhashchimi dobavkami i betony na ikh osnove [Composite portlandcements with carbonate-containing additives and concretes, based on them]. Ph.D. thesis in Engineering Science. Barnaul, 2015. 161 p. (rus)
31. Monkman, S., Makdonald, M., Khuton, D. Ispolzovaniye uglekislogo gaza v kachestve dobavki-uskoritelya [Application of CO2 as a speed-booster additive]. Tsement i yego primeneniye. 2017. No. 1. Pp. 82–89. (rus)

19. Соколова Т.А., Толпешта И.И., Трофимов С.Я. Почвенная кислотность. Кислотно-основная буферность почв. Соединения алюминия в твердой фазе почвы и в почвенном растворе. Тула: Грифи К, 2012. 124 с.
20. Михайлов В.И. Получение и физико-химические свойства материалов на основе нанодисперсных оксидов алюминия и железа (III): дисс. ... на соиск. учен. степ. к.х.н.: Спец. 02.00.04 Сыктывкар, 2016, 129 с.
21. Zhy M., Frandsen A.F., Wallace A.F., et all. Precipitation Pathways for Ferrihydrite Formation in Acidic Solutions // Geochimica et Cosmochimica Acta. 2016. Vol. 172. Pp. 244–264.
22. Starov V.M. Nanoscience: Colloidal and Interfaciel Aspects // London, New York: CRC Press Taylor @Francis Group. 2010. 1187 p.
23. Патент 2323910 C1 Российская Федерация, МПК C04B 28/04, C04B 22/06, C04B 111/20. Высокопрочный бетон / Л.Б. Сватовская, В.Я. Соловьева, И.В. Степанова и др., 2008.
24. Taylor H.F.W. Cement Chemistry. London: Academic Press, 1964. 560 p.
25. Самченко С.В. Формирование и генезис структуры цементного камня: монография. М.: МГСУ, Ай Пи Эр Медиа, ЭБС АСВ, 2016. 248 с.
26. Бабушкин В.И., Матвеев Г.М., Мчедлов-Петросян О.П. Термодинамика силикатов. М.: Стройиздат, 1986. 351 с.
27. Трофимов Б.Я., Муштаков М.И. Коррозия бетона: монография. Челябинск: Изд-во ЮУрГУ, 2008. 310 с.
28. Шпынова Л.Г., Чих В.И., Саницкий М.А. и др. Физико-химические основы формирования структуры цементного камня. Львов: Вища школа, 1981. 160 с.
29. Теория цемента / под ред. А.А. Пащенко. Киев: Будівельник, 1991. 196 с.
30. Малова Е.Ю. Композиционные портландцементы с карбонатсодержащими добавками и бетоны на их основе: дисс. … на соиск. учен. степ. к. т. н: Спец.: 05.17.11. Барнаул, 2015. 161 с.
31. Монкман С., Макдонанд М., Хутон Д. Использование углекислого газа в качестве добавки-ускорителя // Цемент и его применение. 2017. № 1. С. 82–89.

Tatiana Shepelenko,*
+7(3822)64-24-45; shepta72@mail.ru

Nicholas Gorlenko,
+7(3822)64-24-45; Gorlen52@mail.ru

Olga Zubkova,
+7(3822)64-24-45; zubkova0506@mail.ru

Татьяна Станиславовна Шепеленко,*
+7(3822)64-24-45; эл. почта: shepta72@mail.ru

Николай Петрович Горленко,
+7(3822)64-24-45; эл. почта: Gorlen52@mail.ru

Ольга Александровна Зубкова,
+7(3822)64-24-45;
эл. почта: zubkova0506@mail.ru

Shepelenko, T.S., Gorlenko, N.P., Zubkova, O.A. Structurization processes of cement composites modified with electrolytic additives. Magazine of Civil Engineering. 2018. 81(5). Pp. 125–134. doi: 10.18720/MCE.81.13.

doi: 10.18720/MCE.81.14

Ultra-high rockfill dam with combination of the reinforced concrete face and clay-cement diaphragm

Сверхвысокая каменно-набросная плотина с комбинацией железобетонного экрана и глиноцементобетонной диафрагмы

M.P. Sainov*,
V.B. Soroka,
National Research Moscow State Civil Engineering University, Moscow, Russia

Канд. техн. наук, доцент М.П. Саинов*,
студент В.Б. Сорока,
Национальный исследовательский Московский государственный строительный университет, Москва, Россия

Key words: rockfill dam; reinforced concrete face; cutoff wall slurry trench; stress-strain state; numerical modeling

Ключевые слова: каменно-набросная плотина; железобетонный экран; стена в грунте; напряжённо-деформированное состояние; численное моделирование

Abstract. The article deals with design validation of a new type of an embankment dam structural design, i.e. rockfill dam with combination of two types of non-soil seepage-control elements – a reinforced concrete face (in the dam upper part) and a clay-cement diaphragm made of bored piles (in the dam lower part). The dam of the considered design has a number of advantages over classical structural design of concrete faced rockfill dam (CFRD). First of all, conjugation of the seepage-control element with rock foundation does not require arrangement of a pit. Secondly, repairs of the dam lower part may be carried out by arrangement of a grout curtain. But the most important advantage of this design is more favorable conditions of the reinforced concrete operation, i.e. the face is subject to not tensile, but compressive longitudinal force. This decreases the risk of cracking in the face. Design validation of this structural design was conducted on the example of a 235 m high dam. Numerical modeling of the dam stress-strain state (SSS) was performed with consideration of construction and loading sequence, as well as with consideration non-linearity of rockfill deformation. Impact of four main factors on the dam SSS was studied: rockfill deformation, clay-cement deformation, diaphragm height and reinforced concrete thickness. Several alternatives of the dam design parameters were considered. Design of the numerical experiment was conducted by the method of factor analysis. This permitted revealing the impact of the considered factors on the dam SSS, as well as solving the problem on optimization of the dam structural solution. It was revealed that for providing the necessary level of the dam design safety the rockfill deformation modulus should be at least 250 MPa, and the diaphragm should be made of plastic clay-cement concrete. More favorable turned to be the case when the diaphragm height is 20 m but not 35 m.

Аннотация. Статья посвящена расчётному обоснованию нового типа конструкции грунтовой плотины – каменно-набросной плотины с комбинацией двух типов негрунтовых противофильтрационных элементов – железобетонного экрана (в верхней части плотины) и глиноцементобетонной диафрагмы, устроенной из буронабивных свай (в нижней части плотины). Плотина рассматриваемой конструкции имеет ряд преимуществ перед классической конструкцией каменно-набросной плотины с железобетонным экраном. Во-первых, для сопряжения противофильтрационного элемента со скальным основанием не требуется устройство котлована. Во-вторых, ремонт нижней части плотины может быть осуществлён путём создания инъекционной завесы. Но самым важным преимуществом данной конструкции является более благоприятные условия работы железобетонного экрана – экран испытывает не растягивающее, а сжимающее продольной усилие. Это снижает риск образования в экране трещин. Расчётное обоснование конструкции проводилось на примере плотины высотой 235 м. Численное моделирование напряжённо-деформированного состояния плотины велось с учётом последовательности её возведения и нагружения, а также с учётом нелинейности деформируемости каменной наброски. Было исследовано влияние на НДС плотины четырёх основных факторов: деформируемость каменной наброски, деформируемость глиноцементобетона, высота диафрагмы и толщина железобетонного экрана. Рассматривалось несколько вариантов параметров конструкции плотины. Планирование численного эксперимента проводилось методом факторного анализа. Это позволило выявить влияние рассматриваемых факторов на напряжённо-деформированное состояние плотины, а также решить задачу об оптимизации конструктивного решения плотины. Было выявлено, что для обеспечения необходимого уровня надёжности конструкции плотины модуль деформации каменной наброски должен быть не ниже 250 МПа, а диафрагма должна выполняться из пластичного глиноцементобетона. Более предпочтительным оказался случай, когда высота диафрагмы составляет 20 м, а не 35 м. По результатам исследования можно сделать вывод, что рассмотренная конструкция каменно-набросной плотины с составным негрунтовым противофильтрационным элементом является хорошей альтернативой для классической конструкции грунтовой плотины с железобетонным экраном.

1. Introduction

There are cases when the most feasible type of the dam is a rockfill dam with a non-soil seepage-control element. Namely, the dams of this type are feasible for construction of projects in Siberia. Severe climatic conditions of Siberia hinder proper placement of concrete and clayey soils in the dam body, therefore, construction of concrete and rockfill dams in these conditions becomes ineffective.

However, the projects to be constructed in Siberia are as a rule high-head projects. This factor limits the types of non-soil seepage-control elements which may be used in an embankment dam. At present the only type of non-soil seepage-control element which is used in ultra-high embankment dams is a reinforced concrete face (RCF). To date a vast experience has been gained in construction of this type of dams; the theory of their designing was elaborated. In the world at least 6 CFRDs were constructed with height more than 200 m. The highest is Shuibuya dam in China with height 233 m [1].

But CFRD have serious disadvantages. At many ultra-high CFRDs emergency situations took place and were connected with formation of cracks in RCF [2–9]. Therefore, there is an urgent issue regarding improvement of dam designs of this type. Some researchers propose different refinements of the design and methods of CFRD construction [10–14]. However, by the results of our studies [15], various refinements of the classical CFRD design does not permit reaching the guaranteed level of safety. This is connected with a characteristic feature of their SSS: at the dam body deformations the longitudinal tensile force appears in the RCF lower part, which results in formation of cracks in the face. Therefore, it is necessary to search for other ways of refining structural designs of ultra-high embankment dams with RCF.

One of such ways is use of the seepage-control element of combined design consisting of two elements: RCF and clay-cement diaphragm (CCCD). We proposed this type of a dam earlier [16, 17] as an alternative to classical structural design of CFRD. The only example of a real dam with a combination of RCF and CCCD is the Hengshan Dam in China [18]. This dam is the result of reconstruction of the dam with the core in order to increase its height. One of the advantages of the dam structural design is possibility of its construction without a pit, without arrangement of protective cofferdams.

Our design studies [16, 17] showed that the proposed structural design is more efficient than the classical one. In this design RCF is not subject to tensile longitudinal force but is in compressive state. Besides, we studied the possibilities of using the combined structural design of the seepage-control element in ultra-high dams also [17]. It was revealed that in ultra-high dams the SSS of the seepage-control elements may be unfavorable and may not meet the standard requirements:

- Compressive stresses in RCF may exceed ultimate compressive strength of concrete,
- Bending deformations may lead to appearance of tensile stresses in RCF, diaphragm, to formation of cracks in it.

Nevertheless, it was shown that correct selection of structural parameters of a rockfill dam with combination of seepage-control elements may be sufficiently efficient. For example, compressive stresses in RCF may be decreased due to increase of its thickness and bending deformations of seepage-control elements may be minimized by decreasing rockfill deformation. At the same time the deformation characteristics of the diaphragm materials have ambiguous impact on the structure efficiency. Decrease of the diaphragm material modulus of deformation may both decrease and increase of RFC bending deformations. Therefore, there appeared a necessity in formulation of recommendations for selection of the dam parameters with combination of RCF and CCCD.

This article deals with the results of solving the problem on structural optimization of a rockfill dam with combination of RCF and CCCD. The study was conducted on the example of a 235 m high dam (Figure 1). In the upper part of the dam the seepage-control element is presented by a RCF. Its thickness at the dam crest is 0.5 m and it increases as it is deepened below the upstream level. The dam lower part is a cofferdam with a seepage-control element presented by CCCD. The CCCD thickness was adopted to be rather large (1.8 m) in order to provide the seepage strength of clay-cement concrete. The diaphragm of such thickness may be constructed by the “slurry trench” method of two rows of bored piles located in a checkered order.

It was assumed that the dam body was made of rock muck, the diaphragm of gravel-sand mix. Conjugation of the RCF with the diaphragm was provided through the reinforced concrete gallery (Figure 2). RCF and the concrete gallery are separated from each other by a perimeter joint. Conjugation of the gallery with the diaphragm is also envisaged to be flexible; a cavity is provided between them which will be filled with watertight “soft” material (Figure 2).

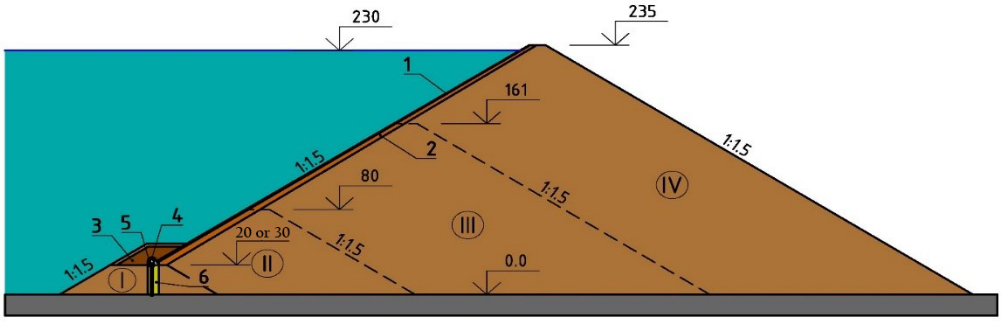

Figure 1. Layout of a rockfill dam with combined seepage-control element:
1 – reinforced concrete face; 2 – under-face zone; 3 – protection shell; 4 – concrete gallery;
5 – clay-cement diaphragm; 6 – gravel-sand core; I, II, III, IV – dam construction stages

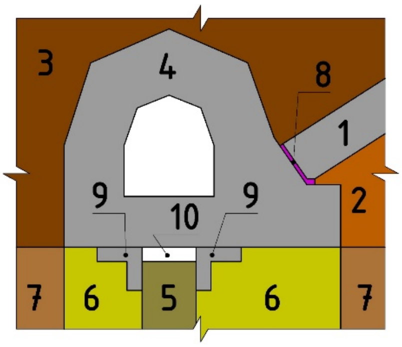

Figure 2. Layout of the interface between the seepage-control elements:
1 – reinforced concrete face; 2 – under-face zone; 3 – material of protection shell;
4 – reinforced concrete gallery; 5 – clay-cement diaphragm ; 6 – gravel-sand core; 7 – rockfill;
8 – perimeter joint; 9 – foreshaft; 10 – cavity.

2. Methods

Studies of the dam structure efficiency with combination of seepage-control elements were conducted with the aid of numerical modeling of the stress-strain state (SSS) by finite element method (FEM). During studies consideration was made of rockfill deformation non-linearity, non-linearity of contacts behavior between the elements of the structure, construction and loading sequence of the structure.

Beside the dam the model of the structure included a limited rock mass foundation under it. During analyses consideration was made of materials dead weight, US and DS hydrostatic water pressure and weighing water action on the upstream shell soil at the reservoir impoundment.

For description of soil deformation non-linearity the use was made of the soil model proposed by Professor L.N. Rasskazov [19]. At description of the contacts behavior its possible opening and sliding along it was taken into account. Coulomb-Mohr strength condition was used as the condition of shear strength failure.

Four construction and loading stages were envisaged. At the initial stage the upstream cofferdam is constructed. Then CCCD is provided in the gravel-sand core, and a reinforced concrete gallery above it. Then the dam of the first stage is constructed with RCF to el. 80 m, and the reservoir is impounded to el.73 m. And then gradually stages II, III, IV are constructed and the reservoir is impounded to FSL 230 m.

Analyses were conducted for several structural alternatives in order to select from them the most feasible one. The alternatives were selected based on the experimental design theory, for the case of full factorial experiment.

Four factors varied:

- rockfill deformation,
- deformation modulus of the clay-cement diaphragm,
- height of the clay-cement diaphragm,
- RCF thickness at the dam foundation.

Rockfill deformation X_1 was considered as the first factor. As the preliminary studies [17] showed, that this factor affects the SSS of non-soil seepage-control elements, three levels of this factor were considered. Value $X_1 = -1$ corresponds to rockfill lowest deformation, the largest one is $X_1 = +1$, and the intermediate value is $X_1 = 0$. As the studies were conducted for non-linear model of rockfill deformation, it is impossible to establish unique dependence between X_1 and rockfill deformation modulus. Conditionally we may say that rockfill deformation decreasing coefficient was used for X_1. It was adopted that at $X_1 = 0$ the parameters of rockfill deformation modulus is 2 times as less, than at $X_1 = +1$, and at $X_1 = -1$ – 4 times as less. Secant deformation modulus of rockfill (E) is tentatively equal to: at $X_1 = -1$ – 100 MPa, at $X_1 = 0$ – 200 MPa, at $X_1 = +1$ – 400 MPa. Thus, a very wide range of rockfill deformation was considered.

Clay-cement deformation modulus X_2 was considered for the second factor, the material, of which the diaphragm was made. It was adopted that the factor lower level ($X_2 = -1$) corresponds to the case, when the diaphragm is made of pored clay-cement with high content of bentonite. The mix of such clay-cement may be as follows: cement – 140 kg/m^3, bentonite – 130 kg/m^3, water – 350 kg/m^3, sand – 650 kg/m^3, gravel – 930 kg/m^3 [20]. The factor upper level ($X_1 = +1$) corresponds to plastic concrete, i.e. concrete with bentonite admixture. Its mix may be as follows: cement – 210 kg/m^3, bentonite – 35 kg/m^3, water – 350 kg/m^3, sand – 700 kg/m^3, gravel – 800 kg/m^3 [21].

Based on the data [20] for plastic clay-cement the deformation modulus was adopted equal to 100 MPa, and for plastic concrete 1000 MPa according to the data [21].

Besides, during studies the dam main geometric parameters varied: the height of the clay-cement diaphragm (CCCD) and RCF maximum thickness. The CCCD height was considered as the third factor X_3. The factor lower level ($X_3 = -1$) corresponded to 20 m height and the upper level ($X_3 = +1$) to the height of 36.5 m. RCF maximum thickness (near the contact with the gallery) was assumed as the fourth variable factor X_4. The factor lower level ($X_4 = -1$) corresponded to 1.2m thickness and the upper level ($X_4 = +1$) to the thickness of 2 m.

The values of all factors with variation boundaries and the main level are given in Table 1.

Table 1. Factors conditioning variation of the optimized parameters

Factor	Factor designation	Lower level (-1)	Middle level (0)	Upper level (+1)
Rockfill deformation	X_1	largest E ≈ 100 MPa	medium E ≈ 200 MPa	lowest E ≈ 400 MPa
Wall deformation	X_2	100	315	1000
Diaphragm height	X_3	20	28.4	36.8
Face maximum thickness	X_4	1.2	1.6	2

The total number of the considered alternatives amounted to 25. Variant 0 corresponded to the case when all 4 factors are on the middle level.

SSS was calculated for each of the alternative. For this purpose the finite element models of the structures were prepared. Finite elements were used there with cubic approximation of displacements inside the element, because the preliminary studies showed that only use of high-order finite elements permits modeling the behavior of rigid thin-wall structures, such as RCF. Contact finite elements of the zero thickness were used for modeling the contact interaction of the structures.

In the dam structure finite element model with the diaphragm height 35 m the number of finite elements amounted to 1040, and with 20 m diaphragm height – 1032. The number of freedom degrees in the structure models was 1057 and 1053 respectively.

Analyses of the dam structure alternatives SSS were conducted with the aid of the software NDS_N, worked out by M.P. Sainov, ph.dr. (tech.sc.) [22].

3. Results and Discussion

Figures 2–5 shows the results of analyses for one of the structural alternatives (var. 0), where the 28.4 m high diaphragm is made of clay-cement with E = 315 MPa. In this alternative the rockfill deformation corresponds to X_1 = 0.

By the results of analyses as of the moment of completion of the reservoir impoundment the maximum construction settlement of the dam is 160 cm. The zone of maximum dam settlements is located in the center of rockfill, because these settlements were determined for the case of the dam body layered construction. Maximum horizontal dam displacement is 64 cm.

RCF SSS is shown in Figures 2–4. Curves of the face displacements have a stepped character, which is due to the adopted sequence of the dam construction in 3 stages.

The values of RCF settlements vary from от 13 cm (at the crest) to 70 cm (Figure 2b). Maximum settlements are confined to the crest of the 2-nd stage dam. The lower point of RCF settles for 38 cm. The values of RCF horizontal displacements are less than those of settlements. Maximum RCF displacement is equal to 36 cm (Figure 2a) at the crest of the 2-nd stage dam.

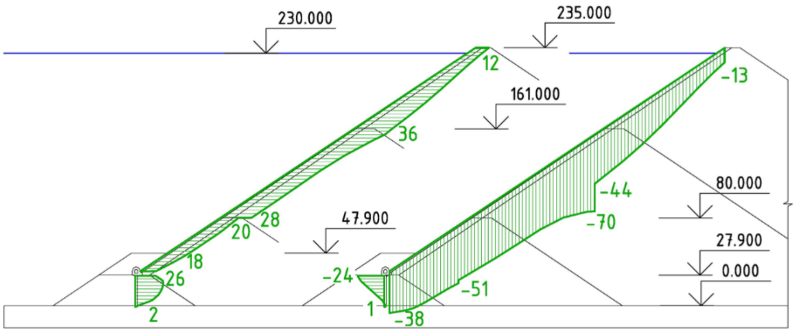

a) **b)**

Figure 2. Horizontal displacements (a) and settlements (b) of the seepage-control elements (cm)

The known RCF settlements and displacement were the basis for calculations of its displacements in direction across the slope (deflections) (Figure 3a) and along the upstream face (Figure 3b). Maximum RCF deflection amounted to 78 cm; deflection of the lower edge of RCF was 40 cm (Figure 3a). The shape of deflection curves evidences about RCF bend toward the downstream side. The strongest bending deformations are typical for RCF lower part.

The shape of RCF longitudinal displacements curve (displacements in the direction along the slope) evidences about its longitudinal compression (Figure 3b). The values of these displacements are rather large: up to 13 cm.

Curves of stresses in RCF, acting in the direction along the slope are given in Figure 4. They show that RCF is subject to compressive force in the direction along the slope. Presence of longitudinal compressive force in RCF is one of the main advantages of the considered dam structure as compared to the classical one. Due to bending deformations the upstream face is compressed more than the downstream one (Figure 4). However, it is the zone of interface with the concrete gallery on the downstream face where the stresses in RCF reach maximum values – 19.1 MPa (Figure 4b).

The diaphragm SSS is shown in Figure 2 and Figure 5. The curve of the diaphragm settlements (Figure 2b) evidences about its compression. The maximum settlement amounts to 24 cm. The diaphragm displaces toward the downstream side: maximum displacement is equal to 26 cm (Figure 2a). The shape of the curve evidences about the diaphragm bend toward the downstream side. However, the greatest bending deformations take place in the zone of embedding the diaphragm into rock foundation. In this zone the diaphragm bends toward the upstream side.

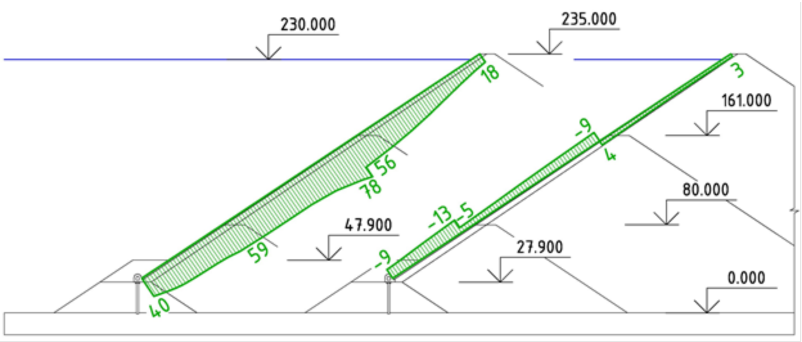

a) b)

Figure 3. Displacements (cm) of the RCF in direction perpendicular to the slope (a) and in the direction along the slope (b)

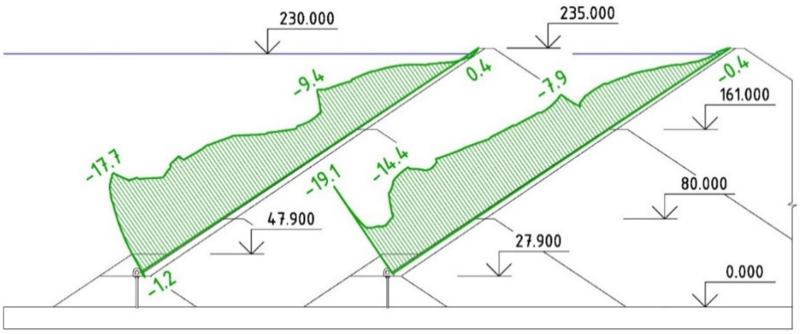

a) b)

Figure 4. Longitudinal stresses in RCF (MPa) on the upstream (a) and downstream (b) faces

Figure 5 shows vertical stresses in the diaphragm. From the Figure it is seen that the diaphragm is subject to longitudinal compressive force: at both diaphragm faces the compressive stresses reach 4.5 MPa. This compressive force appears due to settlements of the surrounding soil and transfers to the diaphragm via the soil friction along the diaphragm lateral surfaces. Bending deformations do not significantly affect distribution of stresses in the diaphragm, except the zone of the diaphragm conjugation with rock foundation. In the embedding zone due to great bending deformations the zone of tensile stresses is formed on the diaphragm upstream face with stress values up to 1.9 MPa (Figure 5a), and compressive stresses reaching the values 6.8 MPa are concentrated on the downstream face (Figure 5b).

At evaluation of CCCD strength there considered the effect of compressive strength increase of clay-cement if there is lateral compression which was established by may experiments [23, 24]. In var. 0 strength of clay-cement at unilateral compression was taken equal 1.8 MPa. From Figure 5 it is seen that due to the diaphragm compression by hydrostatic pressure and soil pressure the clay-cement compressive strength increases to 9 MPa. Comparison of stresses with strength shows that the clay-cement diaphragm compressive strength is provided nearly with double safety factor. Only tensile stresses on the diaphragm upstream face are dangerous, which may lead to crack formation in it.

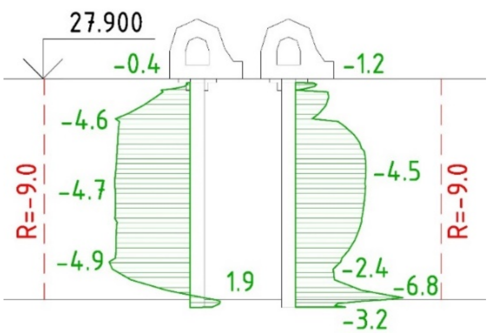

a) b)

Figure 5. Vertical stresses (MPa) on the upstream (a) and downstream (b) faces of the diaphragm.

Red dotted line shows approximate value of clay-cement compressive strength.

SSS analyses permitted evaluating the efficiency of seepage-control elements (RCF and CCCD) under various conditions, for different alternatives of structural design. Strength criteria of the dam seepage-control elements were selected for the strength criteria of the dam efficiency:

- Compressive and tensile stresses in the RCF should not exceed concrete ultimate strength;
- Tensile stresses in CCCD should not exceed concrete ultimate tensile strength,
- Safety factor of CCCD for compressive strength should be less than the standard one.

The following functional relationships were formed to provide the possibility of assigning boundary conditions for the described criteria:

- Function of maximum compressive stresses in RCF – y_2,
- Function of maximum tensile stresses in RCF – y_3,
- Function of safety factor the wall for compressive strength – y_4,
- Function of maximum tensile stresses in the wall – y_5.

The function of the structure one running meter cost was selected for the target function of optimization task – y_1.

The second order polynomial was selected for the mathematical model describing relationship between the response function and variable factors. However, quadratic dependence was used only for factor X_1. Quadratic term was added to increase accuracy of calculations and adequacy. The polynomial has the following form:

$$y_i = a_0 + a_1 * X_1 + a_2 * X_2 + a_3 * X_3 + a_4 * X_4 + a_{12} * X_1 * X_2 + a_{13} * X_1 * X_3 +$$
$$+a_{14} * X_1 * X_4 + a_{23} * X_2 * X_3 + a_{24} * X_2 * X_4 + a_{34} * X_3 * X_4 + a_{123} * X_1 * X_2 * X_3 +$$
$$+a_{124} * X_1 * X_2 * X_4 + a_{134} * X_1 * X_3 * X_4 + a_{234} * X_2 * X_3 * X_4 + a_{1234} * X_1 * X_2 * X_3 * X_4 +$$
$$+a_{11} * {X_1}^2 + a_{112} * {X_1}^2 * X_2 + a_{113} * {X_1}^2 * X_3 + a_{114} * {X_1}^2 * X_4 + a_{1123} * {X_1}^2 * X_2 * X_3 +$$
$$+a_{1124} * {X_1}^2 * X_2 * X_4 + a_{1134} * {X_1}^2 * X_3 * X_4 + a_{11234} * {X_1}^2 * X_2 * X_3 * X_4$$

Here a_0, a_1, a_2 , etc. – coefficients.

Design matrix being the basis of studies is given in Table 2. The matrix meets the requirements of orthogonality.

The cost of structure was determined with the aid of FER-2017[1] and calculated in basic price level of 2000. During calculations of work costs on rockfill filling in the dam body the following relationships were adopted between deformation and the number of roller runs for rockfill compaction: X_1 = -1 – 5 runs; X_1 = 0 – 7 runs; X_1 = +1 – 10 runs. Costs of 1m^3 of materials for seepage-control elements were as follows:

---

[1] State costing standards. Federal unit rates for civil and special civil works. FER-2001. Book 1. Earth moving works. Edition 2017. (FER 81-02-01-2001) Minstroy of Russia. Moscow. 2014-2018. [Electronic source] URL: http://www.minstroyrf.ru/trades/view.state-fer.php (reference date: 28.03.2018);

State costing standards. Federal unit rates for civil and special civil works. FER-2001. Book 5. Piling works, dredging wells, stabilization of soils. Edition 2017. (FER 81-02-05-2001) Minstroy of Russia. Moscow. 2014-2018. [Electronic source] URL: http://www.minstroyrf.ru/trades/view.state-fer.php (reference date: 28.03.2018);

State costing standards. Federal unit rates for civil and special civil works. FER-20011. Book 36. Earth elements of hydraulic structures. Edition 2017. (FER 81-02-36-2001) Minstroy of Russia. Moscow. 2014-2018. [Electronic source] URL: http://www.minstroyrf.ru/trades/view.state-fer.php (reference date: 28.03.2018);

State costing standards. Federal unit rates for civil and special civil works. FER-2001. Book 37. Concrete and reinforced concrete constructions of hydraulic structures. Edition 2017. (FER 81-02-37-2001). Minstroy of Russia. Moscow. 2014-2018. [Electronic source] URL: http://www.minstroyrf.ru/trades/view.state-fer.php (reference date: 28.03.2018);

State costing standards. Federal unit rates for civil and special civil works. FER-2001. Book 38. Stone constructions of hydraulic structures. Edition 2017. (FER 81-02-38-2001) // Minstroy of Russia. Moscow. 2014-2018. [Electronic source] URL: http://www.minstroyrf.ru/trades/view.state-fer.php (reference date: 28.03.2018);

State costing standards. Federal unit rates for materials, items, constructions and equipment used in construction. FSSC. Edition 2017. (FSSC 81-01-2001) Minstroy of Russia. Moscow. 2014-2018. [Electronic source] URL: http://www.minstroyrf.ru/trades/view.state-fer.php (reference date: 28.03.2018).

for pored clay-cement – 314 rub., for plastic concrete – 273 rub., for reinforced concrete – 1042 rub. With consideration of civil work prices the cost of RCF 1m^3 construction amounted to 1077 rub., and 1m^3 of CCCD – about 6200 rub.

Table 2 gives the data on values of response functions (target function and the function of limitations) for each alternative.

Table 2. Design matrix (the first stage of solving the problem)

No	Abs. values of factors				Relative values of factors				Response functions				
	X_1, MPa	X_2, MPa	X_3, m	X_4, m	X_1	X_2	X_3	X_4	y_1, thou.rub.	y_2, MPa	y_3, MPa	y_4	y_5, MPa
1	≈400	100	20	1.2	1	-1	-1	-1	16 139	16.50	1.40	3.47	0.01
2	≈400	100	36.8	1.2	1	-1	1	-1	16 524	15.00	0.50	3.75	0.30
3	≈400	100	20	2	1	-1	-1	1	16 270	12.90	3.30	3.30	0.00
4	≈400	100	36.8	2	1	-1	1	1	16 656	10.80	1.20	5.42	0.20
5	≈400	1000	20	1.2	1	1	-1	-1	16 137	17.60	1.10	1.00	0.80
6	≈400	1000	36.8	1.2	1	1	1	-1	16 522	16.10	0.40	1.53	1.70
7	≈400	1000	20	2	1	1	-1	1	16 269	13.40	2.50	1.00	1.20
8	≈400	1000	36.8	2	1	1	1	1	16 653	11.70	0.90	1.65	1.70
9	≈100	100	20	1.2	-1	-1	-1	-1	16 103	24.30	1.70	2.00	0.00
10	≈100	100	36.8	1.2	-1	-1	1	-1	16 489	24.20	1.60	2.00	0.30
11	≈100	100	20	2	-1	-1	-1	1	16 235	20.50	2.60	2.03	0.00
12	≈100	100	36.8	2	-1	-1	1	1	16 621	16.50	2.30	1.78	0.50
13	≈100	1000	20	1.2	-1	1	-1	-1	16 102	28.60	1.70	1.03	2.40
14	≈100	1000	36.8	1.2	-1	1	1	-1	16 486	29.50	1.60	1.00	4.90
15	≈100	1000	20	2	-1	1	-1	1	16 234	23.70	2.40	1.05	2.20
16	≈100	1000	36.8	2	-1	1	1	1	16 618	21.60	2.40	1.00	4.80
17	≈200	100	20	1.2	0	-1	-1	-1	16 117	19.80	1.20	2.50	0.00
18	≈200	100	36.8	1.2	0	-1	1	-1	16 503	18.20	1.20	2.63	0.30
19	≈200	100	20	2	0	-1	-1	1	16 139	15.90	2.70	2.58	0.00
20	≈200	100	36.8	2	0	-1	1	1	16 524	12.40	2.00	2.60	0.30
21	≈200	1000	20	1.2	0	1	-1	-1	16 270	21.60	0.80	1.10	1.60
22	≈200	1000	36.8	1.2	0	1	1	-1	16 656	21.90	0.40	1.12	3.20
23	≈200	1000	20	2	0	1	-1	1	16 137	17.30	2.10	1.17	1.40
24	≈200	1000	36.8	2	0	1	1	1	16 522	15.90	1.70	1.07	3.20
0	≈200	315	28.4	1.6	0	0	0	0	16 269	19.10	1.60	3.47	1.90

By the values of response functions the polynomial coefficients a_i were determined for response functions. They were determined by solving the system of 24 linear algebraic equations:

$$\begin{cases} y_1 = a_0 + a_1 * X_1 + \ldots\ldots\ldots\ldots\ldots + a_{11234} * {X_1}^2 * X_2 * X_3 * X_4 \\ \ldots\ldots\ldots\ldots\ldots\ldots\ldots\ldots\ldots\ldots\ldots\ldots\ldots\ldots\ldots\ldots\ldots\ldots\ldots\ldots\ldots\ldots\ldots\ldots\ldots\ldots\ldots \\ y_n = a_0 + a_1 * X_{1,n} + \ldots\ldots\ldots\ldots\ldots + a_{11234} * {X_{1,n}}^2 * X_{2,n} * X_{3,n} * X_{4,n} \end{cases}$$

For each of the response function we obtained the system of 24 equations, where values y_n and $X_{i,n}$ are known and values of a_i are unknown. By solving the system equations we obtained the values of coefficients a_i (Table 3).

Table 3. Values of unknown coefficients of response functions (the first stage of solving the problem)

Coeff.	Response functions				
	y_1	y_2	y_3	y_4	y_5
a_0	16 375 067	17.875	1.513	1.874	1.250
a_1	17 748	-4.681	-0.319	0.569	-0.574
a_2	-1 056	1.300	-0.263	-0.746	1.100
a_3	192 530	-0.775	-0.188	-0.019	0.500
a_4	65 879	-2.500	0.613	-0.019	-0.025
a_{12}	0	-0.894	-0.081	-0.428	-0.538
a_{13}	70	-0.094	-0.294	0.253	-0.251
a_{14}	0	0.494	0.094	0.120	0.024
a_{23}	-318	0.500	-0.013	-0.014	0.350
a_{24}	0	-0.075	0.038	0.011	-0.025
a_{34}	0	-0.450	-0.088	-0.001	0.025
a_{123}	0	-0.156	0.019	-0.099	-0.212
a_{124}	0	0.031	-0.044	-0.111	0.063
a_{134}	0	0.381	-0.131	0.131	-0.049
a_{234}	0	0.025	0.088	-0.016	0.025
a_{1234}	0	-0.031	0.006	-0.110	-0.013
a_{11}	3 550	1.056	0.219	0.198	0.063
a_{112}	0	0.044	0.156	-0.171	0.049
a_{113}	14	0.019	-0.181	0.214	-0.013
a_{114}	0	-0.044	-0.144	0.101	0.037
a_{1123}	0	-0.294	0.081	-0.040	-0.024
a_{1124}	0	-0.056	-0.081	-0.072	0.026
a_{1134}	0	-0.031	-0.044	0.115	-0.037
a_{11234}	0	0.056	-0.056	-0.089	-0.051

Analysis of coefficients values (Table 3) and values of response functions (Table 2) permits evaluating the role different factors for response functions. The following may be noted:

- Rockfill deformation (X_1) has impact on the value of maximum compressive stresses in RCF (y_2). Two times decrease of rockfill deformation results in decrease of maximum compressive stresses in RCF by 4.7 MPa, tensile stresses 0.3 MPa. However, in per cent this impact is not large (26 % and 20 % respectively). Impacts of the face thickness (X_4) and the wall rigidness (X_2) are even less. Increase of thickness results in growth of compressive stresses, and increase of the wall rigidness – to their drop;
- The thickness of the face itself (X_4) has great impact on maximum value of tensile stresses (y_3) in RCF. Increase of thickness considerably raises tensile stresses in it. Thus, from the point of view of providing strength it is feasible to have a thin face. Rockfill deformation (X_1) and the wall rigidness (X_2) have less impact on tensile stresses in RCF. Decrease of rockfill deformation and increase of the wall rigidness decrease tensile stresses in RCF;
- Diaphragm height (X_3) among the other factors has the least impact on RCF SSS;
- The diaphragm safety factor for compressive strength (y_4) is subject to the greatest impact from clay-cement deformation (X_2) and rockfill deformation (X_1). Decrease of rockfill deformation (X_1) increases the safety factor for compressive strength, and increase of the wall rigidness (X_2) decreases it;

- Maximum values of tensile stresses in the diaphragm (y_5) are mostly subject to the impact of clay-cement deformation (X_2). Its impact is more than the impact of rockfill deformation (X_1) and the diaphragm height (X_3);
- Use of quadratic dependences of response functions from factor X_1 permitted reflecting their non-linear character especially by responses y_2 and y_3;
- The impact of several factors interaction should not be neglected. Mainly this refers to interaction of factors X_1 with X_2 and with X_3.

Checking the adequacy of the obtained response factors was carried out for the center of factor space. It was carried out by comparison of the value obtained with aid of polynomials with response for var. 0. The information about comparison is given in Table 4.

Table 4. Checking the adequacy of response factors (the first stage of solving the problem)

Estimation method	Response functions				
	y_1, thou.rub.	y_2, MPa	y_3, MPa	y_4	y_5, MPa
Calculation	16 375	17.875	1.513	1.874	1.250
Test	16 362	19.100	1.600	1.950	1.900
Error, %	0.1 %	6.9 %	5.8 %	4.1 %	52.0 %

The analysis shows that the least adequate is function y_5, describing variation of maximum tensile stresses in the diaphragm. From the point of view of relative error the error is rather large (52 %), however, in numerical terms the error is not so large. Therefore, we may consider that the obtained response functions adequately describe variation of the studied values in the selected range of factors.

Construction of functional relations between SSS parameters and factors permitted us solving the problem searching for the optimal parameters of the dam structure. The target function is the function of the dam cost y_1. Limitations were imposed on functions y_2, y_3, y_4, y_5. The following conditions were adopted:

- Maximum values of stresses in the RCF (y_2 and y_3) should not exceed design strength of concrete of class B25. According to Building Code SP 52-101-2003 design compressive strength of concrete amounts to 18.5 MPa, and tensile strength to 1.55 MPa;
- Safety factor of the diaphragm clay-cement compressive strength (y_4) should be at least 1.25;
- Maximum tensile stress in the diaphragm (y_5) should not exceed 0.1 MPa.

The problem of searching for optimal structural parameters was solved by the method of generalized reduced gradient. As a result of solving the problem the structural parameters were obtained which are given in Table 5. It turned out that the determining limitations are RCF compressive strength of concrete and tensile strength of clay-cement (Table 6).

Table 5. Optimal structural parameters

Factors	X_1	X_2	X_3	X_4
coded	0.352	-1.000	-1.000	-1.000
absolute	E ≈ 260 MPa	100	20	1.2

Table 6. Values of response factors for optimal alternative

Functions	y_1, thou.rub.	y_2, MPa	y_3, MPa	y_4	y_5, MPa
Limitations	Tends to min	≤18.5	≤1.55	≥1.25	≤0.1
Values	16 124 065	18.50	1.18	2.92	0.0

Analysis permits arriving to the following conclusion:

- More optimal is the alternative where the diaphragm has the height of 20 m. Increase of the cofferdam height results in worsening of the CCCD strength;
- To provide safety of both seepage-control elements it is necessary anyway to decrease rockfill deformation. Therefore, increase of RCF thickness is the least effective way in reaching its strength;
- Plastic clay-cement should be used for the diaphragm material;

- The fact that value X_1 was not reached to be maximum possible is explained by a complicated character of rockfill deformation impact on the structure working ability. Selection of rockfill deformability (X_1) conditions selection of clay-cement deformability (X_2). If clay-cement deformability turns out to be less than that of rockfill, this may affect the RCF SSS.

Solving the problem on optimization showed that two of four factors do not need to be changed – the optimal solution corresponds to the case when the values of these factors are on the boundary of the factor space. These are the factors characterizing the dam geometry: X_3 (diaphragm height) and X_4 (RCF thickness). The most feasible alternatives are those where the diaphragm height and RCF thickness are minimum (20 m and 1.2 m respectively). These factors were excluded from further consideration.

At the second stage at searching for the optimal structure 2 factors varied: X_1 (dam body rockfill deformation) and X_2 (clay-cement diaphragm deformation). The dam structural design was considered where the diaphragm height is 20 m the RCF thickness is minimal.

At solving the optimization problem it was decided to increase the degree of response functions for factor X_2, in order to represent the complicated impact of factor X_2 on the diaphragm SSS and increase adequacy response functions. According to the obtained design matrix (Table 7) 9 design alternatives (including the check one) were considered.

Table 7. Design matrix (the second stage of solving the problem)

No	Absolute values of factors		Relative values of factors		Response functions				
	X_1, MPa	X_2, MPa	X_1	X_2	y_1, thou.rub.	y_2, MPa	y_3, MPa	y_4	y_5, MPa
1	≈100	100	-1	-1	16 103	24.30	1.80	2.16	0.00
2	≈100	1000	-1	1	16 102	28.60	1.70	1.00	2.40
3	≈200	100	0	-1	16 117	19.80	1.20	2.67	0.00
4	≈200	1000	0	1	16 116	21.60	0.80	1.15	1.60
5	≈400	100	1	-1	16 139	16.50	1.40	3.47	0.01
6	≈400	1000	1	1	16 137	17.60	1.10	1.00	0.80
7	≈100	315	-1	0	16 103	26.90	1.70	1.47	0.20
8	≈200	315	0	0	16 117	23.80	0.90	1.75	0.20
9	≈400	315	1	0	16 138	17.30	0.90	2.32	0.00

By the results of SSS calculations for these alternatives there were plotted relationship curves between the SSS parameters and the considered factors (Figures 6, 7). Analysis of these curves showed that non-linear character is typical for response functions y_3 and y_5, which characterize the level of tensile stresses in RCF (Figure 6b) and CCCD (Figure 7b). Especially vivid this non-linearity is for factor y_5.

On the curves in Figure 6 it is well seen that the determining factor for providing the RCF safety are compressive stresses in the face (y_2). It is seen that compressive strength in RCF may be provided only in the case if coefficient of reduction of rockfill deformation exceeds 2.7. In other words, the secant modulus of rockfill deformation should be at least 270 MPa.

Figure 7 vividly demonstrates that CCCD compressive and tensile strength may be provided only if the diaphragm is made of plastic (pored) clay-cement concrete. Compressive strength condition may be provided at CCCD deformation modulus not exceeding 800 MPa (Figure 7a). But the determining condition is the condition of tensile strength (Figure 7b). To provide the diaphragm tensile strength the CCCD deformation modulus should be at least 250÷400 MPa.

These conclusions were confirmed at using more strict way of searching for solution: i.e. by solving the problem of optimization. After solving the system of linear algebraic equations we found the coefficients of quadratic polynomials of response functions and then using the described above limitations we obtained the parameters of the optimal structural design.

It was found that the optimal structural design if the design where coefficient of reduction of rockfill deformation reaches 3.6, and deformation modulus of clay-cement does not exceed 378 MPa. Thus, it turned out that for reaching optimal SSS of RCF and CCCD deformation moduli of clay-cement and rockfill should be approximately equal.

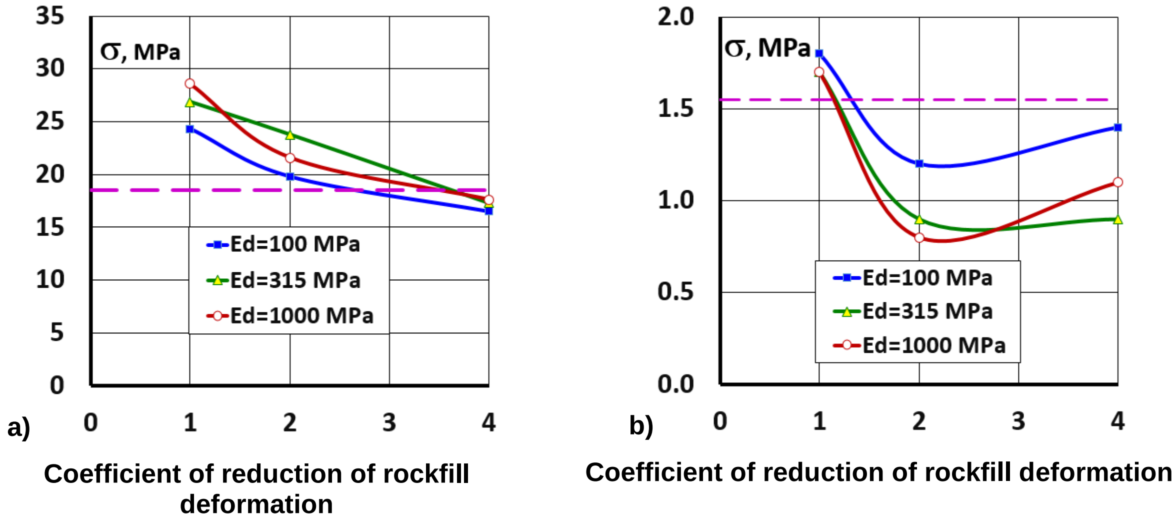

Figure 6. Variation of RCF parameters of SSS depending on rockfill deformation and the diaphragm deformation modulus of clay-cement (Ed)
a – maximum compressive stresses; b – maximum tensile stresses.
The dotted line shows the limitation established for the factor

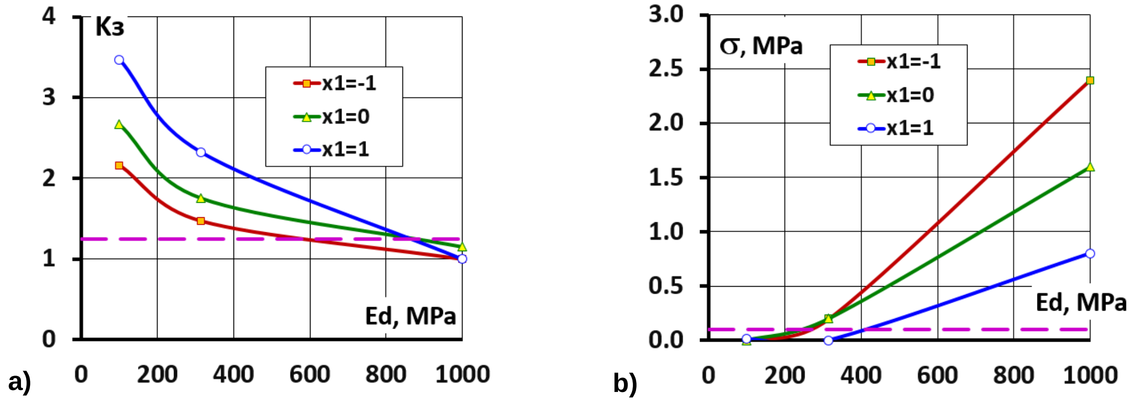

Figure 7. Variation of the diaphragm SSS parameters depending on rockfill deformation and deformation modulus of the diaphragm clay-cement (Ed)
a – safety factor for compression strength; b – maximum tensile stresses. The dotted line shows the limitation established for the factor

Thus solving the problem of optimization permitted revealing main principals in selection of structural design parameters of a rockfill dam with combined seepage-control element, revealing main trends of its optimization. However, the final solution of the problem has not yet reached and there are several reasons for it. First of all, the values of some variable factors in the optimal structural design turned to be at the boundary of the factor space. This means that the structure may be optimized even more extensively. Secondly, there are other ways of enhancing the structure efficiency. Namely, decrease of tensile stresses in the wall may be reached by changing the layout of the diaphragm contact with rock foundation. By the results of studies arrangement of clay-cement «pad» makes the diaphragm free from bending and tensile deformations. This promises the way of further refinement of the dam structural design.

4. Conclusions

1. The rockfill dam with a combined seepage-control element (consisting of a reinforced concrete face and a clay-cement diaphragm) may be a rather safe type of the dam even in conditions of a high head (more than 200 m). For this purpose it is necessary to follow the principles, which were obtained as a result of this study.

2. The main principles of designing the dams of the considered type are as follows:

- Rockfill deformation modulus should be at least 250 MPa in order to provide strength of the reinforced concrete face and the clay-cement diaphragm;

- In spite of the fact that increase of the reinforced concrete face thickness seems to be a simple way of enhancing its strength, there is no need of making it too massive. This is connected with the fact that for providing safety of all structural elements rockfill should be very well compacted. The RCF thickness should be taken equal 0.5 % of the dam height;
- It is desirable that deformation modulus of clay-cement and rockfill were equal. Here the rule may be used, according to which clay-cement deformation modulus should have 2 times difference from rockfill deformation modulus.

3. There are ways of further enhancing safety of a rockfill dam with a combined seepage-control element. Namely, for reducing the danger of appearance in the diaphragm tensile stresses from bending deformations it is feasible to conjugate the diaphragm with rock foundation with the aid of a clay-cement "pad".

References

1. Zhongming, J., Qing J. Shuibuya: The world's highest concrete faced rockfill dam. The International Journal on Hydropower & Dams. 2000. Vol. 7. No. 4. Pp. 94–97.
2. Freitas, M.S.Jr. Concepts on CFRDs Leakage Control – Cases and Current Experiences. ISSMGE Bulletin. 2009. Vol. 3. No. 4. Pp. 11–18.
3. Song, W., Sun, Y., Li, L., Wang, Y. Reason analysis and treatment for the 1st phase slab cracking of Shuibuya CFRD. Journal of Hydroelectric Engineering. 2008. No. 3(27). Pp. 33–37.
4. Markes Filo P., Pinto N. de S. Kharakteristiki kamenno–nabrosnykh plotin s betonnym ekranom, poluchennyye opytnym putem [Features rockfill dam with a concrete screen, obtained by experience]. Mezhdunarodnyy daydzhest po gidroenergetike i plotinam. 2007. Pp. 69–74.
5. Silva da, A.F., Assis de, A.P., Neto, M.P.C. Three–Dimensional Analyses of Concrete Face Rockfill Dams: Barra Grande Case Study. Electronic Journal of Geotechnical Engineering. 2015. Vol. 20. Bund 14. Pp. 6407–6426.
6. Barra Grande Hydropower Plant. Design, Construction and Perfomance. Main Brazilian Dams III. [Online]. System requirements: AdobeAcrobatReader. URL: http://www.cbdb.org.br/documentos/mbdiii/Barra%20grande.pdf.
7. Johannesson, P., Tohlang, S.L. Lessons learned from Mohale. The International Water Power & Dam Construction. August 2007. Vol. 59. No. 8. Pp. 16–18+20–22+24–25.
8. Sobrinho, J.A., Xavier, L.V., Albertoni, S.C., Pereira, R.F. Performance and Concrete Face Repair at Campos Novos. The International Journal on Hydropower & Dams. 2007. No. 14(2). Pp. 39–42.
9. Xavier, L.V., Albertoni, S.C., Pereira R.F., Antunes J. Campos Novos dam during second impounding. The International Journal on Hydropower & Dams. 2008. No. 15. Pp. 53–58.
10. Li, N.-H., Sun, D.-W., Li, D.-H., Deng, Y.-G., Yang, J. Deformation behavior of 300 m high–concrete face rockfill dams. Yantu Gongcheng Xuebao / Chinese Journal of Geotechnical Engineering. 2009. No. 31(2). Pp. 155–160.
11. Luo, D., Luo, L. Study and engineering practice on cracks control measures for concrete face slab of high CFRD. Advanced Materials Research. 2012. Vol. 455–456. Pp. 1606–1611.
12. Li, N.-H. Performance of high concrete face rockfill dams in China and its inspiration. Yantu Gongcheng Xuebao / Chinese Journal of Geotechnical Engineering. 2011. No. 33(2). Pp. 165–173
13. Sun, D., Zhang, G., Wang, K., Yao, H. 3D finite element analysis on a 270m rockfill dam based on Duncan–Chang E–B model. Advanced Materials Research. 2011. Pp. 287–290, 1213–1216.

Литература

1. Zhongming J., Qing J. Shuibuya: The world's highest concrete faced rockfill dam // The International Journal on Hydropower & Dams. 2000. Vol. 7. № 4. Pp. 94–97.
2. Freitas M.S.Jr. Concepts on CFRDs Leakage Control – Cases and Current Experiences // ISSMGE Bulletin. 2009. Vol. 3. № 4. Pp. 11–18.
3. Song W., Sun Y., Li L., Wang Y. Reason analysis and treatment for the 1st phase slab cracking of Shuibuya CFRD // Journal of Hydroelectric Engineering. 2008. № 3(27). Pp. 33–37.
4. Маркес Фильо П., Пинто Н. де С. Характеристики каменно–набросных плотин с бетонным экраном, полученные опытным путем // Международный дайджест по гидроэнергетике и плотинам. 2007. С. 69–74.
5. Silva da A.F., Assis de A.P., Neto M.P.C. Three–Dimensional Analyses of Concrete Face Rockfill Dams: Barra Grande Case Study // Electronic Journal of Geotechnical Engineering. 2015. Vol. 20. Bund 14. Pp. 6407–6426.
6. Barra Grande Hydropower Plant. Design, Construction and Perfomance. Main Brazilian Dams III. [Электронный ресурс]. Сист.требования: AdobeAcrobatReader. URL: http://www.cbdb.org.br/documentos/ mbdiii/Barra%20grande.pdf.
7. Johannesson P., Tohlang S.L. Lessons learned from Mohale // The International Water Power & Dam Construction. August 2007. Vol. 59. № 8. Pp. 16–18+20–22+24–25.
8. Sobrinho J.A., Xavier L.V., Albertoni S.C., Pereira R.F. Performance and Concrete Face Repair at Campos Novos // The International Journal on Hydropower & Dams. 2007. № 14(2). Pp. 39–42.
9. Xavier L.V., Albertoni S.C., Pereira R.F., Antunes J. Campos Novos dam during second impounding // The International Journal on Hydropower & Dams. 2008. № 15. Pp. 53–58.
10. Li N.-H., Sun D.-W., Li D.-H., Deng Y.-G., Yang J. Deformation behavior of 300 m high–concrete face rockfill dams // Yantu Gongcheng Xuebao / Chinese Journal of Geotechnical Engineering. 2009. № 31(2). Pp. 155–160.
11. Luo D., Luo L. Study and engineering practice on cracks control measures for concrete face slab of high CFRD. Advanced Materials Research. 2012. Vol. 455–456, Pp. 1606–1611.
12. Li N.-H. Performance of high concrete face rockfill dams in China and its inspiration // Yantu Gongcheng Xuebao / Chinese Journal of Geotechnical Engineering. 2011. № 33(2). Pp. 165–173.
13. Sun D., Zhang G., Wang K., Yao H. 3D finite element analysis on a 270m rockfill dam based on Duncan–Chang E–B model // Advanced Materials Research. 2011. Pp. 287–290, 1213–1216.

14. Zhang, Z. Development of super–high concrete face rockfill dams in China. 14th Asian Regional Conference on Soil Mechanics and Geotechnical Engineering. 2011.
15. Zhang, Z.-L. Design and technical innovation of rockfill dam projects. Yantu Gongcheng Xuebao / Chinese Journal of Geotechnical Engineering. 2007. No. 29(8). Pp. 1184–1193.
16. Sainov, M.P. Impact of dam site configuration on 3D stress-strain state of concrete faced rockfill dam. Magazine of Civil Engineering. 2016. No. 3. Pp. 16–39. doi: 10.5862/MCE.63.2 (rus)
17. Sainov, M.P. Analysis of normal operation of a rockfill dam with combination of seepage-control elements: reinforced concrete face and a clay-cement-concrete wall. Magazine of Civil Engineering. 2016. No. 4. Pp. 3–9. doi: 10.5862/MCE.64.1
18. Sainov, M.P., Soroka, V.B. Rabotosposobnost sverkhvysokoy kamenno–nabrosnoy plotiny s kombinatsiyey negruntovykh protivofiltratsionnykh ustroystv [Workability of a ultra–high rockfill dam in combination with non–soil seepage–control facilities]. Privolzhskiy nauchnyy zhurnal. 2017. No. 3(43). Pp. 70–76.
19. Tang, J.-S., Ding, B.-M. Design of concrete face rockfill dam of the expansion project of Hengshan Reservoir. Water Power. 2002. No. 28(7). Pp. 35–37. (chinese)
20. Rasskazov, L.N., Dzhkha, Dzh. Deformiruyemost i prochnost grunta pri raschete vysokikh gruntovykh plotin [Deformability and Strength of Soils in High Soil Dam Calculation]. Gidrotekhnicheskoye stroitelstvo. 1987. No. 7. Pp. 31–36.
21. Malyshev, L.I., Shishov, I.N., Kudrin, K.P., Bardyugov, V.G. Tekhnicheskiye resheniya i rezultaty rabot po sooruzheniyu protivofiltratsionnoy steny v grunte v yadre i osnovanii Kureyskoy GES [Technical Solutions and Working Results in the Process of Building Filtration–proof Wall in the Soil of the Core and Foundation of Kureyskaya Water Power Plant]. Gidrotekhnicheskoye stroitelstvo, 2001. No. 3. Pp. 31–36.
22. Mirghasemi, A.A., Pakzad, M., Shadravan, B. The world's largest cutoff wall at Karkheh dam. The International Journal on Hydropower & Dams. 2005. No. 2. Pp. 2–6.
23. Sainov, M.P. Vychislitelnaya programma po raschetu napryazhenno–deformirovannogo sostoyaniya gruntovykh plotin: opyt sozdaniya, metodiki i algoritmy [Computer program for the calculation of the stress–strain state of soil dams: the experience of creation, techniques and algorithms]. International Journal for Computational Civil and Structural Engineering. 2013. No. 9(4). Pp. 208–225.
24. Kahl, T.W., Kauschinger, J.L., Perry, E.B. Plastic concrete cutoff walls for Earth Dams. Departament of the Army US Army Corps of Engineers. 1991. 119 p.
25. Rasskazov, L.N., Radzinskiy, A.V., Sainov, M.P. Strength and Deformability of Clay–cement in Complex Stress State. Technology and Engineering. 2015. Vol. 48(5). Pp. 29–33.

14. Zhang Z. Development of super–high concrete face rockfill dams in China // 14th Asian Regional Conference on Soil Mechanics and Geotechnical Engineering. 2011.
15. Zhang Z.-L. Design and technical in№vation of rockfill dam projects // Yantu Gongcheng Xuebao / Chinese Journal of Geotechnical Engineering. 2007. № 29(8). Pp. 1184–1193.
16. Саинов М.П. Влияние формы створа на напряжённое состояние железобетонного экрана каменно-насыпной плотины // Инженерно-строительный журнал. 2016. № 3(63). С. 16–39.
17. Саинов М.П. Анализ работоспособности каменной плотины с комбинацией противофильтрационных элементов – железобетонного экрана и глиноцементобетонной стены // Инженерно-строительный журнал. 2016. № 4(64). С. 3–9.
18. Саинов М.П., Сорока В.Б. Работоспособность сверхвысокой каменно– набросной плотины с комбинацией негрунтовых противофильтрационных устройств // Приволжский научный журнал. 2017. № 3(43). С. 70–76.
19. Tang J.-S., Ding B.-M. Design of concrete face rockfill dam of the expansion project of Hengshan Reservoir // Water Power. 2002. № 28(7). Pp. 35–37.
20. Рассказов Л.Н., Джха Дж. Деформируемость и прочность грунта при расчете высоких грунтовых плотин // Гидротехническое строительство. 1987. № 7. С. 31–36.
21. Малышев Л.И., Шишов И.Н., Кудрин К.П., Бардюгов В.Г. Технические решения и результаты работ по сооружению противофильтрационной стены в грунте в ядре и основании Курейской ГЭС // Гидротехническое строительство. 2001. № 3. С. 31–36.
22. Mirghasemi A.A., Pakzad M., Shadravan B. The world's largest cutoff wall at Karkheh dam // The International Journal on Hydropower & Dams. 2005. № 2. Pp. 2–6.
23. Саинов М.П. Вычислительная программа по расчёту напряжённо–деформированного состояния грунтовых плотин: опыт создания, методики и алгоритмы // International Journal for Computational Civil and Structural Engineering. 2013. № 9(4). С. 208–225.
24. Kahl T.W., Kauschinger J.L., Perry E.B. Plastic concrete cutoff walls for Earth Dams. Departament of the Army US Army Corps of Engineers. 1991. 119 p.
25. Рассказов Л.Н., Радзинский А.В., Саинов М.П. Прочность и деформируемость глиноцементобетона в сложном напряженном состоянии // Гидротехническое строительство. 2014. №8. С. 29–33.

Mikhail Sainov,*
+7(926)607-89-31; mp_sainov@mail.ru

Vladislav Soroka,
+7(929)503-49-72; vastion08@yandex.ru

Михаил Петрович Саинов,*
+7(926)607-89-31;
эл. почта: mp_sainov@mail.ru

Владислав Борисович Сорока,
+7(929)503-49-72;
эл. почта: vastion08@yandex.ru

doi: 10.18720/MCE.81.15

Computational modelling of stiffness and strength properties of the contact seam

Численное моделирование жесткостных и прочностных свойств контактного шва

A.A. Lukashevich,
St. Petersburg State University of Architecture and Civil Engineering, St. Petersburg, Russia

Д-р техн. наук, профессор
А.А. Лукашевич,
Санкт-Петербургский государственный архитектурно-строительный университет, Санкт-Петербург, Россия

Key words: contact problem; unilateral constraints; step-by-step analysis; contact seam; nonlinear deformability; initial strength

Ключевые слова: контактная задача; односторонние связи; пошаговый анализ; контактный шов; нелинейная податливость; начальная прочность

Abstract. The problem of contact interaction of structures taking into account the deformation and strength properties of the contact seam material is considered. To discretize the contact layer, frame-rod contact finite elements (CFE) are used, by means of which the physical properties of the seam material (initial strength, line and nonlinear deformability) are modelled. By means of CFE are also modelled various contact conditions – separation, clutch, friction-sliding, etc. On the base of the proposed discrete contact model and the method of step-by-step analysis, a numerical algorithm for solving the contact problem has been developed taking into account the deformation and strength properties of the seam material. This approach allows in one step-by-step cycle to perform simultaneous account of the initial strength of the contact seam, as well as the conditions of unilateral deformable constraints and friction-sliding of its surfaces in areas where the strength of the contact seam is broken. The use of frame-rod contact elements allows the physical nonlinearity of the contact layer to reduce to the internal nonlinearity of only the system of contact elements, while the nonlinear properties of the seam are set by means of the nonlinear characteristics of the individual rods of contact elements. Iterative refinement of the nonlinear solution for the current level of loading is performed by the method of compensating loads. With the help of the proposed approach, the numerical solution of the problem of contact of the structure with the base under different conditions of the contact seam has been obtained and analyzed.

Аннотация. Рассматривается задача контактного взаимодействия конструкций с учетом деформативных и прочностных свойства материала контактного шва. Для дискретизации контактного слоя используются рамно-стержневые контактные конечные элементы (ККЭ), посредством которых моделируются физические свойства материала шва (начальная прочность, линейная и нелинейная податливость). С помощью ККЭ также моделируются различные условия контакта – отрыва, сцепления, трения-скольжения и т.п. На основе предложенной дискретной модели контакта и метода пошагового анализа разработан численный алгоритм решения контактной задачи с учетом деформативных и прочностных свойств материала шва. Данный подход позволяет в одном пошаговом цикле выполнить одновременный учет начальной прочности контактного шва, а также условия односторонних податливых связей и трения-скольжения его поверхностей на участках, где прочность контактного шва нарушена. Использование рамно-стержневых контактных элементов позволяет физическую нелинейность контактного слоя свести к внутренней нелинейности только системы контактных элементов, при этом нелинейные свойства шва задаются через нелинейные характеристики отдельных стержней контактных элементов. Итерационное уточнение нелинейного решения для текущего уровня нагружения выполняется посредством способа компенсирующих нагрузок. С помощью предложенного подхода получено и проанализировано численное решения задачи контакта сооружения с основанием при различных условиях работы контактного шва.

Лукашевич А.А. Численное моделирование жесткостных и прочностных свойств контактного шва // Инженерно-строительный журнал. 2018. № 5(81). С. 149–159.

1. Introduction

The problems of contact interaction of structures and their parts have a wide range of applications in construction and other fields of engineering. For example, deformation and technological seams can be opened and closed, both with slippage, and with clutch of contacting surfaces, at various combinations of external loadings. The same can happen at interaction of the cracks coasts, on contact of a sole of the construction with the basis or on the supports allowing a separation or slippage of the construction leaning on them. Herewith, it is often the state of the contact zone can be determining when assessing the stress-strain state, strength and reliability of structures and construction [1–8]. In turn, the state of contact is also influenced by the deformation and strength properties of the material of the contact seam, the accounting of which approximates the design scheme to the real working conditions of construction.

The deformation of the contact seam can be conditioned by the presence of the locally deformable layer between the contact surfaces, the roughness of the boundary surfaces of interacting bodies and other reasons. Similar calculation schemes can be used for structures where an opening and closing of seams, friction and sliding of surfaces, formation of cracks, etc. The corresponding problems (taking into account the deformation of the contact layer, both in normal and tangential directions) were considered in the works [2, 9–15]. They used numerically-analytical or iterative methods for solving the contact problem, particularly, the method of iterations over the gaps [9, 12], the method of iterations on limit friction forces [2, 13–15].

In some cases it is necessary to consider nonlinear properties of the contact seam. Using the finite element method allows to take into account this kind of physical nonlinearity, reducing it to the internal nonlinearity of the system of contact elements discretizing the intermediate layer. The solution of such problems leads to the solution of a nonlinear system of equations at each step of loading or iterative approximation. Various iterative schemes of accounting of nonlinear effects on the contact were considered in the works [16–21]. The nonlinear relationship between the deformation of the contact layer and the contact stresses is given here by means of the corresponding nonlinear dependencies or diagrams.

The contact seam may have some initial strength as well, both in the normal and tangential direction. It should be emphasized that issues related directly to destruction of construction are not considered here. The strength of the seam is described by simple dependencies, which, however, may be useful in solving some practical problems. Account of the strength of unilateral constraints was discussed in several papers [22–25], where the rather complex algorithms of successive approximations were proposed. For example, in [23] a combined algorithm consisting of four nested iterative cycles is presented, for practical implementation of which it is recommended to apply a preliminary lowering of the order of discretization of the problem.

The numerical solution of contact problems is usually realized on the basis of different schemes of the finite element method (FEM). In this case, the continuum problems of contact of elastic bodies are reduced to finite-dimensional problems with discrete unilateral constraints [10–14, 17–26]. In this paper, for the modeling of the contact seam contact finite elements (CFE) of the frame-rod type have been used, that allows to calculate the forces and displacements in the contact zone with the sufficiently high accuracy. By means of the FEM both physical properties of the seam material (initial strength, line and nonlinear deformability), and a variety of contact state (separation, clutch, friction-sliding) are modeled.

The purpose of this work is to develop an algorithm for the numerical realization of the proposed finite element model, which allows simultaneous accounting of the strength and nonlinear deformability of the contact seam, as well as the conditions of unilateral constraints and friction--sliding in the contact areas. To achieve this purpose, numerical studies, as well as a comparison of the results with the solutions having been obtained by alternative methods, have been carried out.

2. Methods

Let us consider the case of contact between the boundary surfaces S_g^+ and S_g^- of the elastic bodies V^+ and V^-. It is believed that the surface data are connected by contact seam having thickness ζ^0, possessing deformability ρ_n and ρ_τ (in the normal and tangent direction respectively) and the initial tensile strength (break) $R_n > 0$ and shift $R_\tau > 0$ ($\alpha_R = R_\tau / R_n$). Under the assumption that the destruction of the material of the contact seam occurs according to the fragile scenario, we use the strength criterion of the Coulomb-Mohr:

Lukashevich, A.A. Computational modelling of stiffness and strength properties of the contact seam. Magazine of Civil Engineering. 2018. 81(5). Pp. 149–159. doi: 10.18720/MCE.81.15.

$$\sigma_n + \frac{1}{\alpha_R}\left|\sigma_\tau\right| \le R_n; \quad \left|\sigma_\tau\right| \le R_\tau - \alpha_R\,\sigma_n. \tag{1}$$

The property of the contact problem with seams having an initial strength is that the process of breaking bonds is an irreversible phenomenon. The solution of such problems depends on the sequence of application of external loads, and the form of boundary conditions having been implemented for contact surfaces at the moment depends on whether the destruction of the initial clutch of constraints from the beginning of loading happened or not. If there was no destruction, then the surfaces at this point remain of clutched, and if there was, then the usual conditions for unilateral constraints with friction (without taking into account their strength) are fulfilled.

The contact finite elements proposed by the author – in the form of a flat or spatial frame are used to model the contact interaction in the seam zone. The CFE data interacts with the usual finite elements of a discrete calculation scheme and thus providing a connection between the mesh nodes located on the boundary surfaces of the contacting bodies (Figure 1).

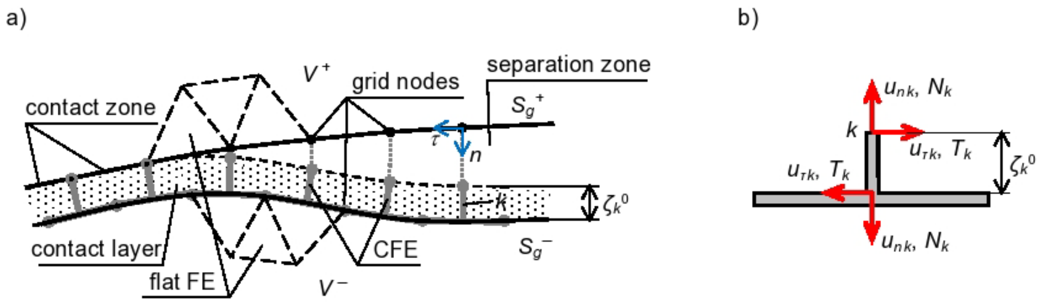

Figure 1. Modeling of contact by means of frame-rod CFE:
a – CFE in the contact zone; b – displacement and forces in the CFE

When using the contact elements data, there is no need to match the coordinates of the nodes of the contacting surfaces, i.e. inconsistent grids can be used. Various properties of the contact seam, such as deformability, initial strength, physical nonlinearity, etc., can be taken into account with the help of CFE. Modeling of various contract conditions is carried out by changing the physical properties of the contact layer, which, in turn, are expressed through the stiffness and strength characteristics of individual rods of frame CFE [26, 27].

Considering the *k* contact element as the *k* discrete unilateral deformable constraint (in normal and tangential directions) between interacting bodies, we express the conditions (1) through contact forces in *k* CFE ($k \in S_g$, $S_g = S_g^+ \cup S_g^-$)

$$N_k + \frac{1}{\alpha_R}\left|T_k\right| \le N_{Rk}; \quad \left|T_k\right| \le T_{Rk} - \alpha_R\,N_k. \tag{2}$$

Let us write down the conditions on the contact in terms of forces and displacements for the *k* contact element:

$$u_{nk} + u_{nk}^c \le 0; \quad N_k + \frac{\left|T_k\right|}{\alpha_R} \le N_{Rk}; \quad (u_{nk} + u_{nk}^c)(N_k + \frac{\left|T_k\right|}{\alpha_R} - N_{Rk}) = 0; \tag{3}$$

$$\left|T_k\right| \le T_{Rk} - \alpha_R\,N_k; \quad T_k\,(u_{\tau k} + u_{\tau k}^c) \ge 0; \quad (T_k - T_{Rk} + \alpha_R\,N_k)\,(u_{\tau k} + u_{\tau k}^c) = 0; \tag{4}$$

$$u_{nk}^c = N_k / C_{nk}; \quad u_{\tau k}^c = T_k / C_{\tau k}. \tag{5}$$

Here u_{nk}, $u_{\tau k}$ is the mutual displacement of the opposite nodes at S_g^+ and S_g^- in the normal and tangential direction; u_{nk}^c, $u_{\tau k}^c$ is the longitudinal and transverse deformation in *k* CFE; N_k, T_k is the forces in the support rod of *k* CFE; $T_{Uk} = -f_k N_k$ is the ultimate «Coulomb» friction force; $f_k \geq 0$ is the coefficient of friction in *k* contact; $N_{Rk} = R_n\,\omega_k$, $T_{Rk} = R_\tau\,\omega_k$ are the ultimate tensile and shear contact forces for *k* discrete unilateral constraint (i.e. CFE). An additional group of conditions Eq. (5) characterize the deformability of the contact seam: C_{nk}, $C_{\tau k}$ is the normal and tangential stiffness; ω_k is the contact area related to *k* CFE. At linear deformability of the seam material $C_{nk} = \omega_k / \rho_{nk}$, $C_{\tau k} = \omega_k / \rho_{\tau k}$.

The conditions in the form (3) – (4) are valid only until the initial strength of unilateral constraints on the *k* contact is reached, and after the destruction the conditions (6) – (7), describing unilateral constraints with additional deformability without taking into account the strength, are valid [27]:

$$u_{nk} + u_{nk}^c \leq 0; \quad N_k \leq 0; \quad (u_{nk} + u_{nk}^c)\,N_k = 0; \tag{6}$$

$$|T_k| \leq |T_{Uk}|; \quad T_k\,(u_{\tau k} + u_{\tau k}^c) \geq 0; \quad (|T_k| - T_{Uk})\,(u_{\tau k} + u_{\tau k}^c) = 0. \tag{7}$$

Thus, in one step cycle simultaneous account of the strength of the seam, as well as the disclosure or friction of its surfaces in areas where the strength of the seam is broken are provided.

Modeling of physical and strength properties, as well as contact states, is carried out by assigning of the corresponding stiffness characteristics of frame-rod CFE. The stiffness of the contact seam in the normal and tangential directions to the boundary surfaces is expressed by the longitudinal and bending stiffness of the support rod CFE. In the state of contact with the clutching, the stiffness values of this rod in *k* CFE must correspond to the corresponding stiffness of the contact layer:

$$EA_k = C_{nk}\zeta_k^0 = \omega_k \zeta_k^0 \big/ \rho_n; \quad EI_k = C_{\tau k}\,(\zeta_k^0)^3 \big/ 3 = \omega_k\,(\zeta_k^0)^3 \big/ 3\rho_\tau. \tag{8}$$

With the disengagement of the contact surfaces or slippage, respectively assigned a «zero» hardness.

The computational implementation of the conditions (3) – (5) is performed using a step-by-step analysis of changes in the state of the contact in the process of sequential application of a given load. In this case, the friction conditions can be satisfied to the best extent, since the solution of the friction problem depends on the history of loading of the structure. The moment of transition from one state to another is, respectively, the event of destruction of unilateral constraints, separation or contact, slippage or clutching. The method of step-by-step analysis is the most effective for the considered class of contact problems, besides, it is possible to monitor the current state of the contact seam in the process of loading the structure.

The algorithms of step-by-step analysis, including the sequence of actions at each step, both under static and dynamic loading, are described in sufficient detail in [27–31]. In the foundation of these algorithms is the representation of constructively nonlinear contact problem in the form of a sequence of finite number of linear problems with a sequential change of the working schemes of the structure. The analysis of the working scheme behavior determines the time of the next event on the contact. As a result of the next step, the working scheme is changed and the new state of the contact is set, while the method of compensating loads is used to fulfill the contact friction-slip conditions [27, 29].

Below are some expressions of the step-by-step algorithm determining, in particular, the moments of the occurrence of the closest event on the contact (change in the state of contact), taking into account the deformability and strength of the contact seam.

The moment of destruction for the bond (in the direction of normal and tangential respectively), which has been earlier in the state of initial strength

$$\left.\begin{aligned} \Delta\lambda_k^{s+1} &= \Delta\tilde{\lambda}^{s+1}\left(\frac{N_{Rk} - N_k^s - \left|T_k^s\right| \big/ \alpha_R}{\Delta\tilde{N}_k^{s+1}}\right) \\ \Delta\lambda_k^{s+1} &= \Delta\tilde{\lambda}^{s+1}\left(\frac{T_{Rk} - T_k^s - \alpha_R\,N_k^s}{\Delta\tilde{T}_k^{s+1}}\right) \end{aligned}\right\}, \quad k \in S_{1g}. \tag{9}$$

The slippage torque for connection in the state of the clutching

$$\Delta\lambda_k^{s+1} = \Delta\tilde{\lambda}^{s+1}\left(\frac{T_{Uk}^s - T_k^s}{\Delta\tilde{T}_k^{s+1} - \Delta\tilde{T}_{Uk}^{s+1}}\right), \quad k \in S_{2g}. \tag{10}$$

The separation torque for constraint, which has been earlier in the contact

$$\Delta\lambda_k^{s+1} = \Delta\tilde{\lambda}^{s+1}\left(\frac{-N_k^s}{\Delta\tilde{N}_k^{s+1}}\right), \quad k \in S_{2g}, S_{3g}. \tag{11}$$

The moment of contact for constraint, which has been earlier in of the separation

$$\Delta\lambda_k^{s+1} = \Delta\tilde{\lambda}^{s+1}\left(\frac{-(\Delta u_{nk} + \Delta u_{nk}^c)^s}{(\Delta\tilde{u}_{nk} + \Delta\tilde{u}_{nk}^c)^{s+1}}\right), \quad k \in S_{4g}. \tag{12}$$

Here the sign "tilda" denotes the values corresponding to the trial step of loading $\Delta\tilde{\lambda}^{s+1}$, the force values T_{Uk}^s, T_k^s and N_k^s correspond to the *s* level of loading. $k \in S_{1g}$ are the connections in the state of initial strength of the contact seam; $k \in S_{2g}$ are the constraints in the state of pre-ultimate friction (clutching); $k \in S_{3g}$ – in conditions of ultimate friction (sliding); $k \in S_{4g}$ – in the state of separation.

The estimated loading step corresponds to the minimum of the obtained values, i.e., the one at which the nearest event occurs on the contact:

$$\Delta\lambda_{S_g}^{s+1} = \min(\Delta\lambda_k^{s+1}), \quad k \in S_{1g}, S_{2g}, S_{3g}, S_{4g}. \tag{13}$$

In other respects, the computational algorithm for solving the contact problem, including the implementation of limiting friction conditions by means of compensating loads, corresponds to the algorithms used in [26–29].

Under the nonlinear law of deformation of the contact layer of stiffness in the direction of the normal and tangential there will be functions from the values respectively compression and shear of the contact seam: $C_n = C_n(u_n^c)$; $C_\tau = C_\tau(u_\tau^c)$. Using a frame-rod CFE allows the physical nonlinearity of the contact layer to reduce the internal nonlinearity of the system, only the contact elements, herewith the nonlinear properties of the weld are determined through the nonlinear characteristics of the single members of the CFE.

When the step-by-step solution of the contact problem (based on the discrete model of FEM) for each (*s*+1) level of loading, the following matrix equilibrium equation is valid:

$$\left[\boldsymbol{K}_{lin} + \boldsymbol{K}_{nel}(\boldsymbol{u}^{s+1})\right]\Delta\boldsymbol{u}^{s+1} = \boldsymbol{P}^{s+1} - \left[\boldsymbol{K}_{lin} + \boldsymbol{K}_{nel}(\boldsymbol{u}^{s+1})\right]\boldsymbol{u}^s. \tag{14}$$

Here $\boldsymbol{u}^{s+1}$ and $\boldsymbol{P}^{s+1}$ are respectively the vectors of nodal displacements and external loads at the end of step (*s*+1); $\Delta\boldsymbol{u}^{s+1}$ is the increment of displacement at step (*s*+1); $\boldsymbol{K}_{lin}$, $\boldsymbol{K}_{nel}(\boldsymbol{u}^{s+1})$ are linear and non-linear components of the stiffness matrix of the system of finite elements.

By moving the nonlinear component of the equation $\boldsymbol{K}_{nel}(\boldsymbol{u}^{s+1})\,\Delta\boldsymbol{u}^{s+1}$ to the right side, it is possible to write the following recurrent equation to determine the increments of displacements $\Delta\boldsymbol{u}^{s+1}$ at step (*s*+1):

$$\boldsymbol{K}_{lin}\,\Delta\boldsymbol{u}_i^{s+1} = \boldsymbol{P}_{lin}^{s+1} - \boldsymbol{P}_{i-1}^{s+1}(\boldsymbol{u}_{i-1}^{s+1}), \tag{15}$$

where $\Delta\boldsymbol{u}_i^{s+1}$ are the values of increments of displacements on the current iteration *i*; $\boldsymbol{P}_{lin}^{s+1} = \left(\boldsymbol{P}^{s+1} - \boldsymbol{K}_{lin}\,\boldsymbol{u}^s\right)$ is the constant (linear) part of the vector of right parts; $\boldsymbol{P}_{i-1}^{s+1}(\boldsymbol{u}_{i-1}^{s+1}) = \boldsymbol{K}_{nel}(\boldsymbol{u}_{i-1}^{s+1})\left(\boldsymbol{u}^s + \Delta\boldsymbol{u}_{i-1}^{s+1}\right)$ is the changeable part of the vector of right parts.

Let us present a nonlinear matrix, $\boldsymbol{K}_{nel}(\boldsymbol{u})$ corresponding to a discrete layer, as the sum of the nonlinear components of the CFE stiffness matrices

$$\boldsymbol{K}_{nel}(\boldsymbol{u}) = \sum_k \left\lfloor \boldsymbol{K}_{n\,nel}^{(k)}(u_n^c) + \boldsymbol{K}_{\tau\,nel}^{(k)}(u_\tau^c) \right\rfloor. \tag{16}$$

In turn, the nonlinear component of the stiffness matrix of *k* CFE, for example, $\boldsymbol{K}_{n\,nel}^{(k)}(u_n^c)$, can be written as follows:

$$\boldsymbol{K}_{n\,nel}^{(k)}(u_n^c) = C_n(u_n^c)\begin{bmatrix} 1 & -1 \\ -1 & 1 \end{bmatrix}. \tag{17}$$

Here, the contribution of the separate CFE to the changeable (nonlinear) part of the right-hand side vector $\boldsymbol{K}_{nel}(\boldsymbol{u}_{i-1}^{s+1})\left(\boldsymbol{u}^s + \Delta\boldsymbol{u}_{i-1}^{s+1}\right)$ will be as follows:

$$C_n(u_n^c)\begin{bmatrix} 1 & -1 \\ -1 & 1 \end{bmatrix}\begin{Bmatrix} (u_n^+)^s + (\Delta u_n^+)_{i-1}^{s+1} \\ (u_n^-)^s + (\Delta u_n^-)_{i-1}^{s+1} \end{Bmatrix} = C_n(u_n^c)\begin{Bmatrix} -(u_n^c)^s - (\Delta u_n^c)_{i-1}^{s+1} \\ (u_n^c)^s + (\Delta u_n^c)_{i-1}^{s+1} \end{Bmatrix}, \tag{18}$$

where $(u_n^+)^s$, $(u_n^-)^s$ are moving opposite points to S_g^+, S_g^- at the end of the step *s*; $(\Delta u_n^\pm)_{i-1}^{s+1} = (u_n^\pm)_{i-1}^{s+1} - (u_n^\pm)^s$ are respectively the increments of displacements of opposite points in (*i*–1) approximation for step (*s*+1); $(u_n^c)^s$ is the layer compression between boundary surfaces for *s* loading level; $(\Delta u_n^c)_{i-1}^{s+1} = (u_n^c)_{i-1}^{s+1} - (u_n^c)^s$ is the increment of layer compression in (*i*–1) approximation for step (*s*+1).

Taking into account the nonlinear deformation of the contact layer, both in the normal and tangential direction, according to (16), the iterative expression (15) takes the following form:

$$\boldsymbol{K}_{lin}\,\Delta\boldsymbol{u}_i^{s+1} = \boldsymbol{P}_{lin}^{s+1} - \left(\sum_{k\,\in\, S_{2g},\,S_{3g}} \begin{Bmatrix} F_{nk}^+ \\ F_{nk}^- \end{Bmatrix} + \sum_{k\,\in\, S_{2g}} \begin{Bmatrix} F_{\tau k}^+ \\ F_{\tau k}^- \end{Bmatrix}\right)_{i-1}^{s+1}. \tag{19}$$

Here F_{nk}^+, F_{nk}^-, $F_{\tau k}^+$, $F_{\tau k}^-$ are the forces applied on the iteration *i* (in the process of iterative refinement of the value $\Delta\boldsymbol{u}^{s+1}$ for step (s+1) of loading) to the opposite nodes of contact surfaces and, respectively, normal and tangential.

The left part of equations (19) for the given working scheme of contact here is not changed that makes it able to hold the factorization of the stiffness matrix once, and then adjusting the value $\Delta\boldsymbol{u}_i^{s+1}$ until the difference between two subsequent iterations does not satisfy the given accuracy of calculation. The values of the correcting forces F_{nk}^+, F_{nk}^-, $F_{\tau k}^+$, $F_{\tau k}^-$ are calculated based on the results of the previous iteration (*i*–1):

$$\begin{Bmatrix} F_{nk}^+ \\ F_{nk}^- \end{Bmatrix} = C_n(u_n^c)\begin{Bmatrix} -(u_n^c)^s - (\Delta u_n^c)_{i-1}^{s+1} \\ (u_n^c)^s + (\Delta u_n^c)_{i-1}^{s+1} \end{Bmatrix}; \quad \begin{Bmatrix} F_{\tau k}^+ \\ F_{\tau k}^- \end{Bmatrix} = C_\tau(u_\tau^c)\begin{Bmatrix} -(u_\tau^c)^s - (\Delta u_\tau^c)_{i-1}^{s+1} \\ (u_\tau^c)^s + (\Delta u_\tau^c)_{i-1}^{s+1} \end{Bmatrix}. \tag{20}$$

Thus, the corresponding expressions to clarify the moment of occurrence of the next event on the contact (switching off, switching of constraint, slipping or clutching) will now be put down in the form of iterative formulas. So, expression (10), (11) will take respectively the following form:

$$(\Delta\lambda_k^{s+1})_i = (\Delta\lambda_k^{s+1})_{i-1}\left(\frac{T_{Uk}^s - T_k^s}{(\Delta T_k^{s+1} - \Delta T_{Uk}^{s+1})_{i-1}}\right), \quad k \in S_{2g}; \tag{21}$$

$$(\Delta\lambda_k^{s+1})_i = (\Delta\lambda_k^{s+1})_{i-1}\left(\frac{-N_k^s}{(\Delta N_k^{s+1})_{i-1}}\right), \quad k \in S_{2g}, S_{3g}\,. \tag{22}$$

Here T_k^s, N_k^s are the values of contact forces for the "*s*" level of loading; $(\Delta T_k^{s+1})_{i-1}$, $(\Delta N_k^{s+1})_{i-1}$ are the increment of forces on the iteration (*i*–1) to the step (*s*+1); $(\Delta\lambda_k^{s+1})_i$ is the iterative refinement of the step value (*s*+1). In other respects step-by-step algorithm defining expressions also take the iterative form. The end of the iterative refinement for the loading step is to achieve the specified accuracy of calculations. In other respects, the sequence of computational solution of the contact problem with a nonlinearly deformable layer corresponds to the algorithms described in [26–29].

In fact the nonlinear deformation law of the contact layer can be much more complicated than that recorded in the form of Eq. (17). First of all, this applies to tangential forces, which should take into account not only the shear deformation, but also the compression of the contact layer. In this case, using the method of step-by-step analysis allows us to establish the dependence of the forces on the deformation at each individual step of loading, then iterative refinement of the solution for the current level of loading.

3. Results and Discussion

Using the stated algorithm, numerical solutions for the model problem of the contact interaction of the structure with the base are obtained. Conditions of Coulomb friction-sliding (friction coefficient f = 0.2), as well as separation of boundary surfaces from each other, are possible at the contact areas. The representation by finite elements is shown in Figure 2a (to the right of the axis of symmetry). Contact seam was simulated by nine frame-rod CFE. The aim of the calculations was to assess the various conditions of contact interaction on the stress state of the soles of the structure.

The comparative analysis of the results of calculations obtained under the following conditions of the contact seam was conducted:

1. with zero deformability of the contact seam (hard unilateral contact taking into account the Coulomb friction);

2. with linear deformability of the contact seam in normal and tangential directions;

3. with nonlinear deformability of the contact seam in the direction of normal to the contact surfaces (at constant deformability in the tangential direction);

4. simultaneously with deformability the initial tensile strength and shear strength of the contact seam were taken into account.

The results of calculations - mutual displacements and stresses on the contact are shown in Figure 2b–d. The solid line corresponds to the calculation of the first option, dashed – on the second, dash-dotted – on the third, dotted – on the fourth.

As it can be seen from the results of the calculation, the area of separation of contact surfaces has the largest dimensions in the first variant – with the hard contact of the structure with the base. When taking into deformability of the seam (thickness is ζ^0 = 2 mm, deformability is ρ_0 = 1.25·10^{-7} m^3/MN, modulus of elasticity of material of structure is 3.06·10^3 MPa) the area of separation is slightly reduced. At the same time, due to shear deformations of the intermediate layer, the mutual displacement of the contact surfaces horizontally increases by 20%. The intensity of contact stresses here is slightly less than in the case of hard contact. It should be noted that the calculation results for the first and second variants fully correspond to the solutions of the problem under consideration, obtained in a number of works by iterative methods [12–14, 23].

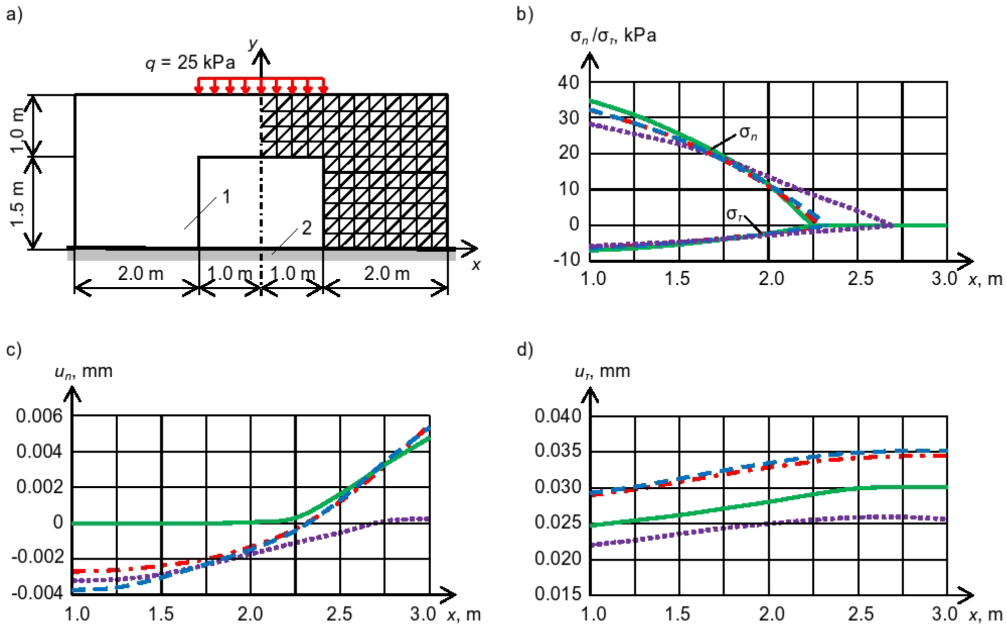

Figure 2. The problem of the interaction of a structure (1) with a hard base (2): a – design scheme; b – contact stresses; c – displacement in the normal direction; d – displacement in the tangential direction

The nonlinear law of deformation of the seam material in the direction of the normal to the boundary surfaces was conditionally set by the following function [17]:

$$C_{nk}(u_{nk}^c) = \omega_k \Big/ \left[\rho_0 \left(1 - \sqrt[3]{\left| u_{nk}^c \right| / \zeta^0} \right) \right]. \tag{21}$$

In the tangential direction the stiffness of the contact seam was taken constant $C_{\tau k} = \omega_k / \rho_0$. The comparison of the calculation results shows that taking into account the nonlinear deformation of the contact seam leads to some redistribution of deformations when it is compressed. If the initial tensile strength of the contact seam R_n = 10 kPa and shear strength R_τ = 5 kPa are taken into account, the opening of the seam surfaces is significantly reduced: the separation zone is reduced by 3 times, the maximum separation value – by 20 times. Due to the redistribution of contact stresses their intensity also decreases.

The given calculations confirm that taking into account the malleability and strength of the contact seam (in particular, between the structure and the base) is important in assessing the stress-strain state and, therefore, for the normal operation of the structure. Alongside this, the strength characteristics of the contact layer are insufficiently defined factors, first of all, due to the irregularity of the properties of the actual contact of the structure with the base. For its evaluation the integral criteria having been derived from experiments are generally used, local strength criteria are not developed sufficiently. Under these conditions, it is quite acceptable – as another approximation to the solution of this problem – to use the model of the initial strength of the contact layer as described here.

4. Conclusion

1. A finite element model of contact interaction of structures and facilities has been proposed, taking into account the physical properties of the contact seam, including initial strength, linear and nonlinear deformability of the seam material. For the modeling of unilateral constraints with the relevant physical properties has been used to contact finite elements of the frame-rod type that allows to calculate the forces and displacement in the contact zone with the same accuracy, apply an incoordinate finite element mesh, to consider the various types and conditions of contact.

2. The numerical algorithms developed on the basis of the proposed discrete contact model and of the stepping method provide the possibility of step-by-step analysis of the contact interaction and have

advantages in cases where the solution of the problem depends on the loading history, in particular, taking into account the initial strength and friction of the contact seam surfaces.

3. The proposed approach allows in one step-by-step cycle to perform simultaneous accounting of the initial strength of the contact seam, as well as the conditions of unilateral deformable constraints and friction-sliding of its surfaces in areas where the strength of the contact seam is broken. It should be noted that the results of the model problem calculations performed using the constructed algorithms are in good agreement with the numerical solutions having been obtained by alternative methods.

4. In the case of nonlinear deformability of the contact layer, the proposed numerical model allows a physically nonlinear problem to reduce to the internal nonlinearity of only the system of frame-rod contact elements, while the nonlinear properties of the seam material will be set through the nonlinear characteristics of the individual rods of the contact elements. Iterative refinement of the nonlinear solution at each step of loading for the system of contact elements is performed by means of the method of compensating loads.

References

1. Vovkushevskiy, A.V., Shoykhet, B.A. Raschet massivnykh gidrotekhnicheskikh sooruzheniy s uchetom raskrytiya shvov [Analysis of massive hydraulic engineering constructions taking into account disclosure of joints]. Moscow: Energoizdat, 1981. 136 p. (rus)
2. Vovkushevskiy, A.V., Rozin, L.A., Rukavishnikov, V.A. Razrabotka metodov rascheta sooruzheniy s uchetom slozhnykh kontaktnykh vzaimodeystviy [Development of methods for calculation of structures taking into account the complex contact interactions]. Izvestiya vuzov. Stroitelstvo. 1994. No. 12. Pp. 25–29 (rus)
3. Tolstikov, V.V. Modelirovaniye raboty shvov i treshchin v raschetakh napryazhenno-deformirovannogo sostoyaniya betonnykh plotin [Modeling the performance of joints and cracks in analyzing the stress-strain state of concrete dams]. Vestnik MGSU. 2006. No. 2. Pp. 123–132 (rus)
4. Bukhartsev, V.N., Vu Man Khuan. Stability assessment of concrete structures on not bedrock foundation. Magazine of Civil Engineering. 2013. No. 1(36). Pp. 57–64. (rus)
5. Yavarov, A.V, Kolosova, G.S., Kuroyedov, V.V. Stress-strain state of buried pipelines. Construction of Unique Buildings and Structures. 2013. No. 1(6). Pp. 1–6. (rus)
6. Kolosova, G.S., Lalin, V.V., Kolosova, A.V. The effect of construction joints and cracks on the stress-strain state of the arch-gravity dam. Magazine of Civil Engineering. 2013. No. 5(40). Pp. 76–85. doi: 10.5862/MCE.40.9 (rus)
7. Lalin, V.V., Savchenko, A.V., Yavarov, A.V., Zdanchuk, Ye.V., Belyayev, D.I. Reliability of low pressure waterworks with earthen dams. Construction of Unique Buildings and Structures. 2013. No. 7(12). Pp. 30–37. (rus)
8. Sainov, M.P., Zverev, A.O. Workability of high rockfill dam with a polymer face. Magazine of Civil Engineering. 2017. No. 7(75). Pp. 76–83.
9. Vovkushevskiy, A.V. Variatsionnaya postanovka i metody resheniya kontaktnoy zadachi s treniyem pri uchete sherokhovatosti poverkhnostey [Variational formulation and solution methods for contact problems with friction when accounting for the roughness of the surfaces]. Izvestiya AN USSR. MTT. 1991. No. 3. Pp. 56–63. (rus)
10. Kikuchi, N., Oden, J.T. Contact Problems in Elasticity: A study of variational inequalities and finite element methods. Philadelphia: SIAM, 1988. 495 p.
11. Podgornyy, A.N., Gontarovskiy, P.P., Kirkach, B.N., Matyukhin, Yu.I., Khavin, G.L. Zadachi kontaktnogo vzaimodeystviya elementov konstruktsiy [Problems of contact interaction of structural elements]. Kiyev: Naukova Dumka, 1989. 232 p. (rus)
12. Rozin, L.A. Smirnov, M.S. Resheniye kontaktnykh zadach teorii uprugosti s podatlivostyu v odnostoronnikh svyazyakh [Solution of contact problems of elasticity with with compliance in unilateral constraints]. Izvestiya vuzov. Stroitelstvo. 2000. No. 5. Pp. 27–31. (rus)

Литература

1. Вовкушевский А.В., Шойхет Б.А. Расчет массивных гидротехнических сооружений с учетом раскрытия швов. М.: Энергоиздат, 1981. 136 с.
2. Вовкушевский А.В., Розин Л.А., Рукавишников В.А. Разработка методов расчета сооружений с учетом сложных контактных взаимодействий // Изв. вузов. Строительство. 1994. № 12. С. 25–29.
3. Толстиков В.В. Моделирование работы швов и трещин в расчетах напряженно-деформированного состояния бетонных плотин // Вестник МГСУ. 2006. № 2. С. 123–132.
4. Бухарцев В.Н., Ву Мань Хуан. Оценка устойчивости бетонных сооружений на нескальном основании // Инженерно-строительный журнал. 2013. № 1(36). С. 57–64.
5. Яваров А.В, Колосова Г.С., Куроедов В.В. Напряженно-деформированное состояние подземных трубопроводов // Строительство уникальных зданий и сооружений. 2013. № 1(6). С. 1–6.
6. Колосова Г.С., Лалин В.В., Колосова А.В. Влияние строительных швов и трещин на напряженно-деформированное состояние арочно-гравитационной плотины // Инженерно-строительный журнал. 2013. № 5(40). С. 76–85.
7. Лалин В.В., Савченко А.В., Яваров А.В., Зданчук Е.В., Беляев Д.И. Расчет напряженно-деформированного состояния арочно-гравитационной плотины в программном комплексе SOFiSTiK // Строительство уникальных зданий и сооружений. 2013. № 7(12). С. 30–37.
8. Саинов М.П., Зверев А.О. Работоспособность высокой каменно-набросной плотины с полимерным экраном // Инженерно-строительный журнал. 2017. № 7(75). С. 76–83.
9. Вовкушевский А.В. Вариационная постановка и методы решения контактной задачи с трением при учете шероховатости поверхностей // Изв. АН СССР. МТТ. 1991. № 3. С. 56–62.
10. Kikuchi N., Oden J.T. Contact Problems in Elasticity: A study of variational inequalities and finite element methods. Philadelphia: SIAM, 1988. 495 p.
11. Подгорный А.Н., Гонтаровский П.П., Киркач Б.Н., Матюхин Ю.И., Хавин Г.Л. Задачи контактного взаимодействия элементов конструкций. Киев: Наукова думка, 1989. 232 с.
12. Розин Л.А. Смирнов М.С. Решение контактных задач теории упругости с податливостью в одно-сторонних связях // Изв. вузов. Строительство. 2000. № 5. С. 27–31.

13. Wriggers, P., Nackenhorst, U. Analysis and Simulation of Contact Problems. Berlin-Heidelberg: Springer, 2006. 394 p.
14. Wriggers, P. Computational Contact Mechanics. Berlin-Heidelberg: Springer, 2006. 521 p.
15. Kravchuk, A.S. Variatsionnyy metod v kontaktnykh zadachakh. Sostoyaniye problemy, napravleniya razvitiya [The variational method in contact problems. The present state of the problem and trends in its development]. Journal of Applied Mathematics and Mechanics. 2009. Vol. 73. No. 3. Pp. 492–502. (rus)
16. Wriggers, P., Panagiotopoulos, P. New Developments in Contact Problems. Wien: Springer, 1999. 246 p.
17. Babin, A.P. Konechno-elementnyy algoritm resheniya kontaktnykh zadach s uchetom nelineynykh effektov [Finite element algorithm for the solution of contact problems taking into account nonlinear effects]. Dinamika, prochnost i nadezhnost transportnykh mashin: sb. nauch. tr. [Dynamics, strength and reliability of transport vehicles: Sat. sci. tr.]. Bryansk: BGTU, 2002. Pp. 138–148. (rus)
18. Zernin, M.V., Babin, A.P., Mishin, A.V., Burak, V.Yu. Modelirovaniye kontaktnogo vzaimodeystviya s ispolzovaniyem mekhaniki «kontaktnoy psevdosredy» [Modelling of contact interaction with the use of mechanics "contact pseudo-environment"]. Prochnost i nadezhnost mashin. Vestnik BGTU. 2007. No. 4(16). Pp. 62–72. (rus)
19. Babin, A.P., Zernin, M.V. Konechno-elementnoye modelirovaniye kontaktnogo vzaimodeystviya s ispolzovaniyem polozheniy mekhaniki kontaktnoy psevdosredy [Finite-element simulation of contact interaction with the use of concepts of contact pseudomedium mechanics]. Izvestiya RAN. Mekhanika tverdogo tela. 2009. No. 4. Pp. 84–107. (rus)
20. Laursen, T.A., Kim, T.Y., Dolbow, J.E. A mortared finite element method for frictional contact on arbitrary surfaces. Computational Mechanics. 2007. No. 39. Pp. 223–235.
21. Wriggers, P., Rust, W.T., Reddy, B.D. A virtual element method for contact. Computational Mechanics. 2016. No. 58(6). Pp. 1039–1050.
22. Kats, C., Werner, H. Implementation of nonlinear boundary conditions in finite element analysis. Computers and structures. 1982. Vol. 15. No. 3. Pp. 299–304.
23. Vovkushevskiy, A.V. Uchet prochnosti shvov pri raschete massivnykh sooruzheniy s odnostoronnimi svyazyami [Accounting for the strength of joints in the calculation of massive structures with unilateral constraints]. Izvestiya VNIIG im. B.Ye. Vedeneyeva. 1982. Vol. 155. Pp. 9–13. (rus)
24. Laursen, T., Yang, B. A contact searching algorithm including bounding volume trees applied to finite sliding mortar formulations. Computational Mechanics. 2008. No. 41. Pp. 189–205.
25. Wriggers, P., Schroder, J., Schwarz, A. A finite element method for contact using a third medium. Computational Mechanics. 2013. No. 52(4). Pp. 837–847.
26. Lukashevich, A.A. Postroyeniye i realizatsiya skhem pryamogo metoda konechnykh elementov dlya resheniya kontaktnykh zadach [Construction and realization of schemes of the direct finite element method for the decision of contact problems]. Izvestiya vuzov. Stroitelstvo. 2007. No. 12. Pp. 18–23. (rus)
27. Lukashevich, A.A., Rozin, L.A. On the decision of contact problems of structural mechanics with unilateral constraints and friction by step-by-step analysis. Magazine of Civil Engineering. 2013. No. 1(36). Pp. 75–81. doi: 10.5862/MCE.36.9 (rus)
28. Bukhartsev, V.N., Lukashevich, A.A. Resheniye zadachi o vzaimodeystvii vodoboynoy plity krepleniya s osnovaniyem pri pulsatsii davleniya v sbrasyvayemom potoke [The solution of problem on interaction of water-fight plate at a pressure pulsation in dumped stream].

13. Wriggers P., Nackenhorst U. Analysis and Simulation of Contact Problems. Berlin-Heidelberg: Springer, 2006. 394 p.
14. Wriggers P. Computational Contact Mechanics. Berlin-Heidelberg: Springer, 2006. 521 p.
15. Кравчук А.С. Вариационный метод в контактных задачах. Состояние проблемы, направления развития // Прикладная математика и механика. 2009. Т. 73. № 3. С. 492–502.
16. Wriggers P., Panagiotopoulos P. New Developments in Contact Problems. Wien: Springer, 1999. 246 p.
17. Бабин А.П. Конечно-элементный алгоритм решения контактных задач с учетом нелинейных эффектов // Динамика, прочность и надежность транспортных машин: сб. науч. тр. Брянск: БГТУ, 2002. С. 138–148.
18. Зернин М.В., Бабин А.П., Мишин А.В., Бурак В.Ю. Моделирование контактного взаимодействия с использованием механики «контактной псевдо-среды» // Прочность и надежность машин. Вест-ник БГТУ. 2007. № 4(16). С. 62–72.
19. Бабин А.П., Зернин М.В. Конечно-элементное моделирование контактного взаимодействия с использованием положений механики контактной псевдосреды // Изв. РАН. Механика твердого тела. 2009. № 4. С. 84–107.
20. Laursen T.A., Kim T.Y., Dolbow J.E. A mortared finite element method for frictional contact on arbitrary surfaces. Computational Mechanics. 2007. № 39. Pp. 223–235.
21. Wriggers P., Rust W.T., Reddy B.D. A virtual element method for contact. Computational Mechanics. 2016. № 58(6). Pp. 1039–1050.
22. Kats C., Werner H. Implementation of nonlinear boundary conditions in finite element analysis. Computers and structures. 1982. Vol. 15. № 3. Pp. 299–304.
23. Вовкушевский А.В. Учет прочности швов при расчете массивных сооружений с односторонними связями // Изв. ВНИИГ им. Б.Е. Веденеева. 1982. Т. 155. С. 9–13.
24. Laursen T., Yang B. A contact searching algorithm including bounding volume trees applied to finite sliding mortar formulations. Computational Mechanics. 2008. № 41. Pp. 189–205.
25. Wriggers P., Schroder J., Schwarz A. A finite element method for contact using a third medium. Computational Mechanics. 2013. № 52(4). Pp. 837–847.
26. Лукашевич А.А. Построение и реализация схем прямого метода конечных элементов для решения контактных задач // Изв. вузов. Строительство. 2007. № 12. С. 18–23.
27. Лукашевич А.А., Розин Л.А. О решении контактных задач строительной механики с односторонними связями и трением методом пошагового анализа // Инженерно-строительный журнал. 2013. № 1(36). С. 75–81.
28. Бухарцев В.Н., Лукашевич А.А. Решение задачи о взаимодействии водобойной плиты крепления с основанием при пульсации давления в сбрасываемом потоке // Гидротехническое строительство. 2010. № 4. С. 52–55.
29. Lukashevich A.A., Rozin L.A. Numerical decision of problems of structural mechanics with nonideal unilateral constraints. Applied Mechanics and Materials. Advances in Civil and Industrial Engineering IV. 2014. Vol. 580–583. Pp. 2932–2935.
30. Bukhartsev V.N., Lukashevich A.A. Stability assessment of a structure subject to asymmetric load application on a rock-free bed. Power Technology and Engineering. Springer New York Consultants Bureau. 2012. Vol. 45. № 5. Pp. 346–350.
31. Лукашевич А.А. Расчетные модели контактного взаимодействия и разрушения деформируемых тел с

Gidrotekhnicheskoye stroitelstvo. 2010. No. 4. Pp. 52–55. (rus)

29. Lukashevich, A.A., Rozin, L.A. Numerical decision of problems of structural mechanics with nonideal unilateral constraints. Applied Mechanics and Materials. Advances in Civil and Industrial Engineering IV. 2014. Vol. 580–583. Pp. 2932–2935.
30. Bukhartsev, V.N., Lukashevich, A.A. Stability assessment of a structure subject to asymmetric load application on a rock-free bed. Power Technology and Engineering. Springer New York Consultants Bureau. 2012. Vol. 45. No. 5. Pp. 346–350.
31. Lukashevich, A.A. Raschetnyye modeli kontaktnogo vzaimodeystviya i razrusheniya deformiruyemykh tel s primeneniyem KKE [Computational models of contact interaction and destruction of deformable bodies using the contact finite elements]. Nauchno-tekhnicheskiye vedomosti SPbGPU. 2013. No. 2(171). Pp. 60–65. (rus)

применением ККЭ // Научно-технические ведомости СПбГПУ. 2013. № 2(171). С. 60–65.

Anatoliy Lukashevich,
+7(911)821-25-53; aaluk@bk.ru

Анатолий Анатольевич Лукашевич,
+7(911)821-25-53; эл. почта: aaluk@bk.ru

Лукашевич А.А. Численное моделирование жесткостных и прочностных свойств контактного шва // Инженерно-строительный журнал. 2018. № 5(81). С. 149–159.

doi: 10.18720/MCE.81.16

The modeling method of discrete cracks in reinforced concrete under the torsion with bending

Метод моделирования дискретных трещин в железобетоне при кручении с изгибом

V.I. Kolchunov*,
A.I. Dem'yanov,
Southwest State University, Kursk, Russia

Д-р техн. наук, профессор В.И. Колчунов*,
канд. техн. наук, доцент А.И. Демьянов,
Юго-Западный государственный университет, г. Курск, Россия

Key words: reinforced concrete plane-stressed composite constructions; spatial cracks; torsion with bending; double-console scheme; distance between cracks; width of crack opening

Ключевые слова: железобетонные плосконапряженные составные конструкции; пространственные трещины; кручение с изгибом; двухконсольная схема; расстояние между трещинами; ширина раскрытия трещин

Abstract. The most famous of computer systems for the design of reinforced concrete structures in the world are taken into account only regular dispersed cracks. Completely different criteria should be used when analyzing the appearance and development of discrete cracks in reinforced concrete, the modeling methodology of which has not been developed to date. Therefore, the article provides working prerequisites, a methodology for simulating discrete cracks and calculating their rigidity. Several levels of cracking are considered. The development of spatial cracks is carried out on special bilinear surfaces. Then they fit in the approximating spatial finite elements that "expand", modeling a spatial crack, the opening of which is given in the form of a deformation effect with allowance for the discontinuity effect. When solving the inverse problem of determining the crack opening width, the deformation effect is not specified, and only the presence of a gap of the minimum possible width is modeled by means of an embossing; its opening, with appropriate loading, determines the width of the crack opening as the divergence of the shores of this gap. It is considered another variant of simulation of discrete spatial cracks in the article, in case of their implicit manifestation. Here pairs of finite elements adjacent to such a crack are distinguished from opposite sides. It is a special two-element design console model. These pairs are considered in two states: before their "expand" and after their "expand" taking into account the deformation effect and the discontinuity effect of concrete. It is introduced the classification of basic spatial cracks in spatial reinforced concrete composite constructions, cracks that develop to zones or from zones of geometric concentration; cracks that develop to zones or from zones of force and strain concentration of loading; cracks that develop in zones of inter-medial strain concentration. Their scheme is supplemented and based on these basic cracks by applying adjacent cracks, which are sought using the deformation criterion for their formation and the method of finding the extremum of a function of many variables using the Lagrange multipliers.

Аннотация. В большинстве известных в мире вычислительных комплексов при проектировании железобетонных конструкций учитываются лишь регулярные дисперсные трещины. Совершенно иные критерии необходимо использовать при анализе появления и развития дискретных трещин в железобетоне, методика моделирования которых на сегодняшний день не разработана. Поэтому в статье разработаны рабочие предпосылки, методика моделирования дискретных трещин и расчета их жесткости. При этом рассматривается несколько уровней трещинообразования. Развитие пространственных трещин осуществляется по специальным билинейным поверхностям. Затем в них вписываются аппроксимирующие пространственные конечные элементы, которые «расшиваются», моделируя пространственную трещину, раскрытие которой задается в виде деформационного воздействия с учетом эффекта нарушения сплошности. При решении обратной задачи определения ширины раскрытия трещин, деформационное воздействие не задается, а с помощью расшивки моделируется лишь наличие щели минимально возможной ширины, ее раскрытие при соответствующем нагружении и определяет ширину раскрытия трещины, как расхождение берегов этой щели. В статье рассмотрен и другой вариант моделирования дискретных пространственных трещин, при их неявном проявлении. Здесь выделяются пары конечных элементов, прилегающих к такой трещине с противоположных сторон,

Колчунов В.И., Демьянов А.И. Метод моделирования дискретных трещин в железобетоне при кручении с изгибом // Инженерно-строительный журнал. 2018. № 5(81). С. 160–173.

– специальная расчетная двухэлементная консольная модель. Эти пары рассматриваются в двух состояниях: до их «расшивки» и после их «расшивки» с учетом деформационного воздействия и эффекта нарушения сплошности бетона. Вводится классификация базовых пространственных трещин в пространственных железобетонных составных конструкциях, – трещины, которые развиваются к зонам или из зон геометрической концентрации; трещины, которые развиваются к зонам или из зон концентрации силового и деформационного нагружения; трещины, которые развиваются в зонах межсредовой концентрации деформаций. Опираясь на эти базовые трещины их схема дополняется путем нанесения смежных трещин, которые отыскиваются с привлечением деформационного критерия их образования и метода отыскания экстремума функции многих переменных с использованием множителей Лагранжа. Для отыскания уровневого расстояния между трещинами и ширины их раскрытия вырезается представительный объем из железобетонной конструкции, подверженной кручению с изгибом (расчетная модель второго уровня), и в итоге записывается дифференциальное уравнение, необходимое для определения искомых параметров.

1. Introduction

In connection with the recommendations of bionics, more and more unique reinforced concrete buildings are being introduced into construction practice in recent decades, which are experiencing complex resistance, necessitating the use of their spatial design scheme [1, 2]. Alongside with them, flat-stressed reinforced concrete (including composite) structures (FSRCCS, bearing walls occupy up to 40% of the total volume of reinforced concrete) are used in a very wide scale in construction. The problem of determining their rigidity in the presence of cracks remains practically unexplored [3], therefore its development is an urgent problem and the need, which is one of the most important problems of capital construction [4, 5].

The resulting cracks significantly reduce the rigidity of reinforced concrete structures [6]. In most computer systems known in the world [7], accounting for the formation of cracks in reinforced concrete structures is performed using criteria for achieving the main stresses or the main deformations of the elongation of concrete of its limit values [8]. However, such criteria reflect the appearance of only dispersed, regular cracks in reinforced concrete structures.

Absolutely different criteria should be used when analyzing the appearance and development of discrete cracks in reinforced concrete [9]. Here the main role is played by the concentration of deformations at the places of sharp changes in geometric dimensions, zones of concentration of force and deformation loading, inter-medial concentration [10], and the like. Nevertheless, to this day, the technique for modeling discrete cracks, including the use of computer systems known in the world, has not been developed.

In order to fill the existing gap in reinforced concrete under conditions of complex torsional resistance with bending [11–13], including under seismic influences [4, 5, 14], the essence of the proposed technique for simulating discrete cracks is described below, taking into account the effect of discontinuity and inconsistency of deformations of concrete and reinforcement. The need to develop this technique is also due to the fact that finding the width of the discrete crack opening with the help of the known computer systems in the world (direct and inverse problem) is absent.

The article is also devoted to the construction of a method for calculating the rigidity of reinforced concrete structures, buildings and structures in the presence of discrete cracks under conditions of complex resistance, torsion with bending arising in conditions of seismic influences (Figure 1).

The basis of this technique is the scheme of discrete cracks, which takes place during seismic actions in buildings and structures made of reinforced concrete, obtained as a result of an analysis of a number of earthquakes [4, 14, 15].

Analysis shows [4, 5, 14, 15] that, as a rule, the development of discrete cracks under seismic actions occurs according to the "envelope" scheme, which manifests itself in the resistance of flat-strained reinforced concrete constructions, and not only, as already known scheme of the "envelope", as applied to slabs with static vertical load. overlapping with a static vertical load.

In the future, based on these basic diagonal cracks (Figure 1, b, position 1), the scheme of discrete cracks ("envelope" scheme) can be refined by applying adjacent cracks (Figure 1, b, position 2), which are sought with the use of the deformation criterion for their formation and the method of finding the extremum of a function of several variables using the Lagrange multipliers. Definition of the scheme of discrete cracks will undoubtedly contribute to the classification of basic cracks for reinforced concrete plane-stressed composite structures, proposed by I.A. Iakovenko [16, 17]. This classification is based on the geometric, force (deformation) and interspersed concentration of the stress-strain state with the corresponding sources-concentrators.

The cracking scheme, based on the envelope scheme, is used as the main one if flat-stressed finite elements (panel buildings, pylons, etc.) are used in the design model of a building, structure or reinforced concrete construction, Figure 2, a, b.

If the modeling of buildings and volumetric reinforced concrete constructions is performed with the help of volumetric finite elements taking into account their complex resistance, it becomes necessary to develop a technique for calculating the rigidity in the presence of already spatial cracks.

2. Methods

If the modeling of buildings and volumetric reinforced concrete structures is performed with the help of volumetric finite elements taking into account their complex resistance, it becomes necessary to develop a technique for calculating the rigidity in the presence of already spatial cracks. Considering that at present the development of the finite element model of reinforced concrete in the calculation of spatial and plane-stressed structures with allowance for nonlinear deformation has reached a rather high level, therefore it is advisable to focus on the use of the most sophisticated software complexes for the calculation of their stiffness and simulation of discrete cracks. In this case, it is necessary to adequately take into account the nature of the development and the opening of cracks in them.

The method of modeling discrete cracks and calculating the rigidity of spatial reinforced concrete structures, buildings and structures with their complex resistance, under the action torsion with bending, will be based on the following design positions:

1. The formation of a subsequent level of spatial cracks occurs after the concrete fibers stretched along the axes of the working reinforcement (longitudinal or transverse) of their ultimate deformations $\varepsilon_{bt,u}$ are reached. There may be several levels of cracking. The development of spatial cracks is carried out on special bilinear surfaces. For this purpose, knowing the equation of a bilinear surface in parametric form [19], the value of the corner points of the cross-section of the reinforced concrete **constructions –** points A, B, C, D is inscribed in it; the equation of a bilinear surface is concretized with respect to a given cross-section.

$$\begin{gathered}[x_k; y_k; z_k] = [x_A; y_A; z_A]\cdot(1-u_k)\cdot(1-w_k) + [x_B; y_B; z_B]\cdot(1-u_k)\cdot w_k + \\ + [x_C; y_C; z_C]\cdot u_k \cdot (1-w_k) + [x_D; y_D; z_D]\cdot u_k \cdot w_k .\end{gathered} \tag{1}$$

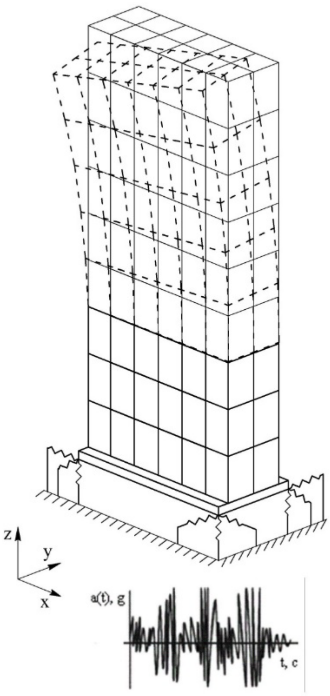

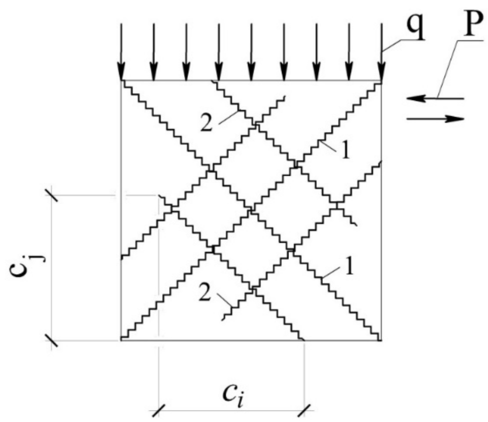

Figure 1. The calculation model of the aboveground and underground parts of the building under seismic action (*a*) and the scheme of basic and adjacent discrete cracks in RC wall panels (*b*)
1 – basic cracks; 2 – adjacent cracks

Then the spatial cracks are the surfaces which approximated by the parallelepipeds inscribed in them after modeling the reinforced concrete construction with the same spatial finite elements (Figure 2, c).

2. The classification of basic discrete spatial cracks is introduced. In spatial reinforced concrete composite structures [10, 16], such basic cracks can occur: 1) cracks that develop to zones or from zones of geometric concentration of stress-strain state, etc.); (in places where the cross-sectional dimensions change, in the incoming corners, in the areas of non-circular holes and the state (in places where cross-sectional dimensions change, in the incoming corners, in zones of non-circular holes, and 2) cracks that develop to zones or from zones of concentration of power and deformation loading (the location of the supporting reactions and concentrated, the place of the change in the loading intensity along the contour of the structure, the place of deformation loading from the subsidence, the type of loading is of particular importance-bending, shearing 3) longitudinal cracks that develop in zones of inter-medium stress concentration (in joints between concrete in flat-strained reinforced concrete composite constructions, along longitudinal reinforcement in anchoring zones, etc.).

In construction practice (for example, in complex engineering-geological conditions), the most often encountered are schemes of force and deformation loading, which, as a rule, cause the imposition of different cracks [17].

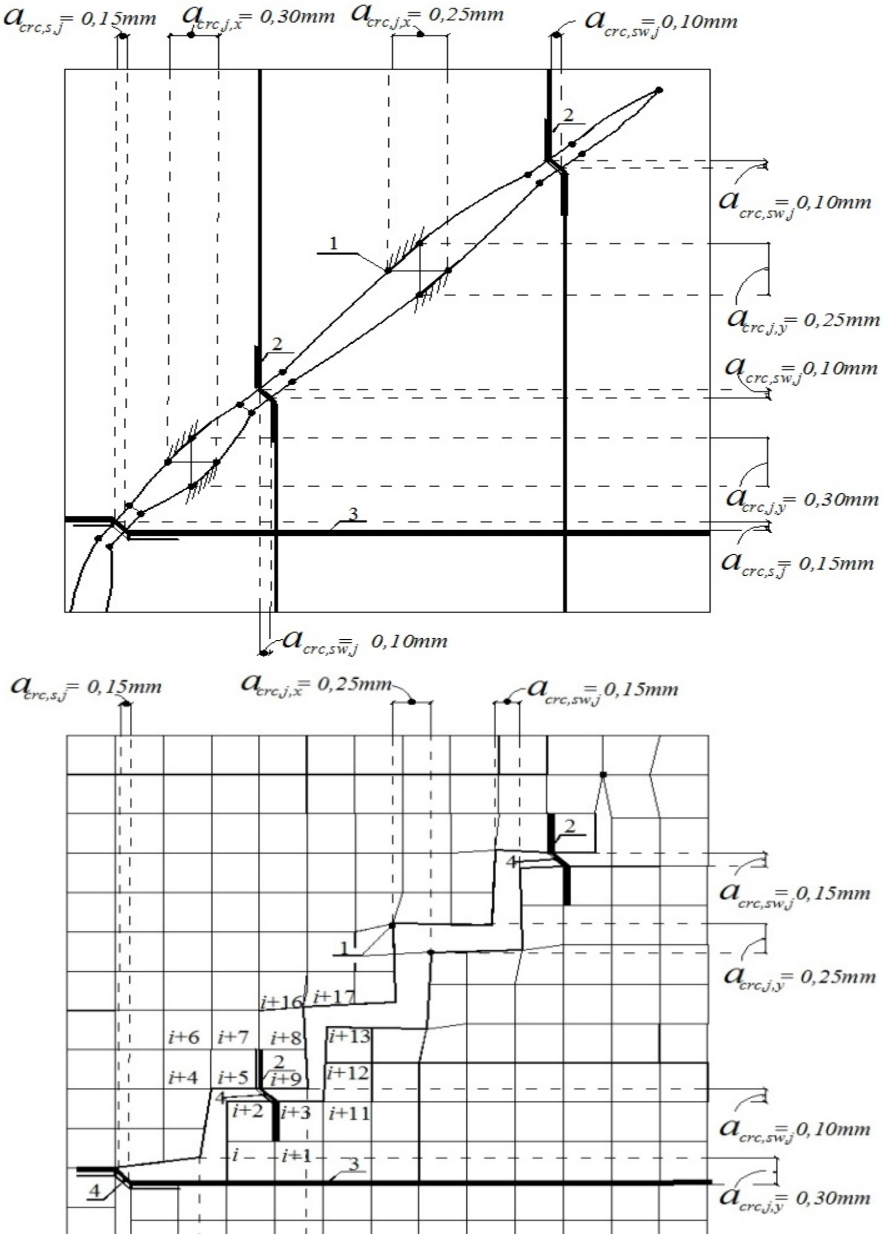

a)

b)

Kolchunov, V.I., Dem'yanov, A.I. The modeling method of discrete cracks in reinforced concrete under the torsion with bending. Magazine of Civil Engineering. 2018. 81(5). Pp. 160–173. doi: 10.18720/MCE.81.16.

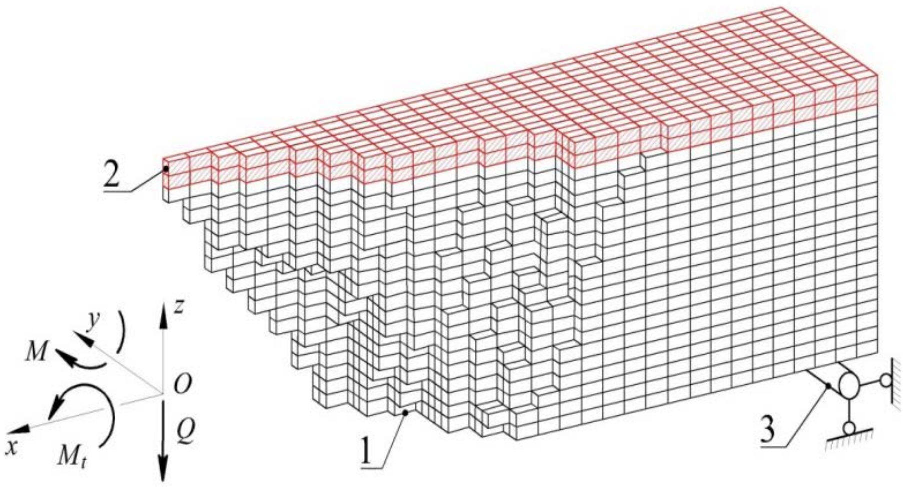

c)

Figure 2. The proposed model of cracks: a – real crack; b – modeled with the help of " disconnection" plane-stressed finite elements (FE) and deformation effects $\Delta = a_{crc,j}$; c – modeled with the help of "disconnection" spatial finite elements (FE) and deformation effects; $\Delta_1 = a^l_{crc}$; $\Delta_2 = a^m_{crc}$; $\Delta_3 = a^n_{crc}$ in a block design model with a spatial and normal section passing through the end of the spiral-shaped crack; 1 – crack; 2 – transverse reinforcement and its simulation with 201 FE, 3 – longitudinal reinforcement and its simulation with 201 FE; 4 – possible closure of the fracture and its simulation with the help of 255 FE

3. With a complex resistance, as already noted above, the building (Figure 1, a) can be modeled with the help of flat ones, or with the help of spatial finite elements.

The essence of the proposed model of cracks [20, 21] is that the actual crack (Figure 2, a for flat reinforced concrete structures and described by (2) formula for spatial reinforced concrete constructions) is replaced by a model in the form of a broken line corresponding to inscribed finite elements (Figure 2, b for planar and Figure 2, c for spatial, is considered on the example of the computer complex "Lira-CAD"), which "expand" by modeling a crack, and its expansion is given in the form of a deformation action $\Delta = a_{crc,j}$, directed perpendicular to the surface of the spatial cracks [19], described by the dependence (1). The effect of discontinuity [23, 24] is taken into account by means of introducing a variable crack width opening depending on its distance from the axis of the working (longitudinal or transverse) reinforcement.

The solving of inverse problem [21, 22] is determining the width of crack opening; the deformation effect is not specified, and only the presence of disconnection of the minimum possible width is modeled with the help of an embossing, and its opening, with the appropriate loading, determines the opening width of the crack, as the divergence of the shores of this gap.

4. There is another possible variant of simulation of discrete cracks [14, 21, 22]. It is used in the case when the renumbering of the nodes of the design scheme of the reinforced concrete construction (building or structure), connected with the necessity of "disconnection", considered in the first variant, is undesirable.

In this variant, the final elements do not "expand" along the entire crack, and in the first stage of discrete cracking simulation only imaginary discrete cracks are used, the development of which is predicted by the introduced classification of cracks as applied to a specific calculation.

At the second stage of modeling cracks along the trajectory of an imaginary crack, pairs of finite elements adjacent to such a crack from opposite sides are distinguished. These pairs are considered in two states: before their "barking" and after their "barking".

For this purpose, a special design two-element console model is involved in the calculation (in the first case, a flat one in accordance with Figure 3, a, b.

In the second case, the spatial crack in accordance with Figure 3, c–e, which is used to perform a sequential iterative analysis of the stress-strain state of the spatial console adjacent to the simulated spatial crack on opposite sides and realized with the help of "disconnection" and the deformation effect, which also takes into account the effect of disturbing the continuity of concrete.

In this case, the distributed reinforcement is replaced by two (for the plane model) and four (for the spatial model) by rod finite elements in each mutually perpendicular direction, respectively. The displacement of nodes is determined from the calculation of a two-element design model with the loads specified in the nodes (nodal finite element forces). In this case, the anchoring of two nodes in a flat model and four nodes in a spatial model (alternating with pivotally fixed and pivotally movable supports), for the purpose of averaging, it is necessary to set left, right, front, and bottom-top. It is also important that along with the node loads in the two-element model, deformation effects associated with the width of the crack opening are also specified, which in turn is related to the discontinuity effect [23, 24].

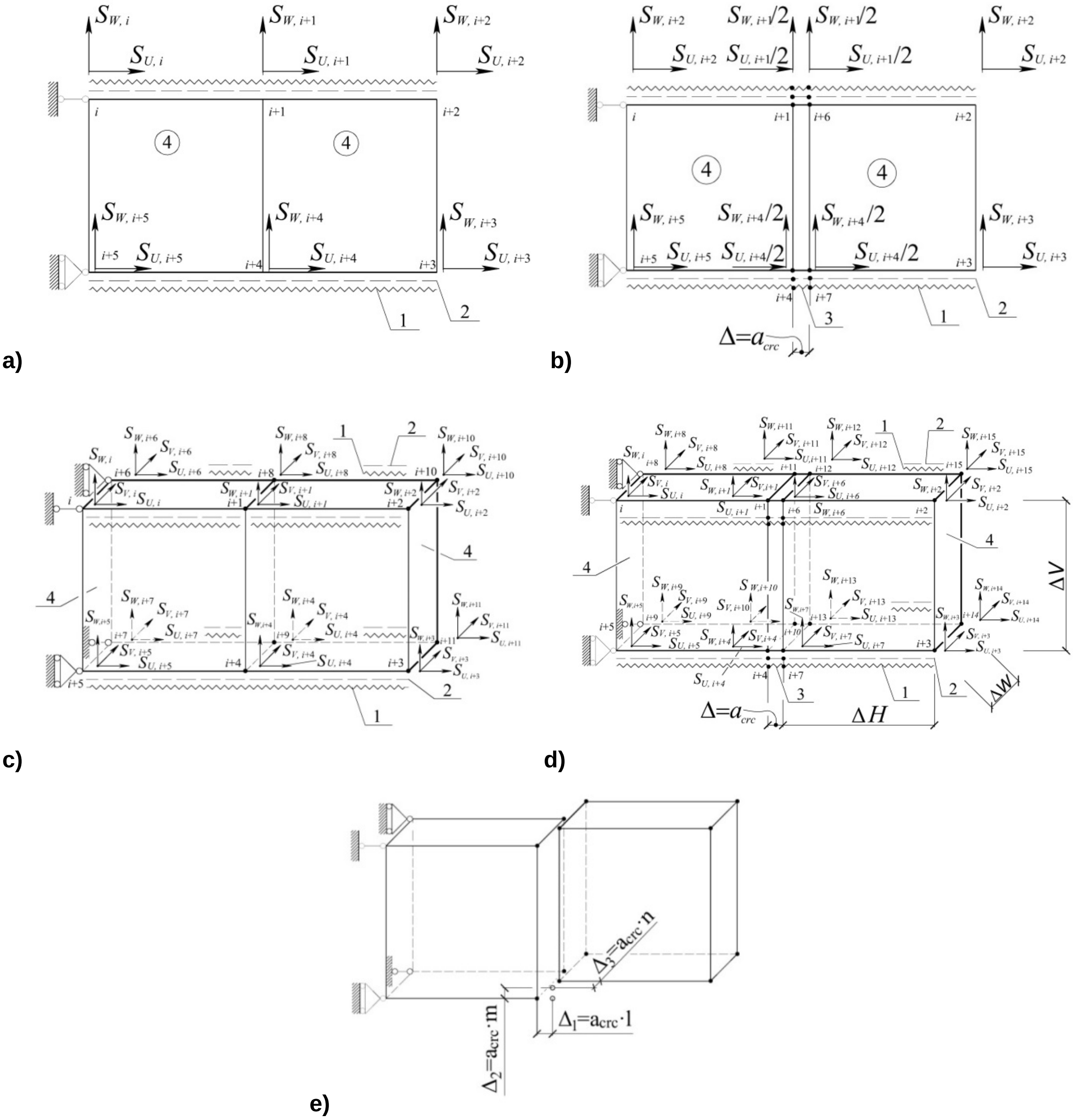

Figure.3. The construction of a two-console flat and spatial model:
a – flat, without "disconnection"; b – the same, after " disconnection";
c –three-dimensional, before "disconnection"; d – the same as (c), after " disconnection";
e – deformation effects; 1 – 255 FE before the "disconnection"; 2 – 201 FE;
3 – 255 FE after the "disconnection"; 4 – 233 FE

The deformation action is set in each node (except the reference ones) in three increments in accordance with Figure 3, e, where l, m and n are the direction cosines of the principal crack opening vector at one or another point to the x, y and z axes, respectively.

Then, having the applied efforts and movements in the nodes of the consoles, the values of the work in two states are compared: "before the disconnection" and "after the disconnection" of the two-element model. From the condition of equality of these works, the thickness of the finite elements in the state "before the disconnection" decreases. This procedure is performed for all pairs of FE adjacent to the fracture (along horizontal, vertical or their lateral surfaces) from different sides. As a result, along the imaginary crack, the thickness of the finite elements decreases, which provokes the formation and development of cracks according by the criterion of regular disperse cracks, without resorting to FE.

The average forces in the nodes in different directions for the two-element console model are determined from the physically non-linear calculation of the entire structure. For this purpose, nodal forces are used in the corresponding FE of concrete and reinforcement.

In the places where the horizontal sections of simulated cracks move vertically and laterally, the robots of the angular finite elements are determined by averaging them.

As a result, a new thickness of the finite elements adjacent to the crack is found by the formula:

$$b = \frac{W_1}{W_2} \cdot b_1, \tag{2}$$

where W_1 and W_2 the work of the two-element model "before disconnection" and "after disconnection", respectively.

The proposed algorithm provides for an iterative process controlled by the achieved accuracy of the thickness of the marked finite elements that are adjacent to imaginary cracks and the dynamic characteristics of the reinforced concrete construction (building or structure).

It is appropriate to note here that the rigidity of the core reinforced concrete structures in areas with inclined cracks, including those that intersect (characteristic for seismic actions for the landing sites and interfaces) is replaced by equivalent rigidity:

$$B(\lambda) = \frac{M^2 \cdot \Delta x}{2 \cdot W_3}, \tag{3}$$

where W_3 – work of forces of selected area.

Here, the iterative process ends after reaching a predetermined error in the determination $B_1(\lambda)$.

In areas with normal cracks, the rigidity of the core reinforced concrete structures is determined using the values of the bending moment M and the radius of curvature ρ and according to the normative technique [22] for the corresponding stretched zone (the section with normal cracks is recommended to be divided into 4 to 6 zones):

$$B_i(\lambda) = M_i \cdot \rho_i \tag{4}$$

5. Projections of different cracks on the horizontal (vertical) are sought on the basis of the block model with the estimated cross sections passing through the beginning and end of the crack (specified in the iteration process, one of these sections, as a rule, is attached to the strongest force – the supporting reaction R_{sup} or goes to one of the faces of the construction) with the use of analytic dependencies, which are based on the extremum of a function of many variables using the Lagrange $F_{1,2} = f\left(q_{sw}, x_B, \sigma_s, x, \sigma_b, \sigma_{s,I}, \sigma_{b,1}, C_2, \lambda_1, \lambda_2, \lambda_3, \lambda_4, \lambda_5, \lambda_6, \lambda_7\right)$ multipliers and $F_3 = f\left(q_{sw}, x_{B,2}, \sigma_{s,3}, c_2, \ , \lambda_1, \lambda_2, \lambda_3\right)$, respectively, and the resulting condition for the equality of the zero partial derivatives [16, 24]:

$$\left.\begin{aligned}&\frac{\partial f}{\partial x_1}+\lambda_1\frac{\partial\varphi_1}{\partial x_1}+\lambda_2\frac{\partial\varphi_2}{\partial x_1}+...+\lambda_m\frac{\partial\varphi_m}{\partial x_1}=0\\&\frac{\partial f}{\partial x_2}+\lambda_1\frac{\partial\varphi_1}{\partial x_2}+\lambda_2\frac{\partial\varphi_2}{\partial x_2}+...+\lambda_m\frac{\partial\varphi_m}{\partial x_2}=0\\&...\\&\frac{\partial f}{\partial x_n}+\lambda_1\frac{\partial\varphi_1}{\partial x_n}+\lambda_2\frac{\partial\varphi_2}{\partial x_n}+...+\lambda_m\frac{\partial\varphi_m}{\partial x_n}=0\end{aligned}\right\} \qquad (5)$$

The result is the formula:

$$(k_1'k_2'k_{21}'+k_1'k_{21}'+k_1'k_{23}')C_2^2+C_2+k_1'k_{22}'-k_1'k_2'k_{21}'=0. \qquad (6)$$

Parameters $k_1',\ k_2',\ k_{21}'-k_{23}'$ depend on the geometric characteristics of the reinforced concrete composite structures, the geometric and mechanical characteristics of concrete and reinforcement, the adhesion parameters, the parameters of the stress-strain state of the calculated sections I-I and II-II that pass through the beginning and end of the inclined (spatial) crack, respectively – $S,\ B',\ B_{a,1}',\ B_{a,2}'$, A_{sw}, E_{sw}, $q_{sw}, q_{sw,hor}, Q_{s,3}',\ h_0,\ \tau_b$, $x\ \ x_{B,2}$, σ_b, σ_S, $\sigma_{S,1}$, $\tau_{xy,2}$, a, b, $R_{\sup}$, $A_{S,i}$, α, ψ_S, v_b.

6. In the flat-stressed and spatial reinforced concrete (including composite) constructions, a multi-level process of development of various spatial cracks takes place [16, 17]. It is determined by the calculated models of their level appearance in the form of representative volumes of concrete with a reinforcing bar long Δx, commensurable with the distance between the clamps (Figures 2 a, b – for plane-stressed and Figure 4 – for spatial reinforced concrete constructions), which allow us to find the distances between the cracks and the width of their opening, taking into account the discontinuity effect.

Then

$$\begin{aligned}\varepsilon_{bt}(y)&=\sigma_{sw}A_{sw}\cdot\frac{1}{D_{13}'}-\sigma_{sw}(y)A_{sw}\cdot\frac{1}{D_{13}'}+\frac{D_{14}'}{D_{13}'}\cdot y+\frac{D_{15}'}{D_{13}'}=\\&=\varepsilon_{sw}\cdot E_{sw}\cdot A_{sw}\cdot\frac{1}{D_{13}'}-\varepsilon_{sw}(y)\cdot E_{sw}\cdot A_{sw}\cdot\frac{1}{D_{13}'}+\frac{D_{14}'}{D_{13}'}\cdot y+\frac{D_{15}'}{D_{13}'},\end{aligned} \qquad (7)$$

where the parameters $D_1'...D_{12}'$ are expressed as functions of the forces in the sections that cut out a representative volume (Figure 4) with the parameters of concrete, reinforcement and clutch.

The level model is used to determine the deformations of stretched concrete $\varepsilon_{bt}(y)$ along the axis of the transverse reinforcement of the i-th level of formation of different spatial cracks, the distance between them and the width of their opening in a reinforced concrete composite structure.

The nature of the diagram $\varepsilon_{sw}(y)$, performed by experiments of other authors [4, 6, 15, 16], shows that for a certain strain load, the deformations on the areas adjacent to the cracks begin to decrease and even change sign, while deformations in the middle of the section between the cracks continue to increase until at this point new crack. Analysis of the nature of the diagram $\varepsilon_{bt}(x)$ shows the necessity (Figure 5) of taking into account the deformation effect in crack [23].

7. After finding different cracks and determining the deformations in the concrete along the axis of the transverse and longitudinal reinforcement, it is possible, according to the accepted criterion for the formation of cracks, to proceed to the calculation of the distance between the spatial cracks.

In this case, knowing the deformations in the transverse reinforcement or the deformation in the longitudinal reinforcement in the section with the y coordinate and the deformation in the concrete (determined using the calculated model of the *i*-th level (Figure 4) by the formula (8), it is possible to find the relative mutual displacements of the reinforcement and concrete:

$$\varepsilon_g(y)=\varepsilon_{sw}(y)-\varepsilon_{bt}(y), \qquad (8)$$

where on the basis of [23]:

$$\varepsilon_{sw}(y) = \varepsilon_{sw} + \frac{\Delta T}{E_{sw}A_{sw}} - \frac{S}{A_{sw}E_{sw}}\int_0^y \tau(y)dy\,. \qquad (9)$$

Here S_s is the perimeter of the cross section of the reinforcement; ε_s – deformation of the reinforcement in crack; ΔT – resultant conditional tangential stresses in the local zone adjacent to the crack [23, 24]; $\tau(x)$ – conditional tangential stresses.

After substituting (8) into (9) and taking into account the accepted criterion for the formation of cracks, after differentiating and solving the inhomogeneous first-order differential equation, we may have:

$$\varepsilon_g(y) = C\cdot e^{-By} + \frac{D_{14}}{D_{13}\cdot B}. \qquad (10)$$

where B – is the parameter of bond reinforcement with concrete, determined in accordance with the formula $B = \dfrac{S_S\cdot G}{K\cdot A_S\cdot E_S}$. The integration constant *C* is found from the boundary condition, according to which, for $y = 0$, $\varepsilon_g(y) = \varepsilon_{sw} + \dfrac{\Delta T}{A_{sw}E_{sw}} - \dfrac{\sigma_{bt,c}}{\nu_b E_b}$.

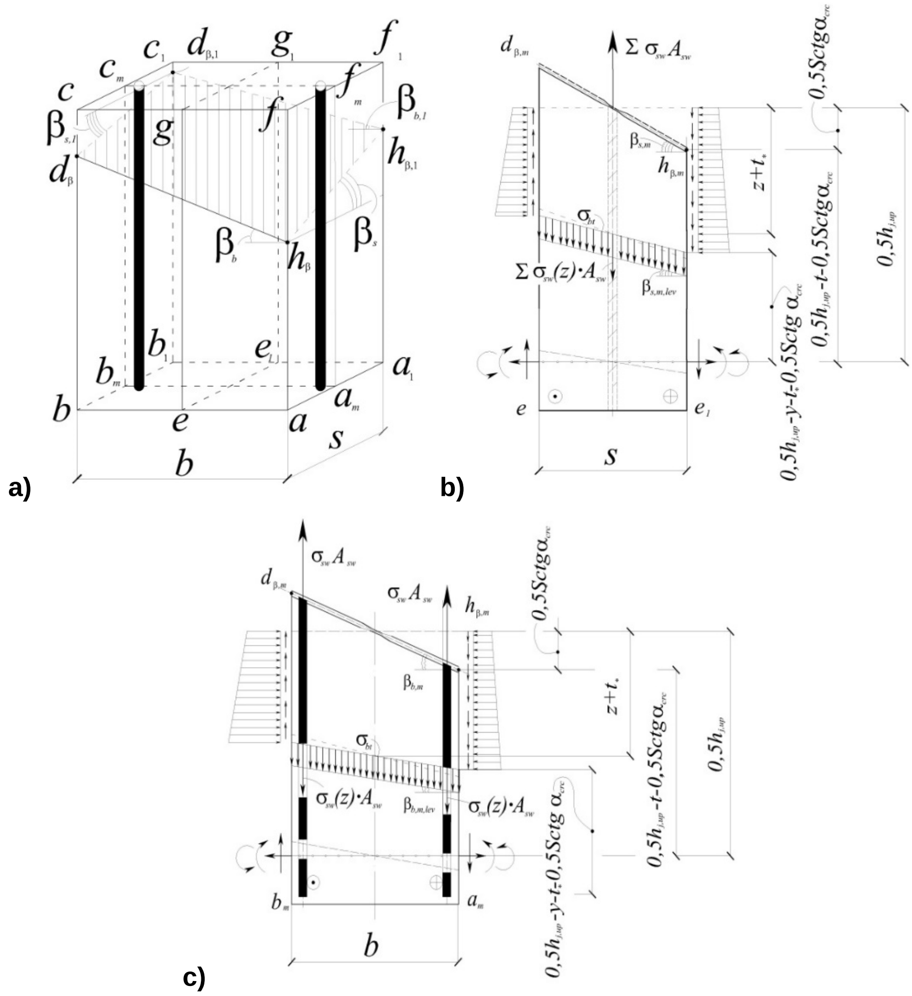

Figure 4. Carving of representative volume from a reinforced concrete structure, subject to torsion with bending: a – representative volume of concrete, including reinforcing bars and part of a spatial crack; b and c are calculated models of the second and subsequent levels for determining deformations of stretched concrete $\varepsilon_{bt}(y)$ between spatial cracks with their longitudinal and transverse sections, respectively

Then

$$C = \varepsilon_{sw} + \frac{\Delta T}{A_{sw} E_{sw}} - \frac{\sigma_{bt,c}}{\nu_b E_b} - \frac{D_{14}}{D_{13} \cdot B}. \qquad (11)$$

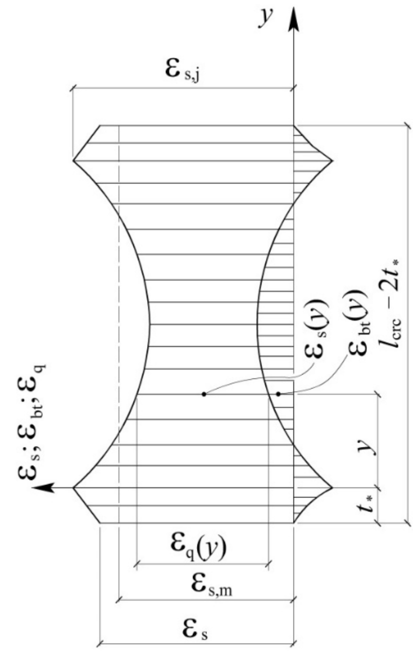

Figure 5. The diagrams of concrete deformation $\varepsilon_{bt}(y)$, reinforcement $\varepsilon_{sw}(y)$ and their relative mutual displacements $\varepsilon_g(y)$ in the area between inclined (for a flat model) or spatial (for a spatial model) cracks in RCC

Here $\frac{\sigma_{bt,c}}{\nu_b E_b}$ corresponds to concrete deformations $\varepsilon_{bt}(y)$ in a section located at a distance t_* from the section with a crack (Figure 5). In this case, the values $\sigma_{bt,c}$ are taken with a “minus” sign here and in all the below formulas.

Then,

$$\varepsilon_g(y) = \left(\varepsilon_{sw} + \frac{\Delta T}{E_{sw} A_{sw}} - \frac{\sigma_{bt,c}}{\nu_b E_b} - \frac{D_{14}}{D_{13} \cdot B} \right) e^{-By} - \frac{D_{14}}{D_{13} \cdot B}. \qquad (12)$$

From the solution of the differential equation (12) and taking into account the criterion for the formation of cracks, distances between cracks of the following level along the axes of the transverse (longitudinal) reinforcement are sought:

$$l_{crc} = \frac{2\left(\ln B_4' - B' t_*\right)}{-B'}. \qquad (13)$$

where the parameters B', B_2', B_3', B_4' are functions of the boundary deformations of the elongation of concrete, the parameters taking into account the effect of discontinuity (through $\sigma_{bt,c}$ and ΔT – the compressive stress and the resultant conditional tangential stress in the local zone adjacent to the crack (they are determined in accordance with the proposals of V.M. Bondarenko and Vl.I. Kolchunov [23]), geometric parameters, the parameters of bond reinforcement with concrete.

Thus, the cracking continues until the moment of destruction. In this case, not one is allocated (as is customary in a number of known techniques), but several levels of crack formation [25]:

$$\left.\begin{array}{c} l_{crc} > l_{crc,1} - no \;\; cracks \\ l_{crc,1} \geq > l_{crc} > l_{crc,2} \;\; - first \;\; level \\ l_{crc,2} \geq l_{crc} > l_{crc,3} - second \;\; level \\ \dots \;\; \dots \;\; \dots \\ l_{crc} \geq 6 \cdot t_{*} - last \;\; level \end{array}\right\}. \tag{14}$$

Comparing the functional and level values of l_{crc}, an analysis is performed of the possible realization of the appearance of subsequent fracture levels.

Having the levels of crack formation along the longitudinal and transverse reinforcement of the reinforced concrete structure, a complete picture of the various cracks adjacent to the concentrated force and to the support is constructed.

The refined and most complete degree of realization of the cracks (whether these cracks intersect the lateral reinforcement or it will be crossed only by a dangerous spatial crack) are determined from the analysis of the stress-strain state along the clamps on the basis of the design scheme, the subsequent level shown in Figure 4, which "closes" to the multi-iterative process provided by the PC.

Crack opening is considered as the accumulation of relative mutual displacements of reinforcement and concrete in areas located on both sides of the crack; this takes into account the effect associated with the violation of the continuity of concrete (the modernized Thomas' hypothesis) [23, 24].

In accordance with this hypothesis, the problem by definition reduces to finding the relative mutual displacements $\varepsilon_g(y)$ of reinforcement and concrete in different sections between the cracks:

$$a_{crc} = 2\int_{0}^{t_*} \varepsilon_g(y_1)dy_1 + \int_{0}^{\eta \cdot l_{crc}} \varepsilon_g(y)dy + \int_{\eta \cdot l_{crc}}^{l_{crc}} \varepsilon_g(y)dy. \tag{15}$$

After integration and some simplifications, we get:

$$a_{crc} = -\frac{2\Delta T}{G} - \frac{2B_{a,2}}{B} - \frac{2B_2}{B}\ln\left(1 + \frac{B_{a,2} \cdot A_{sw}E_{sw}}{q_{sw}S + B_{a,1}A_{sw}E_{sw}}\right), \tag{16}$$

where G – conditional modulus of deformation of bond reinforcement with concrete; S – perimeter of the cross section of the reinforcement; ε_s – deformation of the armature in the crack; A_{sw} – the cross-sectional area of the clamps; other parameters have already been expanded above.

3. Results and Discussion

The algorithm in accordance with the proposed methodology for calculating the rigidity of flat-stressed and spatial reinforced concrete composite structures with the use of the software complex of the PC "LIRA-CAD" was considered in two variants [14, 16, 17, 21, 22].

In the first variant, the rigidity is determined with using the special technique of simulating explicit cracks-gaps when they are opened and closed (Figure 2), taking into account the effect of discontinuity and inconsistency of deformations of concrete and reinforcement. Reinforcing bars are modeled with an additional 201 FE, and a possible closure of the crack is a concrete 255 FE.

The second option involves performing the calculation without changing the order and numbers of the FE. In the FEs adjacent to implicit cracks, their thickness decreases. The work of each pair of FEs is calculated twice using a two-element console model (Figure 3): before "disconnection" FE (W_1) and after "disconnection" FE with applied nodal forces and deformation effects from crack opening, taking into account the discontinuity effect (with distributed the reinforcement is replaced by two (for a planar model) and four (for a spatial model) by rod fibrous FEs.

Efforts at the nodes of the two-element console model are determined from the nonlinear calculation of the entire reinforced concrete construction for the given force and deformation effects. The movements of the nodes are determined from the calculation of the two-element console model (TeCM) with the forces applied and stresses in the nodes (Figure 3). When solving the inverse problem associated with the need to determine the width of the discrete crack opening, deformation effects are not specified, but a gap with its minimum possible width is modeled. In this case, the displacement of its banks along three mutually perpendicular directions as a result of the calculation of the TeCM determines the corresponding components of the width of the discrete crack opening between this FE pair.

As a result, the new thickness of the FEs adjacent to the crack is determined by formula (2). The calculation algorithm assumes the presence of an iterative process, which is controlled by the achieved thickness accuracy of the indicated FEs. In this case, it is also possible to analyze the width of the crack opening, obtained in existing software systems in the finite elements with reduced thickness, which adjoin the imaginary discrete crack [14, 21, 22]. Such a comprehensive comparative analysis of the widths of the disclosure will undoubtedly contribute to an in-depth study of this quantity, which in the theory of reinforced concrete is "obstinate," which is not amenable to description in the form of an acceptable theoretical formula, has been for many decades.

Thus, a method is proposed for calculating the resistance of reinforced concrete structures with the combined effect of transverse force, bending and twisting moments and longitudinal force for the second stage of the stress-strain state, which allows us to reveal the actual stress-strain state in the presence of spatial cracks, with the distance between the cracks and the width of their disclosure.

4. Conclusions

1. It is substantiated the urgency and necessity of technique development for modeling spatial discrete cracks in the case of complex resistance of reinforced concrete structures of buildings and structures, under the action torsion with bending, which have a significant effect on their stress-strain state, and, first of all, on the change in rigidity.

2. The working calculation prerequisites have been developed on the basis of analysis and generalization of experimental and theoretical studies. They allow one to simulate discrete cracks and evaluate the rigidity of reinforced concrete structures, with complex resistance – torsion with bending, which includes:

- modeling of different spatial cracks by bilinear surfaces;
- the proposed classification of basic spatial cracks;
- block calculation model with working sections, to determine the stress-strain state of which the capabilities of existing software complexes are attracted, taking into account the inter-medial disturbance in the seam between the layers of concrete and the incompatibility of deformations of concrete and reinforcement;
- modeling cracks by "shaving" the final elements with the help of cracked cracks and setting the deformation effect, taking into account the effect of discontinuity;
- involvement of a special two-element cantilever model for analyzing the resistance along the fracture path and along the seam between the concrete layers;
- change in the thickness of the final elements adjacent to the crack and the introduction of equivalent rigidities;
- finding the projections of adjacent spatial cracks on the horizontal (vertical) with the use of analytic dependencies, which are based on the extremum of functions of many variables using Lagrange multipliers;
- a special design model for multilevel crack formation, which allows us to search for the distances between the cracks and the width of their openings, taking into account the effect of discontinuity, and to display a multilevel crack development process involving inequalities.

3. The algorithm is developed for calculating the stiffness of plane-stressed and spatial reinforced concrete structures with complex resistance – torsion with bending and the presence of discrete cracks involving existing computer systems, including:

- two options for special modeling of opening and closing of cracks, taking into account the effect of discontinuity and inconsistency of deformations of concrete and reinforcement;
- the iterative process of applying forces in the nodes of the two-element console model, determined from the nonlinear calculation of the entire reinforced concrete structure (or its block design model with working sections-spatial and normal, passing through the end of the spiral-

shaped crack) to given force and deformation effects (in solving the inverse problem , associated with the need to determine the width of the opening of a discrete spiral-like crack, deformation effects are not specified, but a spatial gap is modeled minimally possible opening width, thus moving it coasts along three mutually perpendicularly directions define components width of the cracks between the respective pair of finite elements), which allows you to significantly refine their stress-strain state in the case of force, deformation (including seismic) impacts and, as a consequence, significantly improve the efficiency of reinforced concrete design.

References

1. Kirsanov, M.N. Mathematical model of the truss with hardening elements. Magazine of Civil Engineering. 2015. No. 4(56). Pp. 38–44. (rus)
2. Pavelko, A.D., Rybakov, V.A., Pikht, A.V., Mikhailov, E.S. Non-uniform of thin-walled open-section multi-span beams. Magazine of Civil Engineering. 2016. No. 7(67). Pp. 55–69. doi: 10.5862/MCE.67.6.
3. Kalkan, I., Kartal, S. Torsional Rigidities of Reinforced Concrete Beams Subjected to Elastic Lateral Torsional Buckling. International Journal of Civil and Environmental Engineering. 2017. Vol. 11. No. 7. Pp. 969–972.
4. Nemchinov, Yu.I. Sejsmostojkost' zdanij i sooruzhenij [Seismic stability of buildings and structures]. Kiev, 2008. 480 p. (rus)
5. Vatin, N.I., Ivanov, A.Yu., Rutman, Y.I., Chernogorskiy, S.A., Shvetsov, K.V. Earthquake engineering optimization of structures by economic criterion. Magazine of Civil Engineering. 2017. No. 8(76). Pp. 67–83. doi: 10.18720/MCE.76.7.
6. Salnikov, A., Kolchunov, Vl., Yakovenko, I. The computational model of spatial formation of cracks in reinforced concrete constructions in torsion with bending. Applied Mechanics and Materials. 2015. Vols. 725–726. Pp. 784–789.
7. Pettersen, J.S. Non-Linear Finite Element Analyses of Reinforced Concrete with Large Scale Elements: Including a Case Study of a Structural Wall. Norwegian University of Science and Technology. 2014. 85 p.
8. Nahvi, H., Jabbari, M. Crack detection in beams using experimental modal data and finite element model. International Journal of Mechanical Sciences. 2005. Vol. 47. Pp.1477–1497.
9. Kolchunov, Vl.I., Demyanov, A.I., Iakovenko, I.A., Garba, M.O. Privedenie v sootvetstvie opytnyh dannyh treshchinostojkosti zhelezobetonnyh konstrukcij ih teoreticheskim znacheniyam [Bringing the experimental data of reinforced concrete structures crack resistance in correspondence with their theoretical values]. Science & Construction. No. 1(15). Pp. 42–49. (rus)
10. Jariwalaa, V.H., Patel, P.V., Purohit, S.P. Purohit. Strengthening of RC Beams subjected to Combined Torsion and Bending with GFRP Composites. Procedia Engineering. 2013. Vol. 51. Pp. 282–289.
11. Thomas, A., Hameed, A.S. An Experimental Study On Combined Flexural And Torsional Behaviour Of RC Beams. International Research Journal of Engineering and Technology. 2017. Vol. 04. No. 05. Pp. 1367–1370.
12. Rahal, K. Combined Torsion and Bending in Reinforced and Prestressed Concrete beams Using Simplified Method for Combined Stress-Resultants. ACI Structural Journal. 2007. Vol. 104. No. 4. Pp. 402–411.
13. Santhakumar, R., Dhanaraj, R., Chandrasekaran, E. Behaviour of retrofitted reinforced concrete beams under combined bending and torsion: A numerical study. Electronic Journal of Structural Engineering. 2007. No. 7. Pp. 1–7.
14. Emelyanov, S., Nemchinov, Y., Kolchunov, V., Yakovenko, I. Details of large-panel buildings seismic analysis. Enfoque UTE. 2016. No. 7(2). Pp. 120–134.
15. Li, Y. Final Report Predicting of the Stiffness of Cracked Reinforced Concrete Structures. 2010.147 p.
16. Iakovenko, I., Kolchunov, V., Lymar, I. Rigidity of reinforced concrete structures in the presence of different cracks.

Литература

1. Кирсанов М.Н. Изгиб, кручение и асимптотический анализ пространственной стержневой консоли // Инженерно–строительный журнал. 2014. № 5. С. 37–43.
2. Павленко А.Д., Рыбаков В.А., Пихт А.В., Михайлов Е.С. Стесненное кручение многопролетных тонкостенных балок открытого профиля // Инженерно–строительный журнал. 2016. № 7(67). С. 55–69.
3. Kalkan I., Kartal S. Torsional Rigidities of Reinforced Concrete Beams Subjected to Elastic Lateral Torsional Buckling // International Journal of Civil and Environmental Engineering. 2017. Vol. 11. № 7. Pp. 969–972.
4. Немчинов Ю.И. Сейсмостойкость зданий и сооружений. Киев, 2008. 480 с.
5. Ватин Н.И., Иванов А.Ю., Рутман Ю.Л., Черногорский С.А., Швецов К.В. Оптимизация конструкций сейсмостойких сооружений по экономическому критерию // Инженерно–строительный журнал. 2017. № 8(76). С. 67–83.
6. Salnikov A., Kolchunov Vl., Yakovenko I. The computational model of spatial formation of cracks in reinforced concrete constructions in torsion with bending // Applied Mechanics and Materials. 2015. Vols. 725–726. Pp. 784–789.
7. Pettersen J.S. Non–Linear Finite Element Analyses of Reinforced Concrete with Large Scale Elements: Including a Case Study of a Structural Wall. Norwegian University of Science and Technology, 2014. 85 p.
8. Nahvi H., Jabbari M. Crack detection in beams using experimental modal data and finite element model // International Journal of Mechanical Sciences. 2005. Vol. 47. Pp. 1477–1497.
9. Колчунов В.И., Демьянов А.И., Яковенко И.А., Гарба М.О. Приведение в соответствие опытных данных трещиностойкости железобетонных конструкций их теоретическим значениям // Наука та будівництво. 2018. № 1(15). С. 42–49.
10. Jariwalaa V.H., Patel P.V., Purohit S.P. Strengthening of RC Beams subjected to Combined Torsion and Bending with GFRP Composites // Procedia Engineering. 2013. Vol. 51. Pp. 282–289.
11. Thomas A., Hameed A.S. An Experimental Study on Combined Flexural and Torsional Behaviour of RC Beams // International Research Journal of Engineering and Technology. 2017. Vol. 04. № 05. Pp. 1367–1370.
12. Rahal K. Combined Torsion and Bending in Reinforced and Prestressed Concrete beams Using Simplified Method for Combined Stress–Resultants // ACI Structural Journal. 2007. Vol. 104. № 4. Pp. 402–411.
13. Santhakumar R., Dhanaraj R., Chandrasekaran E. Behaviour of retrofitted reinforced concrete beams under combined bending and torsion: A numerical study // Electronic Journal of Structural Engineering. 2007. № 7. Pp. 1–7.
14. Emelyanov S., Nemchinov Y., Kolchunov V., Yakovenko I. Details of large–panel buildings seismic analysis // Enfoque UTE. 2016. № 7(2). Pp. 120–134.
15. Li Y. Final Report Predicting of the Stiffness of Cracked Reinforced Concrete Structures. 2010.147 p.
16. Iakovenko I., Kolchunov V., Lymar I. Rigidity of reinforced concrete structures in the presence of different cracks. MATEC Web of Conferences // 6th International Scientific Conference “Reliability and Durability of Railway Transport

MATEC Web of Conferences. 6th International Scientific Conference «Reliability and Durability of Railway Transport Engineering Structures and Buildings». Transbud-2017. Kharkiv, Ukraine, 2017. Vol. 0216. 12 p.
17. Kolchunov, V.I., Iakovenko, I.A., Maryenkov, N.G. Analiz skhem treshchin v zhelezobetonnyh konstrukciyah sejsmostojkih zdanij i ih uchet po normam Ukrainy i evrokoda 8 [Analysis of cracks in reinforced concrete construction of seismic resistant buildings and their accounting according to the norms of Ukraine and Eurocode 8]. Bulding Structures. 2015. Vol. 82. Pp. 540–549. (rus)
18. Stepanov, V.B. Metodika opredeleniya shiriny raskrytiya korrozionnykh treshchin dlya otsenki tekhnicheskogo sostoyaniya zhelezobetonnykh konstruktsiy [The method of corrosion crack opening evaluation for the reinforced concrete structures technical state assessment]. Magazine of Civil Engineering. 2012. No 5. Pp. 6–11. doi: 10.5862/MCE.31.1. (rus)
19. Demyanov, A.I., Kolchunov, V.I., Iakovenko, I.A. K zadache dinamicheskogo dogruzheniya armatury pri mgnovennom obrazovanii prostranstvennoj treshchiny v zhelezobetonnoj konstrukcii pri kruchenii s izgibom [To the dynamic loading problem of reinforcement with the instantaneous formation of spatial crack in reinforced concrete construction under the action of torsion with bending]. Industrial and civil engineering. 2017. Vol. 9. Pp. 18–24. (rus)
20. Golyshev, A.B., Kolchunov, V.I., Iakovenko, I.A. Soprotivlenie zhelezobetonnyh konstrukcij, zdanij i sooruzhenij, vozvodimyh v slozhnyh inzhenerno-geologicheskih usloviyah [Resistance of reinforced concrete structures, buildings and structures erected in complex engineering-geological conditions]. Kiev: Talcom, 2015. 371 p. (rus)
21. Kolchunov, Vl.I., Iakovenko, I.A., Lymar, Ya.V. Zhestkost' zhelezobetonnyh sostavnyh konstrukcij pri nalichii razlichnyh treshchin [Rigidity of reinforced concrete composite structures in the presence of various cracks]. Building and Reconstruction. 2015. No. 5(61). Pp. 17–24. (rus)
22. Kolchunov, V.I., Maryenkov, N.G., Tugai, T.V., Iakovenko, I.A. Metodika rascheta zhestkosti ploskonapryazhennyh zhelezobetonnyh konstrukcij s privlecheniem programnogo kompleksa «Lira-Pro» [Resistance of plane-stressed walls to a skew in the presence of a diagonal crack with the use of the Lira-Pro software complex]. Academic journal. Industrial Machine Building. Poltava: Civil Engineering Poltava National Technical Yuri Kondratyuk University. 2015. No. 1(43). (rus)
23. Bondarenko, V.M., Kolchunov, V.I. Raschetnye modeli silovogo soprotivleniya zhelezobetona [The computational model of a power resistance of reinforced concrete]. Moskow: ASV Publ., 2004. 472 p. (rus)
24. Bashirov, H.Z., Kolchunov, V.I., Fedorov, V.S., Iakovenko, I.A. Zhelezobetonnye sostavnye konstrukcii zdanij i sooruzhenij [Reinforced concrete composite constructions of buildings and structures]. Moskow: ASV Publ., 2017. 248 p. (rus)
25. Iakovenko, I., Kolchunov, Vl. The development of fracture mechanics hypotheses applicable to the calculation of reinforced concrete structures for the second group of limit states. Journal of Applied Engineering Science. 2017. Vol. 15. Article 455. Pp. 366–375.

Engineering Structures and Buildings”. Transbud–2017. Kharkiv, Ukraine, April 19–21. 2017. Vol. 0216. 12 p.
17. Колчунов В.И. Яковенко И.А., Марьенков Н.Г. Анализ схем трещин в железобетонных конструкциях сейсмостойких зданий и их учет по нормам Украины и еврокода // Будівельні конструкції. 2015. № 82. С. 540–549.
18. Степанов В.Б. Методика определения ширины раскрытия коррозионных трещин для оценки технического состояния железобетонных конструкций // Инженерно–строительный журнал. 2012. № 5. С. 6–11.
19. Демьянов А.И., Колчунов В.И., Яковенко И.А. К задаче динамического догружения арматуры при мгновенном образовании пространственной трещины в железобетонной конструкции при кручении с изгибом // Промышленное и гражданское строительство. 2017. № 9. С. 18–24.
20. Голышев А.Б., Колчунов В.И., Яковенко И.А. Сопротивление железобетонных конструкций, зданий и сооружений, возводимых в сложных инженерно–геологических условиях. Киев: Талком, 2015. 371 с.
21. Колчунов В.И., Яковенко И.А. Лымарь Я.В. Жесткость железобетонных составных конструкций при наличии различных трещин // Строительство и реконструкция. 2015. № 5(61). С. 17–24.
22. Колчунов В.И., Яковенко И.А., Тугай Т.В. Методика расчета жесткости плосконапряженных железобетонных конструкций с привлечением програмного комплекса «Лира–Pro» // Зб. наук. праць (галузеве машинобудування, будівництво). Полтава: ПолтНТУ, 2014. Т. 2. № 3(42). С. 55–66.
23. Бондаренко В.М., Колчунов В.И. Расчетные модели силового сопротивления железобетона. М.: Изд. АСВ, 2004. 472 с.
24. Баширов Х.З., Колчунов В.И., Федоров В.С., Яковенко И.А. Железобетонные составные конструкции зданий и сооружений. М.: Изд. АСВ, 2017. 248 с.
25. Iakovenko I., Kolchunov Vl. The development of fracture mechanics hypotheses applicable to the calculation of reinforced concrete structures for the second group of limit states. Journal of Applied Engineering Science. 2017. Vol. 15. article 455. Pp. 366–375.

Vladimir Kolchunov,*
+7(471)222-24-61; sjs28@mail.ru

Alexey Dem'yanov,
+7(471)222-24-61; speccompany@gmail.com

Владимир Иванович Колчунов,*
+7(471)222-24-61; эл. почта: sjs28@mail.ru

Алексей Иванович Демьянов,
+7(471)222-24-61;
эл. почта: speccompany@gmail.com

Kolchunov, V.I., Dem'yanov, A.I. The modeling method of discrete cracks in reinforced concrete under the torsion with bending. Magazine of Civil Engineering. 2018. 81(5). Pp. 160–173. doi: 10.18720/MCE.81.16.

doi: 10.18720/MCE.81.17

Installation diagram of the lattice truss with an arbitrary number of panels

Монтажная схема решетчатой фермы с произвольным числом панелей

M.N. Kirsanov,
National Research University "Moscow Power Engineering Institute", Moscow, Russia

Д-р физ.-мат. наук, профессор М.Н. Кирсанов,
Национальный исследовательский университет "МЭИ", Москва, Россия

Key words: truss; deflection; induction; Maple; exact formula; edge coloring; hypergraph

Ключевые слова: ферма; прогиб; индукция; Maple; точная формула; реберная раскраска; гиперграф

Abstract. Hereby the diagram of a flat statically determinate regular lattice truss with the parallel chords is proposed. The task is to obtain an analytical dependence of the truss deflection and forces in the most tension and compressed bars on the number of panels. In order to solve the problem, the Maple computing mathematical system is used. We have considered the case when the lower truss chord is subject to a uniform load. The forces are determined by the Method of Joint. The Maxwell-Mohr formula is used to determine the deflection. The solution obtained for a set of cases with different successively increasing numbers of panels is generalized to a random number of panels by method of induction. The special operators of the Maple system are used to prepare homogeneous linear recurrence relations that are satisfied with the sequences of coefficients in the required formula. It is shown that for the number of panels in the half-span that are divisible to three, the determinant of the equilibrium equation system is becoming zero. The truss is becoming kinematically changeable that is confirmed by the corresponding diagram of possible joint velocity. The algorithm for the truss installation diagram is described, where the cross bars are in different planes and are connected in the nodes so that the truss elements are not subjected to buckling. The solution of this problem is related to the correct edge coloring of graphs and hypergraphs.

Аннотация. Предлагается схема плоской статически определимой регулярной балочной фермы с параллельными поясами. Ставится задача получения аналитической зависимости прогиба фермы и усилий в наиболее растянутых и сжатых стержнях от числа панелей. Для решения задачи привлекается система компьютерной математики Maple. Рассмотрен случай равномерного загружения узлов нижнего пояса фермы. Усилия определяются методом вырезания узлов. Для нахождения прогиба используется формула Максвелла - Мора. Решение, полученное для серии задач с разным последовательно возрастающим числом панелей, обобщается методом индукции на произвольное число панелей. Используются специальные операторы системы Maple для составления однородных линейных рекуррентных уравнений, которым удовлетворяют последовательности коэффициентов в искомой формуле. Показано, что для чисел панелей в половине пролета, кратных трем, определитель системы уравнений равновесия обращается в ноль. Ферма становится кинематически изменяемой, что подтверждается соответствующей схемой возможных скоростей узлов. Описан алгоритм составления монтажной схемы фермы, при которой пересекающиеся стержни лежат в разных плоскостях и соединяются в узлах так, что элементы фермы не подвергаются изгибу. Решение этой задачи связывается с правильной реберной раскраской графов и гиперграфов.

1. Introduction

The lattice trusses are widely used in civil engineering and mechanical engineering. Well-developed numerical algorithms, mainly based on the finite element method, make it possible to easily and accurately calculate a sufficiently wide range of such structures. Development of the modern computing mathematical systems offers new opportunities for solving the problems of the frame structures that is obtaining of accurate solutions. The value of such solutions is determined by the degree of versatility of the design formulas. In particular, it is quite easy to find an analytical expression for the deflection or force in any truss

Кирсанов М.Н. Монтажная схема решетчатой фермы с произвольным числом панелей // Инженерно-строительный журнал. 2018. № 5(81). С. 174–182.

bar, depending on the truss dimensions and the load, if a specific number of panels is provided. For this purpose, it is sufficient to solve the system of equilibrium equations and all the design equations in symbolic form. It is much more difficult to obtain the dependence of the solution on the number of panels or bars that make up the structure. In [1–3], the induction method is applied in the similar case that substantially extend the scope of application of the final formulas. The resulting symbolic estimates of deflection, support reactions and forces in the bars are free from errors naturally accumulated by the numerical methods, especially when a large number of panels is taken into account. The inductive method can be used for the trusses that have the regularity property [4, 5]. The same method is used in the present paper for the statically determinate truss (Figure 1). During the research process, a case of kinematic degeneration of the truss has been found and an algorithm for designing the installation diagram has been proposed. The formulas for calculating the deflection of building structures are of practical importance for the design engineers when developing the new diagrams and improving the standard diagrams of frame structures. Earlier deflection values in analytical form using the induction method in the Maple system were found in flat trusses [2,3, 6–9] and in spatial ones [1,10–14].

2. Methods

2.1. The truss diagram and the equations to find the forces

The truss diagram shows pin-connected bars. The bars are assumed to be elastic with the same elasticity modulus, the cross-sections of the rods are assumed to be the same. The truss containing n number of panels in the half-span has $4n + 6$ pin connections and $m = 8n + 12$ bars, including three support bars. The truss is statically determinate.

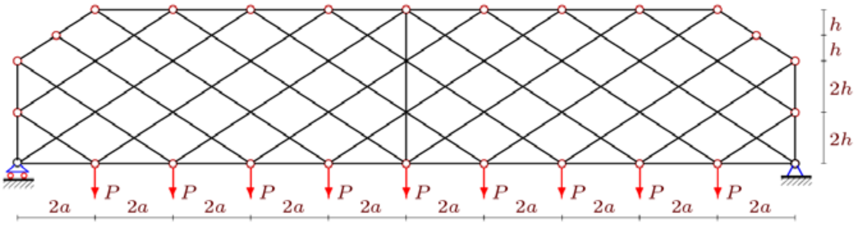

Figure 1. Truss. *n* = 5

The uniform load is applied to the nodes of the lower chord. The Method of Joint is used for determination of forces in the bars with the support of a program compiled in the Maple system [1]. The truss bars and nodes are numbered (Figure 2), the coordinates of the joints and the graph for connection of the bars (edges) and nodes (apex) are provided.

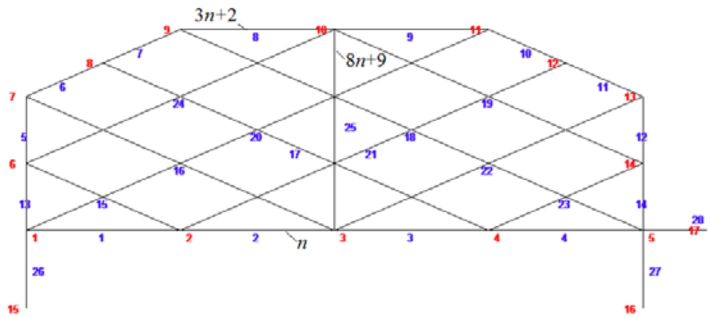

Figure 2. Truss. Numbering of nodes and bars, *n* = 2

The graph of the lattice is represented by conditional vectors $\bar{N}_i,\ i = 1,...,m$ containing the numbers of pin connections at their ends. For example, both chords and side structures are coded with the following vectors:

$$\bar{N}_i = [i, i+1],\ i = 1,..,2n,$$
$$\bar{N}_{i+2n} = [i+2n+1, i+2n+2],\ i = 1,..,2n+4,$$
$$\bar{N}_{4n+5} = [1, 2n+2], \bar{N}_{4n+6} = [2n+1, 4n+6].$$

The matrix of nodes equilibrium equations system $\mathbf{G}$ with the dimensions $m \times m$ consists of the directional cosines of the bars, when projected onto the coordinate axis. The odd matrix rows are projected onto the x-axis, even rows onto the y-axis.

Kirsanov, M.N. Installation diagram of the lattice truss with an arbitrary number of panels. Magazine of Civil Engineering. 2018. 81(5). Pp. 174–182. doi: 10.18720/MCE.81.17.

The directional cosines are calculated using the bars lengths and their vector projections onto the coordinate axes:

$$l_i = \sqrt{l_{1,i}{}^2 + l_{2,i}{}^2}, \ l_{1,i} = x_{N_{2,i}} - x_{N_{1,i}}, \ l_{2,i} = y_{N_{2,i}} - y_{N_{1,i}}, \ \ i = 1,...,m.$$

In the number $N_{i,j}$, the first index i is the bar number, the second one is the number of the vector component $\bar{N}_i$, that takes the value 1 (the beginning of the bar vector) or 2 (the end of the bar). The matrix of the directional cosines $\mathbf{G}$ has the following elements:

$$G_{k,i} = -l_{j,i} / l_i, \ k = 2N_{i,2} - 2 + j, \ \ k \le m, \ j = 1,2, \ i = 1,...,m,$$

$$G_{k,i} = l_{j,i} / l_i, \ \ k = 2N_{i,1} - 2 + j, \ \ \ k \le m, \ \ j = 1,2, \ i = 1,...,m.$$

The forces in the truss bars are determined based on the solution of the system of linear equations $\mathbf{G}\bar{S} = \bar{B}$, where $\bar{S}$ is the vector of unknown forces in the bars, $\bar{B}$ is the vector of external loads.

During calculation of the forces it has been found that the diagram under examination has a hidden and sufficiently dangerous defect. It turns out that for the trusses with a number of panels divisible by three, the determinant of the equation system matrix is becoming equal to zero. With such n values the truss it turned into the instantly changeable mechanism. To confirm this fact, we have obtained the scheme of possible joint velocities for n = 3 (Figure3). It is obvious that the bars 2-8 and 6-18 are rotating around the supports, the rods 12-13, 13-14, 2-3 and 5-6 are rotating around the rigid pin connections. The bars 8-12 and 14-18 make a plane movement. Having considered the rotational motion of the bars 2-8 and 6-18, we obtain that the joint velocities are related to each other: $\omega = v/(2a) = u/(2h)$. The same relation is resulted from the analysis of the plane motion of the bars 8-12 and 14-18 around the instantaneous velocity centers M_1 and M_2.

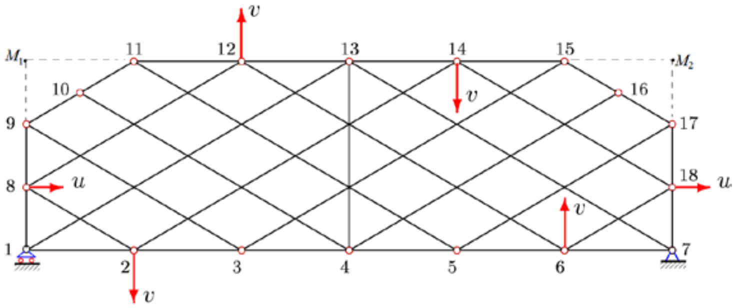

Figure 3. Diagram of possible joint velocities of variable truss at *n* = 3

In order to reveal the regularity of the coefficient formation in the desired formulas for deflection and forces in the typical rods, it is necessary to exclude from the solution sequence the trusses with the number of panels, such as $n = 3i$, i = 1,2,3, ... To meet these requirements, a sequence with common term is taken

$$n = (6k - 3 - (-1)^k)/4, \ k = 1,2,3,... \tag{1}$$

The elements of this sequence take all natural values except for those divisible by three.

2.2. Deflection

In order to determine the deflection of the central joint of the lower chord (the vertical hinge displacement with the number n + 1) we use the Maxwell-Mohr formula

$$\Delta = \sum_{i=1}^{m-3} \frac{S_i s_i l_i}{EF},$$

where S_i, s_i – the forces in the i truss bar from the applied distributed load and from the single vertical force in the central node of the lower chord with the number n + 1, respectively. Summation is carried out over all deformable rods of the truss. Three support rods are assumed to be rigid and are not included into this sum.

The successive solution of truss deflection equation when k, indicating the number of panels in the half-span, is variable gives every time the same equation regardless of k value

$$\Delta = P(A_k a^3 + C_k c^3 + H_k h^3)/(EFh^2),$$

where $c = \sqrt{a^2 + h^2}$. The coefficient values depend on the value of k that determines the number of panels n in the half-span by formula (1). In order to find the common term A_k of the coefficient sequence at a^3, the recurrence equation of the eleventh order, (k > 2), was found using the **rgf_findrecur** operator of the **genfunc** package of rational generating functions of the Maple system.

$$A_k = A_{k-1} + 3A_{k-2} - 3A_{k-3} - 2A_{k-4} + 2A_{k-5} - 2A_{k-6} + 2A_{k-7} + 3A_{k-8} - 3A_{k-9} - A_{k-10} + A_{k-11}.$$

Solution of this equation using the **rsolve** operator provides the general term of the sequence

$$A_k = (30k^4 - 20(\cos 2\varphi + 3)k^3 + 6(5\cos 2\varphi - 29)k^2 + 4(51 - 67\cos 2\varphi)k -$$
$$-144\cos\varphi + 129\cos 2\varphi - 144\sin\varphi + 79)/64,$$

where $\varphi = \pi k/2$ is given. Similarly, on the basis of the solution of homogeneous equations of the seventh order

$$C_k = C_{k-1} + C_{k-2} - C_{k-3} + C_{k-4} - C_{k-5} - C_{k-6} + C_{k-7},$$

$$H_k = H_{k-1} - H_{k-2} + H_{k-3} + H_{k-4} - H_{k-5} + H_{k-5} - H_{k-7}$$

we can obtain other coefficients of the deflection formula:

$$C_k = (-30k^2 + 6(5 - 9\cos 2\varphi)k + 27\cos 2\varphi - 12\cos\varphi - 12\sin\varphi + 33)/16,$$
$$H_k = (2(5 - 3\sin\varphi - 3\cos\varphi)k - 12\cos\varphi + 18\sin\varphi - 39\cos 2\varphi - 5)/4.$$

2.3. Forces in the critical bars

Simultaneously with derivation of the formula for deflection, it is possible to obtain the form of forces in the most compressed and tension bars, depending on the number of panels. These formulas are required to evaluate the structure stiffness and the stability of its bars. The sequences of analyzed solutions, which operator **rgf_findrecur** uses to determine regularity, turns out to be shorter, and the recurrence relations are simpler. Having assumed that the most compressed bar under such a load is located in the middle part of the upper chord (the rod with the number 3*n* + 2, Figure 2), we obtain the following expression:

$$S_{3n+2} = -P(a/h)(6k^2 + 2(6\cos\varphi - 2\sin\varphi - \cos 2\varphi - 3)k + \cos 2\varphi - 4\sin\varphi + 8\cos\varphi + 7)/16.$$

Similarly, the most tension bar appears to have the value of *n* in the middle of the lower chord. The force is also determined by the induction method

$$S_n = P(a/h)(6k^2 + 2(2\sin\varphi - 6\cos\varphi - \cos 2\varphi - 3)k + \cos 2\varphi + 4\sin\varphi - 8\cos\varphi - 17)/16.$$

For comparison, we also obtain formulas for the forces in the bars adjacent to the assumed critical bars:

$$S_{n-1} = P(a/h)(6k^2 - 2(2\sin\varphi + 2\cos\varphi + \cos 2\varphi + 3)k + \cos 2\varphi + 12\sin\varphi - 8\cos\varphi - 17)/16,$$

$$S_{3n+1} = -P(a/h)(6k^2 + 2(2\cos\varphi + 2\sin\varphi - \cos 2\varphi - 3)k + \cos 2\varphi - 12\sin\varphi + 8\cos\varphi + 7)/16,$$

and force in the vertical stand in the middle of the span:

$$S_{8n+9} = P(3\sin\varphi - 2\cos\varphi - k(\cos\varphi + \sin\varphi))/2.$$

2.4. Installation diagram

When assembling a structure, it is necessary to ensure that elements are connected is such a way that the bars are placed in parallel to avoid buckling due to the arrangement of the ends in different planes [15–16]. In discrete mathematics (theory of graph coloring) there is the problem of the graph edge coloring when the graph edges correspond to the natural numbers (colors) so that edges of different colors are incident to one graph vertex (truss joint) [17–19]. In the case of the truss assembly, colors imply the conditional plane level in which the rod is mounted.

In order to solve the installation case, it is possible to apply the special operator **EdgeChromaticNumber** from the GraphTheory package of the Maple system. However, such a solution is suitable only in the cases where the graph of the truss lattice is flat, that is, it does not contain intersectional braces, as in the truss under examination. In order to avoid buckling, cross bars must be in different planes. The following algorithm for the installation diagram is proposed. Information about the rods (graph edges) is provided to the algorithm input in the form of a list of edges with the end numbers. For the truss with *n* = 3 (Figure2), if is the following list $R = \{ R_1, R_2, R_3$, {1,2}, {2,3}, {3,4}, {4,5}, {1,6}, {6, 7}, {7,8}, {8,9}, {9,10}, {10,11}, {11,12}, {12,13}, {13,14}, {14,5 }}. Three separate sets of intersectional rods are determined: ascending edges (upward-directed edges) $R_1 = \{6,10\}$, $\{1,11\}$, $\{2,12\}$, $\{3,13\}$, $\{4,14\}$, descending edges (downward-directed edges) $R_2 = \{2,6\}$, $\{3,7\}$, $\{4,8\}$, $\{5,9\}$, $\{10,14\}$ and a separate vertical middle rod $R_3 = \{3,10\}$ crossing the bars of both first sets. All these edges are placed at the beginning of the general list R. The task of the algorithm is to place the edges in the individual sets (levels) $U_i,\ i = 1,...,n_U$ so that there are no two edges having the same end numbers in every set. Initially, the sets are empty except for the three sets, in which the sets with the pre-reserved places are included $U_i = R_i,\ i = 1,2,3.$. The remaining elements of the list are placed in the sets U_i, based on the condition that the numbers of the edge ends are not repeated on one level. This is done in the cycles by the list elements $R_i,\ i = 4,...,n_R$ and levels $U_i,\ i = 1,...,n_U$. The result of the algorithm operation in relation to the truss *n* = 3 (Figure2) is as follows:

$$U_1 = \{\{1,\ 11\},\ \{2,\ 12\},\ \{3,\ 13\},\ \{4,\ 14\},\ \{6,\ 10\},\ \{7,\ 8\}\},$$
$$U_2 = \{\{2,\ 6\},\ \{3,\ 7\},\ \{4,\ 8\},\ \{5,\ 9\},\ \{10,\ 14\},\ \{11,\ 12\}\}$$
$$U_3 = \{\{1,\ 2\},\ \{3,\ 10\},\ \{4,\ 5\},\ \{6,\ 7\},\ \{8,\ 9\},\ \{12,\ 13\}\},$$
$$U_4 = \{\{1,\ 6\},\ \{2,\ 3\},\ \{9,\ 10\},\ \{13,\ 14\}\},$$
$$U_5 = \{\{3,\ 4\},\ \{5,\ 14\},\ \{10,\ 11\}\}.$$

Indeed, there are no two identical joints numbers on each level $U_i,\ i = 1,...,5$. The index of the obtained partition is equal to five (Figure4). It can be noted that this number is similar to the graph chromatic index, where the edge intersection is not restricted, and only the incidence of one vertex of edges with the same color is not allowed (the rods of the same level in this paper).

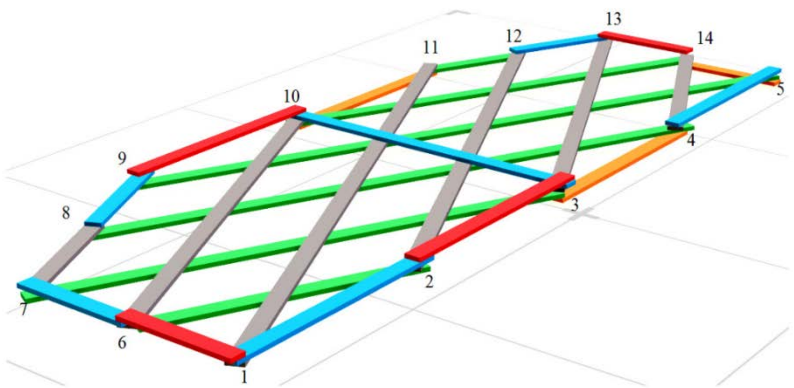

Figure 4. Installation diagram, five levels

Therefore, it is found that in some joints between the bars of different levels there are the gaps in height, requiring additional washers with a thickness equal to the thickness of the bar. It is obvious that the effectiveness of the proposed automatic way to design the installation diagram increases simultaneously with the number of panels, where it is almost impossible to assign the order of the joint assembly manually.

The proposed installation diagram is not the only one. In practice, the short bar elements are not always used in the trusses. For example, the lower chord at *n* = 2 can consist of one bar. In this case, the truss is relevant to the hypergraph that differs from the usual one by the several available vertices near one edge [20, 21]. The algorithm remains the same with the slight difference that the list of vertices of some edges includes more than two numbers:

$R = \{ R_1, R_2, R_3$, {1,2,3,4,5}, {1,6,7}, {7,8,9 }, {9,10,11}, {11,12,13}, {13,14,5}} .

Four sets of bars of the same level are formed at the program output (Figure 5):

U_1 = {{1, 11}, {2, 12}, {3, 13}, {4, 14}, {6, 10}, {7, 8, 9}},

U_2 = {{2, 6}, {3, 7}, {4, 8}, {5, 9}, {10, 14}, {11, 12, 13}},

U_3 = {{3, 10}, {1, 6, 7}, {5, 13, 14}},

U_4 = {{9, 10, 11}, {1, 2, 3, 4, 5}}.

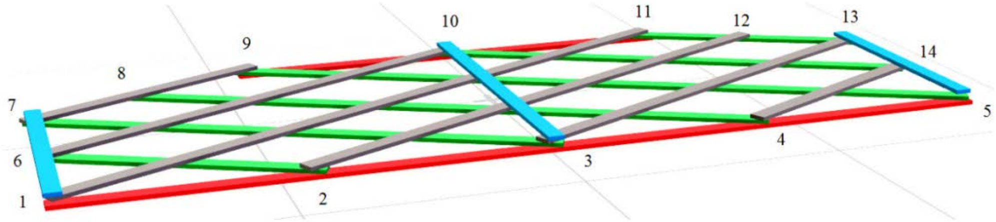

Figure 5. Installation diagram 2, four levels. Hypergraph of truss

3. Results and Discussion

Let us consider some concrete examples, from which the nature of the solution obtained and its features will be clearer.

The curves of the obtained dependence for the non-dimensional deflection $\Delta' = \Delta EF / (P_\Sigma L)$ at a given span length L = 4na = 100m and a fixed total load $P_\Sigma = P(2n-1)$ are plotted in Figure 6. The sharp jumps in the deflection value are typical, especially when a number of panels is small. Moreover, for k = 4 (or for n = 5, that is the same), the node under the load even rises. It means that it is impossible to evaluate the deflection of such structure based on displacement of only one middle node. The adjacent nodes can move in different directions. It is confirmed by the distribution of vertical displacements of the nodes in the lower truss chord at n = 5 (Figure 7).

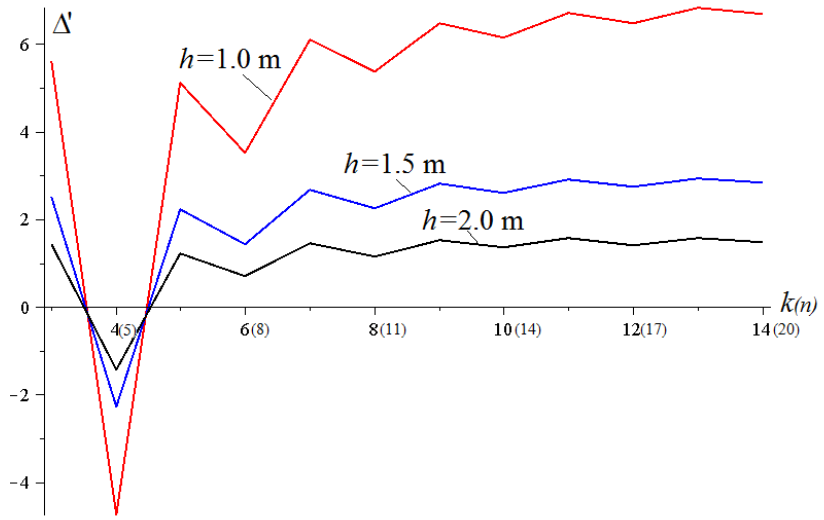

Figure 6. Displacement as a function of number of panels

The formulas for deflections Δ_j of joints j = 1,2,... 11 with due regard to the symmetry have the following form:

$$\Delta_2 = \Delta_{10} = P(57c^3 + 83a^3 + 22h^3)/(EFh^2),$$
$$\Delta_3 = \Delta_9 = -2P(12c^3 + 3a^3 - 4h^3)/(EFh^2),$$
$$\Delta_4 = \Delta_8 = P(69c^3 + 129a^3 + 22h^3)/(EFh^2),$$
$$\Delta_5 = \Delta_7 = 2P(9c^3 + 38a^3)/(EFh^2),$$
$$\Delta_6 = P(a^3 - 33c^3 - 10h^3)/(EFh^2).$$

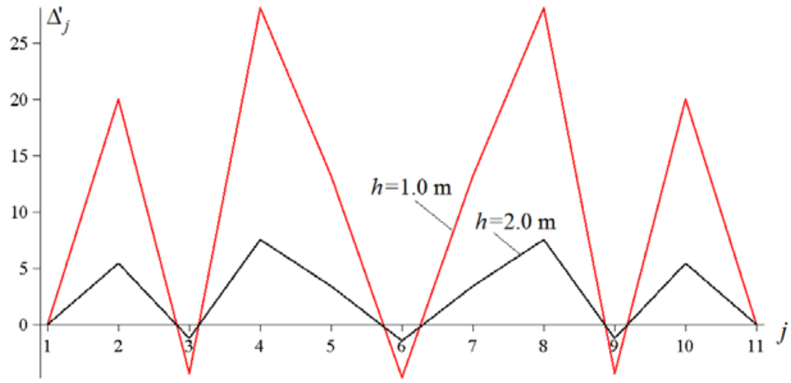

Figure 7. Displacements of the nodes in the lower truss chord. *L*=4*na*=100m, *n*=5, $\Delta'_j = EF\Delta_j/(PL)$

With the increase in the truss height and the value of *n*, the jump rate is decreased. The greatest differences in the values of deflections take place in the middle of the span.

The curves for the non-dimensional values $S'_i = S_i / P_\Sigma$ in Figure 8 show that alternation of the numbers of dangerous bars is possible, depending on the number of panels. Thus, if at k = 5 and k = 6, the bar with the value of *n* in the middle of the span is the most tension rod, then at k = 7 the greatest positive force acts on the adjacent bar *n* – 1. Similarly, the compressed rods in the middle of the upper chord are alternating and are calculated based on the condition of stability loss according to the Euler's formula.

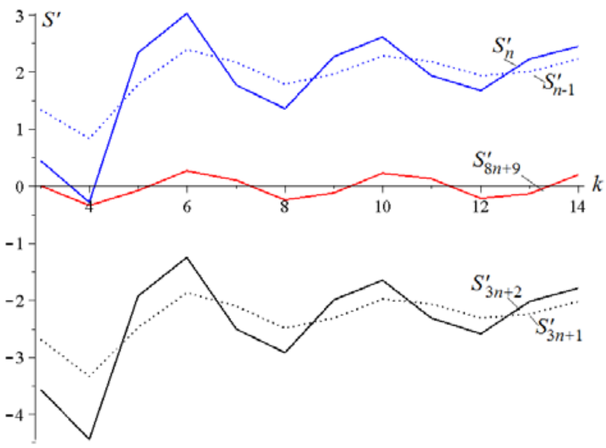

Figure 8. Non-dimensional values of forces in bars

A review of works on the application of the induction method and the computer mathematics system to problems of derivation of exact relations in flat statically determinate trusses is given in [22–24].

4. Conclusions

The obtained formulas for calculation of the deflection and forces in the critical bars when the number of panels are random make it possible to find the values actual for practice in a quite simple way, and what is more important – accuracy, devoid of errors accumulated with a large or very large number of panels and typical for numerical models. A special role here is also played by the induction method. It would seem that if it is necessary to obtain an exact analytical formula with geometric dimensions of the truss as the parameters, then it is simply enough to transfer the calculation program into a symbolic form, and the result is to be ready. However, this is not the case. The peculiarity of symbolic transformations does not allow this to happen even with a very small number of panels (40–50). The period of time for analytical transformations is much longer than for the numerical ones, and, most importantly, the frequently obtained formulas turn out to be unrealistically cumbersome and unsuitable for practice. In addition, the case of kinematic structural variability, revealed in the above example, can not be noticed in calculations (unless the determinant is followed) due to the rounding errors. The problem, solved in this paper, is related to the practice of using the lattice trusses. The truss installation with four panels in the span (Figures 4, 5) is given only as an illustration of the algorithm operation. Such a diagram could be worked out only by listing the possible options without the help of computer methods and concepts of discrete mathematics. However, for the trusses with a large number of panels, the application of the algorithm for automatically preparation of the installation diagram is becoming relevant. All the algorithms considered in this paper can be used in other regular frame structures.

Outside the study of the proposed design, there remained such an important question as the stability of the truss and its elements. The analytical expressions found for the effort make it possible to simply study this question. Regardless of this, the stability of the truss as an element of a spatial construction consisting of individual trusses with horizontal links should also be investigated. Moreover, additional constraints can distort the stress state of a plane model, for which analytical dependencies are obtained. The cases of the found kinematic variability will be valid for the truss and as part of the spatial construction, and the found formulas for the deflection will be an approximate estimate.

References

1. Kirsanov, M.N. Bending, torsion and asymptotic analysis of the cantilever bar. Magazine of Civil Engineering. 2014. No. 5(49). Pp. 37–43. (rus)
2. Salimov, M.S. The formula for deflection of a composite truss, loaded on the bottom flange. Science Almanac. 2017. No. 2-3(28). Pp. 272–274.
3. Smirnova, A.A., Rakhmatulina, A.R Analytical calculation of the displacement of the truss support. Science Almanac. 2017. No. 2-3(28). Pp. 275–278.
4. Hutchinson, R.G., Fleck, N.A. Microarchitectured cellular solids – the hunt for statically determinate periodic trusses. ZAMM Z. Angew. Math. Mech. 2005. No. 9(85). Pp. 607–617.
5. Hutchinson, R.G., Fleck, N.A. The structural performance of the periodic truss. Journal of the Mechanics and Physics of Solids. 2006. Vol. 54. No. 4. Pp. 756–782.
6. Astakhov, S. Vyvod formuly dlya progiba vneshne staticheski neopredelimoy ploskoy fermy pod deystviyem nagruzki v seredine proleta [The derivation of formula for deflection of statically indeterminate externally flat truss under load at midspan]. Construction and Architecture. 2017. Vol. 5. No. 2. Pp. 50–54. (rus)
7. Gorbunova, A.S., Lepetyukha, V.A. The formula for deflection of a composite truss loaded on the upper belt. Innovative science. 2017. Vol. 1. No. 3. Pp. 57–59.
8. Egorov, S.S. The inductive method of solving the problem of deflection of the symmetric core structures of complex shape in the system Maple for arbitrary number of panels. Science Almanac. 2017. No. 3-3(29). Pp. 254–257.
9. Smirnova, A.A., Rakhmatulina, A.R. Analytical calculation of the displacement of the truss support. Science Almanac. 2017. No. 2-3(28). Pp. 275–278.
10. Domanov, Ye.V. Analiticheskaya zavisimost progiba prostranstvennoy konsoli treugolnogo profilya ot chisla paneley [The analytical dependence of the deflection spatial console triangular profile of the number of panels]. Science Almanac. 2016. No. 6-2(19). Pp. 214–217. (rus)
11. Ershov, L.A. Formuly dlya rascheta deformatsiy piramidal'nogo kupola [Formulas for calculating deformations of the pyramidal dome]. Science Almamac. 2016. No. 11-2(25). Pp. 315–318. (rus)
12. Larichev, S.A. Induktivnyy analiz vliyaniya stroitel'nogo pod"yema na zhestkost' prostranstvennoy balochnoy fermy [Inductive analysis of the influence of the building lift

Литература

1. Кирсанов М.Н. Изгиб, кручение и асимптотический анализ пространственной стержневой консоли // Инженерно–строительный журнал. 2014. № 5(49). С. 37–43.
2. Салимов М.С. Формула для прогиба составной фермы, загруженной по нижнему поясу // Научный альманах. 2017. № 2-3(28). С. 272–274.
3. Смирнова А.А., Рахматулина А.Р. Аналитический расчет смещения опоры шпренгельной фермы // Научный альманах. 2017. № 2-3(28). С. 275–278.
4. Hutchinson R.G., Fleck N.A. Microarchitectured cellular solids – the hunt for statically determinate periodic trusses // ZAMM Z. Angew. Math. Mech. 2005. № 9(85). Pp. 607–617.
5. Hutchinson R.G., Fleck N.A. The structural performance of the periodic truss // Journal of the Mechanics and Physics of Solids. 2006. Vol. 54. № 4. Pp. 756–782.
6. Астахов С.В. Вывод формулы для прогиба внешне статически неопределимой плоской фермы под действием нагрузки в середине пролёта // Строительство и архитектура. 2017. Т. 5. № 2. С. 50–54.
7. Gorbunova A.S., Lepetyukha V.A. The formula for deflection of a composite truss loaded on the upper belt // Инновационная наука. 2017. Т. 1. № 3. С. 57–59.
8. Egorov S.S. The inductive method of solving the problem of deflection of the symmetric core structures of complex shape in the system Maple for arbitrary number of panels // Science Almanac. 2017. № 3-3(29). Pp. 254–257.
9. Smirnova A.A., Rakhmatulina A.R. Analytical calculation of the displacement of the truss support // Научный альманах. 2017. № 2-3(28). С. 275–278.
10. Доманов Е.В. Аналитическая зависимость прогиба пространственной консоли треугольного профиля от числа панелей // Научный альманах. 2016. № 6-2(19). С. 214–217.
11. Ершов Л.А Формулы для расчета деформаций пирамидального купола // Научный альманах. 2016. № 11-2(25). С. 315–318.
12. Ларичев С.А. Индуктивный анализ влияния строительного подъема на жесткость пространственной балочной фермы // Trends in Applied Mechanics and Mechatronics. 2015. Т. 1. С. 4–8.

on the rigidity of a spatial beam truss]. Trends in Applied Mechanics and Mechatronics. 2015. Vol. 1. Pp. 4–8. (rus)

13. Kirsanov, M.N. Analiticheskoe issledovanie zhestkosti prostranstvennoy staticheski opredelimoy fermy [Analytical Study on the Rigidity of Statically Determinate Spatial Truss]. Vestnik MGSU. 2017. Vol. 12. No. 2(101). Pp. 165–171. (rus)
14. Kirsanov, M.N. Analysis of the buckling of spatial truss with cross lattice. Magazine of Civil Engineering. 2016. No. 4. Pp. 52–58.
15. Kirsanov, M.N. Staticheskij analiz i montazhnaya skhema ploskoj fermy [Static analysis and mounting diagram of flat truss]. Vestnik gosudarstvennogo universiteta morskogo i rechnogo flota imeni admirala S.O. Makarova. 2016. No. 5(39). Pp. 61–68. (rus)
16. Kirsanov, M. N. Analiz usiliy i deformatsiy v korabel'nom shpangoute modeliruyemogo fermoy [Analysis of forces and deformations in the ship frame simulated by truss]. Vestnik Gosudarstvennogo universiteta morskogo i rechnogo flota imeni admirala S. O. Makarova. 2017. Vol. 9. No.3. Pp. 560–569. (rus)
17. Andersen, L.D. On edge–colourings of graphs. Mathematica Scandinavica. 1977. Vol. 40. No. 2. Pp. 161–175.
18. Baudon, O., Pilśniak, M., Przybyło, J., Senhaji, M., Sopena, É., Woźniak, M. Equitable neighbour–sum–distinguishing edge and total colourings. Discrete Applied Mathematics. 2017. Vol. 222. Pp. 40–53.
19. Venkateswarlu, A., Sarkar, A., Ananthanarayanan, S.M. On acyclic edge–coloring of complete bipartite graphs. Discrete Mathematics. 2017. Vol. 340. No. 3. Pp. 481–493.
20. Koršunov, D.; Ninčák, J. O rackracke gipergrafov [On the coloring of hypergraphs]. Kybernetika, 1976. Vol. 12. No. 1. Pp. 20–30. (rus)
21. Phelps, K.T., Rödl, V. On the algorithmic complexity of coloring simple hypergraphs and Steiner triple systems. Combinatorica. 1984. Vol. 4. No. 1. Pp. 79–88.
22. Kiyko, L.K. Analiticheskaya otsenka progiba arochnoy fermy pod deystviyem vetrovoy nagruzki [Analytical evaluation of deflection of arched trusses under the action of wind loads]. Nauchnyy vestnik. 2016. No. 1(7). Pp. 247–254. (rus)
23. Osadchenko, N.V. Analiticheskiye resheniya zadach o progibe ploskikh ferm arochnogo tipa [Analytical solutions of problems on the deflection of planar trusses of arch type]. Stroitel'naya mekhanika i konstruktsii. 2018. No. 1. Vol. 16. Pp. 12–33. (rus)
24. Tinkov, D.V. Comparative analysis of analytical solutions to the problem of truss structure deflection. Magazine of Civil Engineering. 2015. No. 5(57). Pp. 66–73. (rus)

13. Кирсанов М.Н. Аналитическое исследование жесткости пространственной статически определимой фермы // Вестник МГСУ. 2017. Т. 12. № 2(101). С. 165–171.
14. Кирсанов М.Н. Анализ прогиба фермы пространственного покрытия с крестообразной решеткой // Инженерно-строительный журнал. 2016. № 4(64). С. 52–58.
15. Кирсанов М.Н. Статический анализ и монтажная схема плоской фермы // Вестник Государственного университета морского и речного флота имени адмирала С. О. Макарова. 2016. № 5(39). С. 61–68.
16. Кирсанов М.Н. Анализ усилий и деформаций в корабельном шпангоуте моделируемого фермой // Вестник Государственного университета морского и речного флота имени адмирала С. О. Макарова. 2017. Т. 9. № 3. С. 560–569.
17. Andersen L.D. On edge–colourings of graphs. Mathematica Scandinavica. 1977. Vol. 40. № 2. Pp. 161–175.
18. Baudon O., Pilśniak M., Przybyło J., Senhaji M., Sopena É., Woźniak M. Equitable neighbour–sum–distinguishing edge and total colourings // Discrete Applied Mathematics. 2017. Vol. 222. Pp. 40–53.
19. Venkateswarlu A., Sarkar A., Ananthanarayanan S. M. On acyclic edge–coloring of complete bipartite graphs // Discrete Mathematics. 2017. Vol. 340. № 3. Pp. 481–493.
20. Коршунов А.Д., Нинчак Я. О раскраске гиперграфов // Kybernetika. 1976. Т. 12. № 1. С. 20–30.
21. Phelps K.T., Rödl V. On the algorithmic complexity of coloring simple hypergraphs and Steiner triple systems // Combinatorica. 1984. Vol. 4. № 1. Pp. 79–88.
22. Кийко Л.К. Аналитическая оценка прогиба арочной фермы под действием ветровой нагрузки // Научный вестник. 2016. № 1(7). С. 247–254.
23. Осадченко Н.В. Аналитические решения задач о прогибе плоских ферм арочного типа // Строительная механика и конструкции. 2018. Т. 1. № 16. С. 12–33.
24. Тиньков Д.В. Сравнительный анализ аналитических решений задачи о прогибе ферменных конструкций // Инженерно–строительный журнал. 2015. № 5(57). С. 66–73.

Mikhail Kirsanov,
+7(495)362-73-14; mpei2004@yandex.ru

Михаил Николаевич Кирсанов,
+7(495)362-73-14;
эл. почта: mpei2004@yandex.ru

doi: 10.18720/MCE.81.18

Water vapour by diffusion and mineral wool thermal insulation materials

Диффузионное влагопоглощение теплоизоляционных изделий и минеральной ваты

N.I. Vatin,
I.I. Pestryakov,
Sh.T. Sultanov*,
T. Ogidan,
Y.A. Yarunicheva,
A.P. Kiryushina,
Peter the Great St. Petersburg Polytechnic University, St. Petersburg, Russia

Д-р техн. наук, профессор Н.И. Ватин,
руководитель центра И.И. Пестряков,
аспирант Ш.Т. Султанов*,
студент О.Т. Огидан,
студент Ю.А. Яруничева,
студент А. Кирюшина,
Санкт-Петербургский политехнический университет Петра Великого, г. Санкт-Петербург, Россия

Key words: insulation; water vapour diffusion; humidity; polyisocyanurate; mineral wool; moisture content; water absorption; relative humidity; energy efficiency

Ключевые слова: изоляция; диффузионное влагопоглощение; влажность; полиизоцианурат; минеральная вата; влажность; влагопоглощение; относительная влажность

Abstract. This article is aimed at determining the absorption of moisture by diffusion of mineral wool and polyisocyanurate over a long-term period. The task of increasing the thermal insulation properties of enclosing structures is most relevant for the erection of new buildings or structures, as well as for the repair of existing. The method models operating conditions in which thermal insulation product absorb moisture from both sides at high relative humidity of air (100%) and pressure difference of water vapour over a long-term period. The moisture absorption by diffusion of mineral wool and polyisocyanurate were obtained after 28 days of exposure to temperature and pressure drop of water vapor. Significant changes in moisture content of mineral wool were observed. From the results obtained, it can be concluded that polyisocyanurate has a lesser absorption property of water vapor, which is an important attribute in its operation.

Аннотация. Повышение теплоизоляционных свойств ограждающих конструкций является одной из основных задач строительства на сегодняшний день. Метод, приведенный в данной статье, моделирует условия эксплуатации, при которых теплоизоляционный материал поглощает влагу с обеих сторон при высокой относительной влажности воздуха (100%) и разности давлений водяного пара в течение длительного периода времени. Было произведено сравнение диффузионного влагопоглощения образцов полиизоцианурата (PIR) и минеральной ваты в течение 28 суток. Результаты показали, что диффузионное влагопоглощение у теплоизоляционного материала из полиизоцианурата (PIR) значительно ниже, чем у теплоизоляционного материала из минеральной ваты, что имеет большое значение в ходе его эксплуатации.

1. *Introduction*

The demand for environmentally friendly and healthy products is steadily increasing. This also applies to building materials, which can have great effect on human health. It is not surprising that new environmental friendly construction materials including thermal insulation are still actively studied. Demand for thermal insulation materials is increasing due to the growing costs of energy resources. Obtaining natural and environmentally friendly thermal insulation materials has become a topical issue nowadays, when thermal insulation materials are being extensively used (Muizniece, 2016). The most important challenge in the building sector worldwide is the reduction of the energy consumptions. In 2010, buildings accounted for 32% of total global final energy use (equal to 117 hexaJoules), 19% of energy-related GHG emissions, 51% of global electricity consumption, 33% of black carbon emissions, and an eighth to a third of F-gasses emission according to different accounting conventions in F-gasses data [1]. Control of indoor climate systems, ventilation, heating and air conditioning systems usually implies a high energy and

Ватин Н.И., Пестряков И.И., Султанов Ш.Т., Огидан О.Т., Яруничева Ю.А., Кирюшина А. Диффузионное влагопоглощение теплоизоляционных изделий и минеральной ваты // Инженерно-строительный журнал. 2018. № 5(81). С. 183–192.

economic costs. For heat exchange between the flows of supply and exhaust air are typically used air-to-air heat exchangers. Heat exchangers produce a transfer of tangible (visible) energy due to temperature difference on the surfaces. However, after a long period, the temperature difference between the air flows in the air intake is usually reduced and as a consequence some of the energy becomes insignificant. Another typical energy-saving solution is the introduction of ventilated facades using external or internal air, for reduction of thermal loads [2]. The GHG emissions from the building sector more than doubled between 1970 and 2010, reaching nowadays a value around 10 GtCo2 eq/y (Naldi, 2017). In harsh climatic conditions, the use of thermal insulation in buildings is necessary and is gradually becoming a mandatory requirement in many countries particularly as energy becomes more precious and demand increases (A.Abdou). In this regard, the problem related to the search of technology for energy-efficient construction has become a vital one. It is necessary to introduce not only energy-efficient designs, but also to apply meters and energy-saving technologies that allow to achieve and save on normative indicators of heat energy consumption, the corresponding class assigned to the building [3].

The task of increasing the heat-insulating properties of enclosing structures is most relevant for the erection of new buildings or structures, as well as for the renovation of existing facilities. Thermal protective properties of the fence depend on the design solutions used in this construction materials, the operating conditions of the building. There are many ways to insulate buildings, the most common are insulation with fibrous structure and polymer insulation. Along with the traditional and well-developed materials in the construction industry, new thermal insulation materials are appearing on the market, the physical and mechanical characteristics of which are not fully understood. PIR also belongs to this material. In the technical characteristics of this material, indicated by the manufacturer, there is no such indicator, important from the point of view of thermos-physical properties of the material, as sorption humidity. The manufacturer indicates only the value of the thermal conductivity of the material in the dry state. Meanwhile, it is known that, depending on the level of humidity under operating conditions and the sorption properties of the thermal insulation material, its actual (operational) value of thermal conductivity can differ significantly from the experimental values in the dry state.

The thermal conductivity of insulation materials is greatly affected by their operating temperature and moisture content, yet limited information is available on the performance of insulating materials when subjected to actual climatic conditions. Many parameters should be considered when selecting thermal insulation, including cost, compression strength, water vapor absorption and transmission and, most importantly, the k-value of the material when considering thermal performance of buildings and relevant energy conservation measures [2]. Together with heat transfer modes, phase changes of vapor moisture, although not strictly an energy transfer mechanism, should also be considered in heat transfer analysis since state changes absorb and release large quantities of heat [9]. This means that both vapour flow and moisture absorption are important, and they typically are more critical in insulating materials with open cell structures than with closed cell ones (Naldi, 2017).

The way thermal insulating materials resist to heat flow depends on microscopic cells in which air or other gasses are trapped. Thermal insulating materials resist heat flow as a result of the countless microscopic dead air-volumes. In fact, the thermal resistance of the air entrapped within insulating materials is mainly responsible for their low thermal conductivity. Meanwhile, creating small cells or a closed cell structure within the thermal insulation across which the temperature difference is not large, reduces the radiation heat transfer mode (Naldi, 2017).

Typically, air-based insulating materials do not exceed the thermal resistance of still air. However, some foam insulations such as the polyurethane encapsulate fluorocarbon gas instead of air within the insulation cells to obtain higher thermal resistance (R-value) than the air (Naldi, 2017).

PIR plate based on polyisocyanurate, as the thermal insulation material with the lowest the indicator of heat conductivity, has been extensively used in the USA and Western Europe for a long time, more than 10 years (Nastya). In North America, the roof insulation market shows that polyisocyanurate is the most widely used roof insulation, covering more than 50 % of all commercial new or re-roofing applications. This is probably due to the often nominal double of thermal resistance of the polyisocyanurate when compared to fiberglass or rock wool insulation. These last products have generally a larger market share for vertical building elements and in several European countries (Naldi, 2017).

Due to high performance indicators, the insulation is a considerable interest both for developers wishing to improve the energy efficiency of the constructed buildings, and for private clients interested in the most effective heat insulating material (Nastya). Many benefits justify the adoption of thicker layers of thermal insulation in buildings. In fact, the use of thermal insulation in buildings helps in reducing the reliance on mechanical air-conditioning systems to realize comfortable buildings, and it allows to save energy by reducing the heat flux through the building envelope. Meanwhile, the reduced energy demand achieved by using more effective thermal insulating layers also reduces the needed HVAC equipment. The thermal insulation in building enclosure extends the periods of indoor thermal comfort, especially between seasons, and by keeping buildings with smaller temperature fluctuations, it helps in preserving the integrity of building structures, increasing their lifetime (Naldi, 2017).

The basis for the preparation of polyisocyanurate is methylene diphenyl diisocyanate, which at a high temperature and in the presence of catalysts is able to react with itself, partially transforming into a tri-isocyanate-isocyanurate chemical compound. It is a rigid molecule of the ring structure, which is positively reflected on the physical properties of the final product.

This high-tech insulation polyisocyanurate (abbreviated – PIR) – a close a relative of a well-known polyurethane foam (PUR). Polyurethane possesses exceptional properties such as the high resistance to open fire (group combustibility G1) and low thermal conductivity (in the dry state) among the polymers is not more than 0.024 W/m^2. In addition, the PIR plate does not absorb moisture and is distinguished by a high resistance to compression.

At present, a number of articles have been written on the sorption humidity of insulating materials with a fibrous structure showing a change in this parameter over time during operation, which leads to its increase [4], or reflecting the efficiency of using multi-layered enclosing structures with mineral wool insulation in comparison with with an unheated wall, in which the sorption characteristics are greater [5]. For polymer insulation, foam polyisocyanurate, only the main characteristics characterizing the material have been studied and determined, such as: low flammability (G1), high heat-saving capacity, lightness and strength [6, 7].

Many of the works are related to the determination of the thickness of thermal insulation by calculating the temperature fields and aimed at improving the individual bearing elements of the enclosing structure [8].

The purpose of this work was to determine the thermo-physical properties of slabs from foam polyisocyanurate with soft liners (PIR) with a density of between 30 and 45 kg/m_3 and analogues. plates from mineral wool ROCKWOOL Facade Batts, density ρ = 130 kg/m_3

To achieve this goal, it was necessary to solve the following tasks:

1. Using experimental methods based on National Standards of Russia GOST and GOST EN methods, to determine physical and mechanical characteristics of two types of insulation.

2. Analyze the results and obtain the main evidence base for the correction of normative documents in the field of heat-insulation materials. At this stage, experimental studies were carried out to determine water absorption, diffusion moisture absorption for a long time, sorption humidity and thermal conductivity of the samples.

2. Methods

The test methods were selected in accordance with the work program presented by NAPPAN-Russian Association of Manufactures of Polyurethane Sandwich Panels.

The method simulates the operating conditions under which the samples absorb moisture from both sides at high relative humidity, approximately 100 % and the difference in water vapor pressure over a long period of time, from water to the form. The sample is subjected to a temperature and pressure drop of water vapor for 28 days while maintaining the water temperature (50 ± 1) °C and the temperature on the opposite side of the sample (1 ± 0.5) °C.

Materials:

- plates of mineral wool with a thickness of 50 mm;
- PIR plates 50 mm thick with double-sided lining aluminum foil 50 μm thick;
- PIR plates with a thickness of 50 mm without lining.

The experiments were carried out according to the requirements of the National Standard of Russia EN 12088-2011 Thermal insulating products in building applications. Method for determination of long-term moisture absorption by diffusion.

Sizes of samples were measured in accordance with EN 12085. A panel of mineral wool was cut using an insulation knife, in order to obtain the required lengths and widths equal to 500 and 500 mm, respectively. Samples were weighed to the nearest 0.1 g to determine the initial mass. The sample was then placed on the frame of the container. Since the sample was lined on both sides, experiments will be proceeded with a lined surface, with either side of the sample being placed on the frame facing upwards. The lower edge of the sample is sealed around the perimeter of the frame. The width of the sealant was equal to 10 mm. A thermally insulated cooling plate is placed on the upper surface of the sample.

The sample is exposed to temperature level and pressure drop of water vapor for 28 days, while maintaining the water temperature (50 ± 1) °C and the temperature on the opposite side of the sample (1 ± 0.5) °C. Every 7 days the sample is turned over. After 28 days, the sample is removed from the container and the water with its surface is removed with a paper or other suitable tissue. The sample is weighed and the final mass is determined.

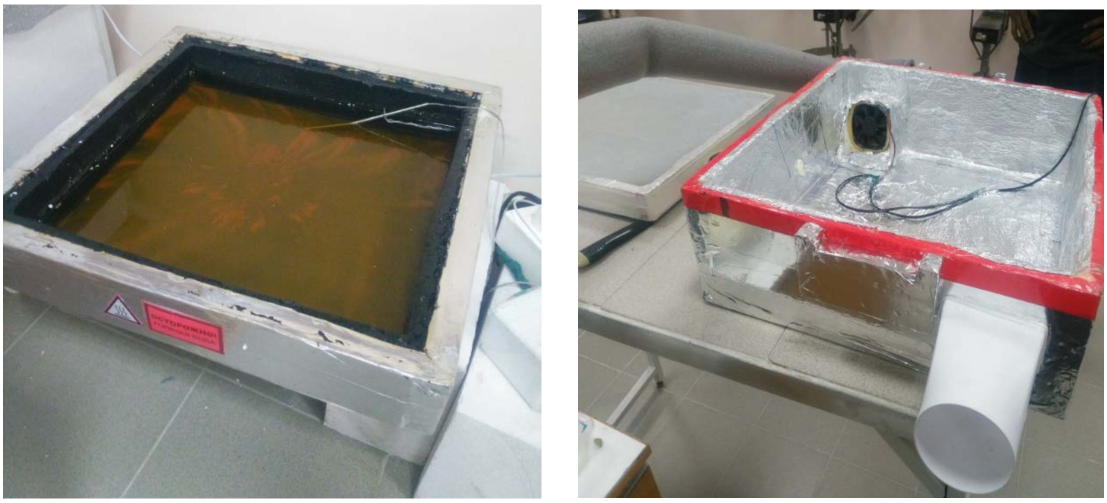

Figure 1. Heating plate with water and Cooling plate

A panel of mineral wool was cut using an insulation knife, in order to obtain the required lengths and widths equal to 500 and 500 mm, respectively. The size and shape of the specimens were determined according to the standard EN 12085. Linear dimensions of the PIR panels were received in prefabricated sizes of 500 and 500 mm. The apparatus for providing hot air, i.e. the hot disk, does not require particular restrictions regarding the shape but must be capable of heating the container with water at a constant temperature of (50 ± 1) °C: for this reason, a thermostat was connected to regulate the temperature inside the container.

The samples were conditioned for at least 6 hours at a temperature of (23 ± 5) °C before the test in a climatic chamber. In case of disagreement, the samples were kept at a temperature of (23 ± 2) °C and relative air humidity (50 ± 5) % for the time specified in the standard, and in its absence – in the technical conditions for the product of a particular type, but not less than 6 h. The samples were then weighed to an accuracy of 0.1 g to determine the initial mass (m0). A thermally insulated cooling plate is then placed above the upper surface of the sample to subject the sample to a lower temperature as a simulation of the winter period. Figure 1 shows a picture of the cooling plate with the sample thermally insulated to prevent air from escaping and support a balanced temperature and humidity conditions. On the other hand, the opposite side of the sample is placed in a thermally insulated container holding with water. Temperature in the container is controlled by a thermostat regulator at 50 °C. The sample is subjected to a temperature and differential pressure of water vapor for 28 days while maintaining the water temperature (50 ± 1) °C and the temperature on the opposite side of the sample (1 ± 0.5) °C. The sample is turned in the opposite direction every 7 days. After 28 days, the sample is removed from the container and water is removed from its surface with a paper or other suitable tissue. The sample is weighed and the mass after 28 days (mD) is obtained. For each sample, the amount of absorbed moisture is estimated by mass W_{dp} in kg/m_2 or by volume W_{dv} in percentage.

Figure 2 shows a flowchart scheme of the experiment to obtain the long-term moisture absorption by diffusion.

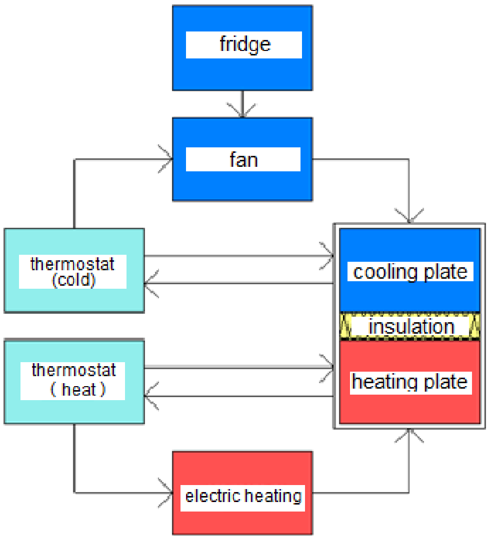

Figure 2. Flowchart scheme of the experiment

The thickness of the samples is equal to 50 mm for mineral wool and PIR (Table 1). Figure 5 shows a picture of the investigated samples.

In a second stage, the same samples were conditioned by setting temperature at (23 ± 5) °C and relative humidity at (50 ± 5) % under environmental conditions for the time necessary to reach the weight stabilization, in order to obtain moist samples.

Figure 3. Cooling plate with mineral wool

Water content (WC) was measured using the gravimetric method by means of Equation (1):

$$WC = (Ws - Wd)/Wd \cdot 100\% \qquad (1)$$

where Ws and Wd are the weights of the examined and of the dried samples, respectively. A precision scale with a graduation of 0.01 g was used to measure weights.

Measurements of water vapour diffusion were performed on samples after different number of days for one of the PIR panels. In particular, four stages of measurements were performed: after 7 days, after 14 days, after 21 days and after 28 days.

In view of the fact that the samples were received with a delay, to date only one PIR sample has been exposed to temperature and a pressure drop of water vapor for 28 days. Table 2 shows the amount of moisture absorbed after 28 days.

Figure 4. Installation for testing in accordance with GOST EN 12088-2011

Sizes of samples were measured in accordance with EN 12085. Samples were weighed to the nearest 0.1 g to determine the initial mass. The sample was then placed on the frame of the container. Since the sample was lined on both sides, experiments will be proceeded with a lined surface, with either side of the sample being placed on the frame facing upwards. The lower edge of the sample is sealed around the perimeter of the frame. The width of the sealant was equal to 10 mm. A thermally insulated cooling plate is placed on the upper surface of the sample.

The sample is exposed to temperature level and pressure drop of water vapor for 28 days, while maintaining the water temperature (50 ± 1) °C and the temperature on the opposite side of the sample (1 ± 0.5) °C. Every 7 days the sample is turned over. After 28 days, the sample is removed from the container and the water with its surface is removed with a paper or other suitable tissue. The sample is weighed and the final mass is determined.

3. Results and Discussion

In view of the fact that the samples were received with a delay, to date only one PIR sample has been exposed to temperature and a pressure drop of water vapour for 28 days. Table 1 shows the amount of moisture absorbed after 28 days.

Table 1. Moisture absorption after 28 days

Sample	A, m^2	D, m	m_0, kg	m_d, kg	W_{dv}, %
PIR 1.1	0.25	0.05	0.53	0.563	0.3
PIR 1.2	0.25	0.05	0.52	0.566	0.4
MW 1	0.25	0.05	1.66	3.864	17.6
MW 2	0.25	0.05	1.69	3.622	15.5

A similar result is expected after 28 days. It is also predicted that mineral wool panels will absorb more moisture than both PIR panels.

Previously, no one has tested the diffusion moisture absorption of samples from polyisocyanurate. The obtained results confirm the presence of the dependence of the vapour content of thermal insulation materials of PIR and mineral wool on the relative thermal properties of the material. PIR with polymer structure of closed pores absorbs less moisture. MW with fibrous structure absorbs more moisture. Absolute values of the moisture absorption of the MW significantly exceed the analogous values for mineral wool by about 50 times

4. Conclusion

The obtained results testify to the differences in physical and thermal properties of the materials. It is shown that the PIR is more reliable than mineral wool by this indicator. However, due to the difference in structure of this material compared with mineral wool, it is not possible to make a final conclusion about which of the materials considered is more efficient in heat-insulating structures without additional studies. For a final conclusion, it is necessary to conduct a study to determine the thermal conductivity of the PIR in the wet state and compare these values with the analogous values for mineral wool or other competing materials. This will be used in the further of this material especially during operating conditions. The increase in the thermal insulation characteristics of the materials of the enclosing structures also makes it possible to avoid the costs of upgrading the sources of thermal energy.

5. Acknowledgements

Authors would like to acknowledge the support of Innovative Technologies Laboratory at the Institute of Civil Engineering. This work was carried out within the framework of the MARUEEB Erasmus + project 561890-EPP-1-2015-1-IT-EPPKA2-CBHE-JP.

References

1. Muizniece, I., Blumberga, D. Thermal Conductivity of Heat Insulation Material Made from Coniferous Needles with Potato Starch Binder. Energy Procedia. 2016. Vol. 95. Pp. 324–329.
2. Petritchenko, M.R., Nemova, D.V., Kotov, E.V., Tarasova, D.S, Sergeev, V.V. Ventilated facade integrated with the HVAC system for cold climate. Magazine of Civil Engineering. 2018. No. 1. Pp. 47–58. doi: 10.18720/MCE.77.5
3. Abdou, A., Budaiwi, I. The variation of thermal conductivity of fibrous insulation materials under different levels of moisture content. Construction and Building Materials. 2013. № 43. Pp. 533–544.
4. Anoprieva, I.L. Vybor effektivnogo uteplitelya dlya proektiruemogo zdaniya [The choice of effective insulation for the projected building]. Proceedings of VIII Mezhdunarodnogo nauchno–prakticheskogo konkursa. 2017. Penza: Izdatelstvo: "Nauka i Prosveshcheniye". (rus)
5. Nik, V.M., Kalagasidis, A.S., Kjellström, E. Assessment of hygrothermal performance and mould growth risk in ventilated attics in respect to possible climate changes in Sweden. Building and Environment. 2012. No. 55. Pp. 96–109.
6. Vereecken, E., Roels S. Capillary Active Interior Insulation Systems for Wall Retrofitting: A More Nuanced Story. International Journal of Architectural Heritage. 2016. Vol. 10. No. 5. Pp. 558–569.
7. Zach, J., Hroudová, J., Brožovský, J., Krejza, Z., Gailius, A. Development of Thermal Insulating Materials on Natural Base for Thermal Insulation Systems. Procedia Engineering. 2013. No. 57. Pp. 1288–1294.
8. Petritchenko, M.R., Kotov, E.V., Nemova, D.V., Tarasova, D.S., Sergeev, V.V. Numerical simulation of ventilated facades under extreme climate conditions. Magazine of Civil Engineering. 2018. No. 1. Pp. 130–140. doi: 10.18720/MCE.77.12.
9. D'Alessandro, F., Baldinelli, G., Bianchi, F., Sambuco, S., Rufini, A. Experimental assessment of the water content influence on thermo–acoustic performance of building insulation materials. Construction and Building Materials. 2018. No. 158. Pp. 264–274.
10. Hroudová, J., Sedlmajer, M., Pařílková, J., Zach, J. Laboratory testing of developed thermal insulation plasters on pillars built from masonry bricks. Procedia Engineering. 2017. No. 172. Pp. 377–384.
11. Gorshkov, A.S., Vatin, N.I., Datsuk, T.A., Bezrukov, A.Yu., Nemova, D.V., Käkelä, P., Viitanen, A. Album of technical

Литература

1. Muizniece I., Blumberga D. Thermal Conductivity of Heat Insulation Material Made from Coniferous Needles with Potato Starch Binder // Energy Procedia. 2016. Vol. 95. Pp. 324–329.
2. Петриченко М.Р., Немова Д.В., Котов Е.В., Тарасова Д.С., Сергеев В.В. Вентилируемые фасады, интегрированные с инженерными системами здания для холодного климата // Инженерно-строительный журнал. 2018. № 1(77). С. 47–58. doi: 10.18720/MCE.77.5
3. Abdou A., Budaiwi I. The variation of thermal conductivity of fibrous insulation materials under different levels of moisture content // Construction and Building Materials. 2013. № 43. Pp. 533–544.
4. Аноприева И.Л. Выбор эффективного утеплителя для проектируемого здания // Сборник статей VIII Международного научно–практического конкурса: в 2 частях. Пенза: Издательство: "Наука и Просвещение" (ИП Гуляев Г.Ю.), 2017.
5. Nik V.M., Kalagasidis A.S., Kjellström E. Assessment of hygrothermal performance and mould growth risk in ventilated attics in respect to possible climate changes in Sweden // Building and Environment. 2012. № 55. Pp. 96–109.
6. Vereecken E., Roels S. Capillary Active Interior Insulation Systems for Wall Retrofitting: A More Nuanced Story // International Journal of Architectural Heritage. 2016. Vol. 10. № 5. Pp. 558–569.
7. Zach J., Hroudová J., Brožovský J., Krejza Z., Gailius A. Development of Thermal Insulating Materials on Natural Base for Thermal Insulation Systems // Procedia Engineering. 2013. № 57. Pp. 1288–1294.
8. Петриченко М.Р., Котов Е.В., Немова Д.В., Тарасова Д.С., Сергеев В.В. Численное моделирование вентилируемых фасадов в экстремальных климатических условиях // Инженерно-строительный журнал. 2018. № 1(77). С. 130–140.
9. D'Alessandro F., Baldinelli G., Bianchi F., Sambuco S., Rufini A. Experimental assessment of the water content influence on thermo–acoustic performance of building insulation materials // Construction and Building Materials. 2018. № 158. Pp. 264–274.
10. Hroudová J., Sedlmajer M., Pařílková J., Zach J. Laboratory testing of developed thermal insulation plasters on pillars built from masonry bricks // Procedia Engineering. 2017. № 172. 377 – 384.

solutions for the application of polyurethane foam thermal insulation products in construction of residential, public and industrial buildings. Construction of Unique Buildings and Structures. 2014. No. 5. Pp. 71–441.

12. Maia, J., Ramos Nuno, M.M., De Freitas, V.P., Sousa, A. Laboratory tests and potential of thermal insulation plasters. Energy Procedia. 2015. No. 78. Pp. 2724–2729.
13. Saber, H.H., Swinton, M.C., Kalinger, P., Paroli, R.M. Long–term hygrothermal performance of white and black roofs in North American climates. Building and Environment. 2012. No. 50. Pp. 141–154.
14. Latif, E., Tucker, S., Ciupala, M.A, Wijeyesekera, D.C., Newport, D.J., Pruteanu, M. Quasi steady state and dynamic hygrothermal performance of fibrous Hemp and Stone Wool insulations: Two innovative laboratory based investigations. Building and Environment. 2016. No. 95. Pp. 391–404.
15. Cardoso, G.T., Neto, S.C., Vecchia, F. Rigid foam polyurethane (PU) derived from castor oil (Ricinus communis) for thermal insulation in roof systems. Frontiers of Architectural Research. 2012. No. 1. Pp. 348–356.
16. Pescari, S., Tudor, D., Tölgyi, S., Maduta, C. Study Concerning the Thermal Insulation Panels with Double–side Anti–condensation Foil on the Exterior and Polyurethane Foam or Polyisocyanurate on the Interior. Key Engineering Materials. 2015. Vol. 660. Pp. 244–248.
17. Russian State Standard GOST EN 12088–2011 Thermal insulating products in building applications. Method for determination of long–term moisture absorption by diffusion.
18. Russian State Standard GOST EN 12085–2011 Thermal insulating products for applications in building. Methods for determination of linear dimensions of test specimens.
19. Stockton, G.R. The case for using a sacrificial layer of absorbent insulation in the design of flat and low–sloped roofing. Proceedings of SPIE – The International Society for Optical Engineering. 2013. Vol. 8705. No. 870504.
20. Hejnaa, A., Kirpluks, M., Kosmela, P., Cabulis, U, Haponiuk, J, Piszczyka, L. The influence of crude glycerol and castor oil–based polyol on the structure and performance of rigid polyurethane–polyisocyanurate foams. Industrial Crops and Products. 2017. No. 95. Pp. 113–125.
21. Kiryudcheva, A.E, Nemova, D.V. Energy service contracts in Russia and in the European Union. Construction of Unique Buildings and Structures. 2017. No. 10(61). Pp. 7–21. (rus)
22. Gafiyatullina, N.M., Kostenko, V.A., Petrochenko, M.V., Strelets, K.I. European Thermal Insulation Technology Implementation to Green Building Concept. Construction of Unique Buildings and Structures. 2017. No. 5(56). Pp. 47–55.
23. Sulakatko, V., Lill, I., Liisma, E. Analysis of on–site construction processes for effective external thermal insulation composite system (ETICS) installation. Procedia Economics and Finance. 2015. Vol. 21. Pp. 297–305.
24. Green Public Procurement – Thermal Insulation Technical Background Report. Brussels: European Commission. 2010. Pp. 42.
25. Burns, S.B., Singh, S.N., Bowers, J.D. The influence of temperature on compressive properties and dimensional stability of rigid polyurethane foams used in construction. Journal of Cellular Plastics. 1998. Vol. 34. No. 1. Pp. 18–37.
26. Zhang, Z., Ashida, K. Amide–modified polyisocyanurate foams having high thermal stability. Journal of Cellular Plastics. 1997. Vol. 33(5). Pp. 487–500.
27. Vatin, N.I., Nemova, D.V., Rymkevich, P.P., Gorshkov, A.S. Vliyaniye urovnya teplovoy zashchity ograzhdayushchikh konstruktsiy [The effect of the thermal

11. Горшков А.С., Ватин Н.И., Дацюк Т.А., Безруков А.Ю., Немова Д.В., Käkelä P., Viitanen A. Альбом технических решений по применению теплоизоляционных изделий из пенополиуретана в строительстве жилых, общественных и промышленных зданий. АТР – СПУ – 02 – 14: материалы для проектирования (издание второе, переработанное и дополненное) // Строительство уникальных зданий и сооружений. 2014. № 5. С. 71–441.
12. Maia J., Ramos Nuno M. M., De Freitas V. P., Sousa A. Laboratory tests and potential of thermal insulation plasters // Energy Procedia. 2015. № 78. С. 2724–2729.
13. Saber H.H., Swinton M.C., Kalinger P., Paroli R.M. Long–term hygrothermal performance of white and black roofs in North American climates // Building and Environment. 2012. № 50. С. 141–154.
14. Latif E., Tucker S., Ciupala M.A, Wijeyesekera D.C., Newport D.J., Pruteanu M. Quasi steady state and dynamic hygrothermal performance of fibrous Hemp and Stone Wool insulations: Two innovative laboratory based investigations // Building and Environment. 2016. № 95. Pp. 391–404.
15. Cardoso G.T., Neto S.C., Vecchia F. Rigid foam polyurethane (PU) derived from castor oil (Ricinus communis) for thermal insulation in roof systems // Frontiers of Architectural Research. 2012. № 1. Pp. 348–356.
16. Pescari S., Tudor D., Tölgyi S., Maduta C. Study Concerning the Thermal Insulation Panels with Double–side Anti–condensation Foil on the Exterior and Polyurethane Foam or Polyisocyanurate on the Interior // Key Engineering Materials. 2015. Vol. 660. Pp. 244–248.
17. ГОСТ EN 12088–2011: Изделия теплоизоляционные, применяемые в строительстве. Метод определения диффузионного влагопоглощения в течение длительного времени.
18. ГОСТ EN 12085–2011: Изделия теплоизоляционные, применяемые в строительстве. Методы определения линейных размеров образцов, предназначенных для испытаний.
19. Stockton G.R. The case for using a sacrificial layer of absorbent insulation in the design of flat and low–sloped roofing // Proceedings of SPIE – The International Society for Optical Engineering. 2013. Vol. 8705. № 870504.
20. Hejnaa A., Kirpluks M., Kosmela P., Cabulis U., Haponiuk J., Piszczyka L. The influence of crude glycerol and castor oil–based polyol on the structure and performance of rigid polyurethane–polyisocyanurate foams // Industrial Crops and Products. 2017. № 95. Pp. 113–125.
21. Кирюдчева А. Е., Немова Д.В., Энергосервисные контракты в России и в Европейском Союзе // Строительство уникальных зданий и сооружений. 2017. № 10(61). С. 7–21.
22. Гафиятуллина Н.М., Костенко В.А., Петроченко М.В., Стрелец К.И. Реализация европейской теплоизоляционной технологии в концепции "Зелёного строительства" // Строительство уникальных зданий и сооружений. 2017. № 5(56). С. 47–55.
23. Sulakatko V., Lill I., Liisma E. Analysis of on–site construction processes for effective external thermal insulation composite system (ETICS) installation // Procedia Economics and Finance. 2015. Vol. 21. Pp. 297–305.
24. Green Public Procurement – Thermal Insulation Technical Background Report. Brussels: European Commission. 2010. 42 p.
25. Burns S.B., Singh S.N., Bowers J.D. The influence of temperature on compressive properties and dimensional stability of rigid polyurethane foams used in construction // Journal of Cellular Plastics. 1998. Vol. 34. № 1. Pp. 18–37.

protection level of the building envelopes on the magnitude of heat losses in the building]. Magazine of Civil Engineering. 2012. No. 8. Pp. 4–14. (rus).

28. Barreira, E., de Freitas, V.P. External Thermal Insulation Composite Systems: Critical Parameters for Surface Hygrothermal Behaviour. Advances in Materials Science and Engineering. 2014. Pp. 1–16.
29. Spiridonova, T.I., Kurasova, E.V., Duvanova, I.A., Vilinskaya, A.O. Energy efficiency heating installation of country house in Northern–East region. Construction of Unique Buildings and Structures. 2013. No. 7. Pp. 133–140.
30. Papadopoulos, A.M., Giama, E. Environmental performance evaluation of thermal insulation materials and its impact on the building. Building and Environment. 2007. No. 42. Pp. 2178–2187.
31. Russian State Standard SP 50.13330.2012 Thermal protection of buildings. The updated edition of SNiP 23–02–2003.
32. Russian State Standard SP 131.13330.2012 Building climatology. The updated edition of SNiP 23–01–99*.
33. Russian State Standard GOST 30494–2011 Residential and public buildings. Microclimate parameters in the premises.
34. Russian State Standard GOST R 54851–2011 Construction building envelope heterogeneous. The calculation of the reduced thermal resistance.
35. Anikina, I.D., Sergeyev, V.V., Amosov, N.T., Luchko, M.G. Use of heat pumps in turbogenerator hydrogen cooling systems at thermal power plant. International Journal of Hydrogen Energy. 2017. Vol. 42(1). Pp. 636–642. doi: 10.1016/j.ijhydene.2016.04.256
36. Kostenko, V.A., Gafiyatullina, N.M., Zulkarneev, G., Gorshkov, A.S. Solutions to Improve the Thermal Protection of the Administrative Building. MATEC Web of Conferences. 2016. No. 73.
37. Startsev, S.A. Analiz prichin neblagopoluchnogo sostoyaniya podvalov v Sankt-Peterburge [Analysis of the causes of the unfavorable state of basements in St. Petersburg]. Magazine of Civil Engineering. 2009. No. 2. Pp. 31–42. (rus)
38. Csoknyai, T., Hrabovszky–Horváth, S. Building stock characteristics and energy performance of residential buildings in Eastern-European countries. Energy and Buildings. 2016. No. 132. Pp. 39–52.
39. Sassine, E., Younsi, Z. Frequency domain regression method to predict thermal behaviour of brick wall of existing buildings. Applied Thermal Engineering. 2017. No. 114. Pp. 24–35.
40. Asdrubali, F., Ferracuti, B. A review of structural, thermo–physical, acoustical, and environmental properties of wooden materials for building applications. Building and Environment. 2017. No. 114. Pp. 307–322.
41. Moradias, P.A. Experimental study on hygrothermal behaviour of retrofit solutions applied to old building walls. Construction and Building Materials. 2012. No. 35. Pp. 864–873.
42. Slepchenko, P.D., Sinyakov, L.N., Influence of temperature and humidity conditions on building structures of basements. Construction of Unique Buildings and Structures. 2017. No. 3(54). Pp. 18–34. (rus)
43. Vilches, A., Garcia–Martinez, A. Life cycle assessment (LCA) of building refurbishment: A literature review. Energy and Buildings. 2016. No. 135. Pp. 286–301.
44. Csoknyai, T., Hrabovszky–Horváth, S. Building stock characteristics and energy performance of residential buildings in Eastern–European countries. Energy and Buildings. 2016. No. 132. Pp. 39–52.

26. Zhang Z., Ashida K. Amide–modified polyisocyanurate foams having high thermal stability // Journal of Cellular Plastics. 1997. № 33(5). Pp. 487–500
27. Ватин Н.И., Немова Д.В., Рымкевич П.П., Горшков А.С. Влияние уровня тепловой защиты ограждающих конструкций на величину потерь тепловой энергии в здании // Инженерно–строительный журнал. 2012. № 8. С. 4–14.
28. Barreira E., de Freitas V.P. External Thermal Insulation Composite Systems: Critical Parameters for Surface Hygrothermal Behaviour // Advances in Materials Science and Engineering. 2014. Pp. 1–16.
29. Спиридонова Т. И., Курасова Е. В., Дуванова И. А., Вилинская А. О. Эффективная тепловая установка для загородного дома СевероЗападного региона России // Строительство уникальных зданий и сооружений. 2013. № 7. С. 133–140.
30. Papadopoulos A.M., Giama E. Environmental performance evaluation of thermal insulation materials and its impact on the building // Building and Environment. 2007. № 42. Pp. 2178–2187.
31. СП 50.13330.2012 Тепловая защита зданий. Актуализированная редакция СНиП 23–02–2003.
32. СП 131.13330.2012 Строительная климатология. Актуализированная редакция СНиП 23–01–99*.
33. ГОСТ 30494–2011. Здания жилые и общественные. Параметры микроклимата в помещениях.
34. ГОСТ Р 54851–2011. Конструкции строительные ограждающие неоднородные. Расчет приведенного сопротивления теплопередаче.
35. Anikina I.D., Sergeyev V.V., Amosov N.T., Luchko M.G. Use of heat pumps in turbogenerator hydrogen cooling systems at thermal power plant. International Journal of Hydrogen Energy. 2017. Vol. 42(1). Pp. 636–642. doi: 10.1016/j.ijhydene.2016.04.256
36. Kostenko V.A., Gafiyatullina N.M., Zulkarneev G., Gorshkov A.S. Solutions to Improve the Thermal Protection of the Administrative Building // MATEC Web of Conferences. 2016. № 73.
37. Старцев С.А. Анализ причин неблагополучного состояния подвалов в Санкт-Петербурге // Инженерно-строительный журнал. 2009. № 2. С. 31–42.
38. Csoknyai T., Hrabovszky–Horváth S. Building stock characteristics and energy performance of residential buildings in Eastern–European countries // Energy and Buildings. 2016. № 132. Pp. 39–52.
39. Sassine E., Younsi Z. Frequency domain regression method to predict thermal behaviour of brick wall of existing buildings // Applied Thermal Engineering. 2017. № 114. Pp. 24–35.
40. Asdrubali F., Ferracuti B. A review of structural, thermo–physical, acoustical, and environmental properties of wooden materials for building applications // Building and Environment. 2017. № 114. Pp. 307–322.
41. Moradias P.A. Experimental study on hygrothermal behaviour of retrofit solutions applied to old building walls. Construction and Building Materials. 2012. № 35. Pp. 864–873.
42. Слепченко П.Д., Синяков Л.Н., Влияние температурно-влажностного режима на строительные конструкции подвалов зданий старого фонда Санкт-Петербурга. Строительство уникальных зданий и сооружений. 2017. № 3(54). С. 18–34.
43. Vilches A., Garcia–Martinez A. Life cycle assessment (LCA) of building refurbishment: A literature review // Energy and Buildings. 2016. № 135. Pp. 286–301.
44. Csoknyai T., Hrabovszky–Horváth S. Building stock characteristics and energy performance of residential

45. Burtseva, M.A. Mednikova, Ye.A. Sendvin–paneli na osnove penopoliizotsianura i mineralnoy vaty [Sandwich panels based on polyisocyanure foam and mineral wool]. Proceedings of 5–oy mezhdunarodnoy nauchno–prakticheskoy konferentsii. Moscow: Izd–vo Nauka i praktika, 2017. Pp. 44–46. (rus)
46. Mizyuryayev, S.A., Zhigulina, A.Yu., Ganechkina, K.V. Traditsii i innovatsii v stroitelstve i arkhitekture [Traditions and innovations in construction and architecture]. Sbornik statey. Samarskiy gosudarstvennyy tekhnicheskiy universitet. Samara: Izd–vo Samarskiy gosudarstvennyy arkhitekturno–stroitelnyy, 2017. Pp. 112. (rus)
47. Igokhina, Ye.O. Sravnitelnyy analiz samykh populyarnykh utepliteley v stroitelstve [Comparative analysis of the most popular heaters in construction]. Zhurnal kolomenskogo instituta (filiala) federalnogo gosudarstvennogo byudzhetnogo obrazovatelnogo uchrezhdeniya vysshego professionalnogo obrazovaniya «Moskovskiy gosudarstvennyy mashinostroitelnyy universitet (MAMI)». 2016. No. 3. Pp. 7–11. (rus)

buildings in Eastern–European countries // Energy and Buildings. 2016. № 132. Pp. 39–52.
45. Бурцева М.А. Медникова Е.А. Сэндвин–панели на основе пенополиизоцианура и минеральной ваты // Материалы 5–ой международной научно–практической конференции. Москва: Изд–во Наука и практика, 2017. С. 44–46.
46. Мизюряев С.А., Жигулина А.Ю., Ганечкина К.В. Традиции и инновации в строительстве и архитектуре // Сборник статей. Самарский государственный технический университет. Самара: Изд–во Самарский государственный архитектурно–строительный, 2017. С. 112.
47. Игохина Е.О. Сравнительный анализ самых популярных утеплителей в строительстве // Журнал коломенского института (филиала) федерального государственного бюджетного образовательного учреждения высшего профессионального образования «Московский государственный машиностроительный университет (МАМИ)», 2016. № 3. С. 7–11.

Nikolai Vatin,
+7(921)964-37-62; vatin@mail.ru

Igor Pestryakov,
+7(812)535-6334; iscvisota@mail.ru

Shukhrat Sultanov,*
+7(905)212-31-13; sultanov.sht@edu.spbstu.ru

Olamipe Timothy Ogidan,
+7(911)096-77-45; ogidano@gmail.com

Yuliya Yarunicheva,
+7(911)231-49-77; julija.jarunicheva@gmail.com

Anastasia Kiryushina,
+7(921)927-77-90; nastyakik97@mail.ru

Николай Иванович Ватин,
+7(921)964-37-62; эл. почта: vatin@mail.ru

Игорь Иванович Пестряков,
+7(812)535-63-34; эл. почта: iscvisota@mail.ru

Шухрат Тахирович Султанов,*
+7(905)212-31-13;
эл. почта: sultanov.sht@edu.spbstu.ru

Оламипе Тимоти Огидан,
+7(911)096-77-45;
эл. почта: ogidano@gmail.com

Юлия Алексеевна Яруничева,
+7(911)231-49-77;
эл. почта: julija.jarunicheva@gmail.com

Анастасия Кирюшина,
+7(921)927-77-90;
эл. почта: nastyakik97@mail.ru

Vatin, N.I., Pestryakov, I.I., Sultanov, Sh.T., Ogidan, T.O., Yarunicheva, Y.A., Kiryushina, A.P. Water vapour by diffusion and mineral wool thermal insulation materials. Magazine of Civil Engineering. 2018. 81(5). Pp. 183–192. doi: 10.18720/MCE.81.18.

doi: 10.18720/MCE.81.19

Wooden beams with reinforcement along a curvilinear trajectory

Деревянные балки с армированием по криволинейной траектории

A.A. Koshcheev*,
S.I. Roshchina,
M.V. Lukin,
M.S. Lisyatnikov,
Vladimir State University named after Alexander and Nikolay Stoletovs, Vladimir, Russia

Ассистент А.А. Кощеев*,
д-р техн. наук, заведующая кафедрой С.И. Рощина,
канд. техн. наук, доцент М.В. Лукин,
канд. техн. наук, доцент М.С. Лисятников,
Владимирский государственный университет имени Александра Григорьевича и Николая Григорьевича Столетовых, г. Владимир, Россия

Key words: construction materials; building construction; reinforcement of wooden beams; strength; elasticity; seismic resistance; resource-saving

Ключевые слова: строительные материалы; строительство зданий; армирование деревянных балок; прочность; эластичность; сейсмостойкость; ресурсосбережение

Abstract. The article is devoted to the investigation of a new type of reinforcement of wooden beams for floors and coatings with using steel cable reinforcement located in a solid wood along a curved S-shaped trajectory. The basic principles of a new type of reinforcement are set up. The schemes of various reinforcement paths are given. Mathematical models of studied structures are formed. The stress-strain state of several beams with different variants of reinforcing paths in the working environment of the software complex SCAD, which calculates the beams studied by the finite element method, has been studied. The results of the work are presented in the form of indicators of deflections of beams and isopoles of stresses. A comparative analysis of the studied structures with non-reinforced beams and the traditional reinforcement method is carried out. Conclusions are made about the increase in the strength characteristics of the beams, in which the steel cable armature is used. The optimal trajectory path for the reinforcement groove is selected. The competitive advantages and prospects of using a new type of reinforcement are determined.

Аннотация. Статья посвящена исследованию нового вида армирования деревянных балок для перекрытий и покрытий с использованием стальной канатной арматуры, расположенной в массиве древесины по криволинейной S-образной траектории. Сформированы основные принципы нового вида армирования. Приведены схемы различных траекторий армирования. Сформированы математические модели изучаемых конструкций. Изучено напряженно-деформированное состояние нескольких балок с различными вариантами траекторий армирования в рабочей среде программного комплекса SCAD, выполняющего расчет исследуемых балок методом конечных элементов. Результаты работы представлены в виде показателей прогибов балок и изополей напряжений. Проведен сравнительный анализ изучаемых конструкций с неармированными балками и традиционным способом армирования. Сделаны выводы о повышении прочностных характеристик балок, в которых использована стальная канатная арматура. Выбрана оптимальная траектория паза врезки для арматуры. Определены конкурентные преимущества и перспективы применения нового вида армирования.

1. Introduction

For historical reasons wood has been used in the form of such constant cross-section units as beams, rafters, curved structures in the construction for centuries. Until the beginning of the 20th century there were no written references about the use of wood reinforcement. However, the high rates of construction and the growth of the construction industry technological level have led to a step change in the requirements for buildings and structures. Need for large-span buildings in public and industrial construction arose [1–4]. Economic conditions and a limited amount of natural resources have produced the desire to save construction materials in the mass low-rise construction. Steel and reinforced concrete structures became the most popular, but aesthetic requirements also grew along with the strength and economic ones. New concepts in the construction of buildings consisted in the principles of ecological compatibility and the maximum ambience of the habitable human environment with natural materials. All these requirements have led to interest in increasing the initial natural strength and deformation characteristics of timber structures.

In some degree the solution to this problem was the widespread use of glued wooden structures in construction that surpassed metal and reinforced concrete units for a number of reasons - they had a small installation weight due to the low wood density, relatively high rigidity and strength with sufficient reliability and durability and low cost. However, some wood properties, such as defects, a small yield of high-quality lumber from round timber, sectional massiveness, creep under sustained loading have also formed a number of drawbacks limiting the use of glued wooden structures [5–8].

Qualitatively new leap in the development of wooden structures occurred with the invention of reinforcing wooden structures with steel or fiberglass reinforcement. Reinforcement allowed to reduce wood consumption significantly, improve the quality and reliability of wooden structures, mainly working in bending and bending compression. Such structures have increased strength and rigidity in combination with a small installation weight that sets them apart from metal and reinforced concrete products and allows to mount an enlarge assembly in the construction of buildings and structures. This makes them indispensable in the construction of scattered structures in places remote from main communication lines in hard-to-reach areas, for use in large-span systems of buildings experiencing significant loads in the junctions.

It should be noted that wood today is one of the most popular construction materials. The volume of this natural resource consumption is constantly growing alongside with the growing volumes of low-rise suburban construction in Russia. Wood is extensively used: it is used in the construction of enclosing structures, covering and blanking beam systems, rafter systems [9]. Despite the fact that wood is a renewable natural resource, the volume of its reproduction is very limited.

At the proper time, the problem of saving wood when erecting buildings and structures led to the invention of the technology of reinforcing wooden beams. The question of introducing rigid steel reinforcement bars into the wood solid was thoroughly studied, by gluing them into milled grooves at the stage of gluing the beams structural parts. The use of the investigation and the emergence of the reinforced wooden structures school in Russia can not be overestimated [10]. These technologies provide substantial material savings and increase in strength and deformation characteristics, but require a factory, labor-intensive process for the manufacture of structures consisting of multistage processes: wood preparation, glueing layers, reinforcement, milling, etc. As a result, beams are much more expensive than their unreinforced counterparts. Therefore, reinforced wooden structures carved out a niche of similar products, especially when constructing public facilities and large-span structures, but they can not displace the beams from ordinary timber in the segment of low-rise construction.

In addition, the issues of reinforced wooden structures fragile destruction, their fire resistance due to the fluidity of adhesive compositions under the influence of high temperatures, the problem of strengthening the bearing zones during reinforcement, continue to be relevant today.

Workings intended to solution of similar problems such as strengthening the beams bearing zones, as well as investigation of the beams work with various longitudinal and transverse reinforcement has been carried out at Vladimir State University, at the Department of Building Structures under the guidance of V.Yu. Shchuko and S.I. Roshchina taking into consideration the increased strength of the reinforced beams in the central zones subjected to tensile deformation with bending, destruction of such beam construction often occurs in the bearing zones because of shear fracture stresses directed along the fibers [10–13]. Therefore, to date, the problem of strengthening the bearing zone of reinforced wooden beams is particularly timely.

The use of wood reinforcement due to the difference in the modulus of elasticity or the difference in the relative strain of wood fibers and reinforcement in mechanical tensile and compression tests (1.15 and 0.84 % for wood and 6-16 for reinforcement (deformations corresponding to the yield strength of 0.15 to 0.35 %)) leads to the fact that in all cases of combined work provided by glue bond of reinforcement with wood, the bearing capacity of the reinforcement will be rationally used. Stresses in the reinforcement will reach the yield point earlier than the strength of the wood will be exhausted. However, the reinforcement will prevent fragile destruction of the beam structure, because even in the area of extreme loads, when the strength of the wood is exhausted, the reinforcement will partially retain its load-bearing capacity, even if it exceeds the yield strength, demonstrating the effect of a strut-framed beam or strengthened bent. The investigations show that the reinforced beam does not collapse even after the destruction of the wood of the stretched zone and the increase in the effective stresses by 60–70 % of the magnitude of the destructive load. This property is extremely useful for the construction of buildings and structures in areas with increased seismic activity and responsible public facilities.

The article considers a new type of wooden beams reinforcement – the wire rope reinforcement along the original curvilinear path. Having analyzed the existing shortcomings of the traditional type reinforcement, it has been suggested to change the approach to reinforcing wooden beams: to use plain lay flexible cable instead of rigid steel reinforcement. The introduction of cable reinforcement into the solid wood will allow to obtain higher strength characteristics in comparison with the traditional reinforcement methods – ordinary steel reinforcement, since when the area is equal with the reinforcement, the rope cross section has greater tensile strength and due to a more detailed structure – greater adhesion properties with the glued layer between the wood and the reinforcing material. A curvilinear wave form in the bearing zones where the waves bend radius would coincide with the radius that the flexural rigidity of the steel cable armature imposes should be used instead of a rectilinear milling path. Compared with the existing methods of reinforcement, the proposed form makes it possible to increase the anchoring length in the bearing zones by 1.6–1.8 times [14]. All this will reduce the beam structures cross-sectional area which will lead to savings in wood and steel in the construction of ceilings and covering. It has been planned to use that has proven effective and already traditional multicomponent glue composition based on epoxy resin with hardener PEPA and plasticizer as a binder [15–18].

Due to its simplicity, the new reinforcement technology can be used not only in stationary conditions, but also on the construction site. In addition to all of the above, an important competitive advantage is the ecological component of application these structures in construction in addition to saving wood, the technology provides for minimizing the use of glue compounds (in comparison with glued wooden reinforced structures), which will reduce the harmful impact on the environment and people operating buildings with such constructions [18–21].

2. Methods

The main method of studying wooden beams in this work was the analysis of the stress - deformed state arising in the type of reinforcement that is being studied by creating mathematical models of beams with different trajectories of slot grooving for armature and their virtual testing in the SCAD software package.

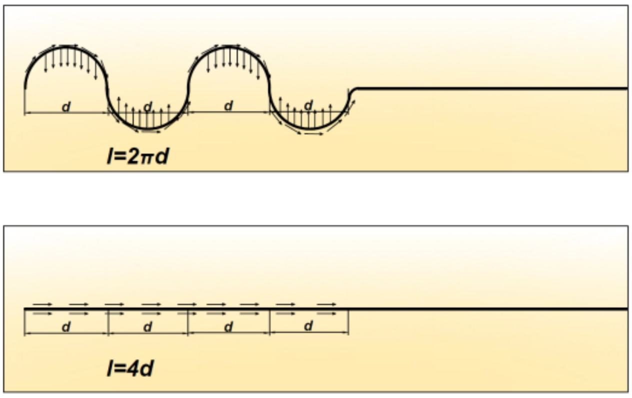

Figure 1. One of the variants of the proposed curvilinear form of anchoring

The proposed form of the reinforcement assumes consideration of the investigated structure volumetric stress, because of the uneven and asymmetric location of the reinforcement along the lower edge of the beam. There are changes in stresses not only in the plane of the longitudinal section of the beam, but also in its cross section. The stress-strain state becomes volumetric that does not allow the construction of diagrams for cross sections, since an infinite set of stress values correspond to each value of the section depth. Such problems are solved only with the help of the finite element method with the use of software systems due to the large (tens of thousands) number of system elements. This method makes it possible to create a realistic model of a reinforced beam with curvilinear reinforcement, to analyze the stresses and deformations arising in the process of loading to the fullest extent possible though the use of the Stress isofield color mapping. It is also possible to perform a comparative analysis of several variants of reinforcement under identical specified ideal conditions - exact geometry, the same loading, the same support fixation.

Figure 2. Demonstration samples of reinforcement along a curvilinear path

The survey objectives were implemented as follows: calculations were carried out for a non-reinforced beam, 3 reinforced beams with rope reinforcement d = 8 mm along a different trajectory (single and double). The beams visualizations are shown in Figures 4–7. The length of the beam is 4.8 m, the cross-section is 100 x 200 mm. The reinforcement is located on the low edge. The beam design model at issue has been constructed by adapting the initial data for the SCAD software running environment. Wood as the beam main material has been assigned as a three-dimensional body obtained by triangulation and extrusion of the beam projecting section. The same grip conditions have been given for all types of reinforcement (on the right - hingedly – a rigid point of support at a distance of 120 mm from the edge of the beam, on the left - hingedly – a simple support at a distance of 120 mm from the edge of the beam). The beam loading – the loading uniformly distributed across the area with the value of 2 tons/m2 is the design load for the ceiling rafters according to CR 64.13330.2011 Wooden structures. Revised edition of SNiP II-25-80. The load works on the upper plane of the beam.

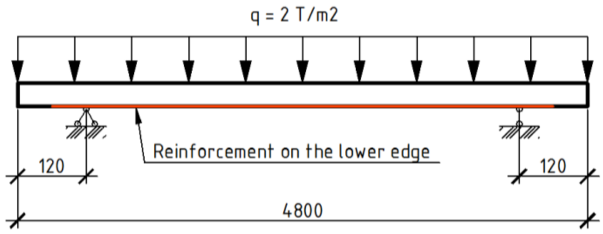

Figure 3. The tests design model

A full calculation by the multifrontal method using finite elements has been performed for the beams presented in the work. It should be noted that the SCAD PC allows to investigate the volumetric stress state of bodies only at the 1 stage of loading - under normal conditions of the structure operation. This is due to the fact that the orthotropic parameters assigned to the volume elements in this program are characterized only by elastic moduli and Poisson's coefficients in different directions.

It is possible to exude a number of indicators according to which the comparative analysis of the stress-strained state of the investigated types of reinforcement has been made from a set of the received results.

1. Isopoles of tensile and compressive stresses operating along the beam fibers. This type of graphical representation of stresses allows to understand how uniformly the stresses are redistributed in the reinforcement zones and throughout the volume of the beam. One can also sit in judgement on the intensity of the stresses at specific points of the beams and make appropriate conclusions about the degree of interaction between wood and reinforcing material according to the contrast grade of the isopoles colour.

2. The beams deflections in the middle of the span (formed by the displacement of the central lower girder connection of the beams along the vertical axis "Z"). It is possible to make a comparative analysis of the deformation parameters of the beams by the size of the deflection.

3. Results

As a result of the comparative analysis these characteristics allow to choose the most advantageous form of the curvilinear trajectory for milling the groove for the steel wire rope reinforcement and make conclusions about the effectiveness of the proposed reinforcement method in comparison with ordinary wooden unreinforced beams and beams with traditional reinforcement.

Consider the results of the study in more detail. Figures 4–19 show the images of longitudinal stresses isopoles in the investigated beams.

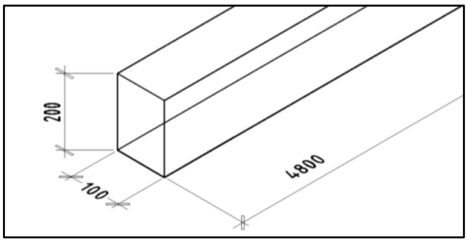

Figure 4. Visualization for an unreinforced beam

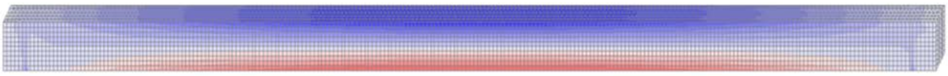

Figure 5. Visualization and the stresses isopoles for an unreinforced beam. General form

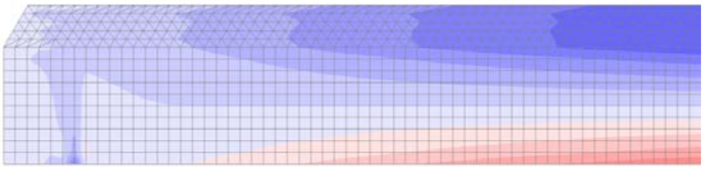

Figure 6. Visualization and the stresses isopoles for an unreinforced beam. View from above

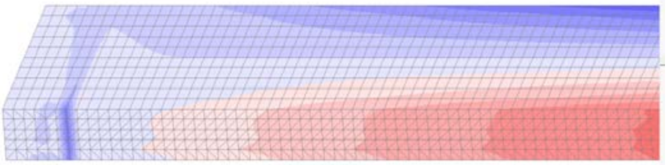

Figure 7. Visualization and the stresses isopoles for an unreinforced beam. Bottom view

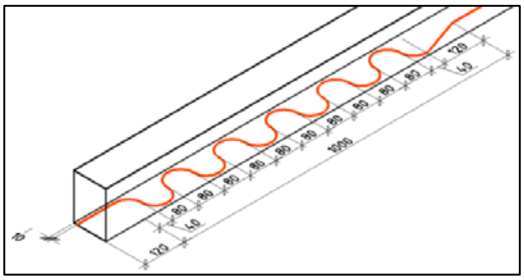

Figure 8. Visualization for a beam with a single reinforcement by wire rope cable

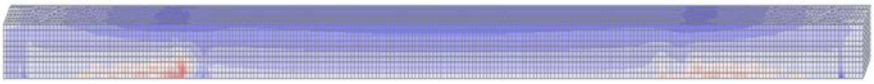

Figure 9. The stresses isopoles for a beam with a single reinforcement by wire rope cable. General form

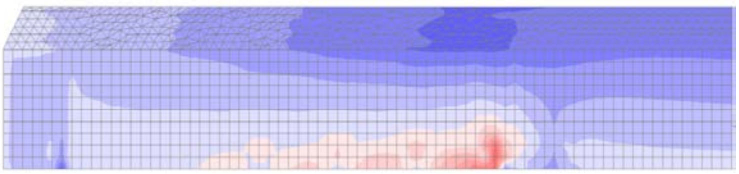

Figure 10. The stresses isopoles for a beam with a single reinforcement by wire rope cable. View from above

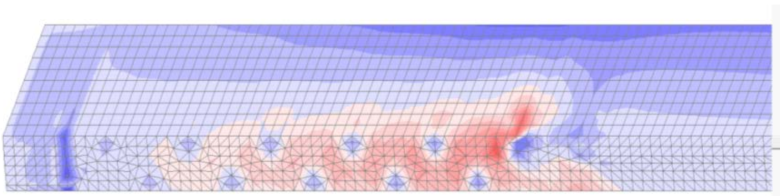

Figure 11. The stresses isopoles for a beam with a single reinforcement by wire rope cable. Bottom view

Кощеев А.А., Рощина С.И., Лукин М.В., Лисятников М.С. Деревянные балки с армированием по криволинейной траектории // Инженерно-строительный журнал. 2018. № 5(81). С. 193–201.

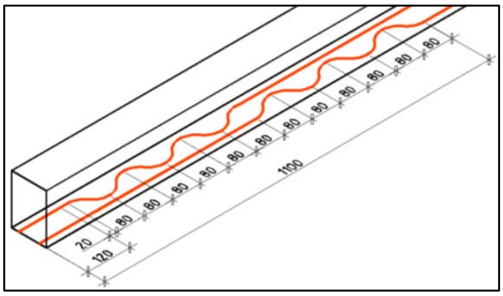

Figure 12. Visualization for a beam with the double unseat reinforcement

Figure 13. The stresses isopoles for a beam with the double unseat reinforcement. General form

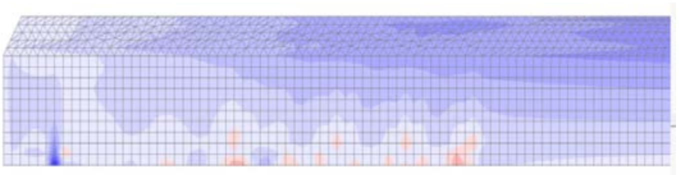

Figure 14. The stresses isopoles for a beam with the double unseat reinforcement. View from above

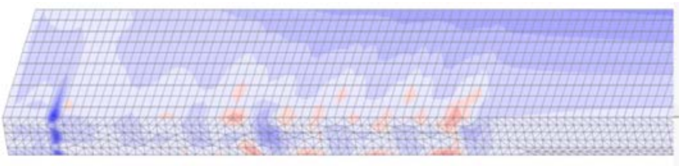

Figure 15. The stresses isopoles for a beam with the double unseat reinforcement. Bottom view

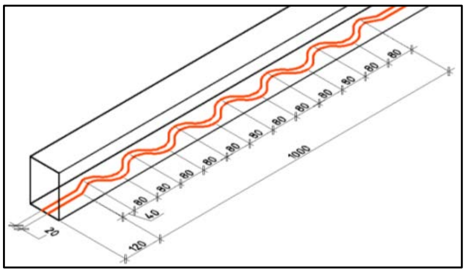

Figure 16. Visualization for a beam with double reinforcement by steel wire rope reinforcement without waves displacement

Figure 17. The stresses isopoles for a beam with double reinforcement by steel wire rope reinforcement without waves displacement. General form

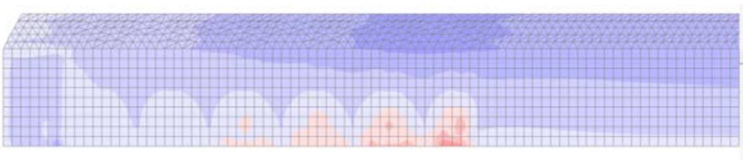

Figure 18. The stresses isopoles for a beam with double reinforcement by steel wire rope reinforcement without waves displacement. View from above

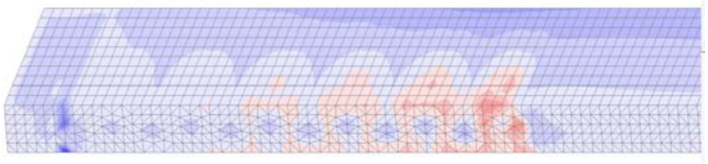

Figure 19. The stresses isopoles for a beam with double reinforcement by steel wire rope reinforcement without waves displacement. Bottom view

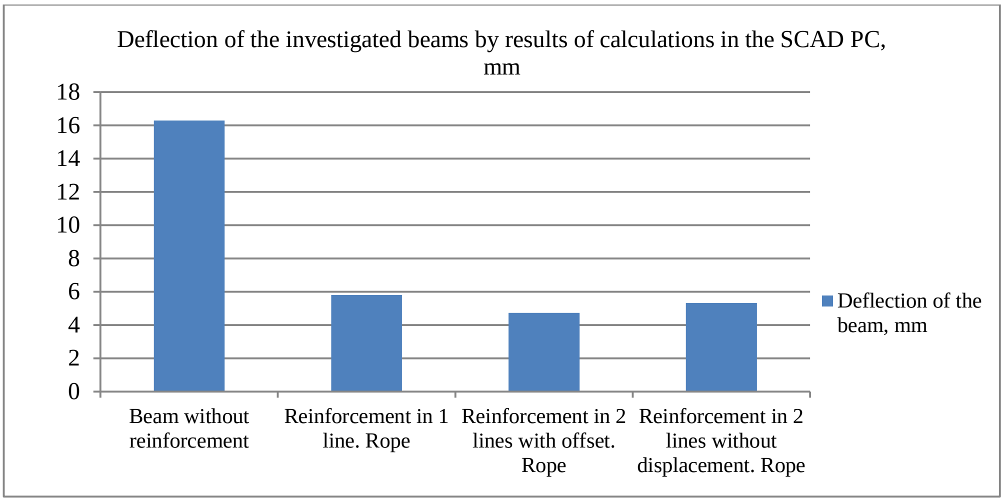

Figure 20. Comparison chart of the beams deflection

4. Discussion

At the Vladimir State University, developments have already been carried out aimed at a similar problem with the subject of this paper – strengthening the bearing zones of beams, as well as studying the work of beams with different types of longitudinal-transverse reinforcement [3, 4, 6–8]. In view of the increased strength of reinforced beams in central zones experiencing deformation of stretching with bending, the destruction of such girder structures occurs often in the prone zones due to shear stresses directed along the fibers. Therefore, to date, the problem of strengthening the piercing zones of reinforced wooden beams is especially urgent.

It has been proposed to perform longitudinal - transverse reinforcement of beams with the use of transverse plates - the use of this type of reinforcement made it possible to reduce the share of tangential stresses perceived by the wood by 20–25 %, which is especially important for high beams or for large transverse forces.

The conducted researches and development have formed a number of conclusive advantages of the wooden reinforced structures before analogues from not reinforced wood. The new technology offers a rational solution to the problem of reinforcing the suspension zones of the beams.

5. Conclusions

Based on the results of calculations, the reinforcement in 1 line with the s-shaped anchoring path turned out to be the most advantageous option from the point of view of strength and deformability (Fig. 5). Based on the obtained data, we can draw the following conclusions:

1. This type of reinforcement significantly changes the work of the timber in the beam;

2. Analysis of emerging strains and stresses shows a 3–4 times increase in strength for a design with a new type of reinforcement;

3. The proposed reinforcement technology provides a 64 % reduction in deformation by comparison with the non-reinforced structure, along with the largest indicator of reinforcement efficiency, harm to all the beams examined.

The prospect of the further investigation is connected with the reliability test of the mathematical model in practice, i.e. performing experimental tests.

In case of experimental verification of the calculation results, beams with a new type of reinforcement will provide a meaningful concurrence to unreinforced wooden structures. Beams of a new type can be used as cheaper and reliable alternative to ordinary wooden beam structures for purposes of strength characteristics with the advantage of reducing the projected floor structure height. The scope of their application is quite extensive – the production of coating and ceiling systems in low-rise, public and industrial construction. Due to the new beams increased elasticity, it is also possible to increase their ability to withstand the action of running value forces, which is important for areas with increased seismic activity.

Construction of energy-efficient buildings and structures is also one of the areas of application of the investigated structures in view of low heat conductivity, aesthetic surface appearance and orientation vector of this technology for resource economy.

Reference

1. Keipour, N., Valipour, H.R., Bradford, M.A. Experimental study of steel–timber composite (STC) beam to steel column joints having a flush end–plate. Engineering Structures. 2018. No. 174. Pp. 906–918.
2. Rescalvo, F.J., Suarez, E., Valverde–Palacios, I., Santiago–Zaragoza, J.M., Gallego, A. Health monitoring of timber beams retrofitted with carbon fiber composites via the acoustic emission technique. Composite Structures. 2018. No. 206. Pp. 392–402.
3. Popova, M.V., Sergeeva, A.N., Sidorov, S.A. Chislennye issledovaniya vysokikh derevokleenykh balok s usileniem priopornykh zon [Numerical studies of glued wood beams with reinforcement of the bearing zones]. BST: Bulletin of construction equipment. 2016 No. 5(981). Pp. 35–37. (rus)
4. Basterra, L.A., Balmori, J.A., Morillas, L., Acuña, L., Casado, M. Internal reinforcement of laminated duo beams of low–grade timber with GFRP sheets. Construction and Building Materials. 2017. No. 154. Pp. 914–920.
5. Melekhov, V.I., Labudin, B.V., Lukin, M.V. Application of glued wood beams in the covering of buildings of textile shops. Technology of the textile industry. 2016. No. 5(365). Pp. 267–271.
6. Sardiko, R., Rocens, K., Iejavs, J., Jakovlevs, V., Ziverts, K. Analysis of the stiffness and load–bearing capacity of glued laminated timber beams reinforced with strands. IOP Conference Series: Materials Science and Engineering. 2017. No. 251(1). Pp. 012104.
7. Gribanov, A.S., Glebova, T.Yu. Raschet i usilenie predel'no – napryazhennykh priopornykh zon vysokikh derevokleyonykh balochnykh konstruktsij [Calculation and amplification of extremely stressed bearing zones of glued wood beams constructions]. Lesotekhnichesky zhurnal. 2015. Vol. 5. No. 1(17). Pp. 187–197 (rus).
8. Solarino, F., Giresini, L., Chang, W.-S., Huang, H. Experimental tests on a dowel–type timber connection and validation of numerical models. Buildings. 2017. No. 7(4). Pp. 116.
9. Lukina, A.V. Vosstanovlenie derevyannoj balki impregnirovaniem polimernoj kompozitsiej na osnove ehpoksidnoj smoly [Restoration of a wooden beam by impregnation with a polymer composition based on epoxy resin]. Lesotekhnichesky zhurnal. 2015. Vol. 5. No. 3(19). Pp. 183–190 (rus).
10. Smirnov, E.A., Lukina, A.V., Gribanov, A.S. Vosstanovlenie destruktivnykh uchastkov opornykh zon derevyannykh balok putem propitki polimernym rastvorom [Restoration of destructive areas of bearing zones of wooden beams by impregnation with a polymer solution]. Scientific and Technical Herald of the Volga Region. 2014. No. 5. Pp. 293–296 (rus).
11. Ottenhaus, L.-M., Li, M., Smith, T. Structural performance of large–scale dowelled CLT connections under monotonic and cyclic loading. Engineering Structures. 2018. No. 176. Pp. 41–48.
12. Roshchina, S.I., Sergeev, M.S., Lukina, A.V. Armirovannye derevyannye konstruktsii [Reinforced wooden structures]. Izvestiya Vysshikh Uchebnykh Zavedenii. Forest Journal. 2013. No. 4(334). Pp. 80–85 (rus).
13. Sergeev, M.S., Lukina, A.V., Gribanov, A.S., Strekalkin, A.A. Razvitie issledovaniya derevokompozitnykh balok s

Литература

1. Keipour N., Valipour H.R., Bradford M.A. Experimental study of steel–timber composite (STC) beam to steel column joints having a flush end–plate // Engineering Structures. 2018. № 174. Pp. 906–918.
2. Rescalvo F.J., Suarez E., Valverde–Palacios I., Santiago-Zaragoza J.M., Gallego A. Health monitoring of timber beams retrofitted with carbon fiber composites via the acoustic emission technique // Composite Structures. 2018. № 206. Pp. 392–402.
3. Попова М.В., Сергеева А.Н., Сидоров С.А. Численные исследования высоких деревоклееных балок с усилением приопорных зон // БСТ: Бюллетень строительной техники. 2016. № 5(981). С. 35–37.
4. Basterra L.A., Balmori J.A., Morillas L., Acuña L., Casado M. Internal reinforcement of laminated duo beams of low–grade timber with GFRP sheets // Construction and Building Materials. 2017. № 154. Pp. 914–920.
5. Melekhov V.I., Labudin B.V., Lukin M.V. Application of glued wood beams in the covering of buildings of textile shops // Technology of the textile industry. 2016. № 5(365). Pp. 267–271.
6. Sardiko R., Rocens K., Iejavs J., Jakovlevs V., Ziverts K. Analysis of the stiffness and load–bearing capacity of glued laminated timber beams reinforced with strands // IOP Conference Series: Materials Science and Engineering. 2017. № 251(1). pp. 012104.
7. Грибанов А.С., Глебова Т.Ю. Расчет и усиление предельно – напряженных приопорных зон высоких деревоклеёных балочных конструкций // Лесотехнический журнал. 2015. Т. 5. № 1(17). С. 187–197.
8. Solarino F., Giresini L., Chang W.-S., Huang H. Experimental tests on a dowel–type timber connection and validation of numerical models // Buildings. 2017. № 7(4). Pp. 116.
9. Лукина А.В., Лисятников М.С. Восстановление деревянной балки импрегнированием полимерной композицией на основе эпоксидной смолы // Лесотехнический журнал. 2015. Т. 5. № 3(19). С. 183–190.
10. Смирнов Е.А., Лукин М.В., Лукина А.В., Грибанов А.С. Восстановление деструктивных участков опорных зон деревянных балок путем пропитки полимерным раствором // Научно – технический вестник Поволжья. 2014. № 5. С. 293–296.
11. Ottenhaus L.-M., Li M., Smith T. Structural performance of large–scale dowelled CLT connections under monotonic and cyclic loading // Engineering Structures. 2018. № 176. Pp. 41–48.
12. Рощина С.И., Сергеев М.С., Лукина А.В. Армированные деревянные конструкции // Известия высших учебных заведений. Лесной журнал. 2013. № 4(334). С. 80–85.
13. Сергеев М.С., Лукина А.В., Грибанов А.С., Стрекалкин А.А. Развитие исследования деревокомпозитных балок с симметричным армированием // Вестник Белгородского государственного технологического университета им. В.Г. Шухова. 2016. № 7. С. 46–49.
14. D'Amico B., Kermani A., Porteous J., Dhonju R., Zhang B. Racking performance of Platform timber framed walls

simmetrichnym armirovaniem [Development of the study of wood–composite beams with symmetrical reinforcement]. Bulletin of the Belgorod State Technological University named after. V.G. Shukhova. 2016. No. 7. Pp. 46–49. (rus)

14. D'Amico, B., Kermani, A., Porteous, J., Dhonju, R., Zhang, B. Racking performance of Platform timber framed walls assessed by rigid body relaxation technique. Construction and Building Materials. 2016. No. 129. Pp. 148–158.
15. Luckina, A.V., Sergeyev, M.S. Experimental research on pressed–bending reinforced timberwork. International Journal of Applied Engineering Research. 2015. Vol. 10. No. 24. Pp. 45307–45312.
16. Ling, Z., Liu, W., Yang, H., Chen, X. Modelling of glued laminated timber joints with glued-in rod considering bond-slip location function. Engineering Structures. 2018. No. 176. Pp. 90–102.
17. Shokhin, P.B., Sergeyev, M.S. Allowance for keeping in the study of the reinforced wood–based constructions. Life Science Journal. 2014. Vol. 11. No. 9s. Pp. 192–195.
18. Ruslantsev, A.N., Portnova, Ya.M., Tairova, L.P., Dumansky, A.M. Analisys of mechanical properties anisotropy of nanomodified carbon fiber–reinforced woven composites / IOP Conference Series: Material Science and Engineering (MSE). 2016. Vol. 153. doi: 10.1088/1757-899.
19. Broutman, L.J., Krock, R.H. Interfaces in polimer matrix composites./ New York and London: Academic press, 1974. Vol. 6.
20. Kelly, A. Interface Effects and the Work of Facture of a Fibrous Composite. N70-29017, 1970.
21. Rosen, B.W. Failure of composite consisting of matrix stiffened by uniaxially oriented fibers, when subjected to uniaxial tensile load parallel to fiber direction. The American Institute of Aeronautics and Astronautics Journal. 1964. Vol. 2. Pp. 64–73.
22. Yao, Z., Wua, D., Chen, C., Zhang, M. Creep behavior of polyurethane nanocomposites with carbon nanotubes. Composites: Part A. 2013. No. 50. Pp. 65.
23. Schapery, R.A. Viscoelastic behavior and analysis of composite materials. Mechanics of Composite Materials. 1974. Vol. 2. Pp. 86–168.
24. Yahyaei–Moayyed, M., Taheri, F. Experimental and computational investigations into creep response of AFRP reinforced timber beams. Composite Structures. 2011. No. 93. Pp. 616–628.
25. Roshchina, S.I., Rimshin, V.I. Calculation of bent reinforced wooden structures with creep. Academy. Architecture and construction. 2009. Pp. 91–92.
26. Lyu, M., Zhu, X., Yang, Q. Bilinear connection stiffness identification of heritage timber buildings with limited strain measurements. Engineering Structures. 2017. No. 151. Pp. 665–681.

assessed by rigid body relaxation technique // Construction and Building Materials. 2016. № 129. Pp. 148–158.

15. Luckina A.V., Sergeyev M.S. Experimental research on pressed–bending reinforced timberwork. International Journal of Applied Engineering Research. 2015. Vol. 10. № 24. Pp. 45307–45312.
16. Ling Z., Liu W., Yang H., Chen X. Modelling of glued laminated timber joints with glued-in rod considering bond-slip location function // Engineering Structures. 2018. № 176. Pp. 90–102.
17. Shokhin P.B., Sergeyev M.S. Allowance for keeping in the study of the reinforced wood–based constructions // Life Science Journal. 2014. Vol. 11. № 9s. Pp. 192–195.
18. Ruslantsev A.N., Portnova Ya.M., Tairova L.P., Dumansky A.M. Analisys of mechanical properties anisotropy of nanomodified carbon fiber–reinforced woven composites // IOP Conference Series: Material Science and Engineering (MSE). 2016. Vol. 153.
19. Broutman L.J., Krock R.H. Interfaces in polimer matrix composites // New York and London: Academic press, 1974. Vol. 6.
20. Kelly A. Interface Effects and the Work of Facture of a Fibrous Composite. N70-29017, 1970.
21. Rosen B.W. Failure of composite consisting of matrix stiffened by uniaxially oriented fibers, when subjected to uniaxial tensile load parallel to fiber direction // The American Institute of Aeronautics and Astronautics Journal. 1964. Vol. 2. Pp. 64–73.
22. Yao Z., Wua D., Chen C., Zhang M. Creep behavior of polyurethane nanocomposites with carbon nanotubes // Composites: Part A. 2013. № 50. Pp. 65.
23. Schapery R.A. Viscoelastic behavior and analysis of composite materials // Mechanics of Composite Materials. 1974. Vol. 2. Pp. 86–168.
24. Yahyaei-Moayyed M., Taheri F. Experimental and computational investigations into creep response of AFRP reinforced timber beams // Composite Structuresno. 2011. Vol. 93. Pp. 616–628.
25. Рощина С.И., Римшин В.И. Расчет изгибаемых армированных деревянных конструкций с учетом ползучести // Академия. Архитектура и конструкции. 2009. С. 91–92.
26. Lyu M., Zhu X., Yang Q. Bilinear connection stiffness identification of heritage timber buildings with limited strain measurements // Engineering Structures. 2017. № 151. Pp. 665–681.

Artyom Koshcheev,*
+7(920)920-34-43; kibole@mail.ru

Svetlana Roshchina,
+7(910)673-35-84; rsi3@mail.ru

Mikhail Lukin,
+7(900)476-22-36; lukin_mihail_22@mail.ru

Mikhail Lisyatnikov,
+7(904)035-83-35; mlisyatnikov@mail.ru

Артем Андреевич Кощеев,*
+7(920)920-34-43; эл. почта: kibole@mail.ru

Светлана Ивановна Рощина,
+7(910)673-35-84; эл. почта: rsi3@mail.ru

Михаил Владимирович Лукин,
+7(900)476-22-36;
эл. почта: lukin_mihail_22@mail.ru

Михаил Сергеевич Лисятников,
+7(904)035-83-35;
эл. почта: mlisyatnikov@mail.ru

Кощеев А.А., Рощина С.И., Лукин М.В., Лисятников М.С. Деревянные балки с армированием по криволинейной траектории // Инженерно-строительный журнал. 2018. № 5(81). С. 193–201.

doi: 10.18720/MCE.81.20

FEM modeling of external walls made of autoclaved aerated concrete blocks

МКЭ-моделирование ограждающих стен, выполненных из автоклавного газобетона

V.A. Pukhkal,
St. Petersburg State University of Architecture and Civil Engineering, St. Petersburg, Russia
A.B. Mottaeva*,
Moscow State University of Civil Engineering, Moscow, Russia

Канд. техн. наук, доцент В.А. Пухкал,
Санкт-Петербургский государственный архитектурно-строительный университет, Санкт-Петербург, Россия
д-р экон. наук, профессор А.Б. Моттаева*,
Московский государственный строительный университет, г. Москва, Россия

Key words: external walls; autoclaved aerated concrete blocks; heating performance uniformity coefficient; reduced thermal resistance; modelling; FEM

Ключевые слова: наружные стены; блоки из автоклавного газобетона; коэффициент равномерности нагрева; снижение термического сопротивления; моделирование; МКЭ

Abstract. The FEM-analysis of factors influencing the heat transfer properties of external walls made of autoclaved aerated concrete blocks is presented. Using the ELCUT program, the external wall temperature fields made of autoclaved aerated concrete blocks were calculated for different values of thermal conductivity for laying cement mortar and laying with adhesive. The temperature field was calculated for a junction of a top floor slab with a two-layer external wall having a facing brick layer and no air cavity. The possibility of condensation of moisture on the surface of the ceiling is established. The values of heating performance uniformity of heat productivity, reduced thermal resistance and heat fluxes for external walls are determined. The calculated values of heating performance uniformity of heat output are obtained depending on the coefficient of thermal conductivity of autoclaved aerated concrete blocks. Further development of the research will be the use of data in calculating the payback period of energy efficiency measures for buildings.

Аннотация. Представлен МКЭ-анализ факторов, влияющих на теплопередающие свойства наружных стен, выполненных из блоков автоклавного газобетона. Используя программу ELCUT получены температурные поля внешней стены, выполненные из блоков автоклавного газобетона, рассчитывались при разных значениях коэффициентов теплопроводности для укладки цементным раствором и укладки клеящим раствором. Температурное поле было рассчитано для соединения верхней плиты перекрытия с двухслойной наружной стенкой, имеющей облицовочный кирпичный слой и воздушную полость. Установлена возможность конденсации влаги на поверхности потолка. Определены значения коэффициентов однородности теплопроизводительности, пониженного теплового сопротивления и тепловых потоков для наружных стен. Расчетные значения коэффициентов однородности теплопроизводительности получены в зависимости от коэффициента теплопроводности блоков автоклавного газобетона. Дальнейшим развитием исследований будет использования данных при расчете периода окупаемости мероприятий по энергоэффетивности зданий.

1. Introduction

1.1 Wall types with autoclaved aerated concrete blockwork applying

Unreinforced wall products of autoclaved aerated concrete (autoclaved aerated concrete blocks) is used as a structural and thermal insulation material in many countries with a cold climate.

The most used types of external walls made of autoclaved aerated concrete (AAC) blocks are shown in Figure 1:

– Type 1 – single-layer walls;

Пухкал В.А., Моттаева А.Б. МКЭ-моделирование ограждающих стен, выполненных из автоклавного газобетона // Инженерно-строительный журнал. 2018. № 5(81). С. 202–211.

- Type 2 – two-layer walls with a facing brick layer; the inner autoclaved aerated concrete layer serves as a thermal protection and bares the load. The outer facing layer protects the structure from atmospheric precipitation; the wall structure may involve an air cavity;
- Type 3 – three-layer walls with a facing brick layer; the inner autoclaved aerated concrete layer serves as a thermal protection and bares the load; thermal insulation is provided to increase the thermal protection properties; the outer facing brick layer protects from atmospheric precipitation; the wall structure may involve an air cavity;

Type 1.

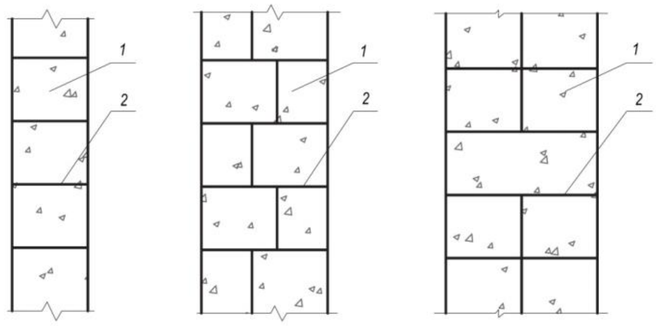

Type 2.

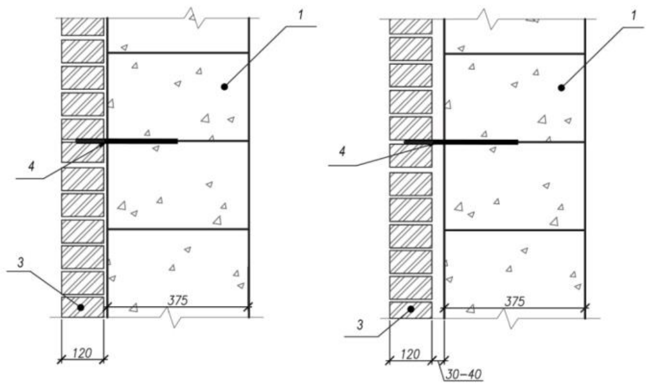

Type 3.

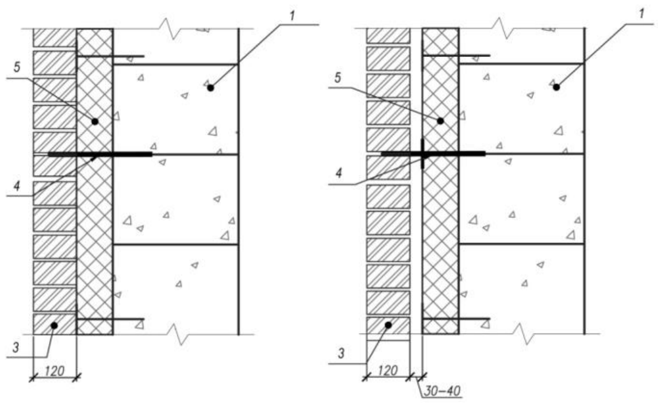

Figure 1. External walls types with autoclaved aerated concrete blockwork applying
1 – autoclaved aerated concrete blocks; 2 – joints; 3 – facing brickwork layer; 4 – flexible connections; 5 –thermal insulation

The peculiarity of external walls structural solutions, the quality and properties of the materials used, and the technology of building's erection have a significant effect on the physical processes of heat transfer in the structures of such walls and, accordingly, on their energy efficiency.

The main factors influencing the heating performance indicators are coefficient of thermal conductivity of autoclaved aerated concrete λ, W/(m·°C).

1.2 Coefficient of thermal conductivity of autoclaved aerated concrete

The thermal properties of autoclaved aerated concrete may vary depending on the materials used [1–5]. For a fixed composition of concrete, the coefficient is significantly dependent on humidity.

The fraction of pore volume in autoclaved aerated concrete products covers the range from 65 to 90 % [4] As a result, concrete easily absorbs water [6] and the thermal conductivity increases with increasing the moisture content [7, 8]. At the temperature below zero. one of the basic mechanisms of moving water for cellular concrete with a moisture content over 30 % by weight is non-isothermal liquid transport [9]. The moisture diffusivity of autoclaved aerated concrete is a function of both temperature and moisture content [10, 11].

The humidity and thermal conductivity of autoclaved aerated concrete given in the manufacturers' lists include mostly just the thermal conductivity in dry state and generic data for the specific heat capacity and water vapor diffusion resistance factor [12]. A Humidity of autoclaved aerated concrete products during the erection of buildings is 2–3 times higher [13, 14] than the design humidity in normative and reference documents used in the calculation of thermal insulation of buildings due to release moisture content of concrete is generally higher than 40 % [15]. Heat transfer through the exterior building envelope in real operating conditions is always unsteady [12]. Values of the thermal conductivity will reach the normalized values only in few years after the erection of the building [16, 17].

Russian Construction Rules SP 50.13330.2012 [18] use the coefficient of heating performance uniformity of the enclosing structure is the indicator of thermal properties of the entire enclosing structure:

$$r = \frac{R_0^r}{R_0^{con}}, \tag{1}$$

where R_0^r is reduced thermal resistance of the enclosing structure section (m^2·°C)/W,

$$R_0^r = \frac{A}{\sum_1^m \frac{A_i}{R_{0,i}^r}}, \text{ (m}^2\text{·°C)/W}, \tag{2}$$

where A is a total area of indicative partition of the enclosing structure equal to sum of areas of separate sections, m^2; A_i – area of ith section of indicative partition of enclosing structure, m^2; $R_{0,i}^r$ – reduced thermal resistance of ith section of indicative partition of the enclosing structure (m^2·°C)/W;

R_0^{con} – thermal resistance of section of uniform enclosing structure (m^2·°C)/W.

Thermal resistance of the uniform enclosing structure

$$R_0^{con} = \frac{1}{\alpha_{\text{int}}} + \sum_i \frac{\delta_i}{\lambda_i} + \frac{1}{\alpha_{ext}}, \text{ (m}^2\text{·°C)/W}, \tag{3}$$

where α_{int} – heat transfer coefficient of the inner surface of the enclosing structure W/(m^2·°C);

α_{ext} – heat transfer coefficient of external surface of enclosing structure W/(m^2·°C);

δ_i – thickness of the ith layer of the enclosing structure, m;

λ_i – thermal conductivity coefficient of the ith layer of the enclosing structure, W/(m·°C);

m –, the number of sections of the building envelope with different reduced thermal resistance.

In works [5, 13, 19], a significant heating performance heterogeneity of autoclaved aerated concrete blockwork is indicated. According to the calculation results given in [20], an increase in the coefficient of thermal conductivity (density) of autoclaved aerated concrete blocks leads to an increase in the coefficient of thermotechnical uniformity coefficients. The results of the calculation differ from the values indicated in [19] up to 10 %. However, these data were obtained only for blockwork with cement-sand mortar having a density of 1,800 kg/m^3 and a 10 mm thickness of horizontal and vertical joints. The work [21] gives data only for joints on cement mortar; blockwork with adhesive solutions providing a joint thickness of 2 ± 1 mm is not considered.

Due to the fact that the thermal conductivity of cement mortars and adhesives is significantly higher than the thermal conductivity of autoclaved aerated concrete products, their effect must be considered when designing the external wallis [15]. The thermotechnical uniformity coefficients of autoclaved aerated concrete walls depends on the thickness and thermal conductivity of mortar joints in stationary and non-stationary conditions [15].

The use of polyurethane foam adhesive to bond the concrete blocks in the masonry walls is technically and economically feasible [19, 22].

Plastering of type 1 external walls (Figure 1) made of autoclaved aerated concrete blocks is performed directly on autoclaved aerated concrete laying (when homogeneous walls provide the required parameters of thermal protection) or on thermal insulation fixed on laying (two-layer structure). Both thick-layered (with an average layer thickness of more than 7 mm) and thin-layered plasters (with an average layer thickness of 7 mm or less) are implemented. External finishing of walls made of autoclaved aerated concrete blocks is obligated, because when there is no finishing, walls have high air permeability.

Different surface coatings [23] and exterior plaster [24–26] can contribute to moisture and thermal performance of external walls made of autoclaved aerated concrete.

1.3 Aims and objectives of the study

In [27–29] A.S.Gorshkov and others developed a mathematical model for estimating the discounted payback period of investments for reducing energy resources needed in building's development. The model allows to perform quickly and efficiently a comparison of various energy-saving solutions based on economic viability.

In order to use this model, in the case of autoclaved aerated concrete blocks, detailed initial data are required. This data must include the heat transfer performance uniformity factors and the coefficient of thermal conductivity with taking into account the influences of mortar joints, surface coatings and exterior plaster, floor slabs perforations, etc.

For fast calculations of all these parameters, a model based on the finite element method (FEM) was proposed.

In 2018 the first results of FEM analysis of data on the effect of joints of the autoclaved aerated concrete blocks on the heat transfer uniformity of exterior walls was carried out [21] with the use of "ELCUT" software.

The task of this research is the further development of the approach and its comparison with experimental data.

2. Materials and Methods

The coefficient of thermal conductivity of autoclaved aerated concrete is taken as a function of density. Data for thermal insulation material (of grade with an average density of not higher than D400), structural and thermal insulation material (of grade with an average density above D400 and below D700) and structural material (of grade with an average density of D700 and above) are given in Table 1.

Table 1. Coefficient values of thermal conductivity of autoclaved aerated concrete blocks

Bulk humidity of the material	Thermal conductivity coefficient, λ, W/(m·°C), a grade of the autoclaved aerated concrete block							
	D200	D300	D400	D500	D600	D800	D1000	D1200
In dry condition (recommended by [30])	0.048	0.072	0.096	0.120	0.140	0.190	0.240	0.280
4% [30]	0.056	0.084	0.113	0.141	0.160	0.223	0.282	0.329
5% [30]	0.059	0.088	0.117	0.147	0.183	0.232	0.293	0.342
8% [31]	-	-	0.140	-	0.220	0.330	0.380	-
12% [31]	-	-	0.150	-	0.260	0.370	0.430	-

According to Russian State Standard SP 50.13330.2012 while designing structures, the coefficient of thermal conductivity of autoclaved aerated concrete blocks is taken when bulk humidity is 12% [18].

The coefficient of heating performance uniformity of the enclosing structure can be determined on the basis of calculation of the temperature field of the structure.

In this case, the calculations are performed according to the dependencies:

- - reduced thermal resistance of a non-uniform section of the enclosing structure

$$R_0^r = \frac{t_{\text{int}} - t_{ext}}{q_0^r}, \text{ (m}^2\cdot{}^\circ\text{C)/W,,} \tag{4}$$

where q_0^r – heat flow rate of non-uniform section of enclosing structure, W/m^2;

- thermal resistance of a uniform section of enclosing structure, (m^2·°C)/W

$$R_0^{con} = \frac{t_{\text{int}} - t_{ext}}{q_0^{con}}, \text{ (m}^2\cdot{}^\circ\text{C)/W,} \tag{5}$$

where q_0^{con} – heat flow rate for uniform section of enclosing structure, W/m^2;

- heating performance uniformity coefficient of enclosing structure

$$r = \frac{q_0^{con}}{q_0^r} \tag{6}$$

Let us consider as an example a two-dimensional temperature field of a single-layer external wall structure made of autoclaved aerated concrete blocks (St. Petersburg, Russian Federation):

- design temperature of outside air is –26 ° C;
- design temperature of inside air is +20 ° C;
- the outer wall is made of 375 mm thick autoclaved aerated concrete blocks of density grade D300;
- the thickness of the horizontal and vertical joints of the laying: with cement mortar – 10 mm; with adhesive solution – 2 mm.

For the block laying, a cement-sand mortar and adhesive cement with density of 1800 kg/m^3 are used.

The coefficients of thermal conductivity of materials are determined for the operating conditions of the enclosing structure:

- for blocks (λ_b, W/(m·°C)) – when bulk humidity of the material is 12 %,
- for cement-sand mortar and adhesive cement (λ_m, W/(m·°C)) – when bulk humidity of the material is 4 % [20].

Blockwork joint thickness is taken:

- with adhesive solution: horizontal and vertical – within 2 ± 1 mm;
- with cement mortar: horizontal - not less than 10 mm and not more than 15 mm; vertical – from 8 to 15 mm.

Calculation of the temperature field and heat fluxes of the external wall structure is carried out in the program of simulation of two-dimensional thermal fields by the ELCUT finite element method which is widely used in thermal fields calculation in constructions [32–36].

3. Results and Discussion

3.1. Results of calculation

The temperature fields of the external wall were calculated using ELCUT program within the range of values of the thermal conductivity coefficient of autoclaved aerated concrete blocks from 0.088 (D300 block) to 0.6 W/(m•°C). The example of calculation results is presented in Figure 2 in the form of fields of heat flows under design conditions.

According to the calculation data, the heat flow through the enclosing structure and its thermal resistance are determined depending on the coefficient of thermal conductivity of autoclaved aerated concrete blocks (Table 2). In comparison, data on a uniform structure are given (without regard to joints).

The temperature field of the junction of the top floor slab with the wall is calculated when the thermal insulating insert is placed along the entire length of the structure (plane problem – Figure 3). A two-layer external wall with a facing brick layer without an air cavity has been set. The grade of autoclaved aerated concrete block is D400. The calculation did not take into account the heterogeneity of the blockwork of autoclaved aerated concrete, which corresponds to the laying with adhesive solution applying. The values of thermal conductivity coefficients of autoclaved aerated concrete blocks are λ_b=0.117 W/(m·°C). The calculation is carried under the outside air temperature, which was –24 °C. The graph of the variation of the ceiling surface temperature is shown in Figure 4.

a) cement mortar blockwork **b) adhesive solution blockwork**

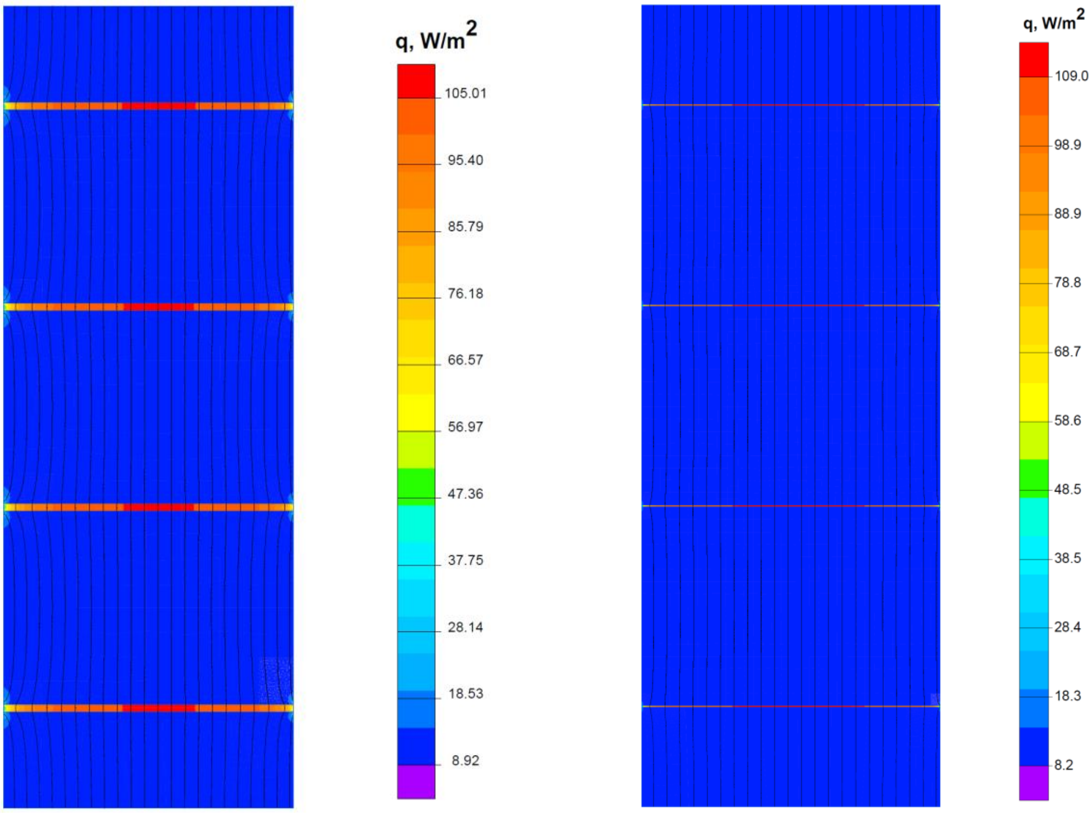

Figure 2. The example of heat flow calculation for external wall made of autoclaved aerated concrete blocks of density grade of D300

Table 2. Heat flow through the autoclaved aerated concrete blockwork and the thermal resistance of the structure

Thermal conduction coefficient of a block, λ_b, W/(m·°C)	Heat flow rate, q_i, W/m^2			Thermal resistance, (m^2·°C)/W		
	Uniform structure	laying: With cement mortar	laying: With adhesive solution	Uniform structure	laying: With cement mortar	laying: With adhesive solution
0.088	10.408	14.302	11.255	4.420	3.216	4.087
0.117	13.676	17.581	14.513	3.364	2.616	3.170
0.147	16.978	20.870	17.804	2.709	2.204	2.584
0.183	20.837	24.700	21.650	2.208	1.862	2.125
0.208	23.454	27.291	24.257	1.961	1.686	1.896
0.3	32.661	36.391	33.431	1.408	1.264	1.376
0.4	41.974	45.590	42.713	1.096	1.009	1.077
0.5	50.637	54.153	51.351	0.908	0.849	0.896
0.6	58.717	62.150	59.410	0.783	0.740	0.774

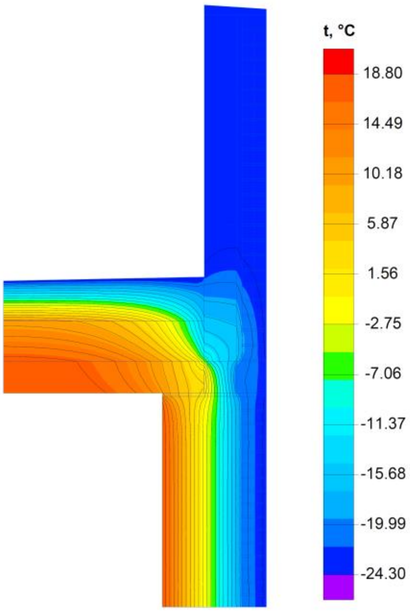

Figure 3. Temperature field of the junction of the top floor slab with an external wall made of autoclaved aerated concrete blocks of D400 grade of density and a brick facing layer

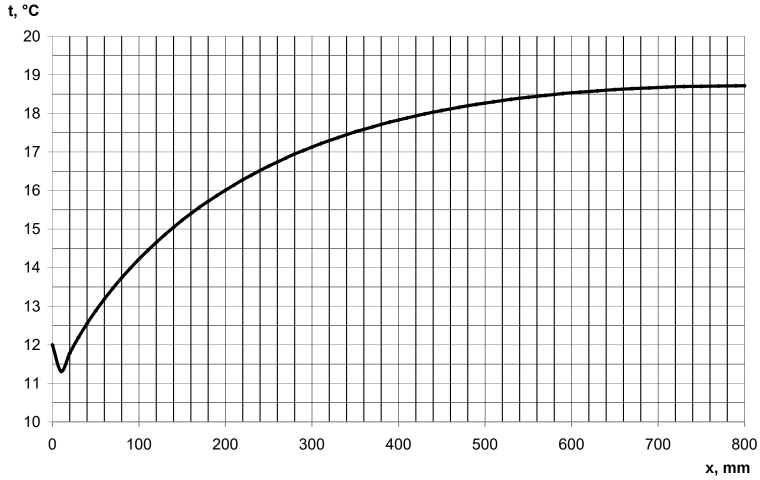

Figure 4. The graph of ceiling surface temperature changing (x – distance from the corner, mm)

3.2. Discussion

As it follows from the calculations performed, an increase in the coefficient of thermal conductivity (density) of autoclaved aerated concrete blocks leads to a decrease in the coefficient of heating performance uniformity (Table 2). The correlation between thermal conductivity coefficients of the joint material and of autoclaved aerated concrete blocks significantly affects the values of the heating performance uniformity coefficients of the blockwork with given thickness of joints (Figure 5).

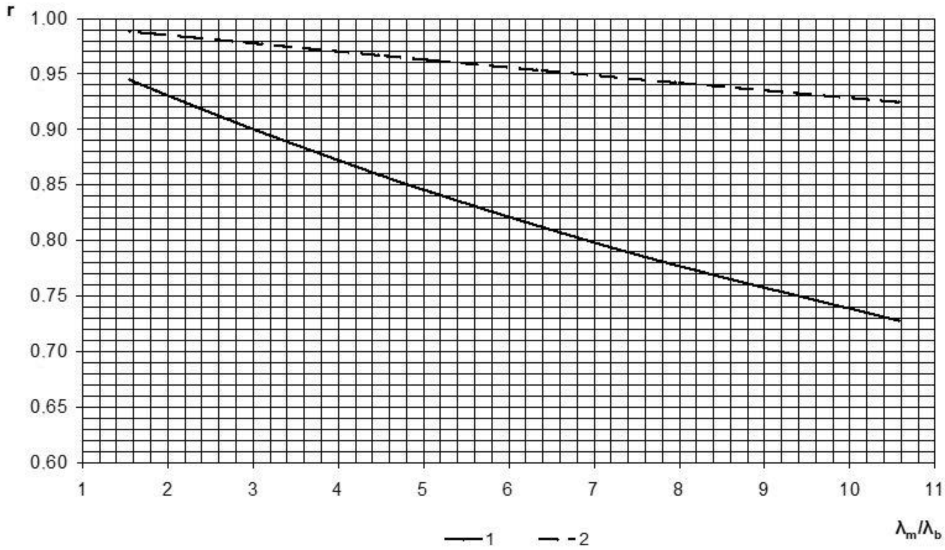

Figure 5. Dependence of the coefficient of heating performance uniformity on the ratio of the coefficients of thermal conductivity of the junction material and autoclaved aerated concrete blocks
1 – laying with using cement mortar with joint thickness of 10 mm; 2 – laying with using adhesive solution with joint thickness of 2 mm

During investigating the temperature field of the junction of top floor slab with the external wall made of autoclaved aerated concrete blocks of D400 density grade and the facing brick layer, the minimum surface temperature of the ceiling in the corner was determined equaling +11.3 °C (Figure 4). In this case, under internal air temperature of +20 °C and relative humidity of 58%, condensate falls out on the surface of the ceiling.

For junctions of intermediate floor slabs with an external wall, the minimum temperatures on the inner surface of the wall and the floor depend primarily on the thickness of the wall and the presence of perforation, or other thermal protective measures.

To further improve the laying of autoclaved aerated concrete blocks, it is required to develop adhesive solutions that are characterized by low values of the thermal conductivity coefficients [19, 22], while ensuring the required adhesion between the blocks and not impairing the performance of the enclosing structures in strength, stability, crack resistance, fire resistance, etc.

4. Conclusions

1. Design values of heating performance of buildings' external walls can be determined using the program of simulation of thermal fields by the ELCUT finite element method.

2. Thermal state of the external enclosing structures made of autoclaved aerated concrete was calculated and the design values of the coefficients of heating performance uniformity for laying with the use of cement mortar and adhesive solution were obtained depending on the ratio of the thermal conductivity coefficients of junction material and autoclaved aerated concrete blocks.

3. It was established that it is necessary to model thermal fields of junctions of building structural elements made of autoclaved aerated concrete blocks in order to test them for condensation of moisture on the surface.

Reference

1. Tasdemir, C., Sengul, O., Tasdemir, M.A. A comparative study on the thermal conductivities and mechanical properties of lightweight concretes. Energy and Buildings. 2017. Vol. 151. Pp. 469–475. DOI:10.1016/j.enbuild.2017.07.013
2. Qu, X., Zhao, X. Previous and present investigations on the components, microstructure and main properties of autoclaved aerated concrete – A review. Construction and Building Materials. 2017. Vol. 135 Pp. 505–516. DOI:10.1016/j.conbuildmat.2016.12.208
3. Walczak, P., Szymański, P., Rózycka, A. Autoclaved Aerated Concrete based on Fly Ash in Density 350kg/m3as an Environmentally Friendly Material for Energy - Efficient Constructions. Procedia Engineering. 2015. Vol. 122. Pp. 39–46. DOI:10.1016/j.proeng.2015.10.005
4. Schober, G. Poros ity in autoclaved aerated concrete (AAC): A review on pore structure, types of porosity, measurement methods and effects of porosity on properties. Cement, Wapno, Beton, (SPEC.ISSUE). 2011. Pp. 39–43.
5. Grinfeld, G.I. Perfomance characteristics of autoclaved aerated concrete with density 400 kg/cub.m. Construction of Unique Buildings and Structures. 2013. No. 5(10). Pp. 28–57.
6. Agata, S., Jarosław, S. Mathematical description of sorption isotherms of autoclaved aerated concrete. Energy Procedia. 2015. Vol. 78. Pp. 1437–1442. DOI:10.1016/j.egypro.2015.11.167
7. Korniyenko, S.V, Vatin, N.I., Gorshkov, A.S. Heat and power characteristics analysis carried out for the residential building made of autoclaved aerated concrete blocks. Construction of Unique Buildings and Structures. 2016. No. 12(51). Pp. 45–60. DOI:10.18720/CUBS.51.4
8. Jin, H.-Q., Yao, X.-L., Fan, L.-W., Xu, X., Yu, Z.-T. Experimental determination and fractal modeling of the effective thermal conductivity of autoclaved aerated concrete: Effects of moisture content. International Journal of Heat and Mass Transfer. 2016. Vol. 92. Pp. 589–602. DOI:10.1016/j.ijheatmasstransfer.2015.08.103
9. Krutilin, A.B., Rykhlionak, Y.A., Liashkevich, V.V. Thermophysical characteristics of low density autoclaved aerated concrete and their influence on durability of

Литература

1. Tasdemir C., Sengul O., Tasdemir M.A. A comparative study on the thermal conductivities and mechanical properties of lightweight concretes // Energy and Buildings. 2017. Vol. 151/ Pp. 469–475. DOI:10.1016/j.enbuild.2017.07.013
2. Qu X., Zhao X. Previous and present investigations on the components, microstructure and main properties of autoclaved aerated concrete – A review // Construction and Building Materials. 2017. Vol. 135 Pp. 505–516. DOI:10.1016/j.conbuildmat.2016.12.208
3. Walczak P., Szymański P., Rózycka A. Autoclaved Aerated Concrete based on Fly Ash in Density 350kg/m3as an Environmentally Friendly Material for Energy - Efficient Constructions // Procedia Engineering. 2017. Vol. 122. Pp. 39–46. DOI:10.1016/j.proeng.2015.10.005
4. Schober G. Poros ity in autoclaved aerated concrete (AAC): A review on pore structure, types of porosity, measurement methods and effects of porosity on properties // Cement, Wapno, Beton, (SPEC.ISSUE). 2011. Pp. 39–43.
5. Гринфельд Г.И. Эксплуатационные характеристики автоклавного газобетона марки по средней плотности D400 // Строительство уникальных зданий и сооружений. 2013. № 5 (10). С. 28–57.
6. Agata S., Jarosław S. Mathematical description of sorption isotherms of autoclaved aerated concrete // Energy Procedia. 2015. Vol. 78. Pp. 1437–1442. DOI:10.1016/j.egypro.2015.11.167
7. Корниенко С.В., Ватин Н.И., Горшков А.С. Анализ теплоэнергетических характеристик жилого здания из газобетонных блоков // Строительство уникальных зданий и сооружений. 2016. № 12(51). С. 45–60. DOI:10.18720/CUBS.51.4
8. Jin H.-Q., Yao X.-L., Fan L.-W., Xu X., Yu Z.-T. Experimental determination and fractal modeling of the effective thermal conductivity of autoclaved aerated concrete: Effects of moisture content // International Journal of Heat and Mass Transfer. 2016. Vol. 92. Pp. 589–602. DOI:10.1016/j.ijheatmasstransfer.2015.08.103
9. Крутилин А.Б., Рыхленок Ю.А., Лешкевич В.В. Теплофизические характеристики автоклавных ячеистых бетонов низких плотностей и их влияние на

exterior walls of buildings. Magazine of Civil Engineering. 2015. No. 2(54). Pp. 46–55. DOI:10.5862/MCE.54.5

10. Kornienko, S.V., Vatin, N.I., Gorshkov, A.S. Assessment of moisture conditions of walls with fasade's thermoinsulation composite systems with external mortar layers. Construction of Unique Buildings and Structures. 2016. No. 6(45). Pp. 34–54.
11. Kočí, J., Korecký, T., Černý, R. Identification of Moisture Diffusivity of Autoclaved Aerated Concrete in the Form of Smooth Two-Variable Function. Energy Procedia. 2017. Vol. 132. Pp. 219–224. DOI:10.1016/j.egypro.2017.09.758
12. Jerman, M., Keppert, M., Výborný, J., Černý, R. Hygric, thermal and durability properties of autoclaved aerated concrete. Construction and Building Materials. 2013. Vol. 41 Pp. 352–359. DOI:10.1016/j.conbuildmat.2012.12.036
13. Vatin, N.I., Gorshkov, A.S., Kornienko, S.V., Pestryakov, I.I. The consumer properties of wall products from AAC. Construction of Unique Buildings and Structures. 2016. No. 1(40). Pp. 78–101.
14. Jerman, M., Černý, R. Effect of moisture content on heat and moisture transport and storage properties of thermal insulation materials. Energy and Buildings. 2012. Vol. 53. Pp. 39–46. DOI:10.1016/j.enbuild.2012.07.002
15. Gorshkov, A.S., Rymkevich, P.P., Vatin, N.I. Simulation of non-stationary heat transfer processes in autoclaved aerated concrete-walls. Magazine of Civil Engineering. 2014. No. 8(52). DOI:10.5862/MCE.52.5
16. Vatin, N., Gorshkov, A., Rymkevich, P., Nemova, D., Tarasova, D. Nonstationary thermal conductionthrough the building envelope. Applied Mechanics and Materials. 2014. Vol. 670–671 Pp. 365–369. DOI:10.4028/www.scientific.net/AMM.670-671.365
17. Gorshkov, A.S., Sokolov, N.A. Inconsistency in Russian and international standards in the determination of the design values of thermal conductivity of building materials and products. Magazine of Civil Engineering. 2013. No. 7(42). DOI:10.5862/MCE.42.2
18. Russian State Standard SP 50.13330.2012 Buildings Heat Insulation.
19. Grinfeldi, G.I., Gorshkov, A.S., Vatin, N.I. Tests results strength and thermophysical properties of aerated concrete block wall samples with the use of polyurethane adhesive. Advanced Materials Research. 2014. Vol. 941–944 Pp. 786–799. DOI:10.4028/www.scientific.net/AMR.941-944.786
20. Gorshkov, A.S., Gladkikh, A.A. Vliianie rastvornykh shvov kladki na parametry teplotekhnicheskoi odnorodnosti sten iz gazobetona [Influence of mortar joints on the parameters of heat transfer performance uniformity of walls made of aerated concrete]. Magazine of Civil Engineering. 2010. No. 3(13). Pp. 39–42.
21. Pukhkal, V., Murgul, V. Effect of aerated concrete blockwork joints on the heat transfer performance uniformity. E3S Web of Conferences. 2018. Vol. 33. Pp. 02002. DOI:10.1051/e3sconf/20183302002
22. Gorshkov, A.S., Vatin, N.I. Properties of the wall structures made of autoclaved cellular concrete products on the polyurethane foam adhesive. Magazine of Civil Engineering. 2013. No. 5(40). Pp. 5–19. DOI:10.5862/MCE.40.1
23. Kus, H., Nygren, K., Norberg, P. In-use performance assessment of rendered autoclaved aerated concrete walls by long-term moisture monitoring. Building and Environment. 2004. Vol. 39(6). Pp. 677–687. DOI:10.1016/j.buildenv.2003.12.006
24. Kočí, V., Maděra, J., Černý, R. Exterior thermal insulation systems for AAC building envelopes: Computational analysis aimed at increasing service life. Energy and Buildings. 2012. Vol. 47. Pp. 84–90. DOI:10.1016/j.enbuild.2011.11.030

долговечность наружных стен зданий // Инженерно-строительный журнал. 2015. № 2(54). С. 46–55. DOI:10.5862/MCE.54.5

10. Корниенко С.В, Ватин Н.И, Горшков А.С, Оценка влажностного режима стен с фасадными теплоизоляционными композиционными системами // Строительство уникальных зданий и сооружений. 2016. № 6(45). С. 34–54.
11. Kočí J., Korecký T., Černý R. Identification of Moisture Diffusivity of Autoclaved Aerated Concrete in the Form of Smooth Two-Variable Function // Energy Procedia. 2017. Vol. 132. Pp. 219–224. DOI:10.1016/j.egypro.2017.09.758
12. Jerman M., Keppert M., Výborný J., Černý R. Hygric, thermal and durability properties of autoclaved aerated concrete // Construction and Building Materials. 2013. Vol. 41. Pp. 352–359. DOI:10.1016/j.conbuildmat.2012.12.036
13. Ватин Н.И., Горшков А.С., Корниенко С.В., Пестряков И.И., Потребительские свойства стеновых изделий из автоклавного газобетона // Строительство уникальных зданий и сооружений. 2016. № 1(40). С. 78–101.
14. Jerman M., Černý R. Effect of moisture content on heat and moisture transport and storage properties of thermal insulation materials // Energy and Buildings. 2012. Vol. 53. Pp. 39–46. DOI:10.1016/j.enbuild.2012.07.002
15. Горшков А.С., Рымкевич П.П., Ватин Н.И. Моделирование процессов нестационарного переноса тепла в стеновых конструкциях из газобетонных блоков // Инженерно-строительный журнал. 2014. № 8(52). С. 38–48. DOI:10.5862/MCE.52.5
16. Vatin N., Gorshkov A., Rymkevich P., Nemova D., Tarasova D. Nonstationary thermal conductionthrough the building envelope // Applied Mechanics and Materials. 2014. Vol. 670–671. Pp. 365–369. DOI:10.4028/www.scientific.net/AMM.670-671.365
17. Горшков А.С., Соколов Н.А. Несоответствие российских и международных стандартов при определении расчетных значений теплопроводности строительных материалов и изделий // Инженерно-строительный журнал. 2013. № 7(42). С. 7–14. DOI:10.5862/MCE.42.2
18. СП50.13330.2012 Тепловая защита зданий.
19. Grinfeldi G.I., Gorshkov A.S., Vatin N.I. Tests results strength and thermophysical properties of aerated concrete block wall samples with the use of polyurethane adhesive // Advanced Materials Research. 2014. Vol. 941–944 Pp. 786–799. DOI:10.4028/www.scientific.net/AMR.941-944.786
20. Горшков А.С., Гладких А.А. Влияние растворных швов кладки на параметры теплотехнической однородности стен из газобетона // Инженерно-строительный журнал. 2010. № 3(13). С. 39–42.
21. Pukhkal V., Murgul V. Effect of aerated concrete blockwork joints on the heat transfer performance uniformity // E3S Web of Conferences. 2018. Vol. 33 Pp. 02002. DOI:10.1051/e3sconf/20183302002
22. Горшков А.С., Ватин Н.И. Свойства стеновых конструкций из ячеистобетонных изделий автоклавного твердения на полиуретановом клею // Инженерно-строительный журнал. 2013. № 5(40). С. 5–19. DOI:10.5862/MCE.40.1
23. Kus H., Nygren K., Norberg P. In-use performance assessment of rendered autoclaved aerated concrete walls by long-term moisture monitoring // Building and Environment. 2004. Vol. 39(6). Pp. 677–687. DOI:10.1016/j.buildenv.2003.12.006
24. Kočí V., Maděra J., Černý R. Exterior thermal insulation systems for AAC building envelopes: Computational analysis aimed at increasing service life // Energy and Buildings. 2012. Vol. 47. Pp. 84–90. DOI:10.1016/j.enbuild.2011.11.030

25. Paruta, V.A. Fracture mechanics of system ‘aerated concrete masonry - Plaster covering’. Magazine of Civil Engineering. 2014. No. 3(47). Pp. 48–55. DOI:10.5862/MCE.47.5
26. Vatin, N., Gorshkov, A., Nemova, D., Gamayunova, O., Tarasova, D. Humidity conditions of homogeneous wall from gas-concrete blocks with finishing plaster compounds. Applied Mechanics and Materials. 2014. Vol. 670–671 Pp. 349–354. DOI:10.4028/www.scientific.net/AMM.670-671.349
27. Vatin, N.I., Nemova, D.V., Kazimirova, A.S., Gureev, K.N. Increase of energy efficiency of the building of kindergarten. 2014. DOI:10.4028/www.scientific.net/AMR.953-954.1537
28. Vatin, N., Gorshkov, A., Nemova, D., Tarasova, D. Energy efficiency of facades at major repairs of buildings. Applied Mechanics and Materials. 2014. Vol. 633–634. Pp. 991–996. DOI:10.4028/www.scientific.net/AMM.633-634.991
29. Gorshkov, A.S., Vatin, N.I., Rymkevich, P.P., Kydrevich, O.O. Payback period of investments in energy saving. Magazine of Civil Engineering. 2018. No. 2(78). Pp. 65–75. DOI:10.18720/MCE.78.5
30. Russian state standard GOST 31359-2007 Cellular autoclave curing concretes. Specifications.
31. Russian regional guidance documents RMD 23-16-2012.
32. Dudin, M.O., Vatin, N.I., Barabanshchikov, Y.G. Modeling a set of concrete strength in the program ELCUT at warming of monolithic structures by wire. Magazine of Civil Engineering. 2015. No. 2(54). Pp. 33–45. DOI:10.5862/MCE.54.4
33. Portnyagin, D.G. Improving the thermal performance of the building envelopes with the use of foam glass-ceramics. Magazine of Civil Engineering. 2015. No. 8(60). Pp. 56–67. DOI:10.5862/MCE.60.7
34. Konesev, S., Khazieva, R., Konev, A., Kondratyev, E. The research of heating efficiency of different induction heating systems. MATEC Web of Conferences. 2017. Vol. 113. DOI:10.1051/matecconf/201711301002
35. Larionov, A., Minnullina, A. Analysis of heat-conducting inclusions in exterior walls of residential building. IOP Conference Series: Earth and Environmental Science. 2017. No. 1(90). DOI:10.1088/1755-1315/90/1/012188
36. Khalimov, O., Shibaeva, G., Portnyagin, D., Ibe, K. The improvement of aseismic horizontal frame’s thermal insulations. Journal of Physics: Conference Series. 2018. Vol. 365(4). DOI:10.1088/1757-899X/365/4/042071

25. Парута В.А. Механика разрушения системы «газобетонная кладка – штукатурное покрытие» // Инженерно-строительный журнал. 2014. № 3(47). С. 48–55. DOI:10.5862/MCE.47.5
26. Vatin N., Gorshkov A., Nemova D., Gamayunova O., Tarasova D. Humidity conditions of homogeneous wall from gas-concrete blocks with finishing plaster compounds // Applied Mechanics and Materials. 2014. Vol. 670–671. Pp. 349–354. DOI:10.4028/www.scientific.net/AMM.670-671.349
27. Vatin N.I., Nemova D.V., Kazimirova A.S., Gureev K.N. Increase of energy efficiency of the building of kindergarten. 2014. DOI:10.4028/www.scientific.net/AMR.953-954.1537
28. Vatin N., Gorshkov A., Nemova D., Tarasova D. Energy efficiency of facades at major repairs of buildings // Applied Mechanics and Materials. 2014. Vol. 633–634. Pp. 991–996. DOI:10.4028/www.scientific.net/AMM.633-634.991
29. Горшков А.С., Ватин Н.И., Рымкевич П.П., Кудревич О.О. Период возврата инвестиций в энергосбережение // Инженерно-строительный журнал. 2018. № 2(78). С. 65–75. DOI:10.18720/MCE.78.5
30. ГОСТ 31359-2007 Бетоны ячеистые автоклавного твердения. Технические условия.
31. РМД 23-16-2012 Санкт-Петербург. Рекомендации по обеспечению энергетической эффективности жилых и общественных зданий
32. Дудин М.О., Ватин Н.И., Барабанщиков Ю.Г. Моделирование набора прочности бетона в программе ELCUT при прогреве монолитных конструкций проводом // Инженерно-строительный журнал. 2015. № 2(54). С. 33–45. DOI:10.5862/MCE.54.4
33. Портнягин Д.Г. Повышение теплозащиты узлов ограждающих конструкций зданий с применением пеностеклокристаллического материала // Инженерно-строительный журнал. 2015. № 8(60). С. 56–67. DOI:10.5862/MCE.60.7
34. Konesev S., Khazieva R., Konev A., Kondratyev E. The research of heating efficiency of different induction heating systems // MATEC Web of Conferences. 2017. Vol. 113. DOI:10.1051/matecconf/201711301002
35. Larionov A., Minnullina A. Analysis of heat-conducting inclusions in exterior walls of residential building // IOP Conference Series: Earth and Environmental Science. 2017. Vol. 90(1). DOI:10.1088/1755-1315/90/1/012188
36. Khalimov O., Shibaeva G., Portnyagin D., Ibe K. The improvement of aseismic horizontal frame’s thermal insulations // Journal of Physics: Conference Series. 2018. Vol. 365(4). DOI:10.1088/1757-899X/365/4/042071

Viktor Pukhkal,
+7(921)741-42-01; pva1111@rambler.ru

Angela Mottaeva,*
+7(926)203-52-86; angela-1309.m@yandex.ru

Виктор Алексеевич Пухкал,
+7(921)741-42-01;
эл. почта: pva1111@rambler.ru

Анджела Бахауовна Моттаева,*
+7(926)203-52-86; эл. почта: angela-1309.m@yandex.ru

Pukhkal, V.A., Mottaeva, A.B. FEM modeling of external walls made of autoclaved aerated concrete blocks. *Magazine of Civil Engineering*. 2018. 81(5). Pp. 202–211. doi: 10.18720/MCE.81.20

Федеральное государственное автономное образовательное учреждение высшего образования
Санкт-Петербургский политехнический университет Петра Великого

ПОЛИТЕХ
Санкт-Петербургский политехнический университет Петра Великого

Инженерно-строительный институт
Центр дополнительных профессиональных программ

195251, г. Санкт-Петербург, Политехническая ул., 29,
тел/факс: 552-94-60, www.stroikursi.spbstu.ru,
stroikursi@mail.ru

Приглашает специалистов проектных и строительных организаций,
не имеющих базового профильного высшего образования
на курсы профессиональной переподготовки (от 500 часов)
по направлению «Строительство» по программам:

П-01 «Промышленное и гражданское строительство»

Программа включает учебные разделы:

- ***Основы строительного дела***
- ***Инженерное оборудование зданий и сооружений***
- ***Технология и контроль качества строительства***
- ***Основы проектирования зданий и сооружений***
- ***Автоматизация проектных работ с использованием AutoCAD***
- ***Автоматизация сметного дела в строительстве***
- ***Управление строительной организацией***
- ***Управление инвестиционно-строительными проектами. Выполнение функций технического заказчика***

П-02 «Экономика и управление в строительстве»

Программа включает учебные разделы:

- ***Основы строительного дела***
- ***Инженерное оборудование зданий и сооружений***
- ***Технология и контроль качества строительства***
- ***Управление инвестиционно-строительными проектами. Выполнение функций технического заказчика и генерального подрядчика***
- ***Управление строительной организацией***
- ***Экономика и ценообразование в строительстве***
- ***Управление строительной организацией***
- ***Организация, управление и планирование в строительстве***
- ***Автоматизация сметного дела в строительстве***

П-03 «Инженерные системы зданий и сооружений»

Программа включает учебные разделы:

- ***Основы механики жидкости и газа***
- ***Инженерное оборудование зданий и сооружений***
- ***Проектирование, монтаж и эксплуатация систем вентиляции и кондиционирования***
- ***Проектирование, монтаж и эксплуатация систем отопления и теплоснабжения***
- ***Проектирование, монтаж и эксплуатация систем водоснабжения и водоотведения***
- ***Автоматизация проектных работ с использованием AutoCAD***
- ***Электроснабжение и электрооборудование объектов***

П-04 «Проектирование и конструирование зданий и сооружений»

Программа включает учебные разделы:

- ***Основы сопротивления материалов и механики стержневых систем***
- ***Проектирование и расчет оснований и фундаментов зданий и сооружений***
- ***Проектирование и расчет железобетонных конструкций***
- ***Проектирование и расчет металлических конструкций***
- ***Проектирование зданий и сооружений с использованием AutoCAD***
- ***Расчет строительных конструкций с использованием SCAD Office***

П-05 «Контроль качества строительства»

Программа включает учебные разделы:

- ***Основы строительного дела***
- ***Инженерное оборудование зданий и сооружений***
- ***Технология и контроль качества строительства***
- ***Проектирование и расчет железобетонных конструкций***
- ***Проектирование и расчет металлических конструкций***
- ***Обследование строительных конструкций зданий и сооружений***
- ***Выполнение функций технического заказчика и генерального подрядчика***

По окончании курса слушателю выдается диплом о профессиональной переподготовке установленного образца, дающий право на ведение профессиональной деятельности